

UNIVERSITY OF LEICESTER

Excitotoxic ATP and Glutamate Signalling during Central Nervous System Ischaemia

Thesis submitted for the degree of
Doctor of Philosophy in the Faculty of Medicine and Biological Sciences
at the University of Leicester

© **Philipp Julio Vermehren, March 2010**

This thesis is copyright material and no quotation from it may be published
without proper acknowledgement.

Abstract

Excitotoxic ATP and Glutamate Signalling during Central Nervous System Ischaemia

Philipp Julio Vermehren

Neural cell death plays a crucial role in the pathogenesis of various ischaemic disorders of the central nervous system (CNS), most prominently stroke, causing very significant mortality and morbidity. Severe ischaemia rapidly kills both neurons and astrocytes, two CNS cell types whose interactions are essential to normal brain functioning, so ideally a target needs to be found which will protect both. Glutamate mediated excitotoxicity, the process whereby excessive extracellular glutamate causes cell death via the over-activation of ionotropic glutamate receptors, is known to operate during ischaemia. However, there is increasing evidence that ATP mediated excitotoxicity may also occur. Using an *in vitro* model of ischaemia (oxygen-glucose deprivation: OGD) and various murine primary cortical cell cultures, I investigated the hypothesis that parallel pathways of ATP and glutamate mediated excitotoxicity contribute to the death of both astrocytes and neurons during ischaemia. OGD produced rapid and significant ATP and glutamate release from co-cultures of astrocytes and neurons, as measured using microelectrode biosensors. Glutamate release was mainly from astrocytes, whereas the cellular origin of ATP was less clear. Ca^{2+} imaging of Fura-2 loaded cells confirmed functional P2 receptor expression in all astrocytes and 60% of neurons along with glutamate receptor expression in all neurons but only a small proportion of astrocytes. During OGD, blocking NMDA and AMPA/kainate receptors significantly reduced neuronal death, while non-selective P2 receptor antagonists as well as selective P2Y₁ (but not P2X₇) receptor antagonists prevented the death of both neurons and astrocytes. Furthermore, a synergistic protective effect was produced by combining low concentrations of P2 and glutamate receptor antagonists, reducing cell death to control levels. These results suggest that ATP and glutamate, acting at P2 and ionotropic glutamate receptors, are the main mediators of early cell death during severe CNS ischaemia, and thus represent a potential target for powerful neuroprotective strategies.

Dedicated to:

Camille, Catalina, Sebastian, Barbara and Joachim

Acknowledgements

I would like to thank my supervisor Dr. Robert Fern for supporting me throughout this project; I could not have gotten this far without his support, patience, and unerring enthusiasm throughout the good times and the bad. I would also like to thank Dr. Antonio Miguel de Jesus Domingues for assistance with molecular biology experiments and helpful comments on my thesis, Maria and Nestor for advice regarding cell cultures, Professor Nick Hartell for allowing me to use his confocal microscope, and Professor Nicholas Dale at the University of Warwick for technical assistance with the microelectrode biosensors. Lastly, I would like to thank the local charity MediSearch for the studentship which helped fund my PhD.

Table of contents

Abstract	ii
Acknowledgements	iv
List of figures	ix
List of tables	xii
List of abbreviations	xiii
Chapter 1: Introduction	1
The burden of ischaemic brain injury.....	2
Pathophysiology of cerebral ischaemia.....	2
Immediate events.....	2
Ischaemia damages neurons and glial cells.....	4
The importance of glial cells.....	5
Glutamate excitotoxicity during ischaemia	6
A short historical perspective.....	6
Glutamate receptors.....	7
Overview of purinergic signalling.....	9
ATP as a neurotransmitter	9
Purinergic receptors	10
Purinergic signalling in the CNS	11
ATP-mediated excitotoxicity during CNS ischaemia?.....	12
Links between purinergic and glutamatergic signalling.....	13
OBJECTIVES	14
Chapter 2: Methods and Materials	15
Cell culture methods	16
Preparation of cell culture flasks and microscope cover slips	16
Different buffers and growth media.....	16
Dissections and tissue preparation	17
Cortical neuron culture	19
Cortical astrocyte culture.....	19
Co-culture of astrocytes and neurons.....	20
Important observations.....	20
P2Y ₁ -/- cell cultures.....	21
Immunohistochemical characterization of the cell cultures	22
Protocols	23
Imaging.....	24
Image analysis.....	25
Results: cell culture characterisation.....	26
Astrocyte culture IHC.....	27
Neuronal culture IHC.....	28
Co-culture IHC	29
Solutions and pharmacological reagents used.....	33
Fluorescence Microscopy of Cells	36
Fura-2ff and Fura-2.....	36
Problems with Fura-2ff during long experiments at 37°C.....	37
BCECF, Propidium Iodide and CMFDA for cell viability studies	39
Mounting and loading of cells for fluorescence microscopy	43
<i>Oxygen-glucose deprivation (OGD) experiments</i>	43
<i>Short agonist application experiments</i>	43

Cell perfusion set-up	44
<i>OGD experiments</i>	44
<i>Short agonist application experiments</i>	45
Cell imaging set-up	46
Imaging protocols.....	46
<i>OGD experiments</i>	46
<i>Short agonist application experiments</i>	47
Image analysis.....	47
Assessing cell viability/death	48
Identification/differentiation of astrocytes and neurons in co-culture.....	51
eGFP-GFAP transgenic mice: a puzzling loss of eGFP fluorescence in cell cultures.....	51
Pre-loading of astrocytes with CMFDA before neuronal plating.....	55
Phase-contrast light microscopy for cell identification	55
Data analysis and statistics.....	56
Molecular Biology	58
mRNA extraction	58
RT-PCR.....	59
Measuring glutamate and ATP release using microelectrode biosensors	60
Biochemistry and physical structure of the ATP and glutamate microelectrode biosensors.....	61
Experimental set-up and protocols.....	63
Data analysis and statistics.....	67
Chapter 3: ATP and glutamate release from cultured neurons and astrocytes	68
INTRODUCTION.....	69
Foreword.....	69
Glutamate metabolism in the CNS	70
Glutamate transport and the glutamate-glutamine cycle	70
Mechanisms involved only in glutamate release	71
Glutamate transporters.....	71
Cystine-glutamate antiporter	74
Mechanisms involved only in ATP release	74
ATP-binding cassette (ABC) proteins: multidrug resistance-associated protein (MRP), <i>p</i> -glycoprotein and the cystic fibrosis transmembrane regulator (CFTR).....	74
Mechanisms involved in both ATP and glutamate release.....	75
Volume-regulated anion channels (VRACs)	75
Connexin/Pannexin hemichannels.....	76
P2X receptors	78
Exocytosis.....	79
Loss of cell membrane integrity	81
Summary.....	82
Objectives	82
RESULTS	84
Data post-processing of ATP and glutamate electrode recordings	84
ATP and glutamate release from co-cultured astrocytes and neurons	89
ATP and glutamate release from astrocyte cultures	94
ATP and glutamate release from neuronal cultures	97
DISCUSSION	100
Summary of results.....	100
Technical considerations	100
Glutamate release during OGD is mainly from astrocytes	100

ATP release during OGD: a co-operative effect of neurons and astrocytes?.....	104
Chapter 4: Functional P2 and glutamate receptors on cultured neurons and astrocytes.....	109
INTRODUCTION.....	110
Iontropic glutamate receptors	111
Classification and general properties	111
NMDA receptors: structure and function.....	111
AMPA/kainate receptors: structure and function	112
Iontropic glutamate receptor expression in cortical neurons and astrocytes	113
Glutamate receptor agonists and antagonists used.....	114
P2 receptors.....	115
P2X receptors: structure and function	115
P2Y receptors: structure and function.....	116
P2 receptor expression in cortical neurons and astrocytes.....	116
P2 receptor agonists and antagonists used.....	119
Objectives	125
RESULTS.....	126
Glutamate receptors on cultured cortical neurons.....	128
P2 receptors on cultured cortical neurons	132
P2 receptors on cultured cortical astrocytes.....	134
Glutamate receptors on cultured cortical astrocytes	143
Effects of NBQX, MK-801 and PPADS on neuronal glutamate and P2 receptors	145
Effects of suramin, PPADS, KN-62 and MRS-2179 on astroglial P2 receptors.....	148
P2 and glutamate receptor mediated $[Ca^{2+}]_i$ rises in co-cultured astrocytes and neurons.....	155
DISCUSSION.....	156
Functional glutamate receptor responses in cultured neurons and astrocytes.....	156
Functional P2 receptor responses in cultured neurons and astrocytes.....	159
Summary of conclusions.....	163
Chapter 5: Roles of ATP and glutamate during the ischaemic injury of cultured astrocytes and neurons.....	165
INTRODUCTION.....	166
Ischaemic cell death.....	166
Importance of ionic deregulation early during ischaemia	166
Ischaemic neuronal death: a major role for glutamate excitotoxicity.....	167
Ischaemic astrocyte death: controversy over sensitivity to ischaemia.....	168
Mechanisms of ischaemic astrocyte death	170
Shortcomings of the NMDA-AMPA model of ischaemic cell death.....	172
The case for ATP-mediated excitotoxicity during ischaemia	173
Potential involvement of specific P2 receptor subtypes	174
Astrocyte-neuron interactions during ischaemia.....	177
Objectives	180
RESULTS.....	181
OGD causes significant cell death of cultured neurons and astrocytes.....	182
Effect of OGD on astrocyte cultures, neuronal cultures, and co-cultures	182
Comparing effects of OGD and control conditions on cell death in different cultures.....	183
Effect of co-culturing vs. mono-cultures on astrocyte and neuronal death during OGD.....	192
Effect of Neurobasal medium on astrocytes cultures: an increased susceptibility to ischaemic injury	196
Co-culture vs. astrocyte culture in Neurobasal: a re-analysis	115

Cell death was always preceded by an increase in $[Ca^{2+}]_i$	203
Continuous application of P2 and glutamate receptor agonists during OGD and control conditions	209
Continuous ATP application in neuronal cultures during control conditions	209
Continuous ATP and glutamate application in neuronal cultures during OGD	214
Continuous application of glutamate during OGD in co-cultures	219
Continuous application of ATP and MRS-2365 during OGD in co-cultures	224
P2 receptor and ionotropic glutamate receptor antagonists prevent cell death in co-cultures during OGD	229
Effects of non-selective P2 receptor antagonists	229
Effects of P2Y ₁ and P2X ₇ receptor antagonists	234
Effects of glutamate receptor antagonists	239
Combining P2 and glutamate receptor antagonists	244
Summary: P2 and glutamate receptor antagonists during OGD in co-cultures	248
DISCUSSION	252
Astrocytes kept in Neurobasal medium are more sensitive to OGD	252
Lack of increased cell death in the neuronal culture by OGD, ATP, and/or glutamate	253
Significant neuronal death during OGD only occurred in co-cultures: importance of astrocyte-neuron interactions?	256
$[Ca^{2+}]_i$ changes during OGD	258
Exogenous ATP and glutamate application	261
Glutamate receptor antagonists prevent neuronal but not astrocyte death	267
Broad-spectrum P2 receptor antagonists prevent death of both neurons and astrocytes	268
P2X ₇ receptor- possible contribution to neuronal death during OGD	270
Potent reduction of OGD induced neuron and astrocyte death by P2Y ₁ antagonism	273
Synergistic protective effect of P2 and glutamate receptor antagonists during ischaemia	275
Final Summary	276
Chapter 6: Final conclusions, discussion and perspectives	277
Summary of results	278
Protective effect of P2 receptor antagonists does not appear to be mediated by interference with glutamate excitotoxicity	281
Potential roles for purinergic signaling beyond the initial phase of necrotic cell death	281
Potential for ATP-mediated excitotoxicity in white matter oligodendrocytes	282
Possible contributions of microglia to ischaemic cell death	283
Considerations regarding stroke therapy: neuroprotective strategies using a combination of glutamate and P2 receptor antagonists	284
Final thoughts	287
Bibliography	288

List of figures

Figure 1-1: Events in brain ischemia	3
Figure 1-2: Classification of glutamate receptors	8
Figure 1-3: Purinergic receptors, an overview	11
Figure 2-1: Total cell counts in IHC experiments	26
Figure 2-2: Astrocyte culture IHC	30
Figure 2-3: Neuronal Culture IHC	31
Figure 2-4: Co-Culture IHC	32
Figure 2-5: Example of fading in Fura-2ff loaded astrocytes	38
Figure 2-6: Example of CMFDA-loaded astrocytes	41
Figure 2-7: Comparing Fura-2ff and CMFDA retention in astrocytes and neurons	42
Figure 2-8: Perfusion system setup, OGD experiments	45
Figure 2-9: Assessing cell viability using Fura-2ff in co-cultured astrocytes and neurons .	50
Figure 2-10: Imaging eGFP-GFAP astrocytes	53
Figure 2-11: PCR analysis of eGFP-GFAP astrocyte cultures	54
Figure 2-12: Cell identification during fluorescent imaging	57
Figure 2-13: Enzymatic reactions in the glutamate and ATP biosensor microelectrodes .	61
Figure 2-14: Physical structure of the microelectrode biosensors	63
Figure 2-15: Pot calibrations of the different types of electrodes used	64
Figure 2-16: Electrode Setup	66
Figure 3-1: Glutamate metabolism and Na ⁺ -dependant transporters	71
Figure 3-2: Mechanisms of ATP and glutamate release from astrocytes and neurons	83
Figure 3-3: Example recordings and data workflow, co-culture ATP release	86
Figure 3-4: Example traces of ATP and glutamate electrode recordings, including calibrations	87
Figure 3-5: ATP release from co-cultured astrocytes and neurons during OGD	91
Figure 3-6: Glutamate release from co-cultured astrocytes and neurons during OGD	92
Figure 3-7: Effect of PPADS on glutamate release from co-culture during OGD	93
Figure 3-8: ATP release from astrocyte cultures during OGD	95
Figure 3-9: Glutamate release from astrocyte cultures during OGD	96
Figure 3-10: ATP release from neuronal cultures during OGD	98
Figure 3-11: Glutamate release from cultured neurons during OGD	99
Figure 4-0: Resting [Ca ²⁺] _i levels in cultured neurons and astrocytes	127
Figure 4-1: Fura-2 Ca ²⁺ imaging of neuronal culture, glutamate receptor agonists	130
Figure 4-2: Functional glutamate receptors on cultured cortical neurons	131
Figure 4-3: Functional P2 receptors on cultured cortical neurons	133
Figure 4-4: Fura-2 Ca ²⁺ imaging of astrocyte culture, P2 receptor agonists	135
Figure 4-5: Functional P2 receptors on cultured cortical astrocytes	136
Figure 4-6: Multiple sequential applications of ATP	137
Figure 4-7: Ca ²⁺ removal experiments	140
Figure 4-8: P2Y ₁ ^{-/-} astrocytes	142
Figure 4-9: Functional glutamate receptors on cultured cortical astrocytes	144
Figure 4-10: Effects of NBQX, MK-801, and PPADS on neuronal receptors	147
Figure 4-11: Effects of suramin	149

Figure 4-12: Effects of PPADS	152
Figure 4-13: Effects of KN-62 and MRS-2179	154
Figure 5-0: Pathways contributing to ischaemic ionic deregulation of neurons and astrocytes	171
Figure 5-1: Example images of CMFDA loaded co-culture, control	184
Figure 5-2: Example images of CMFDA loaded co-culture, OGD	185
Figure 5-3: Example images of CMFDA loaded astrocyte culture, control	186
Figure 5-4: Example images of CMFDA loaded astrocyte culture, OGD	187
Figure 5-5: Example images of Fura-2ff loaded neuronal culture, control	188
Figure 5-6: Example images of Fura-2ff loaded neuronal culture, OGD	189
Figure 5-7: Effect of OGD vs. control on cell death in co-culture, astrocyte culture and neuronal culture	190
Figure 5-8: Effect of OGD and control conditions on cell death: comparing co-culture, astrocyte culture and neuronal culture	191
Figure 5-9: Effect of co-culturing neurons and astrocytes on cell death during OGD and control conditions	194
Figure 5-10: Effect of co-culturing neurons and astrocytes, timescale	195
Figure 5-11: Example images of CMFDA loaded astrocyte culture in Neurobasal, control	197
Figure 5-12: Example images of CMFDA loaded astrocyte culture in Neurobasal, OGD	198
Figure 5-13: Effect of Neurobasal medium on cell death in astrocyte culture	199
Figure 5-14: Effect of OGD and control conditions on cell death: comparing co-culture, astrocyte culture and neuronal culture, corrected for astrocyte culture in Neurobasal	201
Figure 5-15: Effect of co-culturing astrocytes and neurons: figures corrected for astrocyte culture in Neurobasal medium	202
Figure 5-16: $[Ca^{2+}]_i$ rises and cell death during OGD and control in co-cultures	206
Figure 5-17: Astrocyte vs. neuronal $[Ca^{2+}]_i$ rises and cell death during OGD in co-cultures	207
Figure 5-18: $[Ca^{2+}]_i$ rises and cell death during OGD and control in neuronal cultures	208
Figure 5-19: Effects of prolonged ATP application on cell death in neuronal culture during control conditions	211
Figure 5-20: Effects of prolonged ATP application on timescale of cell death in neuronal culture during control conditions	212
Figure 5-21: $[Ca^{2+}]_i$ rises and cell death in neuronal cultures when adding exogenous ATP during control conditions	213
Figure 5-22: Effects of ATP and glutamate application on cell death in neuronal cultures during OGD	217
Figure 5-23: $[Ca^{2+}]_i$ rises and cell death in neuronal cultures when adding exogenous ATP and glutamate during OGD	218
Figure 5-24: Effects on cell death of adding different concentrations of glutamate to co-cultures during OGD	221
Figure 5-25: Effects of adding different concentrations of glutamate to co-cultures during OGD, cumulative timescale of cell death	222

Figure 5-26: Effects of adding different concentrations of glutamate to co-cultures during OGD on cell death, timescale	223
Figure 5-27: Effects on cell death of adding ATP and MRS-2365 to co-cultures during OGD	226
Figure 5-28: Effects of adding ATP or MRS-2365 to co-cultures during OGD, cumulative timescale of cell death	227
Figure 5-29: Effects of adding ATP or MRS-2365 to co-cultures during OGD, timescale of cell death	228
Figure 5-30: Non-selective P2 receptor antagonists during OGD in co-culture	231
Figure 5-31: Non-selective P2 receptor antagonists during OGD in co-culture, cumulative timescale of cell death	232
Figure 5-32: Non-selective P2 receptor antagonists during OGD in co-culture, timescale of cell death	233
Figure 5-33: Effects of P2X ₇ and P2Y ₁ receptor blockade on OGD induced cell death in co-cultures	236
Figure 5-34: Effects of P2X ₇ and P2Y ₁ receptor blockade on OGD in co-cultures, cumulative timescale of cell death	237
Figure 5-35: Effects of P2X ₇ and P2Y ₁ receptor blockade on OGD in co-cultures, timescale of cell death	238
Figure 5-36: Effects of NMDA and AMPA/Kainate receptor antagonists on OGD induced cell death in co-cultures	241
Figure 5-37: Effects of NMDA and AMPA/Kainate receptor antagonists on OGD in co-cultures, cumulative timescale of cell death	242
Figure 5-38: Effects of NMDA and AMPA/Kainate receptor antagonists on OGD in co-cultures, timescale of cell death	243
Figure 5-39: Effects of combining P2 and glutamate receptor antagonists on OGD induced cell death in co-cultures	245
Figure 5-40: Effects of combining P2 and glutamate receptor antagonists during OGD in co-cultures, cumulative timescale of cell death	246
Figure 5-41: Effects of combining P2 and glutamate receptor antagonists during OGD in co-cultures, timescale of cell death	247
Figure 5-42: Summary of results, P2 and glutamate receptor antagonists during OGD	249
Figure 6-1: Final model of purinergic and glutamatergic events involved in astrocyte and neuronal death during OGD.....	280

List of tables

Table 2-1: Cell Culture Reagents	17
Table 2-2: Antibodies used for Immunohistochemistry	23
Table 2-3: Solutions used in experiments	34
Table 2-4: Pharmacological reagents	35
Table 2-5: List of PCR primers used for RT-PCR	59
Table 3-1: Extracellular glutamate levels during ischaemia, examples from literature	102
Table 3-2: Extracellular ATP levels during ischaemia, examples from the literature	105
Table 4-1: P2 receptor expression in cortical neurons and astrocytes	118
Table 4-2: Agonists at P2X receptors	121
Table 4-3: Agonists at P2Y receptors	122
Table 4-4: Antagonists at P2X receptors	123
Table 4-5: Antagonists at P2Y receptors	124
Table 4-6: Summary, glutamate and P2 receptor responses in neurons versus astrocytes	156
Table 4-7: Summary, P2 and glutamate receptor antagonists in neuronal cultures	156
Table 4-8: Summary, P2 receptor antagonists in astrocyte cultures	162
Table 5-1: Effects of P2 antagonists during <i>in vivo</i> ischaemia	178
Table 5-2: Effects of P2 antagonists during <i>in vitro</i> ischaemia	179
Table 5-3: Summary of results, neuron and astrocyte death in different cultures and effects of long agonist applications	250
Table 5-4: Summary of results, effects of different agonists and antagonists added to co- cultures during OGD.....	251

List of abbreviations

[Ca²⁺]_i: intracellular calcium concentration
aCSF: artificial cerebrospinal fluid
ADP: adenosine diphosphate
AMP: adenosine monophosphate
AMPA: alpha-amino-3-hydroxy-5-methyl-4-isoxazolepropionic acid
ANOVA: analysis of variance
ATP: adenosine triphosphate
ATPγS: adenosine 5'-O-(3-thio)triphosphate
BCECF: 2',7'-bis-(2-carboxyethyl)-5-(and-6)-carboxyfluorescein
BDNF: brain-derived neurotrophic factor
BzATP: 3'-O-(4-benzoyl)benzoyl adenosine 5'-triphosphate
CGN: cerebellar granule neurons
CMFDA: chloromethylfluorescein diacetate
CNPase: 2',3'-cyclic nucleotide 3'-phosphodiesterase
CNS: central nervous system
DIV: days in vitro
DM: DMEM-based culture medium
DMEM: Dulbecco's minimum essential medium
E: embryonic day
EAAT: excitatory amino acid transporter
eGFP: enhanced green fluorescent protein
EGTA: ethylene glycol-bis(2-aminoethylether)-N,N,N',N'-tetraacetic acid
ER: endoplasmic reticulum
FBS: foetal bovine serum
fEPSP: field excitatory post-synaptic potential
Fura-2 AM: fura-2-acetoxymethyl ester
Fura-2ff AM: fura-ff-acetoxymethyl ester
GABA: gamma amino-butyric acid
GDNF: glial-derived neurotrophic factor
GFAP: glial fibrillary acidic protein
GLAST: glutamate-aspartate transporter
GLT-1: glial-type glutamate transporter
GPCR: g-protein coupled receptor
GSH: glutathione
HAIR: hypoxic acidic ion-shifted ringer solution
HBSS: hank's balanced salt solution
HH: hypoxia-hypoglycaemia
IB-4: isolectin-B4
IHC: immunohistochemistry
IMS: industrial methylated spirits
KN-62: 4-[(2S)-2-[(5-isoquinolinesulfonyl)methylamino]-3-oxo-3-(4-phenyl-1-piperazinyl)propyl] phenyl isoquinolinesulfonic acid ester
LDH: lactate dehydrogenase

MCAO: middle cerebral artery occlusion
mGluR: metabotropic glutamate receptor
MK-801: (+)-5-methyl-10,11-dihydro-5*H*-dibenzo[*a,d*]cyclohepten-5,10-imine maleate
mRNA: messenger ribonucleic acid
MRS-2179: 2'-deoxy-N6-methyladenosine 3',5'-bisphosphate tetrasodium salt
MRS-2365: [[[1*R*,2*R*,3*S*,4*R*,5*S*]-4-[6-amino-2-(methylthio)-9*H*-purin-9-yl]-2,3-dihydroxybicyclo[3.1.0]hex-1-yl]methyl] diphosphoric acid mono ester trisodium salt
NANC: non-adrenergic non-cholinergic
Nb: Neurobasal-based culture medium
NBQX: 2,3-dihydroxy-6-nitro-7-sulfamoyl-benzo[*f*]quinoxaline-2,3-dione
NCX: sodium-calcium exchanger
NG-2: nerve/glial antigen-2
NKA: sodium/potassium ATPase
NMDA: N-methyl-D-aspartate
NO: nitric oxide
NSE: neuron-specific enolase
NTPDase: nucleoside triphosphate diphosphohydrolase
OGD: oxygen-glucose deprivation
oxATP: 2',-3',-dialdehyde ATP/oxidized ATP
P: postnatal day
PBS: phosphate buffered saline
PCR: polymerase chain reaction
PI: propidium iodide
PLC: phospholipase C
PMCA: plasma membrane calcium ATPase
PPADS: pyridoxal-phosphate-6-azophenyl-2',4'-disulfonate tetrasodium salt
PS: population spikes
PVL: periventricular leukomalacia
RB-2: reactive blue 2 (also synonymous with- basilen blue, evans blue 2)
RON: rat optic nerve
ROS: reactive oxygen species
RT-PCR: reverse transcriptase polymerase chain reaction
SDEV: standard deviation
SEM: standard error of the mean
SERCA: sarco/endoplasmic reticulum calcium ATPase
siRNAs: small interfering ribonucleic acids
TRP: transient receptor potential
UDP: uridine diphosphate
UTP: uridine triphosphate
VGCC: voltage-gated calcium channel

Chapter 1:
Introduction

The burden of ischaemic brain injury

Neural cell death plays a crucial role in the pathogenesis of various ischaemic disorders of the central nervous system (CNS), causing very significant levels of mortality and morbidity in humans. In neonates, prolonged prenatal or perinatal hypoxia/ischaemia has the potential to produce widespread injury to the central nervous system, often leading to problems such as mental retardation, seizures, and/or motor impairment (Vexler and Ferriero, 2001). One frequent outcome, cerebral palsy, affects between 2 to 2.5 of 1000 live births (Russman and Ashwal, 2004). In particular, white-matter structures in the developing brain are often injured, producing a pattern of neurological injury termed periventricular leukomalacia (PVL), in which there is early damage to axons and glial cells (Banker and Larroche, 1962; Volpe, 2001, 2003, 2009). Most cases of PVL arise during mid-gestation. Between 60% and 100% of infants who show this particular pattern of injury later develop cerebral palsy, and 90% of preterm infants who develop cerebral palsy show signs of PVL-induced gliosis on magnetic resonance imaging (Saliba and Marret, 2001; Obenaus and Ashwal, 2008). In the adult brain, stroke is by far the most common injury involving neural cell death, killing about 5.4 million people worldwide each year (110,000 in the UK) whilst leaving an even larger numbers of survivors debilitated, at an annual cost to the UK economy of £7-8 billion (Flynn et al., 2008). It comes as no surprise that ever increasing amounts of research are underway to try and elucidate the mechanisms that are involved in ischaemia-induced neural cell death in search of effective methods to prevent and treat ischaemic brain injury (Ginsberg, 2008).

Pathophysiology of cerebral ischaemia

Immediate events

The human brain requires enormous amounts of energy, demanding around 25 - 50% of cardiac output to maintain its metabolic needs (Flynn et al., 2008). During acute cerebral ischaemia, a limitation in energy supply to the brain, either focally by arterial blockage (focal ischaemia, for example stroke) or globally (during cardiac arrest) results in a rapid and massive collapse of cellular ion gradients, leading to permanent cell damage and death if not reversed within minutes (Rossi et al., 2007; Hertz, 2008). A lack of oxygen

and glucose delivery to the cells causes a reduction in cellular ATP (adenosine triphosphate) levels, and this is accompanied initially by a gradual drop in pH and accumulation of extracellular K^+ as neurons begin to depolarise (Hansen and Nedergaard, 1988; Pringle, 2004; Rossi et al., 2007). Once intracellular ATP levels reach a critical low point, there is a sudden widespread depolarisation of cells accompanied by massive influx of Na^+ , Ca^{2+} , and Cl^- (Ca^{2+} arguably being the most important in terms of mediating cell death), a large efflux of K^+ , a further fall in both intra- and extracellular pH levels and an increase in extracellular glutamate concentration by a combination of the release of synaptic glutamate, failure of glutamate uptake, and the reversal of glutamate uptake mechanisms (See **Figure 1-1**) (Hansen and Nedergaard, 1988; Goldberg and Choi, 1993; Chidekel et al., 1997; Silver et al., 1997; Martinez-Sanchez et al., 2004; Pringle, 2004; Bano and Nicotera, 2007).

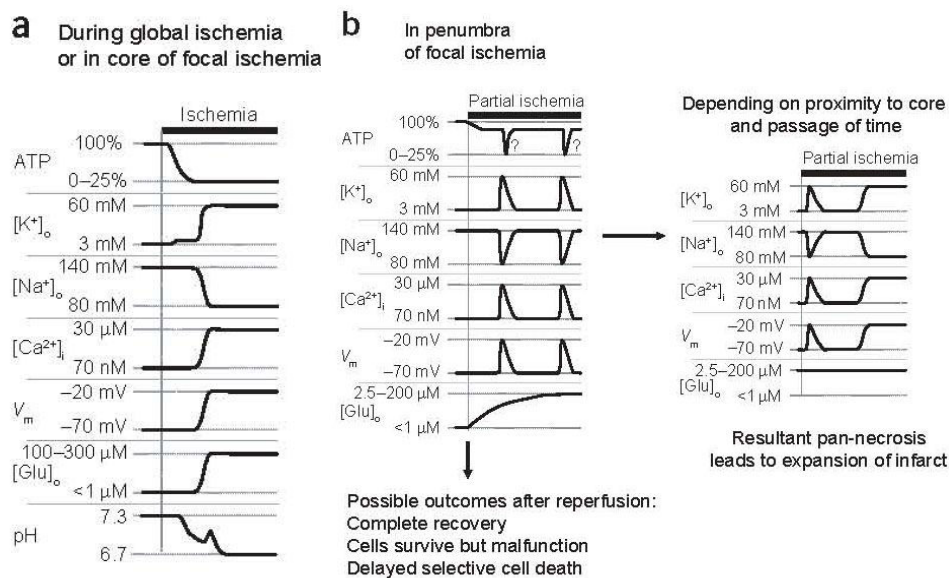


Figure 1-1: Events in brain ischemia

a- events during severe ischaemia: Interruption of ATP production leads to a disruption of transmembrane ion gradients. Initially there is a slow drop in pH and extracellular K^+ accumulation. Later, the anoxic depolarisation occurs, accompanied by massive toxic influx of Na^+ , and Ca^{2+} , K^+ efflux, further acidification and release of large quantities of glutamate into the extracellular space.

b- events in penumbra: Drop in ATP is less severe, but triggers repeated transient depolarisations and ion shifts and slower rise of extracellular glutamate. With increasing duration of ischaemia and proximity to core the transient depolarisations can evolve into terminal depolarisation and ionic disruptions, leading to pan-necrosis and infarct expansion (right panel).

Adapted with permission from Macmillan Publishers Ltd: Nature Neuroscience, (Rossi et al., 2007).

Ischaemia damages neurons and glial cells

The pathophysiological processes leading to eventual injury and death of neurons, glia and endothelial cells include excitotoxicity, acidotoxicity and ionic imbalance, peri-infarct depolarisation, oxidative and nitrative stress, inflammation and apoptosis (Arundine and Tymianski, 2003; Doyle et al., 2008; Brouns and De Deyn, 2009). Each of the above processes occurs over a distinct time frame, lasting from minutes to days, and the extent of cell death during ischaemia is closely related to the severity and duration of the insult (Doyle et al., 2008). During global ischaemia or within the infarct core of a focal ischaemic lesion, where blood flow is most severely restricted, excitotoxicity and necrotic cell death occur within minutes. In the ischaemic penumbra, where collateral blood flow around the core of a focal ischaemic lesion is able to prevent complete oxygen and glucose deprivation, cell death occurs more slowly by mechanisms such as apoptosis and/or inflammation (Doyle et al., 2008; Hertz, 2008). Cells in the penumbra are of particular interest as the slower onset of cell death in these areas ensures a longer window of opportunity for the administration of potentially beneficial therapeutic measures (Weinberger, 2006).

There is also considerable variation in terms of: the susceptibility to and mechanisms of cell death and injury during ischaemia between different CNS regions and cell types and the age/developmental stage of said structures (Towfighi et al., 1997; Johnston et al., 2002; Kahlert and Reiser, 2004; Nedergaard and Dirnagl, 2005; Giaume et al., 2007; Rossi et al., 2007; Hertz, 2008). For example, the delayed death of glutamatergic neurons in the CA1 area of the hippocampus with sparing of CA3 and dentate gyrus neurons is a hallmark of brief global ischaemia followed by reperfusion (Hertz, 2008). There is also still a generally held belief that neurons are the most susceptible to ischaemia whilst astrocytes are more resistant. However, there is ample evidence that astrocyte dysfunction and death in both grey and white matter can occur quickly following the onset of ischaemia, often preceding neuronal death, with astrocytes in earlier developmental stages being particularly vulnerable (Garcia et al., 1993; Martin et al., 1997; Fern, 1998; Petito et al., 1998; Liu et al., 1999; Zhao and Flavin, 2000; Bondarenko and Chesler,

2001a, b; Xu et al., 2001; Lukaszewicz et al., 2002; Thomas et al., 2004; Bondarenko et al., 2005; Shannon et al., 2007; Salter and Fern, 2008). Oligodendrocytes and nerve/glia antigen-2-positive (NG-2⁺) glia are also exquisitely sensitive to ischaemic injury (Lyons and Kettenmann, 1998; Fern and Moller, 2000; Tekkok and Goldberg, 2001; Karadottir et al., 2005; Salter and Fern, 2005; Karadottir et al., 2008). Nevertheless, there is still a relative paucity of research investigating mechanisms leading to glial death during ischaemia compared to neuronal death.

The importance of glial cells

For the better part of the last 150 years, neuroscientists largely ignored the study of glial cells, a population composed of astrocytes, oligodendrocytes (or Schwann cells peripherally), NG-2⁺ glia and microglia, despite the fact that they make up over 50% of the volume of the brain and outnumber neurons in the grey matter by a factor 1.3-1.8 (Giaume et al., 2007; Hertz, 2008). Additionally, phylogenetic advances in brain complexity and capabilities between species coincide with an increase in the ratio of glial to neuronal cells (Nedergaard et al., 2003). Glia, and astrocytes in particular (the most numerous glial cell type in the CNS), were initially thought to serve mainly as a sort of three dimensional scaffolding or 'glue' through which neurons could extend and maintain their synaptic connections, without themselves participating in synaptic transmission or other forms of information processing (Volterra and Meldolesi, 2005). It is now well known that this is far from the truth (Nedergaard et al., 2003).

Oligodendrocytes and Schwann cells produce myelin sheaths which are essential for fast saltatory axonal conduction, whilst microglia represent the primary immune host defence system in the brain. NG-2⁺ glia include oligodendrocyte and astrocyte progenitor cells as well as cells which persist in the mature brain, and they are potentially implicated in neuron-glia signalling (Wigley et al., 2007; Karadottir et al., 2008; Otis and Sofroniew, 2008). Astrocytes are intimately involved in neuronal activity by maintaining an extracellular milieu which is optimal for neurotransmission, terminating the actions of transmitters by various uptake/breakdown mechanisms and providing substrates for

neurotransmitter formation, whilst they are also involved in glial-glia and neuron-glia intercellular communication, the activity dependant control of local blood flow and the blood-brain barrier, and even modulation of synaptic transmission and synapse formation, a process often involving the release of neuroactive agents from astrocytes themselves (Beaman-Hall et al., 1998; Anderson and Swanson, 2000; Auld and Robitaille, 2003; Nedergaard et al., 2003; Araque and Perea, 2004; Fellin et al., 2004; Pellerin and Magistretti, 2004; Reichenbach and Wolburg, 2005; Jessen, 2006; Kozlov et al., 2006). In addition there is increasing evidence that astroglial-like cells in certain regions of the brain, such as the subventricular zone and dentate gyrus, may generate neurons, and astrocytes also influence neuronal growth by releasing neurotrophic factors (Chen and Swanson, 2003; Noctor et al., 2005; Luzzati et al., 2006; Zhang et al., 2008). Neurons in the CNS cannot survive without close interactions with astrocytes (Chen and Swanson, 2003). It comes as no surprise then that astroglial death during or after an ischaemic insult is to the great detriment of adequate functional recovery of the CNS. The lack of glial-protective effects of many neuro-protective agents which have entered into pre-clinical trials has been listed as a possible reason for their repeated failures to show significant benefits (Matute et al., 2006). Accordingly, efforts need to be focused more on protecting astrocytes as well as neurons; indeed, it is eminently likely that any manipulation which leads to increased survival of astrocytes will also be protective of neurons.

Glutamate excitotoxicity during ischaemia

A short historical perspective

Glutamate is the major excitatory neurotransmitter in the mammalian CNS, where it normally mediates physiological signalling. It was first reported in 1957 by Lucas and Newhouse that sustained exposure to parenterally administered L-glutamate resulted in retinal neuron cell death (Lucas and Newhouse, 1957). John Olney and his group then went on to describe how this phenomenon of neuronal death also occurred in other parts of the CNS following application or administration of glutamate, kainate and other excitatory neurotransmitters, coining the term excitotoxicity (Olney, 1969; Olney and Sharpe, 1969; Olney et al., 1971). In 1982, Jorgensen and Diemer noticed that the pattern of selective

neuronal death present after transient cerebral ischaemia corresponded closely to areas of high affinity glutamate-uptake and areas which are selectively injured by the administration of excitatory neurotransmitters, suggesting that glutamate may be involved in this neuronal death (Jorgensen and Diemer, 1982). The same laboratory went on to produce the seminal first paper documenting significantly increased extracellular glutamate (and aspartate) concentrations in the hippocampus during transient cerebral ischaemia in rats using the technique of intracerebral microdialysis (Benveniste et al., 1984). Other groups then used this and other methods to confirm that extracellular glutamate levels rise significantly during ischaemia in other parts of the brain and when using different models or methods of cerebral ischaemia (Hagberg et al., 1985; Globus et al., 1988; Matsumoto et al., 1996; Ooboshi et al., 2000). It has also been demonstrated in humans both *in vivo* and *in vitro* (Castillo et al., 1996; Persson et al., 1996; Marcoli et al., 2004b; Marcoli et al., 2004a).

Glutamate receptors

Glutamate receptors were initially characterised in the central nervous system according to the actions of glutamate, quisqualate, AMPA (α -amino-3-hydroxy-5-methyl-4-isoxazole-propionic acid) and kainate on distinct neuronal populations (Watkins and Jane, 2006). The advent of more selective glutamate receptor antagonists in the 1970s and 80s helped to further define the presence and importance of ionotropic NMDA (*N*-methyl-*D*-aspartate) and non-NMDA (AMPA/kainate) receptors in excitatory CNS pathways, while compelling evidence for the existence of metabotropic glutamate receptors (mGluRs) was first presented in 1985 (Sladeczek et al., 1985; Watkins and Jane, 2006). Following the advent of molecular biology and the cloning of glutamate receptors, the current classification of glutamate receptors was developed which divides receptors broadly into ionotropic and metabotropic receptors (see **Figure 1-2**) (Watkins and Jane, 2006). Ionotropic glutamate receptors are divided into NMDA, AMPA and kainate receptors, all of which are cation-specific ion channels formed by variable assemblies of different subunits which confer specific properties to said receptors, while eight different mGluR subtypes are divided into three groups depending on agonist pharmacology, signal transduction pathways and sequence homology (Watkins and Jane, 2006; D'Antoni et al., 2008).

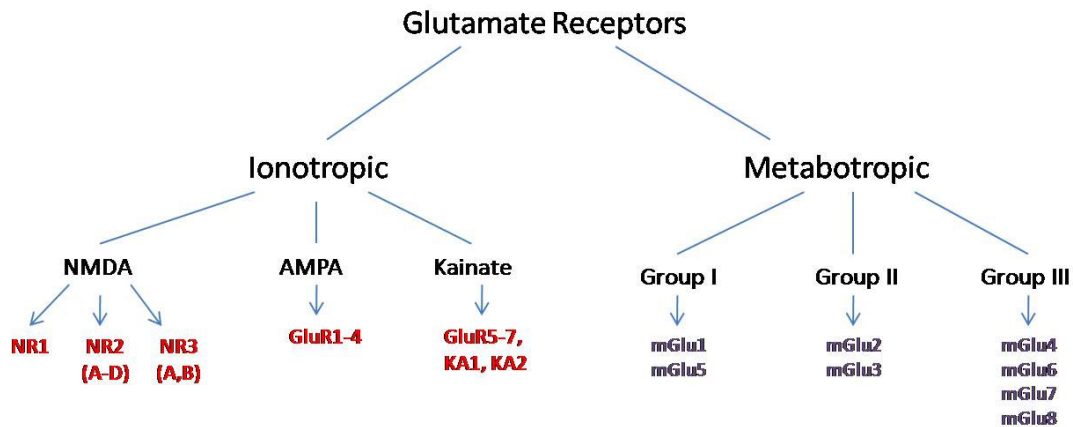


Figure 1-2: Classification of glutamate receptors

Glutamate receptors are divided into ionotropic (ion channels) and metabotropic receptors, with the former consisting of NMDA, AMPA and Kainate receptors and the latter of 8 G-protein coupled receptors (*purple writing*) which are divided into groups I-III according to similarities in second messenger coupling. Ionotropic receptors are composed of combinations of various subunits (*red writing*). Adapted from (Watkins and Jane, 2006)

It is now well established that glutamate-mediated excitotoxicity in neurons is caused by over-activation of ionotropic glutamate receptors, particularly NMDA receptors but also AMPA/kainate receptors, and that this leads to cell death via toxic elevations of intracellular Ca^{2+} (Choi et al., 1988; Nøllgard and Wieloch, 1992; Vornov et al., 1994; Strasser and Fischer, 1995; Vornov, 1995; Pringle et al., 1997). Ischaemia-induced glutamate excitotoxicity, mediated by both NMDA and AMPA/kainate receptors has also been demonstrated to occur in oligodendrocytes and NG-2⁺ glia (McDonald et al., 1998; Fern and Møller, 2000; Tekkok and Goldberg, 2001; Deng et al., 2003; Wilke et al., 2004; Karadottir et al., 2005; Salter and Fern, 2005; Micu et al., 2006; Karadottir et al., 2008). Furthermore, downstream events including reactive oxygen species generation and activation of cell death mediators such as ATPases, proteases, lipases and DNAses are triggered as a result of receptor activation and intracellular Ca^{2+} accumulation (Kahlert et al., 2005; Rossi et al., 2007; Besancon et al., 2008). However, mGluR activation in neurons and oligodendrocytes counteracts glutamate excitotoxicity in these cells (Bruno et al., 1998; Adamchik and Baskys, 2000; Spillson and Russell, 2003; Deng et al., 2004). Antagonists at NMDA and AMPA receptors are highly protective when using animal and tissue culture models of ischaemia, yet they have failed in clinical trials, mainly due to

unacceptable side effect profiles, difficult drug delivery and possibly delays in drug administration following the onset of ischaemia (Choi et al., 1988; Kaku et al., 1991; Nelligard and Wieloch, 1992; Vornov et al., 1994; Strasser and Fischer, 1995; Strijbos et al., 1996; Pringle et al., 1997; Besancon et al., 2008; Ginsberg, 2008). Also, astrocytes are not vulnerable to glutamate-excitotoxicity, so glutamate receptor antagonists will not protect against astrocyte death and dysfunction in this situation (Chen and Swanson, 2003). It is therefore vital that other targets are found for the development of better and safer neuro and glioprotective treatments, and one system which has garnered particular interest in recent years is purinergic signalling.

Overview of purinergic signalling

ATP as a neurotransmitter

The first evidence of ATP-mediated neurotransmission came from observations by Geoffrey Burnstock and colleagues in the 1960's that despite blocking responses of both acetylcholine and noradrenaline at smooth muscle junctions of the taenia coli, inhibitory neurotransmission leading to muscle relaxation occurred (Burnstock et al., 1963, 1964). This could be antagonised by tetrodotoxin, leading to the realisation that the effect must be mediated by a non-adrenergic, non-cholinergic (NANC) inhibitory neurotransmitter (Burnstock et al., 1963, 1964). In the early 1970's ATP was first suggested as the NANC transmitter at various sites including the guinea pig taenia coli and stomach, rabbit ileum, frog stomach and turkey gizzard, and the term 'purinergic' was introduced (Burnstock et al., 1970; Burnstock, 1972). Initially there was resistance to the concept due to the fact that ATP has such important and widespread intracellular biochemical energetic roles, even though it was well known that powerful extracellular enzymes (ectoATPases) capable of breaking down ATP were present (Burnstock, 2006a, b). Direct evidence of ATP-mediated fast synaptic neurotransmission in the CNS was first presented as recently as 1992 by Edwards et al, who demonstrated ligand-gated ion channel responses in the rat medial habenula which could only be abolished by the P2 receptor antagonist Suramin and the desensitising P2 receptor agonist α,β -methylene-ATP (Edwards et al., 1992). Nowadays there is widespread acceptance of purinergic signalling, a field which is quickly

expanding and producing new insights into numerous physiological and pathophysiological processes.

Purinergic receptors

Purinergic receptors were first defined by Burnstock in 1976, with an initial classification of receptors into either P1 (adenosine receptors) or P2 (ATP/ADP receptors) receptors proposed in 1978 (Burnstock, 1976, 2006a). A further sub-classification of P2 purinoceptors into ionotropic P2X and metabotropic P2Y receptors was suggested in 1985 and has been adopted since (Burnstock and Kennedy, 1985). The first ATP receptor to be fully cloned and characterised was the mouse P2Y₂ receptor (Lustig et al., 1993), with the first papers describing the full structure of a cloned P2X receptor following a year later (Brake et al., 1994; Valera et al., 1994). Currently four adenosine receptors, seven P2X subtypes and eight P2Y receptor subtypes are recognised, including receptors which are sensitive to purines and pyrimidines (See **Figure 1-3**) (Burnstock, 2006a; Gever et al., 2006; Roberts et al., 2006; von Kugelgen, 2006).

Adenosine and P2Y receptors are typical 7 transmembrane region G-protein coupled receptors (GPCRs) and are coupled to a variety of intracellular transduction mechanisms, many of which lead to an increase in intracellular Ca²⁺ by release from intracellular stores. P2Y receptors respond to a variety of different agonists including ATP, ADP, UTP, UDP and/or UDP-glucose/UDP-galactose (von Kugelgen, 2006). Adenosine receptors are activated by adenosine (Ralevic and Burnstock, 1998). All P2X receptors are activated only by ATP, and subunits form both homo and heteromultimers which produce a variety of functional trimeric cation pores (North, 2002). P2X₇ only forms homomultimers, while P2X₆ does not form a functional homomultimer (Jarvis and Khakh, 2009). P2X receptors are able to gate a significant Ca²⁺ conductance and P2X₂, P2X₄, and P2X₇ also have the unique ability to undergo a conformational change to form a large pore following prolonged agonist application, allowing the passage of larger molecules up to 900Da in size (North, 2002; Egan and Khakh, 2004; Jarvis and Khakh, 2009). Finally,

widespread P2 receptor expression exists on both neurons and glial cells in the CNS (Burnstock and Knight, 2004; Verkhrasky et al., 2009).

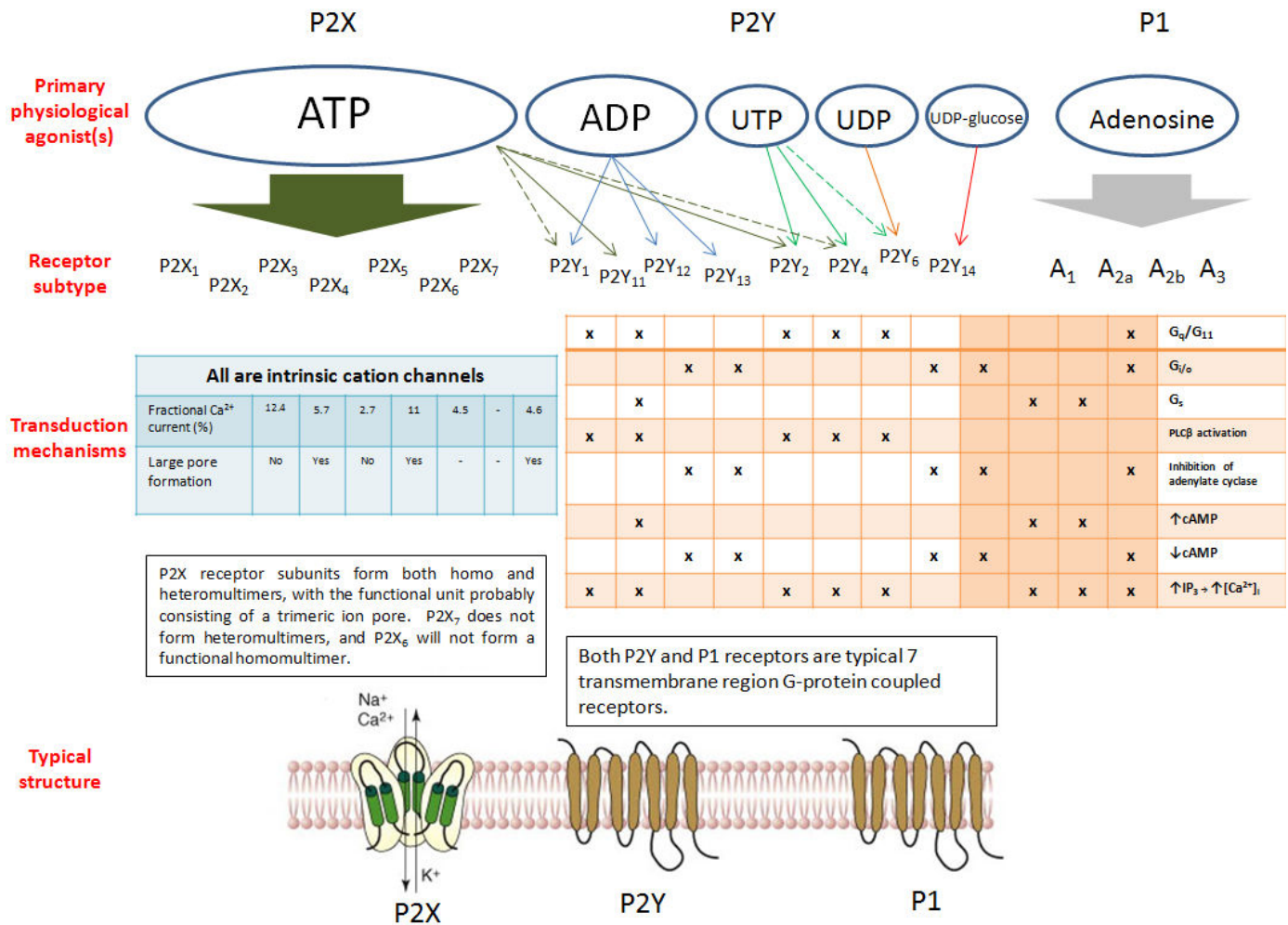


Figure 1-3: Purinergic receptors, an overview

P2X receptors are all gated by ATP, P1 receptors by adenosine, and a number of P2Y receptors can be activated by multiple purines/pyrimidines. Solid arrows indicate principle agonists, dotted lines indicate secondary/less potent agonists. P1 and P2Y receptors are coupled to different transduction/second messenger systems, while ionotropic P2X receptors are all intrinsic cation channels with variable Ca²⁺ permeability. Some P2X receptors form a large diameter pore following prolonged agonist application.

Images of receptor structure adapted from: (Abbracchio et al., 2009)

Data collated from: (Ralevic and Burnstock, 1998; Abbracchio et al., 2006; Jarvis and Khakh, 2009)

Purinergic signalling in the CNS

In the CNS ATP is released by neurons and glial cells, both on its own and during the phenomenon of co-transmission where it is released simultaneously with other transmitters such as glutamate and dopamine, and has key roles in both neurotransmission and neuromodulation as well as glial-glial and neuron-glial communication (Cotrina et al.,

2000; Burnstock and Knight, 2004; Burnstock, 2006b; Pedata et al., 2007). In particular, ATP has been recognised as the main mediator of intercellular glial-glia signalling in the CNS, a process by which astrocytes can propagate long-range Ca^{2+} signals via intercellular Ca^{2+} waves, giving rise to the idea that ATP is a 'gliotransmitter' (Hassinger et al., 1996; Cotrina et al., 2000; Fellin et al., 2006b; Hamilton et al., 2008; Takano et al., 2009). The current understanding of astroglial Ca^{2+} waves suggests that a single astrocyte crosses a threshold of stimulation leading to the release of ATP, which diffuses and activates P2Y receptors on astrocytes in the vicinity, causing the release of Ca^{2+} in these cells from intracellular stores (Arcuino et al., 2002; Nedergaard et al., 2003). In hippocampal neurons, ATP, acting via P2 receptors, has been shown to produce an immediate inhibition of evoked synaptic responses while producing a longer-lasting potentiation of synaptic responses both after ATP removal or during prolonged ATP application (Pedata et al., 2007). The long-term potentiation has been attributed to positive modulation of glutamatergic excitatory neurotransmission in the hippocampus by tonic P2 receptor activation (Pedata et al., 2007). Once ATP is released it is quickly broken down into ADP, AMP and adenosine via the activity of a variety of ectonucleotidases (nucleoside triphosphate diphosphorylases (NTPDases 1, 2, 3, and 8), nucleotide pyrophosphatases (1, 2, and 3), alkaline phosphatase, and 5' ectonucleotidases), thereby terminating their activity at P2 receptors while also producing adenosine which can act at adenosine receptors (Dunwiddie et al., 1997; Zimmermann, 2006).

ATP-mediated excitotoxicity during CNS ischaemia?

There is increasing evidence that ATP-mediated excitotoxicity may occur during CNS ischaemia (Franke et al., 2006). P2 receptor activation has the potential to cause cytotoxic rises in intracellular Ca^{2+} similar to those produced by glutamate receptor activation during glutamate-mediated excitotoxicity. Multiple studies have demonstrated that levels of extracellular ATP increase significantly during periods of ischaemia, both *in vivo* and *in vitro* (Hisanaga et al., 1986; Phillis et al., 1993; Phillis et al., 1996; Lutz and Kabler, 1997; Juranyi et al., 1999; Parkinson et al., 2002; Frenguelli, 2005; Melani et al., 2005; Schock et al., 2007; Schock et al., 2008). Under normal conditions ATP-

metabolising ecto-nucleotidases rapidly remove ATP from the extracellular space, but inflammatory reactions or oxidative stress (such as may occur during ischaemia) may inhibit their activity, leading to the accumulation of extracellular ATP (Zimmermann, 1996; Robson et al., 1997). Prolonged application of relatively high concentrations of exogenous ATP or ATP analogues leads to death of both neurons and glial cells *in vitro* and *in vivo* (Ferrari et al., 1997; Amadio et al., 2002; Ryu et al., 2002; Volonte et al., 2003; Amadio et al., 2005; Matute et al., 2007). The administration of broad-spectrum P2 receptor antagonists via either intravenous or intracerebroventricular routes during *in vivo* models of ischaemia reduce infarct volume and/or improved neurological outcome (Kharlamov et al., 2002; Lammer et al., 2006; Melani et al., 2006). Furthermore, a neuroprotective effect of broad-spectrum P2 receptor blockers has been reported *in vitro* in organotypic hippocampal slice cultures subjected to oxygen-glucose deprivation (OGD) (Runden-Pran et al., 2005). Another group reported that a variety of selective and non-selective P2 receptor antagonists improved the recovery of hippocampal CA1 synaptic transmission in brain slice following transient ischaemia (Coppi et al., 2007). In earlier experiments I also found that the P2 receptor antagonist Suramin was able to significantly reduce neonatal rat optic nerve astrocyte death during ischaemia (Vermehren, 2005).

Links between purinergic and glutamatergic signalling

A number of links have been established between glutamatergic and purinergic signalling. It is well documented that ATP application or P2 receptor activation can stimulate astrocytic glutamate release (Jeremic et al., 2001; Mongin and Kimelberg, 2002; Duan et al., 2003; Kimelberg, 2004; Krugel et al., 2004; Papp et al., 2004; Fellin et al., 2006a; Hamilton et al., 2008; Zeng et al., 2008b; Zeng et al., 2008a). The converse situation (glutamate stimulating ATP release) has been reported in astrocytes and retinal pigment epithelial cells (Queiroz et al., 1997; Queiroz et al., 1999; Reigada et al., 2006). Furthermore, it has been known for a long time that adenosine can inhibit neuronal synaptic glutamate release, although adenosine can also stimulate glutamate release from astrocytes (Dolphin and Prestwich, 1985; Scholz and Miller, 1992; Marcoli et al., 2003; Nishizaki, 2004). P2 receptor antagonists have been shown to protect against glutamate

toxicity in neuronal culture (Volonte and Merlo, 1996). In terms of ATP and P2 receptors, there seems to be a consensus that presynaptic P2Y receptors are inhibitory and P2X receptors are facilitatory of neuronal glutamate release in both the brain and spinal cord (Mendoza-Fernandez et al., 2000; Nakatsuka and Gu, 2001; Pankratov et al., 2002; Koizumi et al., 2003; Nakatsuka et al., 2003; Rodrigues et al., 2005; Xing et al., 2008; Khakh, 2009). In astrocytes, on the other hand, P2Y₁ receptor inhibition reduces ATP-mediated glutamate release (Zeng et al., 2008b; Zeng et al., 2008a). P2Y receptors have also been shown to directly modulate/interact with NMDA receptors (Wirkner et al., 2002; Cavaliere et al., 2004b). ATP itself may even have antagonist properties at some NMDA receptors (Ortinou et al., 2003; Kloda et al., 2004; Lechner and Boehm, 2004). It is therefore important to determine whether any effects attributed to purinergic signalling during ischaemia are actually linked to the glutamatergic system.

OBJECTIVES

Ischaemic brain injury causes much human death and suffering, and despite decades of intense research, effective therapeutic interventions remain elusive and rare. Ideally a target needs to be found which will protect both neurons and glial cells. Purinergic signalling is ubiquitous in the CNS and, as discussed above, may contribute to ischaemic injury. The aim of this project was to test the hypothesis that there is an ATP mediated excitotoxic cascade in the CNS which contributes to ischaemic cell death, functioning in parallel to glutamate mediated excitotoxicity.

To investigate this, I have measured both ATP and glutamate efflux from cultures of cortical astrocytes, neurons, and co-cultures of the two cell types during ischaemia using microelectrode biosensors to elucidate the time-course and cellular origin of their release (**Chapter 3**). I then went on to demonstrate the presence of a variety of functional P2 and glutamate receptors on cultured astrocytes and neurons which are capable of mediating increases in intracellular Ca²⁺ levels (**Chapter 4**). Finally, the effects of a variety of P2 and glutamate receptor agonists and antagonists on ischaemic astrocyte and neuronal death are presented in **Chapter 5**.

Chapter 2:

Methods and Materials

Cell Culture Methods

Preparation of cell culture flasks and microscope cover slips

Inside a sterile laminar airflow cabinet three to four 22 x 40 mm glass cover slips per 92 x 17mm tissue culture dish (Nunc, Roskilde, Denmark) were temporarily submerged in 100% industrial methylated spirits (IMS) and left to dry. To coat the cell culture surfaces a stock solution of poly-L-lysine was prepared at a concentration of 100µg/ml using sterilised millipore water, and 12 ml were placed in each cell culture dish containing the sterilised and now dried cover slips. For the cell culture flasks (175cm² tissue culture flasks with filter caps (Nunc, Roskilde, Denmark)), 20-30 ml of the poly-L-lysine solution were used per flask. The dishes and flasks containing the solution were left for a minimum of 2 hours inside the cabinet, after which time the poly-L-lysine solution was removed and the dishes/flasks were left open in a sterile Class II cabinet to dry out completely before being wrapped in sterile saran wrap and stored until use. The few attempts made to culture astrocytes in flasks that had not previously been coated with poly-L-lysine were unsuccessful, with cells not adhering well to the flask and not growing to confluence adequately.

Different buffers and growth media

All buffers, culture media, and supplements were ordered from GIBCO/Invitrogen (Paisley, Scotland) unless stated otherwise (see **Table 2-1** for details about all cell culture reagents that were used). All the ingredients in the growth media were combined inside a sterile laminar airflow cabinet under sterile conditions, and once made were refrigerated at -4°C until use. For glial cell cultures, a serum-based medium was used consisting of 500ml of Dulbecco's minimum essential medium (DMEM), already containing 4500mg/L glucose, Glutamax (L-glutamine), and pyruvate, to which were added 50 ml of foetal bovine serum (FBS), and 10 ml of a penicillin + streptomycin solution (referred to as DM from here on). For neuronal preparations, a serum-free medium was used consisting of one 500 ml bottle of Neurobasal medium without L-glutamine, to which were added 10 ml of penicillin + streptomycin solution, 10 ml of B27 supplement, and 5 ml of Glutamax I (100x), a solution containing L-glutamine (referred to as Nb from here on). During the

dissections, tissue was buffered using Hank's balanced salt solution (HBSS), which was also kept refrigerated. Media were never used for longer than two weeks to minimize the chance of contamination.

Table 2-1: Cell Culture Reagents

(all from GIBCO/Invitrogen, (Paisley, Scotland) except for Poly-L-lysine (Sigma-Aldrich, St. Louis, USA))

<i>Name</i>	<i>Description</i>	<i>Catalogue Number</i>
Poly-L-lysine hydrobromide	Mol weight 70,000-150,000, for promoting cell adhesion to flasks/cover slips	P6282
Dulbecco's minimum essential medium (DMEM)	Contains 4500mg/L glucose, glutaMAX, and pyruvate	31966-021
Foetal bovine serum (FBS)	Used two different batches	10106-169
Penicillin-Streptomycin solution (Pen/Strep)	5,000 units of both in 100ml of 0.85% saline, Effective against gram-neg and pos bacteria	15070-063
Neurobasal medium (NB)	Without L-glutamine	21103-049
B-27 Supplement	Cocktail of growth factors and anti-oxidants promoting neuronal growth	17504-044
GlutaMAX I	100x, stabilised dipeptide form of L-glutamine	35050-038
Hank's balanced salt solution (HBSS)	With calcium and magnesium	24020-091
Trypsin + EDTA	0.5% Trypsin + 5.3mM EDTA, 1x, Used for removal of cells from flasks	15400-054
Trypsin	2.5% (10x), used to prepare the 1% trypsin + 0.001% DNase aliquots for digestion of the cortices	15090-046
DNase I	Removes DNA released from cells due to overdigestion with proteolytic enzymes	18047-019
Trypan Blue Stain	To differentiate live from dead cells in haemocytometer	15250-061

Dissections and tissue preparation

Cell culture cabinets and all materials to be used were sterilized with 70% IMS, and tools for the dissection were sterilized in pure ethanol and then heated with a gas flame to ensure sterility. Large sterile petri dishes were placed on ice packs, and all but one was filled with refrigerated HBSS. These were the dishes where the tissue was kept at the various

stages of the dissection. A pregnant balb-c mouse was sacrificed humanely according to home office guidelines by cervical dislocation by staff of the Biomedical Services department, soaked and sterilized in 70% IMS, placed in the sterile culture cabinet, and the uterus was taken out via a caesarean section. This contained anywhere between one and fifteen 15-17-day old (E15-17) embryonic mice, which were removed and decapitated, with the heads being placed in the ice-cold buffer. Under a microscope each brain was removed from the skull, and the meninges were carefully peeled off. For all types of cultures the cortices were removed from the rest of the brain. The tissue was placed in sterile 30 ml universal container/centrifuge tubes (Bibby Sterilin Ltd, Stone, UK) containing 5 ml of HBSS and trypsinised with a 1% Trypsin solution (1ml/6 brains, containing DNase as well) for 10 minutes at 37°C. Digestion was then stopped by the addition of at least 5 ml of the DM and the tissue was triturated using a large sterile 10ml pipette and then a needle (bore ~18g) and syringe (10 ml).

After trituration the tube was centrifuged at 1500rpm for 5 minutes, and the pellet re-suspended in 10 ml of growth medium (Nb for cortical neuron culture, DM for astrocytes). The solution was then poured through a 100micron nylon cell-strainer (BD-Falcon) into a fresh sterile universal container to remove debris. The cellular concentration was determined by mixing 20µl of trypan-blue solution with 20µl of the cell suspension. This solution was placed in a haemocytometer, where the non-stained (viable) cells could be counted under the microscope. The factor of dilution needed to achieve the required cellular concentration of 0.7×10^6 cells/ml in the suspension could then be worked out by using the equation:

$$\frac{\text{\#cells}}{\text{\#squares}} \times \text{Factor of dilution} \times 10^4$$

Cortical neuron culture

For the cortical neuron culture, depending on the number of cells available, either 500µl of the suspension was plated onto the centre of each cover slip in the previously prepared petri dishes, and the dishes were placed for 30 minutes in the incubator (humidified, 5%CO₂, 37°C) before being filled to 12 ml with the addition of more growth medium and returned to the incubator, or 5 ml of the cell suspension was mixed with 7 ml of fresh medium and the solution was used to fill a whole petri dish. The first method was used if there was a relative shortage of cells available that particular week, almost always due to there being very few embryos in each pregnant female mouse. Otherwise the second method of plating neurons at equal density over the whole surface area of the cover slips was preferable, as it provided the most homogenous cultures. I found that changing 90% of the culture medium 24 hours after initial plating was beneficial, and from then on the medium was replaced every 3 to 4 days (twice-weekly). These cortical neuron cultures were then used from day 5-6 *in vitro* onwards (at this point the neurons will have formed a network of neurites), up to the age of 14 days *in vitro* (DIV).

Cortical astrocyte culture

For the astrocyte cultures, all the cell suspension was emptied into 175cm² culture flasks (25-30 ml per flask) which were put into a humid 5%CO₂ incubator at 37°C. After two days, I hit the flask 30 times relatively gently against my hand to remove any excess microglial cells, which attach very loosely to the top of the layer of cells, and replaced all of the medium with fresh growth medium. After another 3 to 4 days a confluent layer of astrocytes, oligodendrocyte precursors and microglial cells had formed on the floor of the flask. I developed a protocol for removing most cells except the astrocytes from the flask: I hit the side of the flask moderately hard about 30 times, alternating which side I hit it on every 10 hits, shook it 10 times, and then changed all the medium. This removed the microglial cells and started to dislodge oligodendrocyte precursors from the bottom-most astrocyte layer, as confirmed by intermittent microscopic examination. To remove all of the oligodendrocyte precursors, the flask was hit with increasing force another 30 times, shaken 10 times, hit 40 times, shaken 10 more times, and the medium was changed again.

Once again I would check whether the oligodendrocyte precursors had detached by microscopic examination, and if there were still some left I would continue hitting and shaking the flask and changing the medium until they seemed to have all gone. Then I washed the cells once with HBSS (to remove any traces of the serum-based medium) and added 20 ml of 0.5% trypsin + 5.3 mM EDTA. Cells were incubated for 10 minutes with the trypsin/EDTA solution, and then 20 ml of DM was added to stop the reaction. The solution was removed from the flasks, centrifuged for 5 minutes at 1500 rpm, the pellet resuspended in the desired quantity of medium, and plated the same way as the cortical neuron culture.

Cells were used for experiments from 3 to 14 days after plating, with 50% of the medium changed twice-weekly. Additionally, in some cases the astrocyte cultures were maintained in the Nb for a minimum of three days before being used for experiments. In these situations cells were plated and maintained in DM until confluent before changing all of the medium to Nb. The reasons for this will be discussed further in the results chapters.

Co-culture of astrocytes and neurons

For the astrocyte-neuronal co-cultures, an acute cortical neuron culture was plated directly on top of the slides containing confluent pure astrocytes (plated 1-2 days beforehand), and at that point the medium in the astrocyte dishes was changed from DM to Nb to ensure neuronal growth. Slides were used 3-4 days after the addition of the cortical neuron culture, and were used for up to 14 days. Neurons which were cultured on top of the astrocyte layer were noted to grow neurites at a much quicker rate than neurons in the pure neuronal culture, which is why the co-cultured cells could be used after less time *in vitro*. Astrocytes are known to promote neuronal attachment and growth in culture, with many laboratories using methods such as astrocyte feeder layers or astrocyte conditioned medium to take advantage of this effect (Wang and Cynader, 1999).

Important observations

The age of cell cultures (time *in vitro*) is known to be an important factor in determining the sensitivity of cells to various physiological and pathophysiological stimuli.

In my experiments I noticed that by using cells for a maximum of 14 days in vitro any variability in results due to age of cells could be avoided. Also, it was difficult to culture neurons from mice older than E17, with the theory being that neurons develop too many extensive neurites after this age which are damaged by the mechanical forces involved in trituration, leading to a much lower yield of viable neurons from similar amounts of tissue. In addition there is a proliferation of glial cells after E17, so the relative proportion of glial cells to neurons increases. Finally, it was vital to perform culture medium changes on time, as any delays caused abnormal/poor growth of cells, affecting experimental results. Any cultures which had too high or low a cell density or contained cells that looked of a poor quality (increased numbers of dead cells and/or debris) were not used for experiments.

P2Y₁ ^{-/-} cell cultures

A small number of experiments were performed using astrocyte cultures obtained from transgenic P2Y₁ receptor deficient mice (P2Y₁ ^{-/-}), courtesy of Professor Richard Evans (Atterbury-Thomas et al., 2008). These mice were developed in the laboratory of Christian Gachet (Leon et al., 1999). Due to the fact that these animals needed to be tested postnatally to check whether they were homozygous P2Y₁ ^{-/-}, cultures could only be produced at ages P2 onwards. Cell cultures were performed as detailed above, and gave adequate yields of astrocytes but not of neurons. In addition, due to the small size of the colony and an inconsistent supply of mice, it was unfortunately not possible to produce adequate co-cultures of astrocytes and neurons as the precise timing of each step was critical to obtaining high quality cultures.

Immunohistochemical characterization of the cell cultures

Immunohistochemistry is a technique by which specific proteins of interest are labelled using antibodies. These antibodies are produced by inoculating an animal (such as a mouse or rabbit) with the foreign protein/antigen in question. Large antigens can stimulate the production of antibodies to various different epitopes, leading to a polyclonal mixture of antibodies. Monoclonal antibodies can be generated by isolating B-cells and fusing them with an immortalized cell culture, producing hybridomas that produce antibodies against only one specific epitope. Secondary antibodies are fluorescent or otherwise labelled antibodies which bind to the primary antibodies to allow for visualization of its localization. These are produced by inoculating a different species of animal (such as a goat or donkey) with the primary antibody as an antigen, collecting the antibodies thus generated and labelling them.

Samples to be analysed by this technique are usually fixed to preserve tissue structure before being permeabilised to allow antibodies access to intracellular epitopes. Non-specific antibody binding sites are blocked using animal serum from the species in which the secondary antibodies were produced. Antigens are then detected either directly, where the primary antibody is already labelled with a fluorophore, or indirectly, using an unlabeled primary antibody followed by a labelled secondary antibody.

To determine the exact cellular composition of the three different types of cell cultures which were used in this PhD project, various slides from each type of culture were fixed and labelled with primary antibodies against well known cell-type-specific markers (see **Table 2-2** for details about the primary and secondary antibodies that were used).

Table 2-2: Antibodies used for Immunohistochemistry*Primary Antibodies*

Antibody against:	Species	Monoclonal/ Polyclonal	Dilution	Company	Product Code
GFAP	Mouse	Monoclonal	1:400	Sigma	G3893-.2ml
GFAP (Cy3 conjugate)	Mouse	Monoclonal	1:500	Sigma	C9205
NSE	Rabbit	Polyclonal	Pre-diluted	Sigma	N0649
CNPase	Mouse	Monoclonal	1:100	Chemicon	MAB326R
IB-4 (Alexa-594 conjugate)	<i>Griffonia simplicifolia</i>	Monoclonal	1:100	Molecular Probes	I21413

Secondary Antibodies

Fluorophore	Species	Dilution	Company	Product Code
Alexa-488	Goat anti-mouse IgG (highly cross-adsorbed)	1:1000	Molecular Probes	A11029
Alexa-568	Goat anti-mouse IgG (highly cross-adsorbed)	1:1000	Molecular Probes	A11031
Alexa-568	Goat anti-rabbit IgG (highly cross-adsorbed)	1:1000	Molecular Probes	A11036

Protocols

Microscope cover slips containing the different cells were washed twice in 0.1M phosphate buffered saline (PBS) before fixation. Cells were fixed either by addition of a 4% paraformaldehyde solution (in 0.1M PBS) for 15 minutes at room temperature or by adding a methanol/acetone (1:1) mixture for 10 minutes on ice. The latter method was eventually preferred as it involved handling less toxic substances while providing equally good tissue fixation. Slides were washed three times in PBS to remove any residual chemicals before permeabilisation and staining. The above process was performed with the slides inside their original petri dishes. A solution of 0.1M PBS containing 10% goat serum (Dako, Glostrup, Denmark) and 0.5% Triton-X (Sigma-Aldrich, St. Louis, USA) was used for all further steps and antibody dilutions. This solution will be referred to as PBSGT from now on.

Cover slips were transferred to small custom-made rectangular containers which had space for one cover slip each, with enough liquid put in to always keep the full cover

slip immersed and a box put over the containers to keep them in the dark. In some experiments 1 μ M Hoechst 33342 was added for 15 minutes at this point to label nuclei. This substance binds to DNA, emitting cyan fluorescence around 461nm when excited by ultraviolet light at about 350nm. Cells were washed three times with PBS. PBSGT was added for one hour at room temperature for permeabilisation and blocking. Slides were then incubated overnight at 4°C with the primary antibody (dilutions in **Table 2-2**). The next day slides were washed three times in PBSGT. ‘Washing’ involved removal of all the liquid in each container with a pipette, addition of fresh PBSGT and gentle movement of the fluid around the cover slip. Unless the primary antibody was already fluorescently labelled a secondary antibody was added for one hour at room temperature, after which slides were washed three times again. These steps were repeated for any other antibodies which needed applying. Once all the antibodies had been applied slides were washed three times in normal PBS, excess liquid was allowed to dry off, and the cover slips were mounted onto SuperFrost Plus microscope slides (Menzel-Glaeser, Braunschweig, Germany) using a drop of PermaFluor mountant medium (Thermo Fisher Scientific, Waltham, USA). I waited at least one hour before imaging.

Imaging

In the earlier stages of my project, imaging of stained cells was performed on an older Olympus Fluoview FV300 confocal microscope that only had two lasers (red and green), with no ultraviolet light source for use with conventional nuclear stains. This limited the number of fluorophores that could be used in any one slide to two. Later on I was able to utilize a Leica TCS SP2 confocal microscope (courtesy of Professor Nick Hartell), allowing me to use more fluorophores as well as visualising nuclear staining with Hoechst 33342. Images in figures are labelled for which microscope was used to produce them.

On both microscopes, images were obtained in Z-stacks of usually 8 slices which were then combined into one final image using the software provided with each of the microscopes (Leica LCS Lite, v2.61, Leica Microsystems, Heidelberg, Germany and

Fluoview software, Olympus, Japan) to maximize image quality. Overlays of the different fluorophores in one area were also produced in either the original software or in Metamorph (Molecular Devices, Sunnyvale, USA) to produce final images and aid in analysis.

Image analysis

For each cell culture type (astrocyte culture, neuronal culture and co-culture) multiple areas on a number of cover slips from at least two different cell cultures were imaged to provide an accurate representation of the culture in question. Overall cell numbers were counted either using the Hoechst 33342 nuclear stain or phase contrast light images of the cells. As mentioned before, the Olympus confocal microscope setup was not equipped with a light capable of imaging in the blue spectrum, so for experiments using this microscope the total cell count was performed using a phase contrast light image. To make sure that this method provided numbers of a similar accuracy to counting Hoechst 33342 stained nuclei, cell counts were performed independently on 40x phase contrast light images and Hoechst 33342 images of exactly the same areas of interest in all three of the types of cell cultures used. Both methods produced similar cell counts (see **Figure 2-1**).

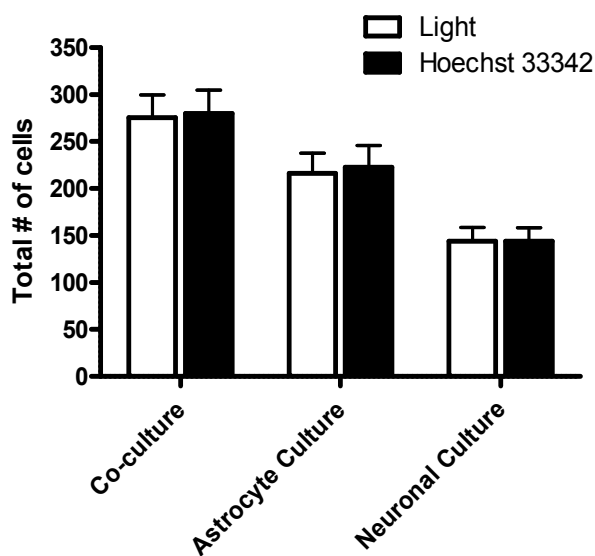


Figure 2-1: Total cell counts in IHC experiments

No significant differences present when comparing total number of cells counted using either phase contrast microscopy or Hoechst 33342 nuclear staining in any of the cell cultures. ($p > 0.05$)

(n:5 areas of interest for each column)

Once overall cell counts had been obtained, antibody-specific counting was performed manually by simply looking at the images and counting the number of cells labelled with each fluorophore. Total cell counts for each cell type are expressed as a percentage of the total number of cells in the area plus or minus the standard error of the mean (SEM). Efforts were made to ensure that for most experiments at least three separate cell cultures and various slides from each culture were analysed. The n-number for each count represents the total number of areas of interest having been imaged.

Results: cell culture characterisation

It seems appropriate to include this section in the materials and methods even though it presents results of IHC experiments. All three of the different cell cultures (cortical astrocytes, cortical neurons and the co-culture of astrocytes and neurons) were analysed to confirm their cellular constituents. Primary antibodies against the following epitopes were used for the selective labelling of the different cell types: neuron-specific enolase (NSE) was used to label neurons, glial fibrillary acidic protein (GFAP) was used to label astrocytes, 2',3'-Cyclic Nucleotide 3'-Phosphodiesterase (CNPase) was used to label oligodendrocytes and Isolectin B-4 (IB-4) was used to label microglia. Whenever possible, nuclei were stained using Hoechst 33342.

Enolase is a glycolytic enzyme catalyzing the reaction pathway between 2 phospho glycerate and phosphoenol pyruvate. In mammals, enolase molecules are dimers composed of three distinct subunits (alpha, beta and gamma). The alpha subunit is expressed in most tissues and the beta subunit only in muscle. The gamma subunit is expressed primarily in neurons, in normal and in neoplastic neuroendocrine cells, making this subunit useful for the identification of neurons (Cooper, 1994). Glial fibrillary acidic protein (GFAP) is a member of the class III intermediate filament protein family (Eng et al., 2000). It is heavily, and specifically, expressed in astrocytes and certain other astroglia in the central nervous system, in satellite cells in peripheral ganglia, and in non myelinating Schwann cells in peripheral nerves (Eng et al., 2000). Antibodies to GFAP are therefore very useful

as markers of astrocytic cells. GFAP is also found in a variety of cells not present in cerebral tissue, including the lens epithelium, Kupffer cells of the liver, in some cells in salivary tumours and has been reported in erythrocytes (Eng et al., 2000). CNPase exists in two forms: 46kDa (CNP1) and 48kDa (CNP2) (Sprinkle, 1989). It is expressed at high levels by oligodendrocytes in the central nervous system and by Schwann cells in the peripheral nervous system and is virtually absent in other cell types (Sprinkle, 1989). Isolectin-B4, obtained from *Griffonia simplicifolia* (a shrub from Africa) recognizes α -D-galactose-containing glycoconjugates on the surface of microglial cells in brain tissue (Ayoub and Salm, 2003).

Astrocyte culture IHC

Immunohistochemical analysis of the astrocyte culture revealed that $93.87 \pm 0.6\%$ of cells were GFAP-positive astrocytes, $2.1 \pm 0.51\%$ were CNPase-positive oligodendrocytes, with NSE-positive neurons made up the lowest proportion of cells with $0.47 \pm 0.36\%$ (see **Figure 2-2** for a graph of overall cell counts and sample images from experiments). It was not physically possible to label and image all cell cultures with all cell-specific antibodies at the same time (as already described in the previous section), hence the slight discrepancy between the total number of cells in each category.

In experiments that used dual labelling for GFAP and either CNPase or NSE, $4.8 \pm 0.5\%$ of cells were *not* positive for either marker, suggesting that these remaining cells could be microglia. When astrocyte cultures were stained for IB-4 and Hoechst 33342, $9.8 \pm 0.64\%$ (54 out of 546 cells) of cells were IB-4-positive, a percentage of microglia higher than expected from the other experiments. The percentage of microglia in this culture is not insignificant, and it has been suggested that any astrocyte culture containing such an amount of microglia should be referred to as an 'astroglial enriched culture' rather than a pure astrocyte culture, since even a relatively low proportion of microglia may have a significant impact on the results of certain experiments (Saura, 2007). For the purpose of this thesis and for ease of discussion this culture will be referred to as the astrocyte culture.

Neuronal culture IHC

In the neuronal culture, NSE-positive neurons accounted for $91.41 \pm 1.2\%$ (3958 out of 4278 cells) of total cells, with GFAP-positive astrocytes making up the second largest contingent with $5 \pm 0.8\%$ (123 out of 2509 cells) (See **Figure 2-3** for a graph of overall cell counts and sample images from experiments). This is within the 5% limit generally considered acceptable in a neuronal culture (Zamzow et al., 2008). CNPase-positive oligodendrocytes ($0.33 \pm 0.22\%$; 3 out of 1769 cells) and IB-4 positive microglia ($1.27 \pm 0.23\%$; 16 out of 1162 cells) accounted for a small proportion of cells.

One interesting observation is that astrocytes in the pure neuronal culture developed a different morphology from those in the astrocyte culture, with the former having many long and thin processes (more akin to fibrous astrocytes *in vivo*) whilst the latter grew into a confluent flat layer of cells with fewer and shorter processes (similar to protoplasmic astrocytes *in vivo*). *In vitro* the situation of astrocyte differentiation and classification is different than *in vivo*. Classically, cultured astrocytes have been classified as either type 1 or type 2 depending on their morphological and immunohistological characteristics (Raff et al., 1983; Fok-Seang and Miller, 1992). The flat astrocytes without many processes seen in the astrocyte culture (**Figure 2-2**), often called fibroblast-like in the literature, have typically been classified as type 1 astrocytes, whereas the type 2 astrocytes have long processes and look exactly like the astrocytes seen in this neuronal culture (Raff et al., 1983). They develop from glial progenitor cells in different proportions depending on the presence or absence of serum and other factors in culture medium; indeed it is suggested that the type 2 astrocyte morphology may be an artefact of cell culture methods (Fok-Seang and Miller, 1992; Hertz et al., 1998).

Co-culture IHC

The aim of the co-culture was to achieve a more evenly balanced combination of astrocytes and neurons in the same culture, and immunohistochemical analysis revealed that this outcome was accomplished. NSE-positive neurons accounted for $51.93 \pm 2.72\%$ (3580 out of 6671) of cells, with GFAP-positive astrocytes making up $43.74 \pm 2.78\%$

(2401 out of 5753) and CNPase-positive oligodendrocytes $0.09 \pm 0.09\%$ (1 out of 918). (See **Figure 2-4** for a graph of overall cell counts and sample images from experiments). Once again, quantification of microglia was difficult for the same reasons already discussed in the astrocyte culture IHC section. In experiments where dual labelling with both NSE and GFAP was undertaken, only $5.05 \pm 0.37\%$ of cells in the co-culture were not positive for either antibody (referred to as 'Other'). Since only 0.9% of cells were CNPase-positive oligodendrocytes, the most likely cell type making up this group would be microglia. Counting of IB-4 labelled cells produced a value of $9.15 \pm 1.1\%$ (105 out of 1166 cells), again a not insignificant quantity of microglia.

Figure 2-2: Astrocyte culture IHC

A1 + A2: Astrocyte culture stained for astrocytes (GFAP/Green), neurons (NSE/red), and nuclei (Hoechst33342/blue). The majority of cells appear to be GFAP positive, with no NSE positive cells visible. Leica microscope.

B1 + B2: Astrocyte culture stained for astrocytes (GFAP/green) and oligodendrocytes (CNPase/red). There are 3 oligodendrocytes in image B2 and none in B1. Olympus confocal microscope.

C1 + C2: Astrocyte culture labelled with the microglial marker IB-4 (red) and the nuclear stain Hoechst 33342. A fairly large proportion of cells seem to be IB-4-positive, but z-stacking and multilobular nuclei make it difficult to accurately count these cells. Leica microscope.

D: Graph showing overall cell-type analysis of the astrocyte culture

GFAP: $93.87 \pm 0.6\%$ (3572 out of 3800 cells)

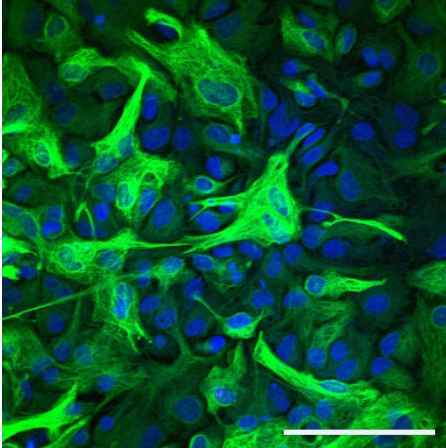
CNPase: $2.1 \pm 0.51\%$ (50 out of 2319 cells)

NSE: $0.47 \pm 0.36\%$ (7 out of 1481 cells)

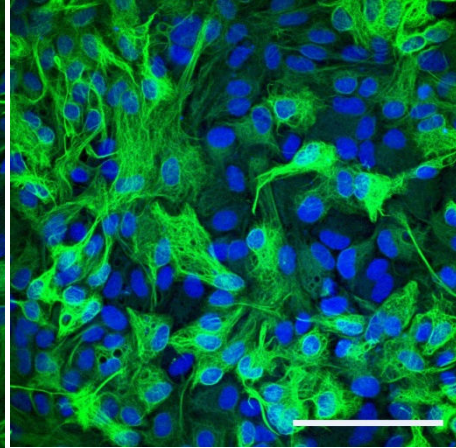
IB-4: $9.8 \pm 0.64\%$ (54 out of 546 cells)

Scale bars: 100uM

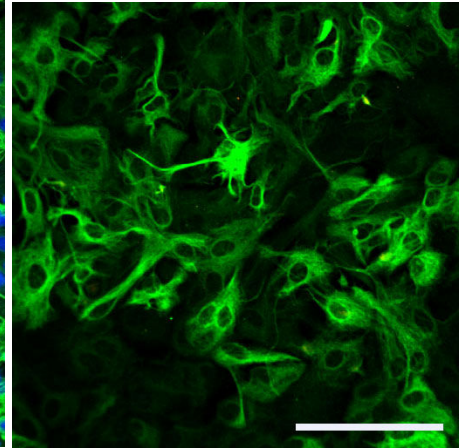
A1 (Hoechst + GFAP + NSE)



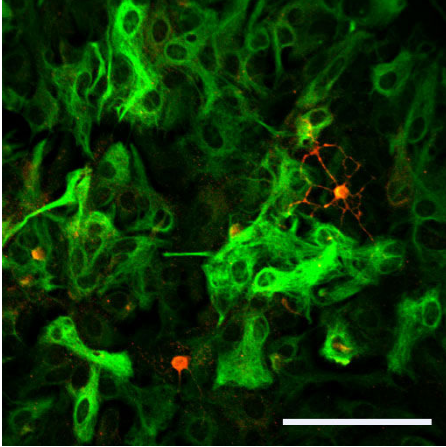
A2 (Hoechst + GFAP + NSE)



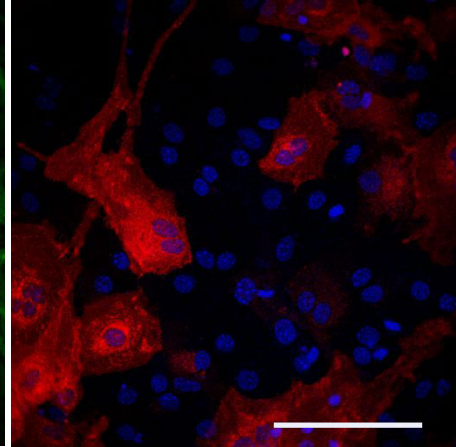
B1 (GFAP + CNPase)



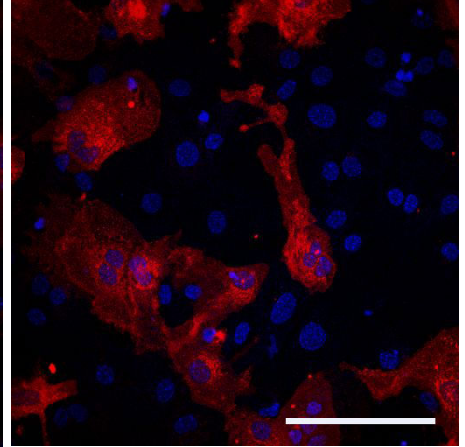
B2 (GFAP + CNPase)



C1 (Hoechst + IB-4)



C2 (Hoechst + IB-4)



D

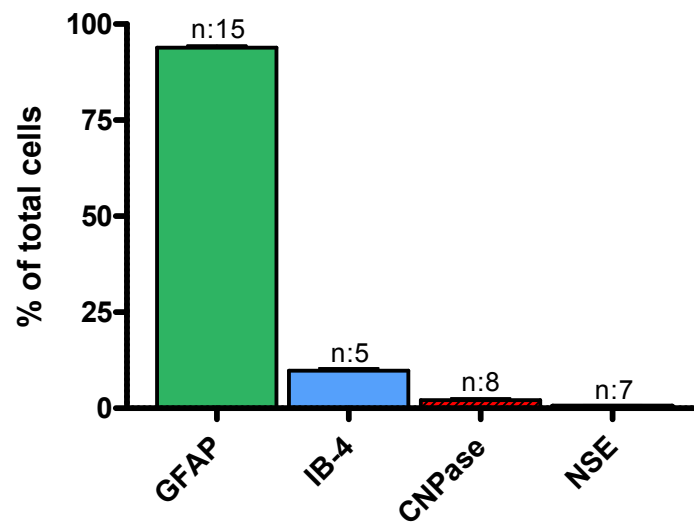


Figure 2-3: Neuronal Culture IHC

A1 + A2: Cortical neuron culture that has been stained for neurons (**NSE/red**) and oligodendrocytes (**CNPase/green**). There are two oligodendrocytes in image A1 and none in A2. This was representative of the very small percentage of oligodendrocytes present in the culture. Olympus microscope.

B1: Cortical neuron culture that has been stained for neurons (**NSE/red**) and astrocytes (**GFAP/green**). Note the relatively low number of astrocytes relative to neurons and the different morphology of the astrocytes in the neuronal culture (Type 2) compared with the astrocyte culture (Type 1). Olympus microscope.

C1 + C2: Cortical neuron cultures which have been labelled for neurons (**NSE/red**), astrocytes (**GFAP/green**) and nuclei (**Hoechst 33342/blue**). The majority of cells are neurons. In image C2 there are also two astrocytes. Leica microscope.

D1 + D2: Cortical neuron cultures stained with the microglial marker IB-4 (**red**) and the nuclear stain Hoechst 33342 (**blue**). Very few cells were stained positively with IB-4, confirming that only a small proportion of cells in the neuronal culture were microglia. Leica microscope.

E: Graph showing overall cell-type analysis of the astrocyte culture

NSE: $91.41 \pm 1.2\%$ (3958 out of 4278 cells)

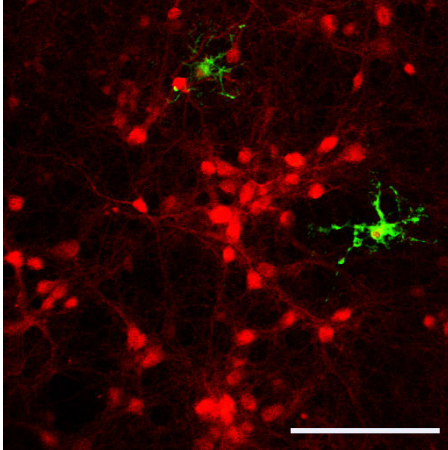
GFAP: $5.02 \pm 0.8\%$ (123 out of 2509 cells)

CNPase: $0.33 \pm 0.2\%$ (3 out of 1769 cells)

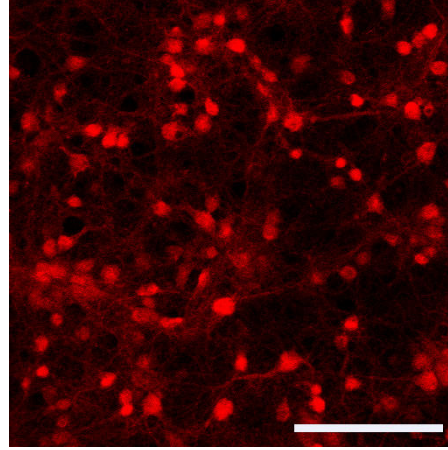
IB-4: $1.28 \pm 0.2\%$ (16 out of 1162 cells)

Scale bars: 100uM

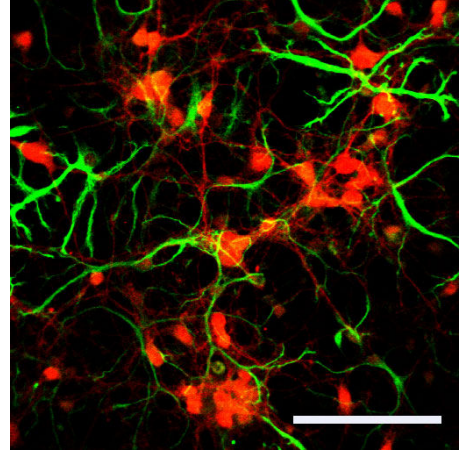
A1 (NSE + CNPase)



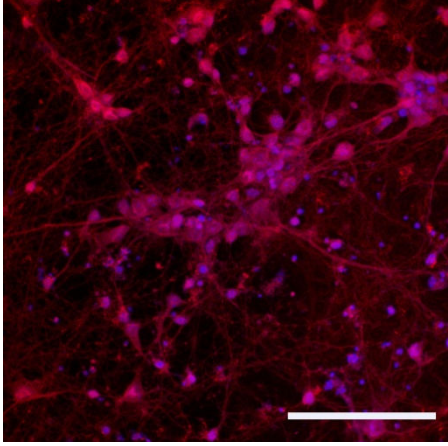
A2 (NSE + CNPase)



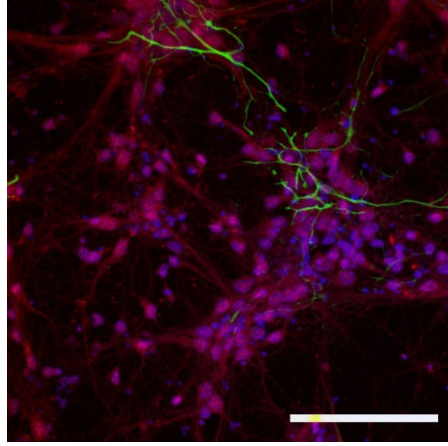
B1 (NSE + GFAP)



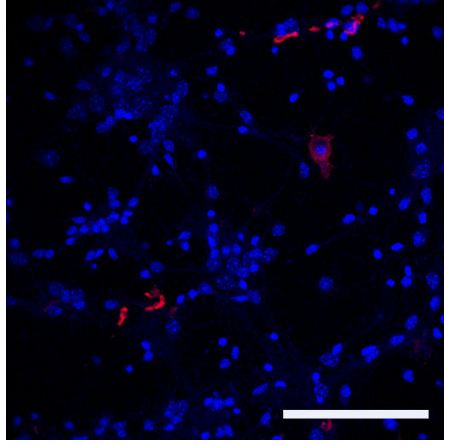
C1 (Hoechst + NSE + GFAP)



C2 (Hoechst + NSE + GFAP)



D1 (Hoechst + IB-4)



D2 (Hoechst + IB-4)

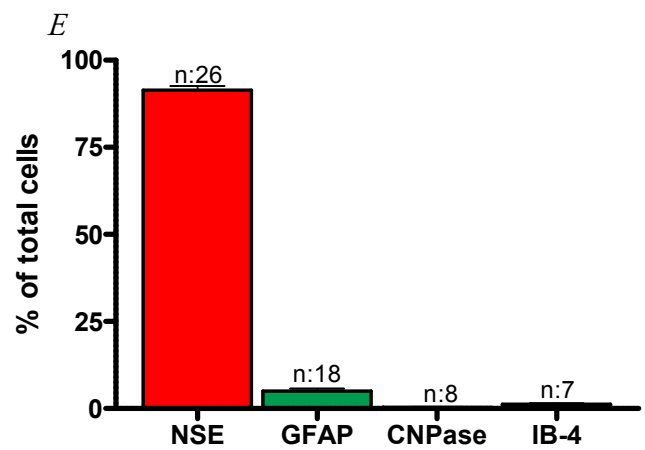
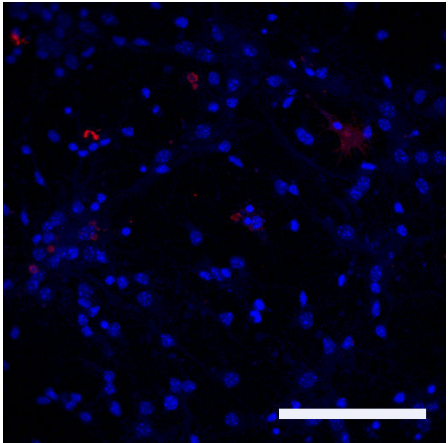


Figure 2-4: Co-Culture IHC

A1-D2: Examples of two areas of interest labelled with GFAP, NSE and Hoechst 33342. Leica microscope.

A1 + A2: GFAP (green) labelling of co-culture.

B1 + B2: NSE (red) labelling of co-culture.

C1 + C2: Hoechst 33342 (blue) in co-culture.

D1: composite of images *A1*, *B1* and *C1*

D2: composite of images *A2*, *B2* and *C2*

Both *D1* and *D2* clearly show that the majority of cells in this culture were either astrocytes or neurons.

E1: co-culture slide that has been stained for neurons (NSE/red) and oligodendrocytes (CNPase/green). Only a very small number of CNPase-positive oligodendrocytes were present. Olympus microscope.

F1 + F2: co-culture labelled for microglia (IB-4/red) and nuclei (Hoechst 33342/blue), confirming that there was a sub-population of microglia present in the co-culture. Leica microscope.

G: Graph showing overall cell-type analysis of the co-culture of astrocytes and neurons

NSE: $51.93 \pm 2.72\%$ (3580 out of 6671 cells)

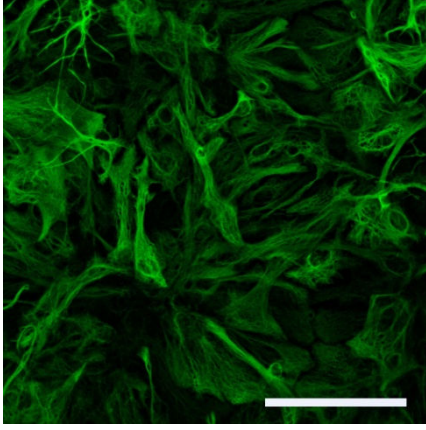
GFAP: $43.74 \pm 2.78\%$ (2401 out of 5753 cells)

CNPase: $0.09 \pm 0.09\%$ (1 out of 918 cells)

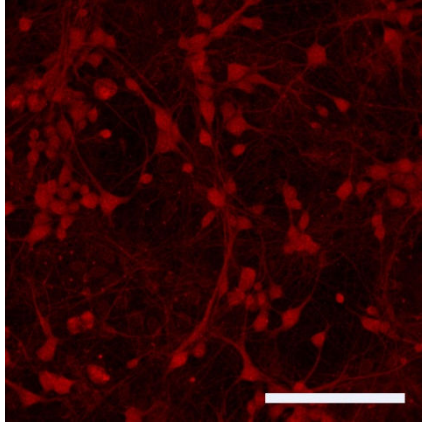
IB-4: $9.15 \pm 1.1\%$ (105 out of 1166 cells)

Scale bars: 100uM

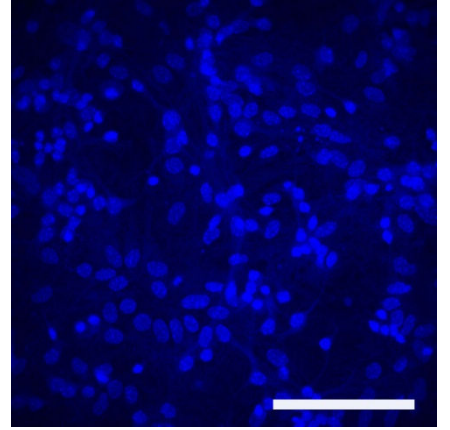
A1 (GFAP)



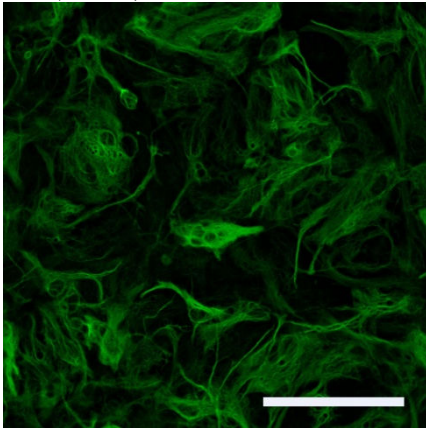
B1 (NSE)



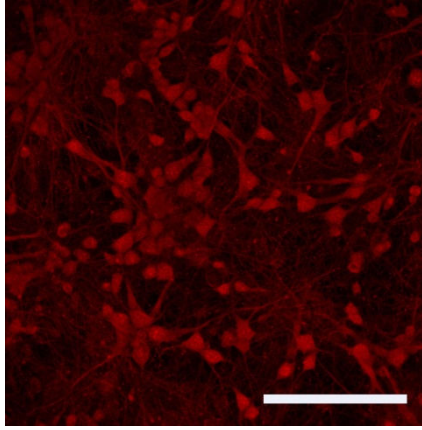
C1 (Hoechst)



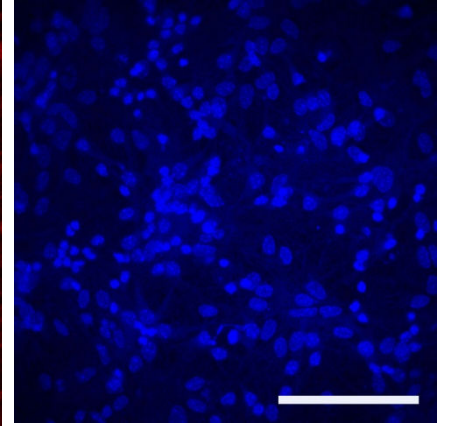
A2 (GFAP)



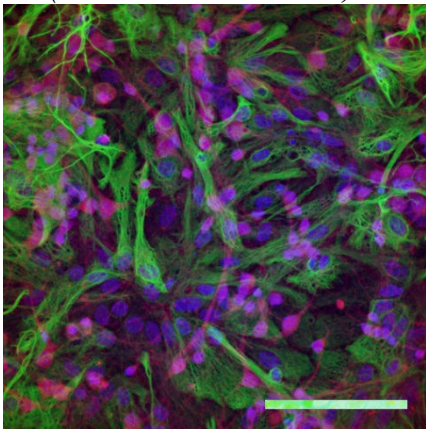
B2 (NSE)



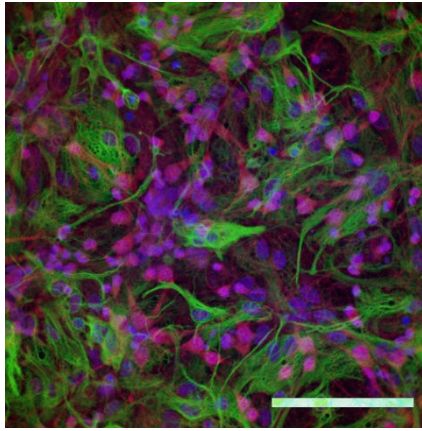
C2 (Hoechst)



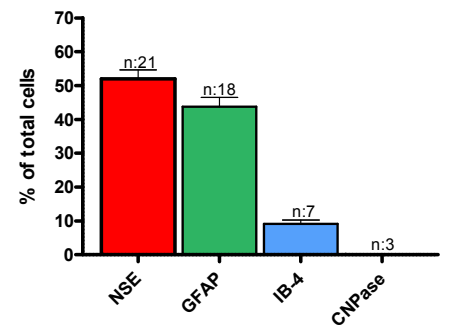
D1 (GFAP + NSE + Hoechst)



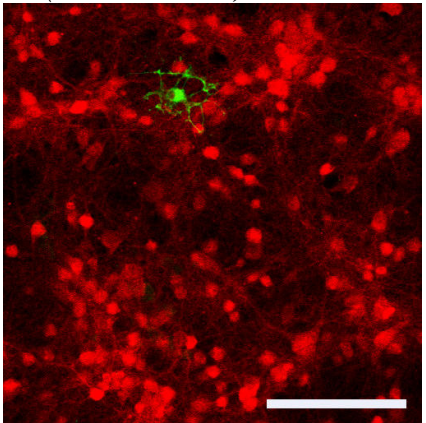
D2 (GFAP + NSE + Hoechst)



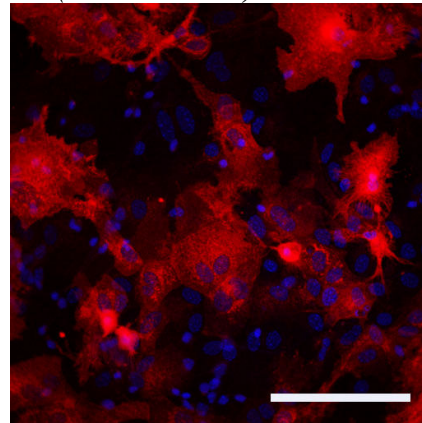
G



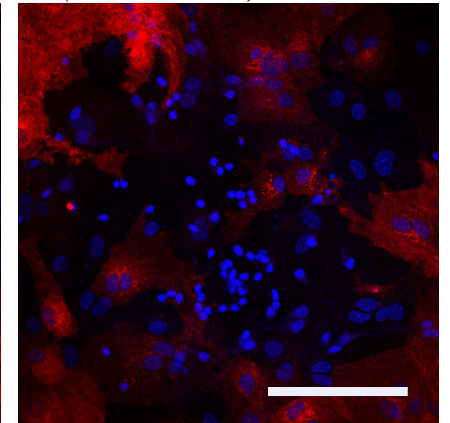
E1 (CNPase + NSE)



F1 (IB-4 + Hoechst)



F2 (IB-4 + Hoechst)



Solutions and pharmacological reagents used

As the experiments undertaken in this project used neural cells, the most appropriate physiological solution to use was artificial cerebro-spinal fluid (aCSF). Three variations were used. To simulate ischaemic conditions aCSF without glucose (aCSF-glucose) was used, which was bubbled with a nitrogen and carbon dioxide mixture (95%N₂/5%CO₂) to remove any oxygen, producing oxygen-glucose deprivation (OGD). Conversely, normal aCSF contained glucose and was bubbled with an oxygen and carbon dioxide mixture (95%O₂/5%CO₂). Both of these solutions are based on the physiologically correct bicarbonate buffer system, hence the need for carbon dioxide to be bubbled through them. However, in higher flow short application agonist experiments a hepes buffered aCSF solution (hepes-aCSF) was used instead as it was impractical and difficult to provide gas flow to the eight different tubes of solution in that particular perfusion system. In experiments calling for zero Ca²⁺ the Ca²⁺ chelator EGTA was used. A special rehydration and wet storage phosphate buffer solution was used for the microelectrodes. **Table 2-3** provides exact details of the chemical composition of all the solutions that were used. Solutions were freshly prepared on a daily basis, with pH kept to 7.4 and osmolarity corrected to 318mosmol using NaCl solution. A wide range of pharmacological reagents were used (see **Table 2-4**), and these were added to solutions either freshly diluted or from aliquots stored at -20°C.

Table 2-3: Solutions used in experiments

Composition shown in mM unless stated otherwise

OGD Experiments/Electrode Experiments

aCSF

153 Na⁺, 3K⁺, 2Mg²⁺, 2Ca²⁺, 131Cl⁻, 26HCO₃⁻, 2H₂PO₄⁻, 10 dextrose.

Bubbled with 95%O₂/5%CO₂ gas mixture to ensure oxygenation and correct pH (7.4)

aCSF-glucose (OGD)

153 Na⁺, 3K⁺, 2Mg²⁺, 2Ca²⁺, 131Cl⁻, 26HCO₃⁻, 2H₂PO₄⁻, 10 dextrose.

Bubbled with 95%N₂/5%CO₂ gas mixture to remove all oxygen and ensure correct pH (7.4)

Agonist Experiments

Hepes aCSF

153 Na⁺, 3K⁺, 2Mg²⁺, 2Ca²⁺, 131Cl⁻, 10Hepes, 2H₂PO₄⁻, 10 dextrose.

pH corrected to 7.4 using HCl and/or NaOH.

Zero Calcium Hepes aCSF

153 Na⁺, 3K⁺, 2Mg²⁺, 131Cl⁻, 10Hepes, 2H₂PO₄⁻, 10 dextrose.

Also contained 50uM EGTA.

pH corrected to 7.4 using HCl and/or NaOH.

(Osmolarity was corrected to 318mosmol using NaCl solution in all four aCSF solutions)

Additional solutions for electrode preparations

Rehydration and storage solution/buffer

Stock solutions of 0.2M monobasic (NaH₂PO₄ * 2H₂O) and 0.2M dibasic (Na₂HPO₄) were prepared and used to make a 0.01M phosphate buffered solution at pH 7.4.

To this were added: 100uM NaCl, 1uM MgCl₂ and, if ATP electrodes were being used, 2mM Glycerol.

Pot calibrations were done using the rehydration buffer.

End calibrations were performed using hepes aCSF.

Table 2-4: Pharmacological reagents

<i>Name</i>	<i>Concentration(s) used</i>	<i>Solvent</i>	<i>Manufacturer</i>	<i>Product Code</i>
(+)-5-methyl-10,11-dihydro-5 <i>H</i> -dibenzo[<i>a,d</i>]cyclohepten-5,10-imine maleate (MK-801)	10uM 1uM	Water	Tocris Sigma	M-107
2,3-dihydroxy-6-nitro-7-sulfamoyl-benzo[<i>f</i>]quinoxaline-2,3-dione (NBQX)	30uM 3uM	DMSO	Tocris	0373
N-methyl-D-aspartate (NMDA)	100uM	Water	Tocris	0114
Adenosine 5'-triphosphate disodium salt (ATP)	1uM, 10uM, 100uM, 1mM	Water	Sigma	A6419
Adenosine 5'-diphosphate monopotassium salt dihydrate (ADP)	100uM	Water	Sigma	A5285
Ethylene glycol-bis(2-aminoethylether)-N,N,N',N'-tetraacetic acid (EGTA)	50uM	Water	Sigma	E3889
Pyridoxal-phosphate-6-azophenyl-2',4'-disulfonate tetrasodium salt (PPADS)	100uM 10uM 1uM	Water	Tocris	0625
Suramin hexasodium salt	100uM	Water	Tocris	1472
4-[(2 <i>S</i>)-2-[(5-isoquinolinylsulfonyl)methylamino]-3-oxo-3-(4-phenyl-1-piperazinyl)propyl] phenyl isoquinolinesulfonic acid ester (KN-62)	1uM	DMSO	Tocris	1277
2'-Deoxy-N6-methyladenosine 3',5'-bisphosphate tetrasodium salt (MRS 2179)	10uM	Water	Tocris	0900
[[[(1 <i>R</i> ,2 <i>R</i> ,3 <i>S</i> ,4 <i>R</i> ,5 <i>S</i>)-4-[6-Amino-2-(methylthio)-9 <i>H</i> -purin-9-yl]-2,3-dihydroxybicyclo[3.1.0]hex-1-yl]methyl]diphosphoric acid mono ester trisodium salt (MRS 2365)	100nM	Water	Tocris	2157
3'-O-(4-benzoyl)benzoyl adenosine 5'-triphosphate triethylammonium salt (BzATP)	100uM	Water	Sigma	B6396
Adenosine 5'-O-(3-thio)triphosphate (ATPγS)	100uM	Water	Sigma	A1388
(<i>RS</i>)-α-amino-3-hydroxy-5-methyl-4-isoxazole propionic acid (AMPA)	100uM	Water	Sigma	A6816
L-glutamic acid (Glutamate)	1mM, 100uM, 10uM, 1uM	Water	Sigma	128430
Thapsigargin	1uM	DMSO	Tocris	1138
Glycine	10uM	Water	Sigma	410225

Fluorescence Microscopy of Cells

Fura-2ff and Fura-2

Since they were developed in the 1980s the use of the ratiometric intracellular Ca^{2+} ($[\text{Ca}^{2+}]_i$) indicators Fura-2 (F1221, Invitrogen, Paisley, UK) and Fura-2ff (F14181, Invitrogen, Paisley, UK) has become widespread, thanks to properties such as good selectivity against other divalent cations and their strong fluorescence, making it easier for a good signal to noise ratio to be achieved at a low probe concentration (Grynkiewicz et al., 1985; Van den Bergh et al., 1995). In addition, thanks to their ratiometric properties, they can be used in samples where the indicator concentration cannot be held constant due to either leakage and/or photobleaching. This is particularly relevant as I used Fura-2ff in experiments lasting nearly two hours, at which point leakage and photobleaching would be almost inevitable. Finally, the addition of an acetoxymethyl ester (AM) group to the indicator molecule making it cell membrane-permeable allows for easy non-invasive loading of the molecules into cells, where the AM group is then subsequently removed by intracellular esterases, preventing the indicator from coming back out of the cell.

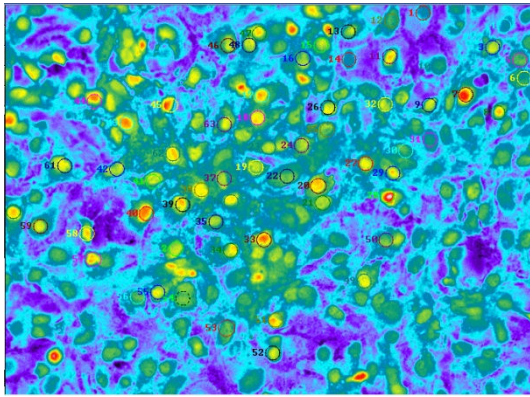
Because Fura-2 is a high-affinity Ca^{2+} indicator (K_d for Ca^{2+} : 0.23 μM) it is more sensitive to smaller fluctuations in $[\text{Ca}^{2+}]_i$, but this also means that it has a significant Ca^{2+} buffering capacity (Paredes et al., 2008). Bondarenko et al (Bondarenko and Chesler, 2001b) found that in astrocyte cultures subjected to the HAIR protocol (subjecting astrocytes to hypoxic acidic ion-shifted ringer solution) Fura-2 loaded astrocytes were significantly protected from Ca^{2+} mediated injury compared with Fura-2ff loaded astrocytes. For this reason all experiments involving the measurement of $[\text{Ca}^{2+}]_i$ levels during OGD were always conducted using the low affinity Ca^{2+} indicator Fura-2ff (K_d for Ca^{2+} : 35 μM) (Paredes et al., 2008). Other advantages of using Fura-2ff compared with Fura-2 during OGD experiments include its high dynamic range (ability to measure moderate-to-high $[\text{Ca}^{2+}]_i$) and low sensitivity to changes in pH, which are known to occur inside cells during OGD (Hyrz et al., 2000). However, in the experiments undertaken to characterize Ca^{2+} flux mediated by different glutamate and P2 receptors in response to the application of receptor agonists, Fura-2 was used as it is more sensitive to smaller

fluctuations in $[Ca^{2+}]_i$ (particularly at physiological $[Ca^{2+}]_i$ levels) and because it is easier to calibrate the fluorescence signals to actual $[Ca^{2+}]_i$ using commercially available static calibration kits. During imaging, Fura-2 and Fura-2ff loaded cells were illuminated at 340, 360, and 380 nm, with emission being recorded at 520nm for each of the three excitation wavelengths.

Problems with Fura-2ff during long experiments at 37°C

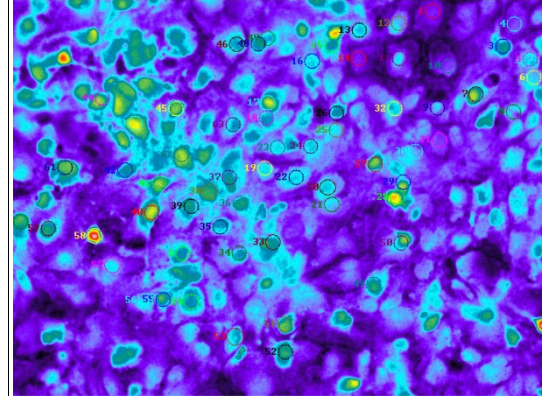
Unfortunately Fura-2ff leaked out of astrocytes over time, manifesting as a gradual drop in 360 signal (F360) to background levels, making it impossible to image them for a full 100 minute experiment without most of them 'fading' (See **Figure 2-5** for example images of fading in astrocytes loaded with Fura-2ff). Increasing the loading time or concentration of Fura-2ff during loading did not prevent this, with only a lowering of the temperature during the experiment reducing indicator efflux. However, dropping the temperature below 36°C also dramatically reduced cell death (the endpoint of interest in the experiments) so this was not a viable option. A different fluorophore needed to be found which would remain intracellular and detectable for the duration of these long experiments at 37°C.

A1



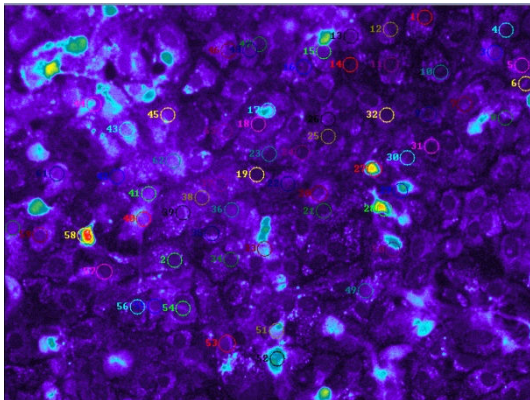
0 minutes

A2



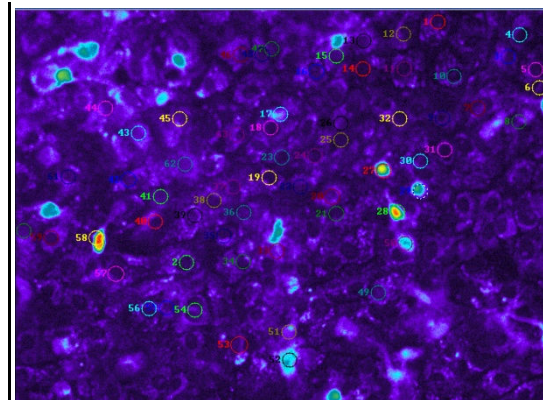
20 minutes

A3



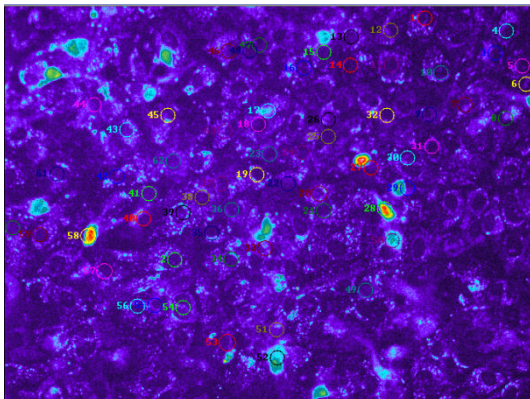
50 minutes

A4



70 minutes

A5



90 minutes

Figure 2-5: Example of fading in Fura-2ff loaded astrocytes

A1-A5: Pseudocolor images of Fura-2ff fluorescence in cultured astrocytes (See pages 43-49 for details of protocols used to obtain these images):

A1: At the start of the experiment the astrocytes show good Fura-2ff loading, but very quickly start to fade. Within 50 minutes (*A3*) the majority of cells are no longer producing enough fluorescence for the purposes of the experiment, making it necessary to find a different dye.

BCECF, Propidium Iodide and CMFDA for cell viability studies

Initially I tried using BCECF (2',7'-bis-(2-carboxyethyl)-5-(and-6)-carboxyfluorescein, B1170, Invitrogen, Paisley, UK) as it had already been used by other groups for imaging astrocytes, assessing intracellular pH and cell viability (Bevensee et al., 1995; Bondarenko et al., 2005). However, the experiments described in these papers were always either significantly shorter (maximum 70 minutes) and/or performed at only 32°C, thereby reducing dye efflux significantly. BCECF was inadequate for these experiments, with astrocytes once again rapidly losing their fluorescence at 37°C.

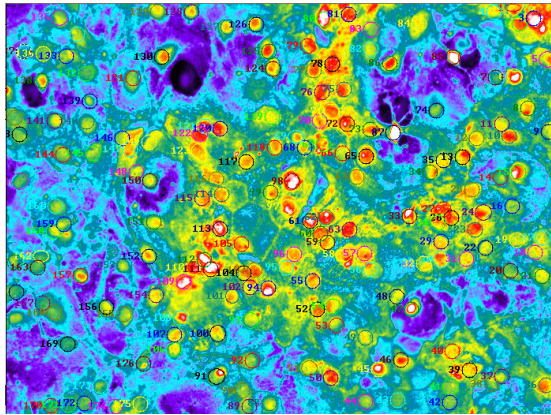
Another method I attempted was using propidium iodide (PI) to monitor cell death, a method which has also been used in this sort of setup by other groups (Bevensee, Schwiening et al. 1995). When PI binds to DNA it emits bright fluorescence at around 570nm when excited at 488nm. Under normal conditions in viable cells PI is unable to cross the cell membrane and bind to DNA, but when the cell dies and membrane integrity is lost it can easily bind. The idea was to have cells loaded with Fura-2ff as well, and then PI could be used as an additional method for inferring the fate of the cells during experiments. Unfortunately during experiments in our system the flow of perfusing solutions seemed to wash away cellular material once the cell had died, so the PI fluorescence would not remain in the same place, making it difficult to localise fluorescence to specific cells or even detect PI fluorescence if it was at all present. It was also very painstaking to manually switch filter cubes every few minutes to measure the different fluorescence emitted between Fura-2ff and PI.

A variety of intracellular probes have been developed which are retained in living cells over a long period of time and through several generations, with the CellTracker™ probes being one of the main groups. These have been used to aid identification of cellular migration patterns over longer periods of time (up to 4 weeks) both *in vivo* and *in vitro* at temperatures around 37°C (Luzzati et al., 2006; Hayes et al., 2007). CMFDA (5-chloromethylfluorescein diacetate, C7025, Invitrogen, Paisley, UK) is one of this group of compounds. According to the product information sheet these dyes contain a

chloromethyl group that reacts with thiols, probably in a glutathione S-transferase-mediated reaction, transforming the probes into cell-membrane impermeant fluorescent dye-thioether adducts, producing cells that are both fluorescent and viable for at least 24 hours. For loading CMFDA was used in its AM ester form.

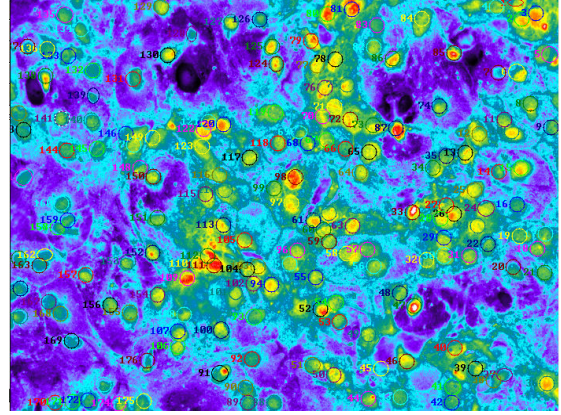
CMFDA proved to be a good choice for long experiments at 37°C (see **Figure 2-6** for example images of CMFDA loaded astrocytes), with all cell types maintaining bright fluorescence for well over 100 minutes (see **Figure 2-7: Comparing Fura-2ff and CMFDA retention in astrocytes and neurons**), despite requiring a shorter loading period and lower loading concentrations than Fura-2ff. Since neurons still maintained adequate Fura-2ff fluorescence during long experiments at 37°C the indicator was still used in the pure neuronal culture.

A1



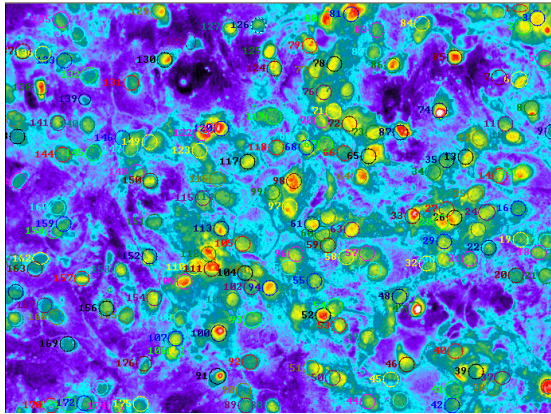
0 minutes

A2



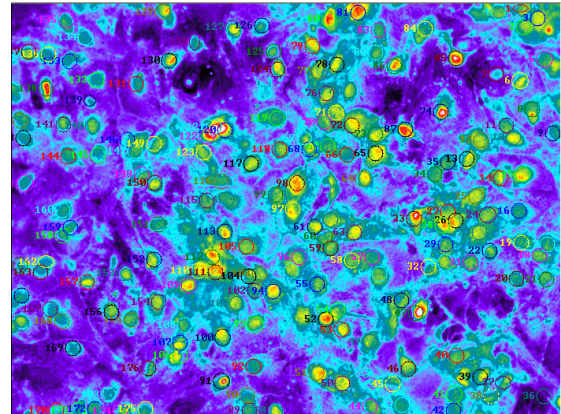
20 minutes

A3



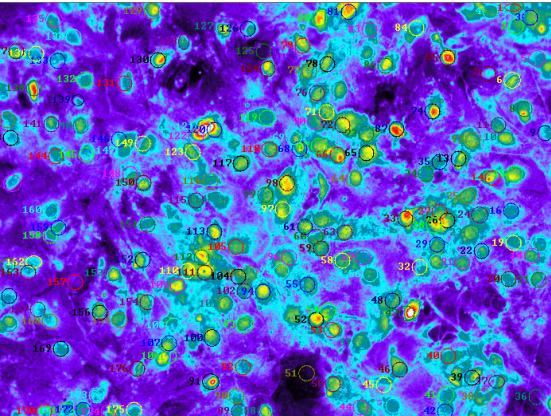
50 minutes

A4



70 minutes

A5



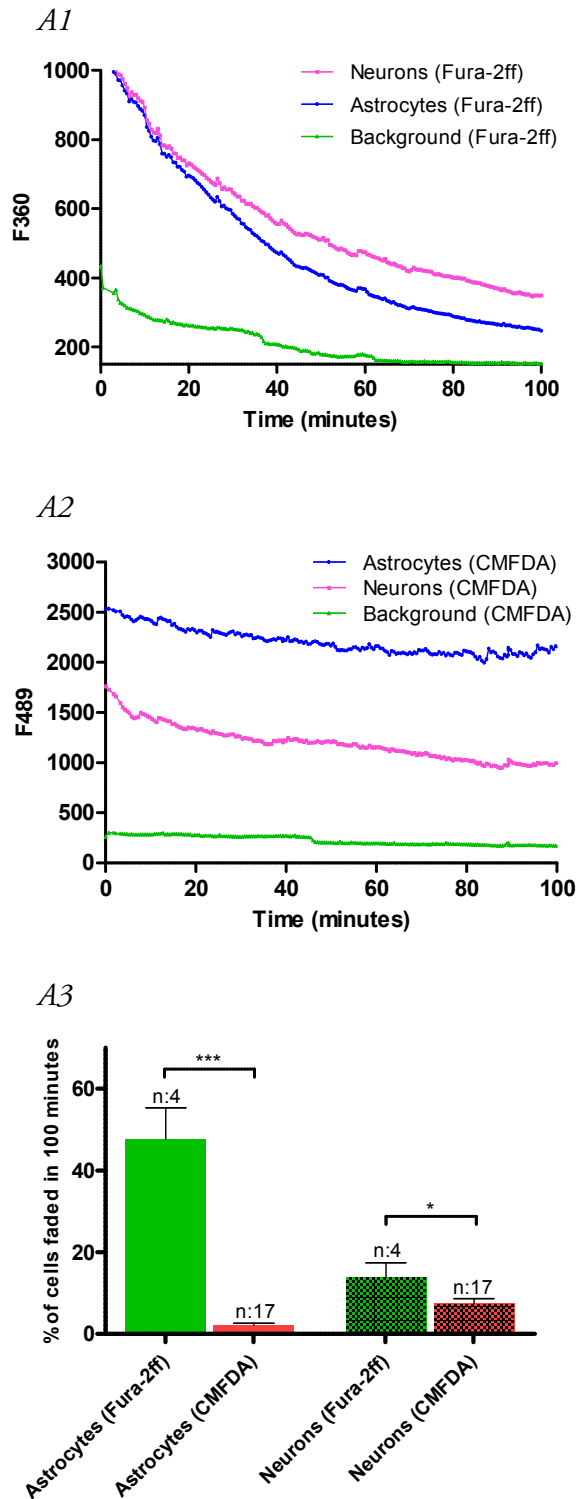
90 minutes

Figure 2-6: Example of CMFDA-loaded astrocytes

A1-A5: Pseudocolor images of CMFDA fluorescence in cultured astrocytes
(See pages 43-49 for details of protocols used to obtain these images)

Throughout the 90 minutes of the experiment the astrocytes maintain adequate fluorescence using the intracellular indicator CMFDA.

Figure 2-7: Comparing Fura-2ff and CMFDA retention in astrocytes and neurons



A1: Fura-2ff retention

Graph demonstrates how within about 25 minutes of starting perfusion experiments Fura-2ff loaded astrocytes (blue line) had a significantly reduced fluorescence intensity compared with neurons (pink line) in co-culture on the same slides (n=3, 240 astrocytes, 126 neurons). There is also a reduced fluorescence overall when compared with CMFDA loaded cells (see A2), and towards the end of the 100 minutes fluorescence, particularly in astrocytes, approaches background levels, making it difficult to identify cells accurately.

A2: CMFDA retention

Loading with CMFDA results in far brighter fluorescence, and in this case the astrocytes (blue line) produce a higher intensity than the neurons (pink line). Both cell types fluoresced at a level high above background. There was only minimal loss of fluorescence over 100 minutes. (n=3, 94 astrocytes, 177 neurons)

A3: Comparing loss of CMFDA and Fura-2ff fluorescence in astrocytes and neurons

Graph comparing what percentages of Fura-2ff vs CMFDA-loaded astrocytes and neurons in co-culture lost enough of their intracellular indicators during the duration of a 100 minute control experiment (see pages 43-49 for protocols of experiments) to no longer be detectable (they 'faded'). Nearly half of all astrocytes ($47.52 \pm 7.8\%$) were unable to retain Fura-2ff for the duration of the experiment, while only $2.14 \pm 0.4\%$ were unable to retain CMFDA, showing that this indicator is superior for imaging cultured astrocytes over a longer period of time at 37°C ($p < 0.001$). Neurons were much better at retaining the dyes, with only $13.8 \pm 3.6\%$ fading when loaded with Fura-2ff and $7.44 \pm 1.2\%$ fading when loaded with CMFDA ($p < 0.05$). In both cell types retention of CMFDA was significantly improved compared with Fura-2ff.

Percentages: Mean \pm SEM.

* $p < 0.05$

*** $p < 0.001$

Mounting and loading of cells for fluorescence microscopy

Oxygen-glucose deprivation (OGD) experiments

Cell culture slides were removed from their petri dishes one at a time when needed for experiments, using sterilised fine forceps. Excess growth medium was removed from the cover slip using tissue paper before sealing it to the bottom of a Plexiglas perfusion chamber (atmosphere chamber, Warner Instruments, Hamden, CT, USA) using silicone grease. The chamber was then filled with some growth medium from the petri dish, and the dish, with any remaining slides, returned to the incubator. The chamber and cells were then mounted into the stage of the microscope, and the growth medium was removed and replaced with aCSF containing either Fura-2ff AM (10ug in 700ul, 14.2uM) or CMFDA AM (2.5ug in 700ul, 7.7uM). All loading solutions also contained 0.01% Pluronic F-127 (P2443, Sigma-aldrich), a non-ionic surfactant, to facilitate loading. The cells were incubated like this in the dark while being oxygenated for a total time of 30 minutes for Fura-2ff or 20 minutes for CMFDA. Before imaging the loading solution was removed and replaced with fresh aCSF.

Short agonist application experiments

A Petri dish containing 4 cell culture slides was removed from the incubator, the growth medium removed and replaced with hepes-aCSF twice to wash away any remaining growth medium before loading cells with hepes-aCSF containing Fura-2 AM (40ug in 6ml, 6.7uM) for one hour at room temperature in the dark. The solution was then replaced again with fresh hepes-aCSF and slides were removed one at a time and attached to the perfusion chamber as detailed above, with unused slides being kept in the dark at room temperature until needed. The cells could be used for up to two hours after loading for these experiments.

Cell perfusion set-up

The perfusion chamber has two sections. The solutions first run into a large chamber, which contains the cells to be imaged, and the solution is then sucked out by a vacuum pump through an opening connected to a smaller chamber on the other side of the apparatus, creating a turbulence-free flow. At the same time, gas is delivered into the atmosphere of the large chamber, with a second cover slip placed over the top of the large chamber ensuring this does not mix with normal atmospheric air (**Figure 2-8**).

OGD experiments

The rig allows for switching between two different perfusing solutions (aCSF and aCSF-glucose) and two different gas mixtures (95%O₂/5%CO₂ and 95%N₂/5%CO₂) to switch between normoxia/normoglycaemia and OGD (see **Figure 2-8** for a diagram of the complete setup). The two bottles containing perfusing solutions are kept in a warm water bath at 37°C and are constantly bubbled with either the 95% O₂ (aCSF) or 95% N₂ (aCSF-glucose) + 5% CO₂. Before reaching the perfusion chamber, the fluid passes through a flow-through feedback heater (Warner Instruments, Hamden CT, USA) set to 37°C, and the objective of the microscope has a heater attached to it (Bioptechs, Butler PA, USA) set to 37°C. In addition to this, the room that the whole rig was being run in was heated up using a simple electrical fan heater and kept at a temperature of around 35-37°C as monitored using an electronic temperature probe which was placed just above the perfusion chamber. I found that this was the only way to ensure that experiments were reproducible as even small changes in the already relatively low flow rate through the chamber could otherwise affect temperatures and thereby results. The highly protective effects of hypothermia during *in vitro* OGD have been described before (Bruno et al., 1994). aCSF was perfused through the perfusion chamber at a rate of 2-3ml/minute, with a fluid level of 1-2 mm in the chamber. It took <3 minutes for the solutions in the chamber to change when switching between perfusing solutions on the rig. Gas was pumped through the chamber at a rate of 1-2l/minute. The tubing used on the rig is not oxygen permeable.

Short agonist application experiments

For the short application agonist experiments a commercially available perfusion system (ValveBank8.2, manufactured by AutoMate Scientific, Berkeley CA, USA) was used. This allowed for electronically activated switching between up to eight different perfusing solutions at precisely controlled flow rates as the solutions were contained within large gas-pressurized syringes. Since these experiments did not measure cell death/survival and were performed at a higher flow rate (approximately 10ml/minute), less stringent temperature control was required. Experiments were performed at normal room temperature (about 25°C) rather than heating the room to 37°C, but the same flow-through feedback heater and objective heater mentioned above were used to maintain chamber temperature at about 37°C.

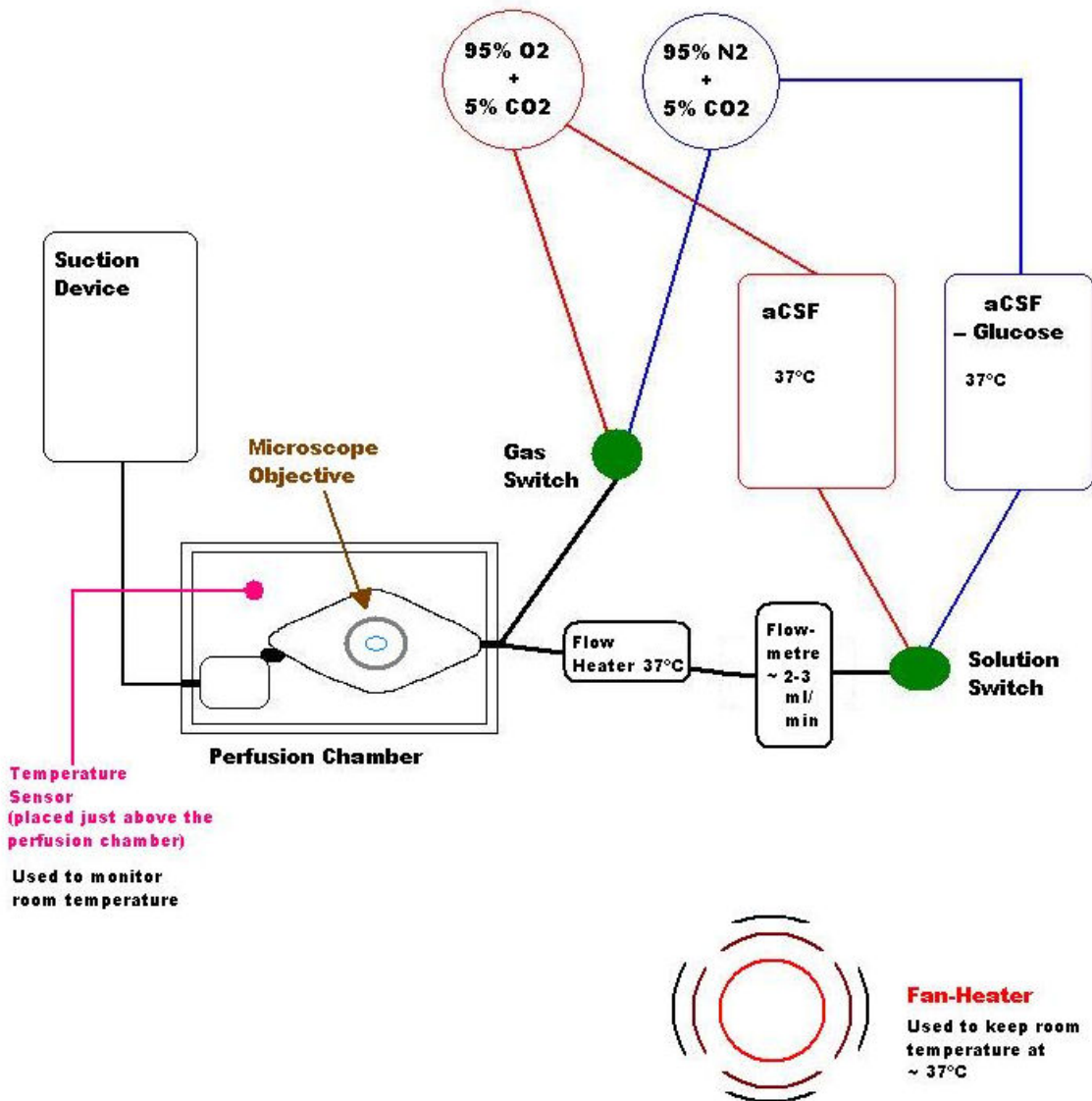


Figure 2-8: Perfusion system setup, OGD experiments

Cell imaging set-up

The chamber containing the specimen was mounted on the stage of either a Nikon Eclipse TE-200 or TE2000-U epifluorescence microscope (Tokyo, Japan). A 20x oil-immersion objective was used for all OGD experiments, whilst a 40x objective was used for agonist experiments. Excitation of the fluorescent indicators was achieved via passage of light from a high-intensity arc lamp through an Optoscan monochromator (both Cairn Research Ltd., Faversham, UK) coupled to the epifluorescence microscope. Emission was recorded at either 520nm through a Fura filter-fitted dichroic mirror or at 508nm through a CMFDA filter-fitted dichroic mirror (Chroma Technology Corporation, Rockingham VT, USA). When using Fura-2ff or Fura-2, cells were illuminated at 340, 360, and 380 nm, with emission being recorded at 520nm for each of the three excitation wavelengths, whilst when using CMFDA cells were illuminated only once at 489nm excitation and 508nm emission. Images were captured by a coolSNAP HQ camera (Roper Scientific, Ottobrunn, Germany) and were stored on a desktop computer running Windows XP. The software that was used to control all the parameters during imaging and to analyse the images was the image acquisition program MetaFluor (Molecular Devices, Sunnyvale CA, USA). Using Metafluor, regions of interest (ROIs) were drawn around individual cells in each experiment, and these regions could be moved between frames to adjust for cell movement due to shifting of the preparation over time.

Imaging Protocols

OGD experiments

Once mounted, cell culture slides were imaged for a total of 100 minutes. The first two or three minutes of imaging were used to focus the cells and choose an area on the slide with as many cells as possible, and cells at this time were perfused with aCSF/O₂. After 10 minutes conditions were switched to OGD, except during control experiments, where cells were constantly perfused with aCSF/O₂. Images were acquired every 30 seconds, at 340, 360, and 380nm excitation when using Fura-2ff or 489nm excitation when using CMFDA.

Short agonist application experiments

After finding a suitable area of Fura-2 loaded cells on a slide, images at 340, 360 and 380nm excitation were acquired every ten seconds for two minutes of perfusion with aCSF + Hepes to calculate a baseline $[Ca^{2+}]_i$. Various P2 and glutamate receptor agonists were then applied sequentially in 20 second bursts, with each application interrupted by five minutes of perfusion with aCSF + Hepes. During the 2 minutes immediately subsequent to the application of every agonist burst, images were acquired every second instead of every ten seconds to increase the recording resolution of any $[Ca^{2+}]_i$ response.

Image analysis

In CMFDA-loaded cells average emissions at 508nm generated by excitation at 489nm (F489) and for Fura-2 and Fura-2ff average emissions at 520nm generated by excitation at 340nm, 360nm (the isosbestic point) and 380nm (F340, F360 and F380 respectively) were collected from individual cells by drawing ROIs around them in MetaFluor. The ratio of the 340:380 fluorescence was then used to calculate $[Ca^{2+}]_i$, either precisely by using a Ca^{2+} calibration kit or simply to show relative changes in $[Ca^{2+}]_i$. A Fura-2 Ca^{2+} calibration kit (F6774, Invitrogen, Paisley, UK) containing 11 pre-diluted buffers was used to do the calibration, as per the instructions supplied. To acquire values for background fluorescence, images at 340nm and 380nm excitation were taken of cells that were not loaded with Fura-2 but were being perfused. These were then used to perform background subtractions on all experimentally obtained values. All settings on the microscope and camera which could affect these values were left unchanged after doing the calibration and obtaining background fluorescence values. Fura-2ff signals in the longer OGD experiments were not calibrated, so changes in $[Ca^{2+}]_i$ reported from these experiments were not quantitative, only qualitative. Calibrations were not performed for Fura-2ff fluorescence in these experiments since the fluorescence properties of Fura-2ff (K_d values) change considerably when the dye is illuminated repeatedly over a long period of time, making calibrated $[Ca^{2+}]_i$ relatively unreliable (Hyrc et al., 2000).

The fluorescence intensity values for each cell over time were exported into Microsoft Excel where traces for each separate excitation wavelength were graphed and further mathematical manipulations of data were performed. 340:380 ratios were calculated and when using Fura-2 were plugged into the calibration equation to convert them to $[Ca^{2+}]_i$. When analysing the short agonist experiments each cell was classified as either a responder or non-responder after each agonist application, and in all that showed a response the change in $[Ca^{2+}]_i$ (ΔCa_i) was precisely calculated by subtracting the baseline $[Ca^{2+}]_i$ from the peak $[Ca^{2+}]_i$ reached (as determined by using the MAX function in Excel) for each separate agonist application.

Assessing cell viability/death

The method for assessing cell viability or death was linked to the ability of living cells to retain intracellular fluorescent indicators, which are suddenly released when the cell dies due to breakdown of the plasma membrane. When using Fura-2ff the F360 signal was monitored to assess the capacity of cells to retain dye, as this is the isosbestic excitation wavelength for Fura-2: at this wavelength any change in the overall signal level is not sensitive to the $[Ca^{2+}]_i$ of the cell, indicating instead the amount of dye present. A sudden and irreversible drop in the F360 level to background therefore correlates with a loss of cell membrane integrity and the release of dye into the extracellular space (Lemasters et al., 1987; Geeraerts et al., 1991). Sudden loss of cell membrane integrity correlates to cell death (Fern, 1998). See **Figure 2-9** for example tracings and images. CMFDA was used in the same way.

Each cell was examined individually to check whether it survived or died during the course of an experiment, both by looking at the fluorescence traces for a sudden drop in fluorescence and by double checking the actual images to make sure that something else had not happened, such as the ROI moving off of the cell in question or the cell detaching and being washed away. Any cells that were lost due to movement of the slide out of the field of view or cells which showed a gradual rather than sudden drop of fluorescence to background levels before the end of an experiment were excluded from any analyses.

Graphs were created comparing the total amount of cell death in different conditions. The specific time at which each cell died was recorded, and this made it possible to create graphs depicting the percent of the total cell death that occurred within each 5 minute interval. The values for each plot were then normalized to reflect the total amount of cell death occurring in each condition.

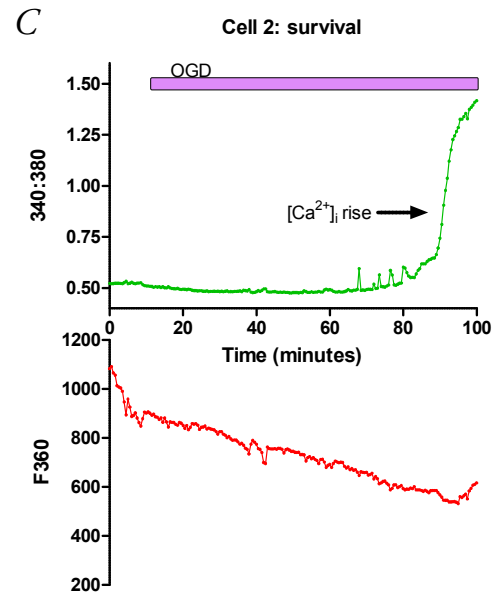
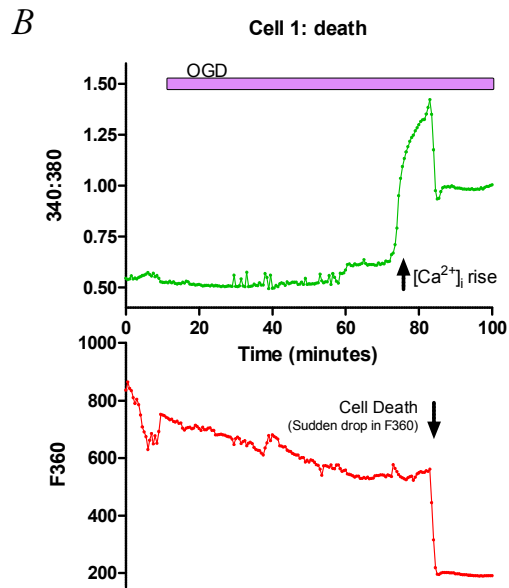
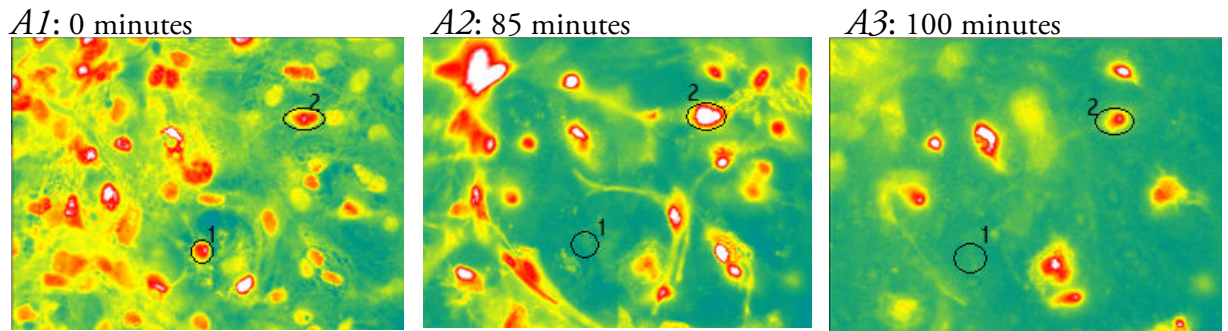


Figure 2-9: Assessing cell viability using Fura-2ff in co-cultured astrocytes and neurons

Examples of cell death and survival in co-cultured astrocytes and neurons loaded with Fura-2ff:

A1-A3: Cells were subjected to 10 minutes of control followed by 90 minutes of OGD (100 minutes total).

B: Cell 1 exhibits the pattern of a short but large rise in $[Ca^{2+}]_i$ starting at about 75 minutes culminating in cell death at about 85 minutes, which is seen as a sudden drop in F360.

C: Cell 2 survived the 90 minutes of OGD (no sudden drop in F360) despite showing a rise in $[Ca^{2+}]_i$ starting at about 90 minutes. If the recording had been allowed to go on for longer this cell would have probably also died.

Identification/differentiation of astrocytes and neurons in co-culture

One of the main aims of this PhD was to be able to differentiate the effects on astrocytes and neurons in co-culture of OGD and various pharmacological/experimental manipulations. I had established in work undertaken during my BSc project that the interactions between the two cell types when combined in culture seemed to be essential, but at the time I was unable to ‘unpick’ the astroglial and neuronal contributions. This method had to be accurate, reproducible, and as simple as possible. In this section I will outline the various methods attempted and the one that was eventually used, including reasons for and against each one.

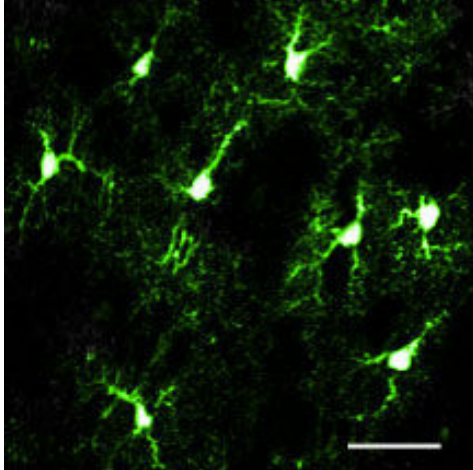
eGFP-GFAP transgenic mice: a puzzling loss of eGFP fluorescence in cell cultures

Since it was first described in 1980 (Gordon et al., 1980) the use of transgenic mice as tools for scientific research has become extremely popular, as it allows for the development of murine models for various human conditions. More recently transgenic mice have been created which selectively express a fluorescent protein under the control of cell-type specific promoters, thereby allowing for labelling and visualization of specific cell types *in vivo* and *in situ* (Brenner et al., 1994; Zhuo et al., 1997; Nolte et al., 2001; Suzuki et al., 2003; Hirrlinger et al., 2005; Salter and Fern, 2005; Shannon et al., 2007; Wigley et al., 2007). In our lab we have a colony of transgenic mice of the strain FVB/N-Tg(GFAPGFP)14Mes/J (jax stock number 003257) which carries eGFP (hGFP-S65T) under the control of the human GFAP promoter (Zhuo et al., 1997; Nolte et al., 2001). The astrocytes in these mice selectively fluoresce brightly (excitation-489nm, emission-508nm) when imaged with a fluorescence or confocal microscope (see **Figure 2-10** for example images) , and have been used for various studies using *in vivo* and *in situ* preparations (Nolte et al., 2001; Shannon et al., 2007; Wigley et al., 2007; Salter and Fern, 2008), but to my knowledge there is no mention in the literature of any of these animals having been used to create cell cultures. I therefore set out to develop a cell culture model using these transgenic mice, where the astrocytes in co-culture with neurons would be easily visualized and identified by their eGFP fluorescence.

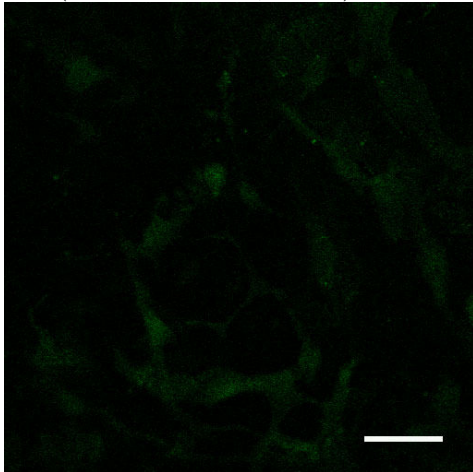
Heterozygous males were mated with wild-type females, with heterozygous transgenic litter mates identified at P0-P1 using a blue light source and appropriate filters in a custom made box, where the transgenic animals were seen to have a characteristic green glow around the eyes and through the thin bones of the skull. Animals were then used at age P0-P1 for astrocyte cultures using the same methods described earlier in this chapter. In terms of growth and survival in cell culture, astrocytes derived from these animals showed no differences to the ones that were cultured from E16 balb-c mice. However, they were devoid of eGFP fluorescence once they had been cultured (**Figure 2-10**). Imaging of eGFP fluorescence was attempted on three different microscopes (including confocal and regular light microscopes) with appropriate filter sets/settings using both live and fixed astrocytes. Cultures were repeated numerous times over a six month period, and were examined for up to 28 days *in vitro* for signs of fluorescence, as GFAP expression increases with age (Eng et al., 2000). I also tried growing astrocytes in Nb, to no avail. GFAP immunostaining of fixed astrocytes revealed sufficient GFAP expression in the cell culture (**Figure 2-10**). I also performed an experiment to detect whether any eGFP mRNA was present in the cell culture, using freshly dissected brains from the transgenic mice as a control (**Figure 2-11**). This demonstrated that mRNA encoding eGFP was present in both the whole brain and cell cultures of eGFP-GFAP transgenic mice, suggesting again that the loss of fluorescence was not due to lack of expression.

Finally, upon consultation with two experts in the field it became apparent that they also had failed to produce cell cultures with these mice that maintained their fluorescence, and that no explanation for this has yet been found (personal communication with Frank Kirchhoff and Arthur Butt). It was apparent at this point that a different method would be required for cell identification.

A1 (eGFP fluorescence, hippocampal slice)



B1 (eGFP fluorescence, culture)



B2 (GFAP IHC labelling, same culture as *B1*)

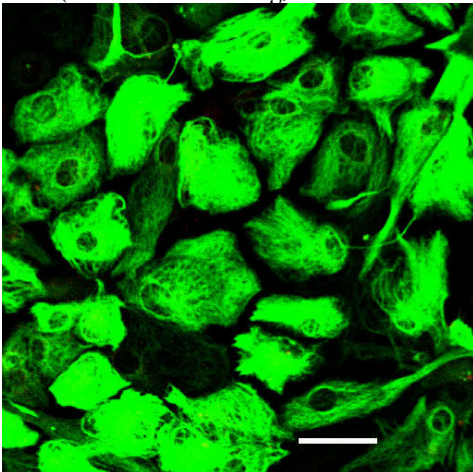


Figure 2-10: Imaging eGFP-GFAP astrocytes

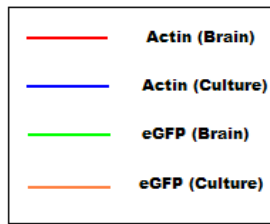
A1: eGFP-expressing astrocytes (green) in a hippocampal slice of a mouse aged P10.

The cells are bright and well defined in this preparation, which was taken using a confocal microscope (Image courtesy of Claire Shannon).

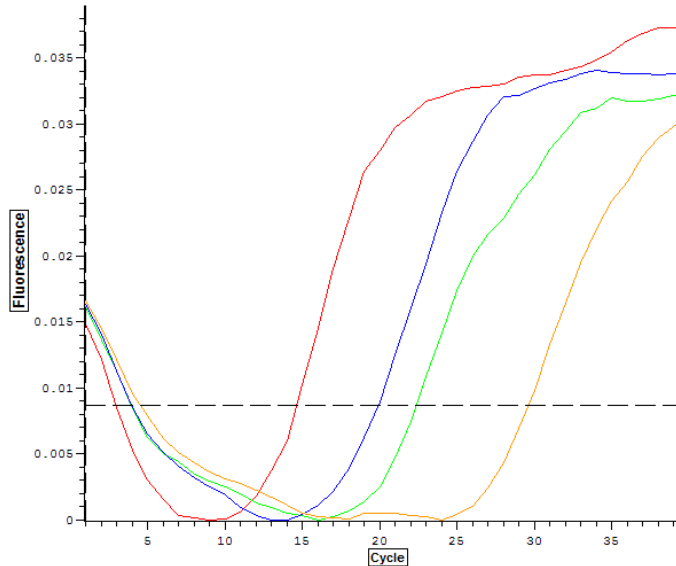
B1: (lack of) eGFP fluorescence of cultured astrocytes. Extremely faint fluorescence was present in the astrocyte culture which was created using the eGFP-GFAP transgenic mice. Image taken using the Olympus confocal microscope, with gain and photo-multiplier tube settings on high. With these settings the fluorescence seen in the image was auto-fluorescence of the cells and not eGFP fluorescence.

B2: GFAP-labelled astrocyte culture. To check whether the lack of eGFP fluorescence seen in *B1* was due to a reduction in GFAP expression, the same culture was fixed and labelled for GFAP. Good GFAP expression is evident in this image, suggesting that the cause of this loss of fluorescence had a different aetiology.

Scale bars: 50uM



A1



A2

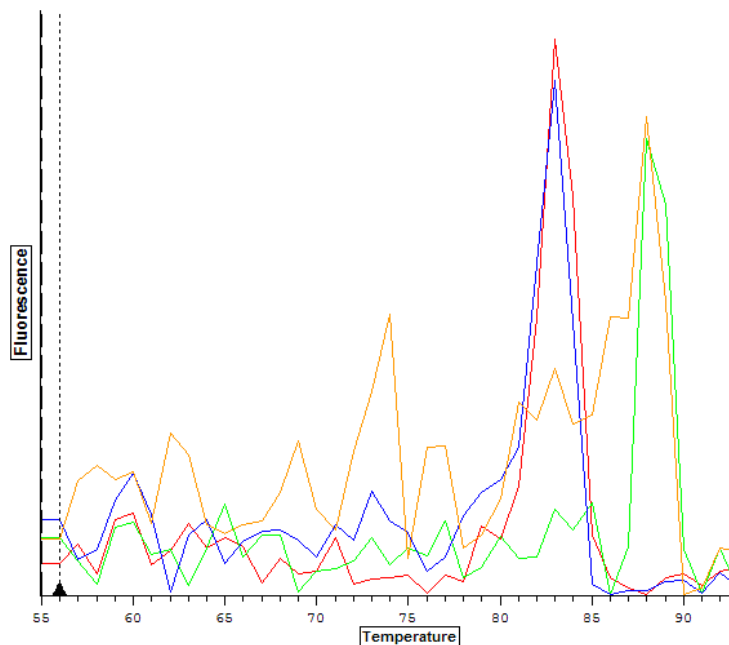


Figure 2-11: PCR analysis of eGFP-GFAP astrocyte cultures

A1: Amplification plots for eGFP and actin in both whole brain and cultured cells, with single representative traces for each. eGFP product accumulation occurs approximately 9 cycles later in the cultured cells than in the brain, whilst actin accumulation occurs about 5 cycles later in the sample taken from cultured cells.

A2: Dissociation curves for eGFP and actin, demonstrating single uniform products in both cases.

Messenger RNA encoding eGFP is present in both the whole brain and cell cultures of eGFP-GFAP transgenic mice, confirming that the loss of fluorescence is not due to lack of expression.

Pre-loading of astrocytes with CMFDA before neuronal plating

As mentioned earlier, CMFDA has been used to aid identification of cellular migration patterns over longer periods of time (up to 4 weeks) both *in vivo* and *in vitro* at temperatures around 37°C (Luzzati et al., 2006; Hayes et al., 2007). This would theoretically make it ideally suited for labelling astrocytes in the co-culture by incubating them with the dye before plating neurons on top of them, so that only astrocytes would subsequently exhibit fluorescence four days later when the co-cultured cells were ready for experiments (Cotrina et al., 2000). Astrocyte cultures were incubated for one hour at 37°C in culture medium containing 12.5uM of CMFDA, washed twice with fresh medium, and then the co-culture was finished as described previously. Unfortunately all of the fluorescence/dye had disappeared by the time the cells were ready to be imaged (4 days after loading).

Phase-contrast light microscopy for cell identification

When viewed with phase-contrast microscopy, cultured astrocytes and neurons are morphologically distinct. Neurons can easily be identified by their characteristic morphology, with the majority having either a pyramidal (triangular perikaryon with one prominent ‘apical’ dendrite at its apex and several shorter ‘basilar’ dendrites), fusiform (dendritic processes emerging from opposite poles of the perikaryon) or multipolar (multiple dendritic processes arising from multiple sites around the perikaryon) characteristics, as well as being very prominently viewable using phase-contrast microscopy (Kriegstein and Dichter, 1983). The cultured astrocytes on the other hand were very difficult to identify with phase-contrast microscopy due to the fact that they are extremely thin, flat, and they form a continuous layer once reaching confluence, making them less prominent compared to the co-cultured neurons. The cultured astrocytes were also much larger than neurons. These criteria for identification (which have been used by others (Fischer et al., 2009)), were tested and confirmed using IHC staining of fixed co-cultures labelled with GFAP and NSE as a control, (**Figure 2-12**) demonstrating that this was indeed an accurate way of differentiating the cells.

The protocol which was adopted thereafter involved taking a phase-contrast image of the field of cells used in any given experiment immediately before the start of the fluorescence imaging (**Figure 2-12**). The phase-contrast and fluorescence images were then overlaid using Photoshop (Adobe) and each cell was individually classified according to its phase-contrast appearance as being either a neuron, astrocyte, or unidentifiable (these were cells which would not exactly fulfil the criteria for either neurons or astrocytes). All unidentifiable cells were excluded from further analysis. The fluorescence images contained all the numbered regions of interest which corresponded to a particular cell, so the fluorescence data could be attributed to either a neuron or an astrocyte. Admittedly this is not a perfect method, since there can be situations where astrocytes and neurons overlap each other in single regions of interest in fluorescence images, but areas where this seemed to be occurring were analyzed very carefully or excluded from the overall data if there was any remaining uncertainty.

Data Analysis and Statistics

GraphPad Prism v5.0 (GraphPad Software Inc, La Jolla, USA) was used to perform all statistical analyses. Experiments were repeated a minimum of three times to ensure accurate results. Results are presented as means \pm the standard error of the mean (SEM). Experiments were compared using either a t-test (when comparing two groups) or a one-way analysis of variance (ANOVA) with Tukey's post-test (when comparing three or more groups), with differences being significant when $p < 0.05$. When comparing the percentages of cells responding to agonists in the short agonist application experiments and when looking at percentages of dead cells in the long OGD experiments, the n-number was the total number of experiments/cover-slips. When calculating the average $\Delta_{\max}[\text{Ca}^{2+}]_i$ in the short agonist application experiments the n-number was the total number of individual cells responding to the agonist in question.

Figure 2-12: Cell identification during fluorescent imaging

A1: Phase-contrast image of fixed co-culture, with green arrows pointing out purported neurons and red arrows pointing out astrocytes.

A2: An overlay of the **NSE** (red) labelled neurons on the phase-contrast image, revealing that the green arrows were indeed pointing at neurons.

A3: An overlay of the **GFAP** (green) labelled astrocytes on the phase-contrast image, revealing that the red arrows were pointing at astrocytes.

All scale bars: 50uM

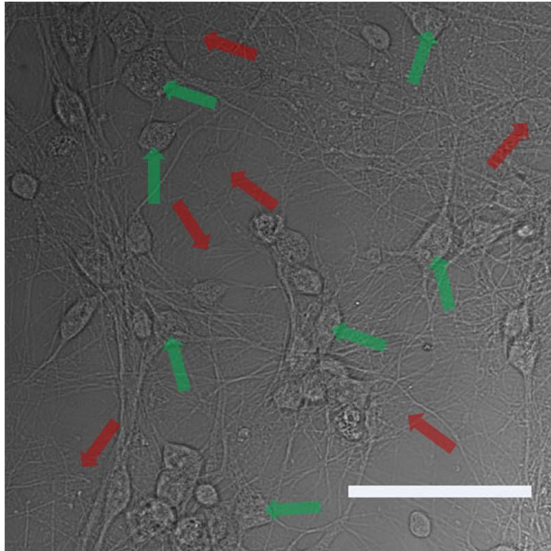
IHC experiments such as these (Images *A1*, *A2*, *A3*) formed the basis for the criteria used to identify/differentiate astrocytes and neurons during fluorescent imaging experiments. NSE labelled cells (neurons) stand out in the phase-contrast images (green arrows) having smaller, more opaque, and either round (granular neurons) or triangular (pyramidal neurons) cell bodies. The GFAP labelled cells (astrocytes) on the other hand appear very faintly and are almost invisible in the phase-contrast images (red arrows), except sometimes for the nuclei.

B1: Phase-contrast image of live co-culture

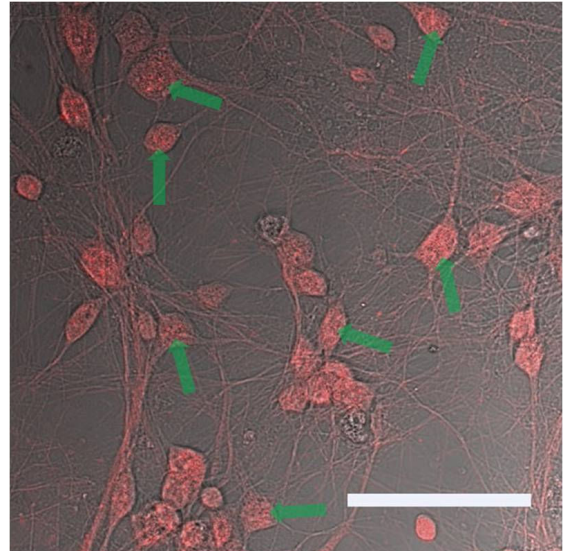
B2: Pseudo-colour image of same cells created by intracellular Fura-2ff fluorescence

B1 and *B2* are examples of the images used to differentiate live astrocytes from neurons during experiments. A phase-contrast image of the field of cells is acquired before the start of every experiment. Cells 46, 47, 48 and 49 in the Fura-2ff image would be classified as neurons because of their characteristic appearance in the phase-contrast images (red arrows) with the obvious round opaque cell bodies. On the other hand, cells 42, 43, 44 and 45 all appear only on the Fura-2ff image and not on the phase-contrast image (green arrows), and would therefore be classified as astrocytes.

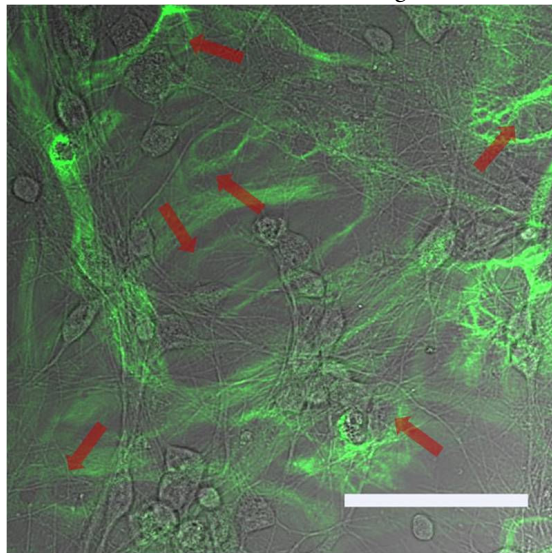
A1 (Phase contrast, fixed cells)



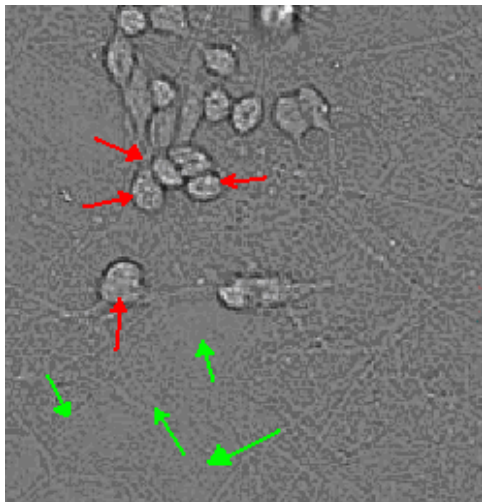
A2 (Phase contrast + NSE labelling)



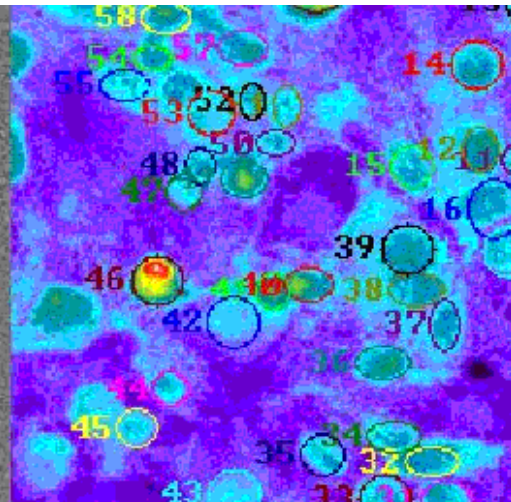
A3 (Phase contrast + GFAP labelling)



B1 (Phase contrast, live cells)



B2 (Fura-2ff fluorescence)



Molecular Biology

I only used this protocol once, comparing GFP-mRNA expression in freshly dissected brains and astrocyte cultures prepared from eGFP-GFAP mice. All materials used were from Qiagen (Hilden, Germany) unless stated otherwise.

mRNA extraction

The Qiagen minikit RNeasy (cat. No. 74104) was used, and the protocol in the handbook was followed. All surfaces were cleaned with DNA-Zap (cat. No. AM9890, Ambion, Austin, USA) to remove any contaminating DNA/RNA.

To isolate RNA from the brain, one brain from an eGFP-GFAP mouse was ground to fine dust using a mortar and pestle cooled in liquid nitrogen. The powder was placed in a 1.5ml eppendorf tube, 1 ml of Qiazol (disrupts lipid tissues, stabilizes RNA in solution) was added for five minutes, followed by 200µl of chloroform, and the solution was centrifuged at 12,000g for 15 min (4°C). Three layers formed, with the upper aqueous phase containing the RNA.

To isolate RNA from the cell culture, a dish containing three cover slips of astrocyte cultures was washed three times with PBS before adding 600µl of RLT Buffer (contained in the RNeasy kit) to lyse the cells. The obtained solution was put into a Qiashredder (for simple and rapid homogenization of cell and tissue lysates and purification of RNA) and centrifuged for two minutes at 14,000g. I then added 600µl of 70% ethanol to the solution, mixed it with the pipette, and used an RNA column to extract the RNA from the solution (as per the RNeasy protocol).

RT-PCR

Both RNA-containing solutions were then treated with TURBO DNA-free (cat. No. AM1907, Ambion, Austin, USA), a recombinant engineered highly efficient form of DNase, to remove any genomic DNA from the samples. The concentration of RNA in the samples was determined using a spectrophotometer, measuring absorbance at 260nm, before preparing samples for RT-PCR. First-strand cDNA was synthesized using the Omniscript kit using an oligo(dT)18 primer. cDNA samples were further purified using the QIAquick PCR purification kit. To prepare the PCR reaction, the same amount of RNA sample (equivalent to 4µg RNA) was added, in separated tubes, to Taq Master Mix SYBR DYE, following the kit instructions (Sigma-Aldrich, St. Louis, USA). The primer sequences are listed in **Table 2-14**. The RT-PCR reaction was run in a PTC-200 thermocycler (MJ Research) coupled to a Chromo 4 fluorescence detector (Bio-Rad), which was operated using Opticon Monitor 3 (MJ Research) software. This software was also used to analyse the results. PCR cycles were the following: 95°C for 45s, 57°C for 30s, 72°C for 45s, for 40 cycles with a dissociation curve at the end. Intensity of fluorescence was read at the end of each cycle and also during each step of the dissociation curve.

Table 2-5: List of PCR primers used for RT-PCR

Primers were designed by Dr. Michael Salter.

Primer	Sequence
Actin for	TGCTCCTCCTGAGCGCAAGTACTC
Actin rev	CGGACTCATCGTACTCCTGCTTGC
EGFP for	TAAACGGCCACAAGTTCAGCGTGTC
EGFP rev	CTCGATGTTGTGGCGGATCTTGAAG

Measuring glutamate and ATP release using microelectrode biosensors

A crucial part of my PhD project involved finding a way to measure both glutamate and ATP net release from cells. A variety of methods have been used in the past to do this, each with their own advantages and disadvantages. Recently a new group of microelectrode biosensors (the *sarissaprobe*[™] sensors, Sarissa Biomedical, Coventry, United Kingdom), developed by the laboratory of Professor Nicholas Dale at Warwick University, have become commercially available (Dale et al., 2005). They allow for real-time *in vivo* and *in vitro* detection of various different neurochemicals, including ATP and glutamate, and are advantageous due to their relative ease of use, high sensitivity (0.5nA/ μ M), broad linear range (0.5 μ M to \sim 100 μ M), fast response times (10-90% rise time \leq 10sec) and capability for repeated use. The microelectrodes themselves have a dry shelf-life of at least 4 months at 4°C and, once hydrated, a wet shelf-life of a maximum of 5 days (although in my experience I was never able to use an electrode for more than three days). The company also provides all the hardware required to set up a virtually complete system, including the Duo-Stat ME-200+ potentiostat (Sycopel International Ltd, Tyne & Wear, United Kingdom) which was purchased and used in all microelectrode experiments. A number of papers have been published which make use of these biosensors, mainly for adenosine and ATP detection (Dale et al., 2000; Frenguelli et al., 2003; Dale et al., 2005; Gourine et al., 2005a, b; Llaudet et al., 2005; Pearson et al., 2006; Frenguelli et al., 2007; Masse et al., 2007; Wall and Dale, 2007; Lin et al., 2008b). At the point of writing this thesis two papers have been published using the glutamate electrodes made by this company as they have only just come on the market (Gourine et al., 2008; Tian et al., 2009).

Biochemistry and physical structure of the ATP and glutamate microelectrode biosensors

According to Dale et al. (Dale et al., 2005), a biosensor can be defined as any sensor that uses a biological component, such as an antibody, enzyme or even a microorganism, to bind specifically an analyte of interest and provide a physical signal that is in proportion to the amount of analyte. The ATP and glutamate biosensors used during this PhD are enzymatic biosensors, which exploit an analyte-dependant step to convert an inert substance to an active product that accumulates in the biosensor where it serves as a measure of the concentration of the analyte in question. **Figure 2-13** shows the enzymatic reactions involved in the two types of electrodes used. In both electrodes the end-product of interest in the final oxidation reaction(s) is hydrogen peroxide (H_2O_2), which in turn can be detected amperometrically by a platinum electrode that has been polarized to 500mV relative to a Ag/AgCl reference electrode. The diagram also demonstrates that unlike the glutamate sensors, the ATP sensors require glycerol as a co-substrate for proper functioning of the enzymatic cascade. Because of this, 2mM glycerol had to be added to all solutions when using the ATP electrodes.

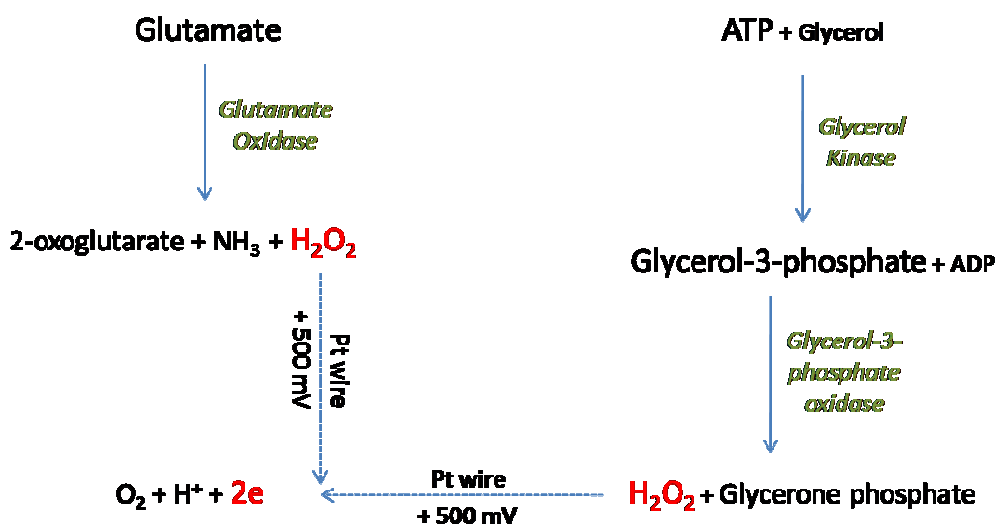


Figure 2-13: Enzymatic reactions in the glutamate and ATP biosensor microelectrodes (adapted from Dale, Hatz et al. 2005 and Llaudet, Hatz at al. 2005)

The actual microelectrodes themselves are made up of a platinum wire held within an insulating hollow glass body by a pin at one end for connection to a potentiostat and with an exposed end of the wire emerging from the other end, giving a defined sensor area (see **Figure 2-14B** for a photo of an electrode). The exposed end of the platinum wire is coated with a combination of three special layers: an innermost permselective layer, an intermediate enzymatic layer which contains a polymer matrix of the enzymes required and an outermost permselective layer (see **Figure 2-14A** for a diagram of these layers and their purpose). The purpose of the permselective layers is to reduce fouling of the sensor surface and prevent electroactive interferants (such as urate, 5-HT, ascorbate, dopamine) from reaching the platinum wire, where they would be oxidized and produce a current themselves, making the sensor non-selective (Dale et al., 2005). The ATP or glutamate diffuses through the outer permselective layer into the enzymatic layer, where hydrogen peroxide is generated which can then diffuse across the inner permselective membrane to the electrode, where it is oxidized to produce a current. Null electrodes which are devoid of the enzymes in the enzyme layer but are otherwise identical to the biosensor electrodes are used as controls, as they should react equally to any electroactive substances whilst not generating any currents in response to ATP or glutamate. Signals are simultaneously recorded from the null and sensor electrodes and the null electrode signal is then subtracted from the sensor electrode signal to give a 'pure' ATP or glutamate mediated signal.

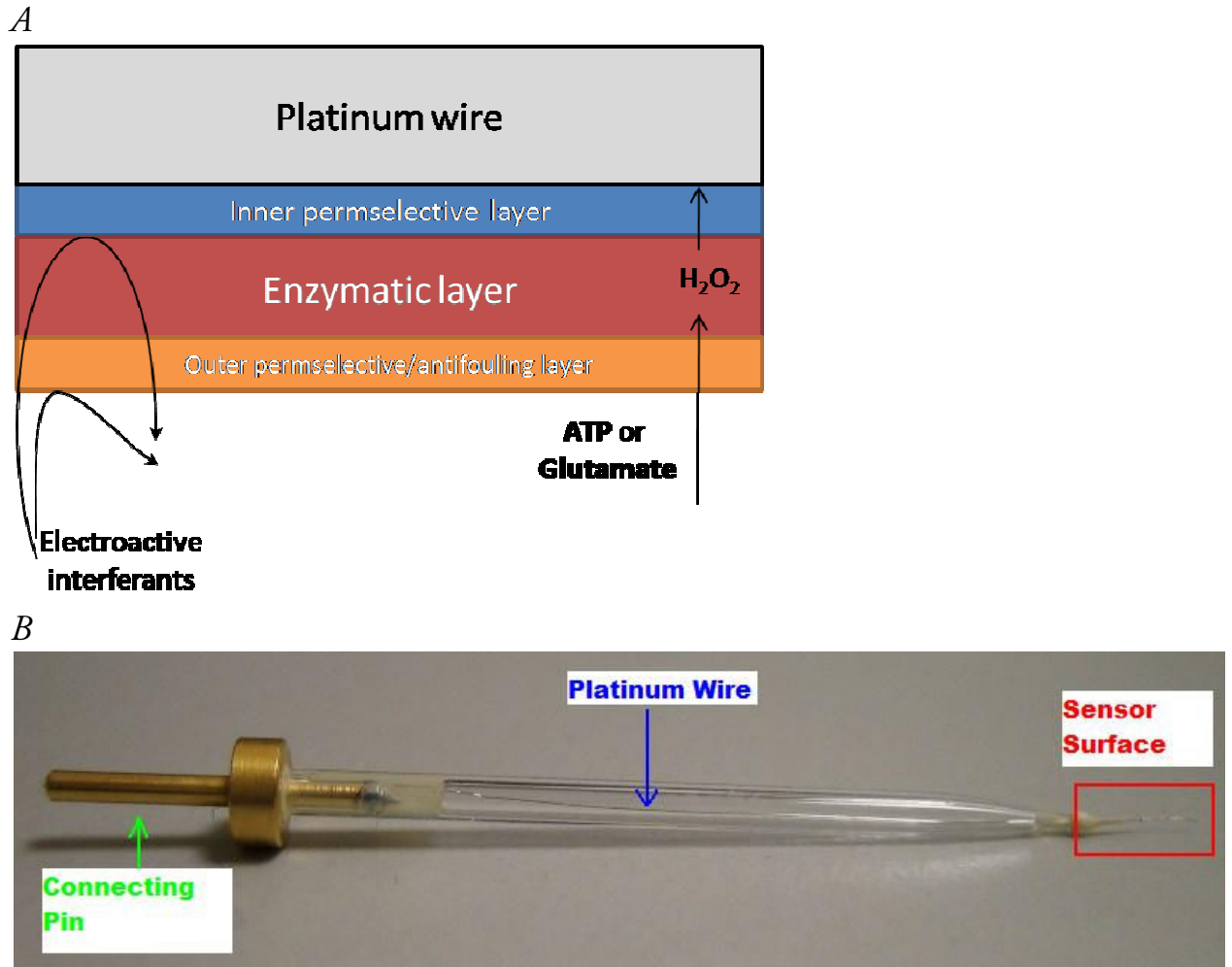


Figure 2-14: Physical structure of the microelectrode biosensors (diagram adapted from Dale, Hatz et al. 2005, photo taken by myself)

Experimental set-up and protocols

Electrodes were used as per the instructions for use that they came with. They were stored at 2-8°C until use at which point they were rehydrated using a rehydration solution (see **Table 2-3**). Stock solutions of 0.2M monobasic ($\text{NaH}_2\text{PO}_4 \cdot 2\text{H}_2\text{O}$) and 0.2M dibasic (Na_2HPO_4) were prepared and used to make a 0.01M phosphate buffered solution at pH 7.4. To this were added 100 μM NaCl, 1 μM MgCl_2 and 2mM glycerol (glycerol was added only if the ATP electrodes were being used). Fresh solution was made using the dibasic and monobasic stocks every day. For rehydration the electrodes were immersed in the solution for a minimum of ten minutes before use, and once rehydrated were stored at 2-8°C in small pots containing the same solution when not being used for experiments.

Stock solutions of 10 μ M, 100 μ M and 1mM ATP or glutamate were prepared using the same buffer solution. The now rehydrated electrodes were mounted in a 40ml ‘calibration pot’ (supplied with the electrodes) containing 30ml of the solution so that the sensor area of the electrode was in the solution, and the sensors were connected to the potentiostat to record a baseline. Once the sensors had polarized (this could take between 5 and 20 minutes depending on how often the electrodes had already been used, with the time to polarization decreasing with repeated usage) they were sequentially calibrated at 1, 10 and 100 μ M by the addition of appropriate quantities of the ATP or glutamate stock solutions to the pot. This was done to make sure the sensors were functional and still responding to low concentrations of the analytes and was especially relevant if the sensors had already been used on previous days, as with repeated usage they would become less sensitive to lower concentrations of ATP or glutamate, at which point they could no longer be used for experiments. Once the electrodes had passed the calibration test they were ready for experimental use. Electrodes with both 0.5mm and 2mm sensor surfaces were used. **Figure 2-15** (pot calibrations of all the different types of electrodes used) confirms the sensitivity and linearity of electrode responses as they were advertised by the manufacturer.

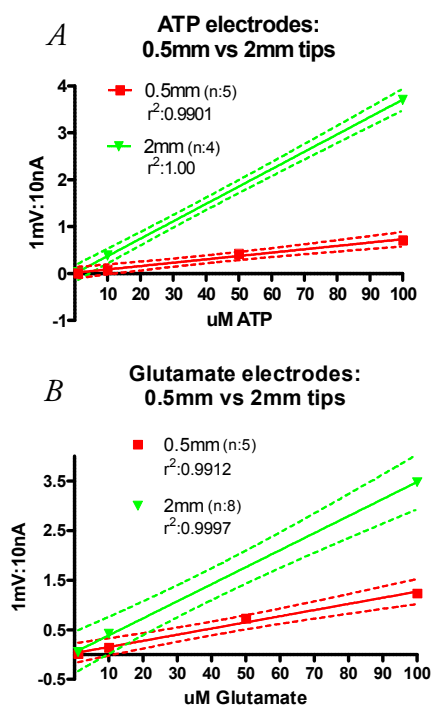


Figure 2-15: Pot calibrations of the different types of electrodes used

A+B: Graphs compare the properties of the ATP (*A*) and glutamate (*B*) electrodes and the 0.5mm (red) versus the 2mm (green) sensor tips.

Due to their larger surface area, the 2mm tips created a larger signal during pot calibrations.

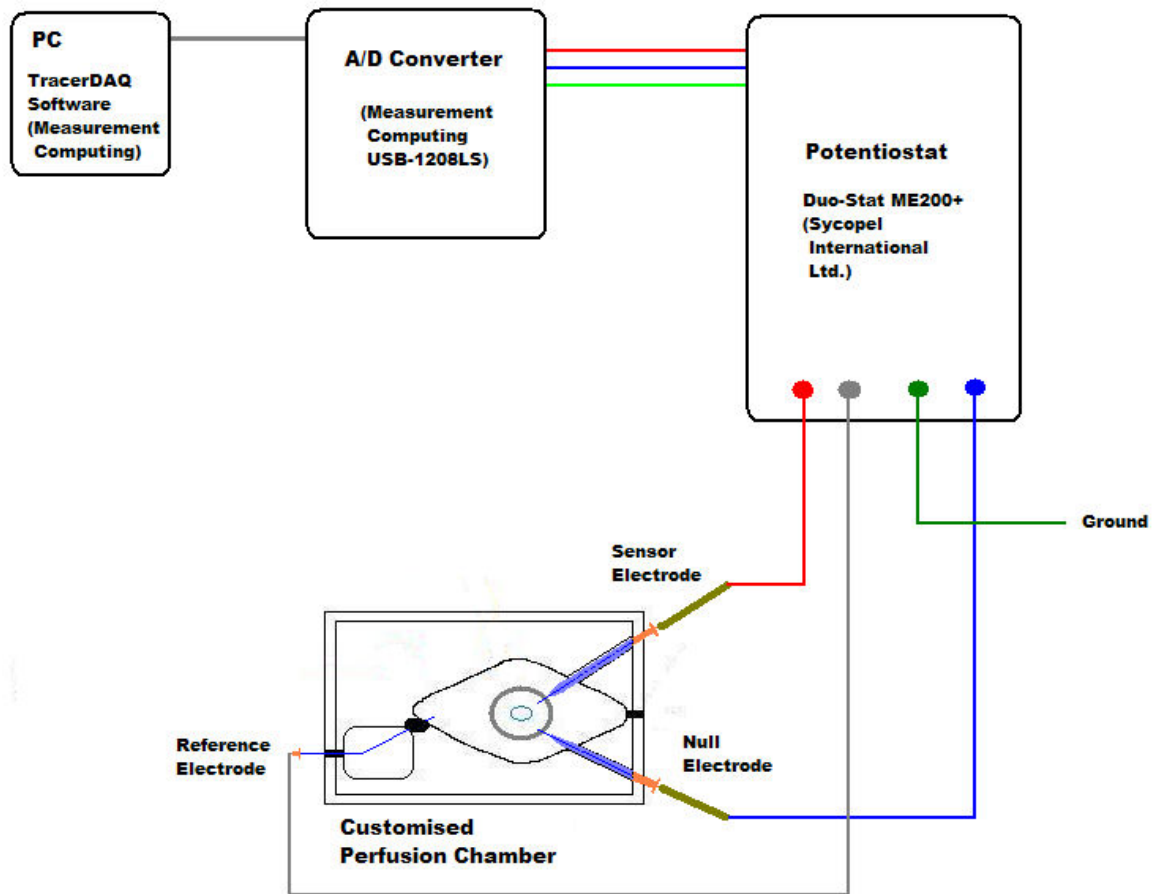
All electrodes were very sensitive and had a linear response ($r^2 > 0.99$) for a range of analyte concentrations between 1-100 μ M.

Dotted lines: 95% confidence intervals

Cell culture slides were prepared and loaded with CMFDA as previously described. However, a modified version of the perfusion chamber was designed and produced with the help of the university workshop (see **Figure 2-16B** for a photo of the chamber). It was slightly wider and had two holes drilled at a downward angle through one side of the chamber for the insertion of electrodes (in parallel with the inflow hole for the solutions entering the chamber). Electrodes (one null and one sensor) were carefully inserted through the holes, with the sensor tips of the electrodes coming gently to rest directly above the layer of cultured cells. An Ag/AgCl reference electrode was introduced through a small hole on the opposite side of the chamber. All three electrodes and a ground were connected to the appropriate inputs on the potentiostat, and the signals from the null, sensor and sensor-minus-null outputs were recorded onto a PC using an analog to digital converter (model USB-1208LS) and TracerDAQ software (both from Measurement Computing, Norton, MA, USA) (see **Figure 2-16A** for a diagram of the hardware setup used for electrode experiments).

OGD and control experiments were performed as before, except for a 20 minute longer period of perfusion with aCSF before imaging to allow for sensor polarization and the acquisition of a good baseline. ATP or glutamate release could then be assessed simultaneously to cell death. At the end of the experiments the sensors were calibrated again in the chamber. To do this the sensors were pulled back slightly to lift them from the cell layer, and all of the solution within the chamber was quickly replaced with fresh aCSF + hepes to give a zero-value before sequentially calibrating with aCSF + hepes containing 10 μ M and 100 μ M of either ATP or glutamate. These end calibrations were used to once again make sure the sensors were still working and to give values which could be used to calculate approximate ATP and glutamate concentrations from the signal recorded during the experiments. If sensors lost their sensitivity by the end of an experiment the results were discarded.

A



B

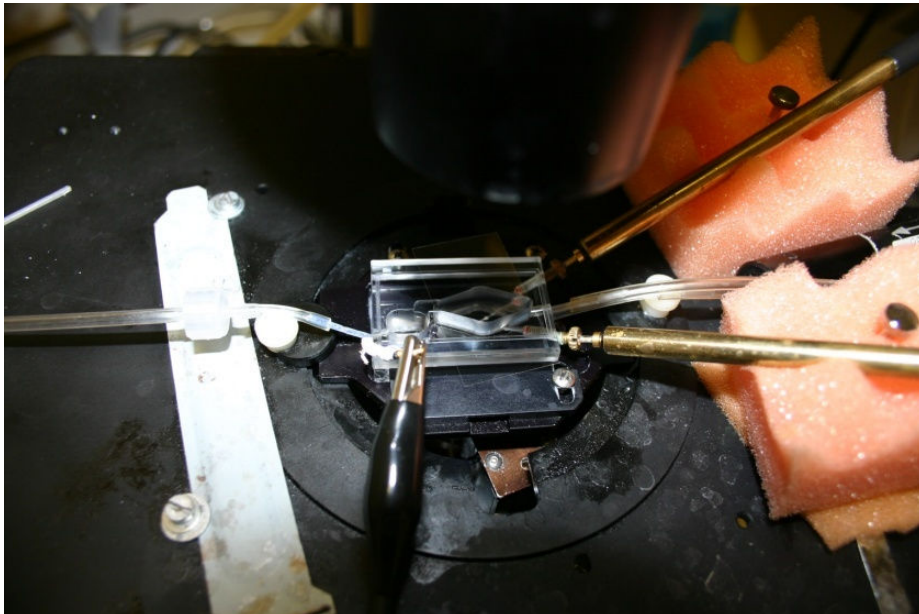


Figure 2-16: Electrode setup (diagram and photo)

Data analysis and statistics

Values from the null, sensor, and sensor-minus-null outputs were recorded every 2 seconds (0.5Hz) using the TracerDAQ software, and following the completion of the experiment the raw numbers were exported into an Excel spreadsheet where all further data manipulations were undertaken. The final raw data recorded by TracerDAQ is in the format of 1mV: 10nA. Data from the sensor-minus-null output was used as the actual ATP or glutamate reading, with the values from the null and sensor outputs obtained as a control, to see whether either the null or sensor electrodes failed at any point during the experiment (which would present as a sudden loss of signal or other unusual large fluctuations in signal intensity). To reduce the amount of noise in the recordings, the data points were binned at a 15:1 ratio: every 15 sequential data points collected at 0.5Hz were averaged to give one reading representative of the 30 second period in question. All data points were aligned so that the first time-point (the point at which OGD began) started at a concentration/current value of zero. Therefore any changes in the electrode signal represent changes in the overall glutamate or ATP concentrations (Δ ATP or Δ glutamate), rather than absolute concentrations of the analytes. Using the calibrations performed at the end of every experiment to make an equation for a line, the voltage readings were converted into approximate concentrations.

For statistics, the data from the individual experiments was entered into GraphPad Prism v5.0 (GraphPad Software Inc, La Jolla, USA). Experiments were repeated a minimum of three times to ensure accurate results. All values collected for a time point during a specific condition/experiment were averaged and a standard deviation (SDEV) was obtained. The SDEV was then used to calculate the standard error of the mean (SEM) for a given data point using the equation $SEM=SDEV/(\sqrt{n})$. The value for n (number of experiments) was obtained by multiplying the actual number of experiments by 15 as this was the number of original data points contained within each 30 second interval before the data was binned. Experiments were compared using unpaired t-tests with differences being significant when $p<0.05$.

Chapter 3:

ATP and glutamate release from cultured neurons and astrocytes

INTRODUCTION

Foreword

ATP and glutamate are known to accumulate extracellularly during ischaemia, suggesting their excessive release from CNS cells (Benveniste et al., 1984; Phillis et al., 1993; Melani et al., 2005). Both neurons and astrocytes have been implicated in mediating ischaemic glutamate and ATP release (Rossi et al., 2000; Bodin and Burnstock, 2001; Parkinson et al., 2002; Parkinson and Xiong, 2004; Fellin et al., 2006b; Montana et al., 2006; Watkins and Jane, 2006; Rossi et al., 2007; Malarkey and Parpura, 2008; Praetorius and Leipziger, 2009). However, a direct comparison of the dynamics of ATP and glutamate release during ischaemia has never been performed, and the relative contribution of astrocytes and neurons remains unclear.

In this chapter's introduction I will first review the many mechanisms of ATP and glutamate release from neurons and astrocytes, with a particular emphasis on those which have been shown to be active during ischaemic conditions. As many mechanisms are involved in both ATP and glutamate release, they have been organised into categories according to whether they are involved only in glutamate release, only in ATP release, or involved in both. My own results demonstrating ATP and glutamate release from cell cultures during OGD will then be presented and discussed.

Glutamate metabolism in the CNS

Glutamate transport and the glutamate-glutamine cycle

Glutamatergic signalling requires the close partnership of astrocytes and neurons. During normal physiological signalling, glutamate released during neurotransmission is rapidly taken up by a number of different Na⁺-dependant high affinity glutamate transporters (excitatory amino acid transporters, EAATs) located on the plasma membrane of most CNS cell types, although the majority of uptake occurs in astrocytes (Anderson and Swanson, 2000; Shigeri et al., 2004) (See **Figure 3-1**). Currently 5 different EAATs (EAAT1-5) have been characterised: EAAT1 and EAAT2 are the principle glial glutamate transporters, EAAT3 (also known as EAAC1) is a neuronal transporter, EAAT4 is found in cerebellar Purkinje cells and EAAT5 is expressed in the retina (Shigeri et al., 2004; Sheldon and Robinson, 2007). In rodents, EAAT1 and EAAT2 are referred to as GLAST (glutamate-aspartate transporter) and GLT-1 (glial-type glutamate transporter), respectively (Shigeri et al., 2004). Glutamate transporters are essential in maintaining the resting concentration of extracellular glutamate in the brain at <1 μ M, a process which has been estimated to consume a large fraction of the brain's energy turnover, as the concentration gradient of glutamate across the plasma membranes is several thousand-fold (Erecinska and Silver, 1990; Sibson et al., 1998; Danbolt, 2001; Rossi et al., 2007; Doyle et al., 2008). Na⁺-independent glutamate transport mechanisms also exist, but probably account for less than 5% of astrocyte glutamate uptake (Cho and Bannai, 1990; Anderson and Swanson, 2000; Sheldon and Robinson, 2007).

The glutamate taken up by astrocytes is then converted to glutamine via glutamine synthetase, an enzyme not expressed in neurons (Chen and Swanson, 2003). Glutamine is then shuttled back to adjacent neurons where it is converted to glutamate by the action of mitochondrial glutaminase, thereby completing what is known as the glutamate-glutamine cycle (Chen and Swanson, 2003). Glutamine released by astrocytes is the main precursor for glutamate synthesis in neurons, underlining the importance of astrocyte-neuronal interactions in glutamatergic signalling (Hertz, 2008).

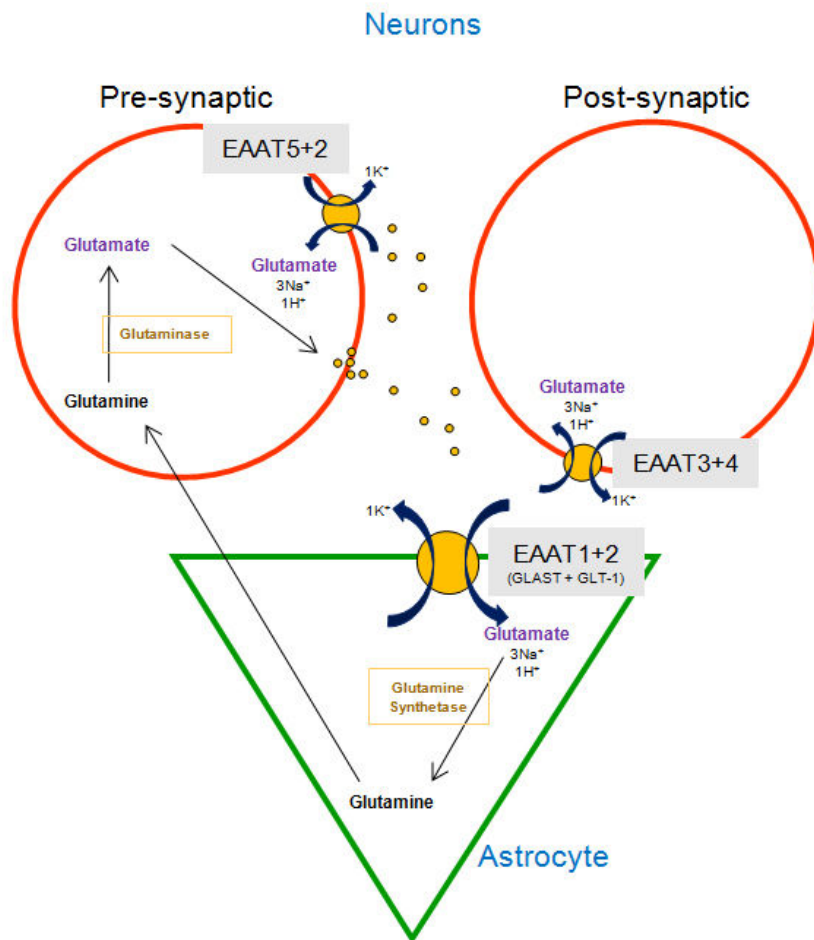


Figure 3-1: Glutamate metabolism and Na⁺-dependent transporters

Glutamate released during neurotransmission is taken up mainly by glial glutamate transporters (EAAT1+2) but also by neuronal transporters (EAAT2-5). In astrocytes glutamate is converted to glutamine by glutamine synthetase, which is not expressed by neurons. Glutamine is then shuttled to neurons where it is deaminated to glutamate by mitochondrial glutaminase.

Mechanisms involved only in glutamate release

Glutamate transporters

Glutamate release via reverse operation of glutamate transporters was first demonstrated by the measurement of glutamate induced currents when extracellular K⁺ levels were raised around glial cells (Szatkowski et al., 1990). Under normal physiological conditions, reversal of glutamate transport cannot occur (Longuemare and Swanson, 1995), but there is plenty of evidence that this happens both *in vivo* and *in vitro* during ischaemia and metabolic blockade (Longuemare and Swanson, 1995; Zeevalk et al., 1998; Li et al., 1999; Seki et al., 1999; Phillis et al., 2000; Rossi et al., 2000; Rao et al., 2001; Kosugi and Kawahara, 2006; Re et al., 2006; Dallas et al., 2007). However, there is still some debate as to which cell type contributes predominantly to this process (Rossi et al., 2007).

The likelihood of reverse transport occurring is dependent on ion shifts, loss of membrane potential and the intracellular glutamate concentration within the cell (Rossi et al., 2007). Although astrocytes express a much higher density of transporters, giving them a higher clearance capacity, neurons have much higher (4-6 fold) intracellular glutamate concentrations, leading to the prediction that neurons are more likely to release glutamate to excitotoxic levels during ischaemia (Ottersen et al., 1996; Rossi et al., 2000; Rossi et al., 2007). However, glutamate may accumulate in astrocytes during ischaemia since its conversion to glutamine by glutamine synthetase is ATP dependent (Rossi et al., 2007). Selectively knocking out GLT-1 in glia or inhibiting GLT-1 with dihydrokainate does not affect the profile of glutamate release during the first 10-15 minutes of severe ischaemia (Rossi et al., 2000; Hamann et al., 2002). Another *in vivo* study using GLT-1 knock-out mice found that in the early stages (5 minutes) of ischaemia, GLT-1 operates to continue clearing glutamate, with reversal and extracellular glutamate accumulation only occurring after 12.5 - 20 minutes of ischaemia (Mitani and Tanaka, 2003). This result concurred with earlier *in vivo* studies by the same group, which found that brain areas low in neuronal synapses (white matter) or where neurons were previously selectively removed did not show glutamate accumulation during the first 5 minutes of ischaemia compared with areas containing neurons (Mitani et al., 1994; Cui et al., 1999). Glutamate accumulation in areas containing mainly glia only occurred later on, after 5-20 minutes of ischaemia (Mitani et al., 1994; Cui et al., 1999). In co-cultures of retinal glial cells and neurons subjected to total metabolic blockade, extracellular glutamate accumulation occurred only after 15 minutes and was mediated by reversal of glial and not neuronal glutamate transporters (Zeevalk et al., 1998). Knocking out the neuronal glutamate transporter EAAC-1, significantly delayed the onset of glutamate-mediated anoxic depolarisation in hippocampal slices, while blocking glial transport as well sped up the time to anoxic depolarisation, suggesting that reversal of neuronal transporters is indeed involved in early glutamate accumulation while glial transporters were still operating normally to clear glutamate at the time (Gebhardt et al., 2002). During longer periods of ischaemia it is possible that GLT-1 reversal in astrocytes may contribute substantially to extracellular glutamate accumulation

in the ischaemic core, as Kimelberg et al. reported a 50% reduction in glutamate accumulation after 30 minutes *in vivo* when the process was blocked (Kimelberg et al., 2004). Overall, this data suggests that in intact preparations, the initial ischaemic glutamate release is by reversal of neuronal glutamate transporters, while astrocyte transporter reversal may contribute later on.

Another reason why glutamate may accumulate during ischaemia is that glutamate transporters are particularly sensitive to acidosis (Swanson et al., 1997). Acidosis or hypoxia+acidosis greatly reduces astrocyte glutamate clearance abilities, even when conditions are not such that reverse operation occurs (Swanson et al., 1997). Hypoxia itself may also downregulate glial EAAT (EAAT1 < EAAT2) expression, thereby reducing glutamate uptake (Dallas et al., 2007). Interestingly, reverse operation of glutamate transporters might actually contribute to astrocyte survival during ischaemia, as this helps to prevent Na⁺ accumulation which mediates cell swelling and astrocyte death (Namura et al., 2002; Kosugi and Kawahara, 2006). On the other hand, in the ischaemic penumbra, continued normal operation of astrocyte transporters is essential for continued glutamate clearance, which enhances cell survival by reducing glutamate excitotoxicity (Rao et al., 2001; Feustel et al., 2004).

Results using cell culture systems paint a different picture. In pure astrocyte cultures, 15 or 45 minutes of chemical ischaemia produced glutamate release which was not by reverse transport (Liu et al., 2006b). Another group demonstrated that glutamate release caused by reverse operation of GLT-1 in astroglial enriched cultures did not occur until after 70 minutes of OGD (Kosugi and Kawahara, 2006). In all studies which investigated glutamate transport reversal during ischaemia, preventing this process was never able to completely prevent ischaemic glutamate release, indicating the presence of other glutamate release mechanisms which are activated simultaneously. It is therefore apparent that reversal of glutamate transporters is one of the main (but not exclusive) sources of glutamate release during ischaemia, with both neurons and astrocytes

contributing to the process with different time courses and depending on the severity of the insult.

Cystine-glutamate antiporter (CGA)

The Na⁺-independent CGA, which imports cystine in exchange for glutamate, has been shown to operate in astrocytes, where cystine uptake is important for the production of the antioxidant glutathione (Malarkey and Parpura, 2008). Addition of cystine into the extracellular space in cerebellum produced currents attributed to glutamate release in Purkinje cells, while putative antagonists of the transporter reduced extracellular glutamate levels in the striatum by 60% under physiological conditions, demonstrating the ability of this transporter to release glutamate (Warr et al., 1999; Baker et al., 2003). However, the contributions of this mechanism to ischaemic glutamate release have not been investigated (Malarkey and Parpura, 2008). Furthermore, the EC₅₀ value for cystine evoked glutamate release via this transporter is much higher (250uM) than physiologically attainable extracellular cystine concentrations, suggesting only a negligible contribution of this transporter to glutamate release (Warr et al., 1999).

Mechanisms involved only in ATP release

ATP-binding cassette (ABC) proteins: multidrug resistance-associated protein (MRP), *p*-glycoprotein and the cystic fibrosis transmembrane regulator (CFTR)

MRP and *p*-glycoprotein (the protein product of the multidrug resistance gene (MDR)), two members of the ABC protein family, are ATP-dependent transmembrane glycoproteins which act as drug efflux pumps and may also mediate ATP release from cells (Darby et al., 2003). MRP and *p*-glycoprotein are both functionally expressed in astrocytes (Decleves et al., 2000; Darby et al., 2003). Darby et al. demonstrated that swelling-induced ATP release from astrocytes could be blocked by MRP transport inhibitors (Darby et al., 2003). However, OGD-induced ATP release in cultured astrocytes was not prevented by a MRP blocker (Liu et al., 2008).

A third member of the ABC protein family, the CFTR chloride channel, has been suggested to either directly conduct ATP or modulate a related ATP-conductive pore, although studies have provided conflicting results (discussed in Praetorius and Leipziger, 2009). In the CNS, glutamate-stimulated ATP release in spinal microglia was significantly reduced in CFTR knockout mice, while another study reported that AMPA (but not NMDA or kainate) induced ATP release from cultured astrocytes could be mediated at least partly by CFTR (Queiroz et al., 1999; Liu et al., 2006a). However, OGD-induced ATP efflux from mouse astrocyte cultures was not reduced when CFTR was pharmacologically blocked (Liu et al., 2008). Therefore, although members of the ABC protein family may mediate ATP release in CNS cell types, there is no evidence as of yet to suggest they contribute to ischaemic ATP release.

Mechanisms involved in both ATP and glutamate release

Volume-regulated anion channels (VRACs)

During ischaemia most cells experience swelling due to hypoosmotic conditions, a process which in itself can be damaging via a variety of mechanisms (Kimelberg, 2005). Astrocytes express a number of VRACs which open in response to cell swelling and are permeable to inorganic and small organic ions, including ATP and glutamate (Abdullaev et al., 2006; Rossi et al., 2007; Praetorius and Leipziger, 2009). Swelling-induced glutamate release, which could be blocked by various anion channel inhibitors, was first reported in astrocytes (Kimelberg et al., 1990). Direct glutamate release from cultured astrocytes via two different VRACs (maxi-anion channels > volume-sensitive outwardly rectifying Cl⁻ channels) during hypotonic and ischaemic stimuli has also been reported, with this study concluding that said mechanisms accounted for the majority of glutamate release (Liu et al., 2006b). Additionally, antagonists at VRACs reduced glutamate efflux during *in vivo* ischaemia, both in the ischaemic core and penumbra (Seki et al., 1999; Feustel et al., 2004; Kimelberg et al., 2004).

In hippocampal slices, VRACs did not contribute significantly to ischaemic glutamate release (Rossi et al., 2000). Furthermore, OGD-induced ATP release from cultured astrocytes could not be prevented by blocking VRACs (Liu et al., 2008). However, there is evidence to suggest that the antagonists used to block VRACs may also have other non-specific effects, such as scavenging for reactive oxygen species (ROS), which may complicate the interpretation of the effects of these compounds (Jentsch et al., 2002; Rossi et al., 2007). Additionally, although it seems intuitive that astrocytes are responsible for most VRAC mediated glutamate or ATP release because they swell more during ischaemia, there is no way to exclude a neuronal contribution to this process (Seki et al., 1999). The development of more specific antagonists or knock-out animals would improve our understanding of their contribution to ischaemic glutamate efflux (Rossi et al., 2007).

Connexin/Pannexin hemichannels

Gap junction channels are pores connecting the cytoplasm of two adjacent cells, and are formed by the joining of two connexons ('hemichannels'), each composed of a hexamer of the protein connexin, of which there are many isoforms (Malarkey and Parpura, 2008). Gap junctions allow the diffusion between cells of molecules up to 1kDa in size (Malarkey and Parpura, 2008). Single unpaired connexons are able to act as functional hemichannels which open up to the extracellular space, allowing for the passage/diffusion of large molecules, such as ATP or glutamate, out of the cells (Spray et al., 2006; Malarkey and Parpura, 2008). Connexin 43 (Cx43) is particularly prevalent in astrocytes, and these channels are permeable to ATP and glutamate (Stout et al., 2002; Ye et al., 2003; Kang et al., 2008). Cx36 forms a neuron-specific channel in the brain that is able to mediate ATP release (Schock et al., 2008). Pannexins are a family of proteins which form conductive channels, including unpaired 'pannexons', with very similar properties as connexons (Malarkey and Parpura, 2008). They are sensitive to many of the same compounds used to block connexin hemichannels, suggesting that many properties attributed to connexons may actually be mediated by pannexons (Malarkey and Parpura, 2008). ATP release from hemichannels was observed in cultured astrocytes and in glioma cells transfected with Cx43 (Stout et al., 2002). Astrocytes from Cx43 knock-out mice show much reduced glutamate

release following stimulation with low divalent solution (Spray et al., 2006). However, using spinal cord astrocytes from Cx43 null mice, another group found no evidence that these mediated ATP release (Suadicani et al., 2006).

Cx43 hemichannels have been shown to open during metabolic inhibition, suggesting that this may occur during ischaemia (Contreras et al., 2002; Contreras et al., 2004). Also, hypoxic/ischaemic insults dephosphorylate Cx43 hemichannels, a process which favours increased channel conductance as well as junctional 'uncoupling' with subsequent decreased gap junctional intercellular communication but increased hemichannel formation (Cotrina et al., 1998; Li et al., 1998b; Li and Nagy, 2000; Lin et al., 2008b). Blocking gap junctions reduced infarct volumes after *in vivo* ischaemia, an effect proposed to have been mediated by a reduction or inhibition of waves of spreading depression (Rawanduzy et al., 1997). However, connexin or pannexin hemichannel opening did not contribute to OGD induced ATP release from cultured astrocytes, although they did contribute to ATP release after reperfusion (Liu et al., 2008; Iwabuchi and Kawahara, 2009b). Additionally, Cx43 heterozygous knockout mice had much increased infarct volume and severe penumbral apoptosis following permanent middle cerebral artery occlusion (Nakase et al., 2003). Authors speculated that the latter result may be due to protective effects of gap junctions in allowing the transfer/distribution of toxic molecules away from compromised cells while substances which aid astrocyte survival are passed in the opposite direction. Pharmacological tools to discern hemichannel-mediated processes from those mediated by other similar channel types are still elusive, hampering further studies (Spray et al., 2006). For example, five different compounds which have classically been used to block gap junctions/hemichannels are all antagonists of P2X₇ receptors (Suadicani et al., 2006). It is also important to mention that hemichannels can only open when low divalent cations solutions are used, so it is unlikely that they would be able to open under the conditions used in my experiments (solutions contained 2mM Ca²⁺ + 2mM Mg²⁺), although this could theoretically be offset by the effects of OGD induced dephosphorylation mentioned above (Liu et al., 2006b).

P2X receptors

The P2X₇ receptor is known to form a non-selective pore which allows the passage of higher molecular weight molecules (up to ~900Da) following prolonged stimulation with high agonist concentrations (North, 2002). P2X₂ and P2X₄ receptors have also been shown to form large pores, although their contributions to transmitter release has been researched much less extensively (Virginio et al., 1999; Jarvis and Khakh, 2009). Expression of all three receptor types has been demonstrated in astrocytes and neurons (Kukley et al., 2001; Lundy et al., 2002; Burnstock and Knight, 2004; Rodrigues et al., 2005; Bianco et al., 2009). Exogenous ATP-induced P2X₇ receptor mediated glutamate release from cultured astrocytes was first reported by Duan et al. (Duan et al., 2003). The more potent P2X receptor agonist, BzATP, also induced glutamate release in hippocampal slices, although it is less clear from this study what cell types are contributing (Fellin et al., 2006a). P2X receptor mediated ATP release was first demonstrated in HEK293 cells expressing membrane-bound luciferase and P2X₇ receptors, with BzATP or ATP application causing the release of large amounts of ATP (100-200uM) from these cells (Pellegatti et al., 2005). Cultured spinal cord astrocytes release ATP directly through P2X₇ receptors, as demonstrated by studies using P2X₇ null mice (Suadicani et al., 2006). ATP release via P2X₇ receptors has also been documented indirectly in white matter astrocytes, where P2X₇ knockouts and a P2X₇ antagonist reduced glutamate mediated increases in ATP release (Hamilton et al., 2008).

There is evidence that the pore-forming properties of P2X receptors may actually be due to a functional link between these receptors and pannexin-1 (Pelegri and Surprenant, 2009). Pannexin-1 physically associates with P2X₇ receptors, and inhibition of pannexin-1 partially attenuates P2X₇ receptor-induced dye uptake and interleukin-1 β release without affecting its ion-channel activation properties (Pelegri and Surprenant, 2006, 2009). This may also explain why P2X₇ receptor antagonists often have variable effects on either ionic flux or pore formation components mediated by P2X₇ receptor activation (Hibell et al., 2000). In P2X₂ receptors this coupling has been shown not to occur; rather, pore formation was due to slow conformational changes in the receptor complex itself

(Chaumont and Khakh, 2008). Yan and colleagues also found that P2X₇ receptor mediated passage of large organic cations was controlled by the receptor pore itself dilating, rather than pannexin channels (Yan et al., 2008).

Since levels of extracellular ATP are raised for a prolonged period of time during ischaemia, P2X receptor pore dilation with consequent release of further ATP and glutamate from either neurons or astrocytes is a theoretical possibility (Le Feuvre et al., 2002; Duan and Neary, 2006; Rossi et al., 2007). To my knowledge, however, there is no evidence in the literature that ATP and/or glutamate are released via this mechanism during ischaemia. A couple of studies have found no reduction in either ATP or glutamate release from cultured astrocytes during ischaemic insults when P2X₇ receptors were blocked (Contreras et al., 2002; Liu et al., 2008).

Exocytosis

Exocytosis is the principal pathway by which both ATP and glutamate are released from nerve terminals, occurring mainly during synaptic transmission (Bodin and Burnstock, 2001; North and Verkhratsky, 2006; Pankratov et al., 2006; Watkins and Jane, 2006; Pankratov et al., 2007). Neuronal Ca²⁺-dependent glutamate release was established in the early 1970s, while ATP release from synaptosomes was first reported in 1977 (White, 1977; Watkins and Jane, 2006). Evidence that exocytotic ATP and glutamate release occurs in astrocytes has been accumulating more recently (Coco et al., 2003; Pascual et al., 2005; Fields and Burnstock, 2006; Montana et al., 2006; Bowser and Khakh, 2007; Jaiswal et al., 2007; Malarkey and Parpura, 2008). Astrocytes possess the secretory machinery for regulated exocytosis, including the SNARE (soluble N-ethyl maleimide-sensitive fusion protein attachment protein receptor) complex and the various proteins required for vesicular glutamate accumulation (Montana et al., 2006; Malarkey and Parpura, 2008). Dense core granules containing glutamate and ATP have been identified in astrocyte electron microscopy studies (Coco et al., 2003; Jourdain et al., 2007). Characteristic quantal release of both ATP and glutamate has been demonstrated in astrocytes (Pasti et al., 2001; Pangrsic et al., 2007). Exocytotic glutamate and ATP release

in astrocytes can be blocked by interfering with molecular players of exocytosis or preventing intracellular Ca^{2+} elevation, while it can be stimulated by raising intracellular Ca^{2+} (Innocenti et al., 2000; Coco et al., 2003; Montana et al., 2006; Praetorius and Leipziger, 2009).

There is evidence that vesicular transmitter release is the earliest mechanism of glutamate or ATP release during ischaemia. Hypoxia produced a profound increase in vesicular transmitter release in the neocortex within 15-30 seconds of onset of hypoxia (Fleidervish et al., 2001). Interestingly, this was not sensitive to tetrodotoxin (TTX) or Ca^{2+} removal, suggesting direct vesicular release stimulated by hypoxia (Fleidervish et al., 2001). Vesicular-like glutamate release may also occur later on during ischaemia. In human cerebro-cortical slices, OGD induced significant glutamate efflux after 18 minutes which was partially inhibited by either TTX (65% reduction) or Ca^{2+} removal (50% reduction) (Marcoli et al., 2004b). Gebhardt and colleagues also found a component of vesicular glutamate release from hippocampal slices during hypoxia (Gebhardt et al., 2002). However, a number of studies have found that exocytosis did not contribute significantly to glutamate or ATP accumulation during ischaemia, both in slices and astrocyte cultures (Rossi et al., 2000; Liu et al., 2006b; Sperlagh et al., 2007; Liu et al., 2008).

A recent paper provided the first evidence that regulated ATP release from astrocytes, stimulated by either ATP, glutamate or KCN (chemical ischaemia) occurs via Ca^{2+} -dependent lysosome exocytosis (Zhang et al., 2007). First, the authors demonstrated that lysosomes contained abundant ATP (while incidentally they could not find clear evidence that these contained significant quantities of glutamate). Lysosomes were selectively fluorescently labelled with FM dyes, and these dyes would dissociate from the lysosome membrane following the brief formation of a transient fusion pore ('kiss-and-run') or full fusion of the lysosome with the plasma membrane. Glutamate and ATP application produced ATP release via 'kiss-and-run' fusion, whereas chemical ischaemia induced both 'kiss-and-run' and full fusion lysosomal exocytosis, as well as the recruitment of new lysosomes from deep cytoplasmic regions. KCN produced a quick (within 4

minutes) and significant accumulation of extracellular ATP and lysosomal enzymes in both cell cultures and acute hippocampal slices that could be largely prevented by pharmacological attenuation of lysosomal exocytosis, suggesting that this mechanism of ATP release is responsible for at least the early component of rises in extracellular ATP following ischaemia. This rise in extracellular ATP during ischaemia preceded ischaemia-induced cell lysis, as determined by concomitant monitoring of lactate dehydrogenase (LDH) levels in these preparations, ruling out the possibility that ATP release from dying cells instead of lysosomal exocytosis may have been responsible for the ATP release in the early phase of the insult.

This data suggests that exocytotic release of glutamate and ATP from neurons is likely to occur during ischaemia, although it may not contribute a quantitatively significant proportion of the total which is released. Astrocytes release significant quantities of ATP by lysosomal exocytosis during ischaemia, while the contribution of exocytotic glutamate release from these cells is not clear.

Loss of cell membrane integrity

Due to the large ATP and glutamate concentration gradient between the intra and extracellular compartments, any situation where cell membrane integrity is compromised will lead to the release of any residual ATP or glutamate still present within the affected cells at the time. During severe ischaemia, necrotic cell death occurs within minutes, suggesting that this mechanism of release must be considered. This may also be relevant in the context of cell process loss independent of complete cellular disintegration (clasmotodendrosis), as has been shown to occur in astrocytes *in situ* during ischaemic insults (Shannon et al., 2007; Salter and Fern, 2008). Additionally, glutamine released by dying astrocytes can be converted to glutamate by glutaminase which has been released by dying neurons, further contributing to glutamate accumulation (Hertz, 2008).

Summary

The mechanisms of ATP and glutamate release from astrocytes and neurons are summarised in **Figure 3-2**, where those which have been shown to directly contribute to ischaemia induced efflux are highlighted in pink boxes. During ischaemia, glutamate release seems to occur initially by exocytosis from intact neurons and reversal of neuronal glutamate transporters, followed by reversal of glial glutamate transporters, with an additional component possibly mediated via release from VRACs and hemichannels in astrocytes (**Figure 3-2: B1 + B2**). Specific mechanisms of ATP release during ischaemia have only been demonstrated in astrocytes (**Figure 3-2: A2**), with exocytosis and VRACs having been implicated thus far. Further release of both substances and/or formation of glutamate during ischaemia following the loss of cell membrane integrity may also contribute.

Objectives

At the time when these experiments were performed, there were no published investigations documenting direct ischaemic ATP release from primary neuron and primary astrocyte cultures. In preparations containing both neurons and astrocytes, the cellular origin of ATP and glutamate, as well as the quantitative contributions of astrocytes and neurons to their release during ischaemia are not completely resolved. Furthermore, a novel comparison of the dynamics of ATP and glutamate release may provide valuable mechanistic insights.

To investigate this, ATP and glutamate release from cultured astrocytes and neurons was measured using microelectrode biosensors. Being 0.5mm thick, they are small enough to be placed directly above the surface of the cultured cells and within an unstirred layer. This would theoretically allow for the detection of ATP before it is enzymatically degraded. The microelectrodes have the further benefit of allowing a detailed analysis and comparison of the time-course, dynamics and quantity of ATP and glutamate release. Employing primary cell cultures is advantageous as it permits the use of astrocyte cultures

or neuronal cultures in the same conditions as the co-culture. This allowed us to try and clarify which cell-types were contributing to the release of ATP and/or glutamate.

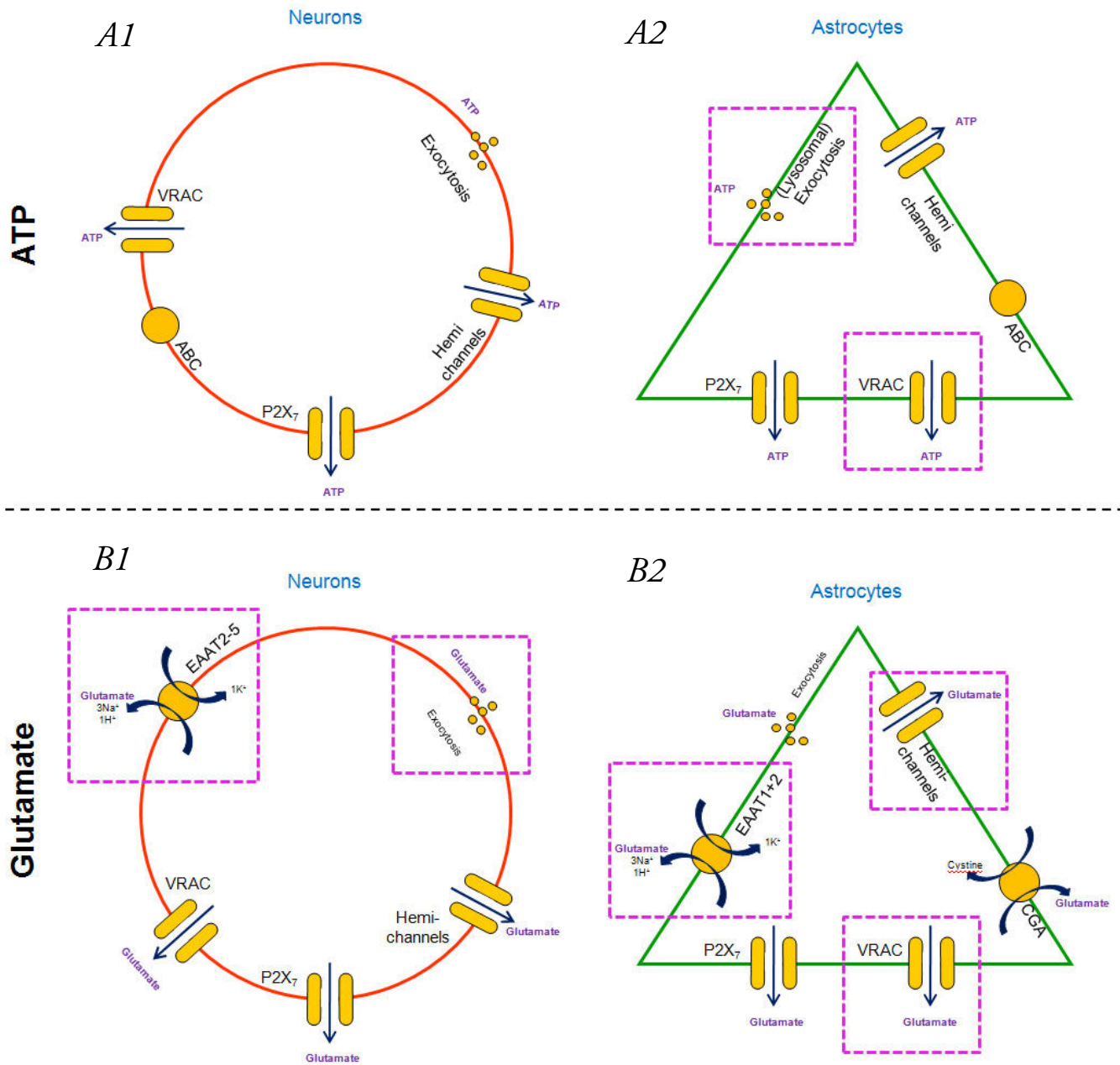


Figure 3-2: Mechanisms of ATP and glutamate release from astrocytes and neurons

Figure depicting potential pathways of ATP and glutamate release from astrocytes (*A2*, *B2*) and neurons (*A1*, *B1*). Mechanisms which have been directly shown to contribute to ischaemic ATP or glutamate accumulation are enclosed by pink boxes. (see text for references)

RESULTS

Data post-processing of ATP and glutamate electrode recordings

As described previously in the materials and methods chapter (see pages 60-65), the potentiostat to which the electrodes are connected outputs a sensor, null, and sensor-null signal to the computer, but these signals need to be further processed to give the final recordings, a procedure which is described in full in **Figures 3-3** and **3-4**. **Figure 3-3: A1 + B1** shows unaltered example recordings from an OGD (**A1**) and a control (**B1**) experiment using the ATP biosensor microelectrodes in co-cultures of astrocytes and neurons. In both experiments there was a certain amount of noise of variable amplitude, as well as an overall shift of the current to a value up to 20nA on both the sensor and null electrode signals. Additionally, the recording from the OGD experiment (**A1**) demonstrates that when OGD was started the overall current shift was reduced. Finally, at the end of experiments flow through the perfusion system was halted, the electrodes were retracted slightly from the cells and an end calibration was performed. Stopping flow through the perfusion system abolished most of the noise and current shift, suggesting that both of these phenomena were somehow caused by the perfusion system, either via fluid flow or component hardware within. An experiment was designed to identify the source of the shift and noise: when the solution was routed directly from the bottle to the chamber using a single length of tubing, bypassing the entire system (see **Figure 2-8** in methods and materials) of tubing/switches/flow metres/flow-through feedback heater, the current shift and noise disappeared. Unfortunately these experiments necessitated the use of all these components, so the noise and shift needed to be eliminated by post-processing of the electrode data.

To remove the noise from the recordings without changing the overall quantitative results, every 15 sequential 0.5Hz data points were averaged to produce one value representative of each 30 second period (**Figure 3-3: A2 + B2**). To compensate for the current shift caused by the perfusion system all of the sensor-null data was then shifted by the value obtained by averaging the current recorded during the first ten minutes (**Figure**

3-3: A3 + B3); time-points of all OGD experiments had previously been aligned so that OGD was always started after this time point. Finally, the current values were converted to actual ATP or glutamate concentrations using the end-calibration. **Figure 3-4** shows example traces of ATP (**A1**) and glutamate (**A2**) recordings, including the initial pot calibration and the final end calibration. A linear regression of the end calibration was performed (**A2 + B2**), and the current values were multiplied by 1/slope, producing the final recordings in the form of $\Delta\mu\text{M}$ ATP (**A3**) or $\Delta\mu\text{M}$ glutamate (**B3**).

There was always a reduction in the sensitivity of the sensors over time, represented by the reduction in the slope of the linear regression when comparing the initial pot calibration with the final end-calibrations (**Figure 3-4: A2 + B2**). For this reason using the end-calibration will tend to over-estimate the concentration of the analyte. However, the current produced by the electrode is also proportional to the surface area of the electrode which is being stimulated, and there is no way in these experiments to ascertain and compensate for this variable. For example, during both the pot and end-calibrations the full surface area of the sensor was exposed to the full concentrations of the analyte, but during the experiments it is likely that only a relatively low proportion of the underside of the sensor's surface area near the cells was being activated, whilst the top surface facing away from the cells was only ever going to be in contact with diluted levels of either ATP or glutamate. It is therefore important to stress that the final values of $\Delta\mu\text{M}$ ATP or glutamate are approximations at best. All example recordings shown in this chapter have undergone all of the above manipulations.

Figure 3-3:

Example recordings and data workflow, co-culture ATP release

This figure demonstrates what the raw data collected using the biosensor microelectrodes looked like and how the data was processed to arrive at the final ATP recordings.

A1 + B1: 0.5Hz recordings of sensor and null electrodes and sensor-null output
In both experiments there is a certain amount of noise of variable amplitude on both electrode signals, as well as an overall shift of the current to a value up to 20nA. Additionally, the recording from the OGD experiment (***A1***) shows that when OGD was induced the overall current shift changed. Finally, at the end of experiments flow through the perfusion system was halted, the electrodes were retracted slightly from the cells and an end calibration was performed. Stopping flow through the perfusion system abolished both the noise and current shift, suggesting that both of these phenomena were somehow mediated by the perfusion system, either via fluid flow or component hardware within.

A2 + B2: 15:1 binning of 0.5Hz data to reduce noise
The 15 consecutive data points collected for every 30 second time period were averaged to produce one value representative of those 30 seconds. This manipulation successfully removed most of the noise from the recording without changing the overall quantitative results of the data.

A3 + B3: Baseline correction and calibration of sensor – null signal to give $\Delta\mu\text{M ATP}$
To compensate for the current shift caused by the perfusion system data was shifted on the x-axis by the average value recorded during the first 10 minutes of the experiment, which was the point after which OGD was started. Then the signal at each time-point was multiplied by 1/slope of the line created by the end-calibration to convert sensor currents to approximate $\Delta\mu\text{M ATP}$.

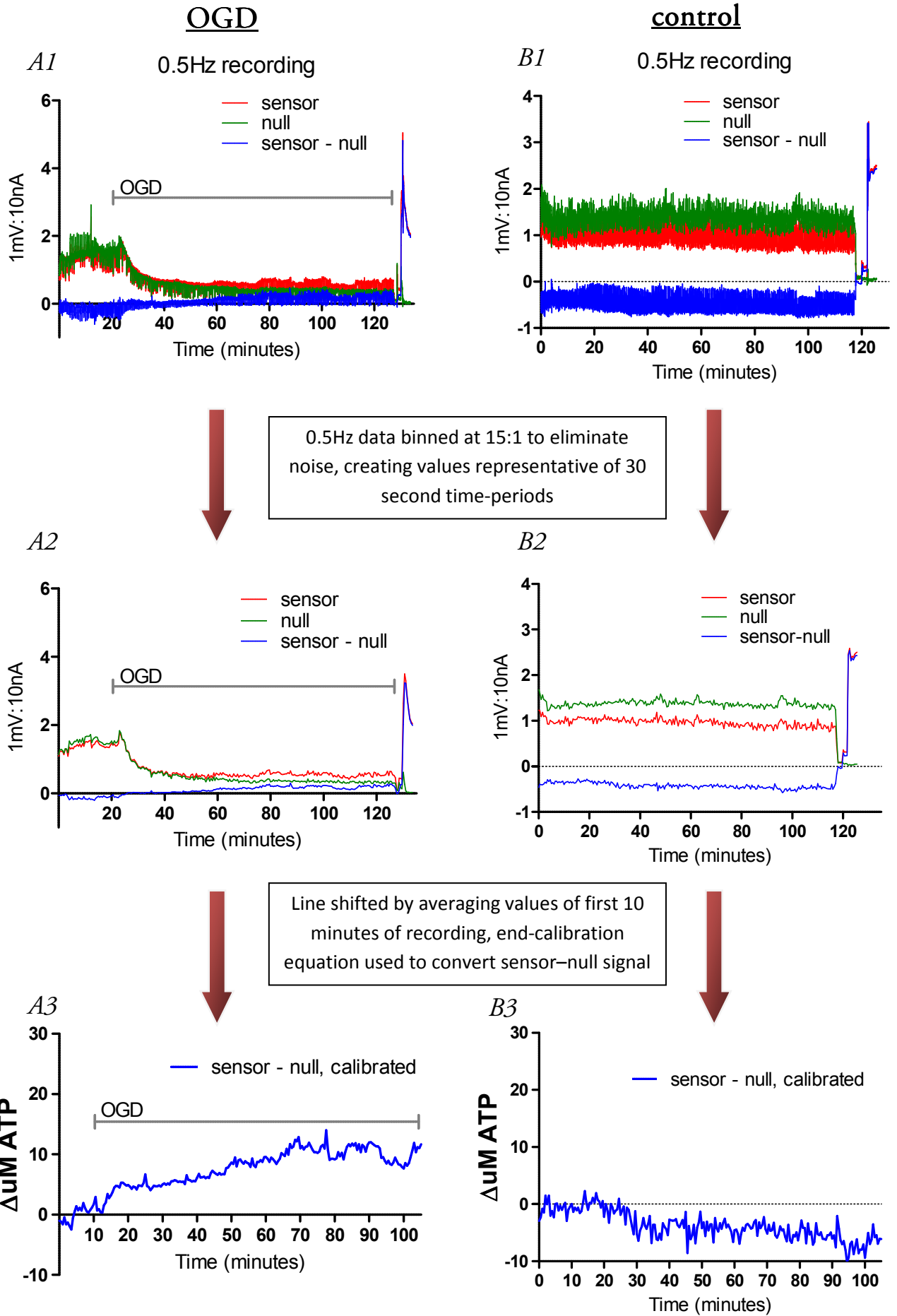


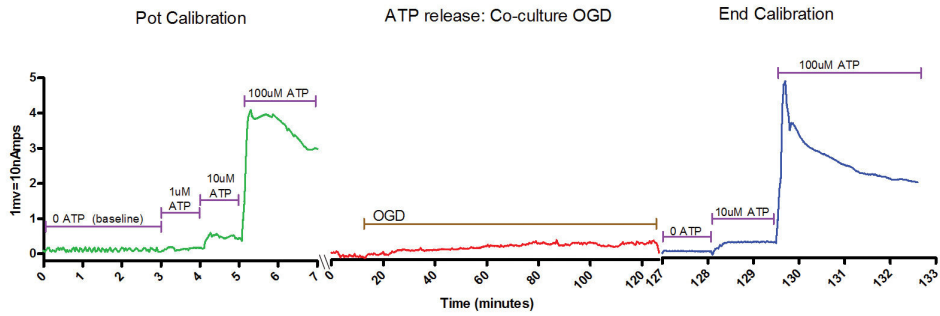
Figure 3-4: Example traces of ATP and glutamate electrode recordings, including calibrations

A1 + B1: Example traces of ATP (A1) and glutamate (A2) recordings, showing the initial pot calibrations, followed by the recording during OGD and finishing with the end calibration which was performed in the perfusion chamber.

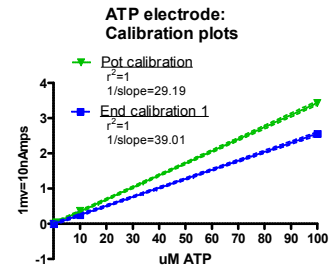
A2 + B2: Linear regressions of the pot and end calibrations recorded during the experiment. The biosensor electrodes always diminished their sensitivity over time, which can be seen here as a reduction in the slope of the linear regression of the end calibration relative to the initial pot calibration in each experiment.

A3 + B3: Final recordings in the form of $\Delta\mu\text{M}$ ATP and $\Delta\mu\text{M}$ glutamate. The current data was converted to ATP or glutamate concentrations by multiplying them by $1/\text{slope}$ of the end calibrations.

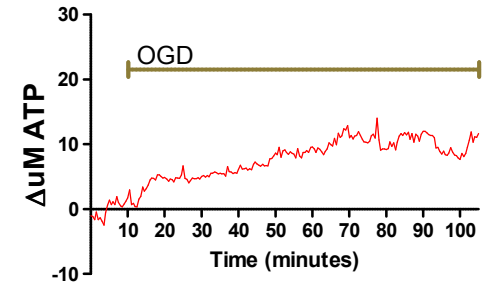
A1



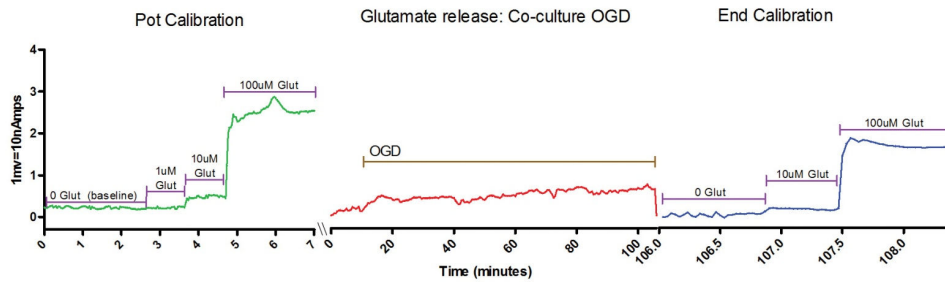
A2



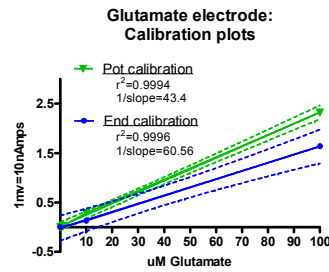
A3



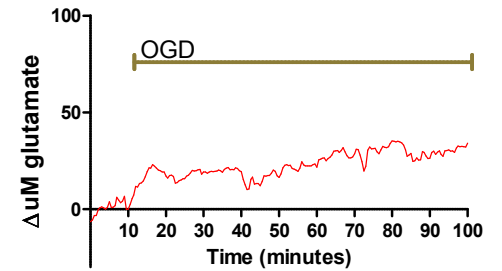
B1



B2



B3



Cell cultures of neurons, astrocytes or co-cultures of the two cell-types were subjected to either 15-30 minutes of perfusion with aCSF before induction of OGD for 90 minutes (OGD) or 110 minutes of perfusion with aCSF (control) while measuring either ATP or glutamate release. Recordings from all the individual experiments for each condition are depicted to show the range of results. For each experiment the overall mean \pm SEM change of ATP or glutamate concentration over time ($\Delta\mu\text{M}$ ATP or glutamate) is presented graphically, showing the mean level of analyte at 30 second intervals. The standard errors for these figures were produced by multiplying the number of experiments (n) by 15 (since each 30 second point was produced by averaging 15 data points). This meant these values could not be used for statistical analyses. For correct statistical comparisons between experiments, the mean ΔATP or $\Delta\text{glutamate}$ values measured during each 10 minute interval over the whole 90 minute period for each condition were calculated and averaged, and are presented as mean \pm SEM. These were then compared using one-tailed unpaired t-tests. An unpaired t-test assumes equal variances between groups, so if the F-test revealed significantly different variances ($p < 0.05$) Welch's correction was additionally used (this was only necessary in a few cases).

ATP and glutamate release from co-cultured astrocytes and neurons

OGD significantly increased the amount of ATP release from co-cultured astrocytes and neurons compared with control conditions (**Figure 3-5**). 5 out of the 7 OGD experiments showed large rises in ATP levels during the 90 minutes of OGD, and in 4 of them this was sustained through most of the experiment (**Figure 3-5: B**). During control conditions (**Figure 3-5: A**, n:5) there were also some rises in ATP in most of the experiments, but these were not as substantial or sustained as those seen during OGD. When all of the recordings were averaged for each time point, the amount of ATP released during OGD was first raised compared to control after 11 minutes, and this was maintained throughout most of the 90 minutes of OGD (**Figure 3-5: C**). A maximum Δ ATP during OGD was reached at 86.5 minutes ($10.47 \pm 0.8\mu\text{M ATP}$). Comparing the effects of OGD vs. control during each of the 10 minute intervals revealed significant increases in ATP release in the 60-70 ($7.41 \pm 2.9\mu\text{M}$ vs. $-0.79 \pm 1.29\mu\text{M}$, $p < 0.05$), 70-80 (8.08 ± 3.1 vs. $-2.05 \pm 3.5\mu\text{M}$, $p < 0.05$), 80-90 ($8.91 \pm 3.05\mu\text{M}$ vs. $-3.38 \pm 2.97\mu\text{M}$, $p < 0.01$) and 90-100 (6.59 ± 3.84 vs. $-4.1 \pm 4.01\mu\text{M}$, $p < 0.05$) minute intervals. (**Figure 3-5: D**).

Glutamate release from the co-culture was also significantly increased during OGD compared with control (**Figure 3-6**). In 9 out of the 10 OGD experiments increases in extracellular glutamate levels were detected, with 3 of them showing particularly large rises (**Figure 3-6: B**). During control conditions none of the 4 experiments showed any comparably large or sustained glutamate rises (**Figure 3-6: A**). As demonstrated by **Figure 3-6: C**, the average Δ uM glutamate was increased compared to control after 12 minutes and throughout the rest of the 90 minutes of OGD, reaching a maximum Δ glutamate level of $31.54 \pm 3.3\mu\text{M}$ at 95.5 minutes. When comparing 10 minute intervals (**Figure 3-6: D**), there were significant increases ($p < 0.05$) in glutamate release during OGD vs. control in the 20-30 ($17.36 \pm 7.4\mu\text{M}$ vs. $-0.15 \pm 2.53\mu\text{M}$), 30-40 ($18.74 \pm 8.17\mu\text{M}$ vs. $-2.18 \pm 2.23\mu\text{M}$), 40-50 (20.35 ± 9.48 vs. $0.04 \pm 1.52\mu\text{M}$), 80-90 (26.63 ± 12.04 vs. $1.1 \pm 2.58\mu\text{M}$) and 90-100 (29.1 ± 13.2 vs. $0.99 \pm 2.52\mu\text{M}$) minute intervals (**Figure 3-6: D**).

Welch's correction was used with these t-tests as variances between controls and OGD were significantly different.

P2 receptors have been implicated in modulating glutamate release from neural cells. To ascertain whether P2 receptor activation might be involved in OGD-mediated glutamate release from co-cultures, 10 μ M PPADS was added to all perfusing solutions. 10 μ M PPADS did not reduce or change the dynamics of glutamate release from the co-culture during OGD (**Figure 3-7**). All 5 experiments with PPADS showed significant increases in glutamate levels following the induction of OGD (**Figure 3-7: B**), and the overall profile of glutamate release over time (**Figure 3-7: C**) was not significantly different from that seen in the absence of PPADS. Similar results were observed when analysing 10 minute intervals, with no significant differences detected (**Figure 3-7: D**). This suggests that P2 receptor activation is not involved in glutamate release from these cells during OGD.

Overall, these results show that significant amounts of ATP and glutamate are released by co-cultured astrocytes and neurons during OGD. Glutamate release reached statistical significance earlier than ATP release. Additionally, glutamate release was not sensitive to PPADS, suggesting P2 receptors are not involved in its release during OGD. The next step was to identify which cell types were releasing ATP and glutamate during OGD, so similar recordings were performed using the astrocyte and neuronal cultures.

Figure 3-5:

ATP release from co-cultured astrocytes and neurons during OGD

A: Control experiments, all recordings (n:5)

15:1 binned sensor-null recordings of all control experiments that were performed. There were still some rises in ATP in some experiments, but these were not as substantial or sustained as those seen during OGD.

B: OGD experiments, all recordings (n:7)

15:1 binned sensor-null recordings of all OGD experiments that were performed. The majority of experiments showed a rise in ATP following the induction of OGD after 10 minutes.

C: Average Δ uM ATP, OGD vs control

The amount of ATP released from the co-culture during OGD (n:7) was increased compared to control (n:5) for the first time at 11 minutes and maintaining this throughout most of the 100 minutes of the experiment. A maximum rise in the ATP level during OGD was reached at 86.5 minutes ($10.47 \pm 0.8\mu\text{M ATP}$).

D: The mean Δ ATP of every 10 minute interval over the 90 minutes:

There were significant increases in ATP release during OGD compared to controls in all four 10-minute intervals between 60 and 100 minutes.

*: $p < 0.05$

** : $p < 0.01$

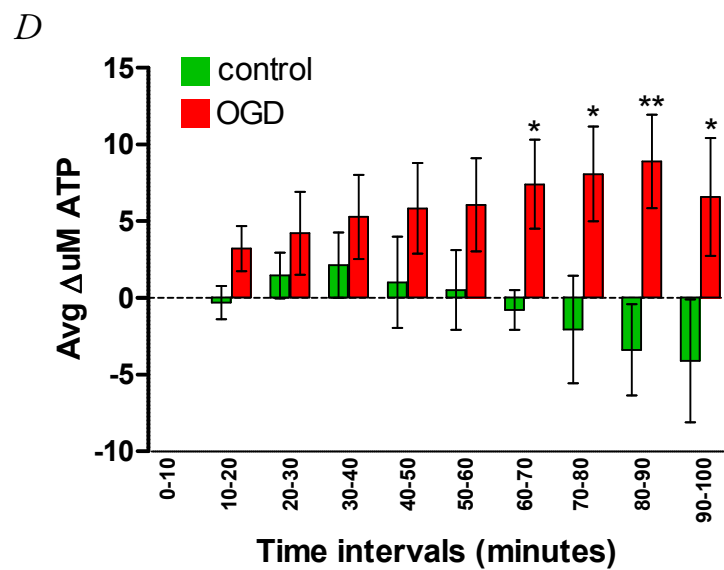
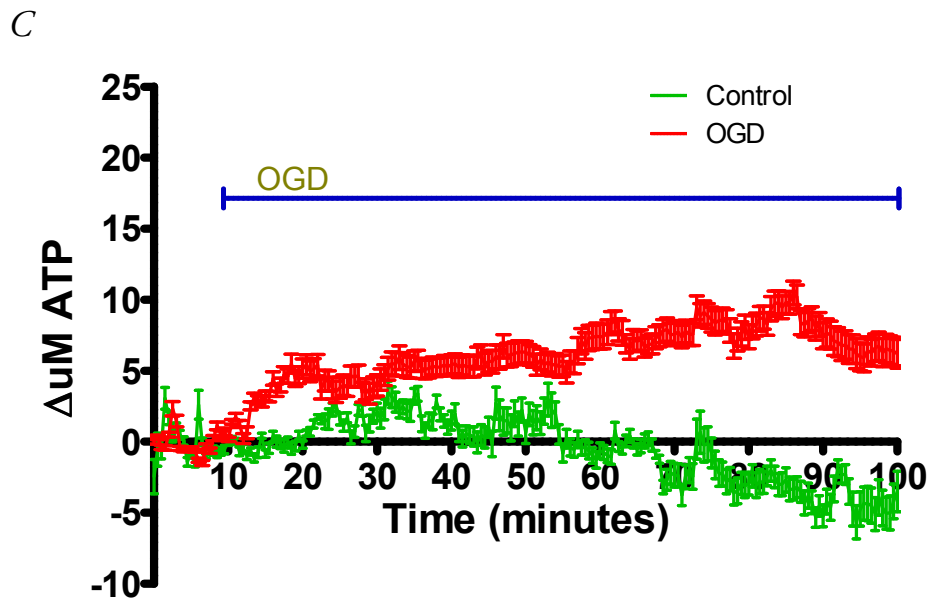
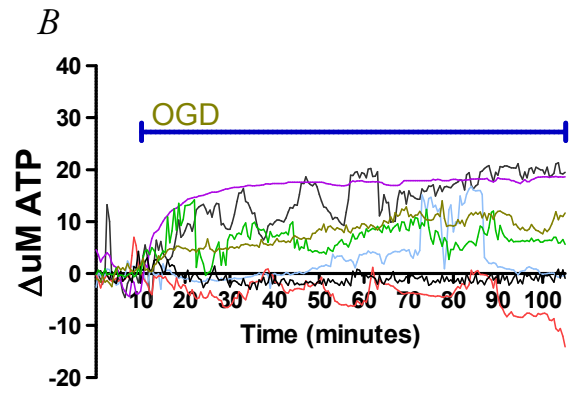
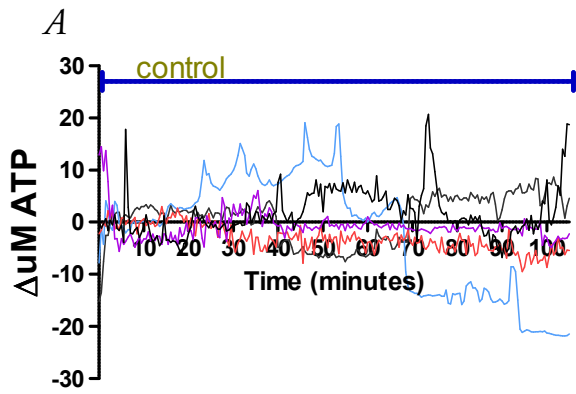


Figure 3-6:

Glutamate release from co-cultured astrocytes and neurons during OGD

A: Control experiments, all recordings (n:4)

15:1 binned sensor-null recordings of all control experiments that were performed. There were rises in glutamate in some experiments, but these were not as substantial or sustained as those seen during OGD.

B: OGD experiments, all recordings (n:10)

15:1 binned sensor-null recordings of all OGD experiments that were performed. Most experiments showed a rise in glutamate following the induction of OGD 10 minutes into the recording.

C: Average $\Delta\mu\text{M}$ glutamate, OGD vs control

The amount of glutamate released from the co-culture during OGD (n:10) was increased compared to control (n:4) for the first time at 12 minutes and maintained this throughout. A maximum rise in the glutamate level during OGD was reached at 95.5 minutes ($31.54 \pm 3.3\mu\text{M}$ glutamate).

D: The mean Δ glutamate during every 10 minute interval of the 90 minutes:

There were statistically significant ($p < 0.05$) differences in glutamate release between OGD and control conditions during the 10 minute intervals between 20-50 and 80-100 minutes.

*: $p < 0.05$

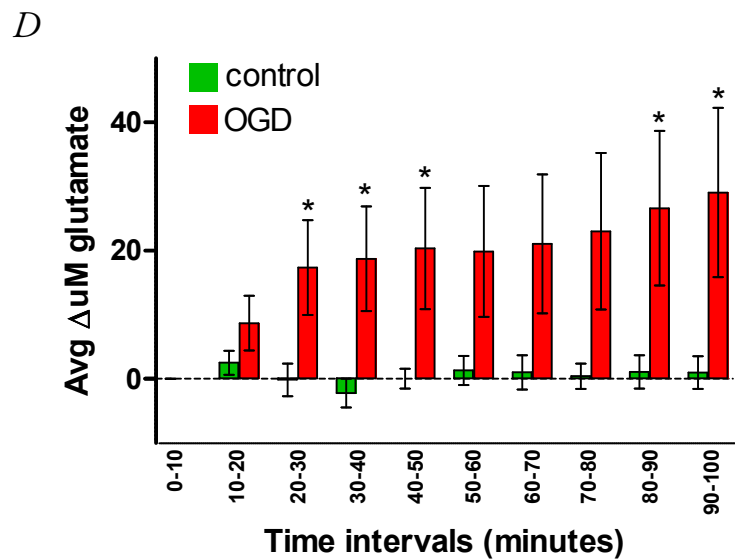
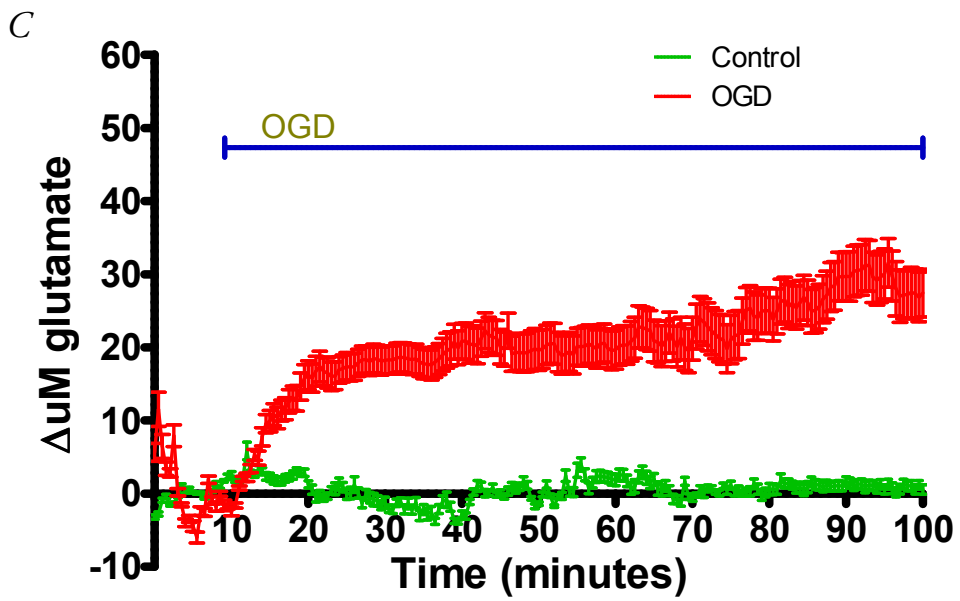
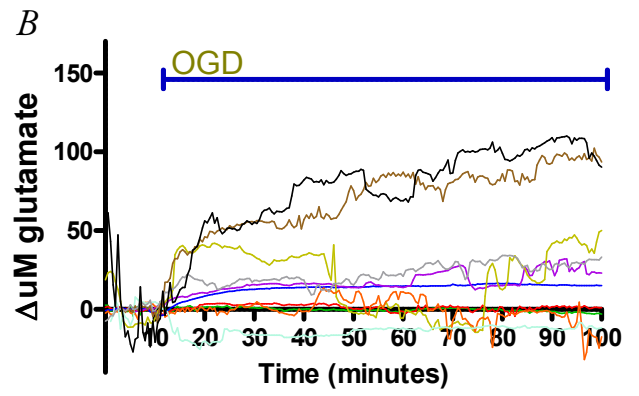
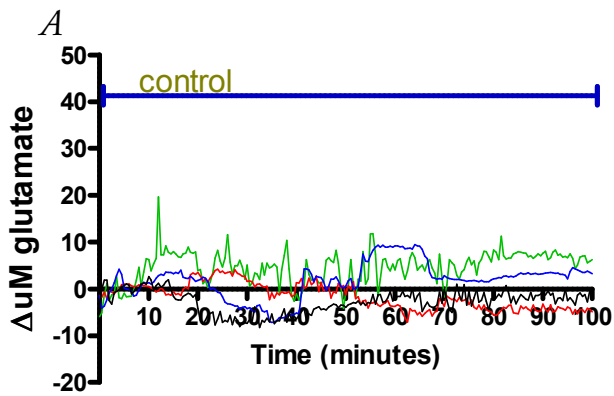


Figure 3-7:

Effect of PPADS on glutamate release from co-culture during OGD

A: OGD experiments, all recordings (n:10)

15:1 binned sensor-null recordings of all OGD experiments that were performed. Most experiments showed a rise in glutamate following the induction of OGD 10 minutes into the recording.

B: OGD + 10uM PPADS, all recordings (n:5)

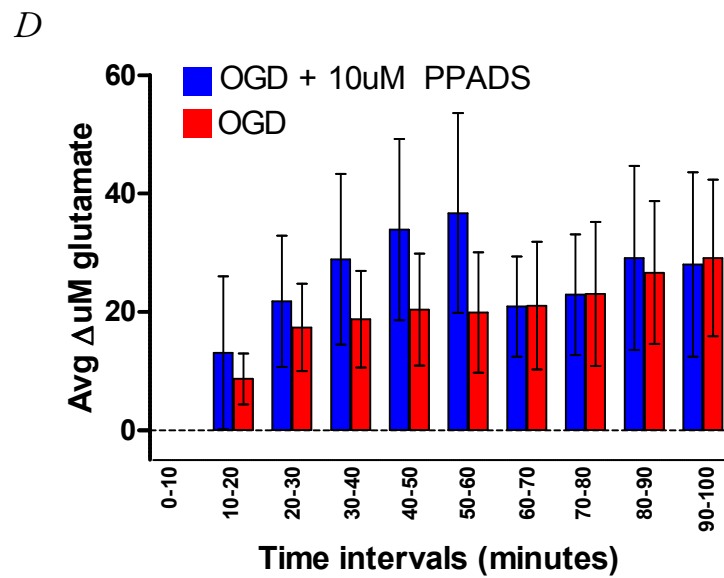
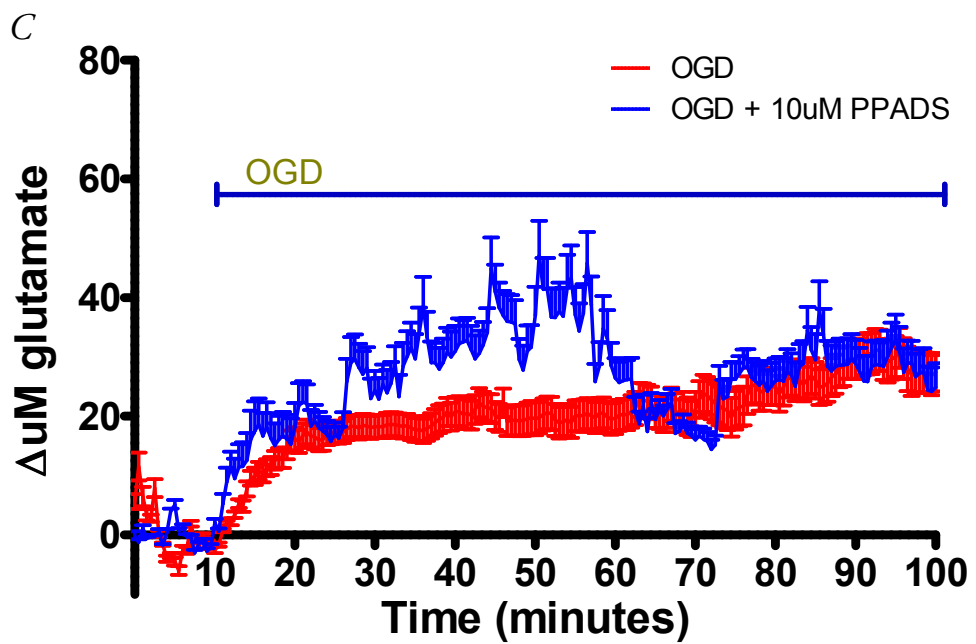
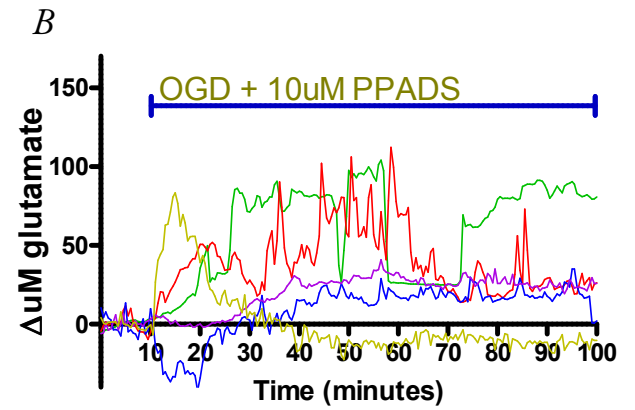
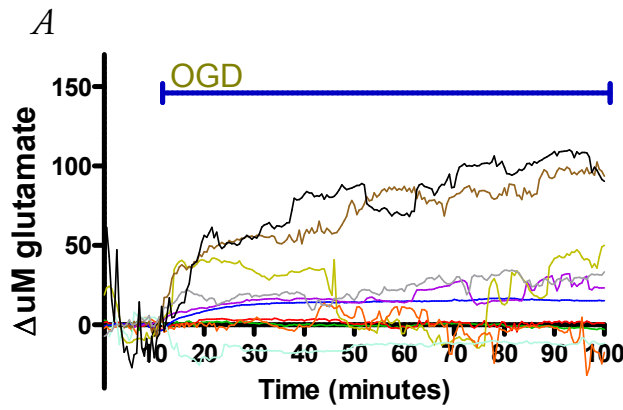
15:1 binned sensor-null recordings of all OGD + 10uM PPADS experiments that were performed. There were rises in glutamate in most experiments, very similar to what was observed during OGD in the absence of PPADS.

C: Average Δ uM glutamate, OGD vs OGD + 10uM PPADS

The amount of glutamate released from the co-culture during OGD (n:10) was not significantly changed by the addition of PPADS (n:5).

D: The mean Δ glutamate during every 10 minute interval over 90 minutes:

There was no significant difference in Δ glutamate during any of the 10 minute intervals, suggesting glutamate release was not affected by P2 receptor activation.



ATP and glutamate release from astrocyte cultures

OGD caused a reduction in ATP release from cultured astrocytes in 3 out of 5 experiments whilst also causing an increase in ATP in 3 experiments at certain time points (**Figure 3-8: B**), There was also significant ATP release during 1 of the 3 control experiments (**Figure 3-8: A**). Overall, the amount of ATP released from the astrocyte culture during OGD (n:5) was reduced compared to control (n:3), even though these differences were small (**Figure 3-8: C**). A maximum reduction in the ATP level during OGD was at 10 minutes ($-10.51 \pm 1.26\mu\text{M ATP}$). There were no significant differences in ATP release between OGD and controls during 10 minute intervals. These results suggest that OGD does not cause significant ATP release from astrocytes on their own.

Glutamate release from cultured astrocytes rose significantly following the onset of OGD (**Figure 3-9**). In 5 of the 8 OGD experiments there were large and sustained increases in extracellular glutamate (**Figure 3-9: B**), whilst during the 6 control experiments there were glutamate increases in just 2 (**Figure 3-9: A**), and these had a later onset than most of those seen during OGD. Consequently the overall profile of average Δ glutamate during OGD was raised compared to control from the 14th minute onward, reaching a maximum level of $16.26 \pm 1.6\mu\text{M}$ at 64 minutes (**Figure 3-9: C**). The mean Δ glutamate during OGD from the astrocyte culture was significantly raised during the 20-30 ($8.41 \pm 3.35\mu\text{M}$ vs. $-5.86 \pm 4.87\mu\text{M}$), 30-40 ($10.74 \pm 4.87\mu\text{M}$ vs. $-4.77 \pm 3.82\mu\text{M}$), 40-50 (12.12 ± 4.88 vs. $-1.33 \pm 3.42\mu\text{M}$) and 50-60 (13.3 ± 6.08 vs. $-1.88 \pm 3.96\mu\text{M}$) minute intervals compared to controls (**Figure 3-9: D**). Overall, these results suggest that astrocytes contribute to the release of glutamate but not ATP during OGD.

Figure 3-8:

ATP release from astrocyte cultures during OGD

A: Control experiments, all recordings (n:3)

15:1 binned sensor-null recordings of all control experiments that were performed. There was considerable variability in the ATP levels during control conditions between experiments.

B: OGD experiments, all recordings (n:5)

15:1 binned sensor-null recordings of all OGD experiments that were performed. Again, there was considerable variability between experiments, with some experiments showing rises in ATP while others had reductions in ATP release.

C: Average Δ uM ATP, OGD vs control

The amount of ATP released from the astrocyte culture during OGD (n:5) appears reduced compared to control (n:3), although the difference between OGD and controls was small. A maximum reduction in the ATP level during OGD was at 10 minutes ($-10.51 \pm 1.26\mu\text{M ATP}$).

D: The mean Δ ATP of every 10 minute interval over the 90 minutes:

There were no significant differences in ATP release between control and OGD during any of the intervals.

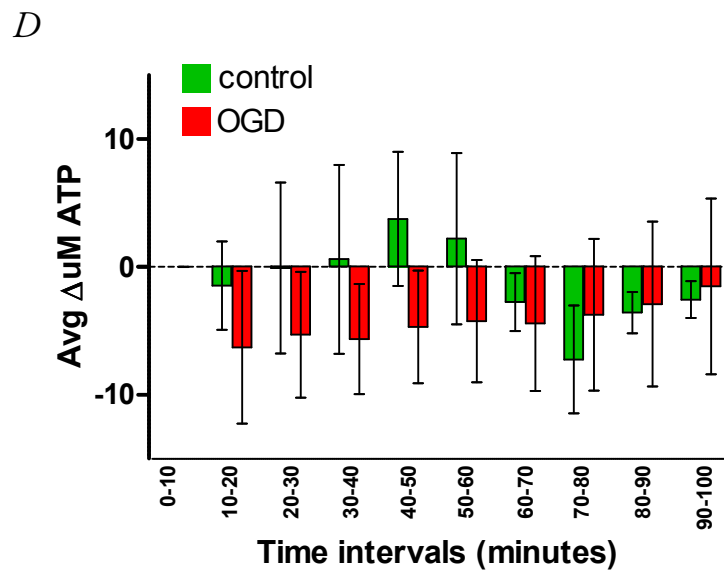
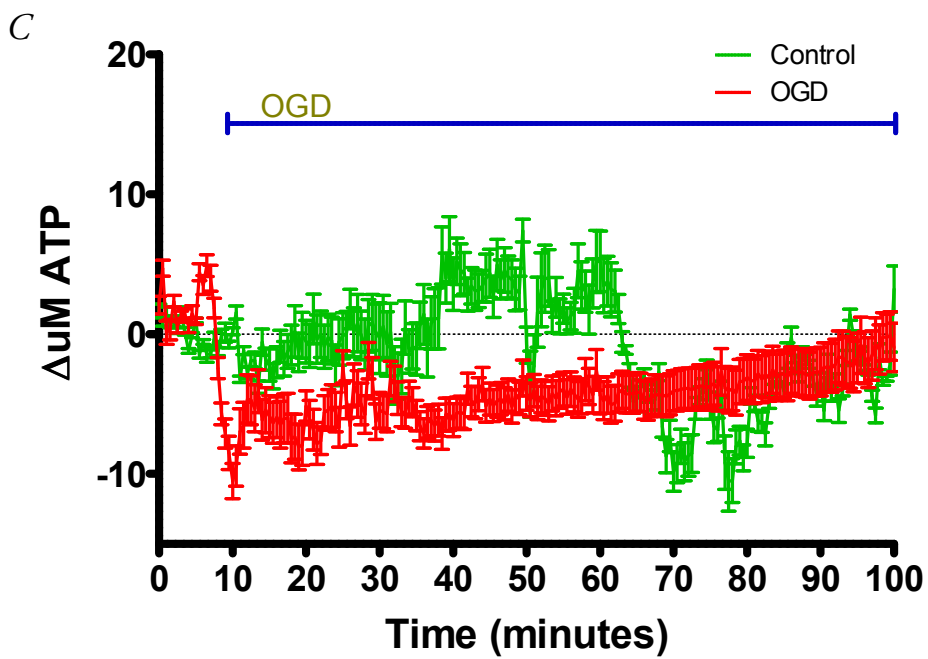
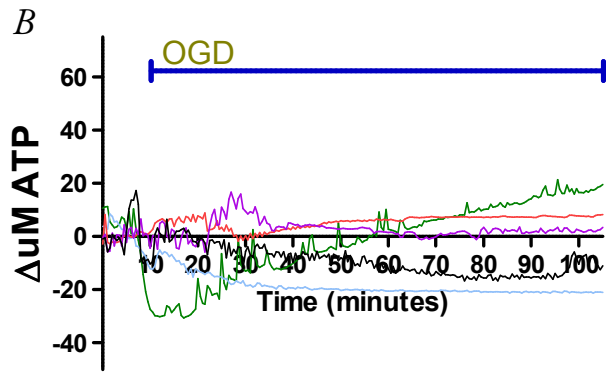
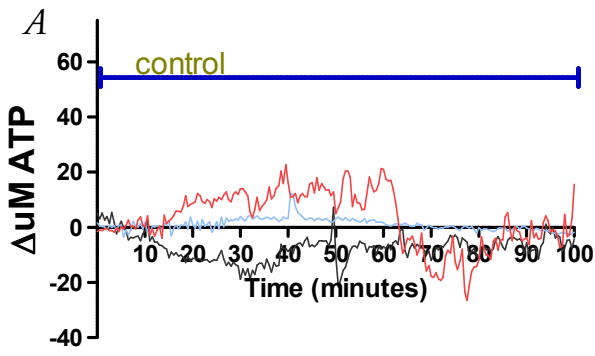


Figure 3-9:

Glutamate release from astrocyte cultures during OGD

A: Control experiments, all recordings (n:6)

15:1 binned sensor-null recordings of all control experiments that were performed. There were rises in glutamate in some experiments, but these were occurring later than those seen during OGD.

B: OGD experiments, all recordings (n:8)

15:1 binned sensor-null recordings of all OGD experiments that were performed. Most experiments showed a rise in glutamate following the induction of OGD 10 minutes into the recording.

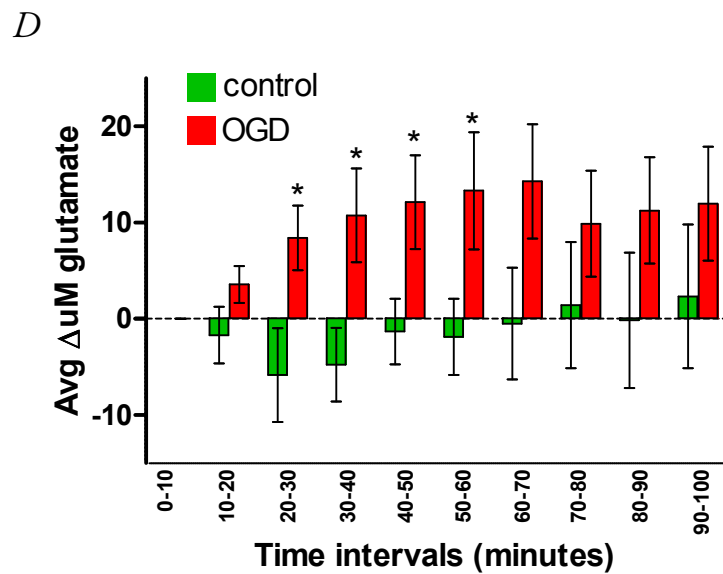
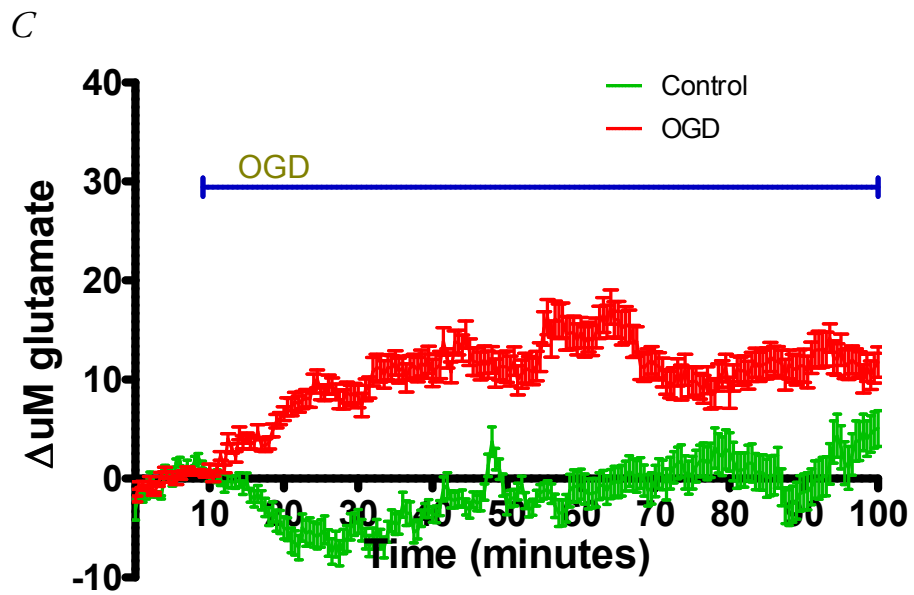
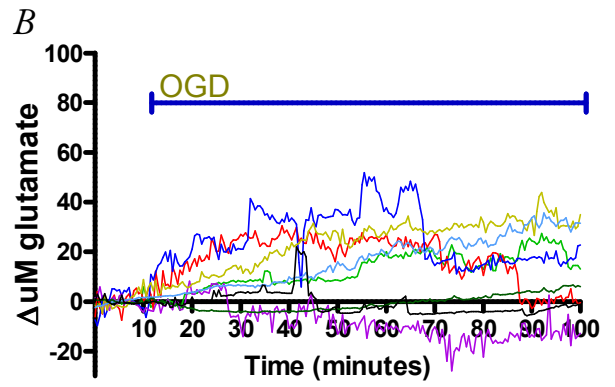
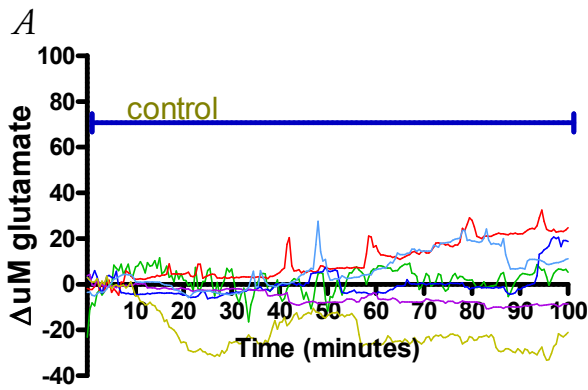
C: Average Δ uM glutamate, OGD vs control

The amount of glutamate released from the astrocyte culture during OGD (n:8) was increased compared to control (n:6) for the first time at 14 minutes and maintained this throughout. A maximum rise in the glutamate level during OGD was reached at 64 minutes ($17.32 \pm 1.7\mu\text{M}$ glutamate).

D: The mean Δ glutamate during every 10 minute interval over 90 minutes:

There were significant increases ($p < 0.05$) in Δ glutamate during OGD compared to control during all intervals in the 20-60 minute period.

*: $p < 0.05$



ATP and glutamate release from neuronal cultures

In contrast with what occurred in co-cultures, OGD caused a *reduction* in ATP release from neuronal cultures (**Figure 3-10**). There was an increase in ATP release from 3 out of the 4 control experiments (**Figure 3-10: A**) while the 4 OGD experiments produced contrasting results, with 2 showing large reductions in ATP release and the other 2 demonstrating increased levels during OGD (**Figure 3-10: B**). The net effect of the recordings was that the Δ ATP over time was reduced during OGD compared to control from 15.5 minutes onwards, with a maximum rise in the ATP level during control being reached at 92 minutes ($15.91 \pm 2.15\mu\text{M ATP}$) and a maximum reduction in ATP during OGD at 55 minutes ($-11.48 \pm 2.36\mu\text{M ATP}$) (**Figure 3-10: C**). There were no significant differences in average Δ ATP between OGD and controls during any of the 10 minute intervals (**Figure 3-10: D**).

OGD did not have a large effect on glutamate release from neuronal cultures (**Figure 3-11**). OGD caused increased glutamate release at some stage in 3 of 4 experiments, with 2 showing immediate increases after the switch to OGD at 10 minutes (**Figure 3-11: B**). During control conditions 3 out of 6 experiments demonstrated increases in glutamate release over time, with 1 of them having an early rise and a particularly large overall increase (**Figure 3-11: A**). Consequently the mean Δ glutamate over time during OGD was not very different from controls (**Figure 3-11: C**). A maximum Δ glutamate during OGD of $7.15 \pm 1.6\mu\text{M}$ was reached after 48 minutes, while during control conditions a level of $13.45 \pm 2.3\mu\text{M}$ was reached at 85.5 minutes. There were no significant differences in glutamate release from neuronal cultures when comparing OGD vs. controls during 10 minute intervals (**Figure 3-11: D**).

These results suggest that neurons in the absence of astrocytes do not release significant quantities of ATP or glutamate during OGD.

Figure 3-10:

ATP release from neuronal cultures during OGD

A: Control experiments, all recordings (n:4)

15:1 binned sensor-null recordings of all control experiments that were performed. There was an increase in ATP release from neurons during most control experiments after 10 minutes.

B: OGD experiments, all recordings (n:4)

15:1 binned sensor-null recordings of all OGD experiments that were performed. Two of the 4 experiments had showed large reductions in ATP release after OGD was induced, with the other 2 experiments showing increases in ATP release during OGD.

C: Average $\Delta\mu\text{M ATP}$, OGD vs control

The amount of ATP released from the co-culture during OGD (n:4) was decreased compared to control (n:4) after 15.5 minutes and throughout the rest of the experiment. A maximum rise in the ATP level during control was reached at 92 minutes ($15.91 \pm 2.15\mu\text{M ATP}$), with a maximum reduction in ATP during OGD at 35.5 minutes ($-11.48 \pm 2.36\mu\text{M ATP}$).

D: The mean ΔATP of every 10 minute interval over the 90 minutes:

There were no significant differences in ATP release from neuronal cultures between control and OGD.

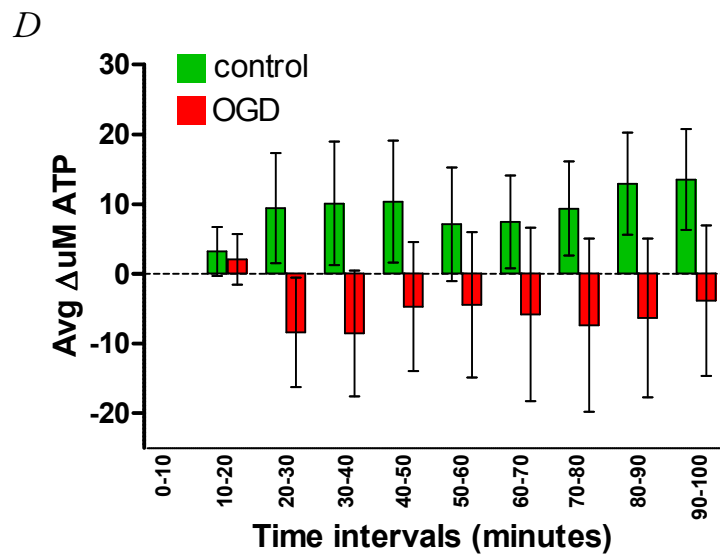
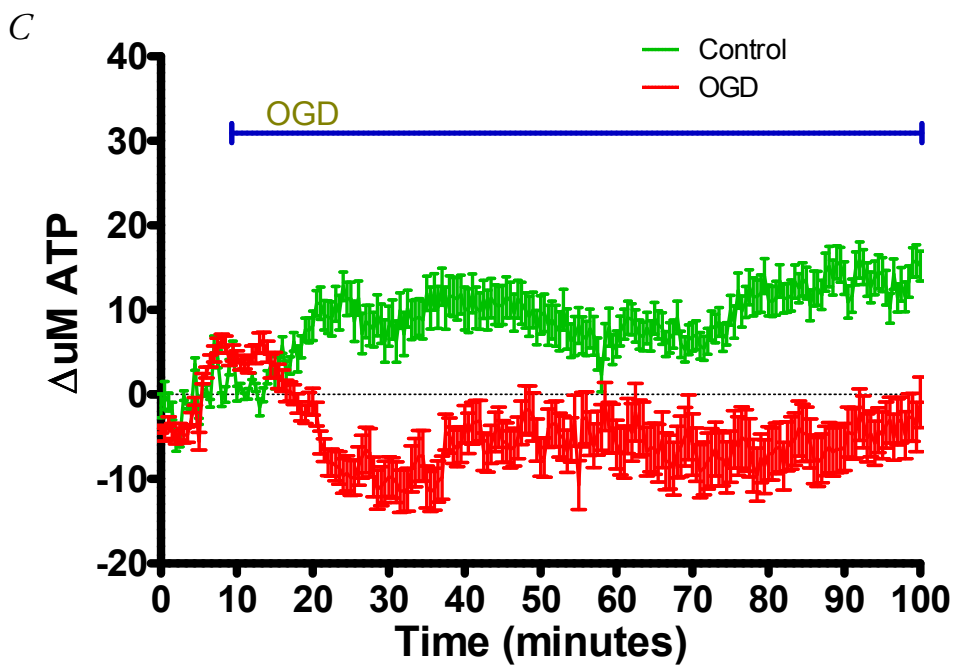
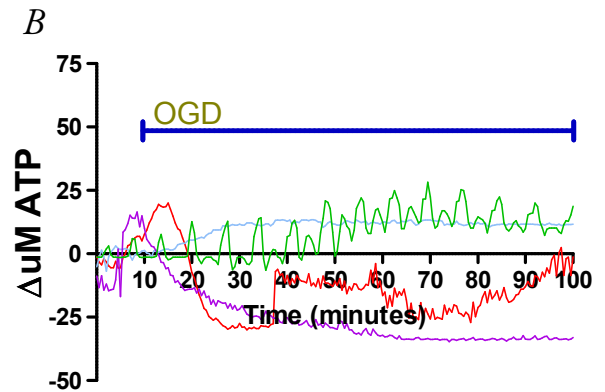
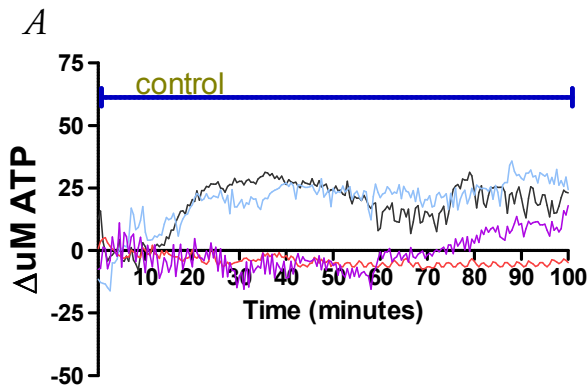


Figure 3-11:

Glutamate release from cultured neurons during OGD

A: Control experiments, all recordings (n:6)

15:1 binned sensor-null recordings of all control experiments that were performed. There were rises in glutamate in most experiments, with a particularly large sustained one in one of them.

B: OGD experiments, all recordings (n:4)

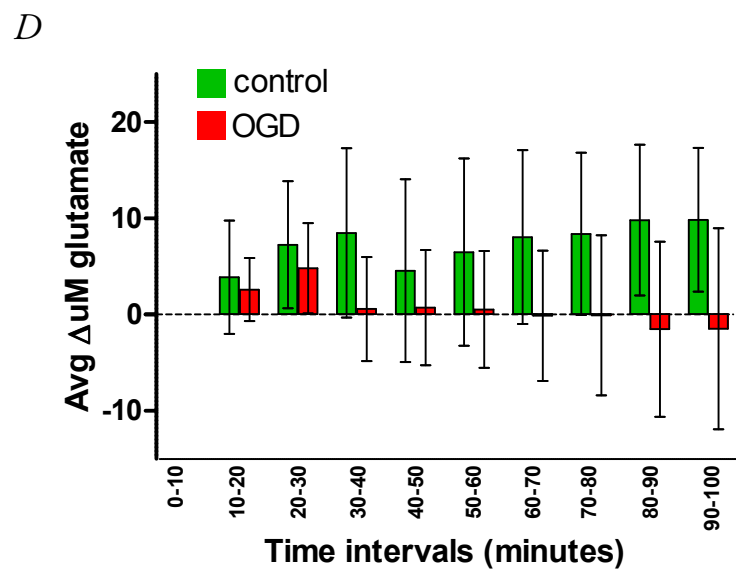
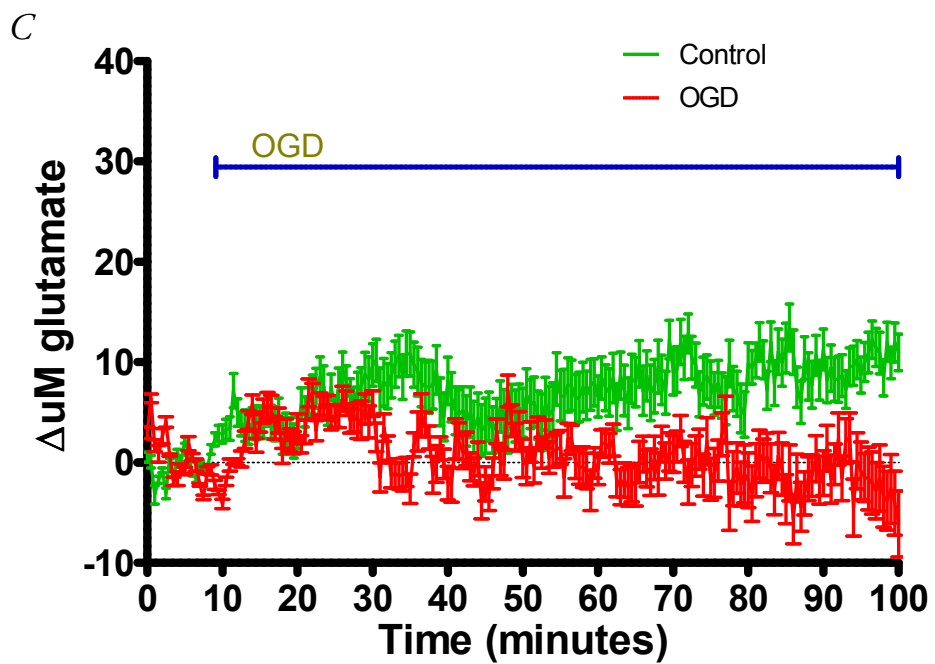
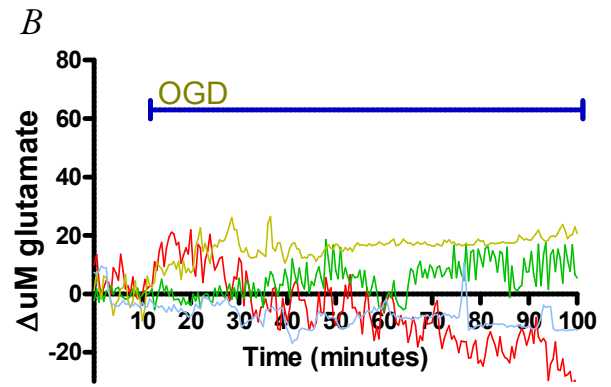
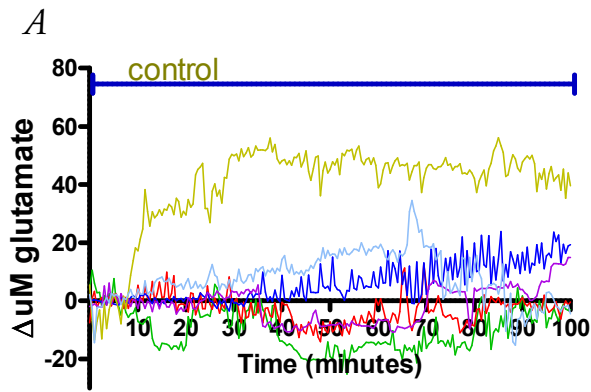
15:1 binned sensor-null recordings of all OGD experiments that were performed. Two experiments showed a rise in glutamate immediately following the induction of OGD 10 minutes into the recording.

C: Average Δ uM glutamate, OGD vs control

The amount of glutamate released from the cultured neurons during OGD (n:4) was not significantly different compared to control (n:6). A maximum rise in the glutamate level during control was reached at 85.5 minutes ($13.45 \pm 2.3\mu\text{M}$ glutamate), and during OGD at 48 minutes ($7.15 \pm 1.6\mu\text{M}$ glutamate).

D: The mean Δ glutamate during every 10 minute interval over 90 minutes:

There were no significant differences in glutamate release from neuronal cultures when comparing OGD and control experiments.



DISCUSSION

Summary of results

OGD caused significant increases in ATP and glutamate release from co-cultured astrocytes and neurons. The majority of glutamate release most likely originated from an astroglial source, since OGD caused an increase in its release from astrocyte cultures but not from neuronal cultures. The glutamate release from co-cultures was not mediated by P2 receptor activation, since it could not be attenuated by PPADS. Neither the astrocyte nor the neuronal culture alone released significant quantities of ATP during OGD, demonstrating the significance of astrocyte-neuronal interactions in mediating ischaemic ATP release in the co-culture.

Technical considerations

These experiments were technically challenging. A few sources of potential error became apparent which may account for some of the variability seen between recordings. The process of inserting the biosensors into the chamber could have damaged at least some of the cells just underneath the sensor. If this occurred, cellular material might have partially coated the biosensor. Also, the cellular density varied between cultures. Neuronal cultures were the least densely populated and contained small cell-free areas, while astrocyte cultures formed a confluent cellular 'carpet' and co-cultures contained the summation of both. As discussed before, the presence of noise and current shifts made data analysis more difficult.

Glutamate release during OGD is mainly from astrocytes

OGD caused significant glutamate release from co-cultured astrocytes and neurons. This result mirrors what has been previously demonstrated by other groups *in vivo* and *in vitro* using a variety of techniques, CNS preparations and models of ischaemia (Benveniste et al., 1984; Hagberg et al., 1985; Globus et al., 1988; Globus et al., 1991; Ueda et al., 1992; Mitani et al., 1994; Matsumoto et al., 1996; Persson et al., 1996; Zeevalk et al., 1998; Melani et al., 1999; Seki et al., 1999; Ooboshi et al., 2000; Phillis et al., 2000; Rossi

et al., 2000; Hamann et al., 2002; Feustel et al., 2004; Marcoli et al., 2004b; Kosugi and Kawahara, 2006). In these studies, ischaemia induced a rapid (within minutes) and substantial accumulation of glutamate, similar to what was observed in my experiments. A few examples of glutamate concentrations measured over time by others are presented in **Table 3-1** for comparison. Most of the data in the table has been collected using the technique of microdialysis, where thin semi-permeable dialysis tubing is inserted into specific brain regions and solutions are constantly run through it which equilibrate with brain extracellular space, allowing the measurement of changes in the concentrations of different analytes, such as glutamate, from samples taken from the tubing.

One advantage of using microelectrode biosensors over microdialysis is that it allows a much more detailed analysis of the timing of glutamate release. Only one other study used an amperometric biosensor to measure glutamate, albeit *in vivo* (Nakayama et al., 2002). The authors used a precursor of the same glutamate biosensor I used to record the highest baseline (~30uM) and ischaemic (up to 200uM) extracellular glutamate levels reported in the literature (Nakayama et al., 2002). Therefore the ability of these sensors to detect glutamate immediately after release, before it is diluted by perfusion media, seems to allow for a more accurate estimate of actual glutamate levels and represents a further advantage of this method.

The majority of glutamate release in the co-culture most likely originated from an astroglial source, since OGD caused an increase in its release from astrocyte cultures but not from neuronal cultures. Neuronal glutamate release early in ischaemia has been postulated by a number of studies showing that both neurotransmitter exocytosis and reversal of neuronal glutamate transporters, in particular, are events which occur early during ischaemia (Rossi et al., 2000; Fleidervish et al., 2001; Gebhardt et al., 2002; Hamann et al., 2002; Rossi et al., 2007). However, these studies do not quantify this contribution.

Table 3-1: Extracellular glutamate levels during ischaemia, examples from literature

Protocol	[Glutamate]	Method of Ischaemia	Animal	Method of Measurement	Ref.
6h permanent occlusion	<i>Baseline:</i> 1.19uM 30m- 5uM 1h- 9uM 1.5h- 12.5uM 2h- 15uM 3h- 20uM 6h- 23uM	Transorbital three-vessel occlusion	Male rabbits	<u>Microdialysis</u> , central region of ischemic distribution	1
10m ischaemia, 60m reperfusion	<i>Baseline:</i> 2uM 5m- 8uM 10m- 16uM 15m- 10uM 20m- 4.5uM	Complete cerebral ischaemia by neck cuff + hypovolaemic hypotension	Male Wistar rats	<u>Microdialysis</u> , dorsal hippocampus	2
20m ischaemia	<i>Baseline:</i> 1-2uM 20m- 32uM	Transient forebrain ischaemia	Male Wistar rats	<u>Microdialysis</u> , dorsal hippocampus	3
20m ischaemia	<i>Baseline:</i> 1-2uM 20m- 38uM	Transient forebrain ischaemia	Male Wistar rats	<u>Microdialysis</u> , somatosensory cortex	3
20m ischaemia	<i>Baseline:</i> 1-2uM 20m- 28uM	Transient forebrain ischaemia	Male Wistar rats	<u>Microdialysis</u> , dorsolateral striatum	3
20m ischaemia	<i>Baseline:</i> 1-2uM 20m- 25uM	Transient forebrain ischaemia	Male Wistar rats	<u>Microdialysis</u> , anterior thalamus	3
20m ischaemia	<i>Baseline:</i> 56nM 15m- 336nM	Bilateral carotid artery occlusion	Female rats	<u>Microdialysis</u> , hippocampus CA1	4
5m ischaemia	<i>Baseline:</i> 2-3uM 5m-35uM	Four vessel occlusion	Male Sprague-Dawley rats	<u>Microdialysis</u> striatum	5
10 m ischaemia	<i>Baseline:</i> 28±9uM 10m- 200uM	Four vessel occlusion	Male Wistar rats	<u>Microdialysis biosensor</u> , hippocampus CA1	6
45m ischaemia	<i>Baseline:</i> 0.1uM 5m- 1.5uM 15-45m- 2uM	Chemical ischaemia (NaCN + iodoacetic acid)	Mouse astrocyte culture	<u>Real-time fluorescent imaging</u>	7

m=minutes, h=hours. References (Ref.):

1 (Benveniste et al., 1984) 2 (Globus et al., 1988) 3 (Ueda et al., 1992) 4 (Matsumoto et al., 1996) 5 (Ooboshi et al., 2000) 6 (Nakayama et al., 2002) 7 (Liu et al., 2006b)

My results, along with evidence in the literature, suggest that neurons do not contribute significantly to ischaemic glutamate release. Periods of ischaemia lasting 5-20 minutes produced rapid (within 2.5 minutes) and significant increases in extracellular glutamate in white matter, an area low in synapses and high in glia (Mitani et al., 1994; Cui et al., 1999). In hippocampus where neurons were selectively eliminated, there was only a slight delay (3-5 minutes) in the onset of ischaemic glutamate release without a significant reduction of the quantity (Mitani et al., 1994; Cui et al., 1999). The overall quantity of glutamate release was only significantly attenuated when astrocyte numbers were also reduced (Mitani et al., 1994; Cui et al., 1999). In animals lacking GLT-1, 5 minutes of ischaemia produced higher glutamate levels compared to wild type mice, while during 20 minutes of ischaemia the opposite was the case, with GLT-1 knockout mice having lower glutamate levels, suggesting that astrocyte glutamate transport reversal contributed significantly to glutamate release during prolonged ischaemia *in vivo* (Mitani and Tanaka, 2003). A similar result was obtained by inhibiting reversal of glial glutamate transporters and preventing release via VRACs pharmacologically *in vivo*: blocking both pathways simultaneously reduced glutamate release by 83% (Seki et al., 1999). In the immature retina, glial cells also contributed more significantly than neurons to glutamate release during total metabolic blockade (Zeevalk et al., 1998). In astrocyte cultures Liu and colleagues demonstrated rapid (within 5 minutes) and significant glutamate accumulation during chemical ischaemia, mainly via VRACs (Liu et al., 2006b).

The glutamate release from co-cultures during OGD was probably not mediated by P2 receptor activation, since it could not be attenuated by PPADS. This excludes direct glutamate release through P2X receptor pores and also makes it unlikely that P2 receptor modulation of glutamate release occurs during OGD. Two other studies have reported that P2X₇ receptor opening during ischaemia did not occur in cultured astrocytes (Contreras et al., 2002; Liu et al., 2008). P2 receptors have been shown to modulate glutamate release, both positively and negatively (Nakatsuka and Gu, 2001; Mongin and Kimelberg, 2002; Sperlagh et al., 2002; Kimelberg, 2004; Krugel et al., 2004; Rodrigues et al., 2005; Fellin et

al., 2006b). For example, P2Y receptor antagonists prevent ATP-induced glutamate release from swollen astrocytes, while P2X receptors enhance glutamate release in a variety of preparations (Mongin and Kimelberg, 2002; Nakatsuka et al., 2003; Kimelberg, 2004; Krugel et al., 2004). However there are no studies investigating whether this sort of modulation occurs during ischaemia. Furthermore, this result suggests that any protective effect of PPADS during OGD (presented in Chapter 5) is not caused by a reduction in glutamate release.

ATP release during OGD: a co-operative effect of neurons and astrocytes?

OGD also caused a significant increase in ATP release from co-cultured astrocytes and neurons, confirming what has been suggested by others using *in vivo* and *in vitro* models of ischaemia (Juranyi et al., 1999; Melani et al., 2005; Frenguelli et al., 2007). The reader is referred to **Table 3-2** for a comparison of ATP measurements during ischaemia reported in the literature. Raised extracellular levels of ATP in the ischaemic mammalian CNS were first measured in rat hippocampal slices subjected to hypoxia/hypoglycaemia using radioactively labelled [³H]purines (Juranyi et al., 1999). ATP levels were first significantly elevated after 6 minutes of ischaemia, demonstrating a similarly sharp rise in ATP levels. An even larger increase in adenosine was also reported, and preceded that of ATP, while ADP and AMP levels were undetectable, suggesting that ATP breakdown did not contribute to adenosine accumulation (Juranyi et al., 1999). Melani et al. have so far provide the only evidence that extracellular ATP levels rise during *in vivo* ischaemia. Using microdialysis from rat striatum, a two-fold increase in ATP was measured (from 3.1 to 5.9nM) after 220 minutes of focal ischaemia, and was further increased when ectonucleotidases were inhibited (Melani et al., 2005).

Table 3-2: Extracellular ATP levels during ischaemia, examples from the literature

Protocol	[ATP]	Method of Ischaemia	Animal/cell culture model	Method of Measurement	Ref.
40m OGD	<i>Baseline:</i> virtually no currents detected OGD- $3.7 \pm 0.1 \mu\text{M}$	OGD	Murine neonatal cortical astrocyte culture	<u>Biosensor</u> - P2X ₂ transfected HEK-293 cell touching surface of a single astrocyte	1
40m OGD	<i>Baseline:</i> <0.25nM 5m- 1.25nM 10m- 1.75nM 15-30m- 2nM 40m- 1.8nM	OGD	Murine neonatal cortical astrocyte culture	<u>Luciferin-luciferase assay</u> of superfusates	1
220m ischaemia	<i>Baseline:</i> $3.1 \pm 0.34 \text{nM}$ 220m- $5.9 \pm 0.61 \text{nM}$	MCA occlusion	Male Wistar rats	<u>Microdialysis</u> , striatum	2
15m OGD + 30m reperfusion	<i>Baseline:</i> unable to detect 15m: $0.7 \pm 0.2 \mu\text{M}$ <i>Reperfusion:</i> $1.8 \pm 0.2 \mu\text{M}$	OGD	Rat hippocampal slices	<u>Enzyme-based Microelectrode biosensor</u> (same one used for this project)	3

m=minutes, h=hours. References (Ref.):

1 (Liu et al., 2008) **2** (Melani et al., 2005) **3** (Frenguelli et al., 2007)

Frenguelli et al. (using the same biosensor electrodes I used), found that both adenosine and ATP release occurred during OGD in hippocampal slices, and that adenosine release preceded and was mechanistically independent from ATP release (Frenguelli et al., 2007). ATP levels first started to rise after approximately 7 minutes of OGD (coinciding with the onset of the anoxic depolarisation) and continued to increase steadily until reperfusion was instated after a total of 15 minutes, reaching a maximum level of $0.7 \pm 0.2 \mu\text{M}$ (Frenguelli et al., 2007). This is less than the $3.8 \pm 2.8 \mu\text{M}$ average which I measured after 15 minutes of OGD. A possible explanation for this discrepancy is that in their study, electrodes were inserted directly into the hippocampal slice, where the cytoarchitecture is much denser, which may influence the ability of ATP to reach the electrode. Also, the ATP electrode requires glycerol to function, and even though this was included in perfusing solutions, it has been demonstrated not to diffuse well into the slice itself, thereby reducing the sensitivity of the electrode to ATP over time (Schock et al., 2007). Finally, the faster onset of ATP release in my experiments may be explained by a faster onset of severe ischaemia in the cell culture system, where the oxygen and glucose content around all cells falls more rapidly than through the full thickness of a slice.

The source of ATP release from the co-culture is less clear than with glutamate, since neither the astrocyte nor the neuronal cultures alone released significant quantities of ATP during OGD. Studies investigating ischaemia-induced ATP release from cultured astrocytes have only recently been published (Zhang et al., 2007; Liu et al., 2008). Chemical ischaemia caused ATP release by lysosomal exocytosis in both astrocyte cultures and acute hippocampal slices (Zhang et al., 2007). Significant ATP accumulation occurred within 4 minutes in both preparations, as measured in supernatant using the luciferase-luciferin assay (LLA), with approximately 15-fold increases in extracellular ATP levels after 15 minutes (Zhang et al., 2007). However, the ectonucleotidase inhibitor dipyridamole was present continuously during these experiments, preventing ATP hydrolysis *in situ* (Zhang et al., 2007). Liu and colleagues measured ischaemia induced ATP release from cultured astrocytes using both the LLA with supernatants and by a novel biosensor technique where P2X₂-transfected HEK293 cells (HEK-P2X₂) were whole-cell patch clamped and placed directly adjacent a single astrocyte (Liu et al., 2008). Basal ATP release was very low using both methods, and during 40 minutes of OGD peak concentrations of 2nM and 3.7 ± 0.1 μM were detected using the LLA and HEK-P2X₂, respectively, with release mainly via maxi-anion channels (Liu et al., 2008).

Indirect evidence of ATP release from cultured astrocytes during ischaemia was also provided by another paper: extracellular adenosine accumulation was prevented by an ectonucleotidase inhibitor, suggesting that release of ATP followed by subsequent extracellular adenosine formation via ectonucleotidase activity was occurring (Parkinson and Xiong, 2004). An earlier study by the same group found no increase in adenine nucleotide (ATP+ADP+AMP) release from cultured astrocytes during OGD (Parkinson et al., 2002). However, this experiment measured nucleotide content at the end of 60 minutes of OGD from superfusates in a static bath without ectonucleotidase inhibitors. In light of their later results demonstrating substantial ectonucleotidase activity in cultured astrocytes, this finding is not surprising.

The aforementioned paper by Parkinson et al. also suggested that ATP may be released from primary neuronal cultures during ischaemia, with OGD, NaCN and IAA application all increasing adenine nucleotide release (Parkinson et al., 2002). However, their methodology did not distinguish between ATP, ADP or AMP, and levels were only measured once after 60 minutes. Furthermore, experiments were performed at 20-22°C, which may significantly affect results. My experiments were therefore the first to investigate direct ATP release from primary neuronal cultures during ischaemia, and the only ones to describe its dynamics over time. My results demonstrating that no significant ATP release occurs from neuronal cultures during ischaemia may be explained by the fact that intracellular ATP levels in primary neuronal cultures fall dramatically during ischaemia. Intracellular ATP content in primary neuronal cultures has been reported to drop to 41% and 17% percent of control following 10 and 60 minutes of OGD, respectively (Parkinson and Xiong, 2004).

The finding that ischaemic ATP release was significantly increased in the co-culture compared with the astrocyte and neuronal culture suggests the presence of a mechanism involving the co-operation of both cell types. One theoretical explanation for why ATP was only released in co-culture is that glutamate released by the astrocytes was causing ATP release from neurons during OGD. Glutamate has been shown to stimulate ATP release from astrocytes and microglia via unclear mechanisms involving ionotropic glutamate receptors, exocytosis, P2X₇ receptors and/or possibly the CFTR (Queiroz et al., 1997; Queiroz et al., 1999; Liu et al., 2006a; Zhang et al., 2007; Hamilton et al., 2008). Ionotropic glutamate receptors and P2X₇ receptors are expressed on neurons, and neuronal CFTR expression has also been reported, opening up this possibility (Conti et al., 1999; Dingledine et al., 1999; Lundy et al., 2002; Burnstock and Knight, 2004; Guo et al., 2009). However, Queiroz et al. saw no change in glutamate-induced ATP release when the numbers of neurons in their cultures was reduced (Queiroz et al., 1999). Nevertheless, their experiments were not performed under ischaemic conditions, so whether or not neurons may participate during OGD is not known. This theory could have been tested by applying glutamate to neuronal cultures during OGD while measuring ATP release.

Another possibility is that the expression of ectonucleotidases or membrane proteins involved in ATP release changes when cells are co-cultured. For example, cultured astrocytes have been shown to possess high ectonucleotidase activity, and this may have made it difficult to detect ATP release with the sensors in this preparation (Parkinson and Xiong, 2004). One could then speculate that co-culturing astrocytes with neurons reduced their expression, making it easier to detect ATP release. Unfortunately, very little is known about the regulation of ectonucleotidase expression (Zimmermann, 2006). The presence of neurons in astrocyte cultures may also change the expression of various ion channels and transporters in astrocytes, so theoretically proteins involved in ATP release may be differentially regulated in the presence or absence of neurons (Barres, 1991). Finally, cultured astrocytes are able to maintain their intracellular ATP levels during 60 minutes of OGD, presumably by utilising their glycogen deposits, suggesting that they would be able to continue lactate production (Kirchhoff et al., 2001; Parkinson and Xiong, 2004; Pellerin and Magistretti, 2004). This lactate could then be utilised by neurons to help maintain production of ATP, which could subsequently be released; indeed, added lactate has been shown to increase neuronal survival during periods of OGD (Cater et al., 2003). However, production of ATP in neurons from lactate still requires oxidative phosphorylation, so it is doubtful whether this process would be able to continue for prolonged periods during OGD (Pellerin and Magistretti, 2004).

In conclusion, these experiments provide the first direct comparison of ATP and glutamate release during ischaemia from cultured neurons, astrocytes, and co-cultures. OGD induced significant release of both ATP and glutamate from co-cultures. Astrocytes, but not neurons, appear to contribute most significantly to glutamate release, with P2 receptor activation apparently not contributing to this process. ATP release was only detectable in the co-culture, giving rise to the novel suggestion that astrocytes and neurons interact by an unknown mechanism to release ATP or enhance extracellular ATP accumulation during ischaemia.

Chapter 4:

Functional P2 and glutamate receptors on cultured neurons and astrocytes

INTRODUCTION

For both ATP and glutamate mediated excitotoxicity to occur in the CNS during ischaemia, cells must express functional P2 and ionotropic glutamate receptors. Although there is a high volume of literature documenting P2 and glutamate receptor expression in cultured astrocytes and neurons, significant variability exists between different brain regions or when using different culturing methods/cellular preparations (Ozawa et al., 1998; Dingledine et al., 1999; James and Butt, 2002; Burnstock and Knight, 2004; Kew and Kemp, 2005; Abbracchio et al., 2006; Burnstock, 2006a; Verkhratsky and Kirchhoff, 2007; Abbracchio et al., 2009; Verkhratsky et al., 2009). Furthermore, evidence of expression at the mRNA or protein level does not always translate into functional responses (discussed later). For these reasons I characterized receptor expression on these cell cultures at the functional level.

Adequate pharmacological tools exist to reliably differentiate ionotropic glutamate receptor subtype responses functionally (Alexander et al., 2008). Accurate determination of functional P2 receptor expression in native cells is more challenging due to the large variety of receptors, many of which are often co-expressed in single cells, and a paucity of pharmacological tools allowing for the discrimination of specific receptor subtype responses (Collo et al., 1997; Lambrecht, 2000; Amadio et al., 2002; Rodrigues et al., 2005; von Kugelgen, 2006; Bianco et al., 2009; Jarvis and Khakh, 2009; Verkhratsky et al., 2009).

The basic structure, function, and CNS expression of P2 and glutamate receptors will be reviewed, and the agonists and antagonists used to functionally characterise their expression introduced, with a particular emphasis on P2 receptors. Results demonstrating widespread functional P2 and glutamate receptor expression in cortical neuron and astrocyte cultures will then be presented and discussed.

Ionotropic glutamate receptors

Classification and general properties

Ionotropic glutamate receptors are divided into three groups according to the names of the agonists which were originally used to selectively activate them: NMDA, AMPA and kainate receptors. It is most likely that native receptors of all three groups are assemblies of four to five specific subunits, with the composition of the subunits determining the functional properties of the receptor (Kew and Kemp, 2005). Subunits of all three receptor types have the membrane topology of an extracellular N-terminus, three transmembrane domains (formed by M1, 3, 4), a channel lining re-entrant loop (M2) located between M1 and M3 that enters and exits the membrane at its cytoplasmic surface, and an intracellular C-terminus (Dingledine et al., 1999; Kew and Kemp, 2005). All three are cation channels, with variable permeability to Na⁺, K⁺ and Ca²⁺ (Kew and Kemp, 2005). Initially, ionotropic glutamate receptors were believed to be expressed solely by neuronal cells, but evidence has mounted in the last two decades that astrocytes and other glial cells also express AMPA and NMDA receptors, suggesting that neurons and glia may act as partners in shaping glutamate mediated information processing within the mammalian brain (Bowman and Kimelberg, 1984; Kettenmann et al., 1984; Kettenmann and Schachner, 1985; Seifert and Steinhauser, 2001; Verkhratsky and Kirchhoff, 2007; Bakiri et al., 2009).

NMDA receptors: structure and function

The NMDA receptor family contains seven subunits: NR1, NR2A-D, and NR3A-B, as well as various functional splice variants of these subunits (Dingledine et al., 1999; Kew and Kemp, 2005). Functional glutamate receptors comprise NR1 and at least one NR2 subunit or a combination of NR1 and NR2 + NR3 (Kew and Kemp, 2005). NMDA receptors have several unique properties. Receptor activation requires the simultaneous presence of both glutamate and the co-agonist glycine at separate binding sites, located on NR2 and NR1 subunits respectively (Dingledine et al., 1999; Kew and Kemp, 2005). At resting membrane potentials the receptor is blocked by Mg²⁺, and this blockage is relieved

by depolarisation (Lester et al., 1990; Dingledine et al., 1999). Finally, NMDA receptors are highly Ca^{2+} permeable, with a ratio of permeability to $\text{Ca}^{2+}/\text{Na}^+$ of 10-11, and show almost no desensitisation (Dingledine et al., 1999; Verkhratsky and Kirchhoff, 2007). These latter properties in particular explain why NMDA receptors have often been found responsible for mediating glutamate excitotoxicity. NR3 subunit inclusion suppresses the Ca^{2+} permeability and reduces Mg^{2+} block compared to NR1/NR2 combinations (Kew and Kemp, 2005). Glial NMDA receptors in particular seem to have low Mg^{2+} block, suggesting a predominance of NR3 subunits (Verkhratsky and Kirchhoff, 2007).

AMPA/kainate receptors: structure and function

Both AMPA and kainate receptors are homo- or heteromeric tetramers composed of distinct subunit combinations (Dingledine et al., 1999; Kew and Kemp, 2005). AMPA receptors are produced by combinations of four possible subunits, GluR1-4, while kainate receptors form from GluR5-7, KA-1 and/or KA-2 subunits (Dingledine et al., 1999; Kew and Kemp, 2005; Pinheiro and Mulle, 2006). AMPA GluR1-4 proteins each have two splice variants, named flip and flop, giving rise to a wide variety of kinetics, while kainate receptors also undergo various post-translational modifications/alternative splicing (Seifert and Steinhauser, 2001; Kew and Kemp, 2005; Pinheiro and Mulle, 2006). AMPA and kainate receptors are predominantly Na^+ and K^+ permeable, although AMPA receptors lacking GluR2 have significant Ca^{2+} permeability (Kew and Kemp, 2005). GluR2 is poorly expressed in various glial preparations, so activation of receptors in these cells produces substantial Ca^{2+} signals (Verkhratsky and Kirchhoff, 2007). AMPA receptors rapidly desensitise, usually within about 100ms, whereas kainate receptors desensitise more slowly (Dingledine et al., 1999; Verkhratsky and Kirchhoff, 2007). The study of AMPA and kainate receptors has been difficult historically due to a lack of selective agonists and antagonists which differentiate between the two, and this is the reason why they are often grouped as 'non-NMDA' receptors (Honore and Drejer, 1988; Kew and Kemp, 2005; Pinheiro and Mulle, 2006).

Ionotropic glutamate receptor expression in cortical neurons and astrocytes

NMDA receptor expression is widespread in cortical neurons, both *in vivo* and *in vitro* (Li et al., 1998a; Ozawa et al., 1998; Conti et al., 1999; Janssens and Lesage, 2001; Kovacs et al., 2001). The recognition of functional NMDA receptors in cortical astrocytes, on the other hand, is a much more recent discovery. NR1 and NR2 protein and mRNA expression was detected in human and mouse cortex, particularly in distal processes of astrocytes (Conti et al., 1996; Conti et al., 1997; Schipke et al., 2001). Both membrane currents and intracellular Ca²⁺ increases were observed in astrocytes from cortical slices in response to NMDA application (Schipke et al., 2001). Finally, a recent paper showed that acutely isolated cortical astrocytes or astrocytes in cortical slices had NMDA-receptor mediated components to their response to glutamate which were sensitive to glycine and NMDA receptor antagonists (Lalo et al., 2006).

AMPA and kainate receptors are widely expressed by neurons, both pre and post synaptically and in various brain regions, including the cortex (reviewed in Dingledine et al., 1999; Pinheiro and Mulle, 2006). Widespread AMPA receptor expression has also been demonstrated in astrocytes throughout the brain, including the neocortex (Holzwarth et al., 1994; David et al., 1996; Porter and McCarthy, 1997; Seifert and Steinhauser, 2001). However, functional kainate receptors have not been reported in astrocytes (Pinheiro and Mulle, 2006; Verkhratsky and Kirchhoff, 2007).

Despite ample evidence for the existence of ionotropic glutamate receptors on cortical cells, particularly neurons, it is often difficult to compare experimental results obtained in different cultures systems, particularly since factors such as the composition of culture medium and the age of cells *in vitro* influence the expression of glutamate receptor subunits, thus changing their functional properties (Kovacs et al., 2001). For this reason it was appropriate to investigate and confirm functional glutamate receptor expression in these cells.

Glutamate receptor agonists and antagonists used

Glutamate, AMPA and NMDA were used as glutamate receptor agonists in the experiments in this chapter. NMDA receptors are activated by glutamate and selectively by NMDA, which acts at the glutamate recognition site of NR2 subunits (Kew and Kemp, 2005). NMDA receptors were selectively inhibited using the highly potent activity-dependent, voltage-dependent non-competitive NMDA receptor antagonist MK-801 (Wong et al., 1986). At AMPA receptors, glutamate and AMPA are both full agonists and induce rapid desensitisation (Kew and Kemp, 2005). Glutamate is a full agonist at kainate receptors, while AMPA can also activate some kainate receptors (Dingledine et al., 1999; Pinheiro and Mulle, 2006). In these experiments I did not seek to fully differentiate between AMPA and kainate receptor responses, so the competitive AMPA/kainate receptor antagonist NBQX was used (Honore et al., 1988; Kew and Kemp, 2005). It has a 30-fold higher affinity for AMPA over kainate receptor binding, and is essentially free of activity at NMDA receptors (Honore et al., 1988; Alexander et al., 2008).

P2 receptors

P2X receptors: structure and function

Ligand-gated ionotropic P2X receptors are composed of homo- and/or heteromeric assemblies containing combinations of seven subunits (P2X₁₋₇) (reviewed in: Jarvis and Khakh, 2009). Subunits range in size from 379 to 595 amino acids (P2X₆ and P2X₇, respectively), and each subunit is thought to consist of two transmembrane domains (TM1/2) separated by an extracellular loop with both N and C termini located intracellularly (Jarvis and Khakh, 2009). The cation pore seems to be formed by the TM2 region (Jarvis and Khakh, 2009). Ionotropic P2X receptor structure has still not been definitively elucidated, but evidence suggests that subunits assemble into functional trimers (Jarvis and Khakh, 2009). Receptors are composed of homo or heterotrimers, with P2X₇ probably only forming homomers and P2X₆ only heteromers, although a recent paper described evidence for functional P2X_{4/7} heteromeric receptors (North, 2002; Illes and Alexandre Ribeiro, 2004; Gever et al., 2006; Guo et al., 2007; Jarvis and Khakh, 2009). Heteromeric functional receptors have so far also been described for P2X_{1/2, 1/4, 1/5, 2/3, 2/6, 4/6} subunit combinations (Le et al., 1998a; Torres et al., 1998; Cockayne et al., 2005; Jarvis and Khakh, 2009).

Upon activation by ATP, (the physiological agonist at all P2X receptors) a transmembrane pore opens, allowing the passage of Na⁺, K⁺ and Ca²⁺ (Egan and Khakh, 2004; Gever et al., 2006). The fractional Ca²⁺ permeability varies between receptors (Egan and Khakh, 2004; Jarvis and Khakh, 2009). Homomeric P2X_{2,4,7} receptors have been shown to undergo a further slower conformational change following prolonged activation, leading to increased permeability through the cation pore itself or an associated transmembrane channel, allowing the passage of larger molecules (Gever et al., 2006; Pelegrin and Surprenant, 2009). P2X₁ and P2X₃ receptors, on the other hand, fully desensitise within a second of agonist application, while many heteromeric assemblies have mixed properties in this respect (Gever et al., 2006; Roberts et al., 2006; Jarvis and Khakh, 2009).

P2Y receptors: structure and function

Eight metabotropic G-protein-coupled P2Y receptor subtypes (P2Y_{1, 2, 4, 6, 11, 12, 13, 14}) have been characterised thus far in human or mammalian tissues (reviewed in: Abbracchio et al., 2006; von Kugelgen, 2006). P2Y receptor proteins show the typical GPCR features of seven transmembrane domains, with an extracellular N-terminus and intracellular C-terminus (Fischer and Krugel, 2007). P2Y_{1,2,4,6,11} couple predominantly via G_{q/11} to activate the PLC β (phospholipase C) /IP₃ (inositol trisphosphate) pathway and release Ca²⁺ from intracellular stores, while P2Y_{12,13,14} almost exclusively couple to G_{i/o}, leading to inhibition of adenylate cyclase, reducing levels of cAMP (cyclic adenosine monophosphate) (Abbracchio et al., 2006; Fischer and Krugel, 2007). P2Y₁₁ may also stimulate adenylate cyclase via G_s (Abbracchio et al., 2006; Fischer and Krugel, 2007). However, there is no rodent ortholog of P2Y₁₁ (Abbracchio et al., 2006). Therefore only P2Y_{1,2,4,6} activation would be expected to induce Ca²⁺ release from intracellular stores in murine receptors.

In contrast to P2X receptors, which are only activated by ATP, P2Y receptors are activated by a variety of adenine and uridine nucleotides. P2Y_{1,12,13} are ADP-preferring, although ATP can also act as a partial agonist or antagonist at these receptors depending on different conditions (Zhang et al., 2002; Marteau et al., 2003; Pausch et al., 2004; Abbracchio et al., 2006). P2Y_{2,4} are UTP-recognising receptors, although murine P2Y_{2,4} are activated equally strongly by ATP and UTP (Lustig et al., 1993; Charlton et al., 1996a; Lazarowski et al., 2001; Suarez-Huerta et al., 2001; Wildman et al., 2003). P2Y₆ is unique as it is most potently and selectively activated by UDP, although it is also potently activated by UTP and, less potently, by ADP (Communi et al., 1996a; Lazarowski et al., 2001). P2Y₁₄ is activated by UDP-glucose, UDP-galactose or UDP-glucosamine (Abbracchio et al., 2006). P2Y₁₄ is therefore not of interest to this project, as it is not activated by ATP or ADP.

P2 receptor expression in cortical neurons and astrocytes

A variety of P2 receptors are expressed by neurons and astrocytes, both *in vitro* and *in vivo* (see **Table 4-1** for collated results from the literature) (for recent reviews see: James

and Butt, 2002; Burnstock and Knight, 2004; Verkhasky et al., 2009). P2X_{1,3,4} and P2Y₁ are the receptors for which evidence of functional expression in cortical neurons has most often been reported, with only one paper each describing P2Y₂ and P2X₇ receptor responses (Lundy et al., 2002; Wirkner et al., 2002; Bennett et al., 2003; Pankratov et al., 2003; Kahlert et al., 2007; Lalo et al., 2007). In cortical astrocytes, functional P2X_{7,1/5} and P2Y_{1,2,4,14} expression have been documented most frequently, while definite P2Y₆ responses have also been reported by one paper (King et al., 1996; Lenz et al., 2000; Zhu and Kimelberg, 2001; Bennett et al., 2003; Fumagalli et al., 2003; Nobile et al., 2003; Kahlert et al., 2007; Lalo et al., 2008; Bianco et al., 2009; Fischer et al., 2009).

Analysing **Table 4-1**, it is clear that variable results have been obtained by different groups when studying P2 receptor expression in cortical neurons and astrocytes. This may be due to differences in the species, tissue preparation, age of the animals/cultures, and/or method of detection. For example, in a preparation of hippocampal synaptosomes, western blotting detected P2X₁₋₆ subunits and P2Y_{1,2,4,6,11,12}, while subsequent evidence of functional expression was only obtained for P2X₁, P2Y₁, and P2Y₂ and/or P2Y₄ but not P2X₇ or P2Y_{6,12,13} (Rodrigues et al., 2005). The same study also reports that single cell RT-PCR experiments detected mRNA for P2X₁₋₄ and P2Y_{1,2,4,6,11,12}, but not P2X₅₋₇ (Rodrigues et al., 2005). P2 expression is also developmentally regulated (Collo et al., 1997; Lalo and Kostyuk, 1998; Zhu and Kimelberg, 2001; Amadio et al., 2002; Rubini et al., 2006; Crain et al., 2009). Additionally, once neurons and glia are transferred into a culture system, the profile of P2 receptor expression quickly changes from that which was present in the intact preparation (Bennett et al., 2003). Furthermore, the only study which investigated P2 receptor expression in cultured cortical neurons used a co-culture of neurons and glial cells and obtained tissue from rats rather than mice (Bennett et al., 2003).

Table 4-1: P2 receptor expression in cortical neurons and astrocytes (contains some data from hippocampal preparations)

Receptor	Neurons				Astrocytes			
	mRNA	protein	IHC	Functional	mRNA	protein	IHC	Functional
<i>P2X (no subtype specified)</i>				<i>31^r</i>				<u>8^r</u>
P2X ₁	<i>21^r, (27^r)</i>	<i>14^r, (27^r)</i>	<i>1^r</i>	<i>14^r, 16^r, 19^r, (27^r)</i>	<i>2^r, 4^r, 5^m</i>	<i>2^r</i>	<i>1^r, (6^r)</i>	<i>1^r, 2^r, 5^m, 16^r, 29^r</i>
P2X ₂	<i>21^r, (27^r)</i>	<i>(27^r)</i>	<i>14^r, (17^r)</i>	<i>19^r</i>	<i>2^r, 4^r, 5^m</i>	<i>2^r</i>	<i>1^r, (6^r)</i>	<u>5^m</u>
P2X ₃	<i>21^r, (27^r)</i>	<i>(27^r)</i>		<i>16^r, 19^r</i>	<i>2^r, 4^r, 5^m</i>	<i>2^r</i>	<i>1^r, (6^r)</i>	<i>1^r, 2^r, 5^m, 16^r, 29^r</i>
P2X ₄	<i>21^r, (27^r)</i>	<i>20^r, (27^r)</i>	<i>(17^r), 20^r</i>	<i>18^m, 18^m, 19^r</i>	<i>2^r, 4^r, 5^m</i>	<i>2^r</i>	<i>1^r, (6^r)</i>	<u>5^m</u>
P2X ₅	<i>21^r, (27^r)</i>	<i>(27^r)</i>		<i>19^r</i>	<i>2^r, 5^m</i>	<i>2^r</i>	<i>1^r, 6^r</i>	<u>5^m</u>
P2X ₆	<i>21^r, (27^r)</i>	<i>(27^r)</i>	<i>(17^r)</i>	<i>19^r</i>	<i>4^r, 5^m</i>		<i>1^r, (6^r)</i>	<u>5^m</u>
P2X ₇	<i>(27^r)</i>	<i>14^r, 15^r, 28^m</i>	<i>14^r, 15^r, 28^m, 13^r</i>	<i>14^r, (27^r)</i>	<i>2^r, 4^r, 5^m</i>	<i>2^r, 11^r, 12^r</i>	<i>1^r, (6^r), 13^r</i>	<i>1^r, 2^r, 5^m, 12^r, 29^r, 13^r</i>
P2X _{1/5}								<u>5^m</u>
<i>P2Y (no subtype specified)</i>				<i>31^r</i>				<u>8^r</u>
P2Y ₁	<i>16^r, (27^r)</i>	<i>(27^r)</i>	<i>22^b, 23^r, 30^r</i>	<i>16^r, (24^r), 26^r, (27^r)</i>	<i>2^r, 4^r, (7^r), 9^r, 10^r, 16^r</i>	<i>2^r, 11^r</i>	<i>1^r, 22^b, 23^r, 30^r</i>	<i>1^r, 2^r, (7^r) 9^r, 10^r, (24^r), 16^r</i>
P2Y ₂	<i>(27^r)</i>	<i>(27^r)</i>	<i>30^r</i>	<i>16^r, 26^r, (27^r)</i>	<i>2^r, 4^r, (7^r), 9^r, 10^r, 16^r</i>	<i>2^r, 11^r</i>	<i>1^r, 30^r</i>	<i>1^r, 2^r, (7^r), 9^r, 10^r, 16^r</i>
P2Y ₄	<i>16^r, (27^r)</i>	<i>(27^r)</i>		<i>16^r, (27^r)</i>	<i>2^r, 4^r, 10^r</i>	<i>2^r</i>	<i>1^r</i>	<i>1^r, 2^r, 10^r, 16^r</i>
P2Y ₆	<i>16^r, (27^r)</i>	<i>(27^r)</i>		<i>16^r, (27^r)</i>	<i>2^r, 4^r, 10^r, 16^r</i>	<i>2^r</i>	<i>1^r</i>	<i>1^r, 2^r, 16^r</i>
P2Y ₁₁	<i>(27^r)</i>	<i>(27^r)</i>						
P2Y ₁₂	<i>25^r, (27^r)</i>	<i>(27^r)</i>		<i>(27^r)</i>	<i>2^r</i>		<i>1^r</i>	<i>1^r, 25^r</i>
P2Y ₁₃				<i>(27^r)</i>			<i>1^r</i>	<i>1^r</i>
P2Y ₁₄					<i>2^r</i>		<i>1^r</i>	<i>1^r, 2^r</i>

Red: definitely not present, Green: definitely present, Purple: probably present / unaltered font: primary cell cultures, underlined: acutely isolated cells, *italicized*: intact preparation, **bold**: synaptosomes / m: mouse r: rat h: human / data from hippocampal preparations is in (parenthesis)

1 (Fischer et al., 2009), 2 (Fumagalli et al., 2003), 4 (Dixon et al., 2004), 5 (Lalo et al., 2008), 6 (Kukley et al., 2001), 7 (Zhu and Kimelberg, 2001), 8 (Kimelberg et al., 1997), 9 (King et al., 1996), 10 (Lenz et al., 2000), 11 (Iwabuchi and Kawahara, 2009b), 12 (Bianco et al., 2009), 13 (Wirkner et al., 2005), 14 (Lundy et al., 2002), 15 (Collo et al., 1997), 16 (Bennett et al., 2003), 17 (Rubio and Soto, 2001), 18 (Lalo et al., 2007), 19 (Pankratov et al., 2003), 20 (Le et al., 1998b), 21 (Collo et al., 1996), 22 (Moore et al., 2000), 23 (Simon et al., 1997), 24 (Kahlert et al., 2007), 25 (Sasaki et al., 2003), 26 (Wirkner et al., 2002), 27 (Rodrigues et al., 2005), 28 (Sim et al., 2004), 29 (Nobile et al., 2003), 30 (Fischer and Krugel, 2007), 31 (Lalo et al., 1998)

P2 receptor agonists and antagonists used

A number of recent reviews contain tables describing and comparing the pharmacology of P2 receptors, including comparisons of the activities of many agonists and antagonists (North, 2002; Abbracchio et al., 2006; Gever et al., 2006; Jarvis and Khakh, 2009). However, these either focus on human P2 receptors or do not specify which species data was obtained from. Considering that significant inter-species variability exists concerning the pharmacological efficacy of agonists and antagonists at some P2 receptors and that most murine P2 receptor orthologues have not enjoyed extensive characterization, I created tables compiling available data about murine P2 receptors in relation to the agonists and antagonists used during this project, including EC₅₀/IC₅₀ values where possible (Garcia-Guzman et al., 1997b; Chessell et al., 1998; Humphreys et al., 1998; Calvert et al., 2004; Donnelly-Roberts et al., 2009). **Tables 4-2/4-3** compare agonists, and **tables 4-4/4-5** compare antagonists at P2X/P2Y respectively. Where data from murine receptors is lacking, values obtained using other species is presented. The reader is asked to refer to these tables when reading the rest of this chapter, particularly for references to individual papers. A number of highly sub-type selective agonists and antagonists have recently become available and are also mentioned in these tables for future reference.

Various P2 receptor agonists were used. ATP activates all P2X receptors as well as P2Y_{2,4,13}, and it also has partial agonist activity at P2Y₁. ADP potently activates P2Y_{1,12,13} and less potently P2Y₆. Both ATP and ADP can be hydrolysed by ectonucleotidases, so the non-hydrolysable ATP analogue ATPγS was also used (Lambrecht, 2000). It activates all P2X receptors, apart from P2X₇, as well as P2Y_{1,2,12}, and may have partial agonist activity at P2Y₄. BzATP is the most potent known agonist at P2X₇, where it is roughly 10-100 times more potent than ATP (Ralevic and Burnstock, 1998; Gever et al., 2006). However, it is not selective, also acting as an agonist at P2X_{1,2,3,4,1/2,2/3} and perhaps P2Y_{2,4}. Finally, MRS-2365 was used as a highly potent and specific P2Y₁ receptor agonist (Chhatriwala et al., 2004).

For non-selective P2 receptor blockade, suramin and PPADS (pyridoxal-5'-phosphate-6-azophenyl-2,4-disulfonate) were used. Suramin, initially developed as a trypanocidal agent, was first shown to act as a P2 receptor antagonist in the mouse vas deferens, and has since been shown to be active at P2Y_{1,2,6,11,12,13} and P2X_{1,2,3,5,7,2/3,1/5,4/6} (Dunn and Blakeley, 1988). Unfortunately, at concentrations which block P2 receptors suramin also has many non-specific effects, including actions at various proteases, ectonucleotidases, growth factors, cytokines, G-protein subunits, and glutamate, GABA, 5-HT and nicotinic receptors (Dunn and Blakeley, 1988; Balcar et al., 1995; Motin and Bennett, 1995; Nakazawa et al., 1995; Beindl et al., 1996; Ong et al., 1997; Gu et al., 1998; Peoples and Li, 1998; Lambrecht, 2000; Zona et al., 2000; Suzuki et al., 2004) PPADS was the first *specific* non-selective P2 receptor antagonist, and has activity at P2Y_{1,4,6,13} and P2X_{1,2,3,4,5,7,2/3,1/5,4/6} (Lambrecht et al., 1992; Lambrecht, 2000). It does not possess as many non-specific effects as Suramin, including little or no activity at glutamate receptors and ectonucleotidases (Motin and Bennett, 1995; Gu et al., 1998; Lambrecht, 2000; Zona et al., 2000). In a number of studies PPADS has erroneously been used as an antagonist with selectivity at P2X over P2Y receptors (Ziganshin et al., 1994; Cavaliere et al., 2001b).

MRS-2179 and KN-62 were used to block P2Y₁ and P2X₇ receptors, respectively. MRS-2179 is a selective competitive P2Y₁ receptor antagonist which appears to have adequate activity at human and murine receptors, with an approximate IC₅₀ of 15-331nM at the human receptor (Boyer et al., 1998; Moro et al., 1998; Baurand et al., 2001; Waldo and Harden, 2004; Atterbury-Thomas et al., 2008). KN-62 is one of the most potent murine P2X₇ receptor antagonists, with approximate IC₅₀ values of 380nM/11nM-1.17uM for prevention of cation channel opening/large pore formation, respectively (Gargett and Wiley, 1997; Chessell et al., 1998; Lambrecht, 2000; Gevers et al., 2006; Donnelly-Roberts et al., 2009). The action of KN-62 is slow in onset and only partially reversible (Lambrecht, 2000). KN-62 is also an inhibitor of calcium/calmodulin-dependent protein kinase II (IC₅₀: 900nM) (Lambrecht, 2000).

Table 4-2: Agonists at P2X receptors

	ATP	ATP _g S	BzATP	Highly selective agonists	Desensitisation *
P2X₁	<i>0.316^c (mouse)</i> 2.2^d (mouse)	<i>3.16^k (human)</i>	<i>.001^k (human)</i> <i>.003^o (human)</i>	L-β,γ-meATP	Fast
P2X₂	<u><i>10^f (rat)</i></u> <i>19.9^g (rat)</i> <i>1.2^o (human)</i>	<i>1.3^k (rat)</i>	<i>5.5^k (rat)</i> <i>0.75^o (human)</i>	No	Slow
P2X_{1/2}	<i>0.5^o (human)</i>	ND	<i>.003^o (human)</i>	No	Slow
P2X₃	<i>0.78^g (human)</i> <i>0.67^g (rat)</i>	<i>0.5-0.63^k (rat/human)</i>	<i>.031^k (rat)</i> <i>.079^k (human)</i>	No	Fast
P2X_{2/3}	<u><i>17.6^f (rat)</i></u> <i>0.501^k (rat)</i>	<i>2.04^k (rat)</i>	<i>0.645^k (rat)</i>	No	Slow
P2X_{2/6}	<i>32^f (rat)</i>	ND	ND	No	Slow
P2X₄	<i>2.3^m (mouse)</i>	<i>10.96^k (human)</i>	<i>0.49^k (human)</i> <i>7^o (human)</i>	No	Slow
P2X_{4/6}	<i>6^o (rat)</i>	ND	ND	No	Slow
P2X₅	<i>0.5ⁱ (rat)</i> <i>15.4ⁿ (rat)</i>	<i>9.3ⁿ (rat)</i>	No activity ^o	No	Slow
P2X_{1/5}	<i>.055-.130^e (rat)</i>	<i>3.2^e (rat)</i>	ND	No	Fast/slow
P2X₆	<i>0.5ⁱ (rat)</i> <i>12ⁿ (rat)</i>	<i>16ⁿ (rat)</i>	ND	No	Slow
P2X₇	(mouse) Cation pore opening: <u><i>2400^a, 734^b, 298^b</i></u> Large Pore Formation: <i>200^a, 214^b, 46.5^b</i>	(mouse) Cation pore opening: <i>>1000^a</i> Large Pore Formation: <i>>1000^a</i>	(mouse) Cation pore opening: <u><i>100^a, 90.4^b, 58.3^b</i></u> Large Pore Formation: <i>60.3^a, 17.3^b, 4.6^b</i>	No	Slow

Numbers represent EC₅₀ values, in uM.

ND: No data available

Methodology= not underlined: electrophysiology, underlined: Ca²⁺ fluorimetry / **bold**: native receptor, *italicized*: recombinant expression system

*Fast desensitization: within 1-2 seconds of agonist application, Slow desensitization: >20seconds (Jarvis and Khakh, 2009)

References:

a (Donnelly-Roberts et al., 2009), **b** (Chessell et al., 1998), **c** (Sim et al., 2008), **d** (Ikeda, 2007), **e** (Surprenant et al., 2000), **f** (Koshimizu et al., 1998), **g** (Garcia-Guzman et al., 1997a), **h** (Soto et al., 1996), **i** (Hausmann et al., 2006), **j** (Roberts et al., 2006), **k** (Bianchi et al., 1999), **l** (Gever et al., 2006), **m** (Jones et al., 2000), **n** (Collo et al., 1996), **o** (Jarvis and Khakh, 2009)

Table 4-3: Agonists at P2Y receptors

	ATP	ADP	ATPgS	MRS-2365	BzATP	UTP	UDP	Highly selective agonists
P2Y₁	<i>Partial Agonist</i> 11 ^{g,1} (human) 17.7 ^{h,2} (human)	0.204^{g,1} (human) 0.92^{h,2} (human)	1.33 ^{h,2} (human)	0.0018 ^{k,3} (human)	No ^L	No	No	MRS-2365
P2Y₂	0.7^{b,4} (mouse)	>1mM ^{b,4} (mouse)	7.9 ^{b,4} (mouse)	No	4.7 ^{m,7} (rat) Maybe ^{n,L}	1.1 ^{b,4} (mouse)	No	MRS-2698 2- ThioUTP
P2Y₄	0.7^{e,3} 0.435^{i,3} (mouse)	No ^{i,3} (mouse)	No ^f (human) 5.4 ^{m,7} (rat) <i>Partial agonist</i>	No	No ^{m,7} (rat)	0.4^{e,3} 0.26^{i,3} (mouse)	No ^{i,3} (mouse)	2'-azido-dUTP
P2Y₆	No ^{i,3} (mouse)	20 ^{i,3} (mouse)	No ^o (rat)	No	Maybe ^{n,L}	0.84 ^{i,3} (mouse)	0.042^{i,3} (mouse)	MRS-2693 MRS-2633 PSB 0474
P2Y₁₂ (no Ca ²⁺ rises)	Antagonist in low receptor density, agonist in high receptor density ^j	0.258^{c,6} 0.027^{c,5} (mouse)	1.5 ^{c,6} 0.32 ^{c,5} (mouse)	No ^{k,3} (human)	ND	No	No	
P2Y₁₃ (no Ca ²⁺ rises)	0.243 ^{d,5} (mouse)	0.0041^{d,5} (mouse)	ND	No ^{k,3} (human)	ND	No	No	
P2Y₁₄	This is a UDP-glucose/galactose receptor, not activated by ATP or ADP.							
P2Y₁₁	Not present in rodent genome ^j							

Numbers represent EC₅₀ values, in uM.

The principal physiological agonist for each receptor is highlighted in **bold**.

ND: No data available

Methodology= **1** [Ca²⁺]_i fluorimetry), **2** inhibition of [3H]MRS2279 binding, **3** InsP₃ accumulation, **4** ⁴⁵Ca²⁺ release, **5** Gαq/i3 construct, **6** *LacZ* system, **7** electrophysiology

References:

a (von Kugelgen, 2006), **b** (Lustig et al., 1993), **c** (Pausch et al., 2004), **d** (Zhang et al., 2002), **e** (Suarez-Huerta et al., 2001), **f** (Communi et al., 1996b), **g** (Leon et al., 1997), **h** (Waldo and Harden, 2004), **i** (Lazarowski et al., 2001), **j** (Abbracchio et al., 2006), **k** (Chhatriwala et al., 2004), **L** (Vigne et al., 1999), **m** (Wildman et al., 2003), **n** (Fischer et al., 2001), **o** (Chang et al., 1995)

Table 4-4: Antagonists at P2X receptors

	Suramin	PPADS	KN-62	Highly selective antagonists ^{a,h,p,s}
P2X₁	No, >1mM ^g (mouse) 0.01-0.3, 0.851 ^{e,t} (human)	0.4 ^g (mouse) 0.01-0.3, 1.29 ^{a,t} (human)	No	NF449, NF864, RO-1
P2X₂	33.1 ^e (rat) 1-32 ^{m,p,t} (human)	3.8 ^e (rat) 0.4-20.4 ^{a,m,p,t} (human)	No	-
P2X₃	0.776 ^e (rat) 14.9, 15.8, >100 ^{e,n,p,t} (human)	3.63 ^e (rat) 1.7-5.13 ^{e,n,t} (human)	No	-
P2X₄	>100 ^q (mouse) 178.1-200 ^{e,o,p} (human)	10.5 ^q (mouse) 10-25,27.5, >100 ^{a,o,p} (human)	No, >3 ^q (mouse)	Benzofuro-1,4- diazepin-2-ones
P2X₅	4.5 ^r (rat) 0.199 ^{p,t} (human)	2 ^r (rat) 0.01-0.3, 3.16 ^{p,t} (human)	No	-
P2X₆	No, >30 ^r (rat)	No, >30 ^r (rat) >0.3 ^t (human)	No	-
P2X₇	40 ^f (mouse) No, >100 ^{e,t} (human)	<i>Cation pore opening</i> 14.79 ^a (mouse) 3.24 ^a (human) <i>Large pore formation</i> 7, 9, >100 ^{a,b} (mouse) 0.015 ^b (human)	<i>Cation pore opening</i> 0.389 ^a (mouse) 0.38 ^a (human) <i>Large pore formation</i> 0.18, 1.17 ^{a,b} (mouse) 0.011 ^b (human)	1A-438079** 1A-740003** A-804590 GSK314181A AZ11645373 1AZ10606120
P2X_{2/3}	33.1 ^e (rat)	1.26 ^e (rat) 16.6 ^a (human)	No	A-317491 RO-3
P2X_{1/5}	1.58 ^p (rat)	0.5-8.6 ^h (mouse)	No	-
P2X_{4/6}	Some activity ^u (rat)	Some activity ^u (rat)	No	-

Numbers represent IC₅₀ values, in uM.

Murine data is presented where available.

** : antagonists with good oral bioavailability

References:

a (Donnelly-Roberts et al., 2009), **b** (Chessell et al., 1998), **e** (Bianchi et al., 1999), **f** (Watano et al., 2002), **g** (Ikeda, 2007), **h** (Lalo et al., 2008), **m** (Lynch et al., 1999), **n** (Garcia-Guzman et al., 1997a), **o** (Garcia-Guzman et al., 1997b), **p** (Gever et al., 2006), **q** (Jones et al., 2000), **r** (Collo et al., 1996), **s** (Jarvis and Khakh, 2009), **t** (Burnstock and Knight, 2004), **u** (Le et al., 1998a)

Table 4-5: Antagonists at P2Y receptors

	Suramin	PPADS	MRS-2179	Highly selective antagonists ^b
P2Y₁	Effective at 100uM ^d (mouse) 1.67 ^t (turkey) 3.16 ^a (human)	Effective at 30uM ^d (mouse) 1.05 ^t (turkey) 2 ^b (human)	Effective at 10uM ^{f,g} (mouse) 0.015-0.331 ^{f,h,p,q,u} (human)	MRS-2279 MRS-2179 MRS-2500 A3P5P
P2Y₂	47.86 ^t (human)	No ^{b,t} (human)	No ^{a,s,u}	AR-C126313 MRS-2576
P2Y₄	No ^{n,o} (mouse/human)	45 ⁿ (mouse) 15 ^o (human)	No ^{a,s,u}	MRS-2577
P2Y₆	Effective at 100uM ^d (mouse)	Effective at 30uM ^d (mouse)	No ^{a,s,u}	MRS-2578 MRS-2575
P2Y₁₂	3.6 ^t (human)	No ^r (human)	No ^{a,s}	MeSAMP AZD6140 INS50589 Clopidogrel
P2Y₁₃	2.3 ^e (human)	11.7 ^c (human)	>100 ^e (human)	MRS-2211

Numbers represent IC₅₀ values, in uM.

Murine data is presented where available.

References:

a (Fischer and Krugel, 2007), **b** (Donnelly-Roberts et al., 2009), **d** (Calvert et al., 2004), **e** (Marteau et al., 2003), **f** (Baurand et al., 2001), **g** (Atterbury-Thomas et al., 2008), **h** (Jacobson et al., 2009), **n** (Suarez-Huerta et al., 2001), **o** (Communi et al., 1996b), **p** (Waldo and Harden, 2004), **q** (Moro et al., 1998), **r** (Abbracchio et al., 2006), **t** (Charlton et al., 1996b), **u** (Boyer et al., 1998)

Objectives

The aim of these experiments was to investigate functional glutamate and P2 receptor expression on cultured cortical astrocytes and neurons. There is a relative lack of data about the functional P2 receptor expression profile of murine cortical cells. Extracellular concentrations of glutamate and ATP are raised during CNS ischaemia, so ionotropic glutamate receptors and P2 receptors activated by ATP and/or ADP are of particular interest. Intracellular Ca^{2+} accumulation during ischaemia is pivotal to excitotoxicity, so demonstration of P2 and glutamate receptors which produce intracellular Ca^{2+} elevations in these cells was a further objective (Pringle, 2004).

RESULTS

Functional glutamate and P2 receptor expression was investigated using Ca^{2+} fluorimetry. Cultures of either neurons or astrocytes were loaded with Fura-2 and subjected to short bursts of a variety of P2 and glutamate receptor agonists. Agonists were applied for 20 second bursts with 5 minutes between each agonist application. In all experiments data is presented showing the percentage of total Fura-2 loaded cells which exhibited a rise in $[\text{Ca}^{2+}]_i$ and the average maximum calibrated $[\text{Ca}^{2+}]_i$ response (avg $\Delta\text{max} [\text{Ca}^{2+}]_i$, shown in nM concentration) of all the cells that responded to any particular agonist. The latter values were calculated by subtracting the resting $[\text{Ca}^{2+}]_i$ from the maximum $[\text{Ca}^{2+}]_i$ reached after every agonist application for each individual cell, as there were significant variations between experiments/conditions and cell-types in terms of the resting $[\text{Ca}^{2+}]_i$ (**Figure 4-0**). When antagonists were applied, their effects on the avg $\Delta\text{max} [\text{Ca}^{2+}]_i$ responses are also presented as a percentage of the normal agonist response (% of control). Representative $[\text{Ca}^{2+}]_i$ recordings for individual cells in each experiment are shown, as well as example images of Fura-2 340:380 fluorescence from some experiments. In addition, a compact disc containing videos of sample experiments is included, each accelerated to last about 1 minute. These show pseudo-colour images of $[\text{Ca}^{2+}]_i$ levels with accompanying embedded text narrating which agonists are being applied, and are best viewed using windows media player. Relatively high concentrations of the different agonists (100uM for all except MRS-2365) were applied to ensure a maximal activation of any receptors (Fischer et al., 2009).

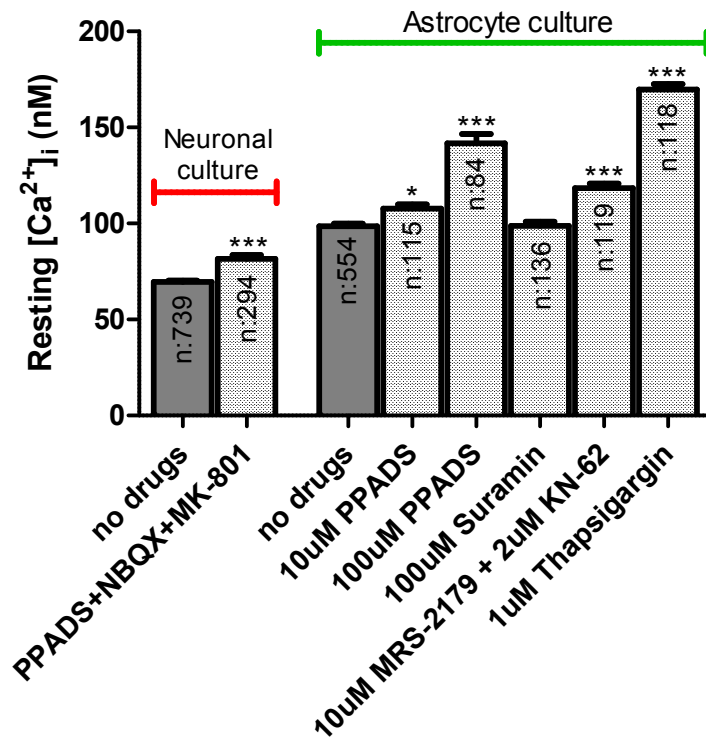


Figure 4-0: Resting [Ca²⁺]_i levels in cultured neurons and astrocytes

Resting [Ca²⁺]_i levels were significantly raised in the astrocyte culture compared to the neuronal culture ($p < 0.001$). They were also significantly ($p < 0.05$) affected by all the combinations of drugs that were used (all applied for 60 minutes), with Suramin in astrocytes being the exception. It is for this reason that [Ca²⁺]_i changes in response to agonist application are always reported as maximum [Ca²⁺]_i reached after stimulation minus the preceding resting [Ca²⁺]_i (avg Δ max [Ca²⁺]_i) rather than actual maximum [Ca²⁺]_i.

n: total number of cells

*: $p < 0.05$

***: $p < 0.001$

Glutamate receptors on cultured cortical neurons

To confirm the presence of NMDA and AMPA type glutamate receptors, cortical neuron cultures were sequentially exposed to 100uM glutamate, 100uM AMPA and 100uM NMDA + 10uM glycine, initially in the presence of 2mM Mg^{2+} (see **Figure 4-1: B1-B4** for example images of Fura-2 340:380 fluorescence, **Figure 4-2: A1-A3** for representative recordings of single cell $[Ca^{2+}]_i$ and **Video 1** for a full-length example experiment). Under these conditions $94.51 \pm 3.8\%$ of cells responded to glutamate, $81.79 \pm 7.8\%$ of cells responded to AMPA, and $62.45 \pm 10.3\%$ of cells responded to NMDA + glycine (**Figure 4-2: C**) (n:7 coverslips, 266 cells), with avg $\Delta_{max} [Ca^{2+}]_i$ responses of 365.4 ± 9 (n:552 cells), 190 ± 9.6 (n:222 cells) and $185.6 \pm 11.2nM$ (n:173 cells) respectively (**Figure 4-2: D**).

To make sure that repeated agonist induced glutamate receptor activation in itself was not responsible for the relative reduction in sequential Ca^{2+} responses, the same cells were subjected to 100uM glutamate application again at the end of the sequence (**Figure 4-2: A1-A3**). This second glutamate application activated exactly the same number of cells as the first one ($94.51 \pm 3.8\%$, n:7 coverslips, 266 cells) (**Figure 4-2: C**) and produced only slightly different ($p > 0.05$) avg $\Delta_{max} [Ca^{2+}]_i$ responses ($376 \pm 12.4nM$, n:252 cells) (**Figure 4-2: D**).

One would expect the vast majority of neurons to respond to glutamate, and the simplest explanation for the 5.5% percent of cells not showing a response was that the Mg^{2+} in the buffer solution was preventing some NMDA receptor mediated responses. To unmask these, the experiment was repeated using solutions containing zero Mg^{2+} (see **Figure 4-1: A1-A4** for example images of Fura-2 340:380 fluorescence, **Figure 4-2: B1+B2** for representative recordings of single cell $[Ca^{2+}]_i$ and **Video 2** for a full-length example experiment). 100% of neurons now responded to glutamate (n:3 coverslips, 181 cells), with $95.58 \pm 2\%$ of cells responding to AMPA and $95.37 \pm 4\%$ of cells responding to NMDA + glycine (n:4 coverslips, 229 cells for both) (**Figure 4-2: C**). Additionally, the avg $\Delta_{max} [Ca^{2+}]_i$ responses for both glutamate ($457 \pm 15nM$, n:181 cells) and NMDA +

glycine ($289.7 \pm 10.9\text{nM}$, n:220 cells), but not AMPA ($207.8 \pm 8.6\text{nM}$, n:220 cells), were significantly increased ($p < 0.001$ for both) in zero Mg^{2+} compared with 2mM Mg^{2+} (**Figure 4-2: E**). These results confirm the presence of functional AMPA and NMDA receptors on cultured cortical neurons in this preparation.

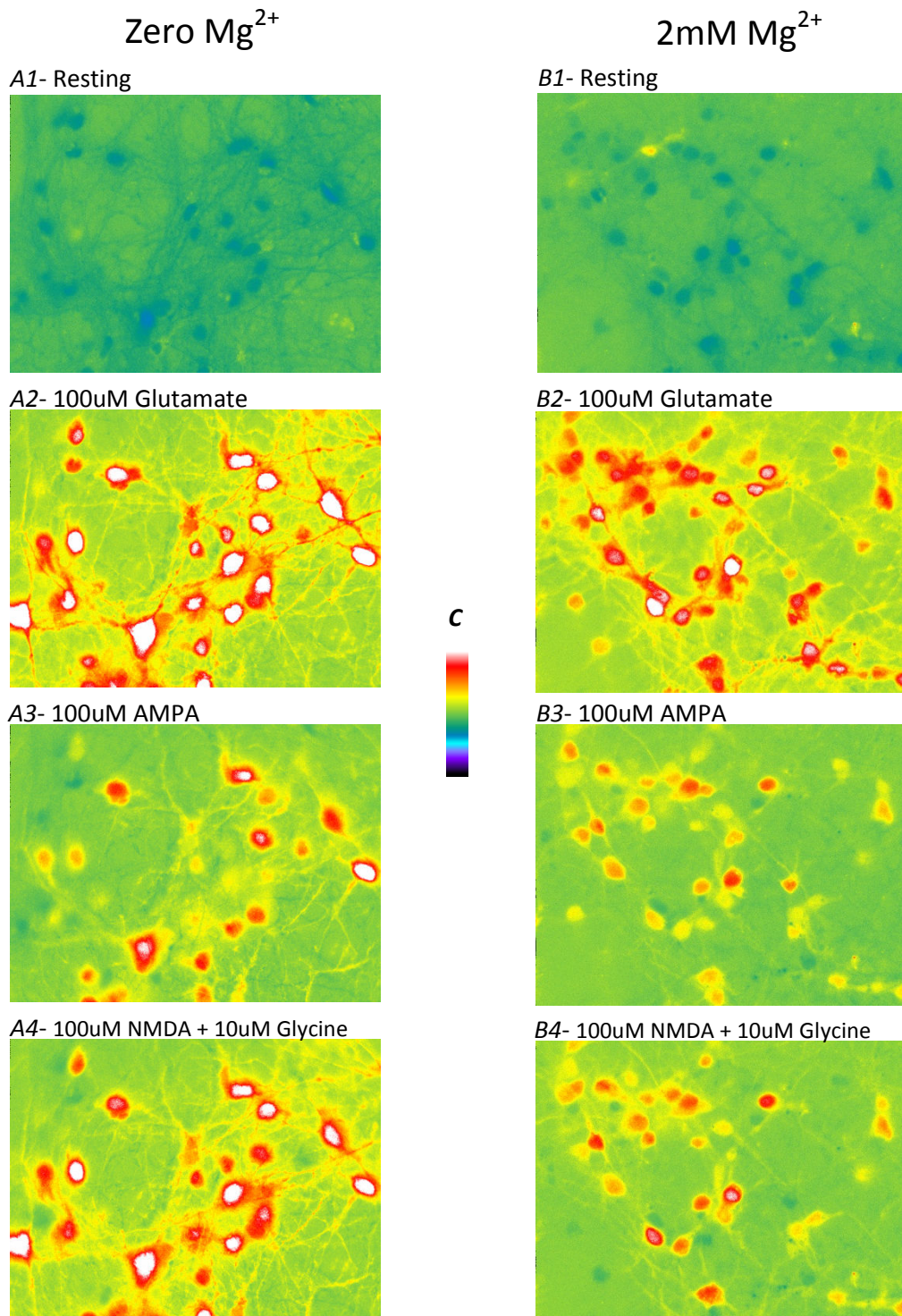


Figure 4-1: Fura-2 Ca^{2+} imaging of neuronal culture, glutamate receptor agonists
 Example images of pseudocolour Ca^{2+} fluorescence (340:380) in Fura-2 loaded neuronal culture subjected to the application of 100uM glutamate, 100uM AMPA, and 100uM NMDA + 10uM Glycine in either the absence (*A1-A4*) or presence of 2mM Mg^{2+} (*B1-B4*).

All cells respond to glutamate with an increase in $[\text{Ca}^{2+}]_i$ (*A2, B2*).
 In the presence of 2mM Mg^{2+} there is a reduced $[\text{Ca}^{2+}]_i$ response to NMDA (*B4*), compared with 0 Mg^{2+} (*A4*). AMPA elicits a similar response under both conditions (*A3, B3*)

C: Pseudocolour scale of fluorescence intensity

Figure 4-2: Functional glutamate receptors on cultured cortical neurons

These experiments were designed to investigate functional glutamate receptor expression in the neuronal culture, more specifically NMDA and AMPA receptors.

A1-B2: Sample recordings of $[Ca^{2+}]_i$ obtained from individual cells.

Cell **A1** is an example of the most commonly seen profile for cultured cortical neurons, with definite and large responses to glutamate, AMPA and NMDA + glycine. The cells in **A2** and **A3** seem to be lacking AMPA and NMDA receptor responses respectively. This was uncommon.

Cells **B1** and **B2** demonstrate the effects of removing Mg^{2+} from the perfusing solutions. The size of both the glutamate and NMDA + glycine induced $[Ca^{2+}]_i$ changes are larger.

C- Percent of cells in the neuronal culture responding to agonists

The majority of cultured cortical neurons expressed functional AMPA and NMDA receptors. As the agonists were applied sequentially a final repeated glutamate application was performed to make sure that responses were not diminishing due to repeated receptor activation.

The removal of Mg^{2+} from perfusing solutions to prevent Mg^{2+} induced NMDA receptor blockade increased the percentage of cells responding, but not significantly ($P > 0.05$).

n: number of coverslips

D- Size of $[Ca^{2+}]_i$ responses

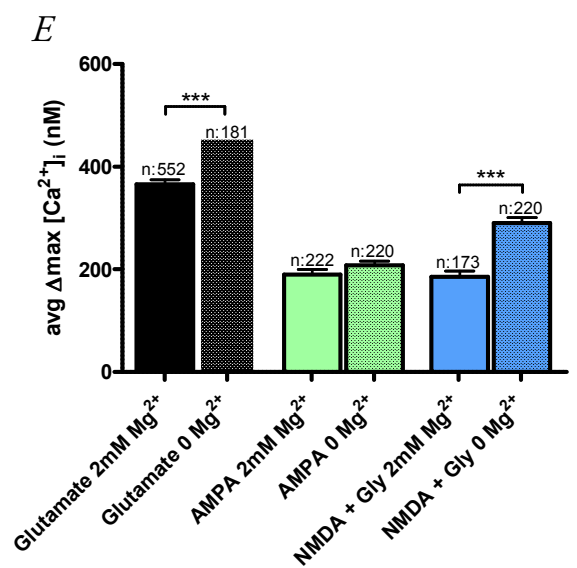
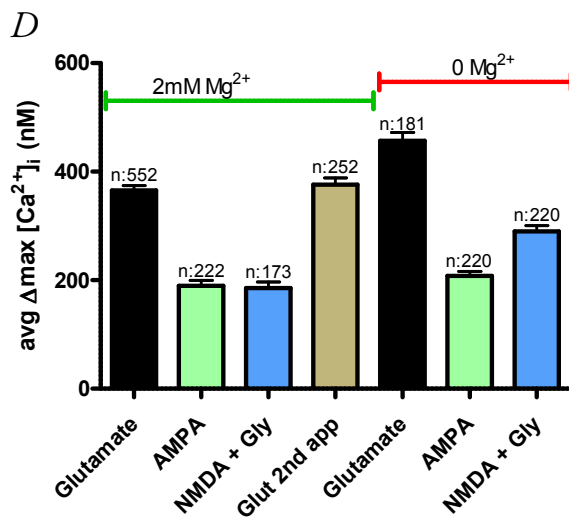
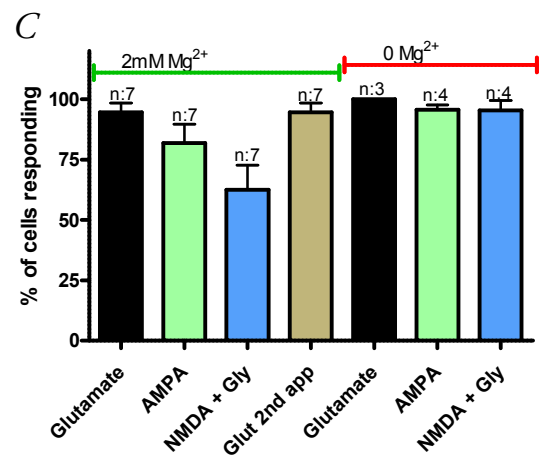
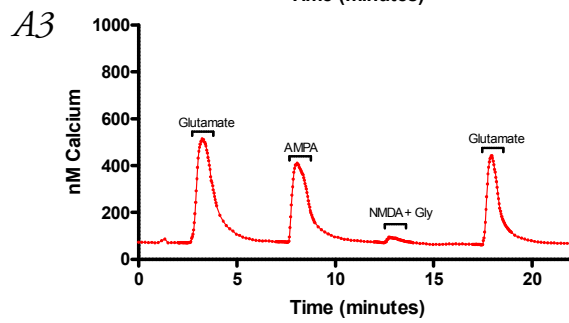
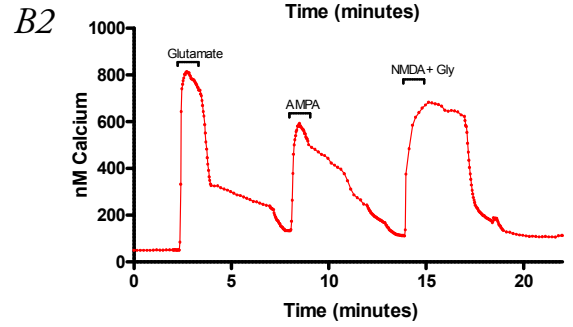
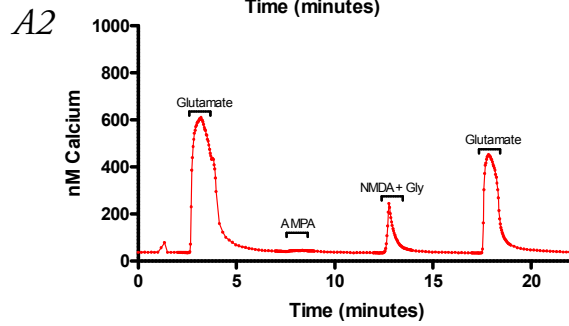
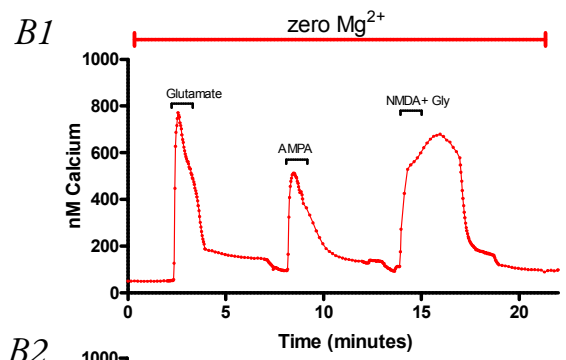
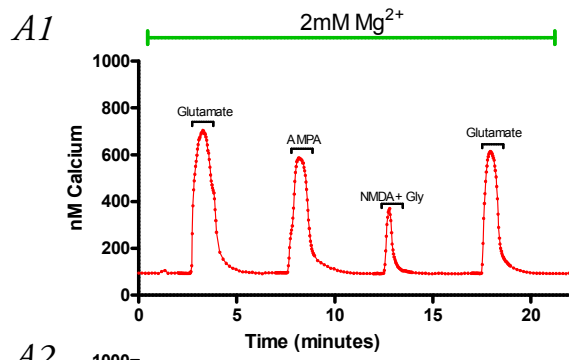
The average maximum increases in $[Ca^{2+}]_i$ (in nM) elicited by the different glutamate receptor agonists. As expected there is always a significantly ($p < 0.001$) greater $\Delta[Ca^{2+}]_i$ with glutamate than with either of AMPA or NMDA + glycine application alone.

n: total number of cells responding

E- Effect of Mg^{2+} removal on size of $[Ca^{2+}]_i$ responses

There was a significantly greater $\Delta[Ca^{2+}]_i$ with both glutamate and NMDA + glycine but not AMPA application in the absence of Mg^{2+} ($p < 0.001$), further documenting the well known effects of Mg^{2+} induced NMDA receptor blockade.

n: total number of cells responding



P2 receptors on cultured cortical neurons

To investigate functional P2 receptor expression on cultured cortical neurons, cells were sequentially exposed to 100uM ATP, 100uM ADP, 100uM ATPgS, 10nM MRS-2365 and 100uM BzATP before a final application of 100uM glutamate to confirm that any non-responding cells were alive (see **Figure 4-3: A1 + A2** for representative recordings of single cell $[Ca^{2+}]_i$ and **Video 3** for a full-length example experiment). Over half of neurons responded to ATP ($57.85 \pm 4.2\%$), ADP ($52.69 \pm 4.9\%$), and ATPgS ($52.04 \pm 4.3\%$) (**Figure 4-3: B**) (n:7 coverslips, 293 cells). Additionally, MRS-2365 caused $[Ca^{2+}]_i$ rises in $32.51 \pm 7.7\%$ of cells while BzATP caused a response in $26.37 \pm 7.1\%$ of cells (**Figure 4-3: B**) (n:7 coverslips, 293 cells). The avg $\Delta_{max} [Ca^{2+}]_i$ responses for the P2 agonists (in nM Ca^{2+}) were 110.9 ± 4.6 for ATP (n:313 cells), 81.22 ± 4.5 for ADP (n:162 cells), 70.32 ± 4.5 for ATPgS (n:155 cells), 62.04 ± 4.8 for MRS-2365 (n:91 cells) and 56.91 ± 4.3 for BzATP (n:80 cells) (**Figure 4-3: C**). These Ca^{2+} responses were significantly smaller than those seen with the application of glutamate ($p < 0.001$). All cells responded to glutamate application at the end of the experiments.

The most commonly seen pattern in these experiments was one where the cell would either respond to most or all of the P2 agonists (**Figure 4-3: A1**) or none of them at all (**Figure 4-3: A2**), suggesting possible separate populations of purinergic and non-purinergic neurons within the cell culture.

Figure 4-3: Functional P2 receptors on cultured cortical neurons

This experiment was designed to investigate for the presence of functional P2 receptors on cells in the cortical neuron culture. Glutamate was applied at the end of every P2 agonist experiment to confirm that any non-responding cells were healthy neurons.

A1+A2: Sample recordings of $[Ca^{2+}]_i$ obtained from individual cells.

Cell **A1** responds to all of the agonists that were applied, although there is only a very small response to BzATP.

Cell **A2** did not respond to any of the P2-receptor agonists, but was responsive to glutamate.

These were the most commonly seen patterns, where a cell was either responsive to most or all of the P2 agonists or was not responsive to any of them, suggesting that there were separate populations of purinergic and non-purinergic neurons.

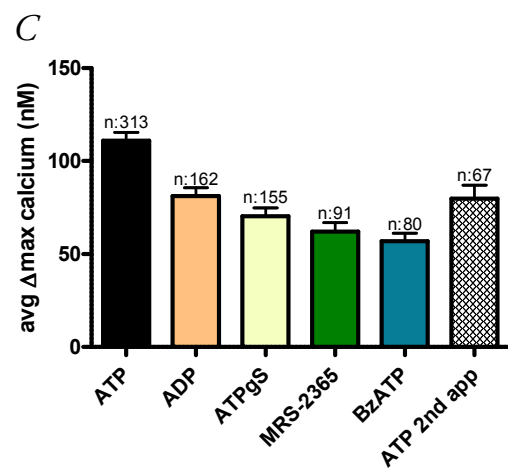
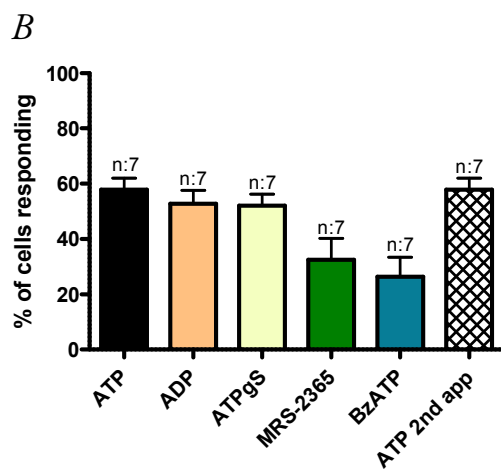
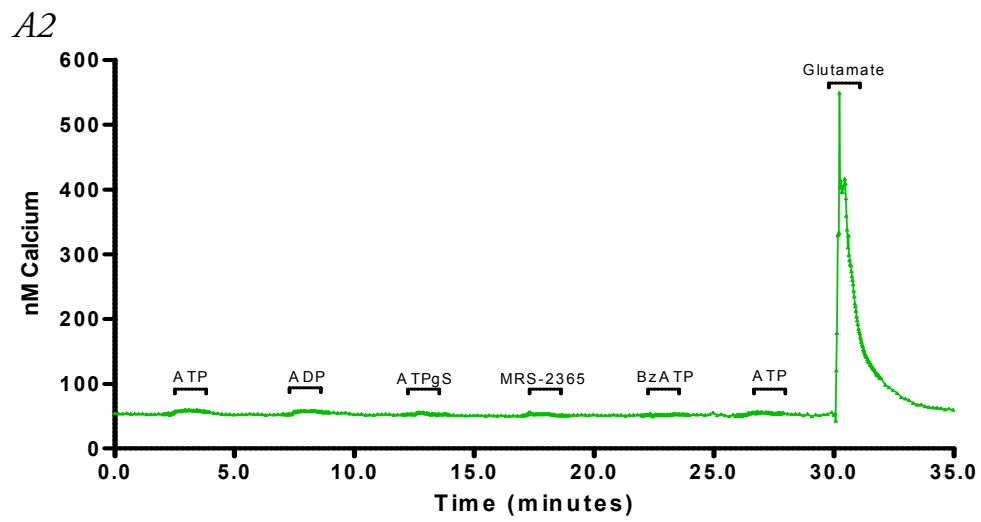
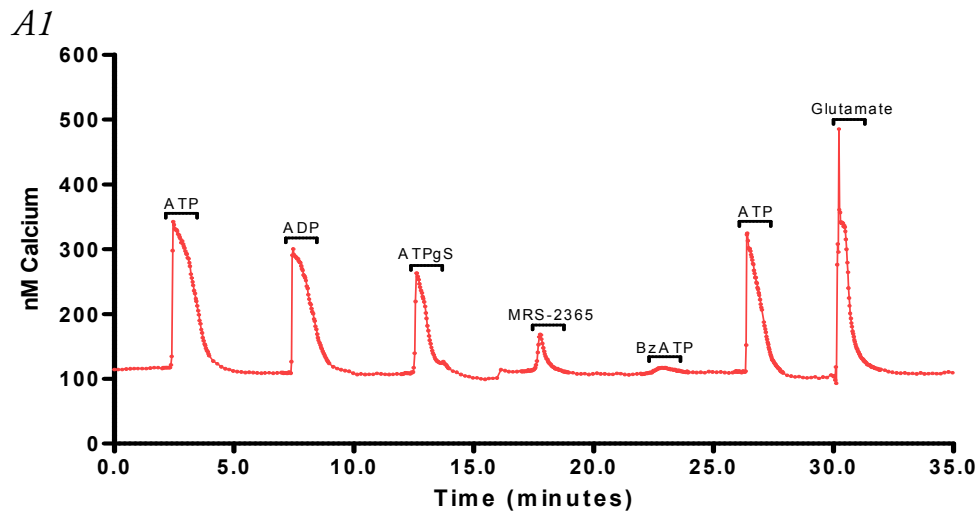
B- Percent of cells in the neuronal culture responding to agonists

Over half of neurons responded to ATP, ADP, and the non-hydrolysable ATP analogue ATP γ S. Additionally, the P2Y₁ agonist MRS-2365 caused calcium rises in over 30% of cells while BzATP only caused a response in just over a quarter of cells.

C- Size of $[Ca^{2+}]_i$ responses

The average maximum increases in $[Ca^{2+}]_i$ (in nM) elicited by the different P2 receptor agonists.

Compared to any glutamate receptor agonists (see **Figure 4-2: D**), the avg $\Delta_{max} [Ca^{2+}]_i$ induced by P2 receptor agonists was much smaller in these neurons.



P2 receptors on cultured cortical astrocytes

To confirm the presence of P2 receptors on cultured cortical astrocytes, cells were sequentially exposed to 100uM ATP, 100uM ADP, 100uM ATPgS, 10nM MRS-2365 and 100uM BzATP (see **Figure 4-4: A1-A6** for example images of Fura-2 340:380 fluorescence, **Figure 4-5: A1 + A2** for representative recordings of single cell $[Ca^{2+}]_i$ and **Video 4** for a full-length example experiment). Functional P2 receptors were present on all cultured cortical astrocytes, with 100% of cells responding to ATP (n:14 coverslips, 438 cells), ADP and ATPgS (both n:7 coverslips, 220 cells), $98.94 \pm 0.7\%$ to MRS-2365 (n:7 coverslips, 220 cells) and $99.56 \pm 0.4\%$ to BzATP (n:6 coverslips, 187 cells) (**Figure 4-5: B**). Contrary to what occurred in the neuronal culture, the avg $\Delta_{max} [Ca^{2+}]_i$ responses were large, with some individual cells reaching $[Ca^{2+}]_i$ levels in the low micromolar range. ATP was the most powerful agonist, with subsequently applied agonists inducing lower $[Ca^{2+}]_i$ rises (**Figure 4-5: C**). The values were (in nM Ca^{2+}) 722.9 ± 29.2 for ATP (n:341 cells), 538.8 ± 19.2 for ADP, 452.1 ± 19.6 for ATPgS (both n:220 cells), 313.7 ± 16.1 for MRS-2365 (n:218 cells) and 328.3 ± 15.2 for BzATP (n:186 cells).

ATP was re-applied at the end of the sequence to make sure that there was no run-down of Ca^{2+} responses due to repeated receptor activation. Unfortunately this did seem to be the case, with a significant reduction ($p < 0.001$) in the avg $\Delta_{max} [Ca^{2+}]_i$ of the ATP application at the end of the sequence compared with the first one. To further investigate this 100uM ATP was applied six times in sequence using the same timings and protocols as above (see **Figure 4-6: A**). This experiment showed that there were significant ($p < 0.05$) reductions in the avg $\Delta_{max} [Ca^{2+}]_i$ following the sequential ATP applications, specifically when comparing the first application with the last four, and this did not recover fully even when an extra 3 minutes were added to the washout time (8 minutes total) before the last application (**Figure 4-6: B**). I performed one experiment in which I left a gap of 25 minutes between ATP applications, and in this case avg $\Delta_{max} [Ca^{2+}]_i$ responses did recover fully. However this sort of protocol was not practicable, as the astrocyte cultures lost their Fura-2 fluorescence during longer experiments.

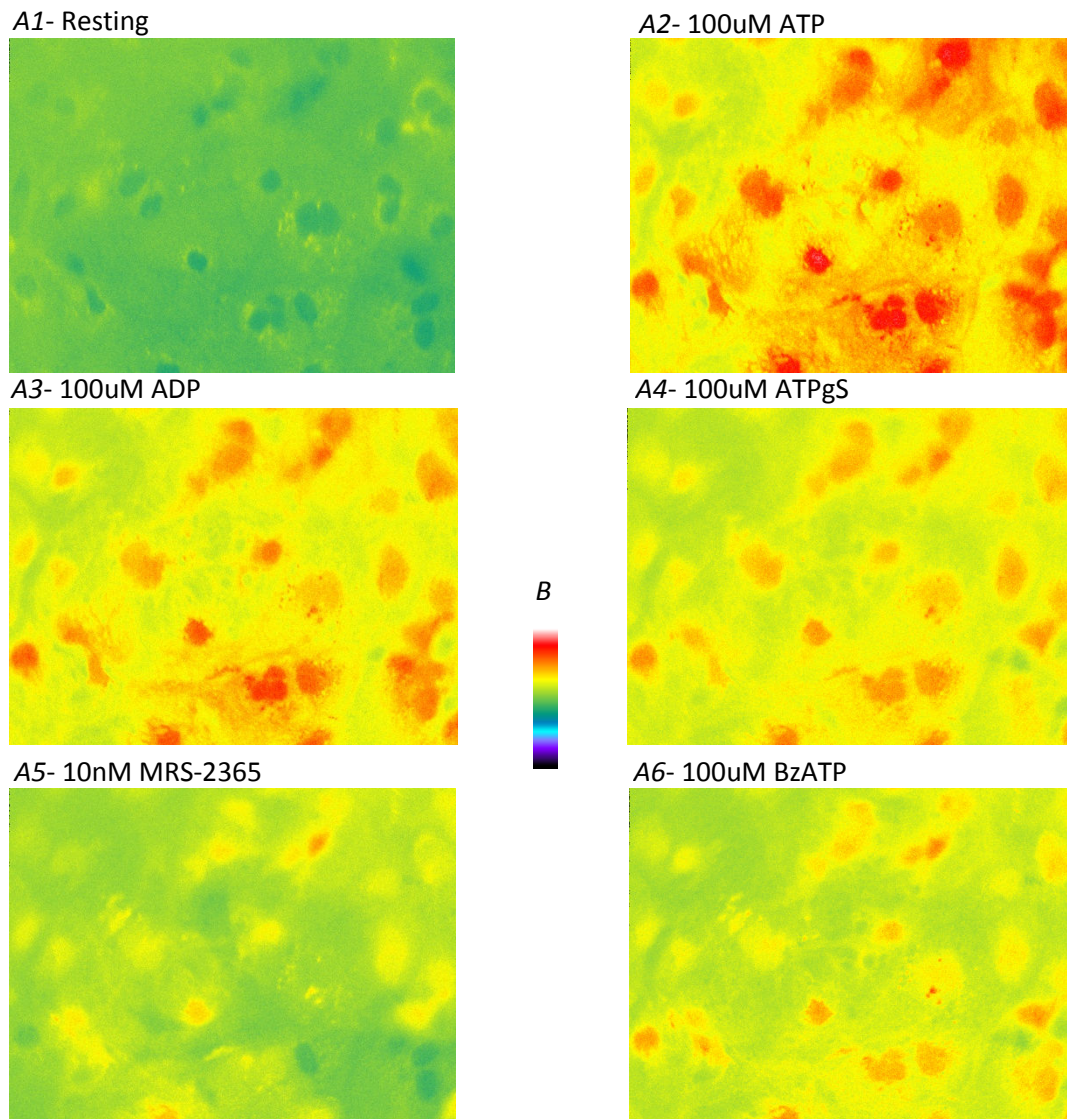


Figure 4-4: Fura-2 Ca^{2+} imaging of astrocyte culture, P2 receptor agonists

Example images of pseudocolour Ca^{2+} fluorescence (340:380) in a Fura-2 loaded astrocyte culture (**A1**) subjected to the application of 100uM ATP, 100uM ADP, and 100uM ATPgS, 10nM MRS-2365 and 100uM BzATP (**A2-A6**).

On this slide, all cells respond to ATP, ADP, ATPgS and BzATP with an increase in $[\text{Ca}^{2+}]_i$ (**A2, A3, A4, A6**). Most cells also responded to MRS-2365 (**A5**).

B: Pseudocolour scale of fluorescence intensity

Figure 4-5: Functional P2 receptors on cultured cortical astrocytes

Here data is presented which shows that functional P2 receptors were present on all cultured cortical astrocytes.

A1+A2: Sample recordings of $[Ca^{2+}]_i$ obtained from individual cells.

Cell **A1** was very much representative of the vast majority of astrocytes, with large $[Ca^{2+}]_i$ increases in response to all P2 receptor agonists and only a very small glutamate induced Ca^{2+} response.

Cell **A2** also showed a more robust response to glutamate, which was unusual.

B- Percent of cells in the astrocyte culture responding to agonists

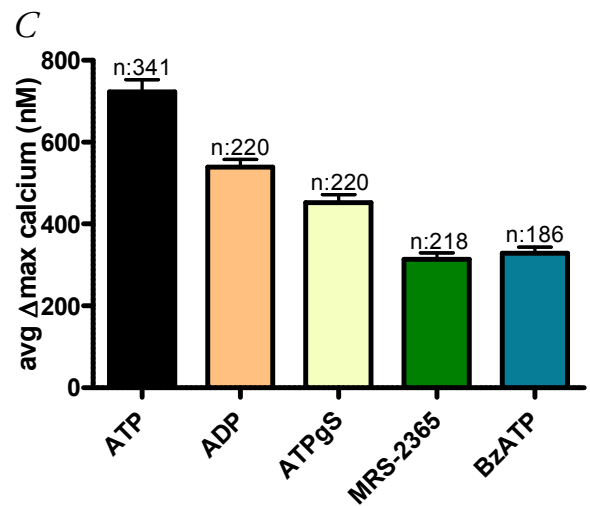
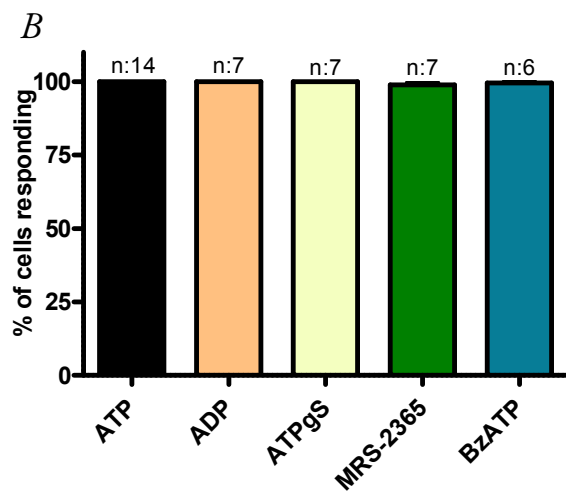
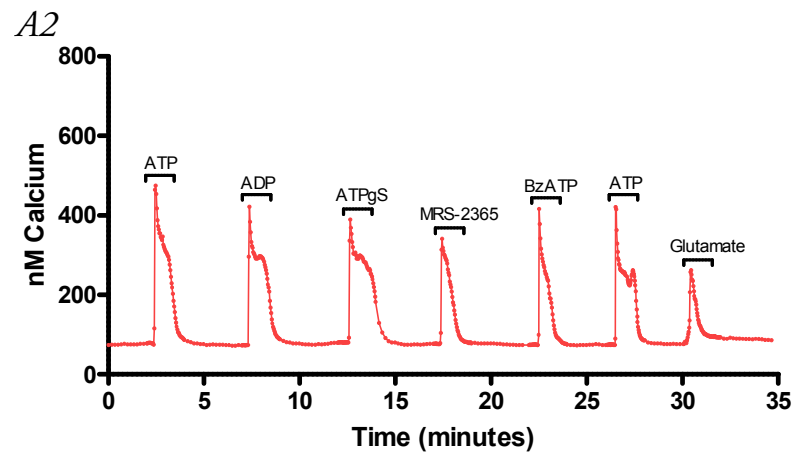
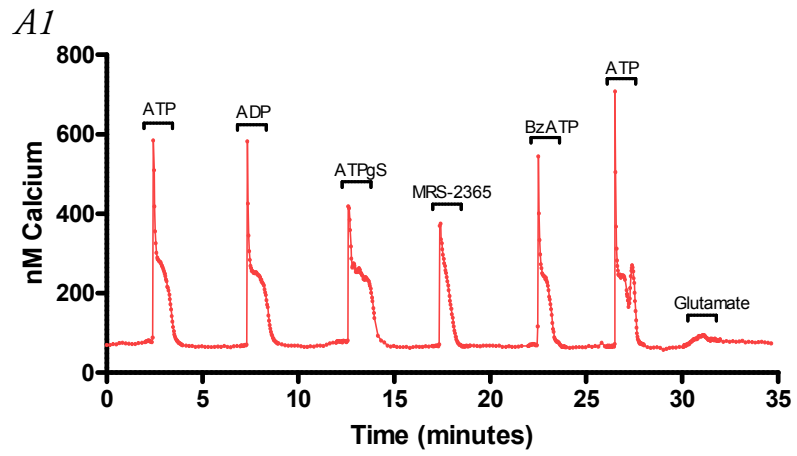
100% of cells in the astrocyte cultures responded to ATP, ADP and ATPgS, with $98.94 \pm 0.7\%$ responding to MRS-2365 and $99.56 \pm 0.44\%$ to BzATP.

n: number of coverslips

C- Size of $[Ca^{2+}]_i$ responses

The average maximum increases in $[Ca^{2+}]_i$ (in nM) elicited by the P2 receptor agonists. The Ca^{2+} responses were large, with some individual cells even reaching $[Ca^{2+}]_i$ in the low micromolar range. ATP was the most powerful agonist with subsequently applied agonists inducing lower $[Ca^{2+}]_i$ rises.

n: total number of cells responding



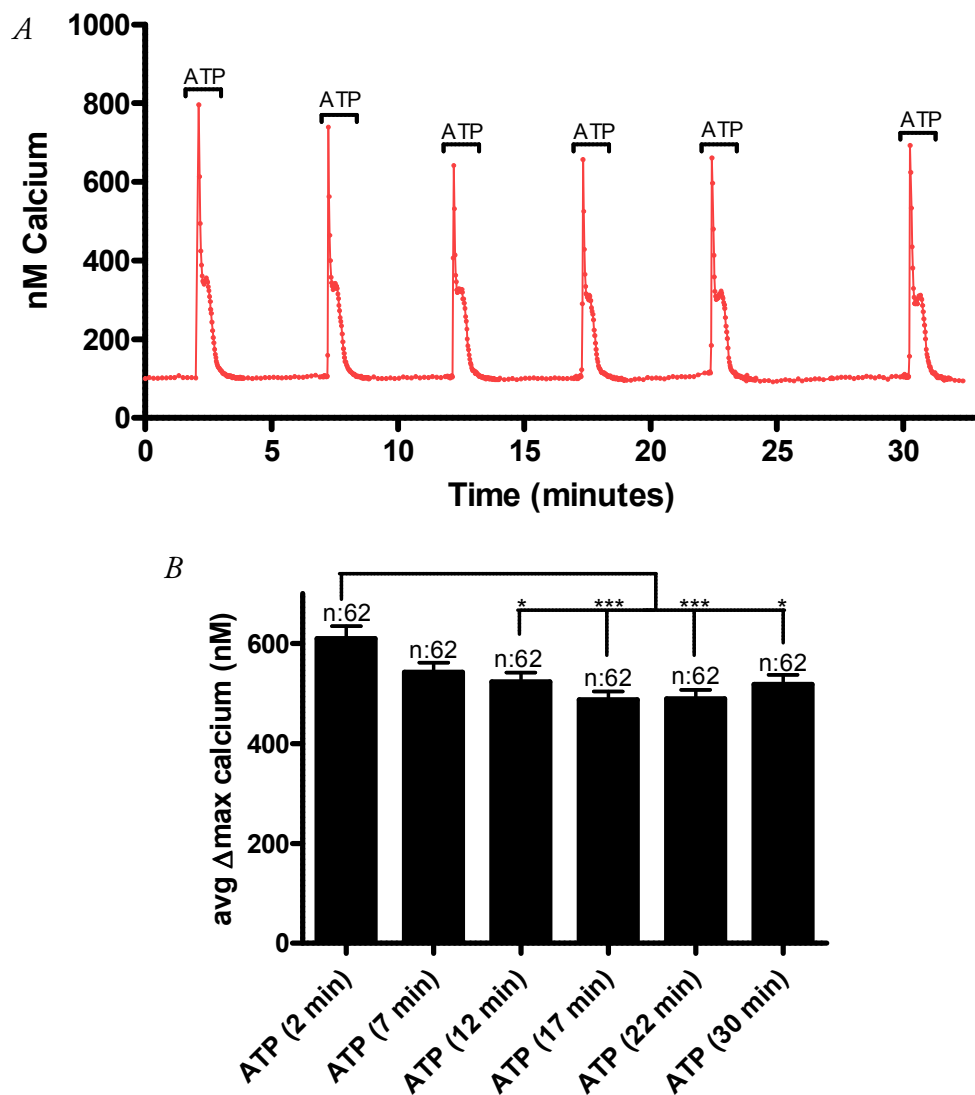


Figure 4-6: Multiple sequential applications of ATP

To investigate whether frequent P2 receptor activation itself may cause Ca^{2+} responses to decrease in size, six sequential applications of 100 μM ATP were performed on Fura-2 loaded astrocyte cultures.

A: Sample recording of $[\text{Ca}^{2+}]_i$ obtained from an individual cell.

B- Size of $[\text{Ca}^{2+}]_i$ responses

There were significant reductions in the average maximum increases in $[\text{Ca}^{2+}]_i$ following sequential ATP applications when comparing the first application with subsequent ones.

Values (in nM Ca^{2+})

1st application: 610 ± 24.1, 2nd: 542.2 ± 19.3, 3rd: 523.4 ± 17.95, 4th: 487.3 ± 16.23, 5th: 489.2 ± 17.76, 6th: 518.1 ± 19.19

(n: 62 cells, 2 coverslips)

*: p<0.05

***: p<0.001

A Ca^{2+} removal experiment was designed to further elucidate whether astrocytes were expressing P2Y or P2X receptors and in what proportion they were present (see **Figure 4-7: A** for a representative recording of single cell $[\text{Ca}^{2+}]_i$ and **Video 5** for a full-length example experiment). Cells were incubated with 1 μM thapsigargin, an inhibitor of the sarcoplasmic/endoplasmic reticulum Ca^{2+} -ATPase (SERCA) in normal aCSF + hepes for one hour to deplete intracellular Ca^{2+} stores, which should theoretically prevent P2Y receptor mediated $[\text{Ca}^{2+}]_i$ rises (Centemeri et al., 1997). The first ATP and ADP applications were performed with thapsigargin and 2mM Ca^{2+} present, so any ionotropic receptor mediated Ca^{2+} changes should still occur. Then a solution containing zero Ca^{2+} + 50 μM EGTA + thapsigargin was used. This should completely inhibit any Ca^{2+} responses at all, confirming that those still present before were indeed mediated by P2X receptors and not by incomplete depletion of intracellular Ca^{2+} stores. For statistics, avg $\Delta\text{max} [\text{Ca}^{2+}]_i$ responses to ATP and ADP measured in **Figure 4-5** were used as controls.

After pre-incubation with thapsigargin $60.06 \pm 13.04\%$ of cells responded to ATP (n:3 coverslips, 118 cells), a significant ($p < 0.001$) reduction compared with controls, suggesting that a high percentage of ATP-induced $[\text{Ca}^{2+}]_i$ rises were P2Y receptor mediated (**Figure 4-7: B**). Removal of extracellular Ca^{2+} abolished all remaining ATP-induced $[\text{Ca}^{2+}]_i$ rises ($p < 0.001$ compared with thapsigargin alone), suggesting that about 60% of astrocytes were expressing functional P2X receptors (**Figure 4-7: B**). However, P2X receptors seemed to only mediated a very small proportion of the overall avg $\Delta\text{max} [\text{Ca}^{2+}]_i$ mediated by the application of ATP, with a reduction in avg $\Delta\text{max} [\text{Ca}^{2+}]_i$ after thapsigargin pre-incubation to $52.94 \pm 2.27\text{nM}$ (n:75 cells) (**Figure 4-7: C**). ADP should only activate P2Y receptors, and therefore thapsigargin preincubation should prevent any ADP induced $[\text{Ca}^{2+}]_i$ rises. A small proportion of cells ($9.85 \pm 9.85\%$, n:3 coverslips, 118 cells) (**Figure 4-7: B**) still responded with very small $[\text{Ca}^{2+}]_i$ rises (only $20.07 \pm 3.01\text{nM}$ Ca^{2+} , n:9 cells) (**Figure 4-7: C**), suggesting that there may have been incomplete depletion of intracellular Ca^{2+} stores, some contamination of the ADP with ATP, or that small amounts of ATP were produced *in situ* by enzymatic activity from ADP. Looking closely at the data, all ADP induced $[\text{Ca}^{2+}]_i$ increases were in one experiment, the one where the

cells had spent least time in thapsigargin, so incomplete depletion of stores seems to be the most likely explanation. These results suggest that P2Y receptors are the main mediators of ATP-induced $[Ca^{2+}]_i$ rises in cultured cortical astrocytes.

Figure 4-7: Ca²⁺ removal experiments

This experiment was designed to further elucidate whether the astrocytes are expressing functional metabotropic P2Y or ionotropic P2X receptors and in what proportion they are present.

Cells were initially incubated with 1 μ M thapsigargin (a SERCA inhibitor) for one hour to deplete intracellular Ca²⁺ stores, which should theoretically prevent P2Y receptor mediated [Ca²⁺]_i changes caused by either ATP or ADP. The first ATP and ADP applications were done with 2mM Ca²⁺ present, so any ionotropic receptor mediated [Ca²⁺]_i changes should still occur. Then a solution containing zero Ca²⁺ + 50 μ M EGTA was used. This should completely inhibit any Ca²⁺ responses at all and confirm that those still present before were indeed mediated by ionotropic P2X receptors and not by incomplete depletion of intracellular Ca²⁺ stores.

A: Sample recording of [Ca²⁺]_i obtained from an individual cell.

There was a small [Ca²⁺]_i rise with ATP application in the presence of thapsigargin and 2mM Ca²⁺, as well as a sudden drop in the 340:380 Fura-2 signal when the solution was switched to the one containing zero Ca²⁺ + EGTA.

B- Percent of cells in the astrocyte culture responding to agonists

60.06 \pm 13.04% of cells were still responding to ATP after thapsigargin (p<0.001 compared with no thapsigargin preincubation) while none did when extracellular Ca²⁺ was also removed (p<0.001), suggesting that these cells were expressing functional P2X receptors. ADP should only activate P2Y receptors and therefore thapsigargin preincubation should prevent any [Ca²⁺]_i rises. However 9.85 \pm 9.85% of cells still responded.

Removing extracellular Ca²⁺ abolished all responses.

n: number of coverslips

C- Size of [Ca²⁺]_i responses

P2X receptors seem to mediate a small proportion (only 52.94 \pm 2.27nM) of the overall [Ca²⁺]_i increase seen by the application of ATP (p<0.001 compared with no thapsigargin preincubation).

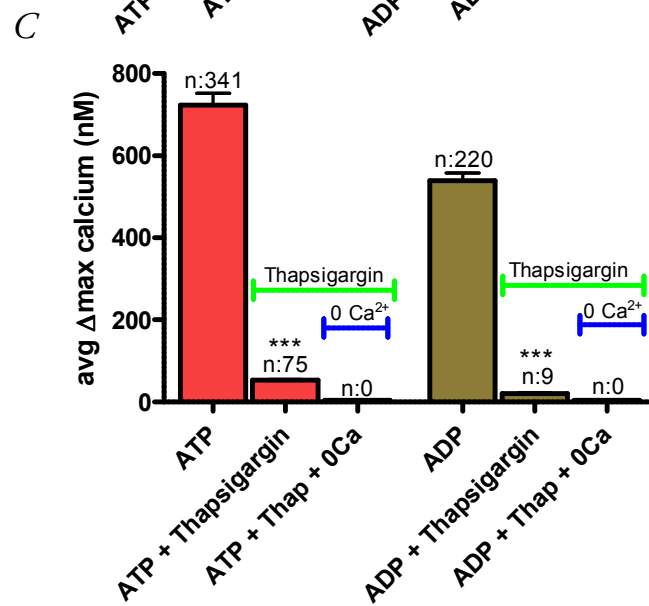
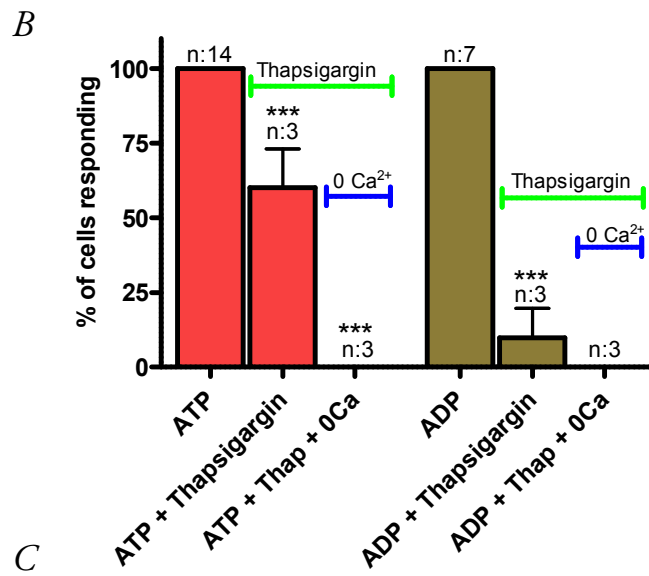
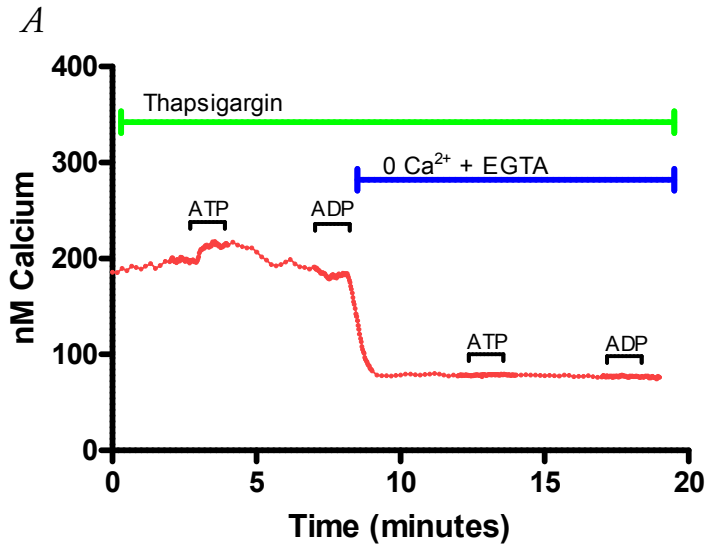
ADP induced an avg Δ max [Ca²⁺]_i rise of 20.07 \pm 3nM.

Removing extracellular Ca²⁺ abolished all responses.

n: total number of cells responding

These results suggest that P2Y receptors are the main mediators of ATP induced intracellular calcium rises in cultured cortical astrocytes.

***. p<0.001



To further characterise the P2Y receptor profile in these astrocytes, cultures were produced from P2Y₁ knock-out mice (-/-) and subjected to the sequential application of 100uM ATP, 100uM ADP and 10nM MRS-2365 (see **Figure 4-8: A1 + A2** for representative recordings of single cell [Ca²⁺]_i and **Video 6** for a full-length example experiment). In P2Y₁ -/- astrocytes there was a significant decrease in the avg Δmax [Ca²⁺]_i response to both ATP (509.1 ± 25.7, n:75 cells) (p<0.001) and ADP (134.3 ± 11.4, n:43 cells) (P<0.001) compared to P2Y₁+/+ astrocytes as well as a complete lack of responses to MRS-2365 (**Figure 4-8: C**), confirming the P2Y₁ selectivity of this agonist. All cells responded to ATP, but there were significantly reduced numbers of cells responding to ADP (57.44 ± 10.34%) (p<0.001) compared with P2Y₁+/+ and none responded to MRS-2365 (n:4 coverslips for all) (**Figure 4-8: B**). These results confirm that P2Y₁ receptors mediate a significant proportion of both the ATP and ADP-induced [Ca²⁺]_i rises in these cultured astrocytes and that P2Y₆ receptors are also present since there were still responses to ADP in some P2Y₁ -/- cells. One other important observation from these experiments is that a number of P2Y₁ -/- cells (such as the one in **Figure 4-8: A2**) responded to ATP but not ADP, suggesting that contamination of ADP with ATP, a well-known problem with some commercially available ADP, was not occurring (Reifel Saltzberg et al., 2003).

Figure 4-8: P2Y₁^{-/-} astrocytes

This experiment was designed to give more insight into the P2Y receptor expression profile in cultured cortical astrocytes. Astrocytes were cultured from P2Y₁ knock-out mice (-/-) and subjected to applications of ATP, ADP and MRS-2365.

A1+A2: Sample recordings of [Ca²⁺]_i obtained from individual cells.

[Ca²⁺]_i traces representative of the two patterns of responses that were seen in these experiments. Neither **A1** nor **A2** showed responses to MRS-2365. **A1** had a small response to ADP while still maintaining large responses to ATP application, whilst **A2** only responded to ATP.

A2 provides evidence for the lack of contaminating ATP in the ADP, since the cell responded to ATP with a large [Ca²⁺]_i rise but not at all to ADP application.

B- Percent of cells in the astrocyte culture responding to agonists

All cells still responded to ATP, but compared with P2Y₁^{+/+} cultures there were significantly reduced numbers of cells responding to ADP (p<0.001) and none responding to MRS-2365. These results suggest that P2Y₁ receptors mediate a significant proportion of both the ATP and ADP-induced calcium rises in these cultured astrocytes.

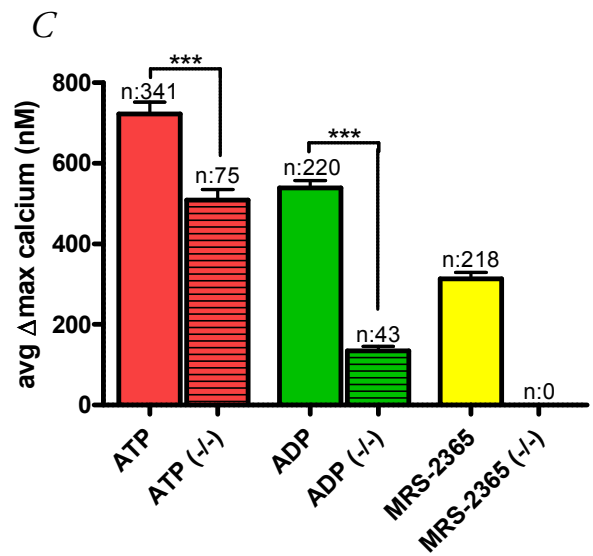
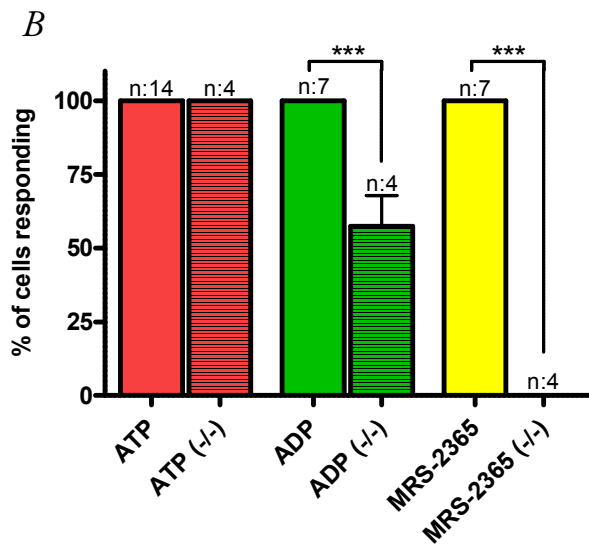
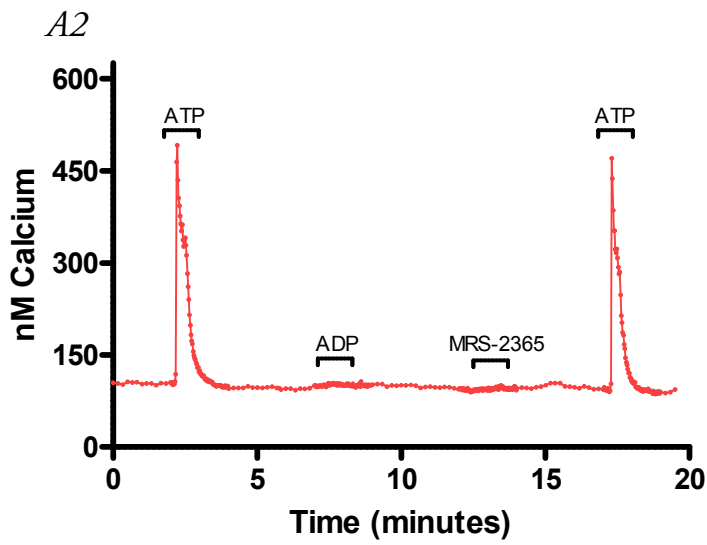
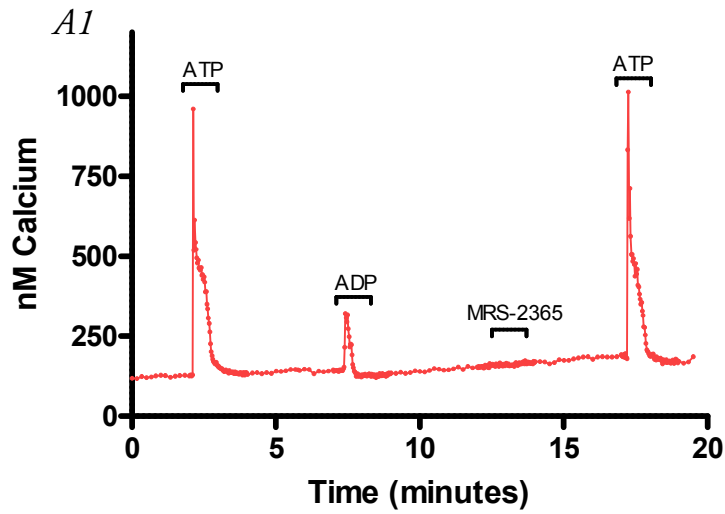
n: number of coverslips

C- Size of [Ca²⁺]_i responses

In P2Y₁^{-/-} astrocytes, there was a significant decrease in the avg Δmax [Ca²⁺]_i to both ATP (p<0.001) and ADP (P<0.001) compared with P2Y₁^{+/+} cells as well as a complete lack of responses to the P2Y₁ selective agonist MRS-2365.

n: total number of cells responding

***: p<0.001



Glutamate receptors on cultured cortical astrocytes

To investigate functional glutamate receptor expression in cultured cortical astrocytes 100uM glutamate, 100uM AMPA, 100uM NMDA + 10uM glycine and 100uM ATP were applied sequentially (see **Figure 4-9: A1 + A2** for representative recordings of single cell $[Ca^{2+}]_i$ and **Video 7** for a full-length example experiment). ATP was used as a control to make sure that any cells that had not responded to glutamate receptor agonists were healthy.

Only a small percentage of these cultured cortical astrocytes exhibited glutamate receptor mediated $[Ca^{2+}]_i$ increases, with $13.91 \pm 6.75\%$ of cells (n:10, 220 cells) responding to glutamate, $8.27 \pm 5\%$ to AMPA and none to NMDA + glycine (n:7, 121 cells for both) (**Figure 4-9: B**). These experiments were performed in zero Mg^{2+} solutions to maximize the chance of finding any NMDA receptor mediated component. All cells responded to ATP application at the end of the experiment with large $[Ca^{2+}]_i$ rises. Compared to ATP, all glutamate receptor agonist induced avg $\Delta_{max} [Ca^{2+}]_i$ changes were relatively small, with values (in nM) of 189.2 ± 14.9 for glutamate (n:32 cells), 34.01 ± 13.4 for AMPA (n:10 cells) and obviously zero for NMDA + glycine, as no cells responded (**Figure 4-9: C**). Additionally, most of the cells which responded to glutamate did not respond to AMPA, suggesting that the majority of glutamate responses were being mediated by metabotropic glutamate receptors.

Figure 4-9: Functional glutamate receptors on cultured cortical astrocytes

A1+A2: Sample recordings of $[Ca^{2+}]_i$ obtained from individual cells.

A1 is representative of the majority of cells in the astrocyte culture, with no $[Ca^{2+}]_i$ changes at all following glutamate, AMPA or NMDA + glycine application, but a large increase in $[Ca^{2+}]_i$ after the application of ATP.

Cell **A2** was representative of those cells which did respond to glutamate, with $[Ca^{2+}]_i$ rises only when glutamate was applied but not AMPA or NMDA + glycine, suggesting that metabotropic glutamate receptors were activated in this particular cell.

B- Percent of cells in the astrocyte culture responding to agonists

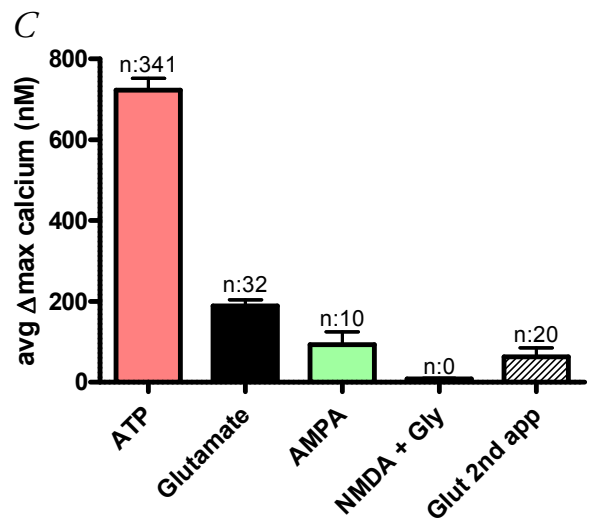
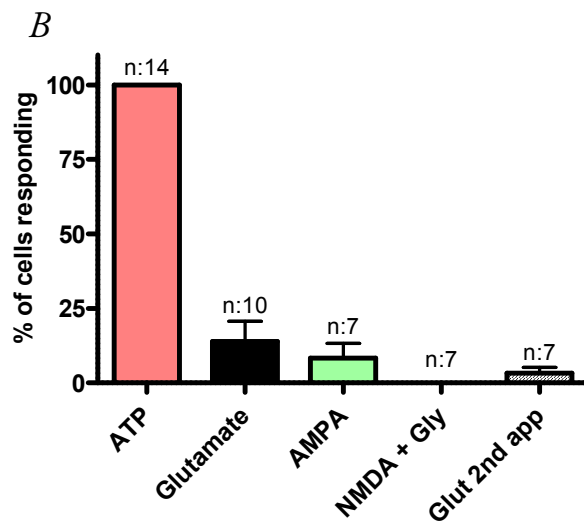
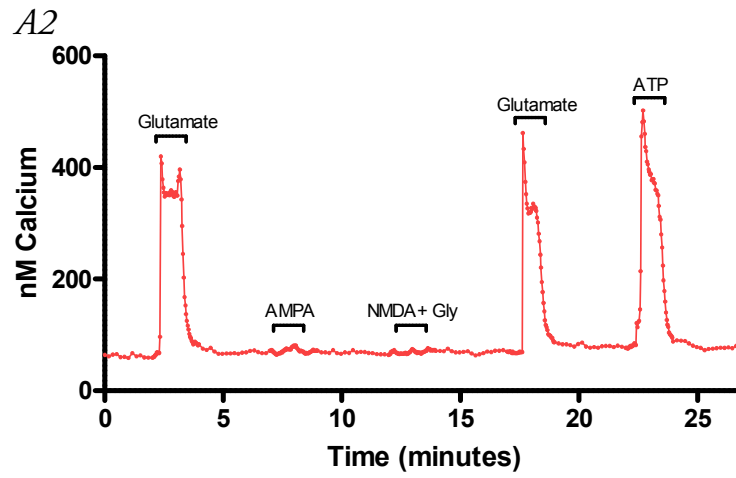
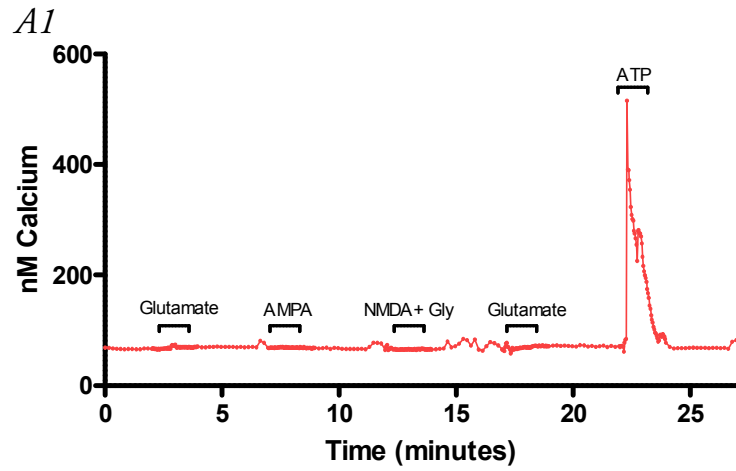
Only a very small percentage of astrocytes seemed to be expressing functional glutamate receptors, and none seemed to have functional NMDA receptors. As a control ATP was applied during each experiment to make sure that the astrocytes were alive. 100% of astrocytes in these experiments responded to ATP.

n: number of coverslips

C- Size of $[Ca^{2+}]_i$ responses

Histogram showing the average maximum increases in $[Ca^{2+}]_i$ (in nM) of the few astrocytes which responded to the glutamate receptor agonists. Ca^{2+} changes were much smaller than those caused by ATP application. In addition, neither AMPA nor NMDA + glycine were able to produce similar Ca^{2+} responses compared with glutamate, suggesting that metabotropic glutamate receptors were the main mediators of the $[Ca^{2+}]_i$ rises induced by glutamate application in these astrocytes.

n: total number of cells responding



Effects of NBQX, MK-801 and PPADS on neuronal glutamate and P2 receptors

These experiments were designed primarily to test the efficacy of the AMPA/Kainate receptor antagonist NBQX, the NMDA receptor antagonist MK-801 and the P2 receptor antagonist PPADS in the cultured cortical neurons, whilst also providing insight into what types of glutamate receptors were present in these neurons. Cells were incubated for one hour in the presence of a combination of 10 μ M MK-801, 30 μ M NBQX and 100 μ M PPADS before 100 μ M Glutamate, 100 μ M AMPA, 100 μ M NMDA + 10 μ M glycine and 100 μ M ATP were applied sequentially (see **Figure 4-10: A1, A2, A3** for representative recordings of single cell $[Ca^{2+}]_i$ and **Video 8** for a full-length example experiment). In some experiments the antagonists were washed out for five minutes prior to a final reapplication of the agonists to check for reversibility (**Figure 4-10: B**). Solutions contained no Mg^{2+} to allow full activation of NMDA receptors. Data about the reduction in the sizes of the Ca^{2+} response in the presence of antagonists is presented as both the actual avg $\Delta_{max} [Ca^{2+}]_i$ and as a % of the control response normally seen by application of the agonist in the absence of any antagonists. Control values were obtained from the experiments depicted in **Figure 4-1**.

The combination of NBQX and MK-801 effectively reduced AMPA ($41.54 \pm 6\%$ of control, $p < 0.001$) and NMDA + glycine ($29.11 \pm 11.4\%$ of control) mediated avg $\Delta_{max} [Ca^{2+}]_i$ rises (86.33 ± 12.7 and 84.32 ± 33 nM Ca^{2+} , respectively) (**Figure 4-10: D**) in these cultured cortical neurons. The reduction of the NMDA + glycine response could not be statistically compared with controls since only two cells showed a $[Ca^{2+}]_i$ rise. There was also a significant ($p < 0.001$) reduction in the numbers of cells responding, with $11.17 \pm 3.76\%$ of neurons responding to AMPA and $0.83 \pm 0.53\%$ responding to NMDA + glycine (n:6, 294 cells for both) (**Figure 4-10: C**). Despite the presence of these two glutamate receptor antagonists $72.01 \pm 3.22\%$ (n:3, 149 cells) (**Figure 4-10: C**) of neurons still displayed glutamate induced $[Ca^{2+}]_i$ increases (123.9 ± 7.36 nM Ca^{2+} , $27.1 \pm 1.5\%$ of control, n:107 cells) (**Figure 4-10: D**), suggesting the presence of metabotropic glutamate receptors and/or incomplete inhibition of ionotropic receptor responses. As expected, MK-801 was irreversible while NBQX could be washed out, with AMPA responses recovering

to $122.6 \pm 6.5\%$ of control. PPADS was able to significantly reduce ($p < 0.01$) the percentage of cells activated by ATP ($13.67 \pm 6.7\%$, n:5, 231 cells) (**Figure 4-10: C**) application but not the size of remaining $[Ca^{2+}]_i$ responses ($79.27 \pm 8.4\%$ of control, 80.15 ± 9.53 nM Ca^{2+} , n:34 cells) (**Figure 4-10: D**). In these experiments the effect of PPADS was not significantly reversible by washout.

Figure 4-10: Effects of NBQX, MK-801, and PPADS on neuronal receptors

Neurons were incubated for one hour in the presence of 10uM MK-801, 30uM NBQX and 100uM PPADS (this combination is labeled as 'Ant' in the figures). 100uM Glutamate, 100uM AMPA, 100uM NMDA + 10uM glycine and 100uM ATP were applied. In a few experiments the antagonists were washed out for five minutes prior to a final reapplication of the agonists to check for reversibility. Solutions contained no Mg^{2+} . Values obtained in experiments from **Figures 4-1** and **4-2** were used as controls for glutamate, AMPA, NMDA + glycine and ATP without antagonists.

A1, A2, A3, B: Sample recordings of $[Ca^{2+}]_i$ obtained from individual cells.

Cells **A1, A2** and **A3** were subjected to the same protocol of pre-incubation with the three antagonists and glutamate, AMPA, NMDA + glycine and ATP application. **A1** had only a very small $[Ca^{2+}]_i$ rise in response to glutamate, with **A2** having the same profile except it had a much larger glutamate response. **A3** also had a response to ATP. None however showed any responses to AMPA or NMDA + glycine.

Cell **B** underwent a period of washout to see if drug actions were reversible. In this cell the AMPA induced current recovered well, P2 receptor mediated currents also did to a smaller degree but NMDA receptor mediated $[Ca^{2+}]_i$ responses did not recover at all.

C- Percent of cells in the neuronal culture responding to agonists

n: number of coverslips

D- Size of $[Ca^{2+}]_i$ responses

n: total number of cells responding

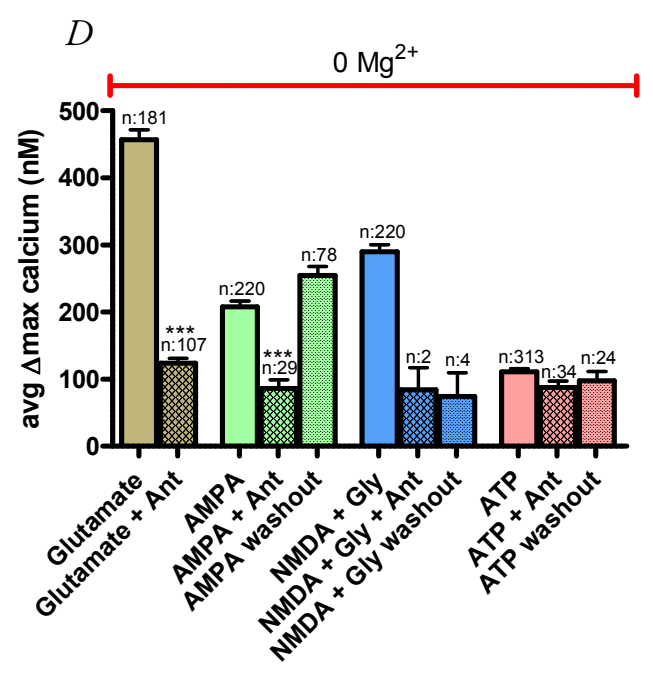
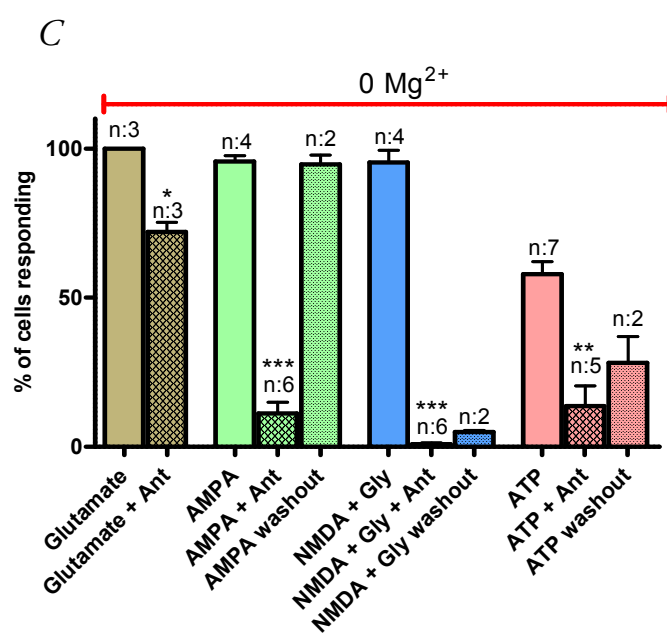
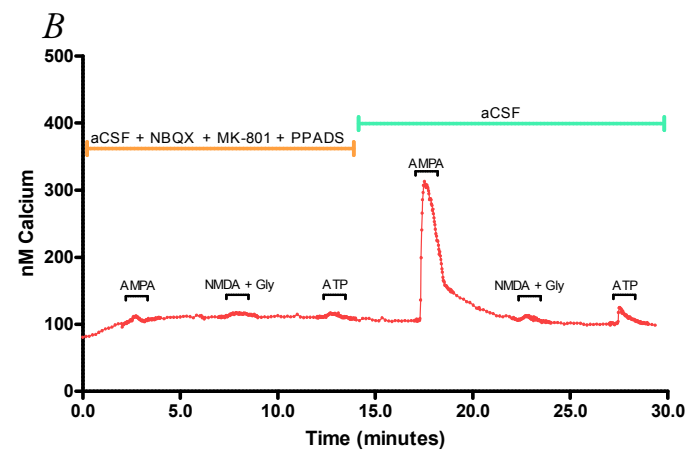
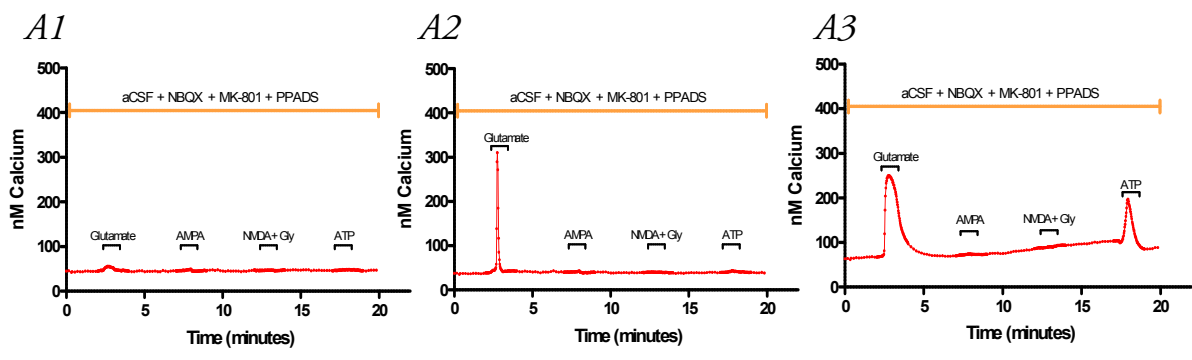
Graphs **C** and **D** show that the combination of 30uM NBQX and 10uM MK-801 was very effective at preventing AMPA and NMDA receptor mediated $[Ca^{2+}]_i$ rises ($p < 0.001$) in these cultured cortical neurons. MK-801 was irreversible while NBQX could be washed out. Despite the presence of these two glutamate receptor antagonists there were still a large number of neurons showing glutamate mediated $[Ca^{2+}]_i$.

PPADS was able to significantly reduce the percentage of cells activated by ATP application ($p < 0.01$) but not the size of remaining $[Ca^{2+}]_i$ responses. In these cells the effect of PPADS was not significantly reversible by washout.

*: $p < 0.05$

**.: $p < 0.01$

***.: $p < 0.001$



Effects of suramin, PPADS, KN-62 and MRS-2179 on astroglial P2 receptors

These experiments were designed primarily to test the efficacy of the broad spectrum P2 receptor antagonists PPADS and suramin, the P2Y₁ receptor antagonist MRS-2179 and the P2X₇ receptor antagonist KN-62 in the cultured cortical astrocytes, whilst also providing insight into what sub-types of P2 receptors were present in these cells. Most of the P2 receptor antagonists were tested only on the astrocyte culture since these cells showed such robust [Ca²⁺]_i responses to all the P2 receptor agonists, whereas neurons showed relatively fewer responses.

Astrocyte cultures were pre-incubated with 100uM of the broad spectrum P2 receptor antagonist suramin for one hour to maximize any effects before being subjected to applications of ATP and ADP (see **Figure 4-11: A** for a representative recording of single cell [Ca²⁺]_i and **Video 9** for a full-length example experiment). Control values for ATP and ADP were obtained from the experiments depicted in **Figure 4-5**. Despite the presence of suramin, 100% of cells responded to both ATP and ADP (n:3 coverslips, 136 cells) (**Figure 4-11: B**). However, the avg Δmax [Ca²⁺]_i responses were significantly (p<0.001) reduced for both ATP (43.93 ± 1.4% of control, 317.5 ± 10.3 nM Ca²⁺) and ADP (59.48 ± 1.9% of control, 320.5 ± 10.36 nM Ca²⁺) (n:136 cells for both) (**Figure 4-11: C**). The effects of suramin could not be significantly reversed by a 5 minute washout period.

Figure 4-11: Effects of suramin

Astrocyte cultures were pre-incubated with 100uM of the broad-spectrum P2 receptor antagonist suramin for one hour to maximize any effects before being subjected to applications of ATP and ADP. Suramin was then removed from all solutions to see if the effects could be reversed. Values obtained in experiments from **Figure 4-5** were used as controls for ATP and ADP without suramin.

A: Sample recording of $[Ca^{2+}]_i$ obtained from an individual cell.

Cell **A** illustrates the exact protocol of this experiment. There were still robust $[Ca^{2+}]_i$ rises in response to ATP and ADP despite the presence of suramin.

B- Percent of cells in the astrocyte culture responding to agonists

Despite the presence of the suramin, 100% of cells responded to both ATP and ADP.

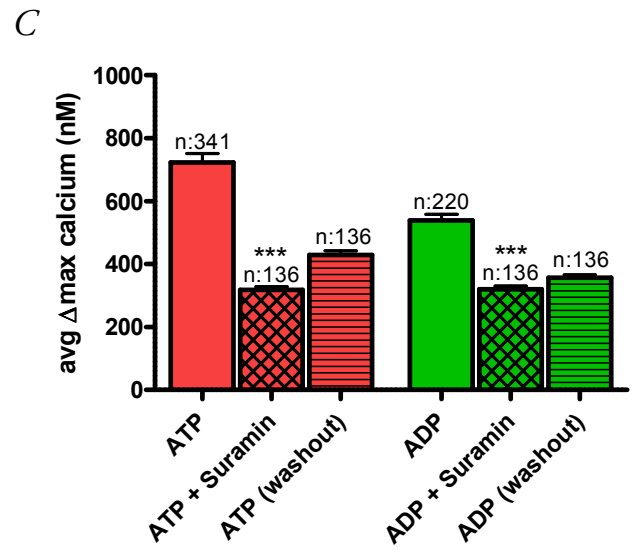
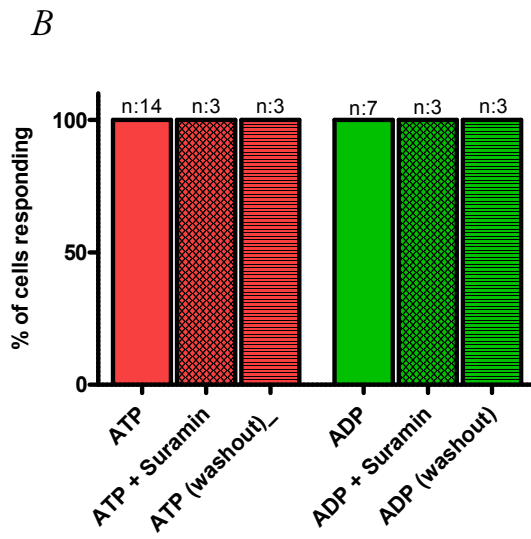
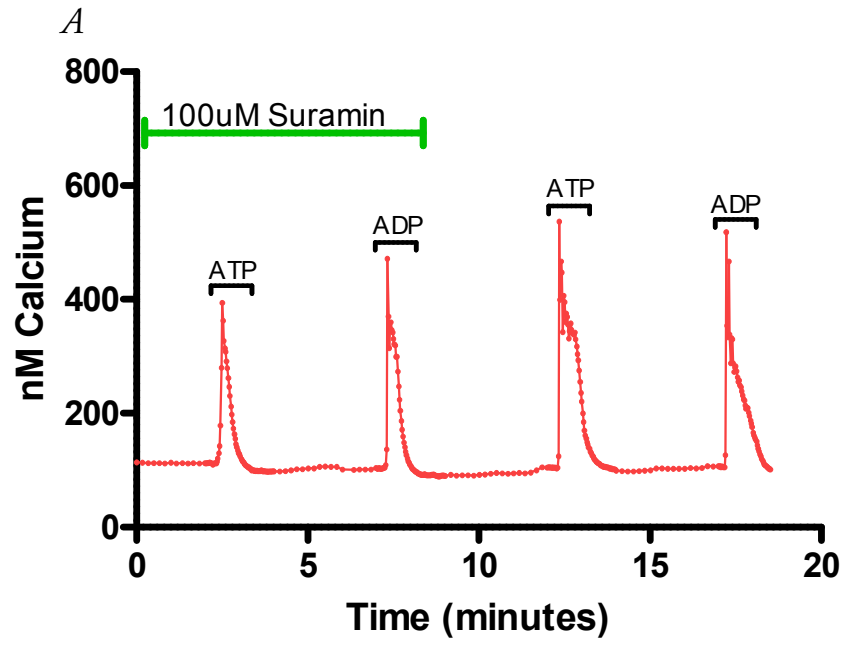
n: number of coverslips

C- Size of $[Ca^{2+}]_i$ responses

Suramin significantly ($p < 0.001$) reduced Ca^{2+} responses to both ATP and ADP. The effects of suramin could not be significantly reversed by a 5 minute washout period.

n: total number of cells responding

***: $p < 0.001$



Two different protocols were used to test the effects of the broad-spectrum P2 receptor antagonist PPADS as an antagonist to the $[Ca^{2+}]_i$ responses induced by 100uM ATP and 100uM ADP application, both using astrocyte cultures. In the first set of experiments (protocol 1), ATP was applied on its own initially, then in the presence of 1, 10 or 100uM PPADS (see **Figure 4-12: A1** for a representative recording of single cell $[Ca^{2+}]_i$ and **Video 10** for a full-length example experiment). In this experiment values were statistically compared to those obtained in the experiment shown in **Figure 4-6** as these astrocytes had shown significant reductions in avg $\Delta_{max} [Ca^{2+}]_i$ responses to sequential ATP applications. To do this, single cell avg $\Delta_{max} [Ca^{2+}]_i$ response were converted to a percent of the mean avg $\Delta_{max} [Ca^{2+}]_i$ response to the first ATP application of all cells in the experiment. In the second experiment (protocol 2) 100uM ATP and 100uM ADP were applied to cells that had been pre-incubated for one hour with either 10uM or 100uM PPADS to maximize any effects of the antagonist (see **Figure 4-12: A2 and A3** for representative recordings of single cell $[Ca^{2+}]_i$ and **Videos 11 + 12** for full-length example experiments). Control values for ATP and ADP were obtained from the experiments depicted in **Figure 4-5**. In both protocols PPADS was then removed from all solutions and the agonists re-applied to see if its effects could be reversed.

In all experiments 10uM and 100uM PPADS significantly ($p < 0.001$) reduced the size of the avg $\Delta_{max} [Ca^{2+}]_i$ responses to ATP and ADP, but 1uM PPADS did not (**Figure 4-12: E, F, G, H**). With protocol 1, PPADS reduced ATP-induced avg $\Delta_{max} [Ca^{2+}]_i$ rises to $87.18 \pm 2.9\%$ of control ($688.7 \pm 23.3\text{nM } Ca^{2+}$, n:115 cells) at 1uM, $63.13 \pm 2.58\%$ of control ($498.7 \pm 20.4\text{nM } Ca^{2+}$, n:115 cells) at 10uM, and $39.53 \pm 1.9\%$ of control ($312 \pm 14.8\text{nM } Ca^{2+}$, n:114 cells) at 100uM, with recovery after washout to $85.68 \pm 3.5\%$ of control ($676.9 \pm 27.4\text{nM } Ca^{2+}$, n:115 cells) (**Figure 4-12: H**).

Pre-incubating cells for one hour with PPADS (protocol 2) did not increase the antagonistic effect, but it did reduce the reversibility following washout, with responses to ATP and ADP recovering to $55.85 \pm 1.8\%$ ($403.7 \pm 12.8\text{nM } Ca^{2+}$) and $63.48 \pm 2\%$ ($342 \pm 11 \text{ nM } Ca^{2+}$) of control respectively with 10uM PPADS (n:115 cells) (**Figure 4-12: F**)

and $62.85 \pm 2.2\%$ ($454.3 \pm 16\text{nM Ca}^{2+}$) and $59.98 \pm 2.4\%$ ($323.2 \pm 12.8\text{nM Ca}^{2+}$) of control with 100uM PPADS (n:84 cells) (**Figure 4-12: G**). Using protocol 2, 10uM PPADS reduced ATP and ADP-induced avg $\Delta_{\text{max}} [\text{Ca}^{2+}]_i$ responses to $50.85 \pm 1.9\%$ ($367.6 \pm 13.6\text{nM Ca}^{2+}$, n:115) and $42.09 \pm 1.8\%$ ($226.8 \pm 9.8\text{nM Ca}^{2+}$, n:112 cells) of control respectively (**Figure 4-12: F**), with 100uM PPADS reducing them to $52.02 \pm 2.4\%$ ($376 \pm 17\text{nM Ca}^{2+}$, n:81 cells) and $31.76 \pm 2.1\%$ ($171.1 \pm 11.4\text{nM Ca}^{2+}$, n:76 cells) (**Figure 4-12: G**). Despite the reduction in the size of avg $\Delta_{\text{max}} [\text{Ca}^{2+}]_i$ responses, ATP-induced responses were still present with 100uM PPADS in $96.43 \pm 3.6\%$ of cells using protocol 1 (n:3 coverslips, 84 cells) and $99.39 \pm 0.6\%$ of cells using protocol 2 (n:3 coverslips, 115 cells), with ADP-induced responses present in $97.28 \pm 1.4\%$ of cells (n:3 coverslips, 115 cells) with 10uM PPADS and $89.76 \pm 5.8\%$ of cells (n:3 coverslips, 115 cells) with 100uM PPADS, demonstrating that this antagonist is unable to block all P2 receptor-mediated Ca^{2+} responses in these astrocytes (**Figures 4-12: B, C, D**).

Figure 4-12: Effects of PPADS

Two different protocols were used to test the effects of the broad spectrum P2 receptor antagonist PPADS as an antagonist to the $[Ca^{2+}]_i$ responses induced by ATP and ADP application. In protocol 1 (Figure **A1**) ATP was applied in the presence of 1, 10 and 100uM of the broad spectrum P2 receptor antagonist PPADS. In protocol 2 ATP and ADP were applied to cells that had been pre-incubated for one hour with either 10uM (Figure **A2**) or 100uM PPADS (Figure **A3**) to maximize any effects of the antagonist and characterize the response to ADP. PPADS was then removed from all solutions and the agonists re-applied to see if its effects could be reversed.

A1-A3: Sample recordings of $[Ca^{2+}]_i$ obtained from individual cells.

A1 shows a cell which was subjected to an initial application of ATP followed by ATP in the presence of 1, 10 and 100uM of PPADS, which was then washed out before a final ATP application at the end. Ca^{2+} responses decrease markedly as the concentration of PPADS increases and this is reversed by the removal of PPADS.

In **A2** and **A3** the cells were pre-incubated for one hour with either 10 or 100uM of PPADS respectively and ATP and ADP were applied, then PPADS was washed out and the agonists re-applied. Again, Ca^{2+} responses were reduced in the presence of PPADS, with **A3** showing a cell where the response to ADP was completely abolished by 100uM PPADS, demonstrating complete antagonism of ADP mediated P2 receptor activation.

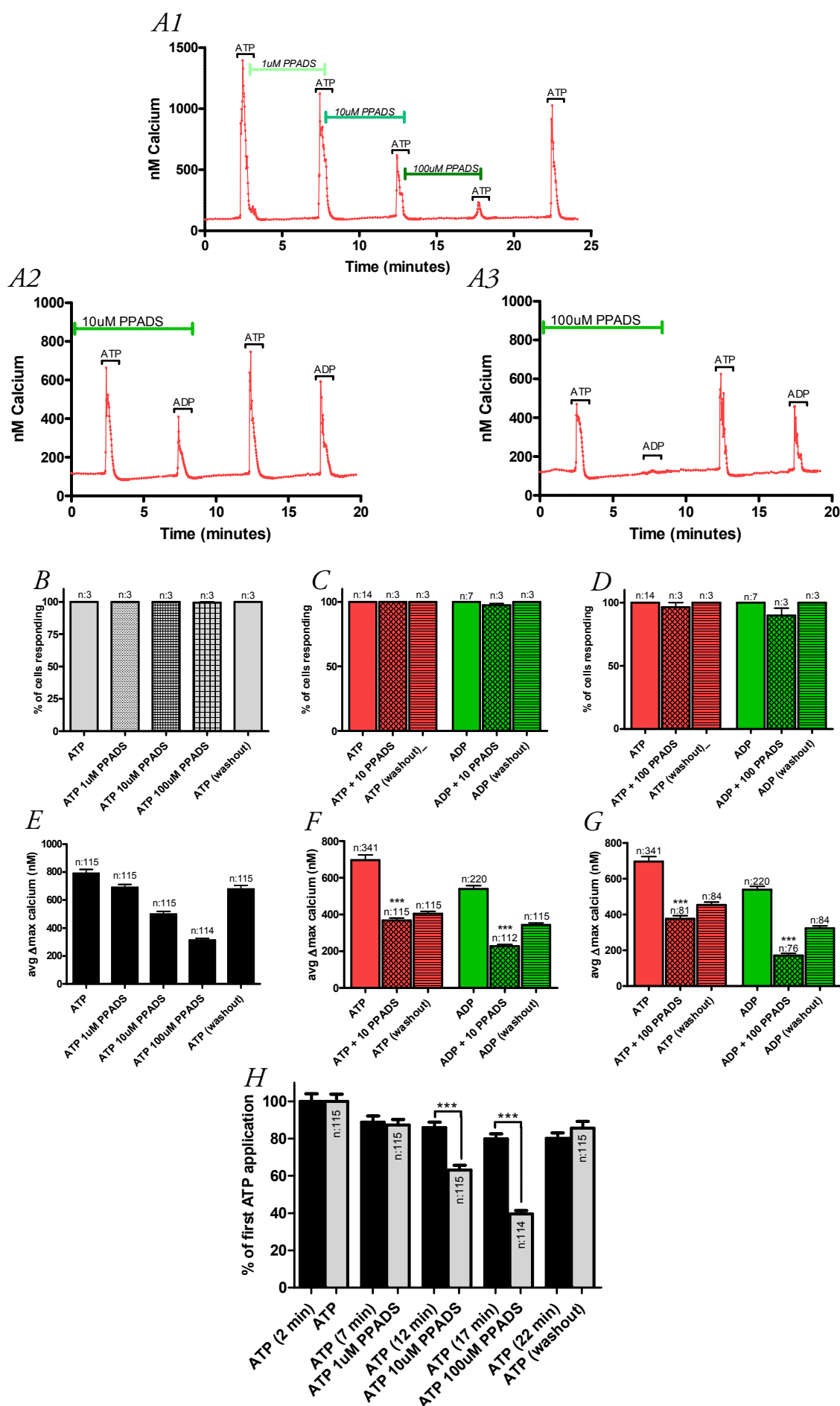
B, C, D- Percent of cells in the astrocyte culture responding to agonists

Despite the reduction in the size of $[Ca^{2+}]_i$ responses to ATP, these were only completely abolished in a tiny number of cells and only at a concentration of 100uM PPADS, suggesting this antagonist is unable to block all P2 receptor responses. Both 10uM and 100uM PPADS were able to completely inhibit ADP responses in a small number of cells. All cells responded to ATP and ADP after washout. (n: number of coverslips)

E, F, G, H- Size of $[Ca^{2+}]_i$ responses

Using protocol 1, both 10uM and 100uM PPADS significantly reduced ($p < 0.001$) the size of the $[Ca^{2+}]_i$ responses to ATP, and this was reversible after PPADS was removed (**E, H**). Figure **H** uses the values for sequential ATP applications from **Figure 4-6** to compare % relative reductions at each time point to overcome the problem of natural run-down of the ATP-induced responses with this protocol. Using protocol 2, 10uM and 100uM PPADS also significantly reduced ($p < 0.001$) the size of the $[Ca^{2+}]_i$ responses to ATP (**F, G**). Pre-incubating cells for one hour with PPADS did not further increase the antagonist effect of PPADS, but it did reduce the level of reversibility following washout, suggesting that long pre-incubation may have a different or added effect, such as internalization of the receptors, which cannot be quickly reversed. (n: total number of cells responding)

***: $p < 0.001$



Finally, to further characterise the profile of P2 receptor expression and to test the efficacy of the P2Y₁ receptor antagonist MRS-2179 and the P2X₇ receptor antagonist KN-62, astrocyte cultures were incubated for one hour in a combination of 10uM MRS-2179 and 1uM KN-62, before being subjected to the application of 100uM ATP, 10nM MRS-2365 and 100uM BzATP (see **Figure 4-13: A1** and **A2** for representative recordings of single cell [Ca²⁺]_i and **Video 13** for a full-length example experiment). The antagonists were washed out for 5 minutes prior to a final reapplication of the agonists to check for reversibility.

MRS-2179 significantly ($p < 0.001$) reduced the size of MRS-2365 induced avg Δ_{\max} [Ca²⁺]_i responses ($45.73 \pm 3.2\%$ of control, $143.5 \pm 9.9\text{nM Ca}^{2+}$, $n:93$ cells) as well as reducing the percentage of responding cells to $72.6 \pm 11.5\%$ ($n:4$ coverslips, 119 cells) (**Figure 4-13: B, C**). This effect was reversible by a 5 minute washout, with 100% of cells responding to MRS-2365 and avg Δ_{\max} [Ca²⁺]_i rises returning to $92.34 \pm 3.6\%$ of control, $289.7 \pm 11.1\text{nM Ca}^{2+}$. KN-62 prevented a very small number of cells from being activated by BzATP ($96.44 \pm 0.5\%$ still responding, $n:4$ coverslips, 119 cells) (**Figure 4-13: B**) but it significantly ($p < 0.01$) reduced BzATP induced [Ca²⁺]_i changes ($59.91 \pm 2.5\%$ of control, $196.7 \pm 8.3\text{nM Ca}^{2+}$, $n:115$ cells) (**Figure 4-13: C**). The effect of KN-62 on BzATP induced avg Δ_{\max} [Ca²⁺]_i was not reversible ($58.17 \pm 2.1\%$ of control, $191 \pm 6.9\text{nM Ca}^{2+}$, $n:119$ cells) (**Figure 4-13: B**) by a 5 minute washout period, even though 100% of cells were now responding to the agonist (**Figure 4-13: C**). The combination of the two antagonists also significantly ($p < 0.001$) reduced ATP induced [Ca²⁺]_i changes ($69.39 \pm 2.2\%$ of control, $483 \pm 15.6\text{nM Ca}^{2+}$, $n:119$ cells) (**Figure 4-13: C**), and this was not reversible by a 5 minute washout, suggesting that a significant proportion of the ATP response is mediated by P2X₇ receptors and that ATP breakdown into ADP by ectonucleotidases and subsequent activation of P2Y₁ receptors is not occurring in significant amounts.

Figure 4-13: Effects of KN-62 and MRS-2179

Astrocytes were incubated for one hour in the presence of 10uM MRS-2179 and 1uM KN-62 (this combination is labeled as 'ant' in the figures). 100uM ATP was applied first, then P2Y₁ receptors were activated by 10nM MRS-2365 and P2X₇ receptors by 100uM BzATP. The antagonists were washed out for five minutes prior to a final reapplication of the agonists to check for reversibility.

A1 + A2: Sample recordings of [Ca²⁺]_i obtained from individual cells

A1 shows reduced responses to MRS-2365 and BzATP, both of which seem to be partially reversed by washout.

A2 shows no response to MRS-2365 suggesting complete blockade of P2Y₁ receptors by MRS-2179. The BzATP induced Ca²⁺ response was still large despite KN-62 and this did not change following washout.

B- Percent of cells in the astrocyte culture responding to agonists

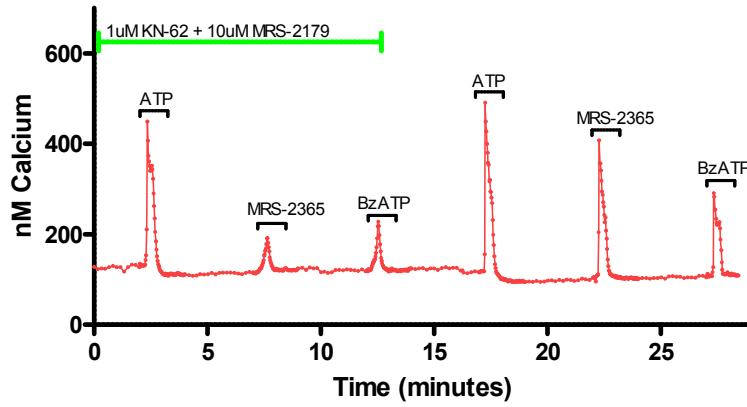
C- Size of [Ca²⁺]_i responses

Graphs **B** and **C** show that MRS-2179 significantly ($p < 0.001$) reduced MRS-2365-induced avg Δ_{\max} [Ca²⁺]_i rises and was able to completely abolish P2Y₁ receptor activation in 27.4% of cells. This effect was largely reversible by washout. KN-62 only prevented 3.56% of cells from being activated, but it also significantly reduced BzATP induced avg Δ_{\max} [Ca²⁺]_i rises ($p < 0.01$). The effects of KN-62 were not reversible by a five minute washout period. The combination of the two antagonists also significantly reduced ATP induced avg Δ_{\max} [Ca²⁺]_i rises ($p < 0.001$), and this was not reversible. This suggests that a significant proportion of the ATP response is mediated by P2X₇ receptors and that ATP breakdown into ADP by ecto-enzymes and subsequent activation of P2Y₁ receptors is not occurring in significant amounts.

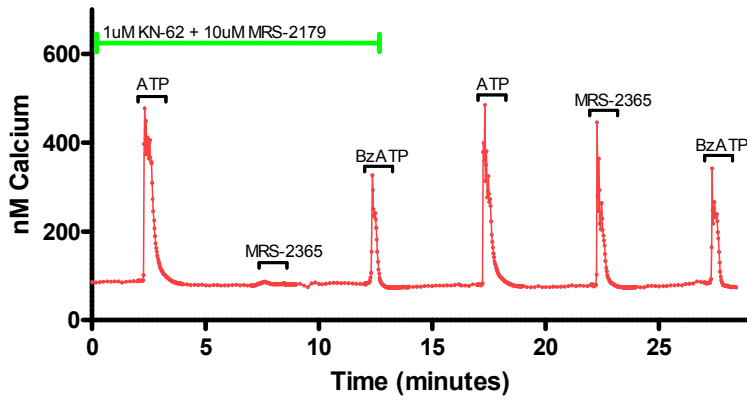
** : $p < 0.01$

*** : $p < 0.001$

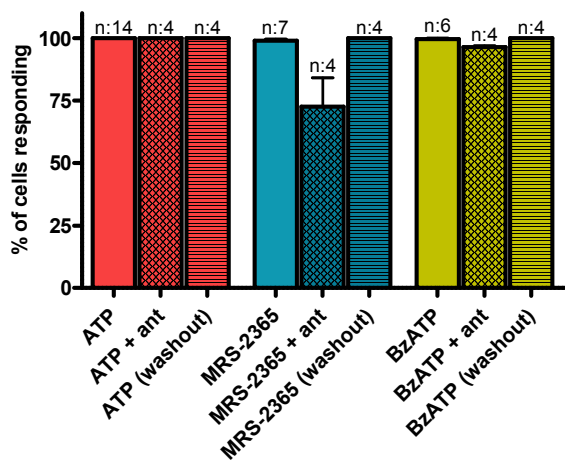
A1



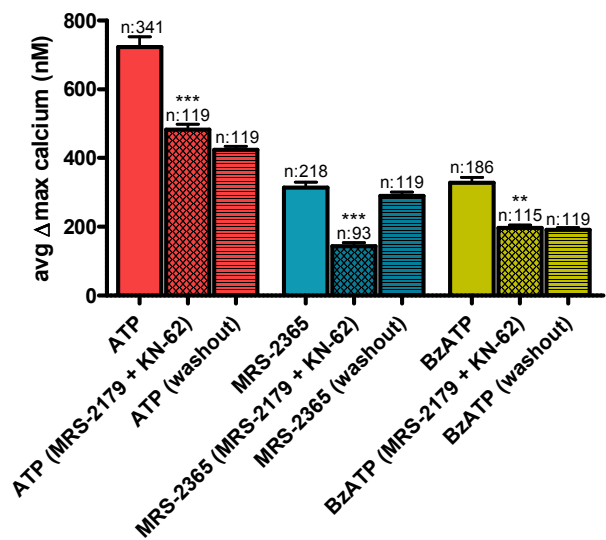
A2



B



C



P2 and glutamate receptor mediated $[Ca^{2+}]_i$ rises in co-cultured astrocytes and neurons

The combined presence of neurons and astrocytes has been proposed to influence the expression and/or function of ion channels and membrane transporters in these cells (Barres, 1991; Daniels and Brown, 2001). Co-cultures of astrocytes and neurons were used in many experiments during this project, so ideally I would have liked to investigate whether there were any changes in P2 or glutamate receptor mediated responses in co-cultures compared with mono-cultures. However, due to the fact that neurons were growing on top of a confluent layer of astrocytes, it was impossible in this imaging system to reliably differentiate whether Fura-2 fluorescence in regions where cells overlapped emanated from the astrocyte below or the neuron above, even when using higher magnification. One way to potentially overcome this problem would be by producing cell cultures where the astrocytes and neurons are grown separately yet in close proximity to one another on culture plate inserts which are then put into the same culture dish/well (Bolanos et al., 1996; Wang and Cynader, 1999; Chen et al., 2001; Daniels and Brown, 2001; Griffin et al., 2005). Cells can then be separated and imaged individually. However, I did not have time to further develop this method.

DISCUSSION

Functional glutamate receptor responses in cultured neurons and astrocytes

Cultured cortical neurons expressed functional ionotropic glutamate receptors of both the NMDA and AMPA/kainate type, as demonstrated by large $[Ca^{2+}]_i$ increases following glutamate, AMPA and NMDA application in almost all cells (see **Table 4-6** for a summary of results). This is in agreement with *in vivo* cortical expression and investigations using primary cortical neuron cultures (Jones and Baughman, 1991; Frandsen and Schousboe, 1993; Durkin et al., 1997; Ozawa et al., 1998; Conti et al., 1999; Fischer et al., 2002; King et al., 2006). NMDA and AMPA responses were potently inhibited by the combination of MK-801 + NBQX, while glutamate induced $[Ca^{2+}]_i$ rises were still evident in over 70% of cortical neurons despite the presence of these antagonists, suggesting the expression of metabotropic glutamate receptors in these cells in addition to NMDA and AMPA/kainate receptors (summarised in **Table 4-7**). This result is not surprising, as metabotropic glutamate receptors enjoy widespread expression in cortical neurons (Ferraguti and Shigemoto, 2006).

Table 4-6: Summary, glutamate and P2 receptor responses in neurons versus astrocytes

	Cortical neuron culture		Cortical astrocyte culture	
	% cells responding	avg. $\Delta_{max} [Ca^{2+}]_i$ (nM)	% cells responding	avg. $\Delta_{max} [Ca^{2+}]_i$ (nM)
Glutamate	100	457 ± 15	13.91 ± 6.8	189.2 ± 14.9
AMPA	95.58 ± 2	207.8 ± 8.6	8.27 ± 5	34.01 ± 13.4
NMDA + glycine	95.37 ± 4	289.7 ± 10.9	0	0
ATP	57.85 ± 4.2	110.9 ± 4.6	100	722.9 ± 29.2
ADP	52.69 ± 4.9	81.22 ± 4.5	100	538.8 ± 19.2
ATPγS	52.04 ± 4.3	70.32 ± 4.5	100	452.1 ± 19.6
MRS-2365	32.51 ± 7.7	62.04 ± 4.8	98.94 ± 0.7	313.7 ± 16.1
BzATP	26.37 ± 7.1	56.91 ± 4.3	99.56 ± 0.4	328.3 ± 15.2

Table 4-7: Summary, P2 and glutamate receptor antagonists in neuronal cultures

	100uM PPADS + 10uM MK-801 + 30uM NBQX		
	% cells responding	avg. $\Delta_{max} [Ca^{2+}]_i$ (nM)	% of control
Glutamate	72.01 ± 3.22	123.9 ± 7.36	27.1 ± 1.5
AMPA	11.17 ± 3.76	86.33 ± 12.7	41.54 ± 6
NMDA + glycine	0.83 ± 0.53	84.32 ± 33	29.11 ± 11.4
ATP	13.67 ± 6.7	80.15 ± 9.53	79.27 ± 8.4

AMPA and NMDA receptor expression in cortical astrocytes has been reported by numerous studies (Jensen and Chiu, 1990, 1991; Petralia and Wenthold, 1992; Martin et al., 1993; Conti et al., 1994; Holzwarth et al., 1994; Conti et al., 1996; David et al., 1996; Conti et al., 1997; Conti et al., 1999; Fan et al., 1999; Schipke et al., 2001; Seifert and Steinhauser, 2001; Lalo et al., 2006; Bakiri et al., 2009). However, in my astrocyte cultures only 14% of cells responded to glutamate application with increases in $[Ca^{2+}]_i$, while 8% responded to AMPA and none to NMDA. AMPA responses were much smaller than those induced by glutamate, suggesting the presence of metabotropic glutamate receptors. Functional metabotropic glutamate receptor expression on astrocytes has been established for many different regions of the brain, including the cortex, and activation of these receptors has been shown to be the main mediator of glutamate induced $[Ca^{2+}]_i$ rises in cultured cortical type 1 astrocytes (Jensen and Chiu, 1991; Holzwarth et al., 1994; Janssens and Lesage, 2001; D'Antoni et al., 2008). Despite this fact, a similarly small percentage of cells demonstrating AMPA or NMDA induced $[Ca^{2+}]_i$ rises has been previously reported in cultured cortical astrocytes (Kettenmann and Schachner, 1985; Glaum et al., 1990; Jensen and Chiu, 1990, 1991; Holzwarth et al., 1994). A number of factors other than a lack of receptor expression may explain why AMPA and NMDA responses could not be detected in these experiments.

For AMPA receptors, a lack of Ca^{2+} permeability and fast receptor desensitisation may be partly responsible for the limited $[Ca^{2+}]_i$ rises seen in astrocytes. AMPA receptor permeability to Ca^{2+} varies inversely with the abundance of GluR2 subunit expression (Deng et al., 2003). Although astrocytes in a number of different brain regions are characterised by a lack of GluR2 expression and enhanced AMPA receptor Ca^{2+} permeability, cortical astrocytes in particular appear to be an exception (Enkvist et al., 1989; Glaum et al., 1990; Jensen and Chiu, 1991; Holzwarth et al., 1994; Jabs et al., 1994; Porter and McCarthy, 1995; Meucci et al., 1996; Haak et al., 1997). A lack of Ca^{2+} permeability has been demonstrated for AMPA receptors in cultured cortical astrocytes, particularly in type 1 astrocytes such as those used here (Glaum et al., 1990; Jensen and Chiu, 1991; Holzwarth et al., 1994; David et al., 1996). Jensen and colleagues

demonstrated large AMPA-induced $[Na^+]_i$ rises but only few $[Ca^{2+}]_i$ rises (Jensen and Chiu, 1991). Additionally, cortical astrocytes appear to widely express GluR2 subunits (Meucci et al., 1996). It has therefore been suggested that cultured cortical astrocytes contain a mixed population of AMPA receptors, most of which are Ca^{2+} impermeable (Holzwarth et al., 1994).

Many early studies demonstrating AMPA receptor expression in astrocytes used kainate, an agonist which causes much slower receptor desensitisation than AMPA (Dingledine et al., 1999). Brief application of AMPA evokes small, and sometimes undetectable, rapidly desensitising inward currents of patch-clamped cortical astrocytes, but no increased $[Ca^{2+}]_i$ as determined by concurrent Fura-2 imaging (David et al., 1996). However, when AMPA receptor desensitisation is prevented by the addition of cyclothiazide, AMPA application produces a large increase in $[Ca^{2+}]_i$ (David et al., 1996). Meucci and colleagues also reported that AMPA induced $[Ca^{2+}]_i$ rises in cultured cortical astrocytes can only be recorded in the presence of cyclothiazide (Meucci et al., 1996). However, this Ca^{2+} accumulation is due to indirect pathways such as reversed operation of the Na^+/Ca^{2+} exchanger and/or L-type voltage-gated calcium channel (VGCC) opening rather than direct entry via the receptor (David et al., 1996).

A further factor which may have hampered detection of AMPA receptor activation is a relatively low density of these receptors in type 1 astrocytes (Jensen and Chiu, 1991). It is possible therefore that AMPA induced $[Ca^{2+}]_i$ responses were prominent in cortical neurons compared with astrocytes due to a higher density and greater $[Ca^{2+}]_i$ permeability of AMPA receptors, and/or concomitant higher density of VGCC expression on neurons whose indirect activation caused a $[Ca^{2+}]_i$ influx. To investigate AMPA receptor responses in the cultured astrocytes more definitively, further useful experiments could have included measuring intracellular Na^+ concentrations and/or the addition of cyclothiazide to prevent desensitisation.

For many years, functional NMDA receptor expression on astrocytes was controversial. In agreement with my experimental results, $[Ca^{2+}]_i$ rises or membrane currents in response to NMDA application could not be detected in cultured or acutely isolated astrocytes (Kettenmann and Schachner, 1985; Seifert and Steinhauser, 1995). Astrocytic responses to NMDA were eventually reported using various *in situ* and *in vitro* preparations, although none could unequivocally attribute these changes to glial NMDA receptor activation and/or reported unusual receptor properties (Porter and McCarthy, 1995; Ziak et al., 1998; Kondoh et al., 2001; Seifert and Steinhauser, 2001; Verkhratsky and Kirchhoff, 2007). Nonetheless, compelling evidence now exists for NMDA receptor expression on cortical astrocytes. Both protein and mRNA of various NMDA receptor subunits has been demonstrated in cortical astrocytes *in situ* (Conti et al., 1996; Conti et al., 1997; Conti et al., 1999; Schipke et al., 2001). Additionally, NMDA induced $[Ca^{2+}]_i$ rises and membrane currents in astrocytes which are sensitive to glycine/ Mg^{2+} and blocked by MK-801 were detected in both cortical slice preparations and acutely isolated cortical cells (Schipke et al., 2001; Lalo et al., 2006). These results suggest that functional NMDA receptor expression on astrocytes present *in vivo* may be lost when cells are cultured.

Functional P2 receptor responses in cultured neurons and astrocytes

Ca^{2+} fluorimetry is a popular method used for detecting functional P2 receptor responses (Centemeri et al., 1997; Lalo et al., 1998; James and Butt, 1999, 2001, 2002; Fumagalli et al., 2003; Rubini et al., 2006; Fischer et al., 2009). However, a few limitations need to be considered. While Ca^{2+} influx via all types of P2X receptors should be detectable, it is most probable that not all P2Y receptors will cause a cytosolic Ca^{2+} rise upon activation, due to differences in G-protein coupling or insensitivity to the agonists used in these experiments. P2Y₁₁ responses can be excluded from the outset, as the rodent genome does not contain this receptor. P2Y₁₄ is only activated by UDP-glucose/galactose. P2Y₁₂ and P2Y₁₃ receptors are coupled to members of the $G_{i/o}$ family of G protein, causing an inhibition of adenylate cyclase, and have previously been shown to not be involved in mediating $[Ca^{2+}]_i$ rises in cultured astrocytes or neurons (Bennett et al., 2003; Abbracchio et al., 2006; Rubini et al., 2006; Fischer et al., 2009). This leaves P2Y_{1,2,4,6} as the main

metabotropic receptors of interest whose activation is detectable by Fura-2 Ca^{2+} imaging. It is also noteworthy that BzATP was the only agonist that theoretically fully activated P2X_7 receptors at the concentrations used in these experiments. Although BzATP probably activates all P2X receptors and has been used in various studies as a $\text{P2X} > \text{P2Y}$ selective agonist, effects at metabotropic P2Y receptors have also been reported, further complicating the interpretation of results (Bianchi et al., 1999; Communi et al., 1999; Fischer et al., 2001; Wildman et al., 2003; Burnstock and Knight, 2004; Fischer et al., 2009). The reader is referred back to **Tables 4-2 to 4-5** for a summary of the agonist/antagonist sensitivities of the various P2 receptor subtypes in relation to experimental results discussed in the remainder of this section.

Experiments using the cortical neuron culture revealed widespread agonist induced P2 receptor responses, indicating the coexistence of various P2 receptor subtypes (results summarised in **Table 4-6**). Of all agonists used, ATP activated the highest number of cells, with 58% responding. Both the percentage of cells responding and the size of the $[\text{Ca}^{2+}]_i$ rises were significantly reduced in the presence of the mixed $\text{P2X}/\text{P2Y}$ antagonist PPADS. PPADS is particularly ineffective at P2Y_2 receptors, suggesting that this subtype may have been partly responsible for the remaining ATP induced $[\text{Ca}^{2+}]_i$ rises. Slightly fewer cells were activated by ATPgS (52%), and the only receptor subtypes which are activated by ATP but not ATPgS appear to be P2Y_4 and/or P2Y_6 , suggesting functional expression of these receptors in at least a small number of cells. 33% of neurons responded to MRS-2365, confirming P2Y_1 receptor expression on these cells. The fact that ADP, which only activates P2Y_1 and P2Y_6 , caused $[\text{Ca}^{2+}]_i$ rises in 52% of cells also suggests the added presence of P2Y_6 receptors. BzATP, an agonist with activity at all P2X but few P2Y receptors, only caused $[\text{Ca}^{2+}]_i$ rises in 26% of cells, suggesting an overall dominance of P2Y over P2X. Furthermore, the lower potency of BzATP in comparison to ATP argues against the involvement of P2X_7 receptors (Fischer et al., 2009). It therefore appears that cells in the cortical neuron culture express a range of P2Y receptors, including P2Y_1 and P2Y_6 , with a possibility of P2Y_2 and P2Y_4 . The subtypes of P2X receptors which may have been expressed could not be reliably elucidated by these experiments.

Functional P2 receptor expression in cortical neurons has been documented using various preparations (see **Table 4-1**). Functional P2X₇ receptors have been reported in cortical synaptosomes (Lundy et al., 2002). Evidence for neuronal expression of functional P2Y₁ and/or P2Y₂ as well as P2X_{1,3,4}, but not P2X_{2,5,6} has been found using cortical slices as well as acutely isolated cortical neurons (Wirkner et al., 2002; Pankratov et al., 2003; Lalo et al., 2007). In partial agreement with my results, the only other paper using cultured cortical neurons reports a similar propensity for P2Y over P2X responses, as well as specific evidence of P2Y₁ and P2X₁ and/or P2X₃, but not P2Y_{2,4,6} subtype expression (Bennett et al., 2003). However, only 9% of neurons tested individually were responsive to ATP in this study, suggesting less widespread receptor expression than in my cultures (Bennett et al., 2003). In a different study, functional evidence of this receptor could only be detected in a very small subset of neurons by electrophysiology and could not be detected at all by fura-2 imaging (Wirkner et al., 2005). This difference may be explained by different cell culture methods, as both used a co-culture of neurons and glia, different growth medium, and/or different species (rat) (Bennett et al., 2003; Wirkner et al., 2005). Consequently, my experiments were the first to investigate P2 receptor expressions in murine cortical neuron cultures, and the first to provide evidence of functional P2Y₆ expression in cortical neurons.

Functional P2 receptor expression was ubiquitous in the astrocyte culture, with all cells responding to ATP, ADP and ATPgS, and almost all to MRS-2365 and BzATP as well (summarised in **Table 4-6**). The non-subtype-selective P2 receptor antagonists suramin and PPADS both significantly reduced P2 agonist responses, suggesting the presence of a variety of receptors (summarised in **Table 4-8**). Evidence from different experiments suggested an overwhelming contribution of P2Y rather than P2X receptor activation to P2 agonist induced [Ca²⁺]_i rises. First of all, depletion of intracellular Ca²⁺ stores by thapsigargin completely prevented ATP induced [Ca²⁺]_i rises in 40% of cells, and reduced the size of remaining responses to just 7.3% of control. Remaining responses to ATP were abolished when extracellular Ca²⁺ was removed, suggesting that 60% of astrocytes expressed functional P2X receptors, but that their overall quantitative contribution to intracellular Ca²⁺ accumulation was minor. Additionally, ADP mediated

responses were entirely prevented by thapsigargin in all but a few cells in which stores appeared to not have been completely depleted. Importantly, this lack of ADP induced $[Ca^{2+}]_i$ rises after store depletion but in the presence of extracellular Ca^{2+} suggest an absence of store-operated calcium influx (Lalo et al., 1998; Rubini et al., 2006).

P2Y₁ receptors in particular contributed significantly, as demonstrated by the potency of the selective agonist MRS-2365 and the antagonist MRS-2179. Furthermore, the presence of P2Y₆ receptors in these cells was confirmed when using cultures derived from P2Y₁^{-/-} animals, where over 50% of cells still responded to ADP. Although the ATP induced avg Δ_{max} $[Ca^{2+}]_i$ was significantly reduced in P2Y₁^{-/-} cells, suggesting P2Y₁ mediated part of the ATP response in wild type astrocytes, ATP application still caused large $[Ca^{2+}]_i$ rises, suggesting the presence of ATP sensitive P2Y receptors such as P2Y₂ and/or P2Y₄. Finally, the presence of functional P2X₇ receptors is suggested by the result that application of the potent P2X₇ antagonist KN-62 significantly reduced the size of BzATP induced Ca^{2+} responses. It therefore appears that the P2 receptor expression profile of these astrocytes is very similar to that seen in the neuronal culture in terms of the dominant P2Y over P2X component. Subtype expression includes P2Y₁ and P2Y₆, P2Y₂ and/or P2Y₄, and possibly P2X₇.

Table 4-8: Summary, P2 receptor antagonists in astrocyte cultures

	ATP			ADP					
	% cells responding	avg. Δ_{max} $[Ca^{2+}]_i$ (nM)	% of control	% cells responding	avg. Δ_{max} $[Ca^{2+}]_i$ (nM)	% of control			
100uM Suramin	100	317.5 ± 10.3	43.93 ± 1.4	100	320.5 ± 10.4	59.48 ± 1.9			
1uM PPADS	100	688.7 ± 23.3	87.18 ± 2.9	-	-	-			
10uM PPADS	100	498.7 ± 20.4	63.13 ± 2.6	-	-	-			
Long preincubation	100	367.6 ± 13.6	50.85 ± 1.9	97.28 ± 1.4	226.8 ± 9.8	42.09 ± 1.8			
100uM PPADS	99.39 ± 0.6	312.3 ± 14.8	39.53 ± 1.9	-	-	-			
Long preincubation	96.43 ± 3.6	376 ± 17	52.02 ± 2.4	89.76 ± 5.8	171.1 ± 11.3	31.76 ± 2.1			
	ATP			MRS-2365			BzATP		
	% cells responding	avg. Δ_{max} $[Ca^{2+}]_i$	% of control	% cells responding	avg. Δ_{max} $[Ca^{2+}]_i$	% of control	% cells responding	avg. Δ_{max} $[Ca^{2+}]_i$	% of control
10uM MRS-2179 + 1uM KN-62	100	483 ± 15.63	66.81 ± 2.2	72.6 ± 11.5	143.5 ± 9.9	45.73 ± 3.2	96.44 ± 0.5	196.7 ± 8.3	59.91 ± 2.5

Similar profiles of P2 receptor subtype expression have been reported of cortical astrocytes in numerous studies (see **Table 4-1**). In particular, the prominence of P2Y over P2X as the main mediators of $[Ca^{2+}]_i$ rises is well documented (King et al., 1996; Centemeri et al., 1997; Kimelberg et al., 1997; Lenz et al., 2000; Bennett et al., 2003; Fumagalli et al., 2003; Fischer et al., 2009). In agreement with results presented in this chapter, all demonstrated the involvement of P2Y₁ receptors, while most also suggest that P2Y_{2,4} are present (King et al., 1996; Lenz et al., 2000; Bennett et al., 2003; Fumagalli et al., 2003; Fischer et al., 2009). A recent study was the first to test for the full spectrum of P2 receptor subtypes in rat cultured cortical astroglia, taking advantage of improved antibodies and agonists/antagonists (Fischer et al., 2009). Immunostaining was reported as strongly positive for P2X_{4,6,7} and P2Y_{1,2}, with weaker, but still positive, staining for P2X₅ and P2Y_{4,6,13,14} (Fischer et al., 2009). Functional characterisation revealed the presence of P2Y_{1,2,4,6,14} as well as unidentified P2X receptor(s), although extensive testing failed to reveal P2X₇ responses (Fischer et al., 2009). However, functional P2X₇ expression has been reported in cortical astrocyte cultures by a number of other studies (Fumagalli et al., 2003; Nobile et al., 2003; Bianco et al., 2009). A similar lack of functional P2X₇ responses was reported in rat cultured cortical astrocytes by Wirkner and colleagues (Wirkner et al., 2005). Additionally, P2X_{1/5} has been identified as the main P2X receptor subtype in acutely isolated murine cortical astrocytes (Lalo et al., 2008). Furthermore, studies using astrocyte cultures prepared from various other areas of the brain have also suggested functional expression of P2Y_{1,2,4,6,14} (Ho et al., 1995; Jimenez et al., 2000; Koizumi et al., 2002; Fam et al., 2003).

Summary of conclusions

In conclusion, functional glutamate receptor responses were detected on all cortical cultured neurons (including ionotropic NMDA and AMPA receptors and metabotropic glutamate receptors) but only a small percentage of astrocytes (mostly metabotropic). The AMPA/Kainate receptor antagonist NBQX and the NMDA receptor antagonist MK-801 effectively blocked AMPA and NMDA induced $[Ca^{2+}]_i$ responses. Additionally, cortical cultured neurons and astrocytes expressed a variety of functional P2 receptors, with 100%

of astrocytes and approximately 60% of neurons responding. In both cell types, there was a dominant contribution of P2Y over P2X receptors. The broad spectrum P2 receptor antagonists PPADS and Suramin significantly reduced $[Ca^{2+}]_i$ responses to ATP and ADP suggesting effects on a wide range of P2 receptors, although neither was able to completely block agonist induced responses. The P2Y₁ receptor antagonist MRS-2179 and the P2X₇ receptor antagonist KN-62 were both able to significantly reduce $[Ca^{2+}]_i$ rises in astrocytes. Neurons and astrocytes appeared to express P2Y₁ and P2Y₆, with a possibility of P2Y₂ and/or P2Y₄, with astrocytes in particular probably also expressing functional P2X₇ receptors.

Chapter 5:

Roles of ATP and glutamate during the ischaemic injury
of cultured astrocytes and neurons

INTRODUCTION

Ischaemic cell death

Cerebral ischaemia produces a complex cascade of neurochemical processes which lead to eventual cell death and dysfunction. The speed of onset and ultimate extent of cell death is proportional to the severity and duration of impairment of oxygen and glucose delivery (Martin et al., 1998; Lipton, 1999; Brouns and De Deyn, 2009). Within areas undergoing severe energy deprivation, such as the core of a focal ischaemic lesion, necrotic cell death ensues within minutes, whereas in areas such as the ischaemic penumbra, cell death occurs less rapidly and involves distinct mechanisms such as apoptosis and inflammation (Doyle et al., 2008). The term 'necrosis' in the context of cell death can be defined loosely as a type of pathological cell death resulting from an extrinsic insult which produces an abrupt perturbation of and departure from physiological conditions and leads to disruption of cell membrane structure and functional integrity, rapid influx of Ca^{2+} and water, and subsequent dissolution of the cell (Martin et al., 1998). The experimental protocol of prolonged OGD without reperfusion used throughout my PhD project leads to rapid and severe energy deprivation, and thus most closely resembles conditions which lead to rapid necrotic cell death. Therefore, in this introduction, I will focus on reviewing mechanisms which are involved mainly in mediating necrotic cell death.

Importance of ionic deregulation early during ischaemia

A number of ionic disturbances occur during the first minutes of ischaemia, of which intracellular Ca^{2+} accumulation appears to be particularly important (Siesjo, 1988; Goldberg and Choi, 1990, 1993; Tymianski et al., 1993a; Tymianski et al., 1993b). Deregulation of Ca^{2+} homeostasis plays a critical role in both neuronal and astrocyte death during and after ischaemia (Goldberg and Choi, 1990; Siesjo, 1990; Goldberg and Choi, 1993; Duffy and MacVicar, 1996; Silver et al., 1997; Fern, 1998; Bondarenko and Chesler, 2001a; Martinez-Sanchez et al., 2004; Pringle, 2004; Bondarenko et al., 2005). Crucially, it is likely that these early changes determine not only cell fate in the short term, such as sub-lethal cell injury and necrosis, but also long term events such as apoptosis or reactive

changes which will impact subsequent functional recovery (Yao and Haddad, 2004). It is therefore vital that the events and mechanisms which contribute to early ionic deregulation are understood, as they provide insights for potential neuroprotective strategies during ischaemia.

Tight control of the composition of brain extracellular milieu as well as intracellular ionic balance is vital to adequate CNS functions, and requires the constant activity and interplay of both neuronal and astrocytic transporters/receptors. Various ATP-dependent membrane transport systems, such as the Na⁺/K⁺-ATPase (NKA), sarco/endoplasmic reticulum Ca²⁺-ATPase (SERCA) and plasma membrane Ca²⁺-ATPase (PMCA), are crucial to this process, and during severe ischaemia they stop working within minutes due to a failure of ATP production (Doyle et al., 2008). One critical consequence of this is cellular Ca²⁺ overload. Normally, the gradients for intracellular/extracellular [Ca²⁺]_i are <0.1µM/1.2mM, but during ischaemia intracellular levels may rise to 50-100µM (Doyle et al., 2008). Since most Ca²⁺-dependent cellular processes have K_m values around 0.1-1µM, such Ca²⁺ overload leads to the activation of various ATPases, proteases, lipases and DNAses which lead to cell death (Lipton, 1999; Besancon et al., 2008; Doyle et al., 2008). Processes which contribute to toxic [Ca²⁺]_i accumulation include (among others): influx through voltage-gated Ca²⁺ channels (VGCCs) and ionotropic receptors, inhibition of active cytoplasmic Ca²⁺ extrusion mechanisms, reversal of the Na⁺-Ca²⁺ exchanger (NCX), and release from intracellular stores (Pringle, 2004; Aarts and Tymianski, 2005). The relative contribution of each during ischaemia varies between cell types. A summary of mechanisms involved in ischaemia induced ionic deregulation of astrocytes and neurons is presented in **Figure 5-0**, and can be referred to when reading the forthcoming text.

Ischaemic neuronal death: a major role for glutamate excitotoxicity

After ischaemia, neurons undergo mainly delayed cell death (Pulsinelli et al., 1982; Garcia et al., 1993; Lipton, 1999). This is why almost all studies investigating ischaemic neuronal injury, assess for the extent of cell death 24 hours after the ischaemic insult. Morphological studies of early neuronal changes *in vivo* and *in vitro* report early shrinking

and scalloping (within 30 minutes), followed by swelling and the formation of vacuoles in dendrites within 45-60 minutes (Garcia et al., 1993; Goldberg and Choi, 1993). In cortical neuron cultures (14-18 DIV), no lactate dehydrogenase (LDH: an intracellular enzyme, released following loss of cell membrane integrity) release could be detected during 70 minutes of OGD; substantial release first occurred after 2 hours of reperfusion and was maximal 12-16 hours later (Goldberg and Choi, 1993). However, hypoxia-hypoglycaemia has been mentioned to lead to rapid cell death of acutely isolated neurons within 15-20 minutes (Duffy and MacVicar, 1996). An element of early neuronal death therefore appears to exist during the initial phase of ischaemia, although the overall lack of data in the literature about this particular component of neuronal death is rather surprising.

One of the earliest events contributing to Ca^{2+} accumulation and cell death during severe cerebral ischaemia is the process of excitotoxicity, where pathological activation of receptors (including NMDA and AMPA receptors) by the excessive extracellular accumulation of excitatory neurotransmitters such as glutamate leads to massive ionic deregulation, particularly of Ca^{2+} , which persist even once the glutamate is removed (Choi, 1985; Choi and Rothman, 1990; Goldberg and Choi, 1990; Benveniste, 1991; Goldberg and Choi, 1993; Choi, 1995; Silver et al., 1997). Neurons have classically been shown to be particularly sensitive to glutamate excitotoxicity during ischaemia, where cell death can largely be prevented by NMDA and AMPA receptor antagonists (Goldberg et al., 1987; Choi and Rothman, 1990; Kaku et al., 1991; Goldberg and Choi, 1993; Gwag et al., 1995; Pringle et al., 1997; Aarts et al., 2003). More recently, oligodendrocytes have also been shown to be particularly sensitive to glutamate toxicity during ischaemia (McDonald et al., 1998; Fern and Moller, 2000; Tekkok and Goldberg, 2001; Wilke et al., 2004; Karadottir et al., 2005; Salter and Fern, 2005; Micu et al., 2006). However, astrocytes are not affected by this process during ischaemia.

Ischaemic astrocyte death: controversy over sensitivity to ischaemia

Based largely on findings from *in vitro* experiments, a widespread belief exists that astrocytes are more resistant to excitotoxic and ischaemic insults than neurons (Fern, 2001;

Matute et al., 2002). Astrocytes cultured from various brain regions are highly resistant to excitotoxic injury induced by glutamate receptor agonist exposures lasting up to 24 hours, although a few conflicting results on this matter have been reported (Prieto and Alonso, 1999; Chen et al., 2000; Beck et al., 2003). Similarly, prolonged periods of OGD lasting anywhere from 2-24 hours have been necessary to induce significant *in vitro* astrocyte death in many studies, while others have reported complete resistance to injury even after such extended periods of ischaemia (Goldberg et al., 1987; Monyer et al., 1989; Yu et al., 1989; Kaku et al., 1991; Goldberg and Choi, 1993; Lyons and Kettenmann, 1998; Ho et al., 2001; Beck et al., 2003; Lenart et al., 2004; Danilov and Fiskum, 2008). However, these latter findings stand in stark contrast to multiple studies using *in situ* (whole mount) or *in vivo* models of ischaemia, as well as more sophisticated models of *in vitro* ischaemia, all of which have demonstrated rapid (within 30-60 minutes) and widespread astrocyte dysfunction and death after energy deprivation, which often precedes neuronal death (Garcia et al., 1993; Fern, 1998; Liu et al., 1999; Bondarenko and Chesler, 2001a; Lukaszewicz et al., 2002; Thomas et al., 2004; Shannon et al., 2007; Salter and Fern, 2008).

One explanation for this discrepancy is that astrocytes are known to be particularly sensitive to acidosis, which occurs *in vivo* during ischaemia but not when using conventional ischaemia models *in vitro*, where an artificially large buffered extracellular space exists (Giffard et al., 1990). In response to this, numerous recent studies have successfully induced rapid ischaemic cell death using hypoxic, acidic, ion-shifted Ringer (HAIR) solution instead of OGD (Swanson et al., 1997; Bondarenko and Chesler, 2001a; Bondarenko et al., 2005; Shannon et al., 2007). Additionally, ischaemia triggers the process of reactive astrogliosis, which is characterised by an increase in astrocyte numbers, hypertrophy of cell bodies and processes, and upregulation of GFAP content (Sofroniew and Vinters, 2009). Since reactive changes can set in within minutes of ischaemic injury, this process may obscure the true extent of astrocyte death reported in many studies, which often only assay for cell death hours or days after the insult (Shannon et al., 2007). Therefore, even if the majority of astrocytes perish within an infarct, the few which survive

can multiply to give a false impression of a lack of astrocyte death. Finally, astrocytes in different regions of the brain seem to be differentially sensitive to ischaemia. For example, protoplasmic gray matter astrocytes appear to be less sensitive than fibrous white matter astrocytes (Shannon et al., 2007).

Mechanisms of ischaemic astrocyte death

Consequent to the difficulties in producing significant ischaemic astrocyte death *in vitro* by conventional protocols, comparatively little is actually known about the mechanisms mediating acute ischaemic injury and death of astrocytes. Using the HAIR protocol, Bondarenko and colleagues have demonstrated that Na⁺ loading by Na⁺-H⁺-exchange and subsequent reversal of Na⁺-Ca²⁺-exchange leads to cytotoxic intracellular Ca²⁺ elevation and death of over 80% of cultured cortical astrocytes within 30-40 minutes (Bondarenko and Chesler, 2001a, b; Bondarenko et al., 2005). Studies using neonatal rat optic nerves (RON) and cultured cortical astrocytes have revealed the involvement of L and T-type voltage gated Ca²⁺ channels, reversal of the Na⁺-Ca²⁺-exchanger, the Na⁺-K⁺-Cl⁻ cotransporter as well as Na⁺ and K⁺ dependent HCO₃⁻ transport in producing ischaemic astrocyte injury at different time points in development, and cell death was found to be preceded by an increase in [Ca²⁺]_i (Haun et al., 1992; Fern, 1998; Thomas et al., 2004; Salter and Fern, 2008). Furthermore, ischaemia induces swelling of astrocytes that can lead to astrocyte death/dysfunction and/or further pathophysiologically relevant events such as neurotransmitter release (Kimelberg et al., 1990; Kimelberg, 2004; Kimelberg et al., 2004; Kimelberg, 2005). Importantly, glutamate receptor antagonists do not reduce astrocyte death during ischaemia. Of particular relevance to this study, there is currently no literature documenting whether or not P2 receptors are involved in mediating acute ischaemic astrocyte death. When one considers the widespread expression of P2 receptors on astrocytes and the important signalling functions they mediate, this question begs to be investigated.

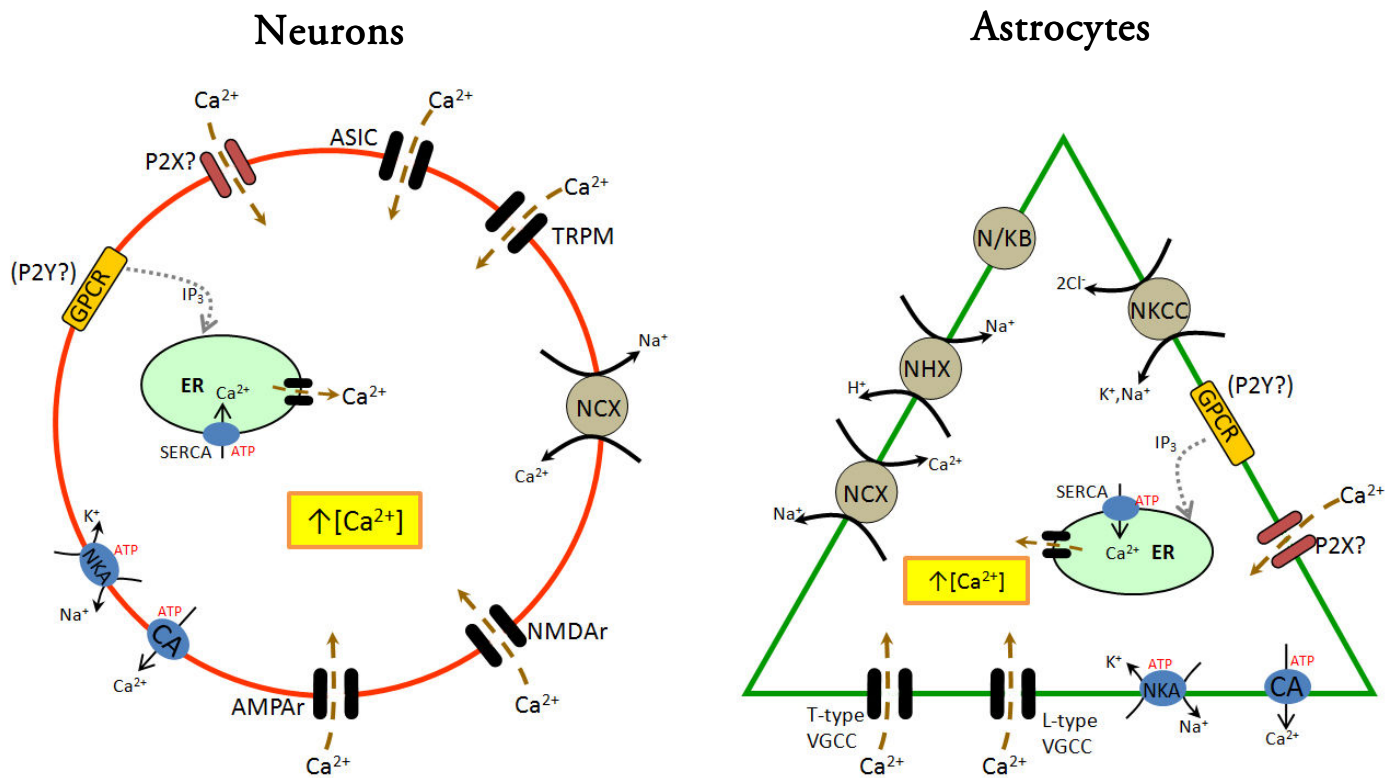


Figure 5-0: Pathways contributing to ischaemic ionic deregulation of neurons and astrocytes

Various pathways are involved in the toxic deregulation of ionic homeostasis which occurs during CNS ischaemia in both neurons and astrocytes (see text for references).

Following the onset of ischaemia in both cell types, intracellular ATP levels fall, inhibiting active transport systems involved in the maintenance of cellular ion homeostasis in both astrocytes and neurons, including the Na^+/K^+ -ATPase, sarco/endoplasmic reticulum Ca^{2+} -ATPase and Ca^{2+} -ATPase, effectively paralysing the ability of cells to remove excess cytoplasmic Ca^{2+} . The loss of ionic gradients leads to reverse operation of the $\text{Na}^+/\text{Ca}^{2+}$ -exchanger and further Ca^{2+} accumulation.

In astrocytes, Na^+/H^+ -exchanger activity contributes to early ionic imbalance, while activation of $\text{Na}^+/\text{K}^+/\text{2Cl}^-$ cotransporter, Na^+ -dependent/ K^+ -dependent HCO_3^- transporters, and voltage-gated Ca^{2+} channel are also involved.

In neurons, excess extracellular glutamate activates AMPA and NMDA receptors, leading to further excessive Ca^{2+} entry. Recently, transient potential channels of the melastatin subfamily (TRPM) and acid sensing ion channels (ASIC) have been shown to contribute significantly to Ca^{2+} entry during ischaemia.

Other ionotropic and metabotropic G-protein coupled receptors capable of mediating Ca^{2+} release from intracellular stores may also be involved. This included ionotropic P2X and metabotropic P2Y receptors, which were the main focus of my investigations.

NKA= Na^+/K^+ -ATPase, CA= Ca^{2+} -ATPase, SERCA=sarco/endoplasmic reticulum Ca^{2+} -ATPase, ER=endoplasmic reticulum, VGCC=voltage-gated Ca^{2+} channel, NCX= $\text{Na}^+/\text{Ca}^{2+}$ -exchanger, NHX= Na^+/H^+ -exchanger, N/KB= Na^+ -dependent and K^+ -dependent HCO_3^- transporters, NKCC= $\text{Na}^+/\text{K}^+/\text{Cl}^-$ cotransporter GPCR=g-protein coupled receptor, IP_3 =inositol-1,4,5-triphosphate, ASIC=acid sensing ion channel, TRPM= Transient receptor potential channel (melastatin subfamily)

Shortcomings of the NMDA-AMPA model of ischaemic cell death

Following the multitude of reports documenting effective neuroprotection by NMDA and AMPA receptor antagonists during experimental ischaemia in animal models, these antagonists entered early phase pre-clinical trials, where they universally failed to produce beneficial effects (Besancon et al., 2008; Ginsberg, 2008). A number of potential reasons for the shortcomings of efforts based primarily around NMDA and AMPA receptor antagonist have been postulated. The protective effect of blocking these receptors seems to decrease with increasing duration of ischaemic episodes: 30-60 minutes of OGD causes widespread delayed death of cultured neocortical neurons which could be significantly prevented by MK-801 or the non-NMDA receptor antagonist CNQX, while after 90-180 minutes of OGD the protective effect of MK-801, CNQX or a combination of both antagonists is overcome (Kaku et al., 1991; Aarts et al., 2003). Furthermore, there is only a short therapeutic window of opportunity for antagonist administration *in vivo* once ischaemia has set in (Margaill et al., 1996). Also, even low doses of glutamate receptor antagonists such as MK-801 produced unacceptable side-effects in humans, making it difficult to attain therapeutic drug levels in the brain (Ginsberg, 2008).

Further complications exist. It has recently emerged that while extrasynaptic NMDA receptor activation during ischaemia is harmful and leads to cell death, synaptic NMDA receptor activation has anti-apoptotic activity (Hardingham et al., 2002; Gouix et al., 2009). Therefore, NMDA receptor antagonists acting simultaneously at both synaptic and extrasynaptic sites may produce less overall benefit. Less intense NMDA and AMPA receptor activation has been shown to protect against glutamate toxicity in cultured neurons by increasing brain-derived neurotrophic factor (BDNF) production, while glutamate preconditioning also protects against future OGD-induced injury by activation of NMDA and AMPA receptors (Wu et al., 2004; Jiang et al., 2005; Lin et al., 2008a). Moreover, NMDA receptors are inhibited by acidic conditions similar to those which occur during *in vivo* ischaemia, so further pharmacological NMDA receptor blockade may not add a significant protective effect *in vivo* (Xiong et al., 2004). In addition, many other channels and pathways can carry large ionic currents and have been postulated to

contribute to ionic imbalance and cell death during ischaemia (Aarts et al., 2003; Xiong et al., 2004; Aarts and Tymianski, 2005; Besancon et al., 2008). These include Na⁺-Ca²⁺ exchangers (NCX), acid sensing ion channels (ASICs), transient receptor potential channels (TRPs) and non-selective cation channels (Aarts et al., 2003; Xiong et al., 2004; Aarts and Tymianski, 2005; Besancon et al., 2008).

A further potentially vital reason for the reduced *in vivo* efficacy of glutamate receptor antagonists is their inability to prevent astrocyte death or dysfunction. In humans, the ratio of astrocytes to neurons in the CNS is much higher than rodents, while single astrocytes are also larger, more complex and more diverse: for example, the domain of a single human astrocyte has been proposed to contain up to 2 million synapses (compared with 20,000-120,000 in rodents), so the death of even a single astrocyte has potentially more severe consequences (Takano et al., 2009). It is becoming increasingly evident then that effective neuroprotective therapies for ischaemic brain injury will need to look beyond AMPA and NMDA receptors and protect both neurons and glial cells. Furthermore, due to the myriad of mechanisms which are involved in mediating ischaemic cell death, an approach where drugs targeting multiple pathways are administered in combination appears to be a promising avenue of research (Doyle et al., 2008). P2 receptors may provide a further target for neuroprotection.

The case for ATP-mediated excitotoxicity during ischaemia

There is increasing evidence that ATP-mediated excitotoxicity may occur during CNS ischaemia. As demonstrated in Chapter 4, P2 receptor activation in astrocytes and neurons has the potential to cause large [Ca²⁺]_i rises similar to those produced by glutamate receptor activation. Furthermore, OGD induced significant ATP release from my co-cultures, a finding which is in agreement with multiple studies demonstrated that levels of extracellular ATP increase significantly during periods of ischaemia, both *in vivo* and *in vitro* (Hisanaga et al., 1986; Phillis et al., 1993; Phillis et al., 1996; Lutz and Kabler, 1997; Juranyi et al., 1999; Parkinson et al., 2002; Frenguelli, 2005; Melani et al., 2005; Schock et al., 2007; Schock et al., 2008). Moreover, prolonged direct application of relatively high

concentrations of exogenous ATP or non-selective P2 receptor agonists leads to delayed death of both neurons and glial cells *in vitro* and *in vivo*, mimicking the excitotoxic effect of glutamate (Ferrari et al., 1997; Amadio et al., 2002; Ryu et al., 2002; Volonte et al., 2003; Amadio et al., 2005; Matute et al., 2007).

The administration of various broad-spectrum P2 receptor antagonists via either intravenous, intraperitoneal or intracerebroventricular routes during *in vivo* models of ischaemia reduces infarct volume and/or improves neurological outcome (Kharlamov et al., 2002; Lammer et al., 2006; Melani et al., 2006). Details concerning the results and methodology from all studies investigating effects of P2 antagonists on ischaemic injury *in vivo* have been collated in **Table 5-1**. In addition, neuroprotective effects of broad-spectrum and more selective P2 receptor blockers has been reported in a variety of *in vitro* models of ischaemia (details collated in **Table 5-2**). For example, in a sequence of papers, Cavaliere and colleagues demonstrated that Suramin, PPADS and/or reactive blue 2 (RB-2) significantly reduce neuronal death in various different dissociated primary neuron cultures and slice cultures, as measured by PI uptake 20-24 hours after a period of hypoglycaemia or OGD (Cavaliere et al., 2001b; Cavaliere et al., 2003; Cavaliere et al., 2005).

Potential involvement of specific P2 receptor subtypes

Numerous P2 receptor subtypes have been implicated in ischaemic neuronal death. P2X₂ and P2X₄ receptors are upregulated on neurons in organotypic hippocampal slice cultures after OGD and *in vivo* on gerbil hippocampal CA1 and CA2 pyramidal cells after cerebral ischaemia (Cavaliere et al., 2003). P2X₂ receptor knock-down using antisense oligonucleotides reduces neuronal death after ischaemia in hippocampal slice culture (Cavaliere et al., 2003). In a different study, P2X₁ was upregulated 24 hours after an ischaemic insult in organotypic hippocampal slice cultures, and this upregulation was inhibited by the moderately selective P2X₁ antagonist TNP-ATP (Cavaliere et al., 2007). However, several lines of evidence along with the availability of specific antagonists/agonists led me to focus my investigations on P2X₇ and P2Y₁ receptor subtype involvement during ischaemia.

As discussed in Chapter 4, P2X₇ receptor expression has been documented in cortical neurons and astrocytes, and my experiments suggest possible functional expression on cultured cortical astrocytes. The P2X₇ receptor has several unique properties which make it particularly interesting in the context of cell death and damage during pathophysiology. P2X₇ is unique among P2 receptors for its low affinity to ATP (EC₅₀ >100uM, full activation >1mM), therefore making it most likely for widespread receptor responses to occur during injurious events such as ischaemia or traumatic injury when ATP levels have the potential to rise most dramatically (Gever et al., 2006). P2X₇ receptors are also characterised by their unique ability to induce the opening of an unusually large transmembrane pore (allowing the passage of molecules up to ~1000Da in size) upon prolonged uninterrupted stimulation by high concentrations of ATP (Surprenant et al., 1996; Duan and Neary, 2006; Ferrari et al., 2006; Pelegrin and Surprenant, 2006; Yan et al., 2008; Pelegrin and Surprenant, 2009).

Many large molecules capable of contributing to cytotoxicity are released by astrocytes and microglia upon P2X₇ large pore formation: astrocytes can release glutamate and ATP, while microglia release toxic agents including interleukin-1 β , tumour necrosis factor- α , superoxide and nitric oxide (Sperlagh et al., 2002; Duan et al., 2003; Murakami et al., 2003; Narcisse et al., 2005; Suadicani et al., 2006; Guerra et al., 2007; Lenertz et al., 2009). Apart from the potential for the release of such molecules, large pore formation can lead to a massive deregulation of cytoplasmic ion homeostasis similar to what is seen in CNS cell types during ischaemia, and when receptor stimulation is prolonged cells become irreversibly injured and committed to death (Surprenant et al., 1996; Ferrari et al., 1997; Di Virgilio et al., 1998; Schulze-Lohoff et al., 1998; Brough et al., 2002; Sperlagh et al., 2002; Duan et al., 2003; Fellin et al., 2006a; Ferrari et al., 2006). This direct toxic effect of P2X₇ over-activation has been described most extensively in immune cells, including microglia in the CNS, and it can lead to both necrotic and apoptotic death, although astrocytes and neurons may also be affected (Ferrari et al., 1997; Humphreys et al., 1998;

Schulze-Lohoff et al., 1998; Humphreys et al., 2000; Ferrari et al., 2006; Franke and Illes, 2006).

A possible involvement of P2X₇ receptors during CNS ischaemia has been suggested by various studies. P2X₇ receptor protein expression is upregulated on cultured cortical neurons but not astrocytes following 2 or 12 hours of OGD, while *in vivo* P2X₇ expression is increased in neurons, astrocytes and microglia in the peri-infarct region 1-7 days after middle cerebral artery occlusion (MCAO) (Franke et al., 2004; Milius et al., 2008). In a different rat *in vivo* study, immunohistochemistry revealed P2X₇ expression in penumbral microglia following MCAO, while no expression could be detected prior to the insult (Collo et al., 1997). Blocking P2X₇ receptors during a short period of OGD in hippocampal slices significantly delays the onset of anoxic depolarisation and prevents failure of neurotransmission in the CA1 region, while it also completely prevents cell death in hippocampal slice cultures measured 20 hours after 40 minutes of OGD (Coppi et al., 2007). However, it is still unclear what effects P2X₇ receptors have during prolonged severe ischaemia and whether blocking these receptors is protective of neurons and/or astrocytes. Furthermore, most studies have investigated cell death 24 hours after a short period of ischaemia (**Table 5-2**), so exact contributions of this receptor to cell death during the initial phase of the ischaemic insult cannot be extrapolated.

The first evidence that P2Y₁ receptors may be involved in mediating cell death and survival came from a study using astrocytoma cells transfected with human P2Y₁ receptors, where agonist induced P2Y₁ receptor activation caused apoptosis via the stimulation of mitogen-activated protein kinases, a finding which was successfully replicated by a second group (Sellers et al., 2001; Mamedova et al., 2006). A possible involvement during energy deprivation has been suggested by further studies. P2Y₁ receptor expression is downregulated in cultured cerebellar granule neurons following a period of hypoglycaemia (Cavaliere et al., 2002). By contrast, in cultured cortical astrocytes, P2Y₁ (and P2Y₂) receptors are transiently upregulated 1 hour (but not 24 hours) after 8 hours of OGD, and this is also coupled functionally to an increase in spontaneous intracellular Ca²⁺ oscillations

mediated by receptor activation in response to increased post-ischaemic extracellular ATP levels (Iwabuchi and Kawahara, 2009b, a). Furthermore, this receptor upregulation significantly increases the propagation speed of intracellular Ca^{2+} waves, leading to the speculation that the detrimental effects of glial Ca^{2+} waves during ischaemia could theoretically be attenuated by blocking these receptors (Nedergaard and Dirnagl, 2005; Iwabuchi and Kawahara, 2009a). Finally, blocking P2Y_1 receptors in hippocampal slices significantly delays and/or reduces the onset of anoxic depolarisation and failure of neurotransmission during a short period of OGD (Coppi et al., 2007).

Astrocyte-neuron interactions during ischaemia

Astrocytes can mediate both protective and damaging effects on neurons during ischaemia. For example, astrocyte glutamate transporters reverse during ischaemia, leading to neuronal death via over-activation of ionotropic glutamate receptors (Rossi et al., 2000; Mitani and Tanaka, 2003; Kosugi and Kawahara, 2006; Gouix et al., 2009). Dysfunction and metabolic paralysis of astrocytes leads to neuronal death, as the normal supportive functions of astrocytes are lost (Haberg et al., 2001; Dugan and Kim-Han, 2004; Pellerin and Magistretti, 2004; Haberg et al., 2006; Suh et al., 2007). On the other hand, astrocytes can use glycogen and glutathione stores and secrete neuroprotective cytokines such as glial-derived neurotrophic factor to promote neuronal survival during ischaemia (Swanson and Choi, 1993; Bolanos et al., 1996; Lucius and Sievers, 1996; Iwata-Ichikawa et al., 1999; Chen et al., 2001; Gegg et al., 2005; Suh et al., 2007; Sun et al., 2008). Furthermore, astrocytes also protect neurons from excitotoxicity during less severe ischaemia by continued glutamate transporter activity (Rosenberg and Aizenman, 1989; Sugiyama et al., 1989; Dugan et al., 1995; Rao et al., 2001). The balance of protective vs. damaging effects of astrocytes appears to be crucial in determining the outcome of ischaemia, so the effects of astrocytes on neuronal death during prolonged severe ischaemia were also investigated.

Table 5-1: Effects of P2 antagonists during *in vivo* ischaemia

Receptor(s)	Antagonist(s)	Methodology	Outcome	Ref.
P2	Suramin, IV, 100mg/kg estimated brain concentration: 10uM	Rat, permanent MCAT + CCA, outcomes tested after 6h	Improved neurological score, decreased infarct and oedema volume	A
P2	PPADS, ICV, 100uM, 10min before insult and twice daily thereafter	Spontaneously hypertensive rats, permanent MCAO, functional and histological analysis after 1, 3, 7 days	Significantly reduced motor deficit, reduced infarct volume after 7 days, reduced numbers of injured cells in penumbra	B
P2	RB-2, IP, 10 or 100mg/kg, 5min before insult	Rat, permanent MCAO, functional and histological analysis after 24h	Significant neurological improvement, reduced infarct volumes in cortex and striatum	C
P2	PPADS, ICV, 30uM, 5min before and 30min after insult	Mouse, 30min MCAO + 24h reperfusion	Increased lesion volume	D
P2X₇	P2X ₇ -/- or oxATP (3mM) or BzATP (30mM)	Mouse, 30-60min MCAO + 24h reperfusion	Equal or slightly increased lesion volume	D,E

min=minutes h=hours IV=intravenous ICV=intracerebroventricular IP=intraperitoneal MCAO=middle cerebral artery occlusion

MCAT + CCA=unilateral occlusion and transection of middle cerebral artery + bilateral occlusion of common carotid arteries

RB-2=reactive blue 2 oxATP=oxidised ATP

Ref: **A** (Kharlamov et al., 2002), **B** (Lammer et al., 2006), **C** (Melani et al., 2006), **D** (Le Feuvre et al., 2003), **E** (Le Feuvre et al., 2002)

Table 5-2: Effects of P2 antagonists during *in vitro* ischaemia

Receptor(s)	Antagonist(s)	Methodology	Outcome	Ref.
P2	RB-2 100, Suramin 100, PPADS 60	R, CGN, 8 DIV, 3h GD + 20h reperfusion, PI uptake	Cell death reduced by: 85% RB-2, 67% suramin, 36% PPADS	G
P2	RB-2 100	R, HNC, 8 DIV, 3h GD + 20h reperfusion, PI uptake	Complete prevention of cell death	G
P2	RB-2 100	R, CNC, 8 DIV, 3h GD + 20h reperfusion, PI uptake	No reduction in cell death	G
P2	Suramin 100	R, HSC, 3h OGD + 20h reperfusion, PI uptake	Complete prevention of cell death	H
P2	RB-2 100	R, CSSC, 40m OGD + 20h reperfusion, PI uptake	Significantly reduced cell death	H
P2	PPADS 100, TNP-ATP 50	R, CSSSN9, 40m OGD + 20h reperfusion, PI uptake	Significantly reduced cell death	I
P2	Suramin 200, PPADS 5-300	R, HSC, 32m OGD + ≤48h reperfusion, PI uptake	Significantly reduced cell death	J
P2	Suramin 100, PPADS 30	R, HS, 7m OGD + 15m reperfusion, function of neurotransmission monitored by fEPSP	Prevention of irreversible failure of neurotransmission, blocked or delayed anoxic depolarisation	K
P2X₇	KN-62 10, oxATP 200	R, CGN, 8 DIV, 3h GD + 20h reperfusion, PI uptake	No reduction in cell death	G
P2X₇	oxATP 100	R, HSC, 40m OGD + 20h reperfusion, PI uptake	Complete prevention of cell death	L
P2X₇	oxATP 200	R, HSC, 32m OGD + ≤48h reperfusion, PI uptake	No reduction in cell death	J
P2X₇	BBG 1	R, HS, 7m OGD + 15m reperfusion, function of neurotransmission monitored by fEPSP	Prevention of irreversible failure of neurotransmission, blocked or delayed anoxic depolarisation	K
P2X₂	P2X ₂ antisense oligonucleotides	R, HSC, 3h OGD + 20h reperfusion, PI uptake	Significantly reduced cell death	H
P2X₁	NF279 5, TNP-ATP 1-40	R, HSC, 32m OGD + ≤48h reperfusion, PI uptake	No reduction in cell death	J
P2X₁	TNP-ATP 10, 50, 200	R, HSC, 40m OGD + 24h reperfusion, PI uptake	Significant dose-dependent reduction in cell death by: 10-15%, 30-40%, 70%	M
P2X₃	TNP-ATP 1-40	R, HSC, 32m OGD + ≤48h reperfusion, PI uptake	No reduction in cell death	J
P2Y₁	MRS-2179 10	R, HS, 7m OGD + 15m reperfusion, function of neurotransmission monitored by fEPSP	Prevention of irreversible failure of neurotransmission, blocked or delayed anoxic depolarisation	K

All drug concentrations are in μM m=minutes h=hours R=rat CGN=cerebellar granule neuron culture HNC=hippocampal neuron culture CNC=cortical neuron culture HSC=hippocampal slice culture CSSC=cortical/striatal slice culture CSSSN9=cortical/striatal/subventricular zone slice + N9 microglial cell line co-culture HS=acute hippocampal slice fEPSP=field excitatory post synaptic potential DIV=days *in vitro* GD=glucose deprivation OGD=oxygen/glucose deprivation PI=propidium iodide RB-2=reactive blue 2 oxATP=oxidised ATP BBG=brilliant blue G TNP-ATP=trinitrophenyl ATP

Ref.: **G** (Cavaliere et al., 2001b), **H** (Cavaliere et al., 2003), **I** (Cavaliere et al., 2005), **J** (Runden-Pran et al., 2005), **K** (Coppi et al., 2007), **L** (Cavaliere et al., 2004a), **M** (Cavaliere et al., 2007)

Objectives

The overwhelming majority of published studies investigating ischaemic cell death of neurons and astrocytes describe levels of death and/or dysfunction hours or days after the insult. Therefore, there is still a lack of detailed information about the early time course of cell death during severe ischaemia. Past efforts which focused solely on preventing glutamate toxicity have failed to produce significant neuroprotection during prolonged *in vitro* and *in vivo* ischaemia, suggesting that other pathways such as ATP-mediated excitotoxicity are involved. Having demonstrated excessive OGD induced glutamate and ATP release (Chapter 3) as well as widespread functional glutamate and P2 receptor expression in these cells (Chapter 4), parallel pathways of glutamate and ATP-mediated excitotoxicity may operate during ischaemia. The involvement of P2 receptors in the early phase of ischaemic cell death and the ischaemic injury of astrocytes is at this point unknown. Therefore, using primary cortical cultures of astrocytes and neurons or co-cultures of both cell types, I investigated in detail the time course of cell death during a 90 minute exposure to OGD, the relative contributions of astrocyte and neuronal death to overall cell death during ischaemia and any involvement/relative contributions of P2 and glutamate receptors in mediating cell death. This study provides novel insights into the contributions of P2 receptors to cell death of astrocytes and neurons during the early phase of severe ischaemia.

RESULTS

Cells in astrocyte cultures, neuronal cultures and co-cultures were loaded with either Fura-2ff or CMFDA and imaged continuously during exposure to 90 minutes of OGD or control conditions, allowing for the precise time of death of each cell to be recorded. Data collected from experiments is presented in a number of ways: graphs demonstrate the amount of cell death, dynamics of cell death over time and, in some experiments, effects on $[Ca^{2+}]_i$. The amount of cell death during the course of the experiments is presented as a percentage of total cells (mean \pm SEM) that died by the end of the imaging period. This is further broken down to illustrate the cumulative amount of cell death after every 5 minute period of the experiment, allowing for statistical comparisons after different time points. The time-course of cell death is also depicted using frequency histograms showing the amount of cell death occurring during every 5 minute period as a percentage of total cell death (non-cumulative), normalised to the amount of cell death during OGD (so that scales are relative to the amount of overall cell death for each condition). The time points of cell death for all cells undergoing a given experiment were averaged to give a mean time to cell death (n: number of cells that died). Finally, it became apparent that some conditions/drugs affected the time to the onset of first cell death: to statistically compare the speed of onset of cell death between conditions the average time to *first* cell death was calculated by recording the time-point of death of the first cell that died during each experiment and averaging them (n: number of slides).

For statistics, when two groups were compared two-tailed unpaired t-tests (with Welch's correction if there was unequal variance) were performed and when three or more groups were compared a one-way ANOVA with Tukey's multiple comparison test was used. Example images of cell fluorescence from representative slides of some experiments are displayed. In most co-culture experiments, individual cells were identified morphologically as either neurons or astrocytes as described in the materials and methods chapter, allowing effects on neurons and astrocytes to be distinguished. Finally, some of the co-culture and all of the neuronal culture experiments were performed using Fura-2ff loaded cells, so for these experiments data is also presented showing changes in $[Ca^{2+}]_i$.

OGD causes significant cell death of cultured neurons and astrocytes

Effect of OGD on astrocyte cultures, neuronal cultures and co-cultures

A period of 90 minutes of OGD caused increased cell death compared to controls in the co-culture (see **Figures 5-1** and **5-2** for example images), but not in the astrocyte or neuronal cultures (see **Figures 5-3** to **5-6** for example images). In co-cultures, $44.46 \pm 3.28\%$ of cells died during OGD (n:36, 5488 cells), compared to $4.15 \pm 1.51\%$ during control conditions (n:22, 3211 cells) ($p < 0.001$) (**Figure 5-7: A**). The timescale of cumulative cell death in co-culture reveals that during OGD significant cell death was present compared to controls after 20 minutes (**Figure 5-7: F**), with both the mean time to cell death (control- 76.25 ± 1.8 minutes, n:92 vs. OGD- 60.06 ± 0.4 minutes, n:2421, $p < 0.001$; **Figure 5-7: B**) and average time to first cell death (control- 43 ± 4.54 minutes, n:22 vs. OGD- 31.25 ± 2.66 minutes, n:36, $p < 0.05$; **Figure 5-7: C**) occurring significantly earlier during OGD. In the astrocyte cultures $17.64 \pm 8.56\%$ of cells died during OGD (n:11, 1323 cells) compared with $0.98 \pm 0.4\%$ during controls (n:10, 1049), a difference which did not reach statistical significance ($p > 0.05$) (**Figure 5-7: A**). The cumulative timescale of cell death revealed that the difference in cell death between OGD and control conditions never reached statistical significance at any point in time (**Figure 5-7: E**). There were also no significant differences in the mean time to cell death (control- 70 ± 3.49 minutes, n:13 vs. OGD- 74.59 ± 0.76 minutes, n:360; **Figure 5-7: B**) or average time to first cell death (control- 66 ± 3.83 minutes, n:10 vs. OGD- 50 ± 7.81 minutes, n:11; **Figure 5-7: C**) in the astrocyte culture comparing OGD vs. controls. In the neuronal cultures the difference in cell death between OGD and control conditions was small, with $10.56 \pm 2.8\%$ cell death during OGD (n:18, 1210 cells) and $9.89 \pm 2.9\%$ during controls (n:10, 1116 cells) (**Figure 5-7: A**), with the cumulative timescales of cell death during both conditions mirroring each other (**Figure 5-7: D**). In the neuronal culture there were no significant differences in the mean time to cell death (control- 65.81 ± 1.91 minutes, n:111 vs. OGD- 68.16 ± 1.74 minutes, n:128; **Figure 5-7: B**) or average time to first cell death (control- 48.75 ± 5.84 minutes, n:10 vs. OGD- 49.23 ± 4.88 minutes, n:18; **Figure 5-7: C**) when comparing OGD vs. controls.

Comparing effects of OGD and control conditions on cell death in different cultures

When comparing cultures, there was significantly ($p < 0.001$) reduced cell death during OGD but not control conditions in both the astrocyte and neuronal cultures compared to co-cultures (**Figure 5-8: A**), with the difference becoming significant for the first time after 40 minutes in the neuronal culture and 45 minutes in the astrocyte culture (**Figure 5-8: D, E**). As demonstrated by **Figure 5-8: F**, cells first started to die in all three cultures within 5-10 minutes of the onset of OGD. However, it was in the co-culture that large amounts of cell death started to occur earliest, rising steadily to a peak rate at 60-65 minutes, whereas in both the astrocyte and neuronal culture substantial death rates are reached later and do not reach a maximum rate until the end of the experiment in the 85-90 minute period. These differences in the timescale of cell death between the astrocyte and neuronal cultures compared with the co-culture are further demonstrated by **Figure 5-8: B, C**: in the astrocyte culture there was a significantly longer delay in the average time to first cell death during OGD ($p < 0.05$) and control ($p < 0.01$) conditions and the mean time to cell death ($p < 0.001$) during OGD, whilst in the neuronal cultures the mean time to cell death was increased during OGD ($p < 0.05$) and decreased during control ($p < 0.001$), with the average time to first cell death during OGD being delayed ($p < 0.05$).

In summary, OGD caused significant quantities of cell death compared to controls solely in the co-culture, with more and earlier cell death occurring in co-culture compared with both the neuronal and astrocyte cultures. These results suggested that something was occurring in the co-culture which caused earlier and more widespread cell death compared with the 'pure' cultures of astrocytes or neurons.

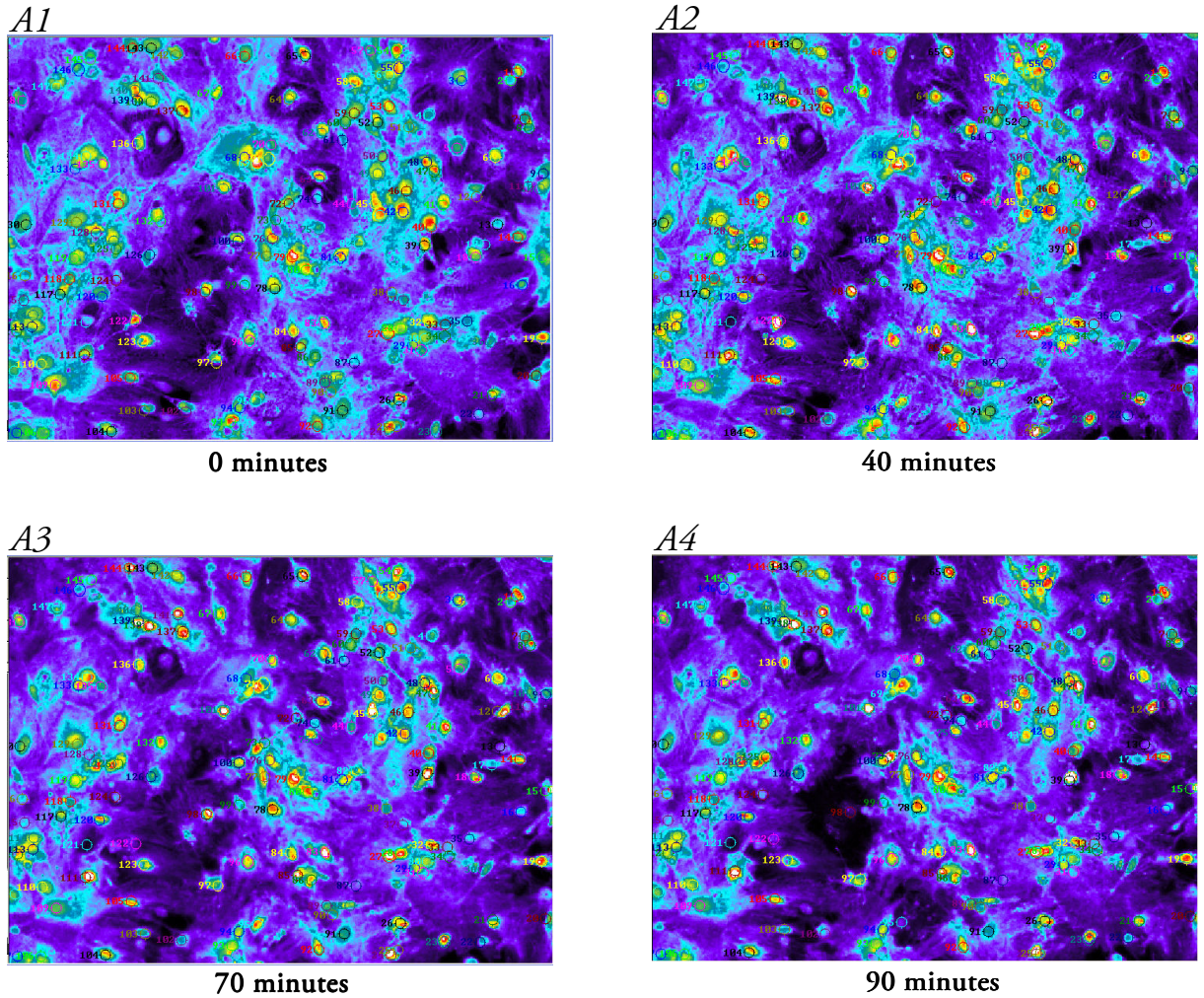


Figure 5-1: Example images of CMFDA loaded co-culture, control

A1-A4: Pseudocolour images of CMFDA fluorescence during a control experiment using the co-culture

All cells are alive at the start of the experiment (**A1**), with only 4 cells dying during the 90 minutes of perfusion with aCSF (control conditions).

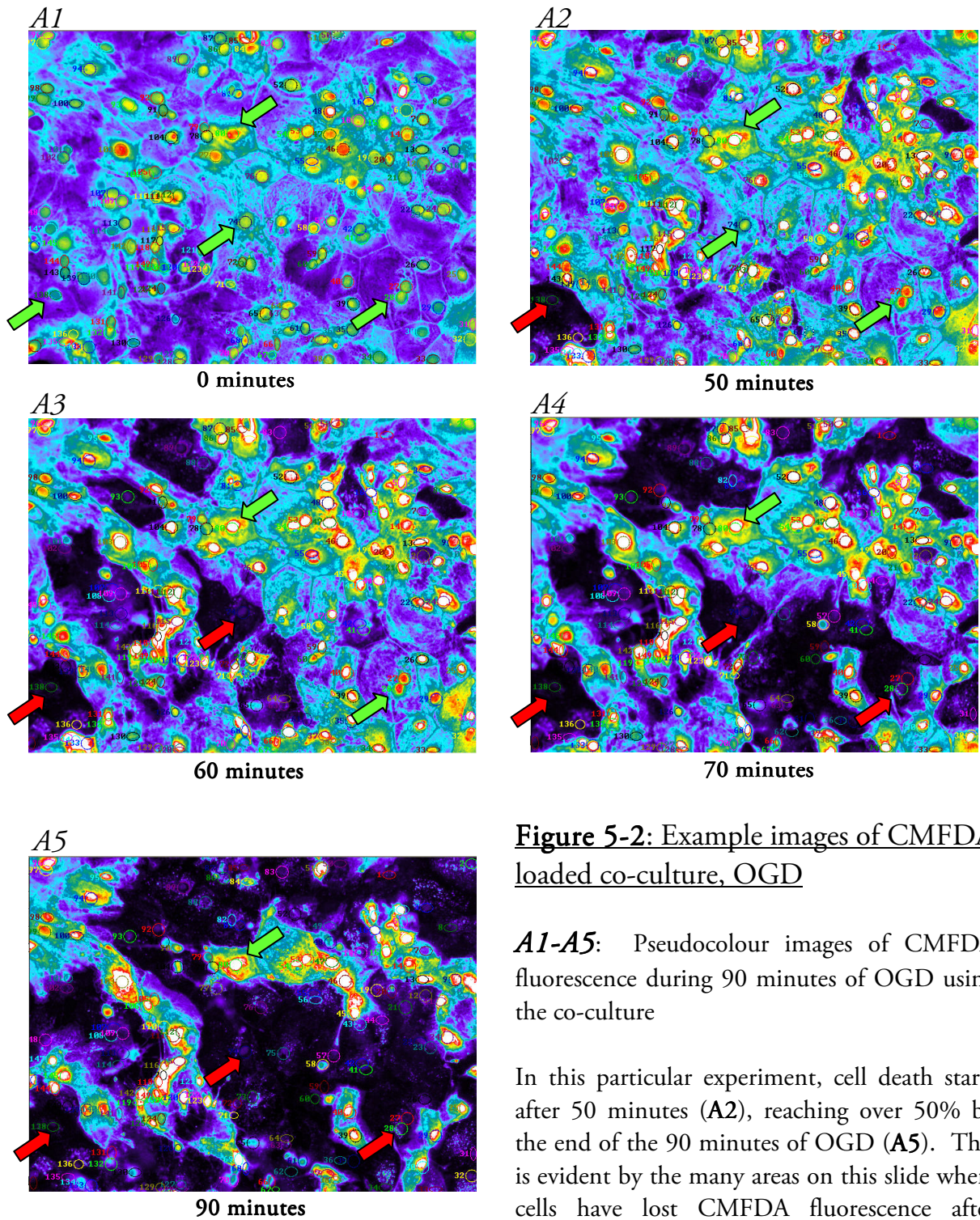


Figure 5-2: Example images of CMFDA loaded co-culture, OGD

A1-A5: Pseudocolour images of CMFDA fluorescence during 90 minutes of OGD using the co-culture

In this particular experiment, cell death starts after 50 minutes (*A2*), reaching over 50% by the end of the 90 minutes of OGD (*A5*). This is evident by the many areas on this slide where cells have lost CMFDA fluorescence after dying.

Green arrows point at sample cells, with arrows turning red when the cell has died.

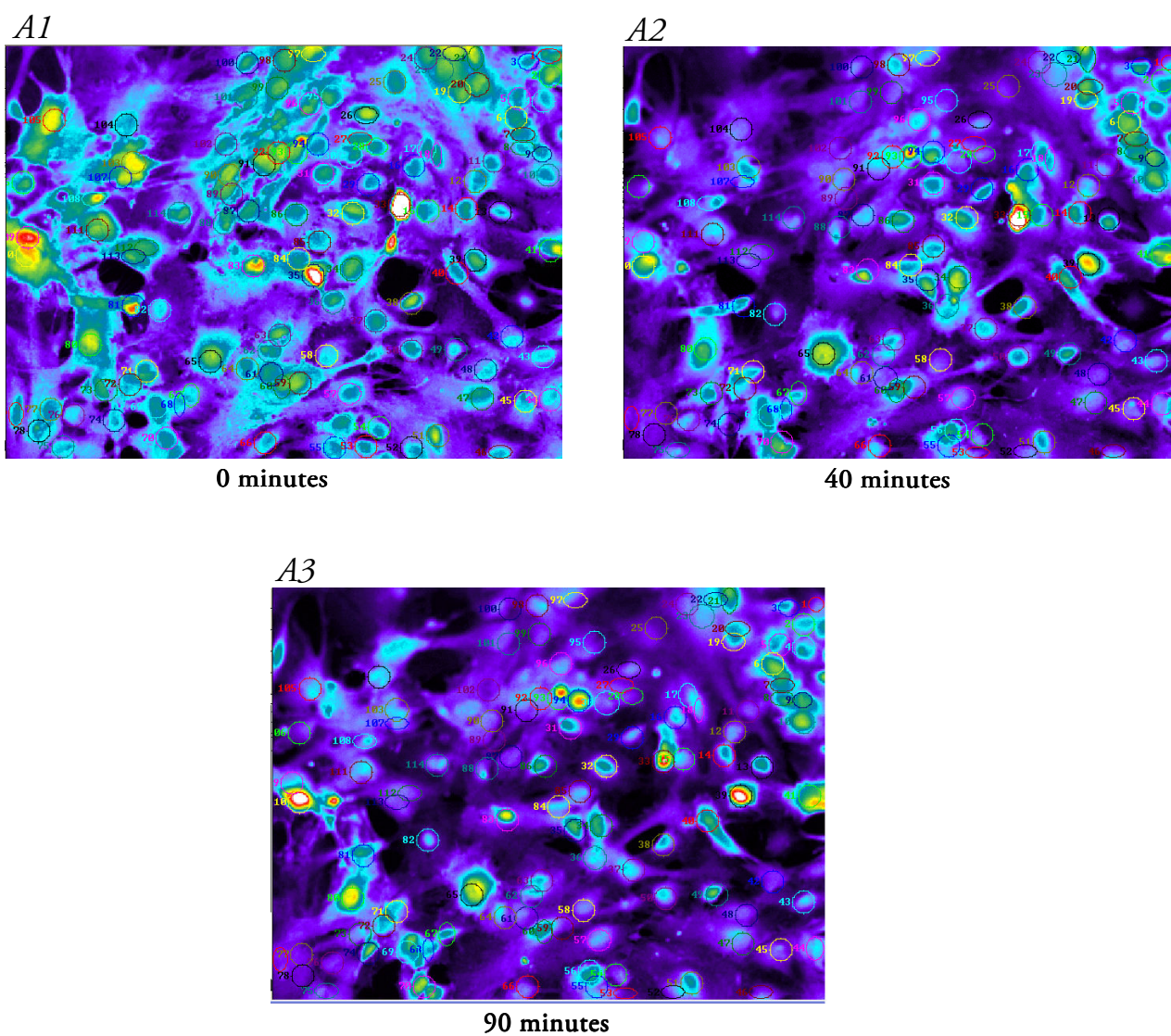


Figure 5-3: Example images of CMFDA loaded astrocyte culture, control

A1-A3: Pseudocolour images of CMFDA fluorescence during a control experiment.

No cells died during this control experiment.

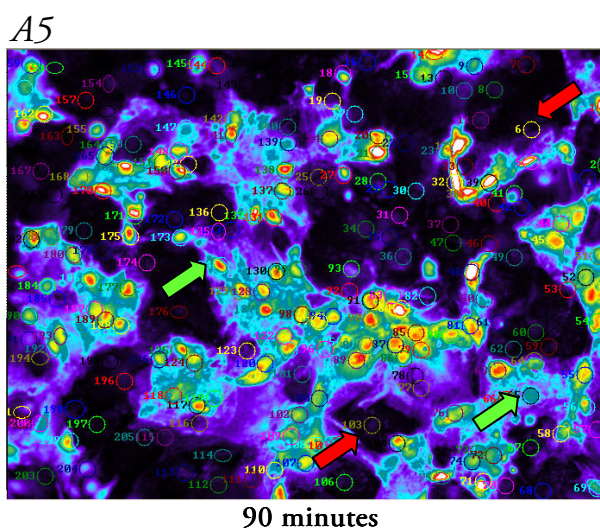
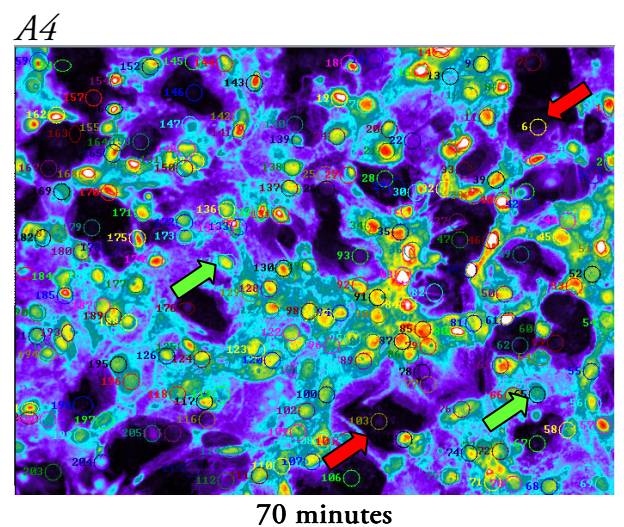
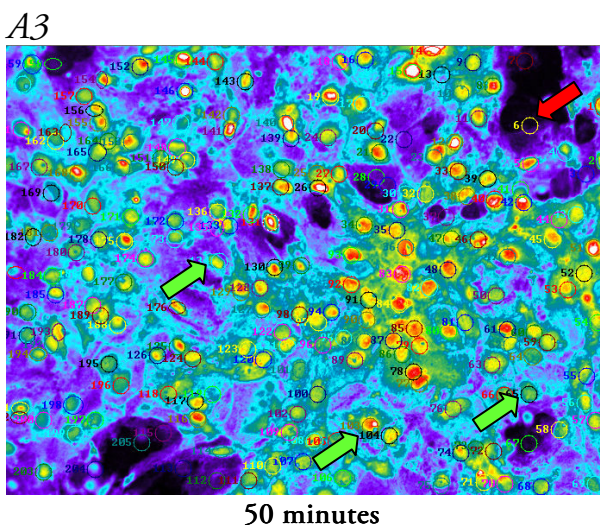
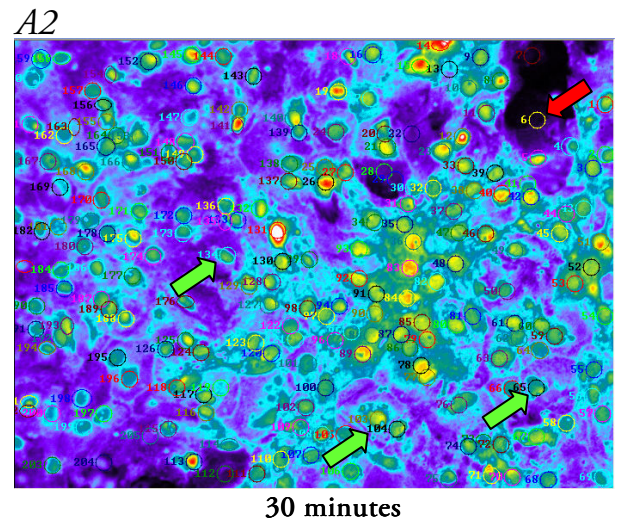
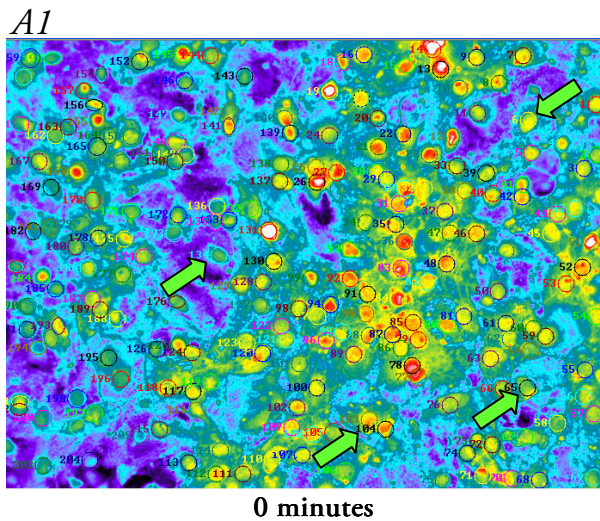


Figure 5-4: Example images of CMFDA loaded astrocyte culture, OGD

A1-A5: Pseudocolour images of CMFDA fluorescence during 90 minutes of OGD.

At the start of the experiment (*A1*) all of the cells are alive, and cells first begin to die after 30 minutes (*A2*). By 90 minutes (*A5*), 85 out of the 205 cells have died (41.46% cell death).

Green arrows point at sample cells- arrows turn red when the cell has died.

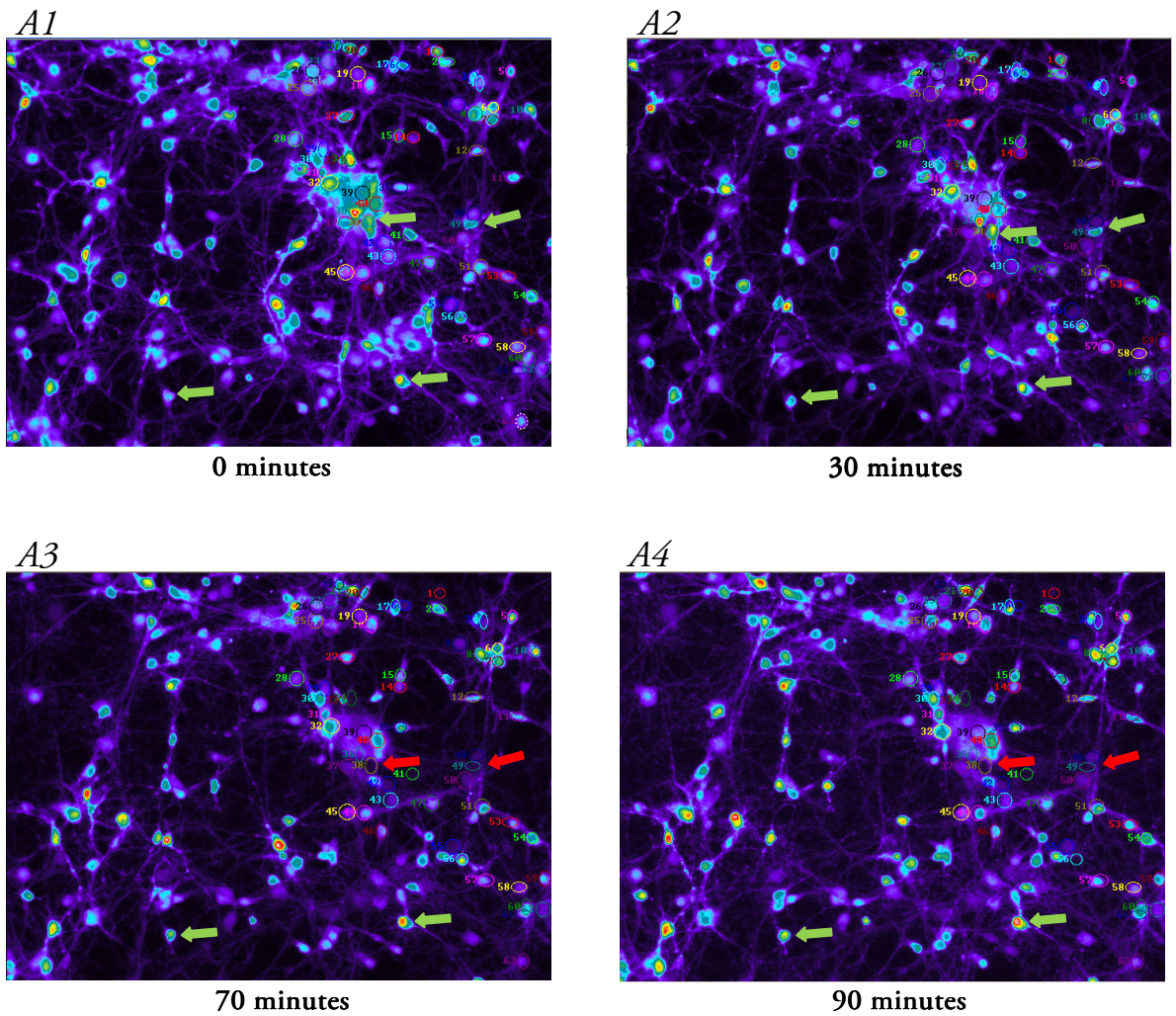


Figure 5-5: Example images of Fura-2ff loaded neuronal culture, control

A1-A4: Pseudocolour images of Fura-2ff fluorescence during a control experiment using the neuronal culture

All cells are alive at the start of the experiment (**A1**), and there are a few cells that died during the 90 minutes of perfusion with aCSF (control conditions). Some example cells are indicated using arrows: green arrows show live cells, with arrows turning red when the cell has died (evident by a sudden lack of fluorescence).

Note also that fluorescence is well-maintained throughout the 90 minutes of the experiment when using Fura-2ff in neurons.

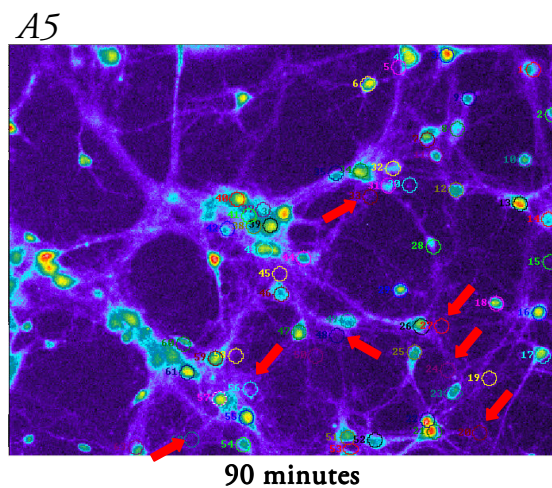
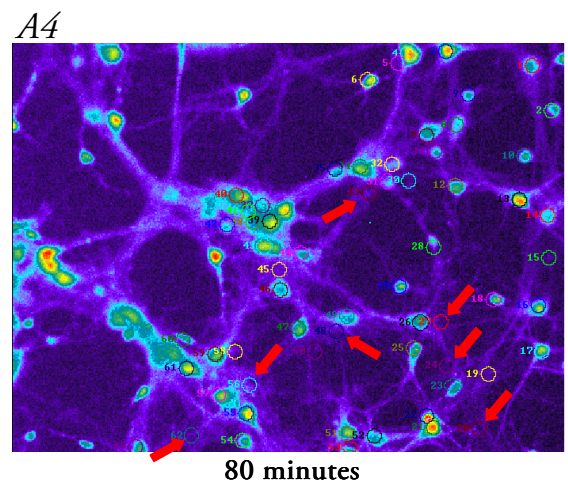
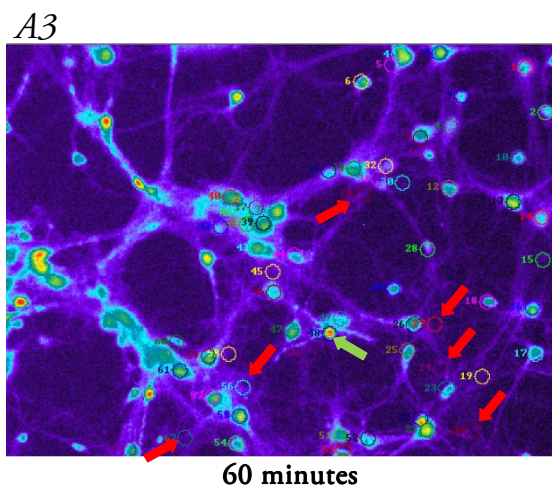
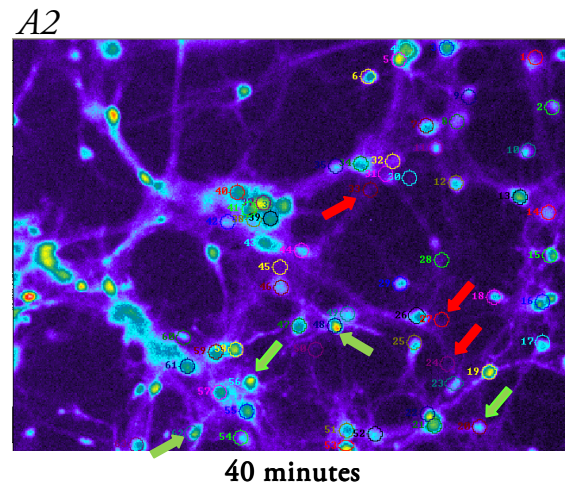
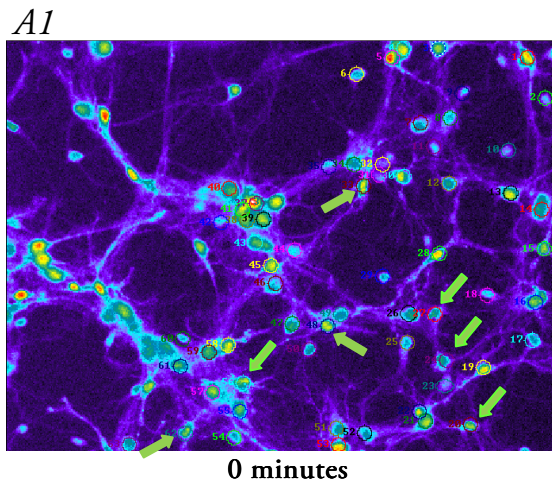


Figure 5-6: Example images of Fura-2ff loaded neuronal culture, OGD

A1-A5: Pseudocolour images of Fura-2ff fluorescence during 90 minutes of OGD in the neuronal culture

At the start of the experiment (**A1**) all of the cells are alive (some examples are highlighted using green arrows), but by 40 minutes (**A2**) some of the cells have died, as evidenced by a lack of fluorescence (when example cells have died arrows turn red).

Most neurons on this coverslip survived 90 minutes of OGD.

Figure 5-7: Effect of OGD vs. control on cell death in co-culture, astrocyte culture and neuronal culture

A: Effect of OGD vs. control on total cell death in different cultures

Both the co-culture and astrocyte culture demonstrate increased cell death during OGD compared to control, although it is only significant in the co-culture ($p < 0.001$). In the neuronal culture OGD did not cause increased cell death.

B: Mean time to cell death

There was a significant reduction in the mean time it took for cells to die during OGD compared to controls in the co-culture ($p < 0.05$).

C: Average time to first cell death

There was a reduction in the average time it took for cells to start dying during OGD compared to controls in the co-culture ($p < 0.05$) and astrocyte culture (not significant).

D,E,F: Timescale of cumulative cell death during 90 minutes of OGD vs. controls, different cultures

Significant cell death started in the co-culture (**F**) after 20 minutes of OGD ($p < 0.05$), with the difference becoming gradually more significant with time. In both the astrocyte (**E**) and neuronal (**D**) culture there were never any significant differences in cell death between OGD and controls after any time point.

It was therefore only in the co-culture that the analysed parameters were significantly different when comparing OGD vs. control conditions.

*: $p < 0.05$

** : $p < 0.01$

***: $p < 0.001$

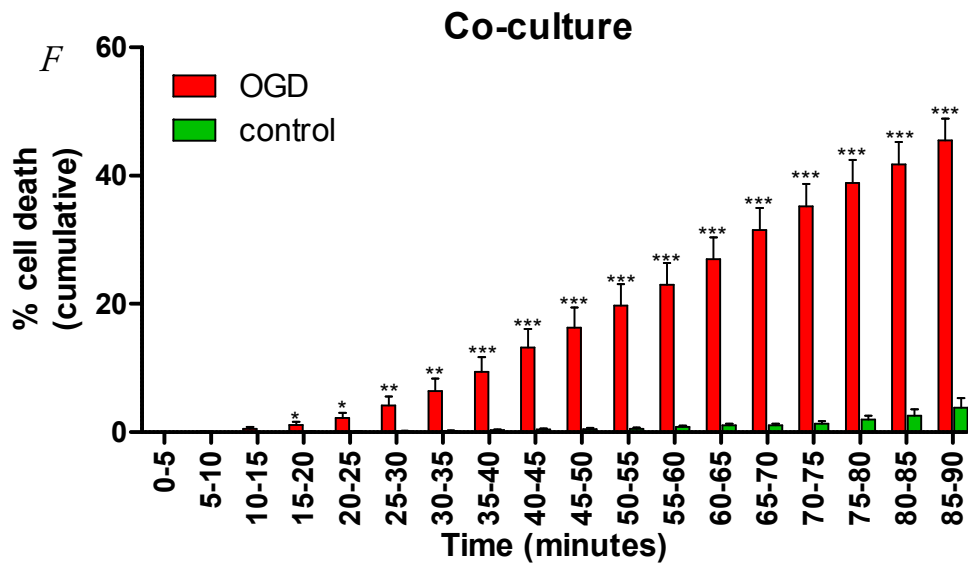
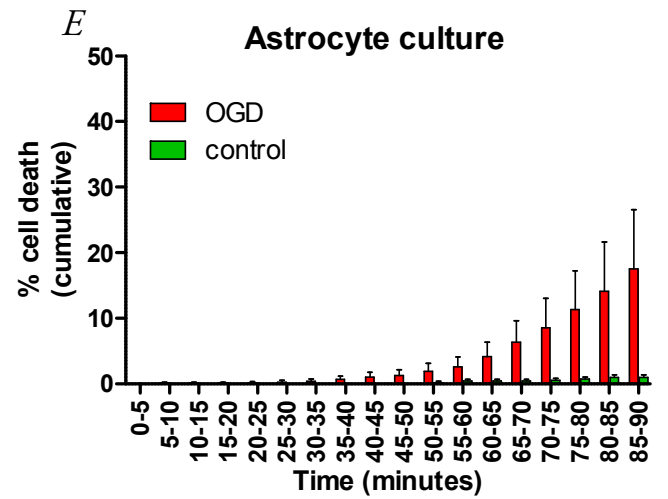
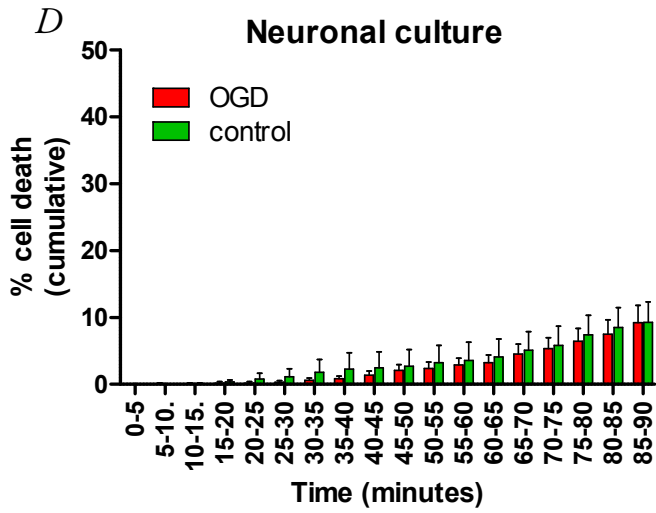
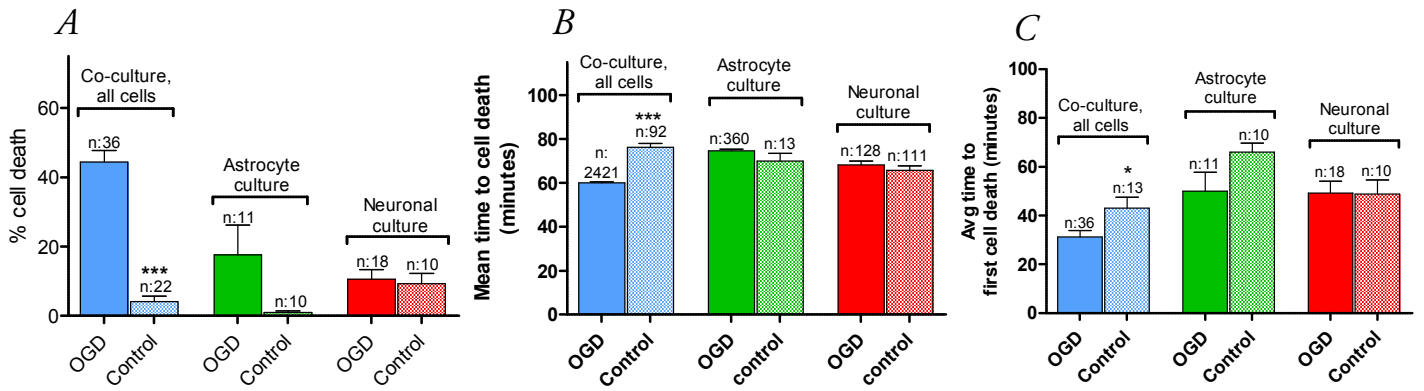


Figure 5-8: Effect of OGD and control conditions on cell death: comparing co-culture, astrocyte culture and neuronal culture

A: Effect of OGD vs. control on total cell death

Both the neuronal culture and astrocyte culture demonstrate significantly ($p < 0.001$) less cell death after 90 minutes of OGD compared to co-cultures. There were no significant differences during control conditions between cultures.

B: Mean time to cell death

There was a significant reduction in the mean time it took for cells in the co-culture to die during OGD compared to both the astrocyte culture ($p < 0.001$) and the neuronal culture ($p < 0.05$). The mean time to cell death during control conditions was significantly reduced ($p < 0.001$) in the neuronal culture compared with the co-culture.

C: Average time to first cell death

There was a reduction in the average time it took for cells to start dying during OGD in the co-culture compared to both the astrocyte and neuronal cultures ($p < 0.05$), whilst during control conditions cells started dying significantly later in the astrocyte culture compared to the co-culture ($p < 0.01$).

D,E: Timescale of cumulative cell death during 90 minutes of OGD, comparing different cultures

Significantly more cell death during OGD occurred in the co-culture compared with the neuronal and astrocyte cultures after 40 and 45 minutes ($p < 0.05$) respectively, with the difference becoming gradually more significant with time. Two versions of this graph are shown as **D** allows for easier labelling of statistical outcomes whilst **E** makes it easier to compare dynamics between cultures.

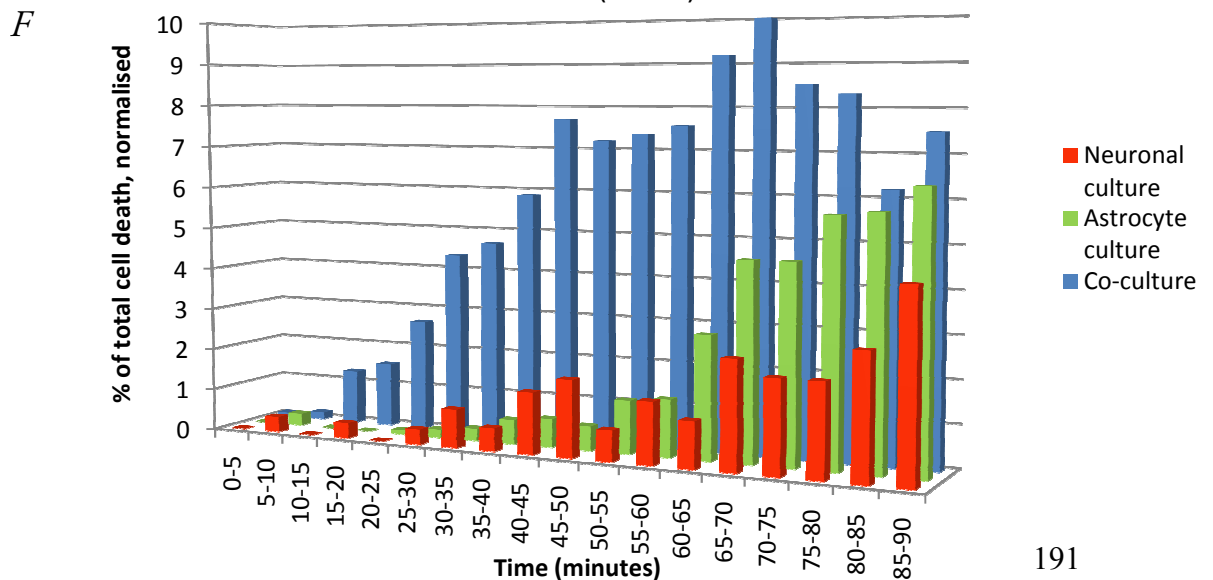
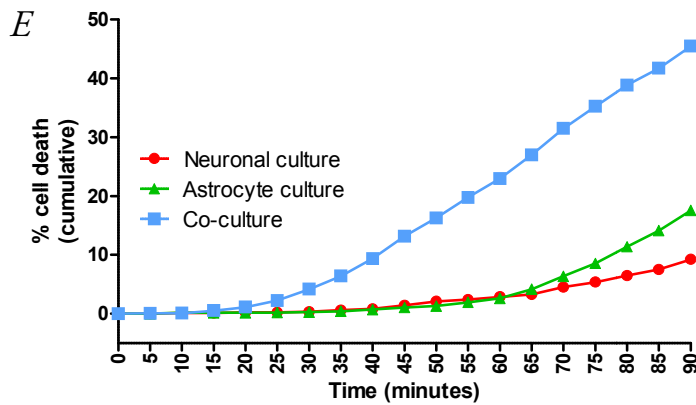
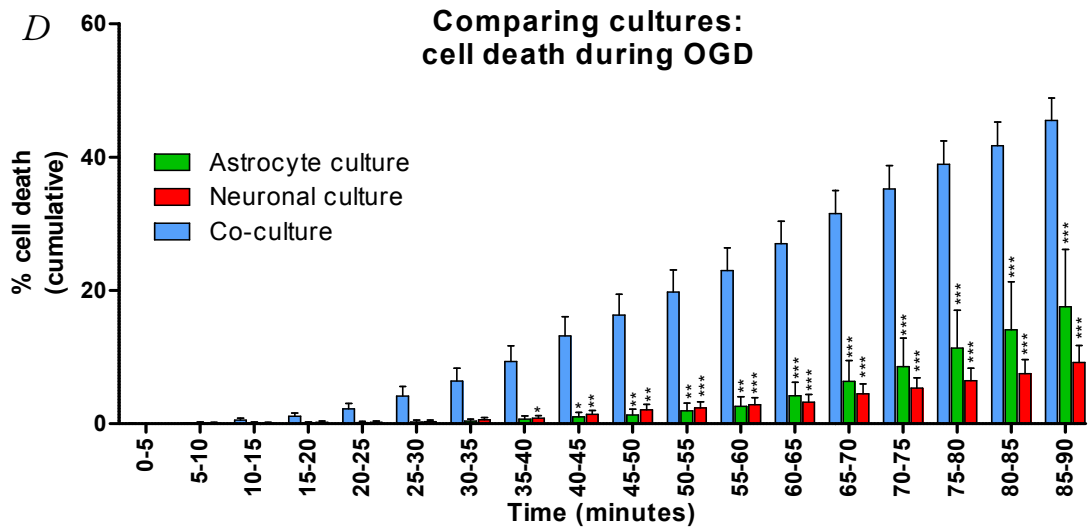
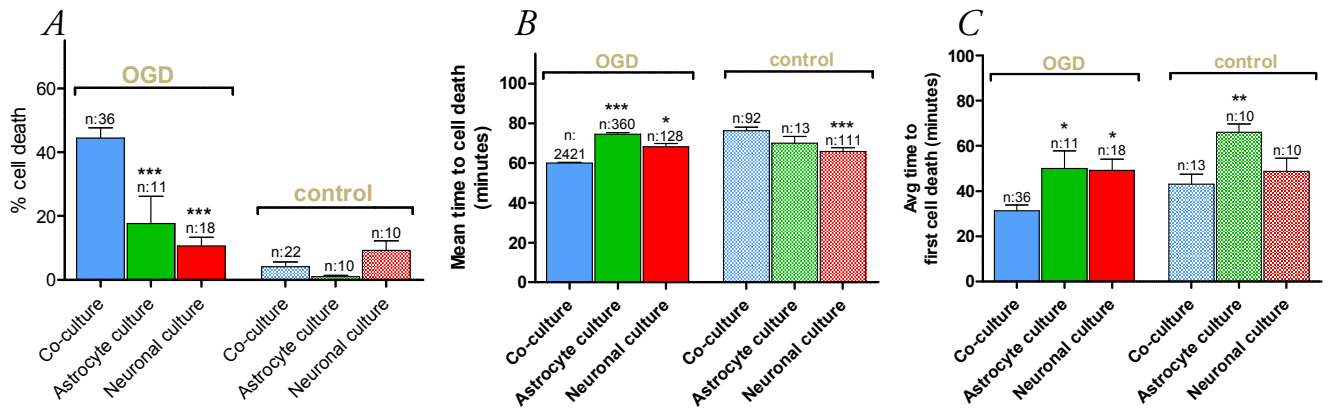
F: Frequency histogram of cell death during 90 minutes of OGD

Significant cell death started earliest in the co-culture, rising steadily to a peak rate at 65-70 minutes. In both the astrocyte and neuronal culture cell death starts later and does not reach a maximum rate until the end of the experiment in the 85-90 minute period.

*: $p < 0.05$

** : $p < 0.01$

***: $p < 0.001$



Effect of co-culturing vs. mono-cultures on astrocyte and neuronal death during OGD

To investigate what cell types were affected by the increased cell death in co-cultures during OGD, individual cells were identified morphologically as either neurons or astrocytes as described in the methods and materials chapter. This analysis revealed that during OGD in the co-culture $23.2 \pm 2.5\%$ of neurons (n:22, 1589 cells) and $50.04 \pm 4.51\%$ of astrocytes died (n:22, 1997 cells), whilst during control conditions $1.73 \pm 0.6\%$ of neurons (n:13, 1052 cells) and $5.77 \pm 2.4\%$ of astrocytes (n:13, 1303 cells) perished (**Figure 5-9: A**). Compared to the astrocyte and neuronal cultures, there was a significant increase in astrocyte death ($p < 0.001$) and neuronal death ($p < 0.01$) in the co-culture during OGD (**Figure 5-9: A**), with astrocyte death first becoming significant after 45 minutes and neuronal death after 50 minutes (**Figure 5-10: A, B**). Interestingly, there was a significant ($p < 0.01$) reduction in neuronal death in the co-culture versus the neuronal culture during control conditions (**Figure 5-9: A**). This suggests that the presence of astrocytes is protective to neurons during control conditions but harmful during OGD. Astrocytes in co-culture had a significantly reduced mean time to cell death (62.23 ± 0.58 minutes, n:1030; $p < 0.001$) and average time to first cell death (34.55 ± 3.08 minutes, n:22; $p < 0.05$) during OGD compared to the astrocyte culture, with the average time to first cell death of astrocytes also significantly earlier during control conditions in co-culture (50.83 ± 5.51 minutes, n:13; $p < 0.01$) relative to the astrocyte culture (**Figure 5-9: B, C**). The mean time to cell death and average time to first death of neurons was not significantly different between the co-culture (66.07 ± 0.95 minutes, n:354/ 38.18 ± 3.15 minutes, n:22 respectively) and neuronal culture (**Figure 5-9: B, C**). Looking at the frequency histograms of astrocyte death once again demonstrates earlier onset in the co-culture, reaching a peak rate at 65-70 minutes, whereas in the astrocyte cultures substantial cell death started after 50 minutes and reached a peak rate at 85-90 minutes (**Figure 5-10: C**). The frequency histograms of neuronal death in the co-culture and neuronal culture are very similar, with the main difference being the increased amount of death in the co-culture (**Figure 5-10: D**).

In summary, there is significantly more astrocyte death during OGD in the co-culture, and it is earlier both in onset and mean time to cell death than in the astrocyte culture. There is also significantly more neuronal death in the co-culture during OGD but significantly less during control conditions compared to neuronal cultures, without the onset or mean time to death being significantly different.

Figure 5-9: Effect of co-culturing neurons and astrocytes on cell death during OGD and control conditions

This figure compares the effects of OGD and control conditions on neuronal and astrocyte death when the cells were either co-cultured or in 'pure' cultures.

A: % total cell death

Co-cultures had significantly more astrocyte ($p < 0.001$) and neuronal ($p < 0.01$) death than the astrocyte or neuronal cultures. Interestingly, there was significantly less neuronal death during control conditions in co-cultures compared with neuronal cultures ($p < 0.01$), suggesting that the presence of astrocytes is neuro-protective during control conditions yet harmful during OGD.

B: Mean time to cell death

There was a significant delay in the mean time it took for astrocytes to die during OGD when comparing the astrocyte culture to the co-culture ($p < 0.001$). There were no significant differences regarding mean time of neuronal death.

C: Average time to first cell death

There was a significant delay in the average time it took for astrocytes to start dying during both OGD ($p < 0.05$) and control ($p < 0.01$) conditions when comparing the astrocyte culture to the co-culture. There were no significant differences regarding onset of neuronal death between the two cultures.

In summary, neuronal death is increased and astrocyte death is increased and earlier in the co-culture.

*: $p < 0.05$

** : $p < 0.01$

***: $p < 0.001$

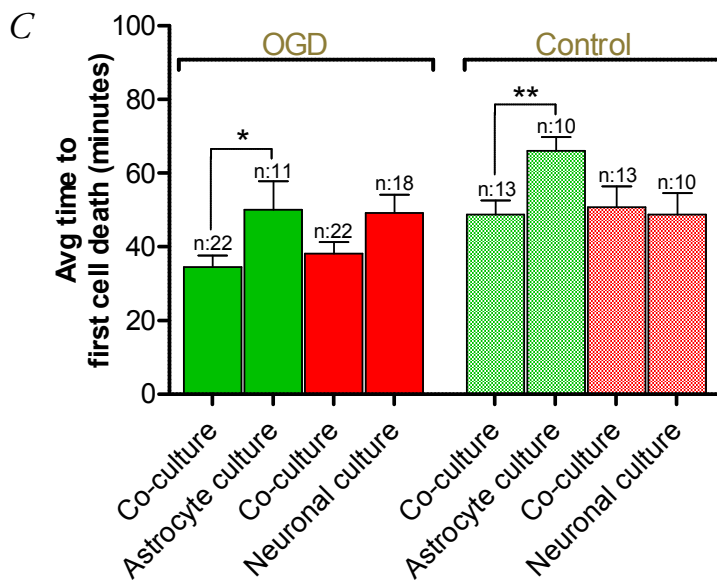
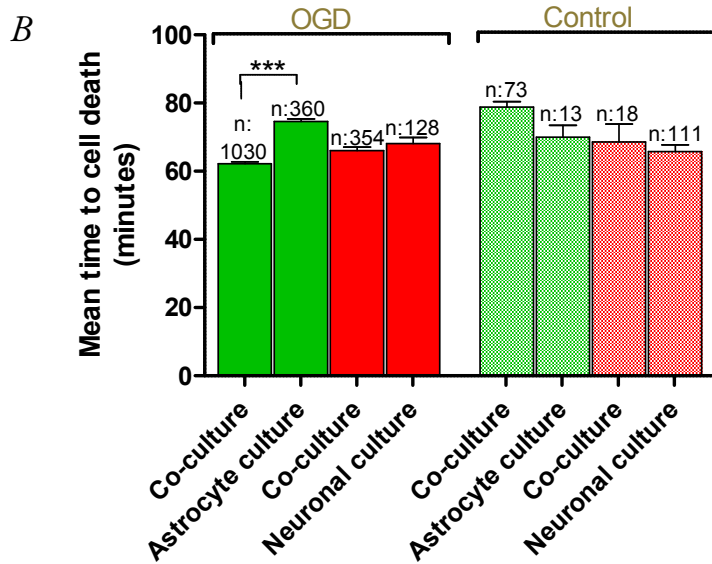
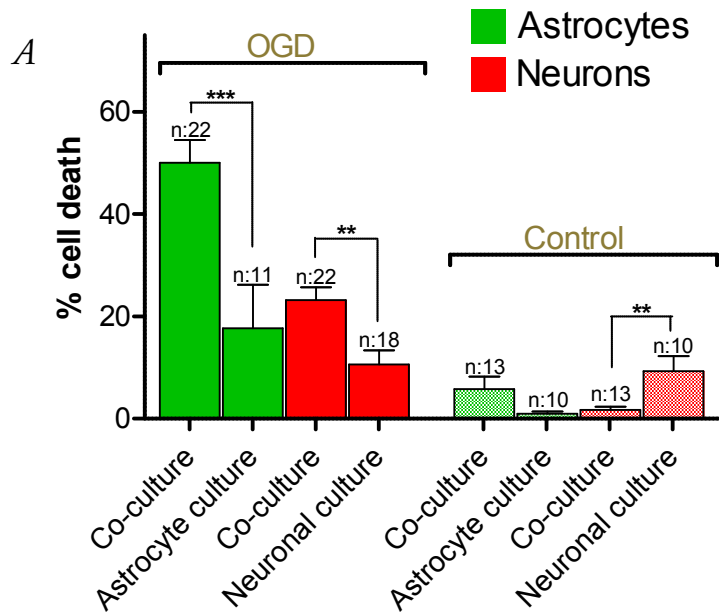


Figure 5-10: Effect of co-culturing neurons and astrocytes, timescale

This figure compares the effects of OGD and control conditions on neuronal and astrocyte death when the cells were either co-cultured or in 'pure' cultures.

A, B: Timescale of cumulative cell death during 90 minutes of OGD: comparing astrocyte death and neuronal death in co-culture vs. 'pure' cultures

Both astrocyte and neuronal death was significantly increased in the co-culture compared with the 'pure' cultures, with astrocyte death being significantly raised after 45 minutes and neuronal death after 50 minutes ($p < 0.05$), with the difference becoming gradually more significant with time.

C: Frequency histogram of astrocyte death, co-culture vs. astrocyte culture OGD

Astrocyte death had a much earlier onset in the co-culture, reaching a peak rate at 65-70 minutes, whereas in the astrocyte cultures substantial cell death started after 50 minutes and reached a peak rate at 85-90 minutes.

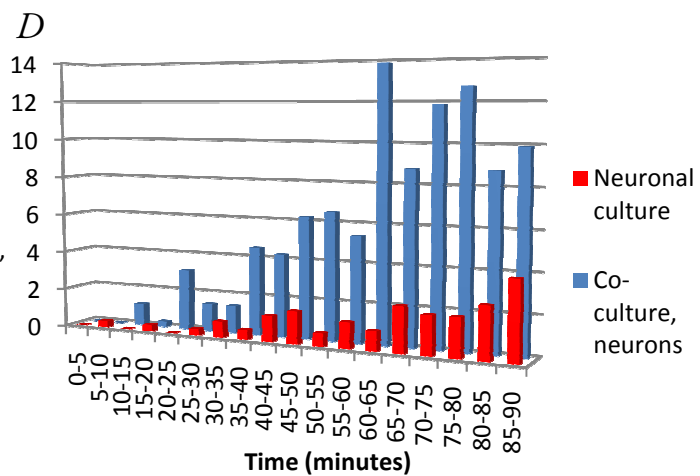
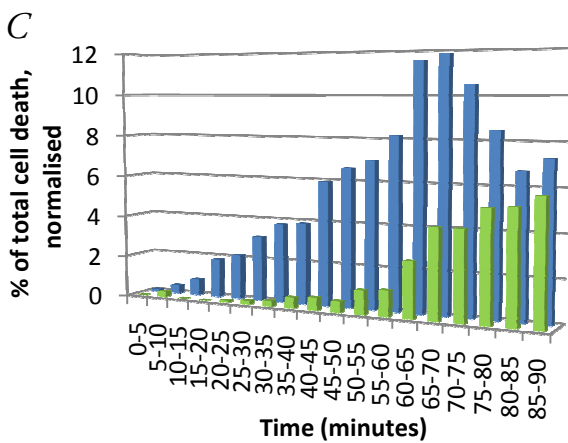
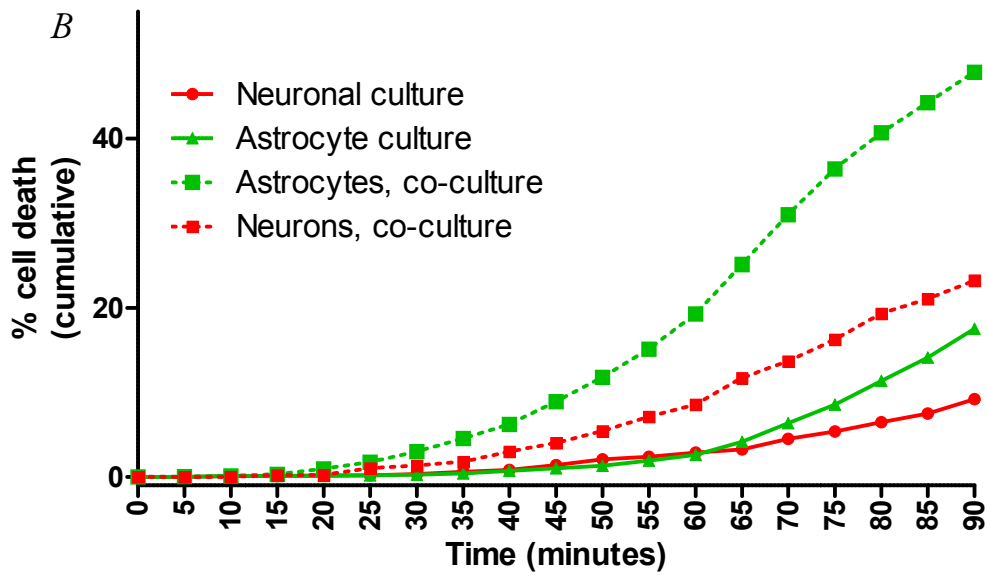
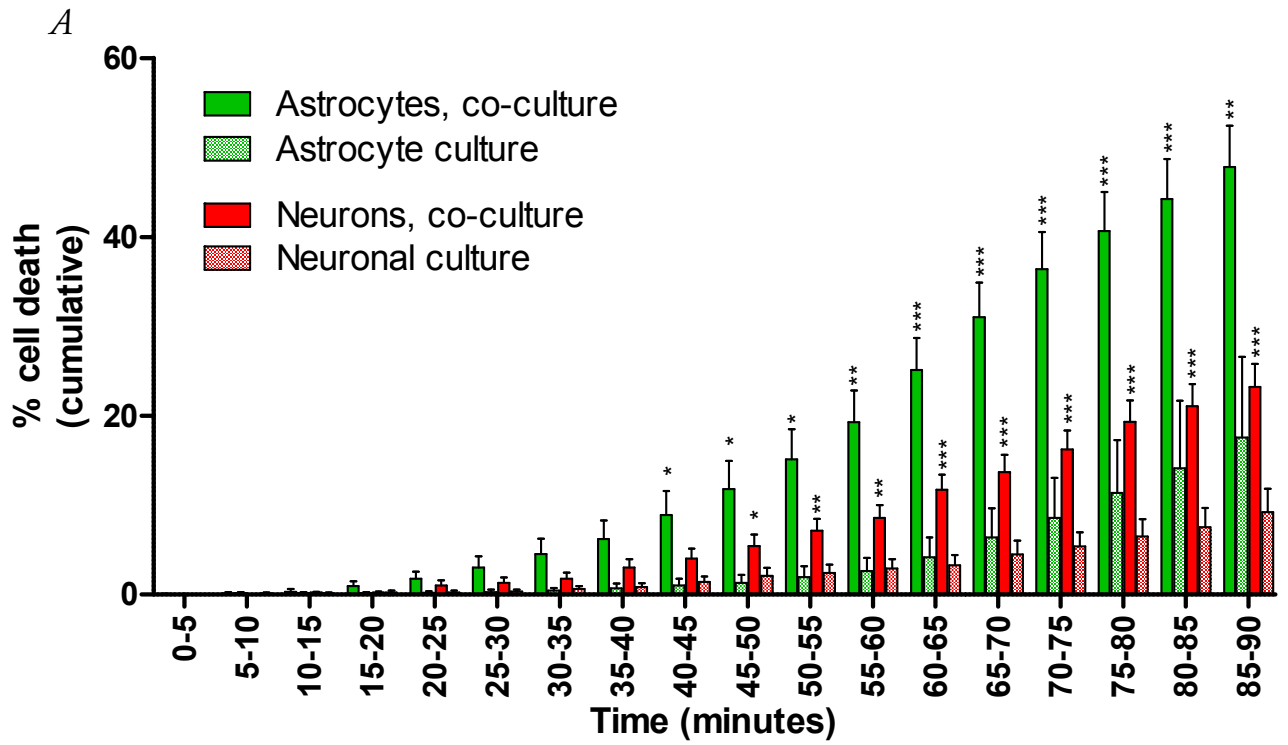
D: Frequency histogram of neuronal death, co-culture vs. neuronal culture OGD

The timescales of neuronal death are not dissimilar between the co-culture and neuronal culture, with the main difference being the increased amount of death in the co-culture. The peak rate of neuronal death occurred at 60-65 minutes in the co-culture and 85-90 minutes in the neuronal culture.

*: $p < 0.05$

** : $p < 0.01$

***: $p < 0.001$



Effect of Neurobasal medium on astrocyte cultures: an increased susceptibility to ischaemic injury

One possible explanation for the substantial reduction in the amount of astrocyte death during OGD in the astrocyte culture compared with the co-culture was the use of different cell growth media in the two preparations. When the neurons were plated onto the astrocytes to produce co-cultures, the culture medium was changed from a serum-containing DMEM-based one to a Neurobasal solution-based medium with added B27 supplement (see *Chapter 2: Methods and Materials* for details). To test this theory, confluent astrocyte cultures were placed in Neurobasal medium for a minimum of three days (as they would be in the co-culture) before being subjected to control and OGD experiments. Keeping astrocytes in Neurobasal medium did not produce any obvious morphological effects on the cultures themselves, although it did seem to reduce the rate of cell division.

Astrocytes in Neurobasal medium had significantly increased cell death during OGD ($58.78 \pm 10.62\%$, n:9, 864 cells) compared with controls ($p < 0.001$) ($0.26 \pm 0.21\%$, n:8, 1191 cells) (**Figure 5-13: A**), with the difference first becoming significant after 35 minutes (**Figure 5-13: D, E**). **Figures 5-11 and 5-12** present example images from control and OGD experiments using astrocytes in Neurobasal. The death rate of astrocytes in Neurobasal during OGD was also significantly increased compared to astrocytes in DMEM ($p < 0.01$) ($17.64 \pm 8.56\%$) (**Figure 5-13: A**), with the difference first becoming significant after 35 minutes (**Figure 5-13: F, G**). The mean time to cell death during OGD of astrocytes in Neurobasal (51.59 ± 1.11 minutes, n:440) was significantly earlier ($p < 0.001$) than for astrocytes in DMEM, and it was also earlier than during control conditions (80 minutes, n:2), although statistical comparisons are not possible since only two cells died (**Figure 5-13: B**). There were no significant differences in the average time to first cell death comparing OGD in Neurobasal and DMEM, but it was significantly later ($p < 0.001$) during control vs. OGD in Neurobasal (80 ± 2.23 minutes, n:8 vs. 33.33 ± 6.79 minutes, n:9) (**Figure 5-13: C**). These differences are also reflected in the timescale of cell death as displayed by the frequency histogram in **Figure 5-13: H**: astrocyte death had the

earliest onset in the astrocyte cultures that were kept in Neurobasal medium, with cell death occurring within the first 5 minutes of OGD, reaching a first peak rate within 35 minutes. In astrocyte cultures in DMEM, substantial cell death started more gradually and later, reaching a peak rate at 85-90 minutes.

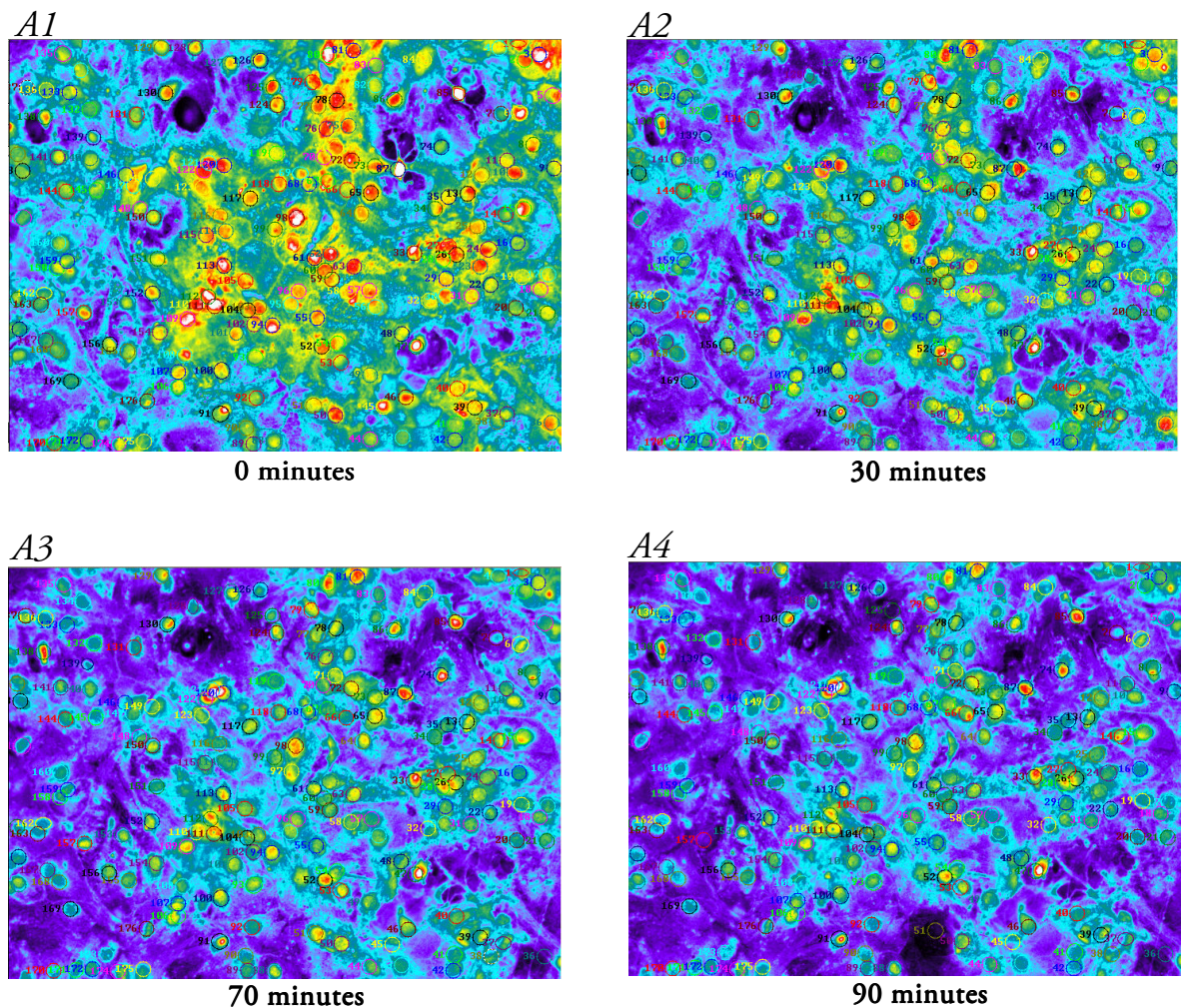


Figure 5-11: Example images of CMFDA loaded astrocyte culture in Neurobasal, control

A1-A4: Pseudocolour images of CMFDA fluorescence during a control experiment using the astrocyte culture in Neurobasal

3 cells died during the 90 minutes of perfusion with aCSF (control conditions) on this coverslip.

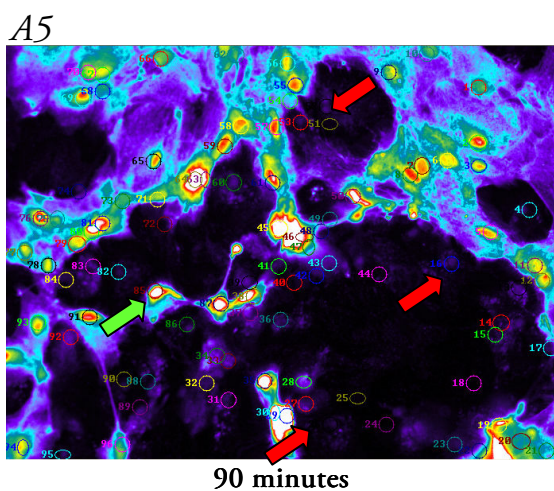
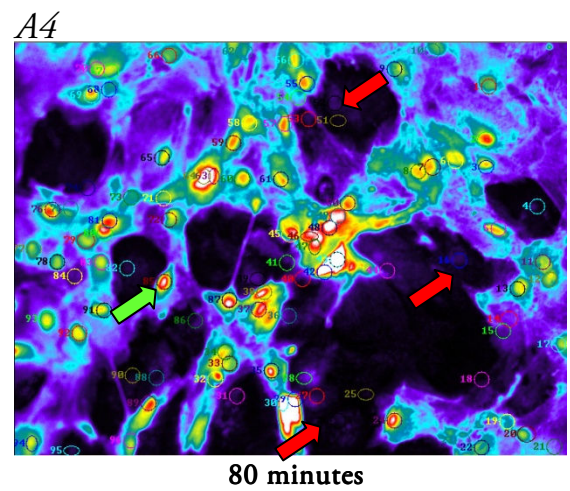
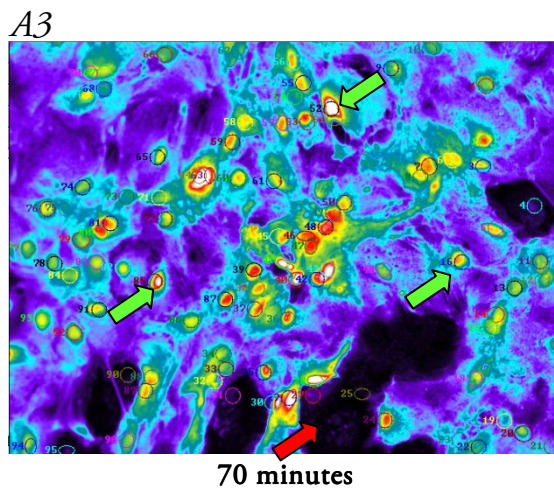
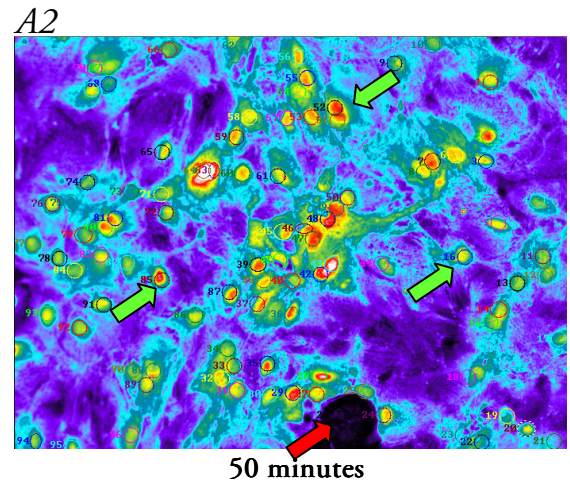
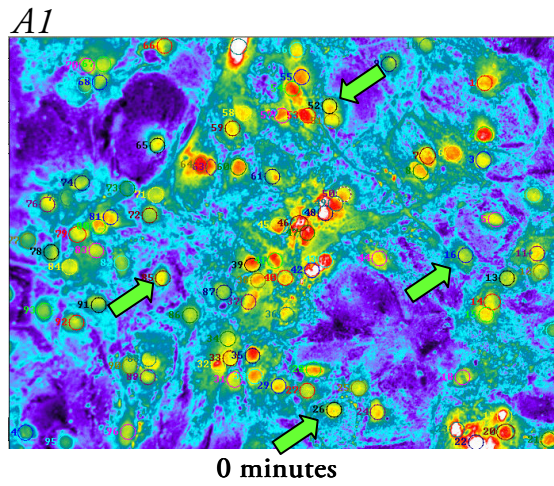


Figure 5-12: Example images of CMFDA loaded astrocyte culture in Neurobasal, OGD

A1-A5: Pseudocolour images of CMFDA fluorescence during 90 minutes of OGD.

Cells first begin to die after 50 minutes (*A2*). By 90 minutes (*A5*), 43 out of the 96 cells have died (45.26% cell death) on this coverslip.

Green arrows point at sample cells- arrows turn red when the cell has died.

Figure 5-13: Effect of Neurobasal medium on cell death in astrocyte culture

A: % total cell death, DMEM vs. Neurobasal medium

There was significantly more cell death during OGD than control conditions in astrocytes that were kept for at least 3 days in Neurobasal medium, and this was also significantly raised compared to astrocytes in DMEM ($p < 0.001$). Control conditions caused almost no cell death in either culture method.

B: Mean time to cell death

Astrocytes in Neurobasal had a significantly earlier mean cell death compared with those in DMEM ($p < 0.001$). Only 2 cells died during control conditions in Neurobasal, making statistical comparisons impossible.

C: Average time to first cell death

Astrocytes in Neurobasal medium had a significantly reduced average time to first cell death during OGD compared to controls ($p < 0.001$). They also died earlier than astrocytes kept in DMEM, although not significantly so ($p > 0.05$).

D, E: Timescale of cumulative cell death of astrocyte in Neurobasal during 90 minutes of OGD vs. control

Cell death of astrocytes in Neurobasal during OGD was first significantly raised after 35 minutes compared to controls ($p < 0.05$), with the difference becoming gradually more significant with time.

F, G: Timescale of cumulative cell death in astrocyte cultures during 90 minutes of OGD: DMEM vs. Neurobasal

Compared to astrocytes in DMEM, those kept in Neurobasal showed significantly more cell death during OGD from 35 minutes onward ($p < 0.05$), with the difference becoming gradually more significant with time.

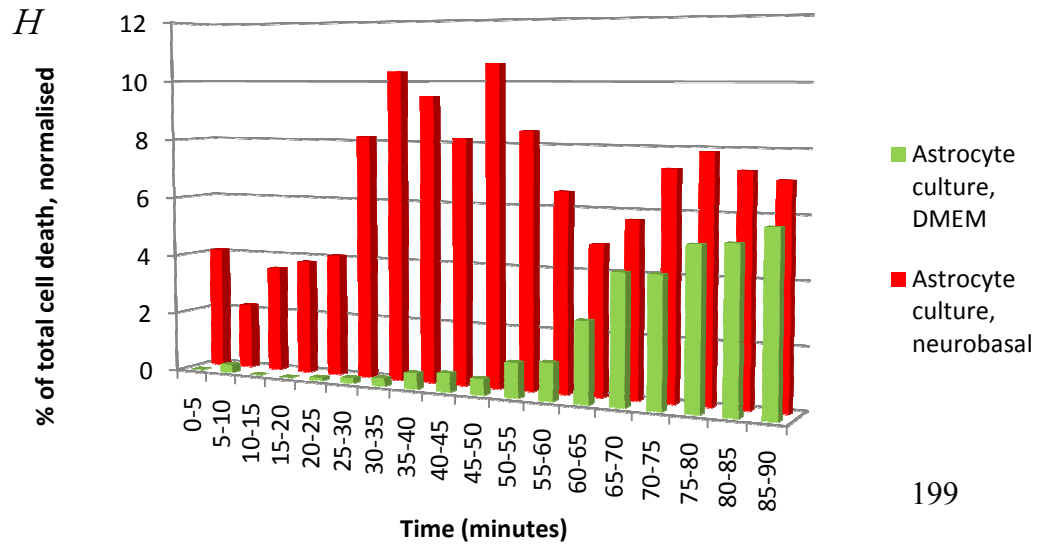
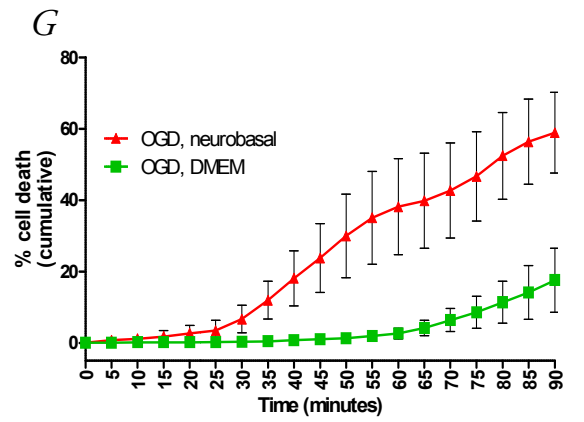
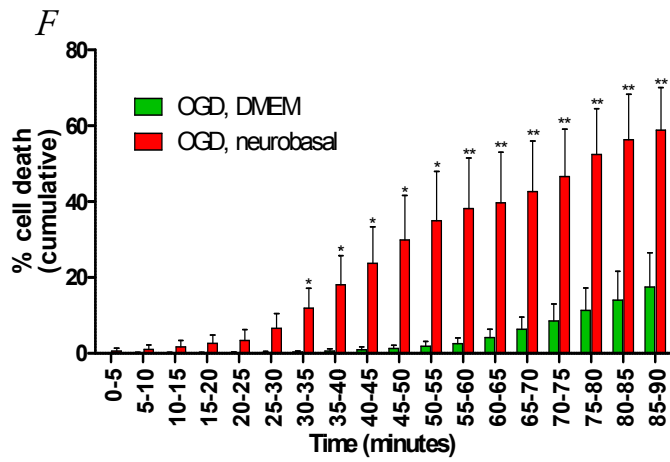
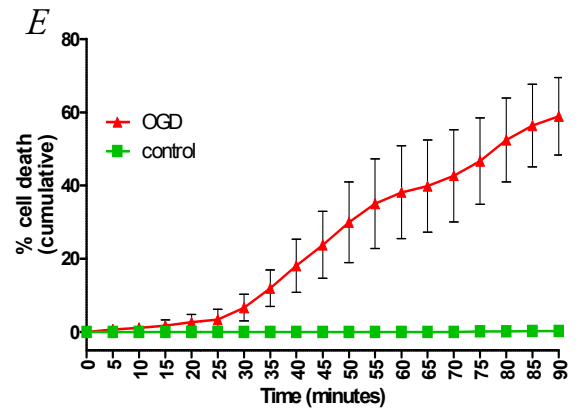
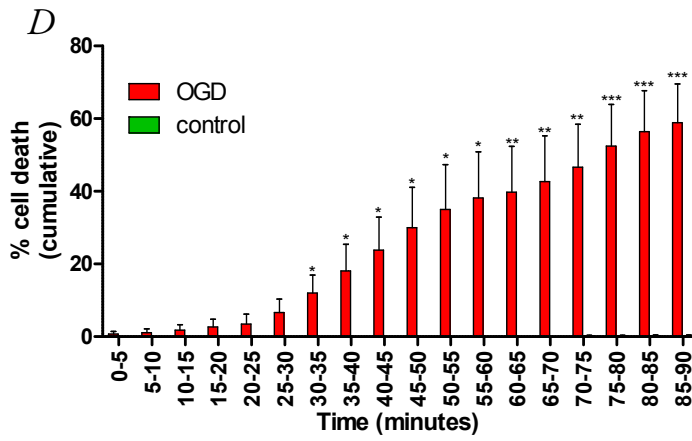
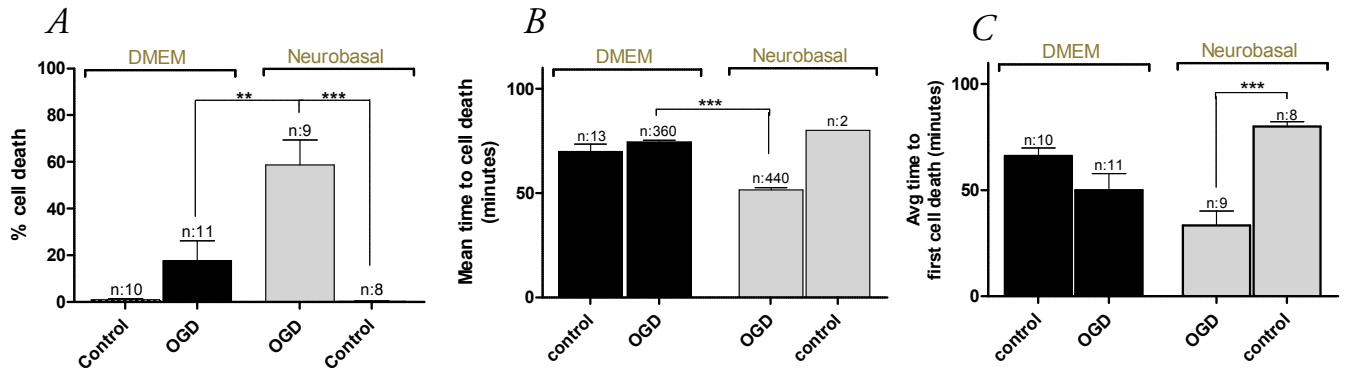
H: Frequency histogram of astrocyte death, astrocytes in DMEM and Neurobasal

Astrocyte death had the earliest onset in the astrocyte cultures that were kept in Neurobasal medium, with cell death occurring within the first 5 minutes and reaching a first peak rate within 35 minutes of OGD. In astrocyte cultures in DMEM, substantial cell death started more gradually and later, reaching a peak rate at 85-90 minutes.

*: $p < 0.05$

** : $p < 0.01$

***: $p < 0.001$



Co-culture vs. astrocyte culture in Neurobasal: a re-analysis

Figures 5-14 and 5-15 contain corrected versions of Figures 5-8, 5-9 and 5-10, using the data from astrocytes kept in Neurobasal instead of DMEM for comparisons of the co-culture with the astrocyte culture. There is now no significant difference in the amount of astrocyte death or total cell death during OGD between the co-culture and astrocyte culture (Figure 5-14: *A, D* and Figure 5-15: *A*), although the cumulative timescale of cell death shows significantly ($p < 0.05$) higher levels of astrocyte death in the astrocyte culture compared with the co-culture during the 40-55 minute periods (Figure 5-15: *D*). Also, the mean time to cell death during OGD is now significantly earlier rather than later in astrocyte cultures compared with astrocytes or all cells combined in the co-culture ($p < 0.001$) (Figure 5-14: *B* and Figure 5-15: *B*), while the average time to first death during OGD is no longer significantly different, although it is significantly later during control conditions in the astrocyte culture vs. astrocytes and all cells combined in the co-culture (Figure 5-14: *C* and Figure 5-15: *C*). Finally the frequency histograms of cell death during OGD reveal that more astrocyte death occurred earlier in the astrocyte culture, with cell death starting within the first 5 minutes and reaching a first peak as early as 30 minutes into OGD, whereas in co-culture the onset was more gradual, reaching a peak at 65-70 minutes (Figure 5-15: *F*).

In summary, there are no significant differences in the overall amount of astrocyte death or average time to first death during OGD in the co-culture compared with the astrocyte culture, but the mean time to cell death is significantly earlier in the astrocyte culture. During control conditions cells in the astrocyte culture had a significantly later average time to first cell death than the co-culture. There is also significantly more neuronal death in the co-culture during OGD but significantly less during control conditions compared to neuronal cultures, without the onset or mean time to death being significantly different.

Figure 5-14: Effect of OGD and control conditions on cell death: comparing co-culture, astrocyte culture and neuronal culture, corrected for astrocyte culture in Neurobasal

This figure provides versions of the graphs previously presented in **Figure 5-8** which have been corrected to now include astrocyte data about astrocyte cultures in Neurobasal rather than DMEM.

A: Effect of OGD vs. control on total cell death

Only the neuronal culture demonstrates significantly ($p < 0.001$) less cell death after 90 minutes of OGD compared to co-cultures. There were no significant differences during control conditions between cultures.

B: Mean time to cell death

Compare to the co-culture, the mean time to cell death in the astrocyte culture was now significantly decreased ($p < 0.001$) and in the neuronal culture it was increased ($p < 0.05$). The mean time to cell death during control conditions was significantly reduced ($p < 0.001$) in the neuronal culture compared with the co-culture.

C: Average time to first cell death

There was a reduction in the average time it took for cells to start dying during OGD in the co-culture compared to the neuronal culture ($p < 0.05$), whilst during control conditions cells started dying significantly later in the astrocyte culture compared to the co-culture ($p < 0.01$).

D, E: Timescale of cumulative cell death during 90 minutes of OGD, comparing different cultures

There is now no significant reduction in astrocyte death at any point compared to the co-culture. Significantly more cell death during OGD occurred in the co-culture compared with the neuronal culture after 40 minutes ($p < 0.05$), with the difference becoming gradually more significant with time. Two versions of this graph are shown as *D* allows for easier labelling of statistical outcomes whilst *E* makes it easier to compare dynamics between cultures.

*: $p < 0.05$

** : $p < 0.01$

***: $p < 0.001$

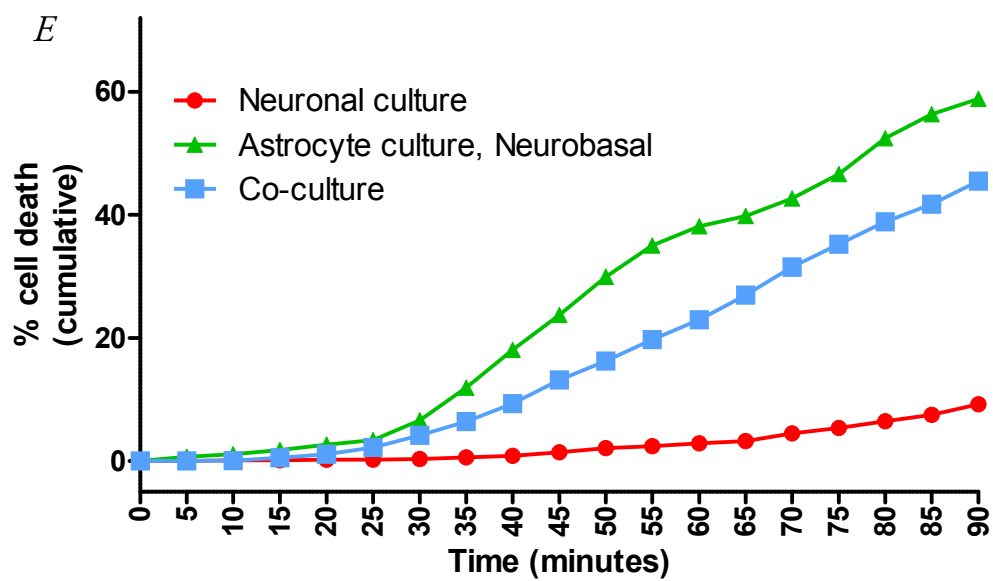
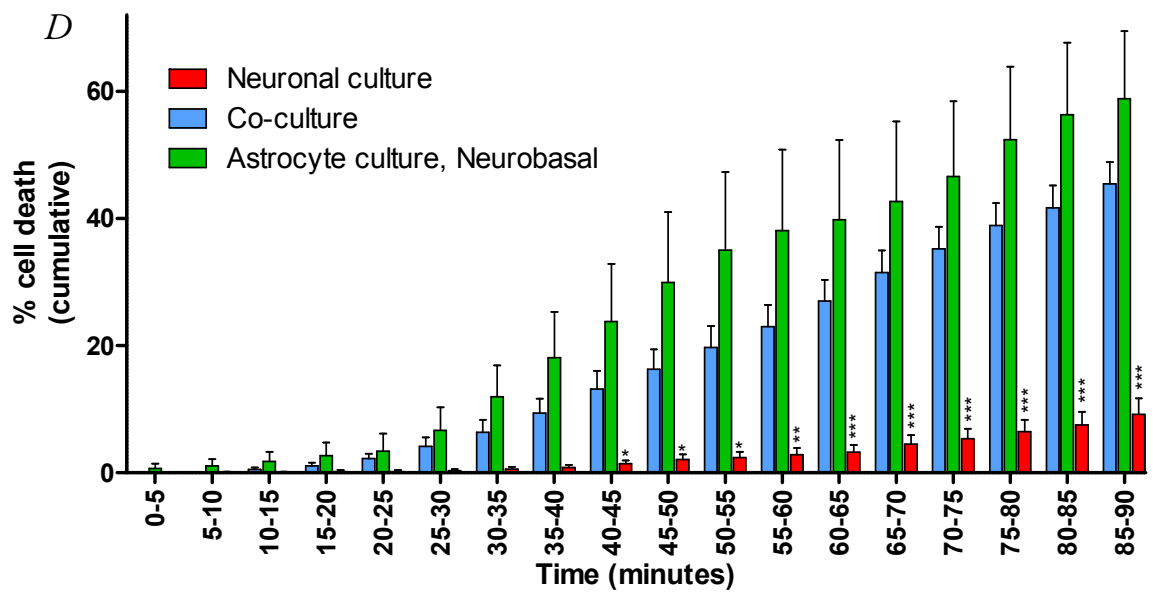
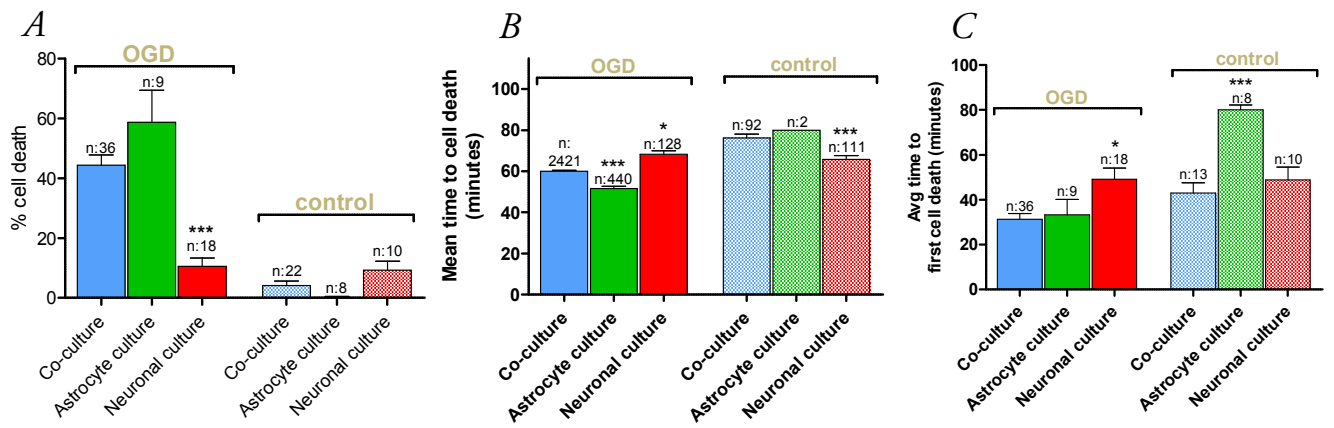


Figure 5-15: Effect of co-culturing astrocytes and neurons: figures corrected for astrocyte culture in Neurobasal medium

This figure provides versions of the graphs previously presented in **Figures 5-9 and 5-10** which have been corrected to now include astrocyte data about astrocyte cultures in Neurobasal rather than DMEM.

A: % total cell death

There is no longer significantly more astrocyte death in the co-culture compared with the astrocyte cultures in Neurobasal. Co-cultures had significantly more neuronal ($p < 0.01$) death than the neuronal cultures. There was significantly less neuronal death during control conditions in co-cultures compared with neuronal cultures ($p < 0.01$), suggesting that the presence of astrocytes is neuro-protective during control conditions yet harmful during OGD.

B: Mean time to cell death

Astrocyte cultures in Neurobasal had significantly earlier average cell death during OGD than astrocytes in co-culture ($p < 0.001$). There were no significant differences regarding mean time of neuronal death between the two cultures.

C: Average time to first cell death

There was delay in the average time it took for astrocytes to start dying during control conditions but not OGD when comparing the astrocyte culture to the co-culture ($p < 0.001$). There were no significant differences regarding onset of neuronal death between the two cultures.

D, E: Timescale of cumulative cell death during 90 minutes of OGD: comparing astrocyte death and neuronal death in co-culture vs. 'pure' cultures

There was a period between 40 and 55 minutes when there was transiently significantly more astrocyte death in the astrocyte culture vs. the co-culture ($p < 0.05$). Neuronal death was significantly increased in the co-culture compared with the 'pure' cultures after 50 minutes ($p < 0.05$), with the difference becoming gradually more significant with time.

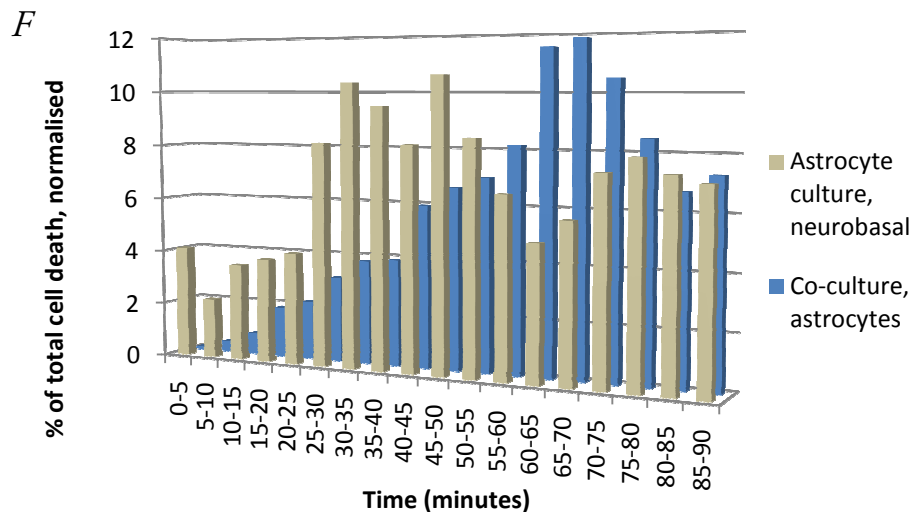
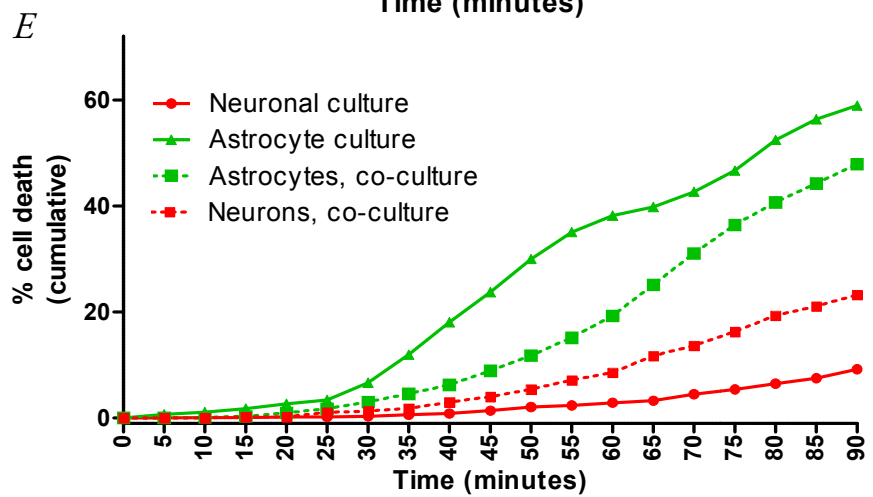
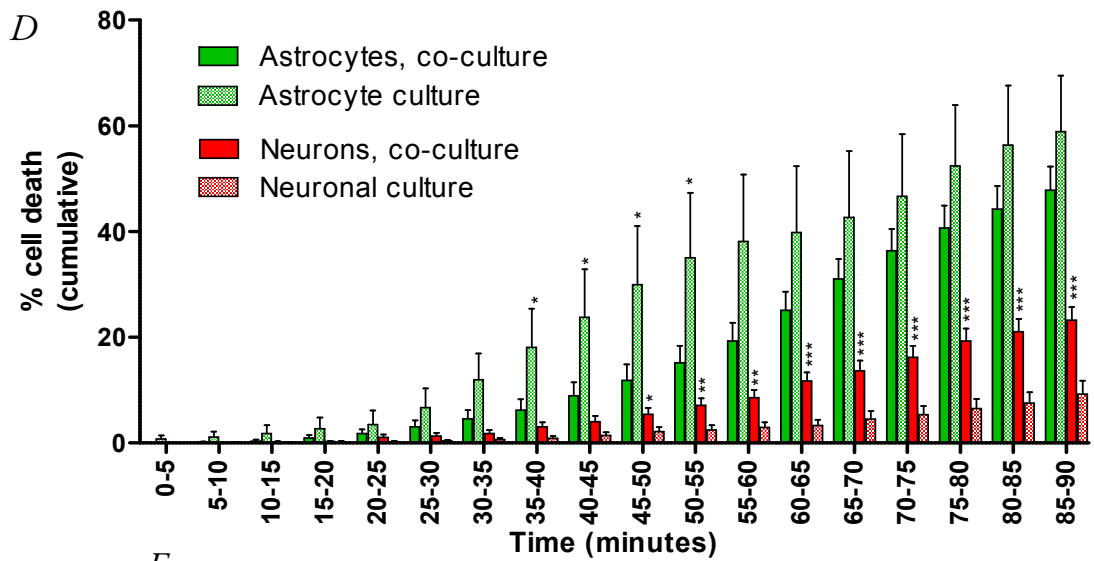
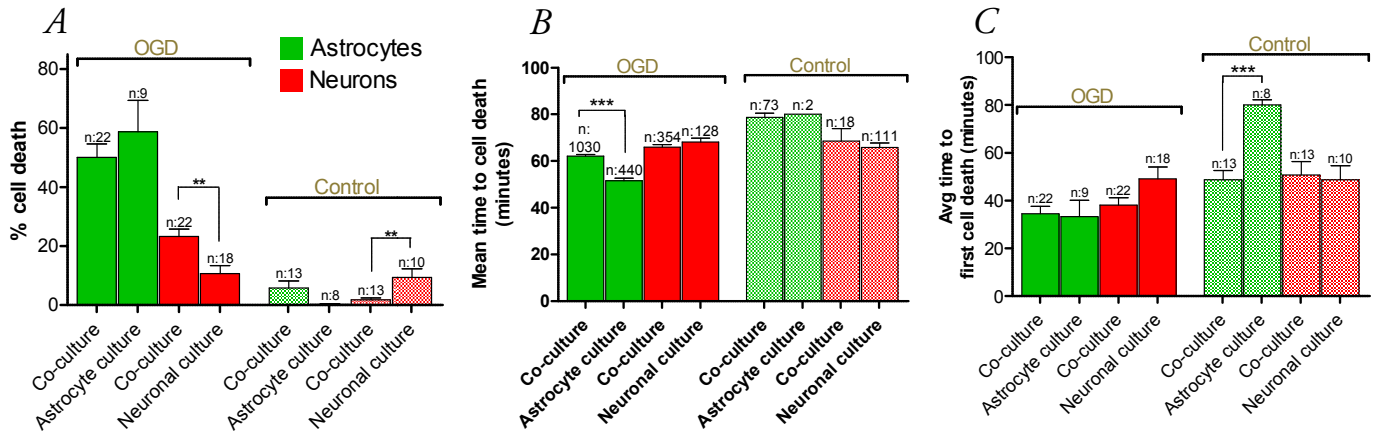
F: Frequency histogram of astrocyte death, co-culture vs. astrocyte culture OGD

More astrocyte death occurred earlier in the astrocyte culture, with cell death starting within the first 5 minutes and reaching a first peak as early as 30 minutes into OGD, whereas in co-culture the onset was more gradual, reaching a peak at 65-70 minutes.

*: $p < 0.05$

** : $p < 0.01$

***: $p < 0.001$



Cell death was always preceded by an increase in $[Ca^{2+}]_i$

Early in my project I used Fura-2ff instead of CMFDA for all experiments. This provided interesting insights into the dynamics of $[Ca^{2+}]_i$ during OGD-induced cell death. However, as already discussed in the Materials and Methods chapter, using Fura-2ff during these long experiments at -36°C was not reliable or efficient due to excessive loss of fluorescence (presumably due to leakage or active extrusion of Fura-2ff from cells) during these experiments, particularly from astrocytes. This meant that in practice, data about the death or survival of a large proportion of the cells, particularly astrocytes in co-cultures or astrocyte cultures, was not available because they had faded during the course of the experiment. However, I continued to use Fura-2ff for all experiments in the neuronal culture, and I was able to gather some information about Ca^{2+} from co-cultured astrocytes and neurons as well. Data is presented in the form of traces of $[Ca^{2+}]_i$ (340:380) and 360nm excitation (F360) from individual representative cells as well as groups of 30 randomly selected cells undergoing each experiment to give an idea of the range of responses. Finally, the average overall $[Ca^{2+}]_i$ trend was calculated by averaging the 340:380 traces of cells, and in some experiments the percentages of cells that had $[Ca^{2+}]_i$ rises is reported.

In all cell types and during all experimental conditions, cell death was invariably preceded by a sudden sharp rise in $[Ca^{2+}]_i$. In co-cultures, $[Ca^{2+}]_i$ rises in cells usually started soon after the onset of OGD, whereas during control conditions they occurred much less frequently and later, in concordance with amounts of cell death which occurred. Examples of this can be seen in **Figures 5-16: A** and **C** for OGD and control respectively. In the OGD experiment (**A**), large quickly rising $[Ca^{2+}]_i$ increases start in individual cells from 35 minutes onwards, with every $[Ca^{2+}]_i$ rise followed by subsequent cell death, which can be seen as a sudden drop in F360 to background levels. In the control experiment (**C**) there are no sharp $[Ca^{2+}]_i$ rises until 80 minutes into the experiment, and only two cells died. Looking at traces from individual cells (**Figure 5-16: B** and **D**), **B1** and **B4** survived the duration of the OGD experiment, and did not have any $[Ca^{2+}]_i$ rises of note, while **B2**, **B3** and **B5** all died, with cells tending to demonstrate an initial $[Ca^{2+}]_i$ rise followed by a

second, usually larger $[Ca^{2+}]_i$ rise which immediately preceded cell death. During control conditions cells **D1-4** all survived and had no $[Ca^{2+}]_i$ rises of note, while cell **D5** died following a short monophasic $[Ca^{2+}]_i$ rise. The $[Ca^{2+}]_i$ trends during OGD (n:421 cells) and control (n:372 cells) in the co-cultures differed after 40 minutes, at which point $[Ca^{2+}]_i$ increased more rapidly during OGD (**Figure 5-16: E**), an effect one would expect due to the much more numerous and earlier $[Ca^{2+}]_i$ rises seen during OGD.

Taking advantage of cell identification, it became apparent that there were some similarities and differences in the $[Ca^{2+}]_i$ responses between astrocytes (**Figure 5-17: A**) and neurons (**Figure 5-17: B**) in the co-culture during OGD. Both cell types tended to have the pattern described above of an initial $[Ca^{2+}]_i$ rise followed by a second, usually larger $[Ca^{2+}]_i$ rise which immediately preceded cell death. The first $[Ca^{2+}]_i$ rise tended to be smaller in astrocytes and larger in neurons, with the final $[Ca^{2+}]_i$ rise being larger relative to the first in astrocytes compared with neurons. In addition astrocytes, but not neurons, often demonstrated Ca^{2+} oscillations, and these would cease soon after the onset of OGD (See examples of this in traces **1,3** and **5** in **Figure 5-17: A**). However, the $[Ca^{2+}]_i$ trend of astrocytes (n:227 cells) and neurons (n:178 cells) in co-culture during OGD was almost identical, perhaps due to the subtle nature of the differences between cells, with a gradual rise in average $[Ca^{2+}]_i$ starting after 10 minutes in both cell types, or due to higher levels of cell death in astrocytes (**Figure 5-17: C**).

Cells in the neuronal cultures had very similar responses to neurons in co-cultures during OGD (**Figure 5-18: A**), with large rises in $[Ca^{2+}]_i$ starting shortly after the onset of OGD, followed by cell death. There were comparable $[Ca^{2+}]_i$ rises during control conditions (**Figure 5-18: C**) as well, and these occurred earlier than they did in co-cultures during control conditions. Looking at the dynamic changes of $[Ca^{2+}]_i$ in individual neurons that died during OGD (**Figure 5-18: B1, 2, 3**) and control (**Figure 5-18: D1, 2**) experiments revealed no change from the pattern already observed in co-cultured astrocytes and neurons, with cells demonstrating an initial $[Ca^{2+}]_i$ rise followed by a second, often larger $[Ca^{2+}]_i$ rise which immediately preceded cell death. The majority of cells that

survived had no $[Ca^{2+}]_i$ rises (**Figure 5-18: D4**) with others sometimes showing $[Ca^{2+}]_i$ rises (**Figure 5-18: B4, D3**) although these were not as large as those seen in cells that died. The $[Ca^{2+}]_i$ trend of all cells during OGD (n:681 cells) and control conditions (n:791 cells) in the neuronal cultures was similar (**Figure 5-18: E**), with a gradual rise in $[Ca^{2+}]_i$ starting after about 25 minutes during OGD and after 50 minutes in controls.

In summary, cell death during OGD and control conditions in co-cultures and neuronal cultures was always preceded by an increase in $[Ca^{2+}]_i$, with the majority of these cells demonstrating an initial $[Ca^{2+}]_i$ rise followed by a second, often larger $[Ca^{2+}]_i$ rise which immediately preceded cell death. In the co-culture, there were more frequent and earlier $[Ca^{2+}]_i$ rises during OGD compared to controls, a fact mirrored by the $[Ca^{2+}]_i$ trend, and when comparing astrocytes and neurons in the co-culture the first $[Ca^{2+}]_i$ rise tended to be smaller in astrocytes and larger in neurons, with the final $[Ca^{2+}]_i$ rise being larger relative to the first in astrocytes compared with neurons. Astrocytes, but not neurons, often showed Ca^{2+} oscillations, and these would cease soon after the onset of OGD. Finally, in neuronal cultures there were similar numbers of $[Ca^{2+}]_i$ rises during control and OGD, and the overall $[Ca^{2+}]_i$ trends were similar.

Figure 5-16: $[Ca^{2+}]_i$ rises and cell death during OGD and control in co-cultures

Traces of $[Ca^{2+}]_i$ (340:380) and 360nm excitation (F360) from 30 randomly selected cells (**A**, **C**) and 4 individual representative examples of cell death (**B**, **D**) demonstrating effects of OGD and control conditions respectively on $[Ca^{2+}]_i$ during OGD in co-cultures.

In the OGD experiment (**A**), large quickly rising $[Ca^{2+}]_i$ increases start in individual cells from 35 minutes onwards, with every $[Ca^{2+}]_i$ rise followed by subsequent cell death, which can be seen as a sudden drop in F360 to background levels.

Cells **B1** and **B4** survived the duration of the OGD experiment, and did not have any $[Ca^{2+}]_i$ rises of note. By contrast **B2**, **B3** and **B5** all died, with cells tending to demonstrate an initial $[Ca^{2+}]_i$ rise (*purple arrows*) followed by a second, usually larger $[Ca^{2+}]_i$ rise (*green arrows*) which immediately preceded cell death. Cell death is indicated by the sudden drop in F360 (*red arrows*) caused by a loss of cell plasma membrane integrity.

In the control experiment (**C**) there are no sharp $[Ca^{2+}]_i$ rises until 80 minutes into the experiment, and only two cells died. This is also reflected in the example traces, with cells **D1-4** all surviving and having no $[Ca^{2+}]_i$ rises of note, while cell **D5** died following a short monophasic $[Ca^{2+}]_i$ rise.

E: Average overall $[Ca^{2+}]_i$ trend, OGD vs. control

The average change in $[Ca^{2+}]_i$ of all cells during OGD and control in the co-cultures differed after 40 minutes, at which point the average $[Ca^{2+}]_i$ increased more rapidly during OGD, an effect one would expect due to the much more numerous $[Ca^{2+}]_i$ rises seen during OGD.

Co-culture

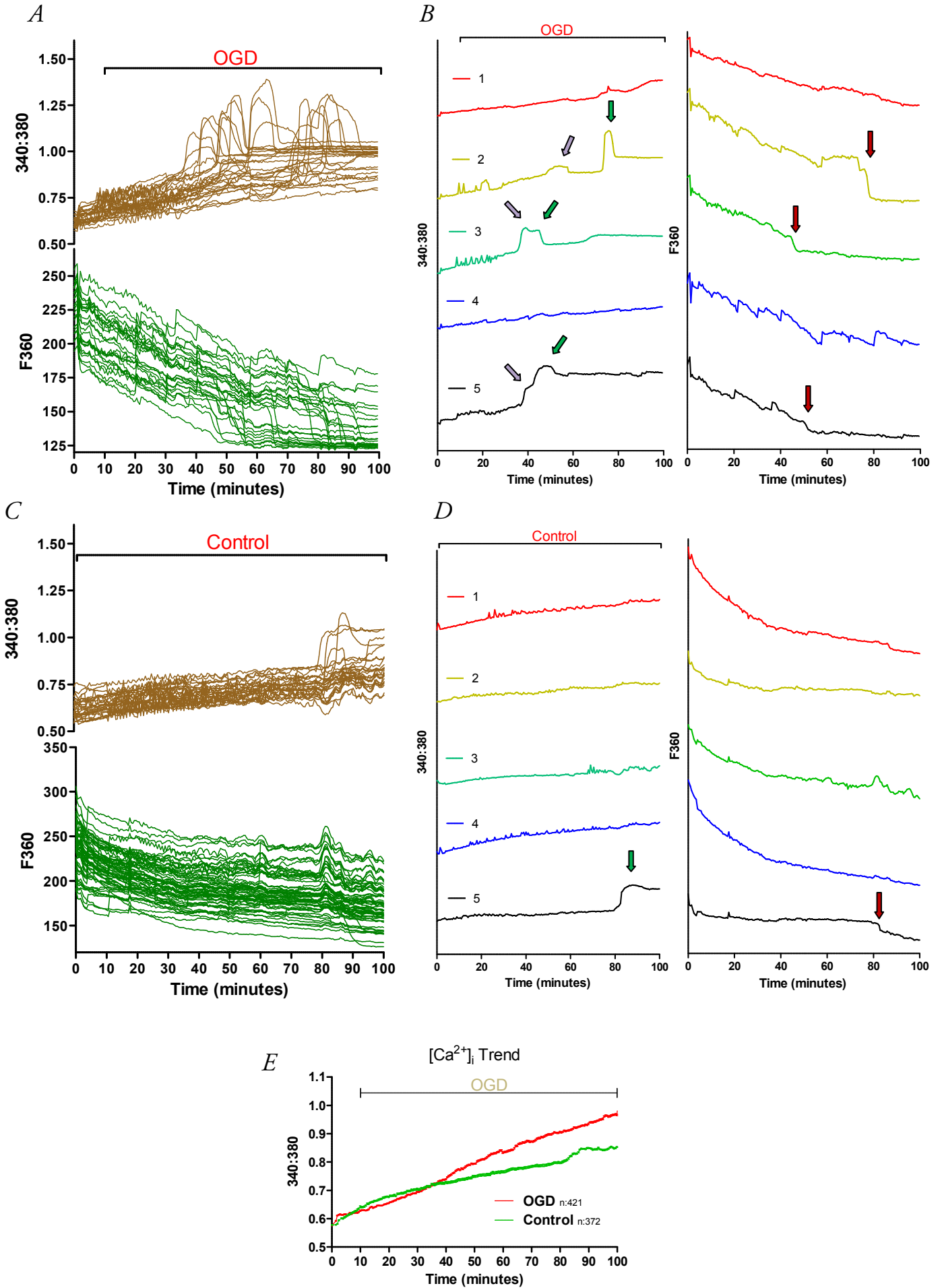


Figure 5-17: Astrocyte vs. neuronal $[Ca^{2+}]_i$ rises and cell death during OGD in co-cultures

A+B: Representative traces each of $[Ca^{2+}]_i$ (340:380) in astrocytes (**A**) and neurons (**B**) that died during OGD. The fluorescence intensity of the 360nm excitation (F360) is presented to indicate cell membrane integrity.

There were some similarities and differences in the $[Ca^{2+}]_i$ responses to OGD between astrocytes and neurons in the co-culture. Both cell types tended to demonstrate an initial $[Ca^{2+}]_i$ rise (*purple arrows*) followed by a second, usually larger $[Ca^{2+}]_i$ rise (*green arrows*) which immediately preceded cell death. Cell death is indicated by the sudden drop in F360 (*red arrows*) caused by a loss of cell plasma membrane integrity. Also, the first $[Ca^{2+}]_i$ rise tended to be smaller in astrocytes and larger in neurons, with the final $[Ca^{2+}]_i$ rise being larger relative to the first in astrocytes compared with neurons. In addition, astrocytes but not neurons often showed $[Ca^{2+}]_i$ oscillations, and these would cease soon after the onset of OGD, just before the first smaller $[Ca^{2+}]_i$ rise (See examples of this in traces **A1,A3** and **A5**).

C: Average overall $[Ca^{2+}]_i$ trend, Astrocytes vs. Neurons

The average change in $[Ca^{2+}]_i$ of astrocytes and neurons in co-culture during OGD was almost identical, with a gradual rise in average $[Ca^{2+}]_i$ starting after 10 minutes in both cell types. This figure was produced using recordings of all cells from 3 coverslips, the same ones which provide the example traces in graphs **A** and **B**.

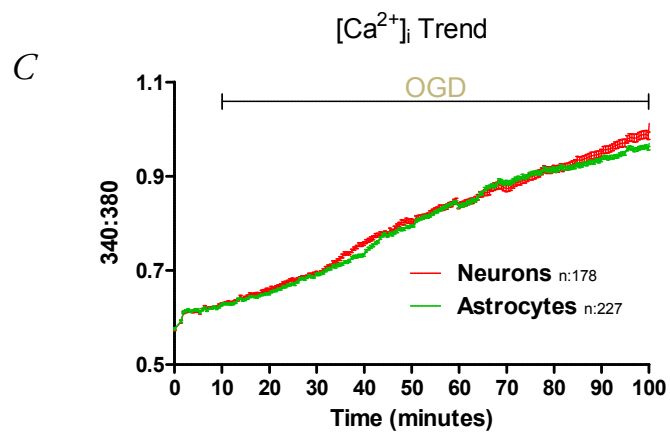
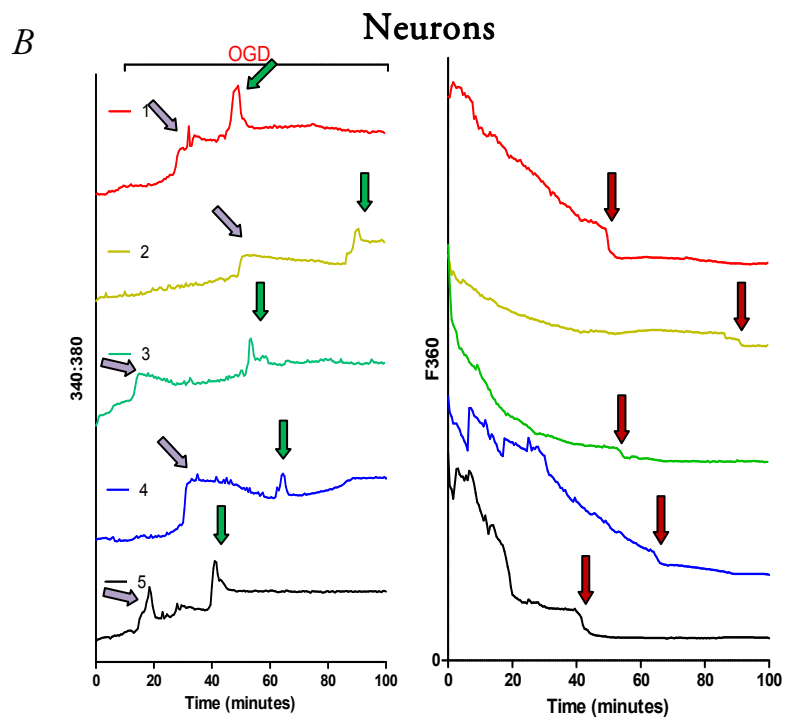
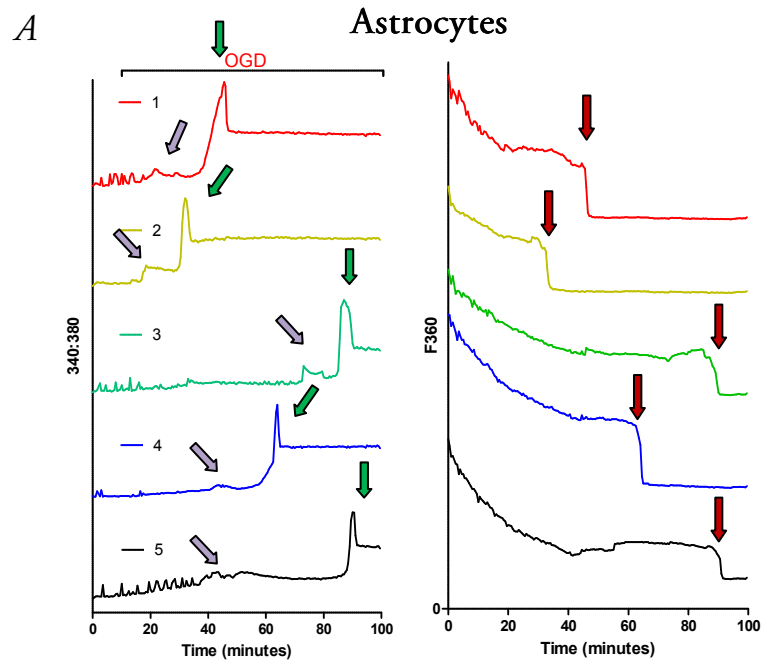


Figure 5-18: $[Ca^{2+}]_i$ rises and cell death during OGD and control in neuronal cultures

Traces of $[Ca^{2+}]_i$ (340:380) and 360nm excitation (F360) from 30 randomly selected cells (**A**, **C**) and 4 individual representative examples of cell death (**B**, **D**) demonstrating effects of OGD and control conditions respectively on $[Ca^{2+}]_i$ during OGD in neuronal cultures.

In the OGD experiment (**A**), large quickly rising $[Ca^{2+}]_i$ increases start in a group of cells from 25 minutes onwards. The $[Ca^{2+}]_i$ rises are of variable duration, with most eventually followed by cell death, which can be seen as a sudden drop in F360 to background levels.

In the control experiment (**C**) there are also a number of $[Ca^{2+}]_i$ rises, although they are less numerous, start later on, and lead to death in fewer cells.

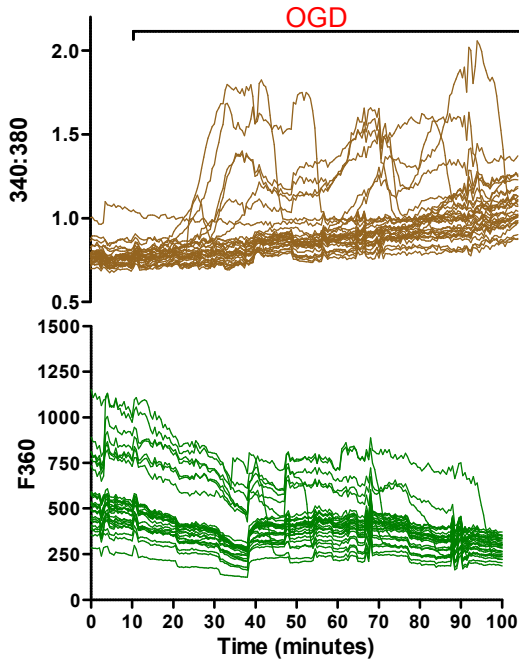
There are few apparent differences in the $[Ca^{2+}]_i$ rises seen before cell death during control (**D1**, **2**) and OGD (**B1**, **2**, **3**) conditions in the neuronal culture. Similar to what happened in the co-cultured astrocytes and neurons, cells in the neuronal culture usually demonstrated an initial $[Ca^{2+}]_i$ rise (*purple arrows*) followed by a second, often larger $[Ca^{2+}]_i$ rise (*green arrows*) which immediately preceded cell death, indicated by the sudden drop in F360 (*red arrows*) caused by a loss of cell plasma membrane integrity. There was a variable delay from the initial $[Ca^{2+}]_i$ rise to cell death in both conditions. The majority of cells that survived either had no $[Ca^{2+}]_i$ rises (**D4**) or sometimes also showed $[Ca^{2+}]_i$ rises (**B4**, **D3**) although these were not as large as those seen in cells that died.

E: Average overall $[Ca^{2+}]_i$ trend, OGD vs. control

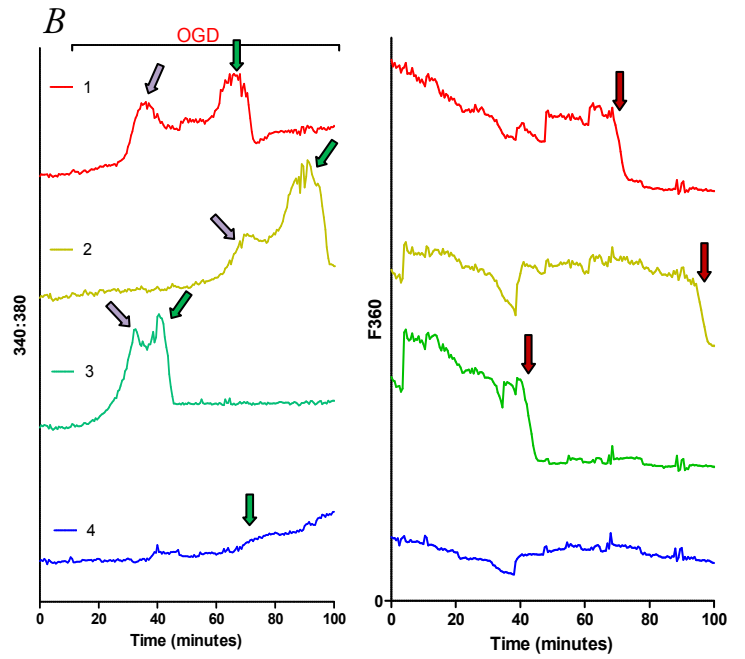
The average change in $[Ca^{2+}]_i$ of all cells during OGD and control in the neuronal cultures was similar, with a gradual rise in $[Ca^{2+}]_i$ starting after about 25 minutes during OGD and after 50 minutes in controls.

Neuronal culture

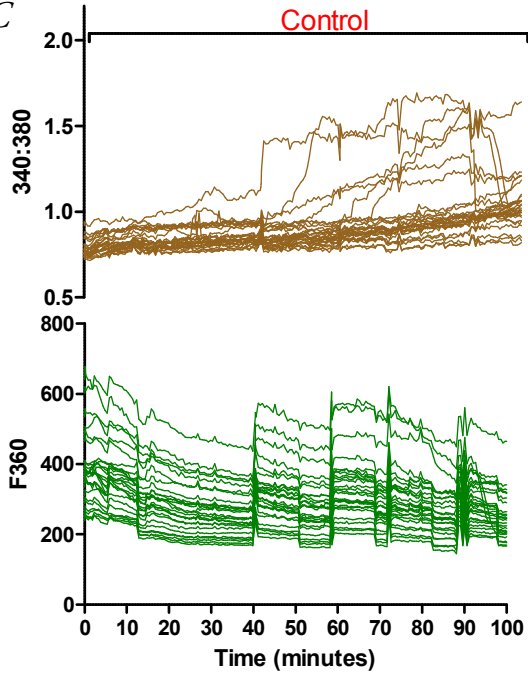
A



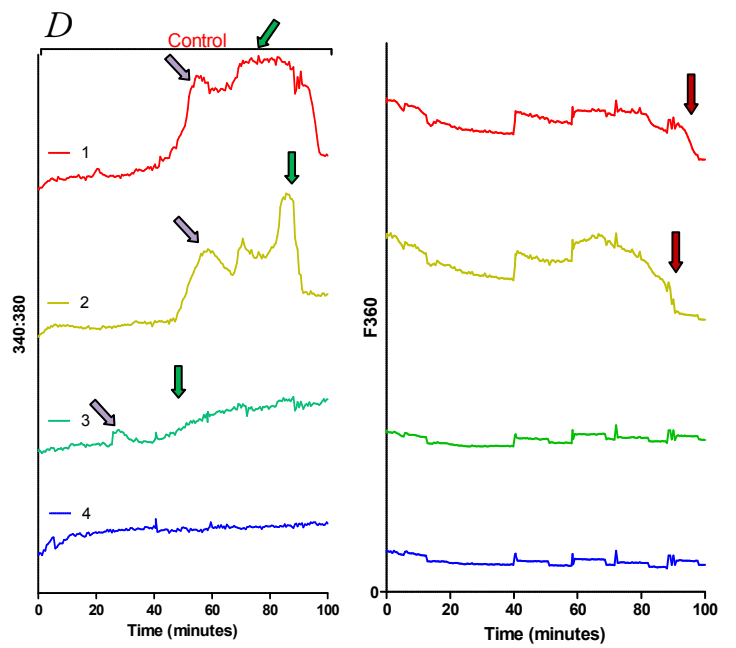
B



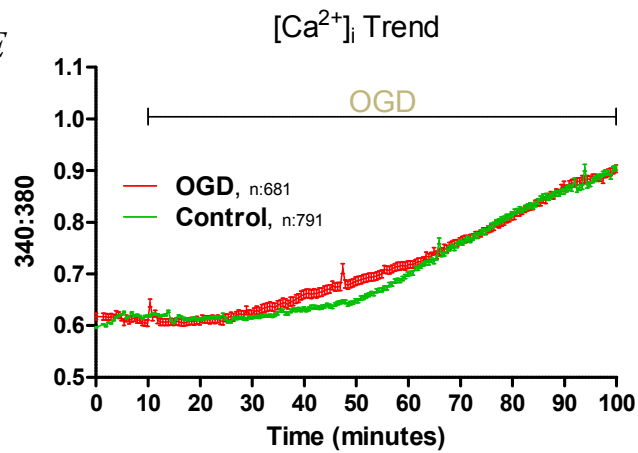
C



D



E



Continuous application of P2 and glutamate receptor agonists during OGD and control conditions

Continuous ATP application in neuronal cultures during control conditions

Having demonstrated that ATP is released during OGD from co-cultures, one hypothesis is that this ATP could act on neuronal P2 receptors to cause or potentiate ischaemic cell death. Different concentrations of ATP (1 μ M-1mM) were added onto neuronal cultures continuously for 90 minutes during control conditions to see if this would lead to increased cell death. None of the concentrations of ATP used were able to significantly increase the amount of cell death although the death rates did rise in a dose-dependent manner up to 100 μ M ATP, before being reduced at 1mM ATP (**Figure 5-19: A**). During control conditions without added ATP 9.28 \pm 2.9% of cells died, with 1 μ M ATP 9.36 \pm 3.5% (n:3, 272 cells), with 10 μ M ATP 10.83 \pm 7.4% (n:3, 280 cells), with 100 μ M ATP 20.67 \pm 7.9% (n:3, 254 cells) and with 1mM ATP 6.23 \pm 0.9% (n:3, 243 cells) ($p > 0.05$ for all [ATP] compared to control). The cumulative timescale of cell death does reveal a transient period of significantly increased cell death in the presence of 1 μ M ATP after 5 and 10 minutes compared to control (**Figure 5-19: D**), a trend which is mirrored by a significant reduction in the average time to first cell death compared to controls with the addition of 1 μ M ATP (10 \pm 6.1 minutes, $p < 0.01$), but not 10 μ M (33.33 \pm 18.1 minutes), 100 μ M (20 \pm 6.1 minutes) or 1mM ATP (36.67 \pm 4.41 minutes) (n:3 for all) (**Figure 5-19: C**). The mean time to cell death was earlier with the addition of 100 μ M (50.54 \pm 3.59 minutes, n:46, $p < 0.01$) and 1mM ATP (52.33 \pm 3.45 minutes, n:15, $p > 0.05$) but not 1 μ M (65.38 \pm 3.92 minutes, n:52) or 10 μ M ATP (62.71 \pm 3.9 minutes, n:24) (**Figure 5-19: B**). Finally, the frequency histograms of cell death demonstrate some very early cell death with 1 μ M (**Figure 5-20: A**) and 10 μ M ATP (**Figure 5-20: B**), while 100 μ M ATP (**Figure 5-20: C**) increased the amount of early cell death and 1mM ATP (**Figure 5-20: D**) reduced the amount of late neuronal death as well as having no cell death in the first 25 minutes.

When comparing the $[Ca^{2+}]_i$ recordings from these experiments (**Figure 5-21: A, C, E**) it is apparent that there are no sudden increases in $[Ca^{2+}]_i$ immediately after the application of any amount of ATP. This is in contrast to the experiments which were performed in Chapter 4, where over half of cells in the neuronal culture had immediate $[Ca^{2+}]_i$ rises following short bursts of ATP application. There are two likely reasons for this: Fura-2ff is a low affinity Ca^{2+} indicator with a reported useful detection range of 0.5-35 μ M, so it will not be able to react to the small changes in $[Ca^{2+}]_i$ which were recorded using Fura-2 (ATP caused avg $\Delta_{max} [Ca^{2+}]_i$ of just 111nM in neurons with resting $[Ca^{2+}]_i$ of about 70nM, see Chapter 4), and secondly the frequency of image acquisition in these experiments was once every 30 seconds, so it is possible that receptor desensitisation may have occurred before any $[Ca^{2+}]_i$ rise was detected (Hyrc et al., 2000). However, later $[Ca^{2+}]_i$ rises were present, and seemed to occur earlier with increasing concentrations of added ATP. Once again, all cells that died had rises in $[Ca^{2+}]_i$ before death (See example cells in **Figure 5-21: B1, D1, F3, F4**) but in these experiments there were also a number of cells which had $[Ca^{2+}]_i$ rises that did not die (See example cells in **Figure 5-21: B3, B4, D4**), although it is possible and probable that most of these would have lead to cell death had the experiments been allowed to continue for longer. The $[Ca^{2+}]_i$ trend of all cells (**Figure 5-21: G**) was actually reduced with both 1 and 10 μ M ATP, whereas with 100 μ M ATP it was similar to controls without added ATP. The $[Ca^{2+}]_i$ data of the 1mM ATP experiments is not present as the original files were lost.

To summarize, none of the added [ATP] could significantly affect death rates in the neuronal culture, although the onset of cell death was earlier with 1 μ M ATP and the mean time to cell death was reduced by both 100 μ M and 1mM ATP, although this latter reduction is more likely because of a reduction in late cell death rather than increased earlier death. The Fura-2ff traces indicate that any effects of Ca^{2+} accumulation on cell death were not caused by an immediate ATP-mediated influx, with the lower concentrations of 1 μ M and 10 μ M ATP actually reducing the $[Ca^{2+}]_i$ trend of cells compared to controls.

Figure 5-19: Effects of prolonged ATP application on cell death in neuronal culture during control conditions

Different concentrations of ATP (1uM-1mM) were added onto neuronal cultures continuously during 90 minute control experiments to see if this would lead to increased cell death.

A: Total cell death, neuronal culture control + ATP

None of the concentrations of ATP used were able to significantly increase the amount of cell death compared to controls, although the death rates did rise in a dose-dependent manner up to 100uM ATP, before being reduced at 1mM ATP

B: Mean time to cell death

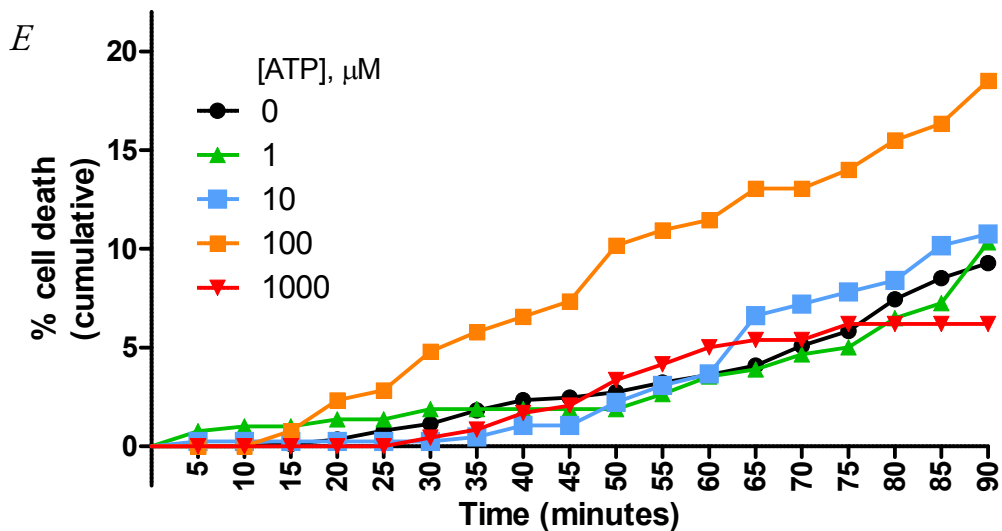
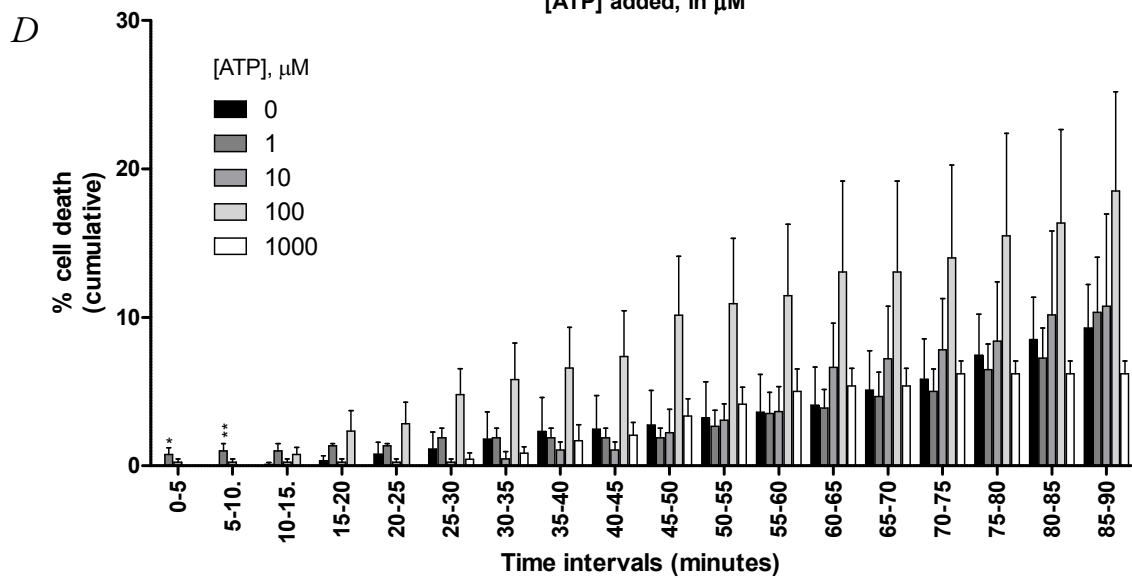
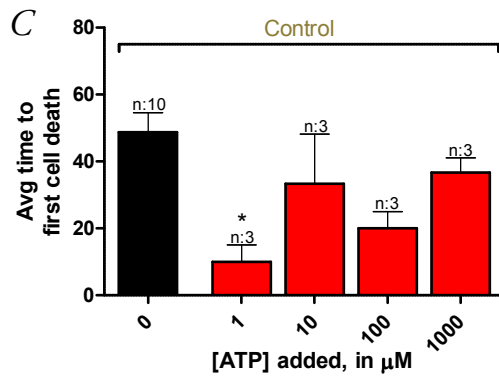
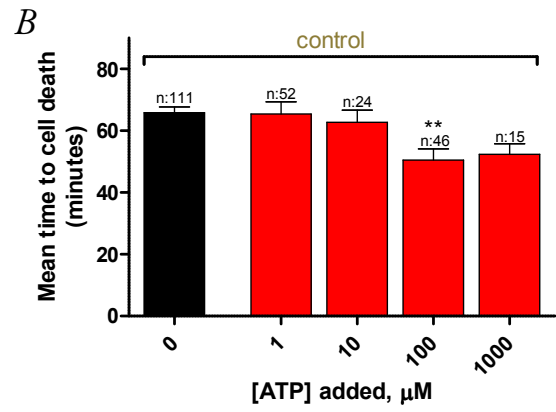
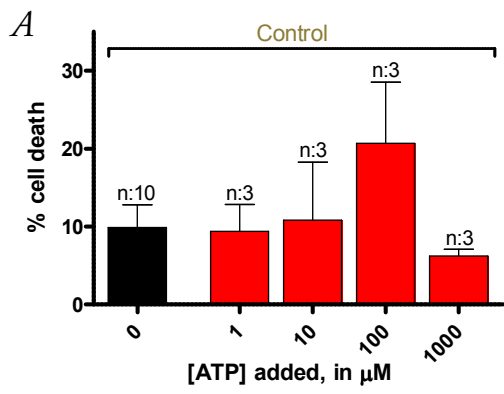
The mean time to cell death was significantly earlier with the addition of 100uM ATP ($p < 0.01$) and there seems to be a general trend for earlier mean time to cell death with increasing [ATP].

C: Average time to first cell death

There was significant reduction in the average time to first cell death with the addition of 1uM ATP ($p < 0.05$), but not 10, 100uM or 1mM ATP, during control conditions, although it was reduced with all [ATP] that were applied.

D, E: Timescale of cell death, 1uM-1mM ATP

Cell death was significantly increased after 5 and 10 minutes in the presence of 1uM ATP. However there were no other significant differences, despite the apparent higher rate of death in the presence of 100uM ATP.



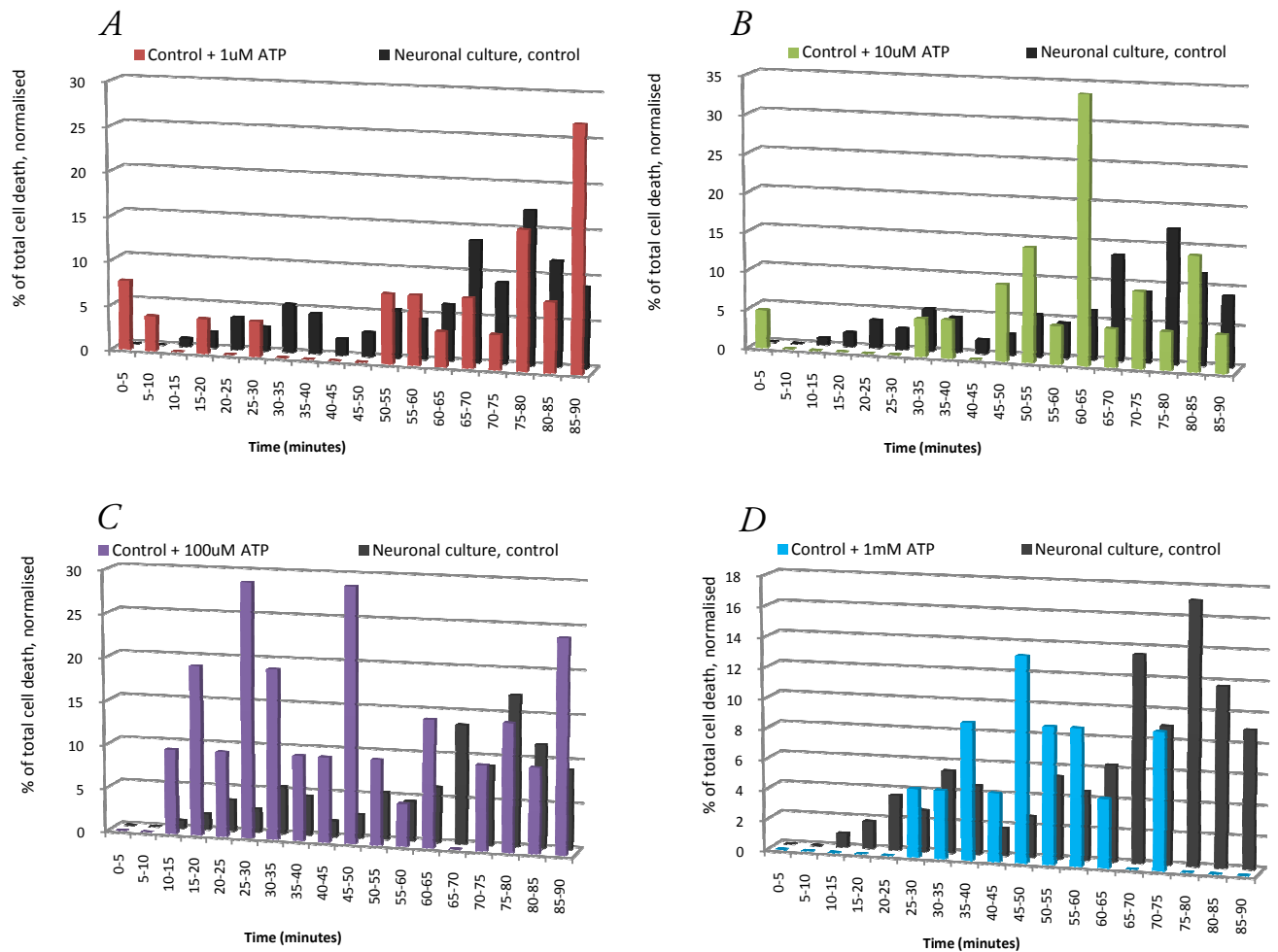


Figure 5-20: Effects of prolonged ATP application on timescale of cell death in neuronal culture during control conditions

A, B, C, D: Frequency histogram of cell death, 1uM-1mM ATP

There was some very early cell death with 1uM (A) and 10uM ATP (B), with 100uM ATP (C) increasing the amount of early cell death. 1mM ATP (D) reduced the amount of late neuronal death and had no cell death in the first 25 minutes.

Figure 5-21: $[Ca^{2+}]_i$ rises and cell death in neuronal cultures when adding exogenous ATP during control conditions

Traces of $[Ca^{2+}]_i$ (340:380) and 360nm excitation (F360) from 30 randomly selected cells (**A**, **C**, **E**) and 4 individual representative examples (**B**, **D**, **F**) demonstrating effects of continuous application of 1, 10 and 100uM ATP respectively on $[Ca^{2+}]_i$ during control conditions in neuronal cultures. Purple arrows point out rises in $[Ca^{2+}]_i$, red arrows the time of cell death (drop in F360).

When comparing these $[Ca^{2+}]_i$ recordings it is apparent that there are no sudden increases in $[Ca^{2+}]_i$ immediately after the application of any amount of ATP. However, later $[Ca^{2+}]_i$ rises seem to occur earlier with increasing concentrations of added ATP. Once again, all cells that died had rises in $[Ca^{2+}]_i$ before death (See example cells **B1**, **D1**, **F3** and **F4**) but in these experiments there were also a number of cells which had $[Ca^{2+}]_i$ rises that did not die (See example cells **B3**, **B4**, and **D4**), although it is possible and probable that most of these would have lead to cell death had the experiments been allowed to continue for longer.

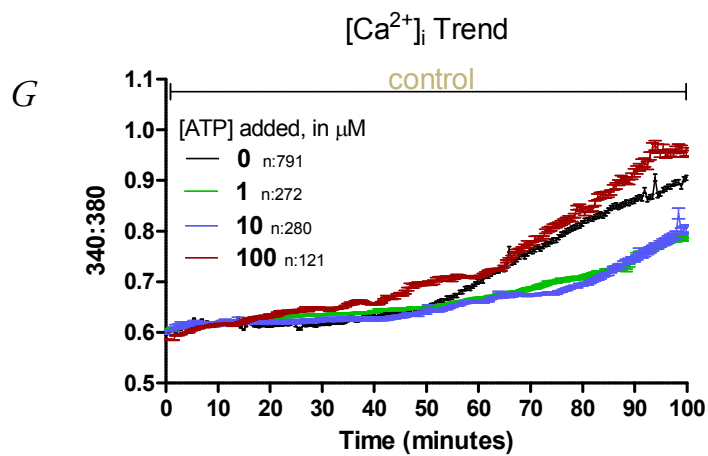
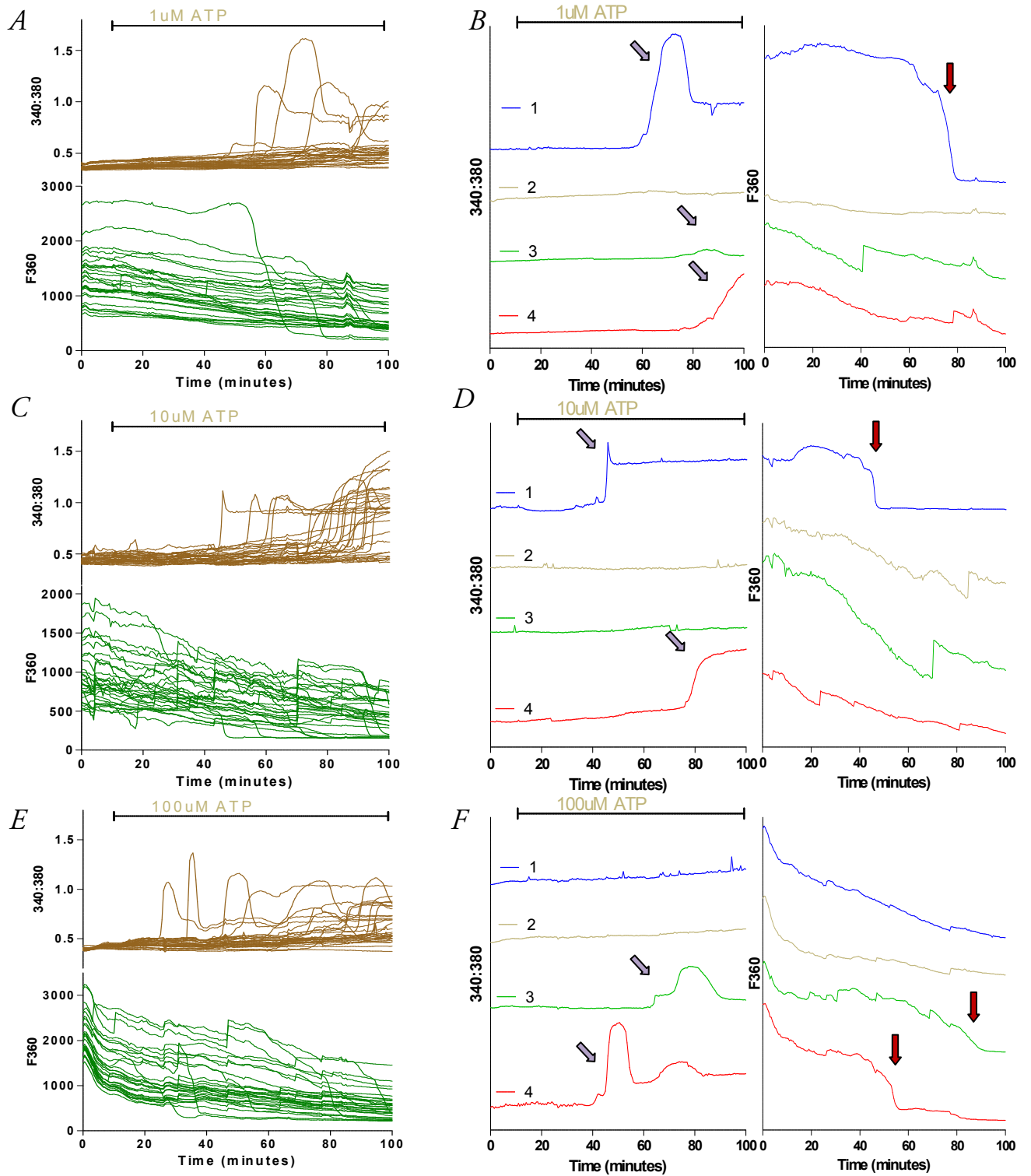
G: Average overall $[Ca^{2+}]_i$ trend

The average change in $[Ca^{2+}]_i$ of all cells was actually reduced with both 1 and 10uM ATP, whereas with 100uM ATP it was similar to controls without added ATP.

*: $p < 0.05$

** : $p < 0.01$

Neuronal culture



Continuous ATP and glutamate application in neuronal cultures during OGD

Since ATP application was not able to significantly increase cell death in the neuronal culture under control conditions, I applied it during OGD. Adding 100uM ATP (the concentration which caused the largest increase in cell death during control conditions) caused a reduction in cell death compared to OGD, with only $3.66 \pm 3.3\%$ of cells dying (n:4, 439 cells), although this did not reach statistical significance ($p > 0.05$) (**Figure 5-22: A**). As well as releasing ATP, co-cultures and astrocytes also released large amounts of glutamate during OGD, so I added 1mM glutamate to the neuronal culture during OGD to see if this would lead to increased death rates. This manipulation did not cause any change in the quantity of cell death, with $10.27 \pm 1.3\%$ of cells dying (n:3, 379 cells) (**Figure 5-22: A**). Finally, I added a combination of 100uM ATP + 1mM glutamate to the neuronal culture during OGD. This led to a slight non-significant reduction in cell death, with $6.05 \pm 0.7\%$ of cells perishing (n:3, 301 cells) (**Figure 5-22: A**). In terms of the effects on the cumulative timescale of cell death compared with OGD alone, the combination of 100uM ATP + 1mM glutamate produced a period of significantly increased death after 5 and 15 minutes (**Figure 5-22: D**). Both 100uM ATP (40.53 ± 5.03 minutes, n:19) and 100uM ATP + 1mM glutamate (43.68 ± 6.41 minutes, n:19), but not 1mM glutamate (60.13 ± 3.31 minutes, n:38) significantly decreased ($p < 0.001$) the mean time to cell death (**Figure 5-22: B**), suggesting that this effect was mediated by ATP. By contrast, the addition of either 1mM glutamate (20 ± 7.64 minutes, n:3) or the combination of 1mM glutamate + 100uM ATP (18.33 ± 10.93 minutes, n:3), but not 100uM ATP (45 ± 21.2 minutes, n:4), reduced the average time to first cell death in neuronal cultures during OGD (although this did not reach statistical significance by ANOVA) suggesting this early death may have been mediated by glutamate (**Figure 5-22: C**). Finally, looking at the frequency histograms of cell death, 100uM ATP (**Figure 5-22: G**) seemed to reduce cell death after 50 minutes, and the combination of 100uM ATP + 1mM glutamate (**Figure 5-22: H**) increased the amount of early cell death and reduced late cell death, while 1mM glutamate (**Figure 5-22: F**) did not greatly affect the timescale of cell death during OGD.

The $[Ca^{2+}]_i$ recordings from these experiments reveal that there were only large sudden increases in $[Ca^{2+}]_i$ immediately after the application of either 1mM glutamate (**Figure 5-23: A**) or 100uM ATP + 1mM glutamate (**Figure 5-23: E**), but not 100uM ATP (**Figure 5-23: C**), where they only occurred in fewer cells and much later on after nearly 80 minutes of OGD. This suggests that glutamate was responsible, a conclusion that coincides with the findings in Chapter 4 where glutamate caused large $[Ca^{2+}]_i$ rises in all cells in the neuronal culture. Interestingly, the combination of ATP + glutamate produced the highest number of $[Ca^{2+}]_i$ rises and these also appear to be larger, although an accurate judgment cannot be made without calibrating the signal. This suggests that even though ATP alone did not cause immediate $[Ca^{2+}]_i$ rises it did somehow potentiate or increase glutamate induced $[Ca^{2+}]_i$ rises. Once again, all cells that died had rises in $[Ca^{2+}]_i$ before death (See example cells in **Figure 5-23: B3, F1 and F3**), and particularly with ATP + glutamate there were cells which died within 5 minutes of agonist application following a large monophasic $[Ca^{2+}]_i$ rise (**Figure 5-23: F1, F3**): this was a quicker time from first $[Ca^{2+}]_i$ rise to cell death than was seen under any other conditions. There were also a number of cells which had long-lasting $[Ca^{2+}]_i$ rises that did not die (**Figure 5-23: B2, B4, and F4**), suggesting that Ca^{2+} accumulation alone during OGD is not sufficient to cause cell death. This observation is further supported by the finding that significantly more cells in the neuronal culture had increased $[Ca^{2+}]_i$ levels during OGD after the application of ATP + glutamate ($65.12 \pm 4.06\%$, n:3) compared with ATP ($13.63 \pm 9.63\%$, $p < 0.01$) or glutamate ($32.36 \pm 2.51\%$, $p < 0.05$) (**Figure 5-23: G**), while the relative quantities of cell death were glutamate > ATP + glutamate > ATP. The $[Ca^{2+}]_i$ trend (**Figure 5-23: H**) was raised in the glutamate and ATP + glutamate experiments compared to ATP and OGD, and there was also a reduction in $[Ca^{2+}]_i$ in the ATP experiment relative to OGD alone after about 60 minutes.

In summary, neither ATP, glutamate nor ATP + glutamate significantly increased overall cell death during OGD in the neuronal culture. As during control conditions, the presence of ATP either alone or together with glutamate caused a reduction in the mean time to cell death in the neuronal culture, this time during OGD, while the average time to

first death was earlier whenever glutamate was added. This effect of ATP reducing the mean time to cell death once again seems to be secondary to a reduction in the amount of late cell death rather than increased early death. The latter effect of glutamate may be linked to the widespread large $[Ca^{2+}]_i$ rises seen following the application of glutamate or ATP + glutamate. The combination of ATP + glutamate in particular caused very early cell death and the largest and most numerous $[Ca^{2+}]_i$ rises, even though this did not correlate with having the highest death rate at the end of the experiment.

Figure 5-22: Effects of ATP and glutamate application on cell death in neuronal cultures during OGD

Agonists were applied continuously during 90 minutes of OGD.

A: Total cell death during OGD

Adding 100uM ATP or a combination of 100uM ATP and 1mM glutamate during OGD reduced the amount of cell death, although the difference was not significant ($p>0.05$). 1mM glutamate during OGD had no effect on overall cell death in these cultures.

B: Mean time to cell death

Despite the reduction in overall cell death, the mean time to cell death was significantly earlier with the addition of ATP and ATP + glutamate but not glutamate alone ($p<0.001$), suggesting this effect is mediated by ATP.

C: Average time to first cell death

The addition of either 1mM glutamate or the combination of 1mM glutamate + 100uM ATP, but not 100uM ATP, reduced the average time to first cell death in neuronal cultures during OGD (although this did not reach statistical significance by ANOVA) suggesting this early death was mediated by glutamate.

D,E: Timescale of cumulative cell death

There were two periods of time (after 5 and 15 minutes) when there was significantly more cell death with the combined application of ATP + glutamate. These were transient effects and there were no other significant differences.

F,G,H: Frequency histogram of cell death

Both 100uM ATP (**G**) and the combination of ATP and glutamate (**H**) increased the amount of early cell death and reduced late cell death, while 1mM glutamate alone (**F**) did not greatly affect the timescale of cell death during OGD.

*: $p<0.05$

** : $p<0.01$

***: $p<0.001$

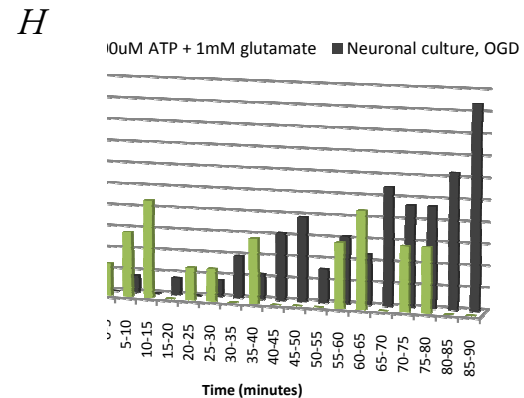
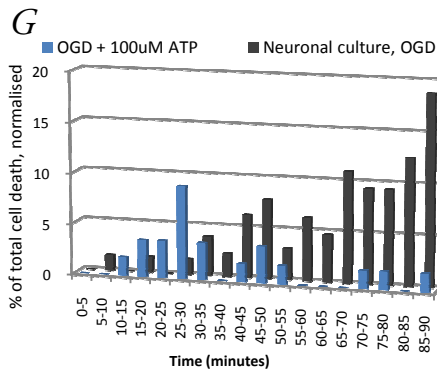
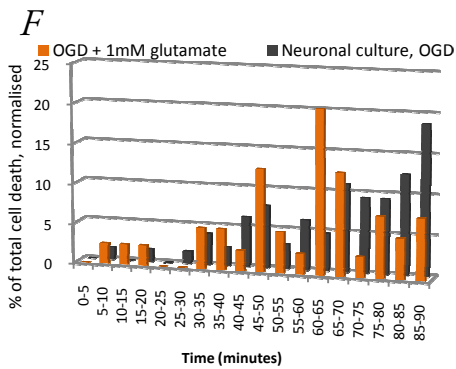
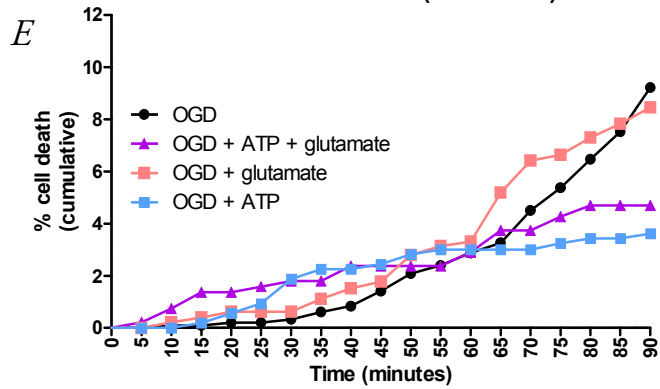
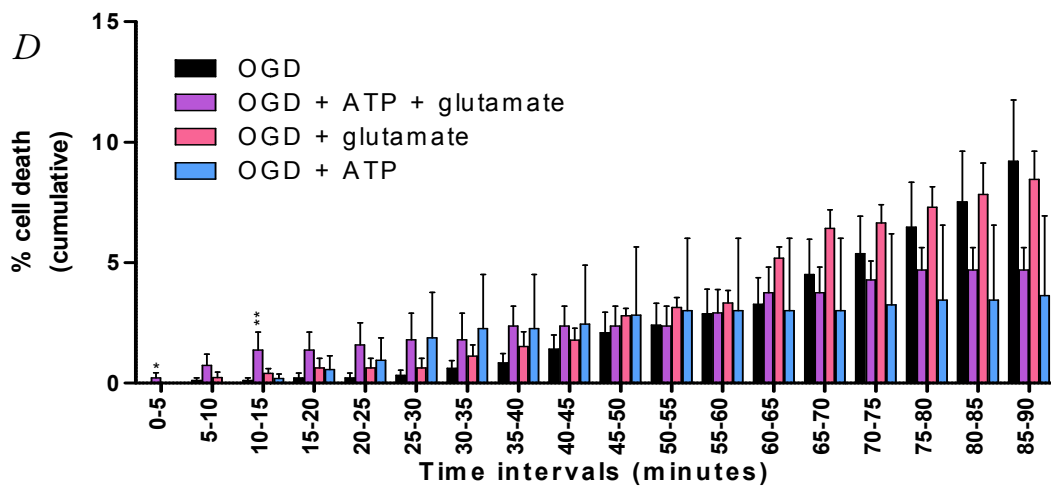
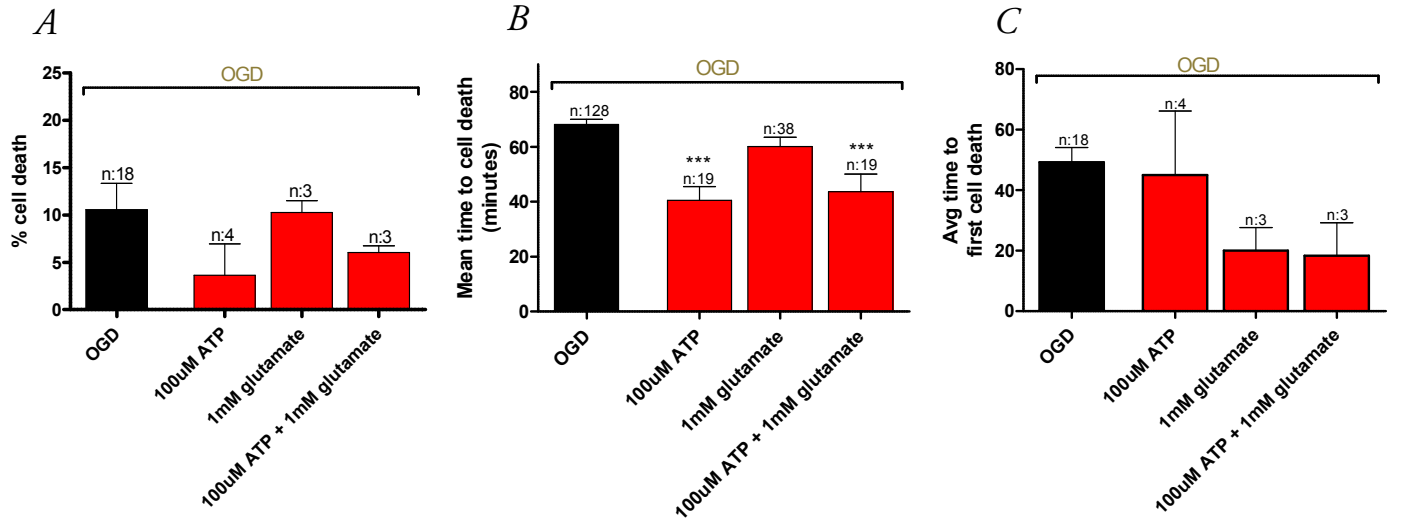


Figure 5-23: $[Ca^{2+}]_i$ rises and cell death in neuronal cultures when adding exogenous ATP and glutamate during OGD

Traces of $[Ca^{2+}]_i$ (340:380) and 360nm excitation (F360) from 30 randomly selected cells (**A**, **C**, **E**) and 4 individual representative examples (**B**, **D**, **F**) demonstrating effects of 1mM glutamate, 100uM ATP and 100uM ATP + 1mM glutamate respectively on $[Ca^{2+}]_i$ during OGD in neuronal cultures. Purple arrows point out rises in $[Ca^{2+}]_i$, red arrows the time of cell death (drop in F360).

When comparing these $[Ca^{2+}]_i$ recordings it is apparent that there are only large sudden increases in $[Ca^{2+}]_i$ immediately after the application of either 1mM glutamate (**A**) or 100uM ATP + glutamate (**E**) during OGD, but not 100uM ATP (**C**), where they only occurred in fewer cells and much later on after nearly 80 minutes of OGD. Once again, all cells that died had rises in $[Ca^{2+}]_i$ before death (See example cells **B3**, **F1** and **F3**) but in these experiments there were also a number of cells which had long-lasting $[Ca^{2+}]_i$ rises that did not die (See example cells **B2**, **B4**, and **F4**), suggesting that Ca^{2+} accumulation alone during OGD is not sufficient to cause cell death. The combination of ATP + glutamate produced the highest number of $[Ca^{2+}]_i$ rises and these also appear to be larger, although accurate judgment cannot be made without calibrating the signal.

G: % of cell that had raised $[Ca^{2+}]_i$

Significantly more cells in the neuronal culture had increased $[Ca^{2+}]_i$ levels during OGD after the application of ATP + glutamate compared with ATP ($p < 0.01$) or glutamate ($p < 0.05$).

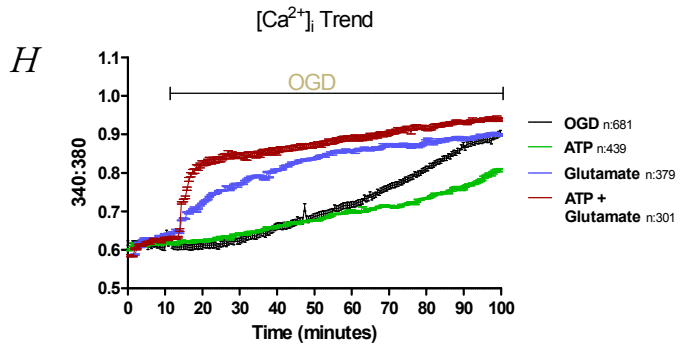
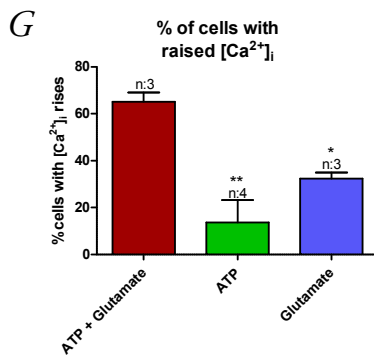
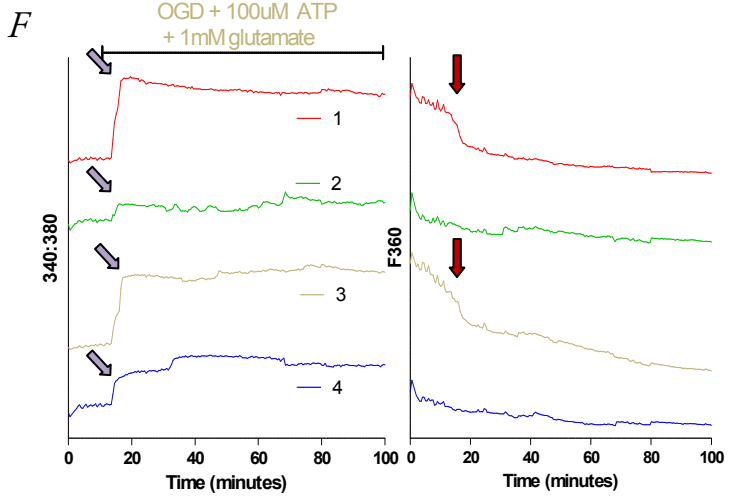
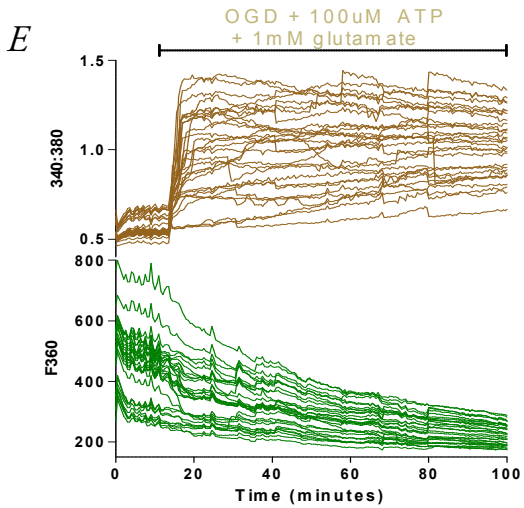
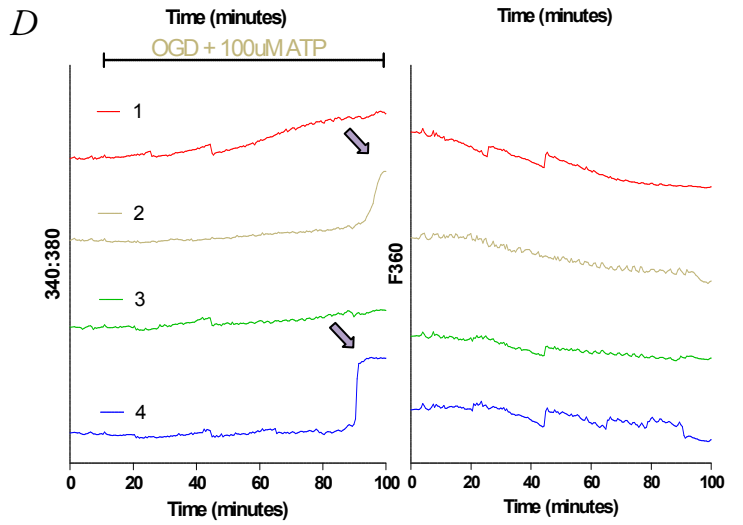
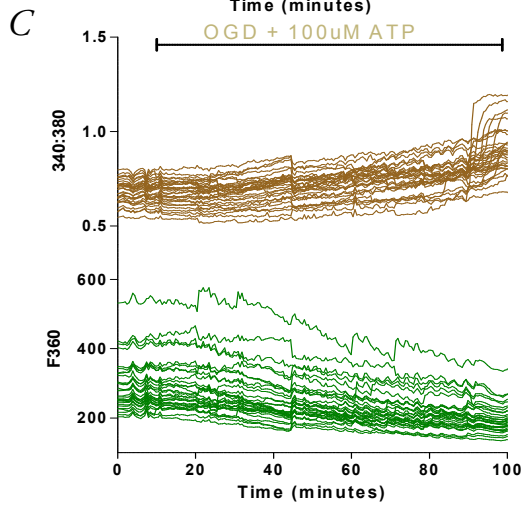
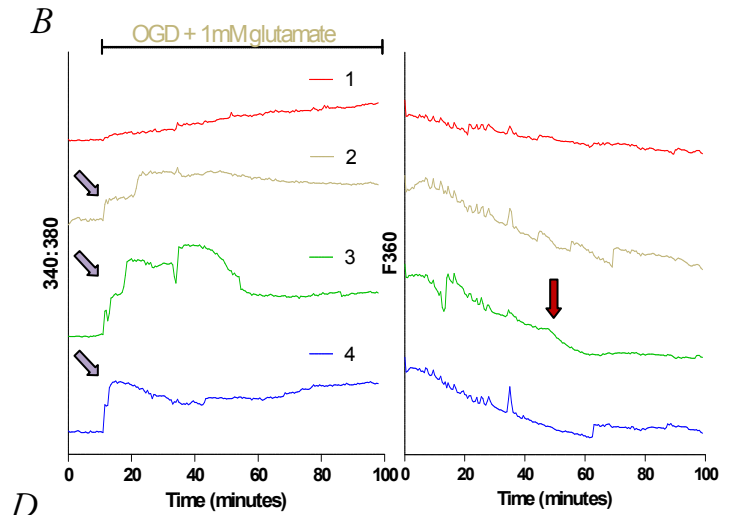
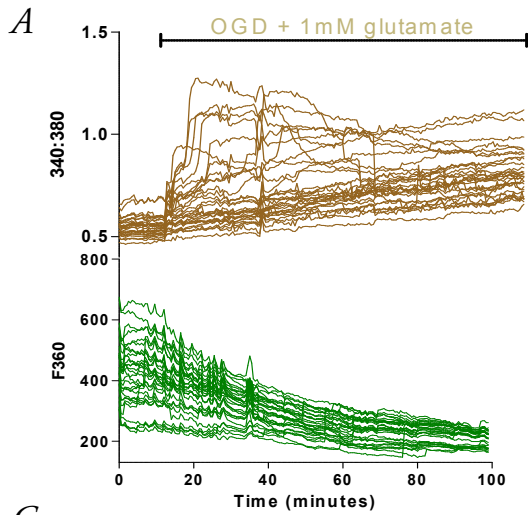
H: Average overall $[Ca^{2+}]_i$ trend, OGD vs. OGD + agonists

The average change in $[Ca^{2+}]_i$ of all cells was raised in the glutamate and glutamate + ATP experiments compared to OGD and ATP. There was also a reduction in $[Ca^{2+}]_i$ in the ATP experiment relative to OGD alone after about 60 minutes.

*: $p < 0.05$

**.: $p < 0.01$

Neuronal culture



Continuous application of glutamate during OGD in co-cultures

Having been unable to significantly affect rates of overall cell death in the neuronal cultures by the application of P2 and glutamate receptor agonists during both OGD and control conditions, I proceeded to add different concentrations of glutamate or P2 receptor agonists to co-cultures during OGD. The addition of 10uM ($7.59 \pm 2.4\%$, n:3, 501 cells), 100uM ($7.95 \pm 4.7\%$, n:3, 505 cells) and 1mM glutamate ($7.62 \pm 2.5\%$, n:6, 775 cells) but not 1uM glutamate ($35.15 \pm 15.1\%$, n:4, 739 cells) significantly reduced overall cell death ($p < 0.05$ for 10uM and 100uM, $p < 0.001$ for 1mM) in co-cultures compared to OGD alone ($44.46 \pm 3.3\%$) (**Figure 5-24: A**), with the difference first becoming significant for 1mM after 70 minutes and for 10uM and 100uM after 85 minutes (**Figure 5-25: A**). This was due to a reduction in the amount of astrocyte death but not neuronal death. The astrocyte death rates were $50.04 \pm 4.5\%$ during OGD, $47.53 \pm 18.7\%$ with 1uM glutamate (n:4, 355 cells, $p > 0.05$), $6.54 \pm 2.9\%$ (n:3, 302 cells, $p < 0.05$) with 10uM glutamate, $5.58 \pm 2.1\%$ (n:3, 300 cells, $p < 0.05$) with 100uM glutamate and $7.55 \pm 2.8\%$ (n:5, 410 cells, $p < 0.01$) with 1mM glutamate (**Figure 5-24: A**), with 1mM significantly reducing astrocyte death earliest after 65 minutes and 10uM and 100uM both first becoming significant after 75 minutes (**Figure 5-25: B**). In terms of neurons the death rates were $23.2 \pm 2.5\%$ with OGD alone, $19.59 \pm 9.6\%$ (n:4, 365 cells) with 1uM glutamate, $9.74 \pm 3.8\%$ (n:3, 185 cells) with 10uM glutamate, $13.12 \pm 10.9\%$ (n:3, 191 cells) with 100uM glutamate and $13.89 \pm 5.9\%$ (n:5, 256 cells) with 1mM glutamate, with none of these differences being statistically significant ($p > 0.05$) (**Figure 5-24: A**), despite there being a transient significant increase in neuronal death with 1mM glutamate after 20 minutes (**Figure 5-25: C**).

In terms of the effects of glutamate on the time of cell death, 1uM glutamate significantly increased the mean time to cell death for astrocytes (73.8 ± 1.05 minutes, n:184, $p < 0.001$), neurons (74.02 ± 2.06 minutes, n:56, $p < 0.05$) and all cell types combined (73.56 ± 0.93 minutes, n:246, $p < 0.001$), while 100uM reduced it for astrocytes (48.44 ± 2.65 minutes, n:16, $p < 0.05$) or when all cells were combined (53.24 ± 2.03 minutes, n:34, $p < 0.05$) and 1mM reduced it for neurons only (55.86 ± 3.36 minutes,

n:35, $p < 0.05$) (**Figure 5-24: B**). The trend was for neurons to die earlier with increasing concentrations of added glutamate. There were no statistically significant differences in the average time to first cell death with the application of glutamate during OGD (**Figure 5-24: C**). When looking at the frequency histograms of cell death of all cell types together (**Figure 5-26: A**), 1uM glutamate delayed the onset of significant cell death during OGD, whilst 10uM, 100uM and 1mM also caused delayed onset of cell death as well as greatly reducing overall rates of cell death, most pronounced towards the end of the experiments. As the overall effect was mainly due to increased astrocyte survival, the effects on the timescale of astrocyte death are the same as for all cell types together, with a delaying of onset and overall reduction in cell death over time (**Figure 5-26: B**). Finally, the frequency histogram of neuronal death does not seem to be affected by 1 or 10uM glutamate (**Figure 5-26: C**). With 100uM the onset was delayed and there was no death in the last 15 minutes, and 1mM glutamate lead to earlier onset of neuronal death but also a slight reduction in late death (**Figure 5-26: C**).

Figure 5-24: Effects on cell death of adding different concentrations of glutamate to co-cultures during OGD

Different concentrations of glutamate (1uM-1mM) were added onto co-cultures continuously during 90 minute OGD experiments.

A: Total cell death, co-culture OGD + glutamate

The addition of 10, 100 (both $p < 0.05$) and 1000 ($p < 0.001$), but not 1uM glutamate ($p > 0.05$) significantly reduced overall cell death during OGD, and this was due mainly to a reduction in astrocyte death, with 10, 100 (both $p < 0.05$) and 1000 ($p < 0.01$) uM glutamate significantly reducing astrocyte death. There were no significant differences in total neuronal death.

B: Mean time to cell death

1uM glutamate significantly increased the mean time to cell death for astrocytes ($p < 0.001$), neurons ($p < 0.05$) and all cell types combined ($p < 0.001$), while 100uM reduced it for astrocytes ($p < 0.05$) or when all cells were combined ($p < 0.05$) and 1mM reduced it for neurons only ($p < 0.05$). The trend was for neurons to die earlier with increasing concentrations of added glutamate.

C: Average time to first cell death

There were no statistically significant differences in the average time to first cell death with the application of glutamate during OGD.

*: $p < 0.05$

** : $p < 0.01$

***: $p < 0.001$

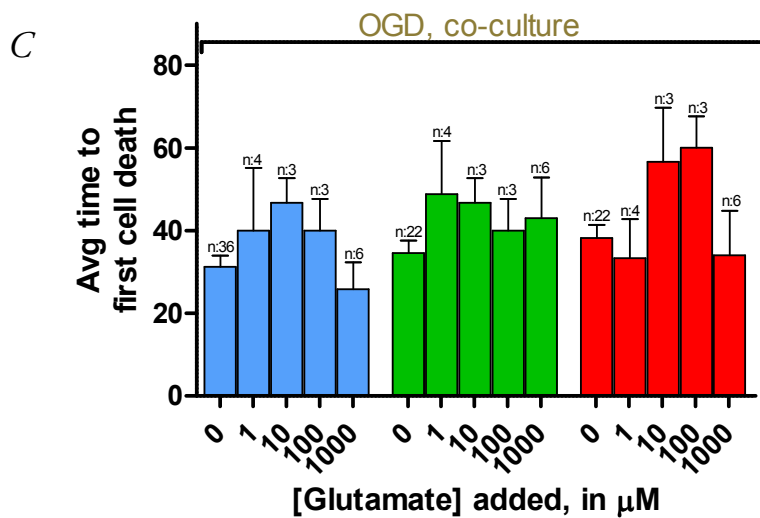
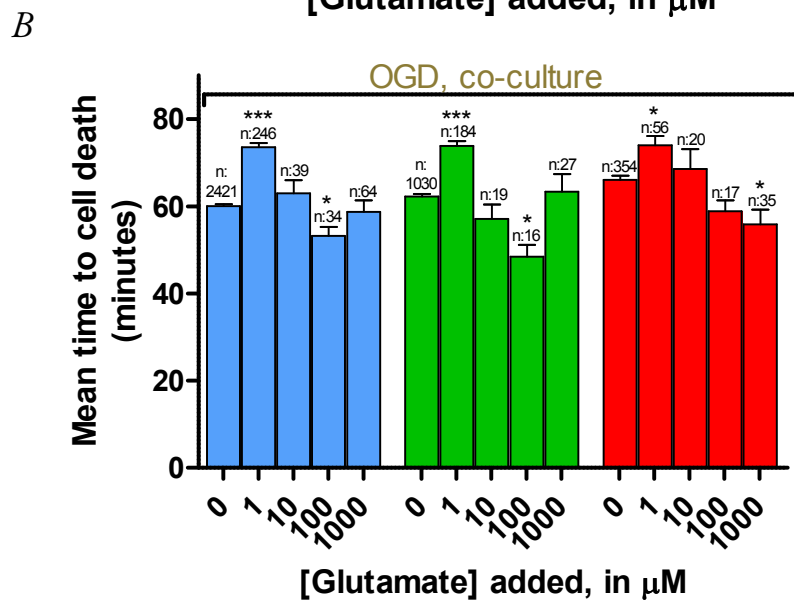
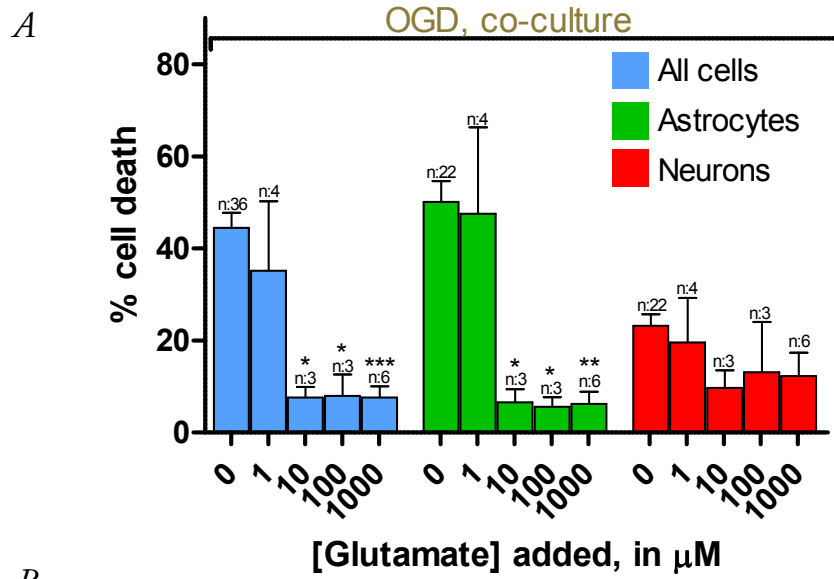


Figure 5-25: Effects of adding different concentrations of glutamate to co-cultures during OGD, cumulative timescale of cell death

Note the different scales on the y-axis for graphs **A-C**.

A: Timescale of death, all cell types

1mM glutamate significantly reduced overall cell death after 70 minutes, with 10 and 100uM doing so after 85 minutes.

B: Timescale of astrocyte death

10,100 and 1000uM glutamate all significantly reduced astrocyte death in co-culture, with 1mM reducing it earliest after 65 minutes and 10 and 100 both first becoming significant after 75 minutes.

C: Timescale of neuronal death

The addition of 1mM glutamate during OGD caused an earlier onset of neuronal death than OGD alone; consequently neuronal death was significantly increased during one timepoint after 20 minutes. There were no other significant differences.

D,E,F: Linear versions of graphs **A-C**, with error bars removed and uniform y-axis scales for easier comparisons.

*: $p < 0.05$

** : $p < 0.01$

***: $p < 0.001$

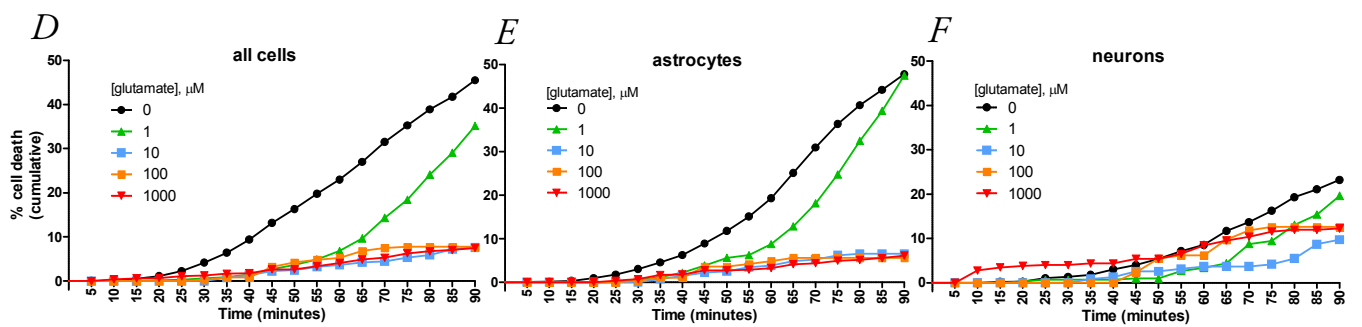
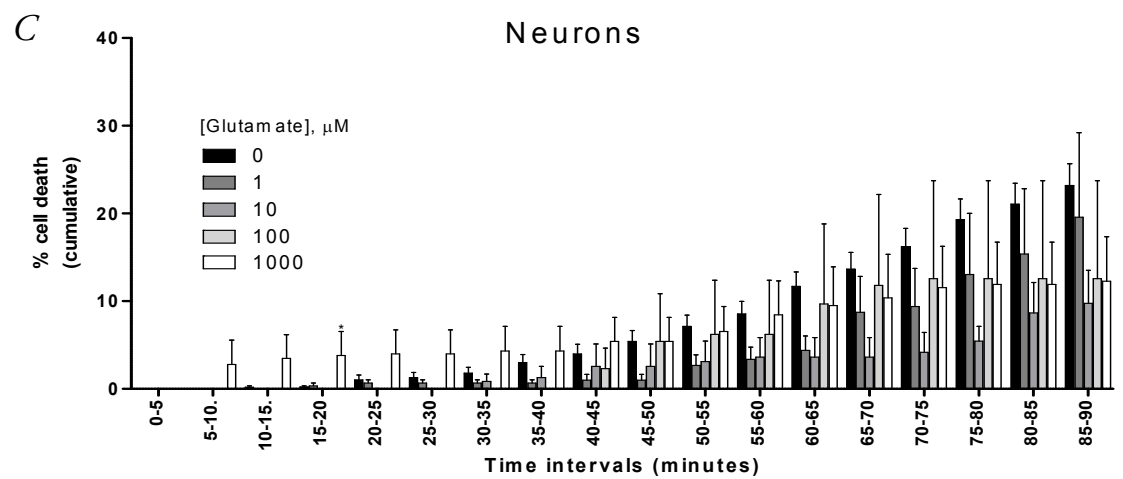
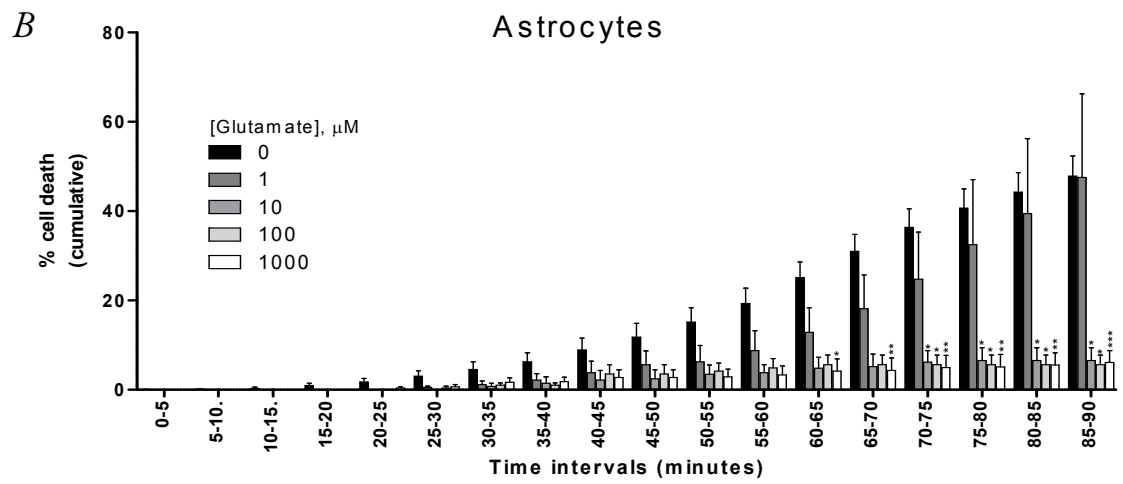
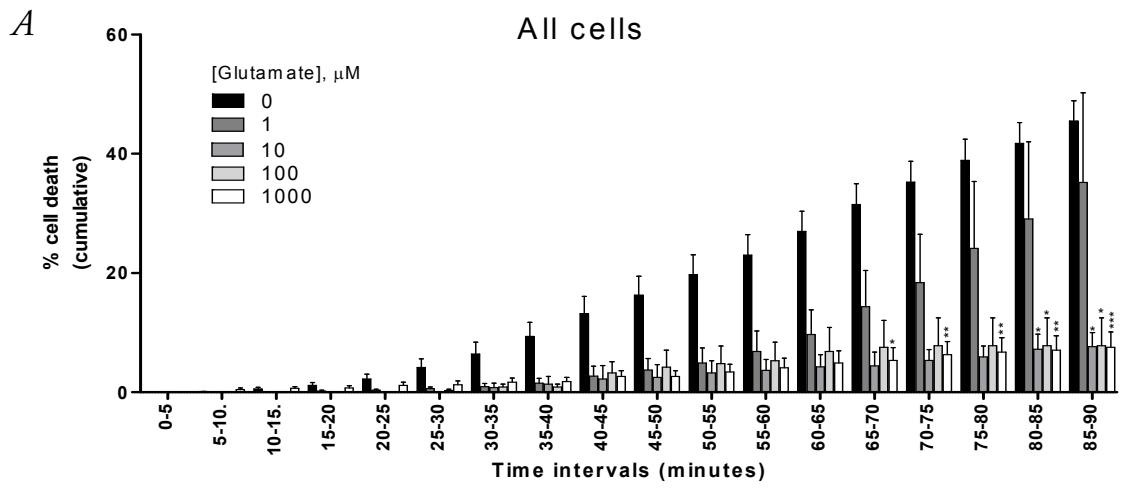


Figure 5-26: Effects of adding different concentrations of glutamate to co-cultures during OGD on cell death, timescale

A: Frequency histogram of death, all cell types

1uM glutamate delayed the onset of significant cell death during OGD, whilst 10, 100 and 1000uM also had delayed onset of cell death as well as greatly reduced overall rates of cell death, most pronounced towards the end of the experiment.

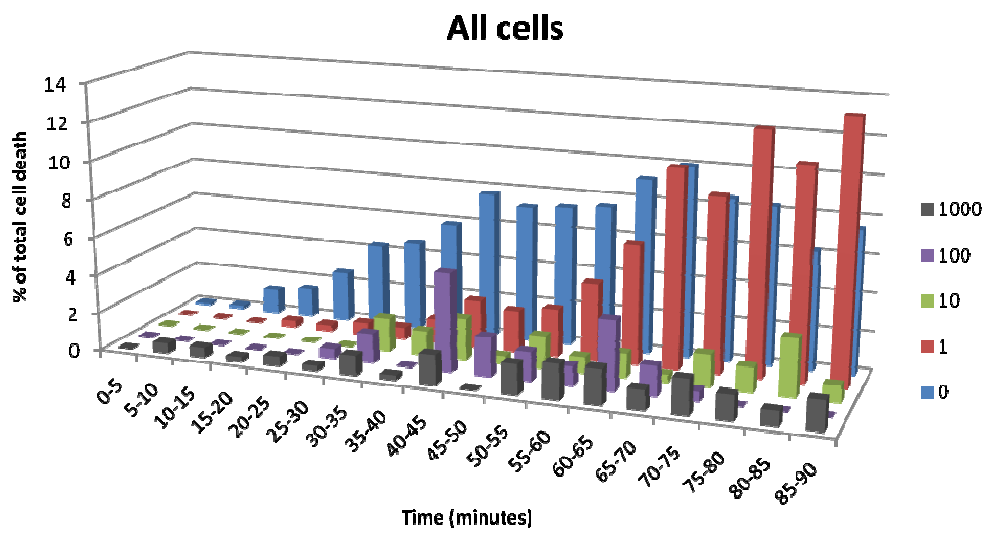
B: Frequency histogram of astrocyte death

Since most effects of added glutamate were protective of astrocytes, the timescale of astrocyte death in co-cultures was affected in the same way as that of all cell types, with a delaying of onset and overall reduction in cell death over time.

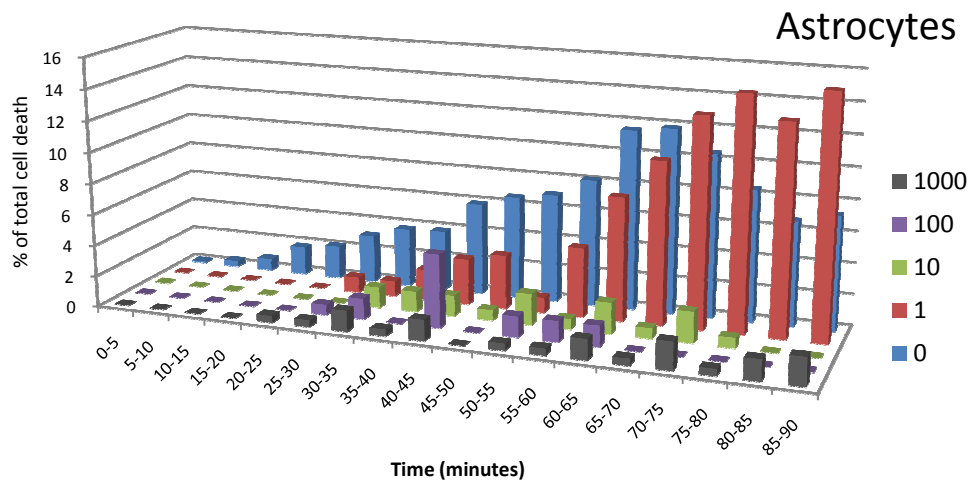
C: Frequency histogram of neuronal death

The timescale of neuronal death was not significantly affected by 1 or 10uM glutamate. With 100uM the onset was delayed and there was no death in the last 15 minutes. 1000uM glutamate lead to earlier onset of neuronal death but also a reduction in late death.

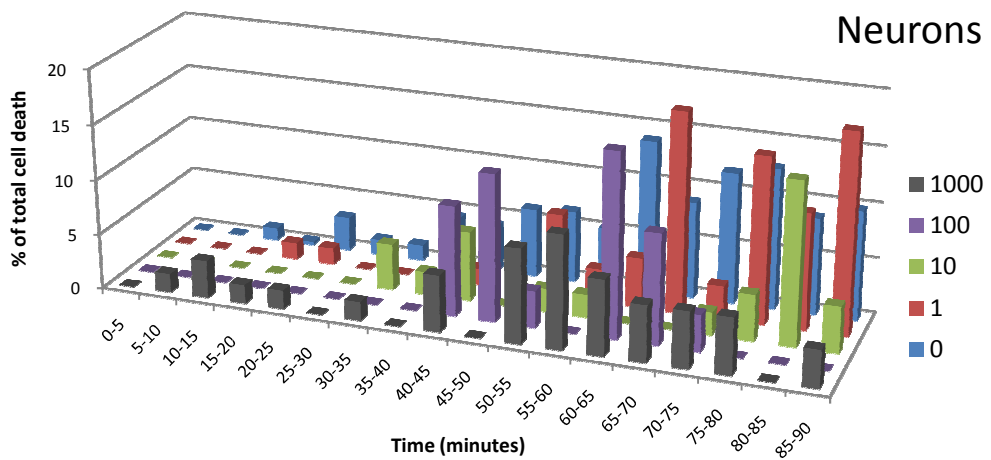
A



B



C



Continuous application of ATP and MRS-2365 during OGD in co-cultures

To finish this group of experiments, I applied either 100uM ATP or 10nM of the P2Y₁ receptor agonist MRS-2365 to co-cultures during OGD. Neither 100uM ATP nor 10nM MRS-2365 significantly changed the amount of cell death during OGD (**Figure 5-27: A**). ATP caused a non-significant reduction in cell death when all cell types were combined ($p > 0.05$), with $30.88 \pm 10.59\%$ death (n:6, 1000 cells), whilst the cell specific analysis revealed $58.71 \pm 12\%$ astrocyte death (n:4, 342 cells) and $26.37 \pm 4.42\%$ neuronal death (n:4, 349 cells) (**Figure 5-27: A**). The addition of MRS-2365 did not significantly affect overall cell death rates ($45.84 \pm 8\%$, n:5, 956 cells), astrocyte death ($54.87 \pm 9.7\%$, n:5, 561 cells), or neuronal death ($32.38 \pm 7.1\%$, n:5, 374 cells) (**Figure 5-27: A**). The cumulative timescale of cell death confirms that neither ATP nor MRS-2365 significantly affected cell death after any time-point during these experiments (**Figure 5-28**). However, both ATP (68.67 ± 0.7 minutes, n:321) and MRS-2365 (66.61 ± 0.68 minutes, n:450) significantly increased the mean time to cell death of all cells combined ($p < 0.001$ for both) and of astrocytes ($p < 0.001$ for ATP (69.04 ± 0.88 minutes, n:204), $p < 0.05$ for MRS-2365 (65.52 ± 0.87 minutes, n:305)) but not of neurons (67.05 ± 1.22 minutes, n:100 for ATP; 69.81 ± 1.05 minutes, n:133 for MRS-2365) (**Figure 5-27: B**). The addition of ATP during OGD significantly delayed the average time to first cell death when all cells were combined (52.5 ± 8.14 minutes, n:6, $p < 0.05$) (**Figure 5-27: C**). There were no other statistically significant differences in the average time to first cell death with ATP (astrocytes: 48.75 ± 3.86 minutes, n:4; neurons: 46.25 ± 5.37 minutes, n:4) or MRS-2365 (all cells: 34 ± 4 minutes, n:5; astrocytes: 34 ± 4 minutes, n:5; neurons: 48 ± 5.39 minutes, n:5) (**Figure 5-27: C**). Finally, the frequency histograms of cell death reveal that both ATP and MRS-2365 were able to delay the onset of death of all cell types during OGD by around 20 minutes without any other apparent effects (**Figure 5-29**).

To summarize, glutamate added to co-cultures during OGD significantly reduced astrocyte death and death of all cells combined in a concentration range from 10uM – 1mM, with 1uM increasing the mean time to astrocyte death and 100uM decreasing it. Overall neuronal death was not significantly affected, although 1mM glutamate did cause

some earlier neuronal death and reduced the mean time to cell death, with the trend being for neurons to die earlier with increasing glutamate concentrations. ATP and MRS-2365 were not able to significantly affect rates of cell death during OGD, although both significantly increased the mean time to cell death of astrocytes but not neurons and ATP also significantly delayed the average time to first cell death.

Figure 5-27: Effects on cell death of adding ATP and MRS-2365 to co-cultures during OGD

100uM ATP or 10nM MRS-2365 (a potent selective P2Y₁ receptor agonist) was added onto co-cultures continuously during 90 minute OGD experiments.

A: Total cell death, co-culture OGD + ATP and OGD + MRS-2365

Neither agonist was able to significantly affect overall cell death during OGD, although 100uM ATP reduced overall cell death.

B: Mean time to cell death

Both ATP and MRS-2365 significantly increased the mean time to cell death of all cells combined ($p < 0.001$ for both) and of astrocytes ($p < 0.001$ for ATP, $p < 0.05$ for MRS-2365) but not of neurons.

C: Average time to first cell death

The addition of ATP during OGD significantly delayed the average time to first cell death when all cells were combined ($p < 0.05$).

*: $p < 0.05$

***: $p < 0.001$

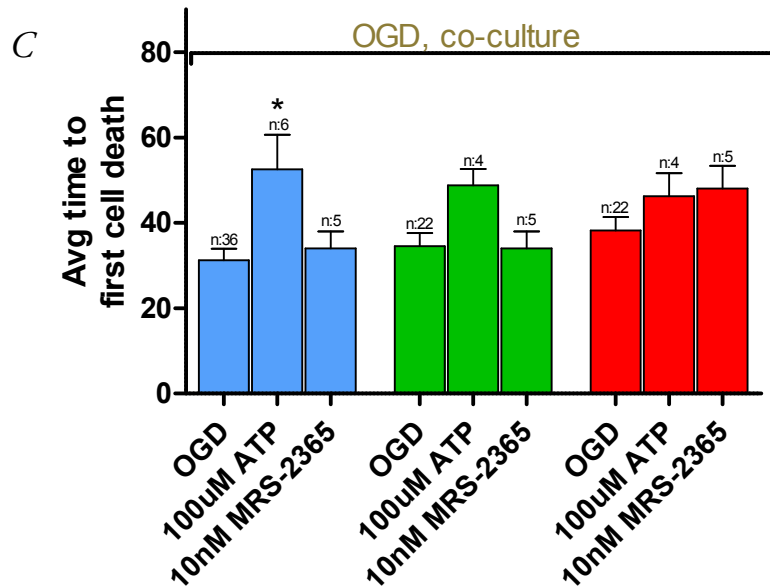
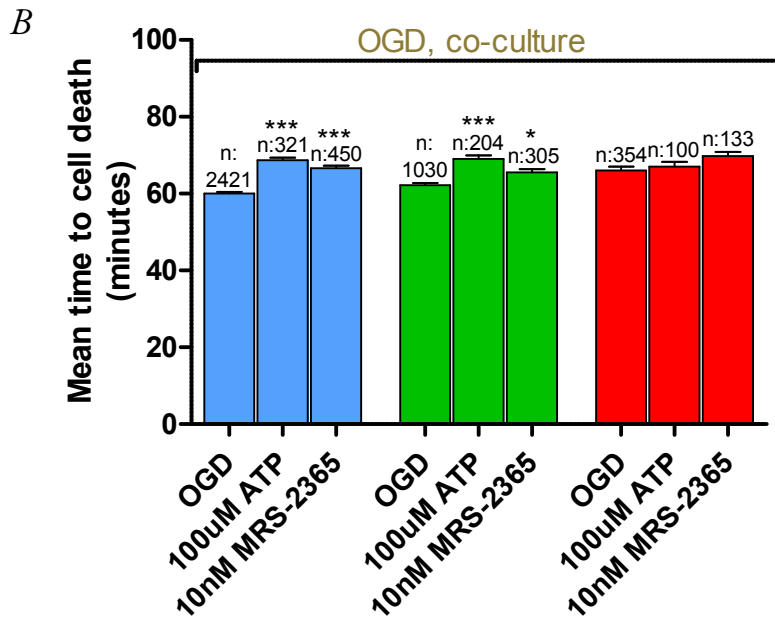
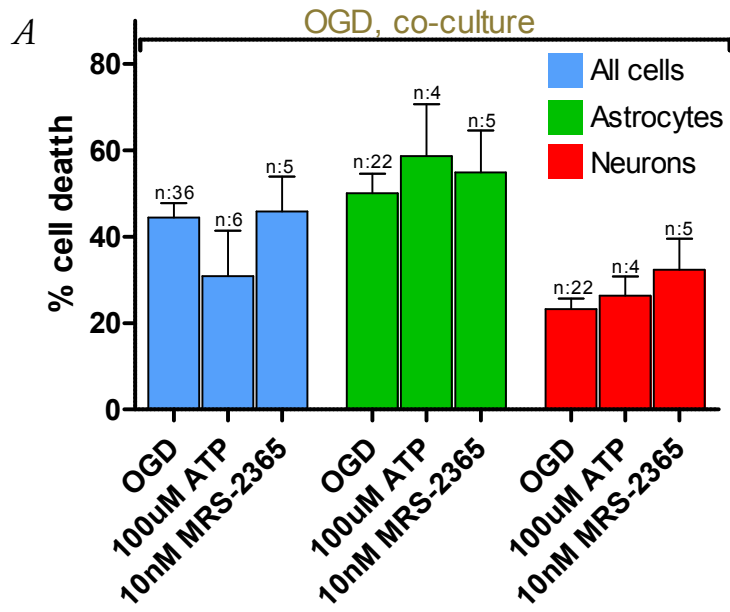


Figure 5-28: Effects of adding ATP or MRS-2365 to co-cultures during OGD, cumulative timescale of cell death

Note the different scales on the y-axis for graphs **A-C**.

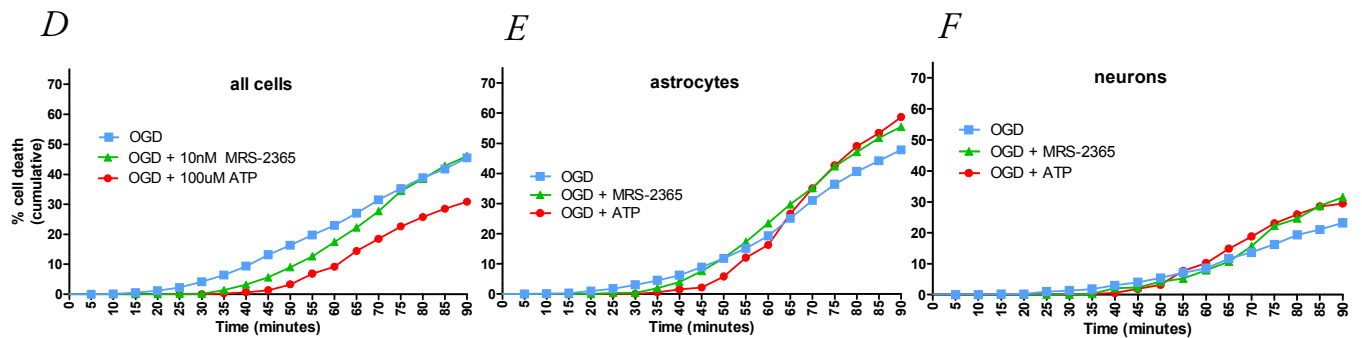
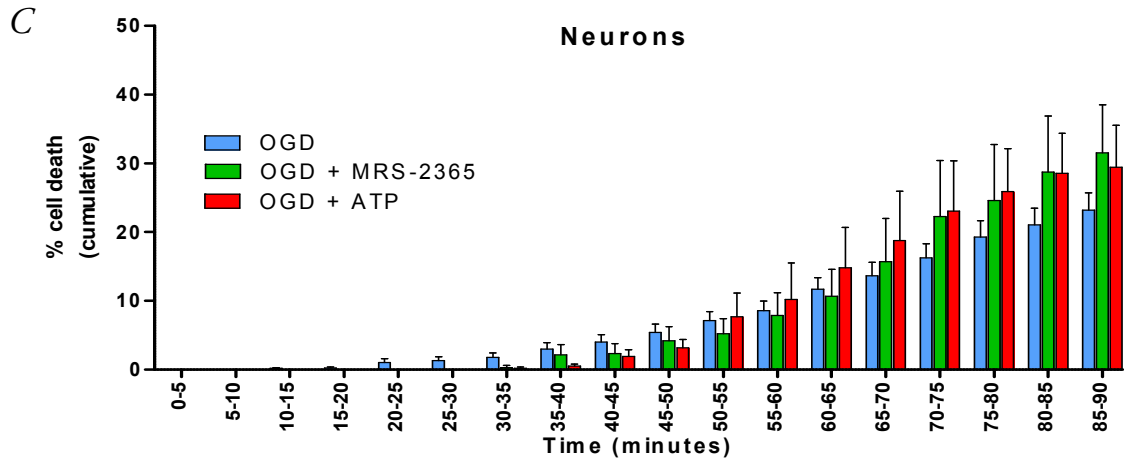
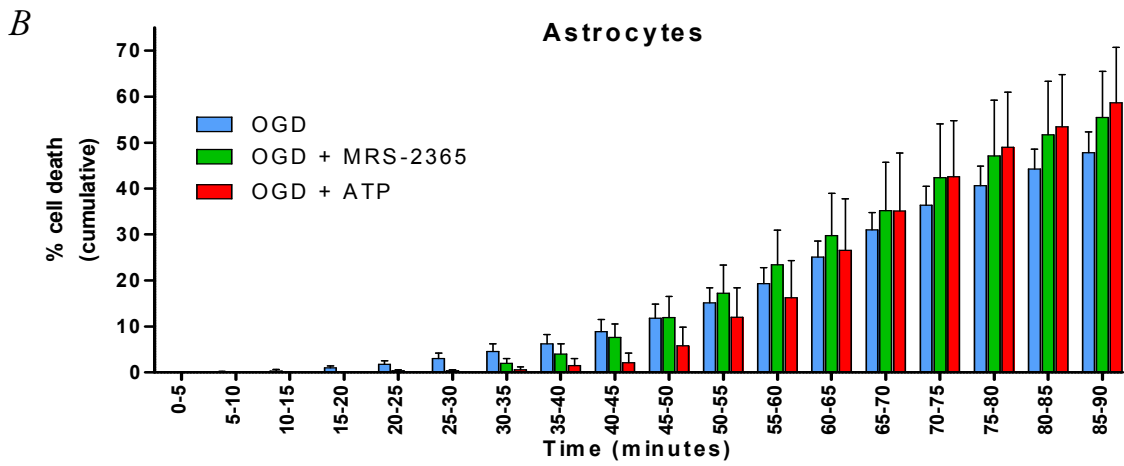
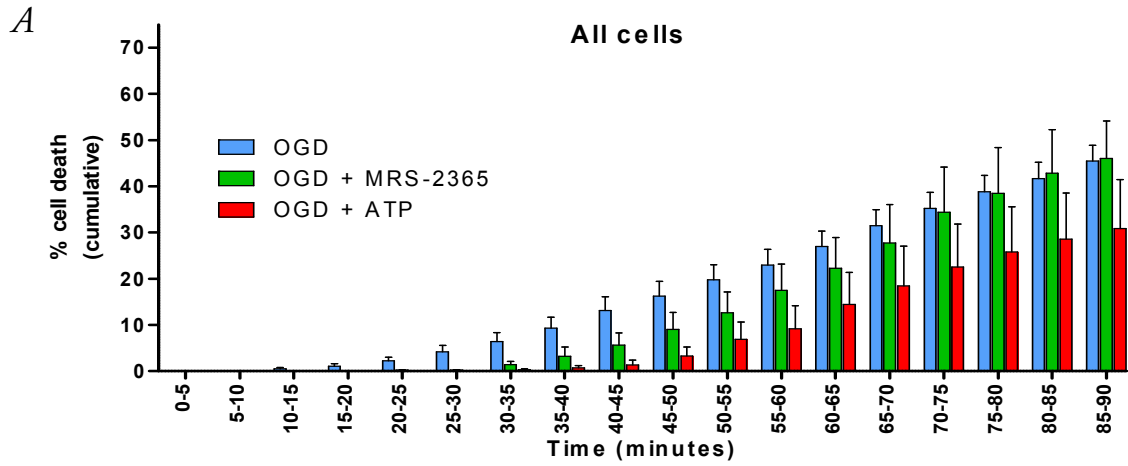
A: Timescale of cell death, all cell types

B: Timescale of astrocyte death

C: Timescale of neuronal death

D,E,F: Linear versions of graphs **A-C**, with error bars removed and uniform y-axis scales for easier comparisons.

Neither ATP nor MRS-2365 significantly affected cell death at any point in these experiments.



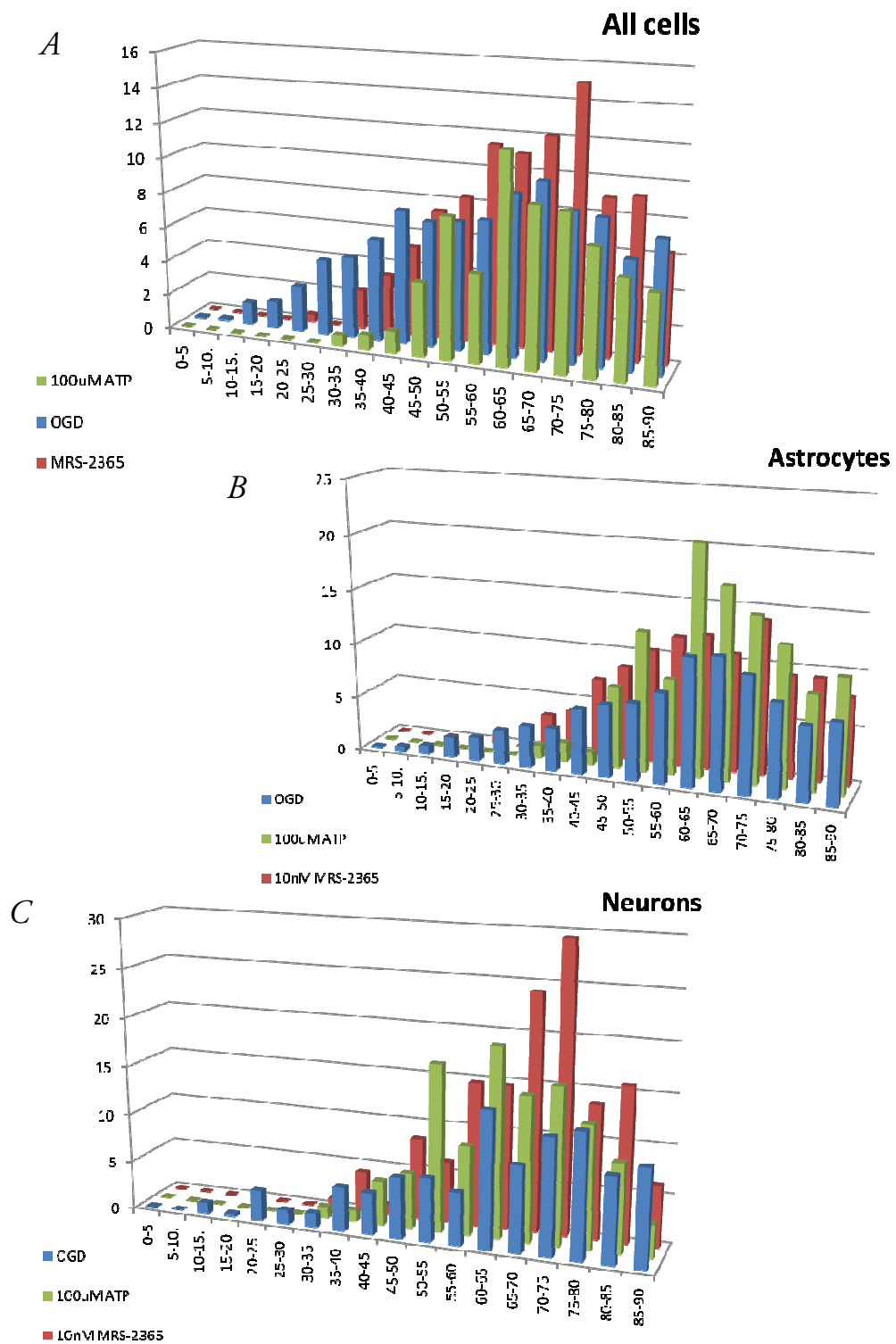


Figure 5-29: Effects of adding ATP or MRS-2365 to co-cultures during OGD, timescale of cell death

A, B, C: Frequency histogram of cell death of all cells (**A**), astrocytes (**B**) and neurons (**C**)

Both ATP and MRS-2365 were able to delay the onset of death of all cell types during OGD by around 20 minutes without any other apparent effects.

P2 receptor and ionotropic glutamate receptor antagonists prevent cell death in co-cultures during OGD

Effects of non-selective P2 receptor antagonists

The non-selective/broad spectrum P2 receptor antagonists PPADS (100uM and 10uM), suramin (100uM) and reactive blue 2 (RB-2, 100uM) were applied to co-cultures during OGD. As previously discussed in Chapter 4, PPADS and suramin have antagonist activities at a wide range of P2X and P2Y receptors, and the same is true for RB-2, which, at 100uM, has activity at P2X_{1, 2, 3, 5} and P2Y_{1, 4, 6, 11, 12} receptors (Burnstock and Knight, 2004). The concentration of PPADS was lowered to 10uM to reduce non-specific effects. Cell identification was only performed on the experiments using 10uM PPADS and suramin. Both 10 (10.64 ± 2.75%, n:16, p<0.001) and 100uM PPADS (0.92 ± 0.55%, n:5, p<0.001) and suramin (17.96 ± 9.99%, n:5, p<0.05), but not RB-2 (57.71 ± 4.54%, n:3), significantly reduced overall cell death during OGD (**Figure 5-30: A**), with 10uM PPADS first being protective after 40 minutes, 100uM PPADS after 60 minutes and suramin after 65 minutes (**Figure 5-31: A**). Astrocyte death was significantly reduced by 10uM PPADS (9.44 ± 4.5%, n:10, p<0.001), becoming significant after 50 minutes, while suramin (35.24 ± 20.54%, n:4) never significantly reduced astrocyte death (**Figure 5-30: A** and **Figure 5-31: B**). Neuronal death was significantly reduced by 10uM PPADS (2.76 ± 1.72%, n:10, p<0.001) for the first time after 50 minutes and by suramin (5.82 ± 4.55%, n:4, p<0.01) after 65 minutes (**Figure 5-30: A** and **Figure 5-31: C**).

All P2 receptor antagonists increased the mean time to cell death during OGD, with 100uM PPADS not reaching statistical significance due to the few cells that died. The values are 74.29 ± 0.7 minutes for suramin (n:182, p<0.001), 74.29 ± 7.82 minutes for 100uM PPADS (n:7, p>0.05), 74.83 ± 0.85 minutes for 10uM PPADS (n:300, p<0.001) and 71.59 ± 0.94 minutes for RB-2 (n:247, p<0.001) (**Figure 5-30: B**). Both 10uM PPADS and suramin significantly increased the mean time to cell death of astrocytes (78.11 ± 1.16 minutes, n:117 for 10uM PPADS; 74.7 ± 0.74 minutes, n:152 for suramin; p<0.001 for both) with only 10uM PPADS doing the same for neurons (83.52 ± 1.38

minutes, n:44, p<0.001) (**Figure 5-30: B**). The mean time to cell death of neurons with suramin was 71.59 ± 2.36 minutes (n:22) (**Figure 5-30: B**). All P2 antagonists except RB-2 (33.33 ± 14.81 minutes, n:3) significantly delayed the average time to first cell death (52.08 ± 4.93 minutes, n:16, p<0.01 for 10uM PPADS; 60 ± 11.83 minutes, n:5, p<0.05 for 100uM PPADS; 56.25 ± 6.54 minutes, n:5, p<0.05 for suramin), with 10uM PPADS, but not suramin, significantly delaying the onset of astrocyte death (58.57 ± 5.14 minutes, n:10, p<0.001; 48.33 ± 1.18 minutes, n:4, p>0.05 for suramin) and both 10uM PPADS (66.25 ± 3.29 minutes, n:10, p<0.001) and suramin (60 ± 4.08 minutes, n:4, p<0.01) significantly delaying the onset of neuronal death (**Figure 5-30: C**). Finally, the frequency histograms of cell death reveal that all non-selective P2 receptor antagonists delayed the onset of cell death during OGD, with all except RB-2 also reducing overall death rates (**Figure 5-32: A**). Both suramin and 10uM PPADS delayed the onset of astrocyte death, but only PPADS reduced death rates during all 90 minutes of OGD (**Figure 5-32: B**). Both suramin and 10uM PPADS delayed the onset of neuronal death, with the effect being most striking with 10uM PPADS (**Figure 5-32: C**).

Figure 5-30: Non-selective P2 receptor antagonists during OGD in co-culture

Various non-selective/broad spectrum P2 receptor antagonists were applied to co-cultures during OGD. Cell identification was only performed on the experiments using 10uM PPADS and Suramin.

A: Total cell death

10 and 100uM PPADS ($p < 0.001$) and suramin ($p < 0.05$), but not RB-2, significantly reduced overall cell death with 10uM PPADS reducing astrocyte death ($p < 0.001$) and both 10uM PPADS ($p < 0.001$) and suramin ($p < 0.01$) significantly reducing neuronal death.

B: Mean time to cell death

All P2 antagonists except 100uM PPADS significantly increased the mean time to cell death ($p < 0.001$ for all), with 100uM PPADS not reaching statistical significance due to the few cells that died ($n:7$). Both 10uM PPADS and suramin significantly increased the mean time to cell death of astrocytes ($p < 0.001$ for both) with only 10uM PPADS doing the same for neurons ($p < 0.001$).

C: Average time to first cell death

All P2 antagonists except RB-2 significantly delayed the time to first cell death ($p < 0.01$ for 10uM PPADS, $p < 0.05$ for 100uM PPADS and suramin), with 10uM PPADS significantly delaying the onset of astrocyte death ($p < 0.001$) and both 10uM PPADS ($p < 0.001$) and suramin ($p < 0.01$) significantly delaying the onset of neuronal death.

*: $p < 0.05$

**.: $p < 0.01$

***.: $p < 0.001$

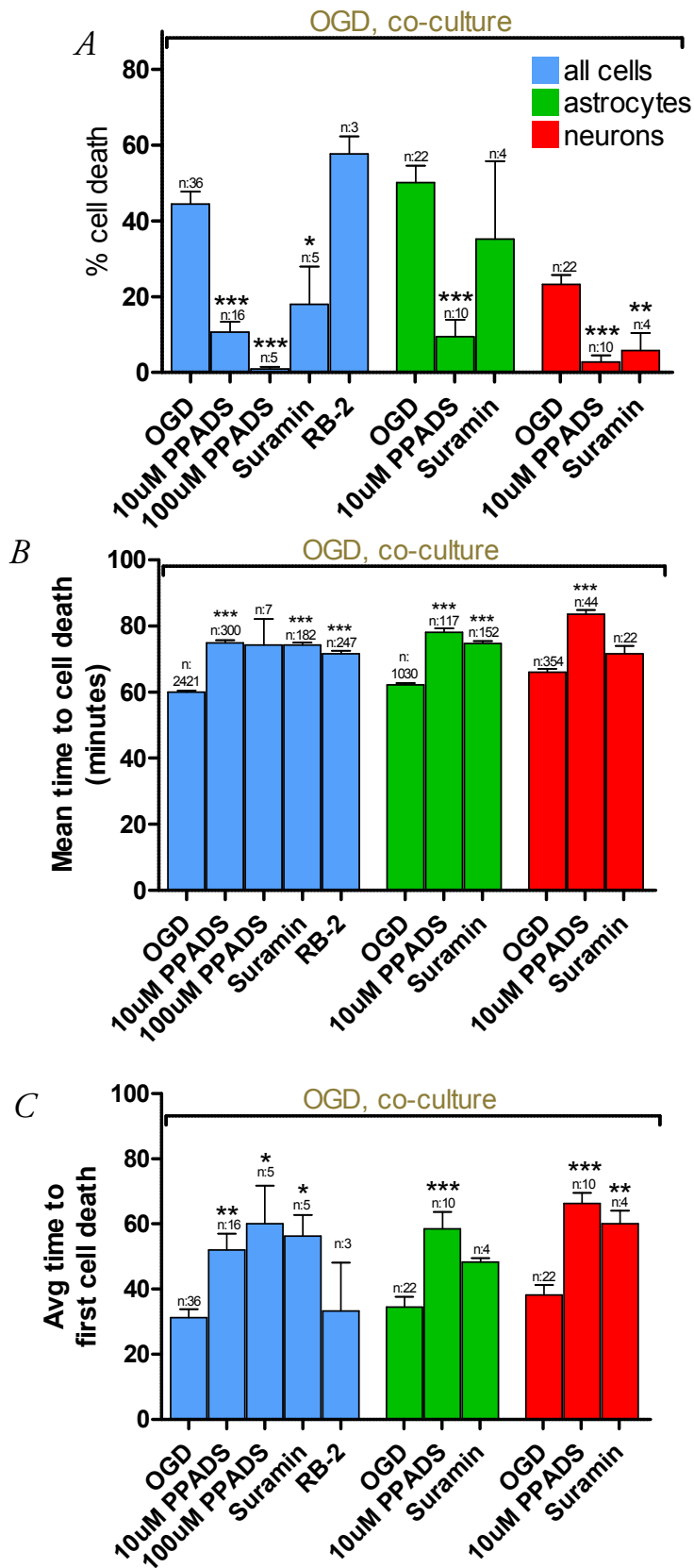


Figure 5-31: Non-selective P2 receptor antagonists during OGD in co-culture, cumulative timescale of cell death

Note the different scales on the y-axis for graphs *A-C*.

A: Timescale of death, all cell types

10uM PPADS was protective earliest, reaching significance compared to OGD for the first time after 40 minutes, with 100uM PPADS doing the same after 60 minutes and 100uM suramin after 65. RB-2 never significantly changed OGD-induced cell death.

B: Timescale of astrocyte death

10uM PPADS was protective of astrocytes in co-culture after 50 minutes, whilst suramin never significantly reduced astrocyte death.

C: Timescale of neuronal death

Both suramin and 10uM PPADS significantly reduced neuronal death in co-culture, with the former doing so after 65 minutes and the latter after 50.

D,E,F: Linear versions of graphs *A-C*, with error bars removed and uniform y-axis scales for easier comparisons.

*: $p < 0.05$

** : $p < 0.01$

***: $p < 0.001$

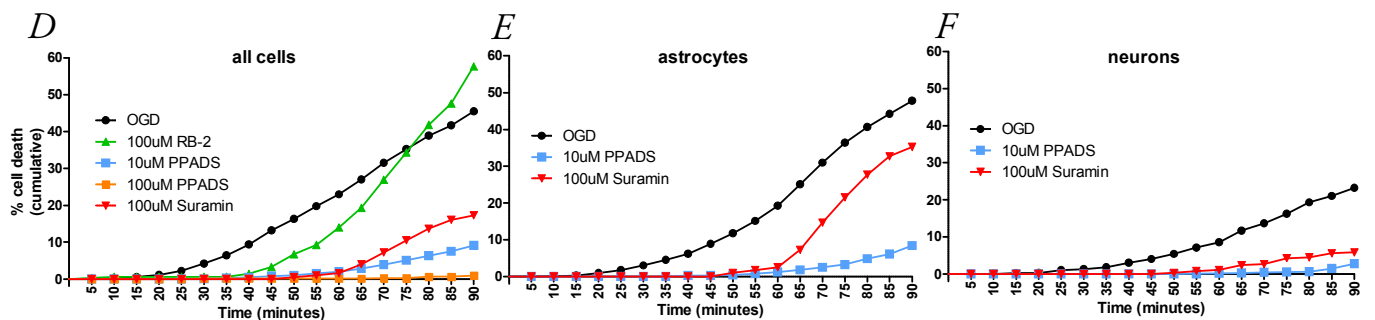
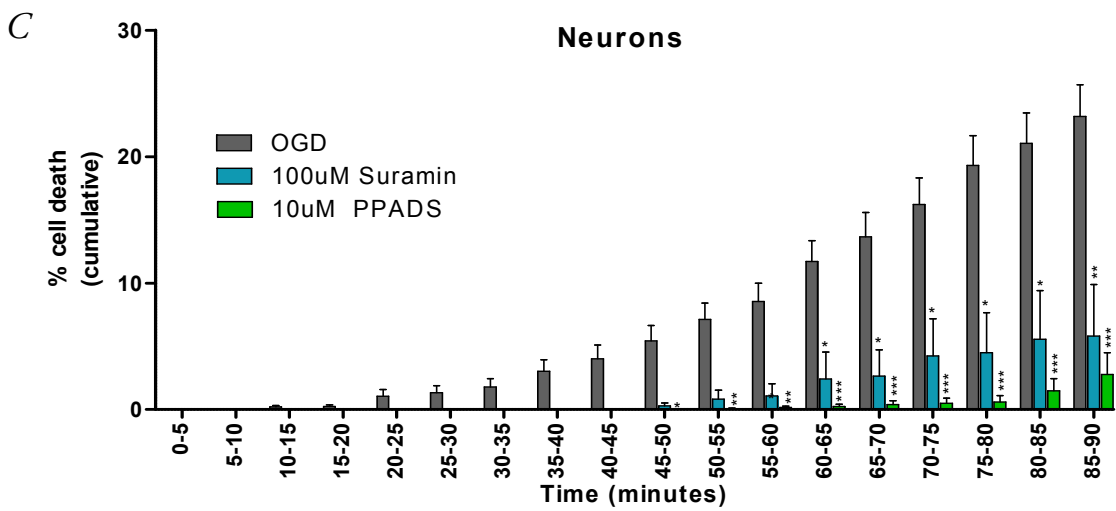
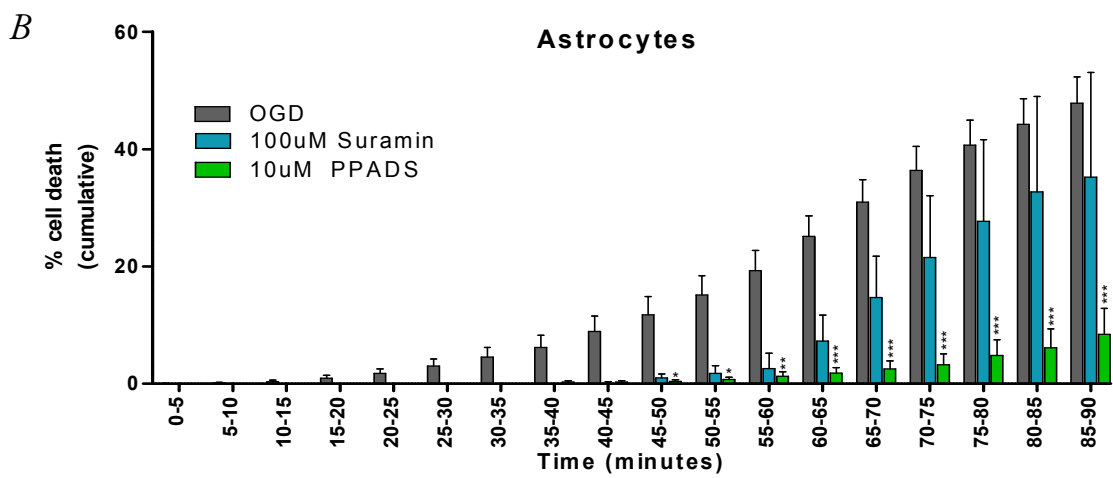
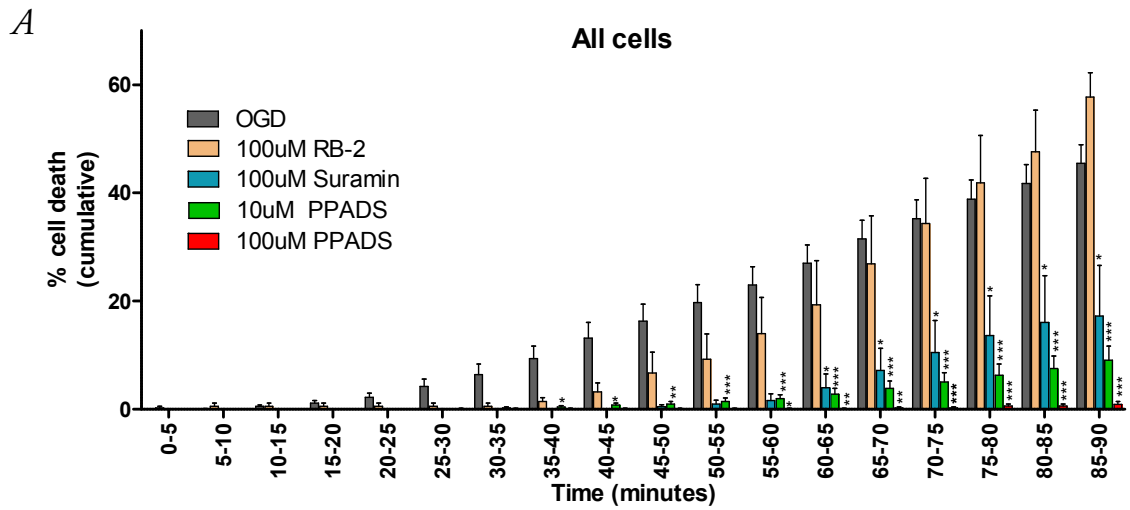


Figure 5-32: Non-selective P2 receptor antagonists during OGD in co-culture, timescale of cell death

A: Frequency histogram of cell death of all cells

All non-selective P2 receptor antagonists delayed the onset of cell death during OGD, with all except RB-2 also reducing overall death rates.

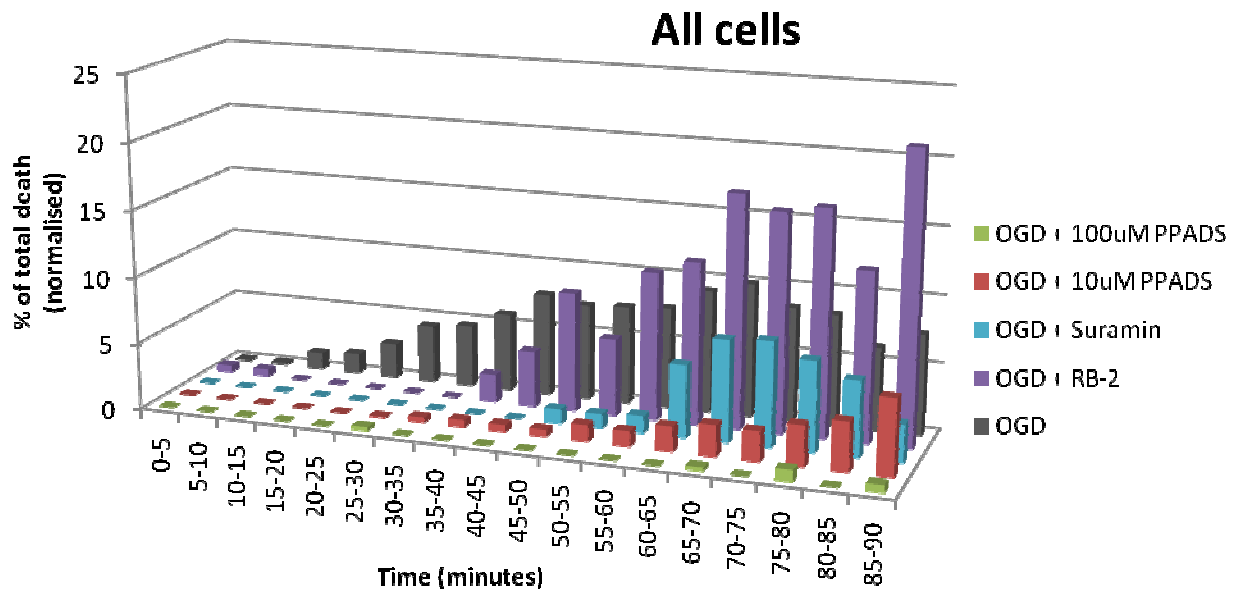
B: Frequency histogram of astrocyte death

Both suramin and 10uM PPADS delayed the onset of astrocyte death, but only PPADS reduced death rates during all 90 minutes of OGD.

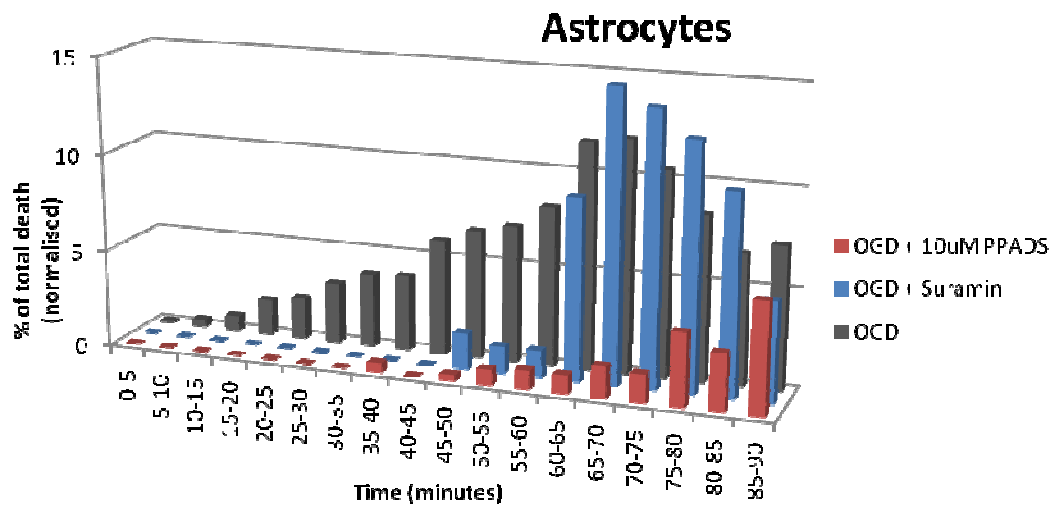
C: Frequency histogram of neuronal death

Both suramin and 10uM PPADS delayed the onset of neuronal death.

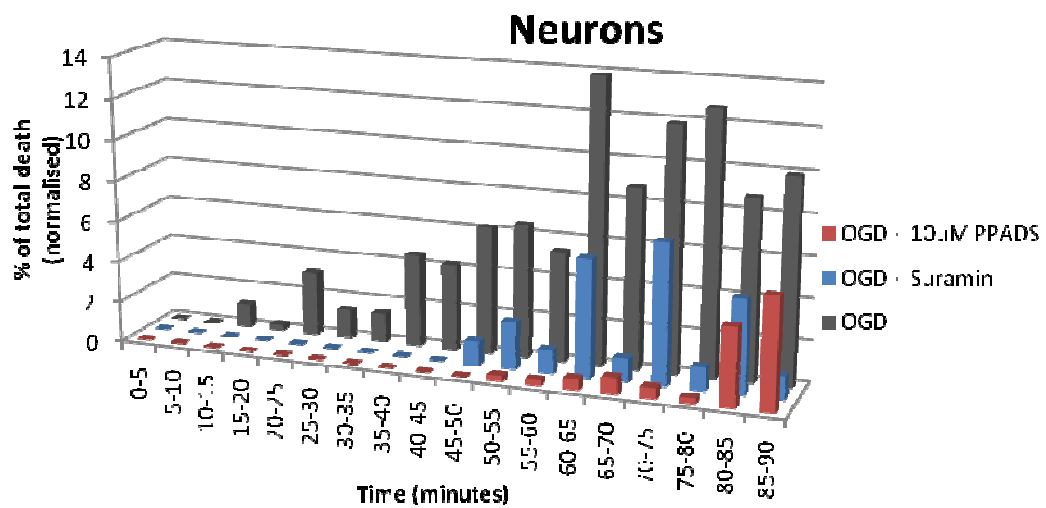
A



B



C



Effects of P2Y₁ and P2X₇ receptor antagonists

Having established that non-selective P2 receptor antagonists can reduce cell death during OGD I made use of two selective P2 receptor antagonists which were available at the time: the P2Y₁ receptor antagonist MRS-2179 (10 μ M) and the P2X₇ receptor antagonist KN-62 (1 μ M). MRS-2179 significantly reduced cell death of all cells combined ($15.45 \pm 6.27\%$, n:8, $p < 0.001$), astrocytes ($16.98 \pm 9.58\%$, n:5, $p < 0.01$) and neurons ($3.51 \pm 2.31\%$, n:5, $p < 0.01$), whilst KN-62 did not significantly reduce cell death ($32.28 \pm 3.6\%$, n:7 for all cells; $44.22 \pm 3.52\%$, n:5 for astrocytes; $12.92 \pm 3.75\%$, n:5 for neurons) (**Figure 5-33: A**). MRS-2179 significantly reduced overall cell death for the first time after 65 minutes compared to OGD, with the difference becoming more significant with time, whilst KN-62 did not reduce overall cell death at any time point (**Figure 5-34: A**). MRS-2179 significantly reduced astrocyte death after 85 minutes and neuronal death after 65 minutes, with KN-62 significantly attenuating neuronal death transiently after 75 and 80 minutes but never significantly reducing astrocyte death (**Figure 5-34: B, C**).

Despite not reducing overall cell death, KN-62 significantly increased the mean time to cell death for all cells combined (70.51 ± 0.92 minutes, n:408, $p < 0.001$), astrocytes (74.75 ± 0.96 minutes, n:241, $p < 0.001$) and neurons (75.87 ± 1.77 minutes, n:63, $p < 0.001$), whilst MRS-2179 was only able to do so when all cells were combined (65.26 ± 1.34 minutes, n:174, $p < 0.001$) (**Figure 5-33: B**). The values with MRS-2179 for astrocytes were 62.07 ± 1.74 minutes (n:111) and for neurons 62.86 ± 9.12 minutes (n:7) (**Figure 5-33: B**). In terms of the onset of cell death, KN-62 significantly delayed the average time to first cell death of neurons during OGD (64 ± 6.99 minutes, n:5, $p < 0.05$); there were no other significant differences with KN-62 or MRS-2179 (**Figure 5-33: C**). The values of average time to first cell death for MRS-2179 were 44.17 ± 4.67 minutes (n:8) for all cells, 46.67 ± 6.69 minutes (n:5) for astrocytes and 47.5 ± 11.25 minutes (n:5) for neurons, whilst for KN-62 they were 35 ± 9.94 minutes (n:7) for all cells combined and 48 ± 8.19 minutes (n:5) for astrocytes (**Figure 5-33: C**). Looking at the frequency histograms of cell death, MRS-2179 uniformly reduced the overall rate without really changing the timing of cell death, with onset and peak rates of cell death occurring at

roughly the same time compared to OGD (**Figure 5-35: A**). KN-62 produced reduced death rates until 80 minutes, with the rates increasing compared to OGD in the 85 and 90 minute periods (**Figure 5-35: A**). The frequency histograms of astrocyte death are very similar to those seen for all cells combined (**Figure 5-35: B**), whilst those of neurons demonstrate that KN-62 delayed the onset of neuronal death until the 40th minute, reaching a peak rate after 85 minutes, and MRS-2179 had an overall reduction in neuronal death although the time points of death were spread out evenly (**Figure 5-35: C**).

Figure 5-33: Effects of P2X₇ and P2Y₁ receptor blockade on OGD induced cell death in co-cultures

The P2X₇ receptor antagonist KN-62 and the P2Y₁ receptor antagonist MRS-2179 were added to co-cultures during OGD.

A: Total cell death

MRS-2179 significantly reduced cell death of all cells combined ($p < 0.001$), astrocytes and neurons ($p < 0.01$ for both), whilst KN-62 also reduced cell death but this did not reach statistical significance.

B: Mean time to cell death

KN-62 significantly increased the mean time to cell death for all cells, neurons and astrocytes ($p < 0.001$), whilst MRS-2179 was only able to do so when all cells were combined ($p < 0.001$).

C: Average time to first cell death

KN-62 significantly delayed the onset of neuronal death during OGD ($p < 0.05$).

*: $p < 0.05$

** : $p < 0.01$

***: $p < 0.001$

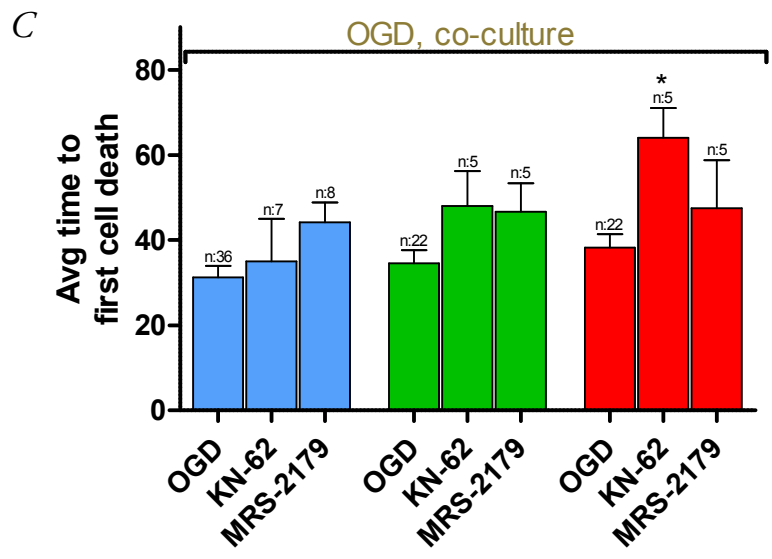
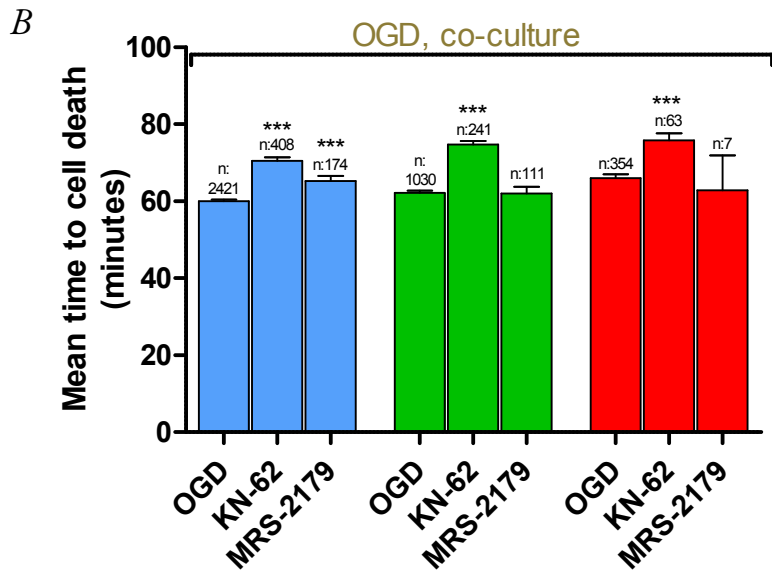
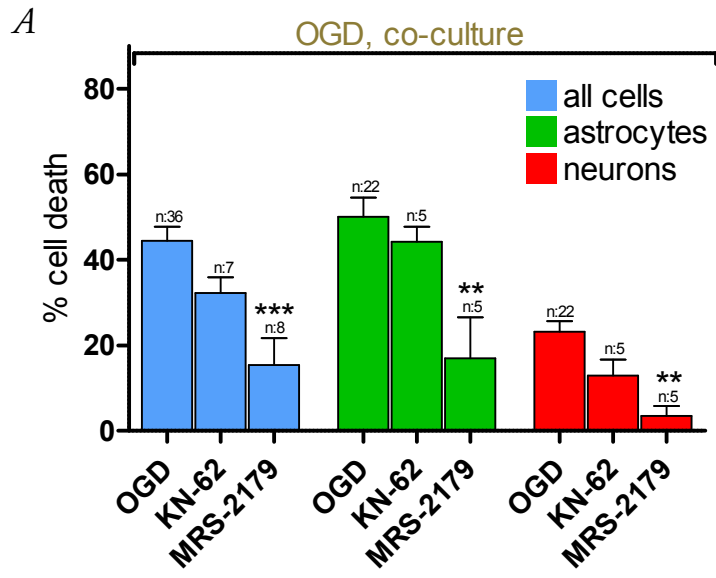


Figure 5-34: Effects of P2X₇ and P2Y₁ receptor blockade on OGD in co-cultures, cumulative timescale of cell death

Note the different scales on the y-axis for graphs **A-C**.

A: Timescale of death, all cell types

MRS-2179 significantly reduced overall cell death for the first time after 65 minutes compared to OGD, with the difference becoming more significant with time. KN-62 had no significant effects.

B: Timescale of astrocyte death

MRS-2179 significantly reduced astrocyte death after 85 and 90 minutes compared to OGD. KN-62 had no significant effects.

C: Timescale of neuronal death

OGD induced neuronal death was significantly attenuated after 65 minutes by MRS-2179, with the difference becoming more significant with time. KN-62 also significantly decreased neuronal death transiently after 75 and 80 minutes.

D,E,F: Linear versions of graphs **A-C**, with error bars removed and uniform y-axis scales for easier comparisons.

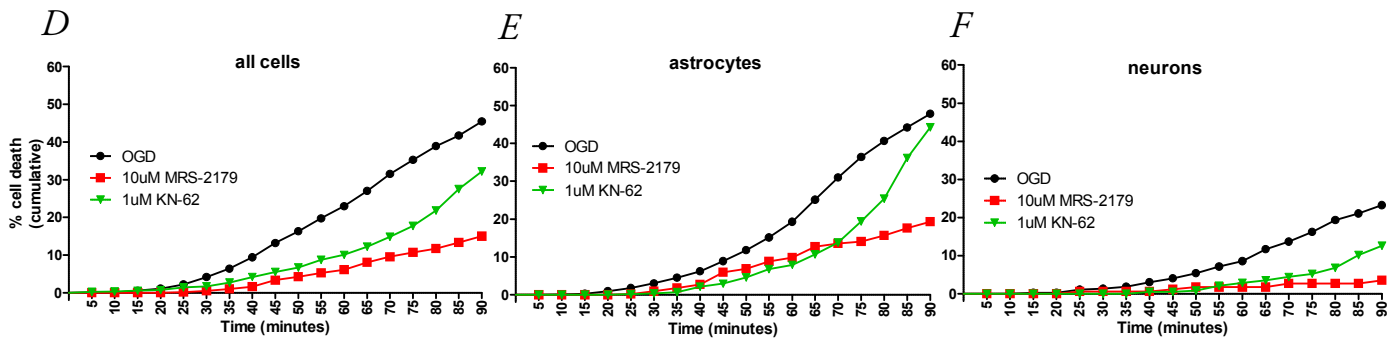
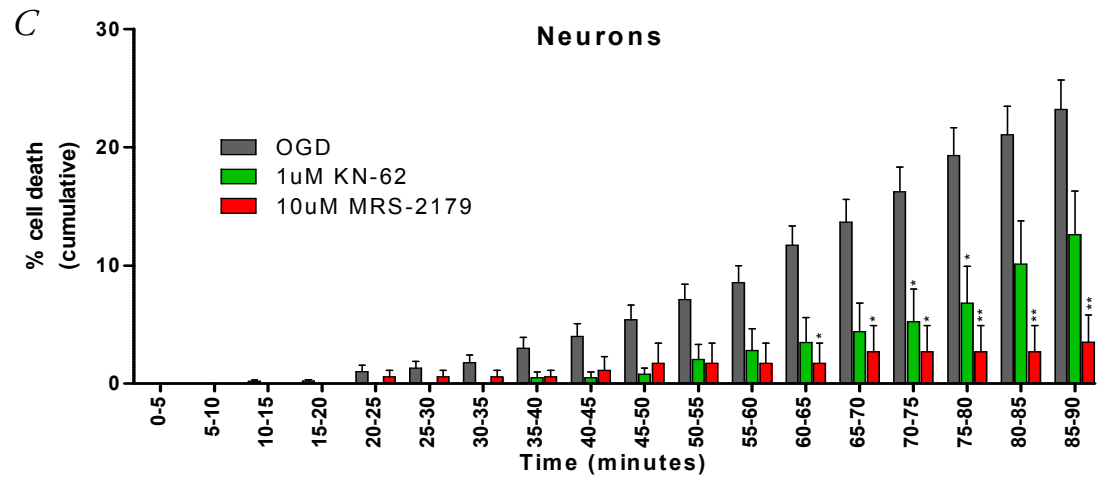
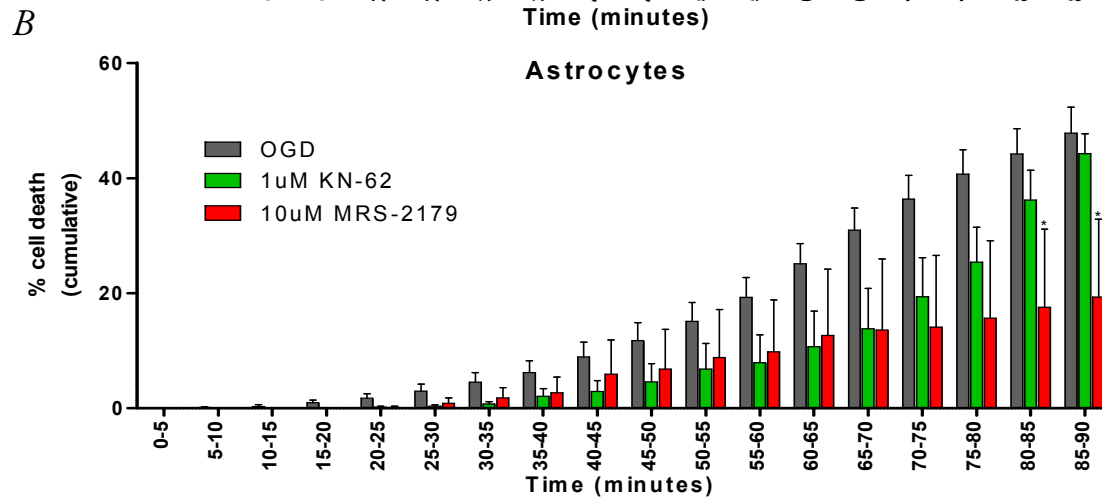
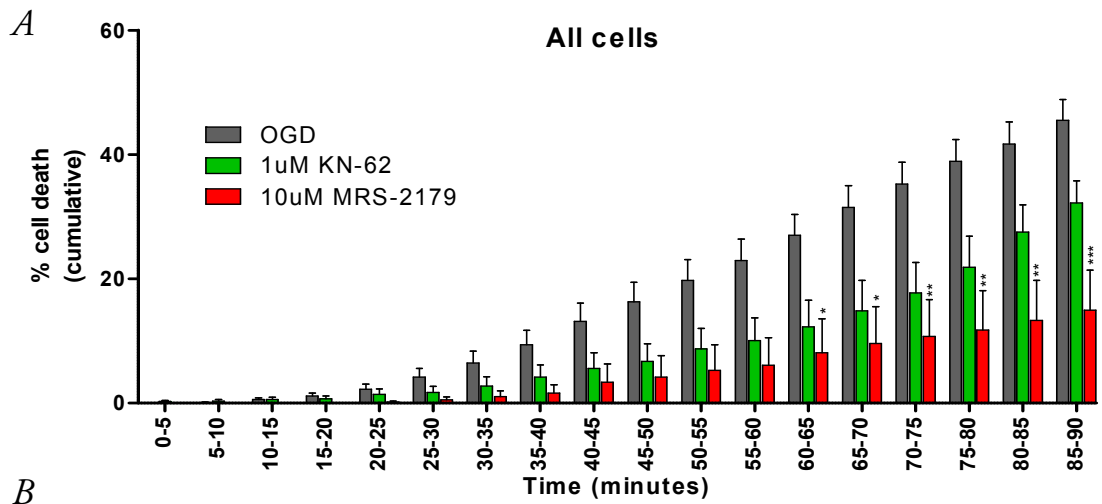


Figure 5-35: Effects of P2X₇ and P2Y₁ receptor blockade on OGD in co-cultures, timescale of cell death

A: Frequency histogram of cell death of all cells

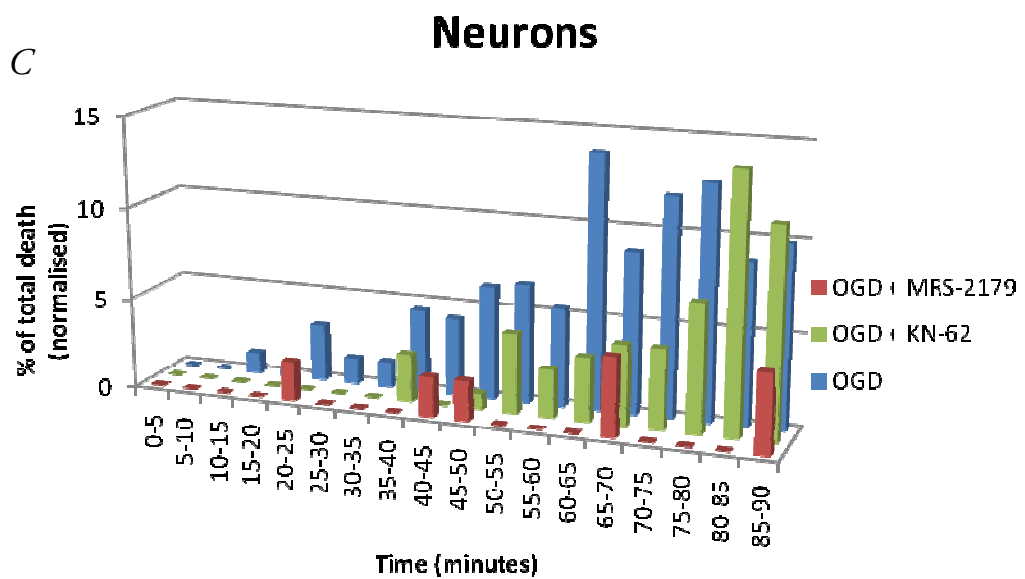
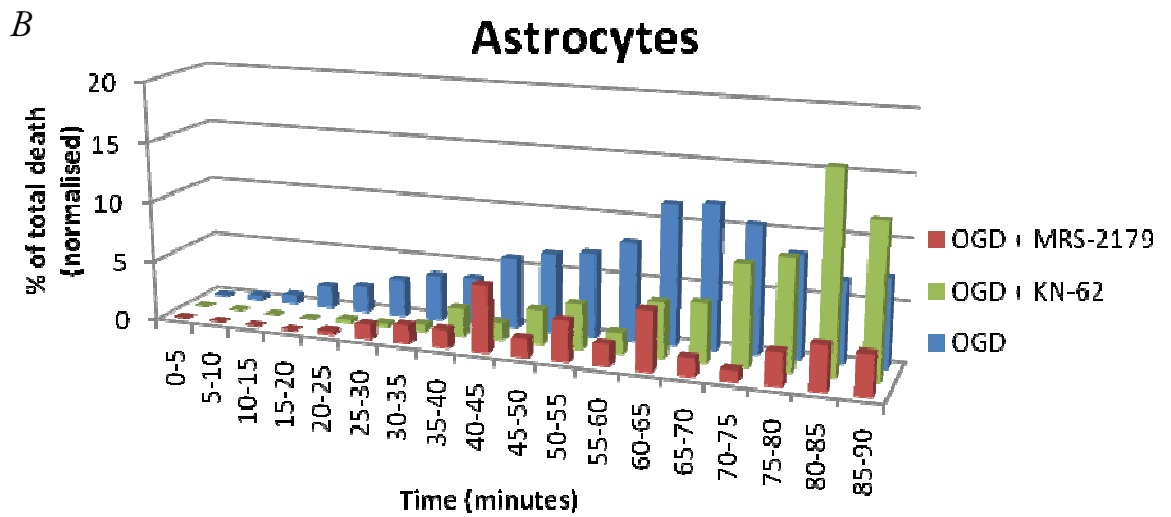
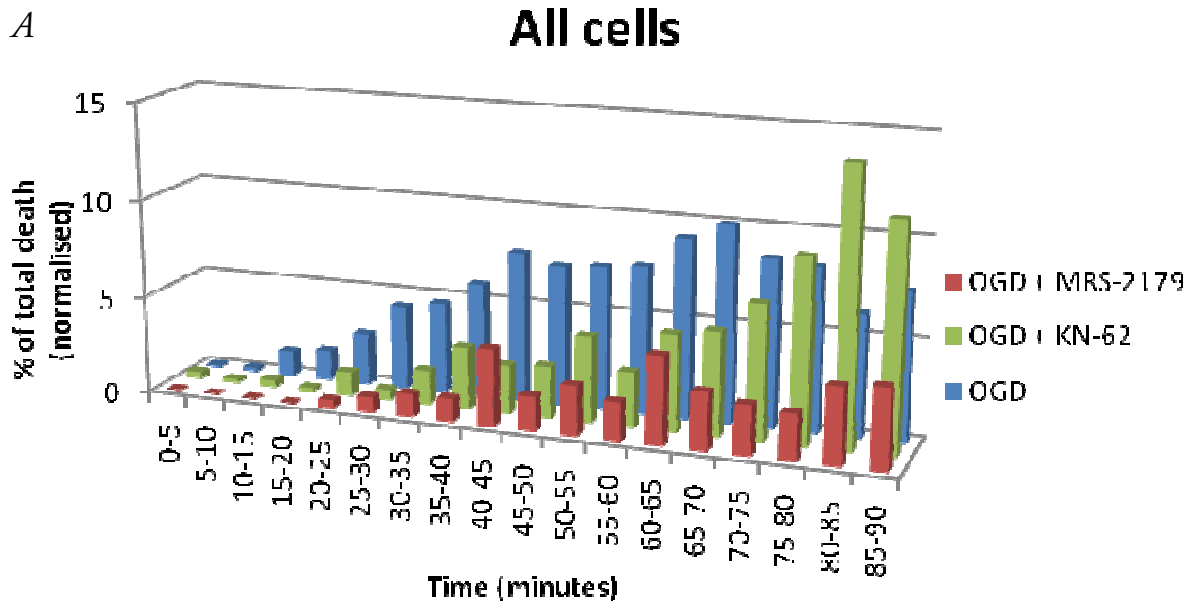
MRS-2179 reduced the overall rate of cell death without really changing the profile, with peak rates at the same time as during OGD. KN-62 had reduced death rates until 80 minutes, reaching a peak rate of death at 85 minutes.

B: Frequency histogram of astrocyte death

The profiles of astrocyte death are very similar to those seen for all cells combined.

C: Frequency histogram of neuronal death

KN-62 delayed the onset of neuronal death until the 40th minute, reaching a peak rate after 85. MRS-2179 had a great overall reduction in neuronal death although the timepoints of death were spread out evenly.



Effects of glutamate receptor antagonists

The contribution of NMDA and AMPA/kainate receptors to OGD-induced cell death was investigated using the non-competitive NMDA receptor antagonist MK-801 (10uM) and the competitive AMPA/kainate receptor antagonist NBQX (30uM). Antagonists were applied separately or in combination during OGD. Death of all cells combined was significantly reduced with NBQX ($15.02 \pm 2.23\%$, n:4, $p < 0.05$) and NBQX + MK-801 ($26.79 \pm 5.12\%$, n:12, $p < 0.05$) with neuronal death rates being significantly reduced by MK-801 ($10.34 \pm 1.29\%$, n:5, $p < 0.05$), NBQX ($6.95 \pm 1.57\%$, n:4, $p < 0.05$) and NBQX + MK-801 ($6.47 \pm 1.62\%$, n:8, $p < 0.001$) (**Figure 5-36: A**). Astrocyte death was not significantly reduced by NBQX ($20.31 \pm 4.33\%$, n:4), MK-801 ($37.03 \pm 10.03\%$, n:5) or the combination of NBQX + MK-801 ($56.16 \pm 8.58\%$, n:8) (**Figure 5-36: A**). Looking at the cumulative timescale of cell death, NBQX significantly reduced overall cell death from 75 minutes onwards, while MK-801 or the combination of MK-801 + NBQX did not (**Figure 5-37: A**). None of the glutamate receptor antagonists conferred significant protection against astrocyte death at any point, despite the reduction with NBQX (**Figure 5-37: B**). All of the glutamate receptor antagonists significantly reduced neuronal death, with MK-801 being protective after 90, NBQX after 65 minutes and the combination of both after 50 minutes (**Figure 5-37: C**).

The mean time to cell death of all cells combined was significantly increased by MK-801 (63.03 ± 1.31 minutes, n:234, $p < 0.05$), NBQX (75.31 ± 1.44 minutes, n:113, $p < 0.001$) and NBQX + MK-801 (70.1 ± 0.61 minutes, n:522, $p < 0.001$), while NBQX and NBQX + MK-801 significantly increased the mean time to cell death for astrocytes (75.52 ± 1.6 minutes, n:87; 69.04 ± 0.66 minutes, n:451 respectively, $p < 0.001$ for both) and neurons (79.21 ± 2.49 minutes, n:19, $p < 0.01$; 78.29 ± 1.73 minutes, n:38, $p < 0.001$ respectively) (**Figure 5-36: B**). The mean time to cell death for astrocytes and neurons was not significantly affected by MK-801 alone (63.15 ± 1.42 minutes, n:189; 62.96 ± 3.6 minutes, n:27 respectively) (**Figure 5-36: B**).

The average time to first cell death of neurons was significantly delayed by both NBQX (67.5 ± 8.78 minutes, $n:4$, $p<0.01$) and the combination of NBQX + MK-801 (69.29 ± 3.11 minutes, $n:8$, $p<0.001$), suggesting that this effect is mediated by AMPA/kainate receptors (**Figure 5-36: C**). The average time to first cell death of astrocytes or all cells combined was not affected by the glutamate receptor antagonists (**Figure 5-36: C**). The values for all cells/astrocytes are: 42.5 ± 11.27 minutes, $n:4/48.75 \pm 5.54$ minutes, $n:4$ for NBQX, 19 ± 4.58 minutes, $n:5/29 \pm 4.85$ minutes, $n:5$ for MK-801 and 43.89 ± 5.12 minutes, $n:12/42.5 \pm 5.27$ minutes, $n:8$ for NBQX + MK-801. The frequency histograms of cell death of all cells combined (**Figure 5-38: A**) reveal that NBQX and NBQX + MK-801 delay the onset of cell death, while MK-801 alone reduces the amount of death up to 50 minutes without delaying its onset. The greatest overall reduction in death rates is apparent with NBQX alone. The histograms of astrocyte death (**Figure 5-38: B**) are very similar to those seen for all cells combined, and they only differ from OGD alone by the delay in onset seen with NBQX and NBQX + MK-801. Looking at the histograms of neuronal death (**Figure 5-38: C**), NBQX + MK-801 caused a marked delay in the onset of neuronal death by around 50 minutes compared to OGD alone, with overall death rates being lower with all antagonists.

Figure 5-36: Effects of NMDA and AMPA/Kainate receptor antagonists on OGD induced cell death in co-cultures

The NMDA receptor antagonist MK-801 and/or AMPA/Kainate receptor antagonist NBQX were added to co-cultures during OGD.

A: Total cell death, co-culture

NBQX and NBQX + MK-801 reduced overall cell death ($p < 0.05$), with MK-801, NBQX ($p < 0.05$ for both) and NBQX + MK-801 ($p < 0.001$) significantly reducing neuronal death. None of the antagonists significantly reduced astrocyte death.

B: Mean time to cell death

MK-801 ($p < 0.05$), NBQX and NBQX + MK-801 ($p < 0.001$ for both) significantly increased the mean time to overall cell death, while NBQX and NBQX + MK-801 significantly increased the mean time to cell death for astrocytes ($p < 0.001$ for both) and neurons ($p < 0.01/p < 0.001$).

C: Average time to first cell death

Both NBQX ($p < 0.01$) and the combination of NBQX + MK-801 ($p < 0.001$) significantly delayed the onset of first cell death of neurons. The time to first cell death of astrocytes was not affected by glutamate receptor antagonists.

*: $p < 0.05$

** : $p < 0.01$

***: $p < 0.001$

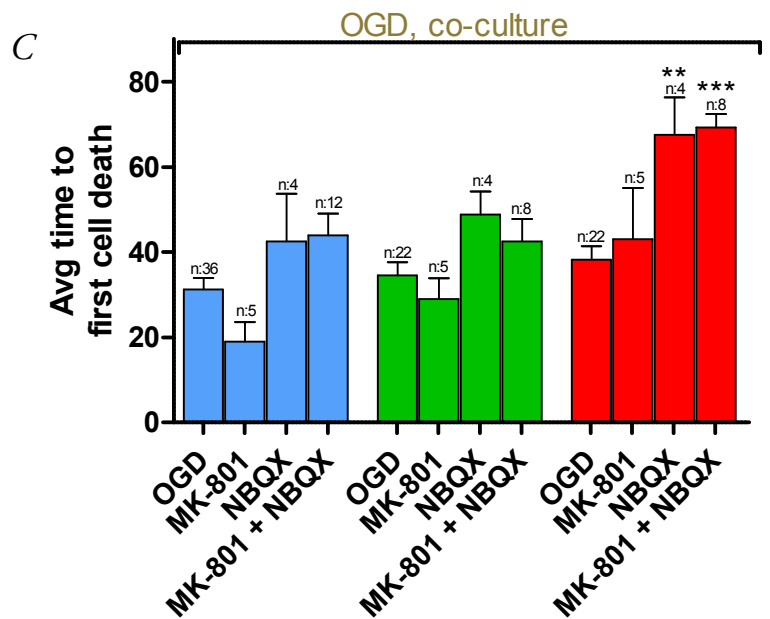
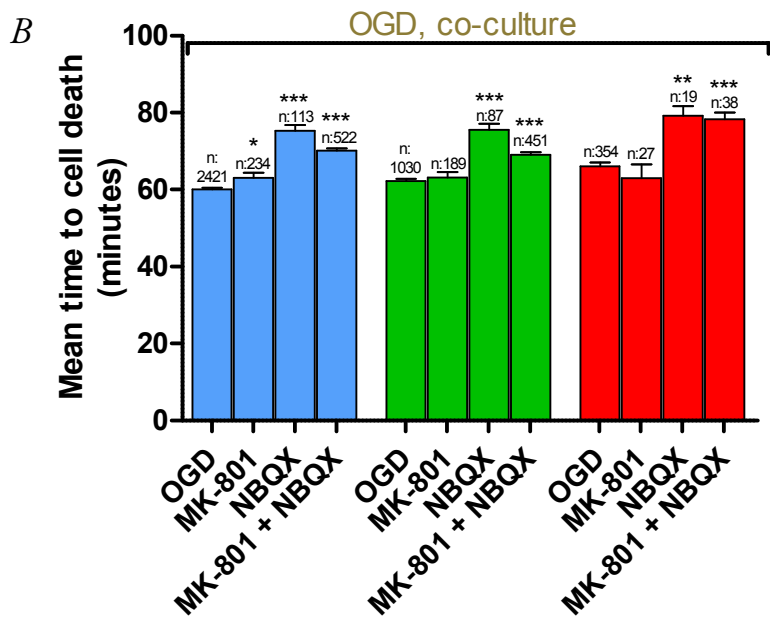
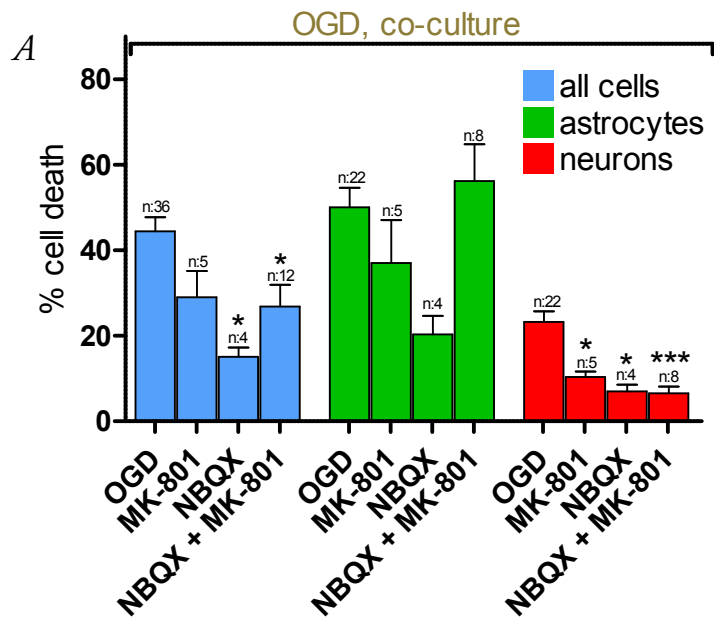


Figure 5-37: Effects of NMDA and AMPA/Kainate receptor antagonists on OGD in co-cultures, cumulative timescale of cell death

Note the different scales on the y-axis for graphs **A-C**.

A: Timescale of death, all cell types

NBQX significantly reduced overall cell death from 75 minutes onwards, while MK-801 or the combination of MK-801 + NBQX did not.

B: Timescale of astrocyte death

None of the glutamate receptor antagonists conferred significant protection to astrocytes at any point, despite the apparent reduction with NBQX.

C: Timescale of neuronal death

All of the glutamate receptor antagonists significantly reduced neuronal death, with MK-801 being protective after 90, NBQX after 65 minutes and the combination of both after 50 minutes compared to OGD.

D,E,F: Linear versions of graphs **A-C**, with error bars removed and uniform y-axis scales for easier comparisons.

*: $p < 0.05$

** : $p < 0.01$

***: $p < 0.001$

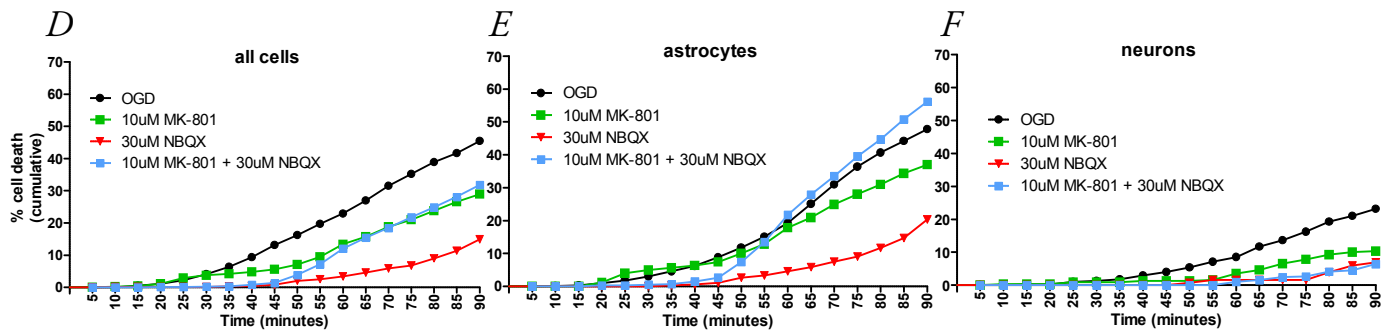
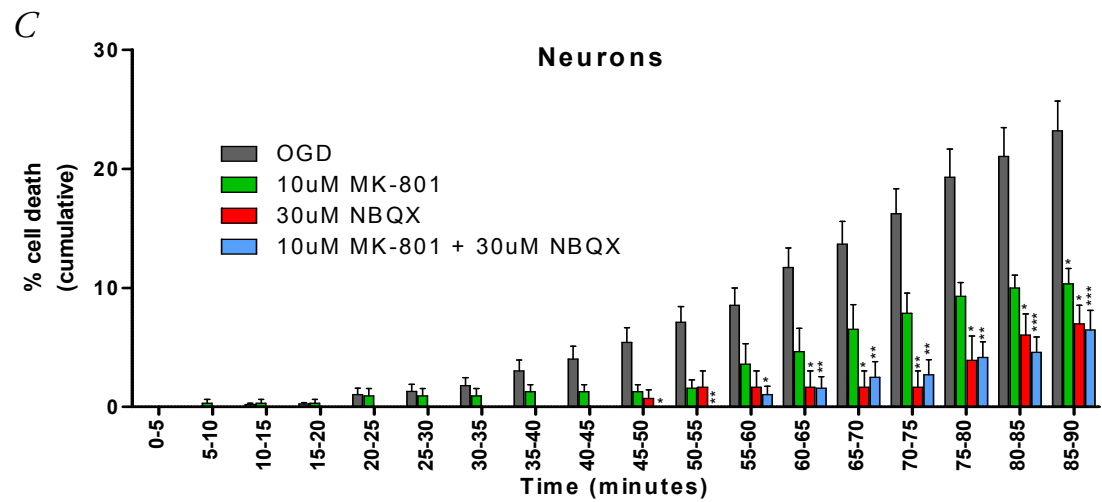
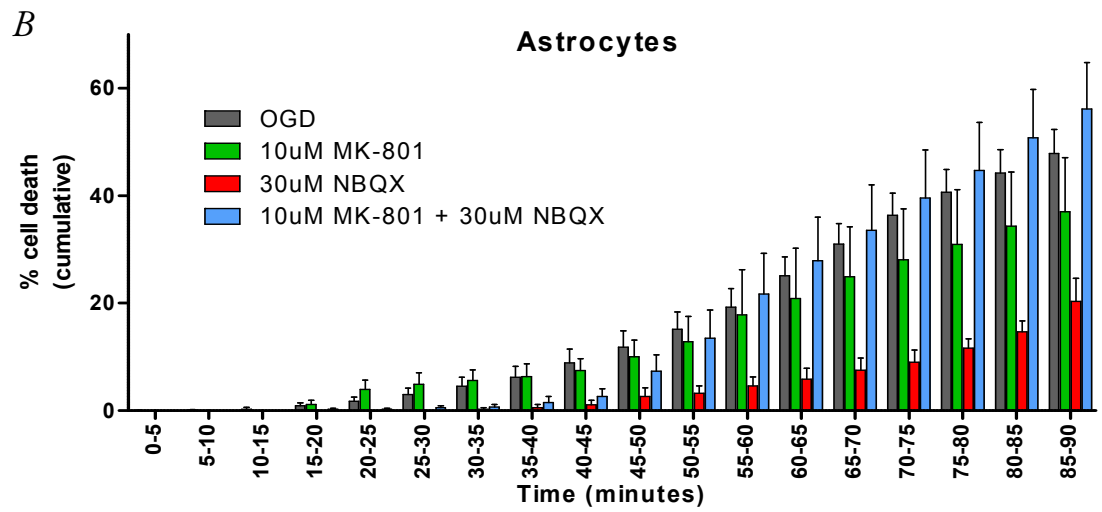
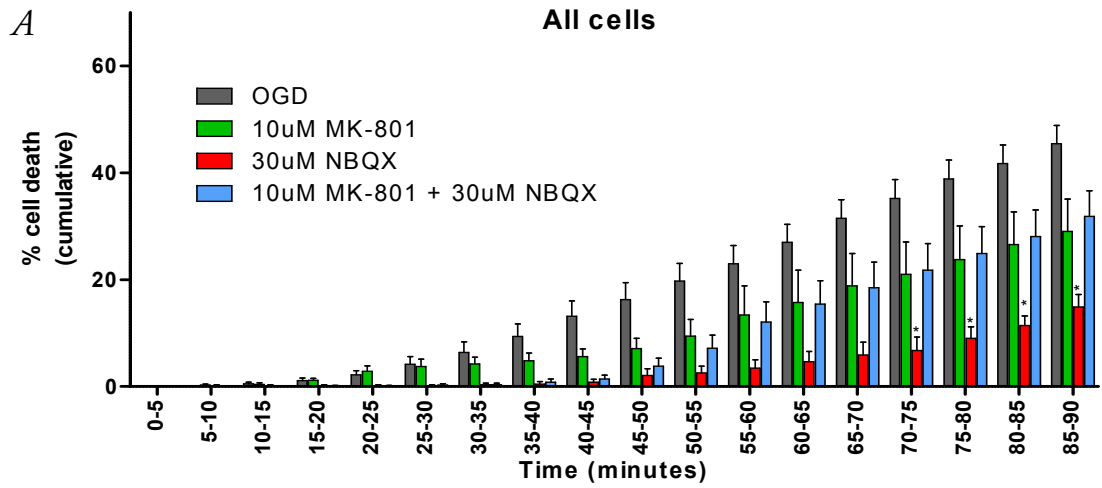


Figure 5-38: Effects of NMDA and AMPA/Kainate receptor antagonists on OGD in co-cultures, timescale of cell death

A: Frequency histogram of cell death, all cells combined

NBQX and NBQX + MK-801 seem to delay the onset of cell death, while MK-801 alone reduces the amount of death up to 50 minutes without delaying its onset. The greatest overall reduction in death rates is apparent with NBQX alone.

B: Frequency histogram of astrocyte death

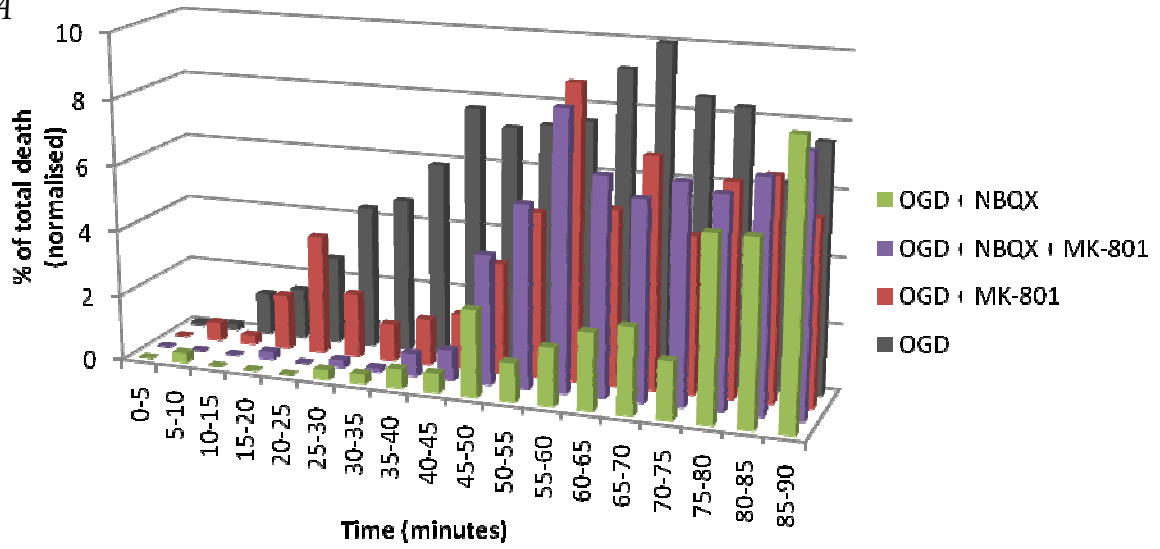
The profiles of astrocyte death are very similar to those seen for all cells combined, and they only differ from OGD alone by the delay in onset seen with NBQX and NBQX + MK-801.

C: Frequency histogram of neuronal death

The combination of NBQX + MK-801 caused a marked delay in the onset of neuronal death by around 50 minutes compared to OGD alone. Overall rates are also lower with all antagonists.

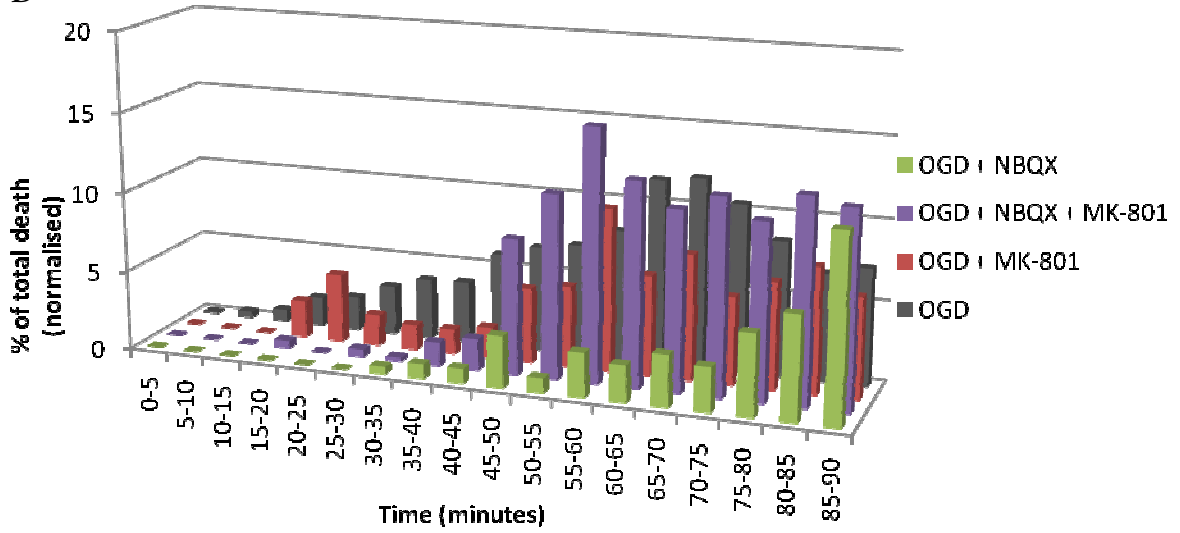
All cells

A



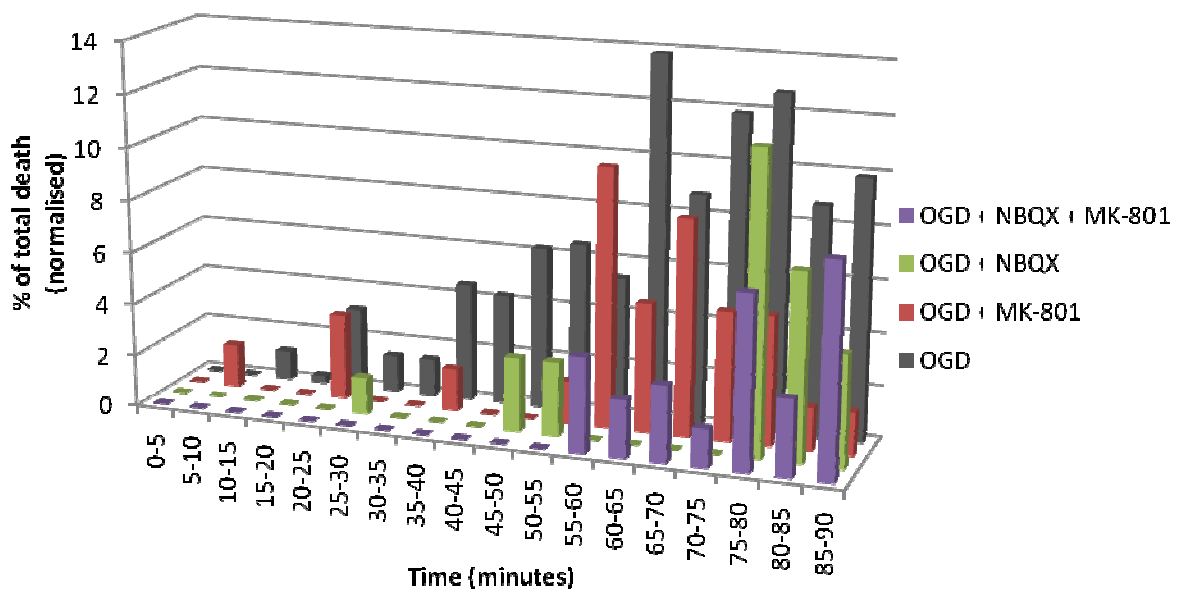
Astrocytes

B



Neurons

C



Combining P2 and glutamate receptor antagonists

Having demonstrated protective effects of both P2 and glutamate receptor antagonists during OGD, the next obvious question was whether combining them would give even more enhanced protection. A combination of 100uM suramin + 10uM MK-801 and 30uM NBQX was first used to test the protective effect of blocking P2 and ionotropic glutamate receptors in unison, and this proved highly protective, with no cell death at all (n:3, 149 cells, $p < 0.001$) (**Figure 5-39: A**). Despite not doing a cell-type analysis in this experiment, this combination of drugs was obviously significantly protective of both neurons and astrocytes in co-culture. To test whether the protective effect of blocking P2 and glutamate receptors during OGD was synergistic, the concentrations of antagonists was reduced, using a cocktail of 1uM PPADS (preferred due to less non-selective effects than suramin) + 1uM MK-801 + 3uM NBQX (combination referred to as 1P1M3N). This was highly protective, with $4.98 \pm 2.93\%$ cell death of all cell types, $8.47 \pm 5\%$ astrocyte death and only $1.05 \pm 0.93\%$ neuronal death (n:8, $p < 0.001$ for all) (**Figure 5-39: A**), with death of all cell types and neurons first becoming significantly reduced after 45 minutes and of astrocytes after 50 minutes (**Figure 5-40**). The combination of 1P1M3N also significantly increased the mean time to cell death for all cells combined (82.16 ± 0.98 minutes, n:58, $p < 0.001$), astrocytes (81.89 ± 1.02 minutes, n:53, $p < 0.001$) and neurons (85 ± 3.87 minutes, n:5, $p < 0.05$) (**Figure 5-39: B**). The same significant effect was produced in terms of delaying the average time to first cell death (n:8 for all) for all cells combined (77 ± 4.07 minutes, $p < 0.001$), astrocytes (77 ± 4.07 minutes, $p < 0.001$) and neurons (77.5 ± 3.75 minutes, $p < 0.001$) (**Figure 5-39: C**). This highly protective effect is further evident in the frequency histograms of cell death, with 1P1M3N significantly delaying and reducing all types of cell death during OGD in co-cultures, with the effect most striking in terms of the reduction in neuronal death (**Figure 5-41**). These results suggest a synergistic protective effect of simultaneously blocking P2, NMDA and AMPA/kainate receptors.

Figure 5-39: Effects of combining P2 and glutamate receptor antagonists on OGD induced cell death in co-cultures

A combination of 100uM suramin + 10uM MK-801 and 30uM NBQX was first used to test the protective effect of blocking P2 and ionotropic glutamate receptors in unison. Then, to test whether this protection was a synergistic effect, the concentrations of antagonists were reduced, giving a cocktail of 1uM PPADS (preferred due to less non-selective effects than suramin) + 1uM MK-801 + 3uM NBQX.

1P 1M 3N= 1uM PPADS + 1uM MK-801 + 3uM NBQX

100S 10M 30N= 100uM Suramin + 10uM MK-801 + 30uM NBQX

It was not possible to calculate mean time to cell death or average time to first cell death for the experiment using 100S 10M 30N as there was no cell death.

Even though cell identification was not performed on the experiment using Suramin + NBQX + MK-801 there was no cell death, so both astrocytes and neurons were comprehensively protected.

A: Total cell death, co-culture

All combinations of P2 and glutamate receptor antagonists were significantly protective of all cell types ($p < 0.001$).

B: Mean time to cell death

The combination of 1P 1M 3N significantly increased the mean time to cell death during OGD for all cells combined, astrocytes ($p < 0.001$ for both) and neurons ($p < 0.05$).

C: Average time to first cell death

The combination of 1P 1M 3N significantly increased the average time to first cell death during OGD for all cell types ($p < 0.001$).

*: $p < 0.05$

***: $p < 0.001$

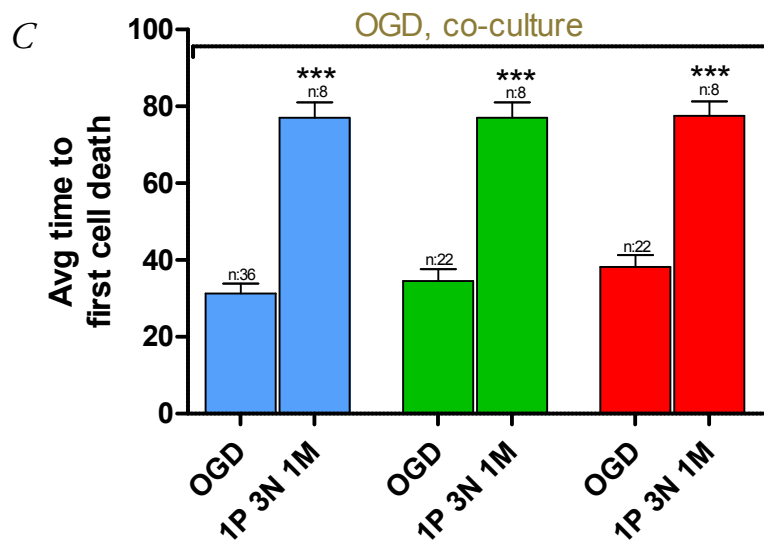
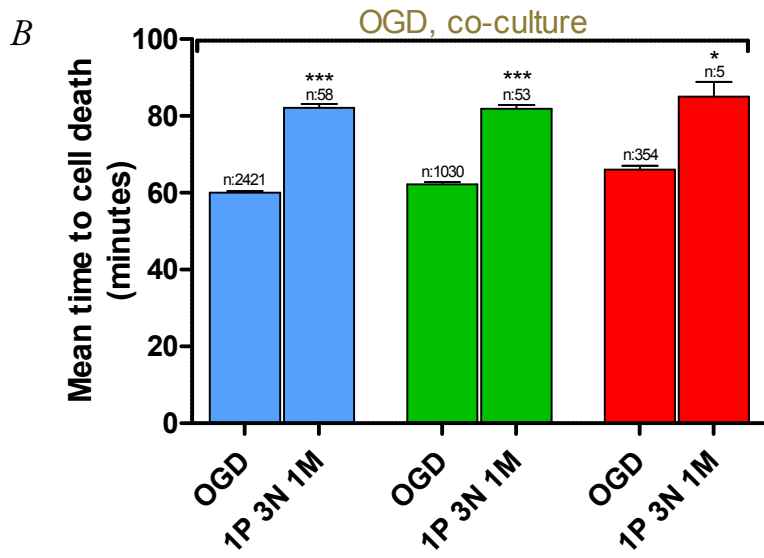
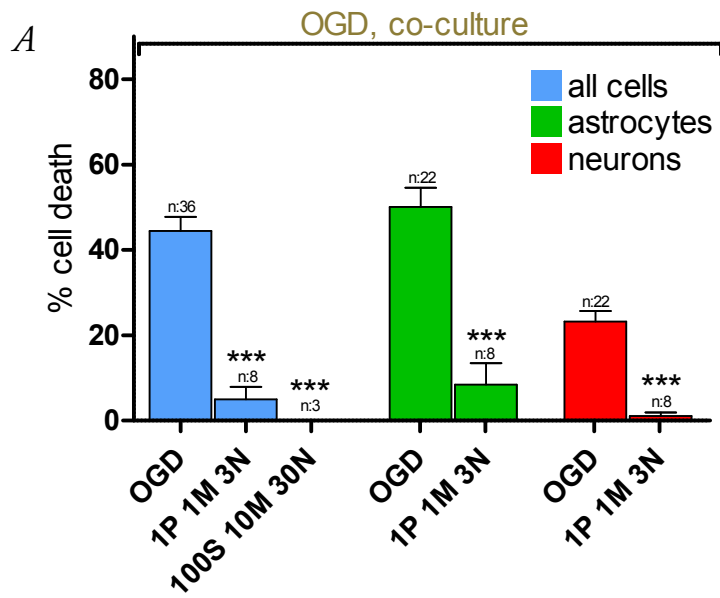


Figure 5-40: Effects of combining P2 and glutamate receptor antagonists during OGD in co-cultures, cumulative timescale of cell death

Note the different scales on the y-axis for graphs *A-C*.

A: Timescale of death, all cell types

B: Timescale of astrocyte death

C: Timescale of neuronal death

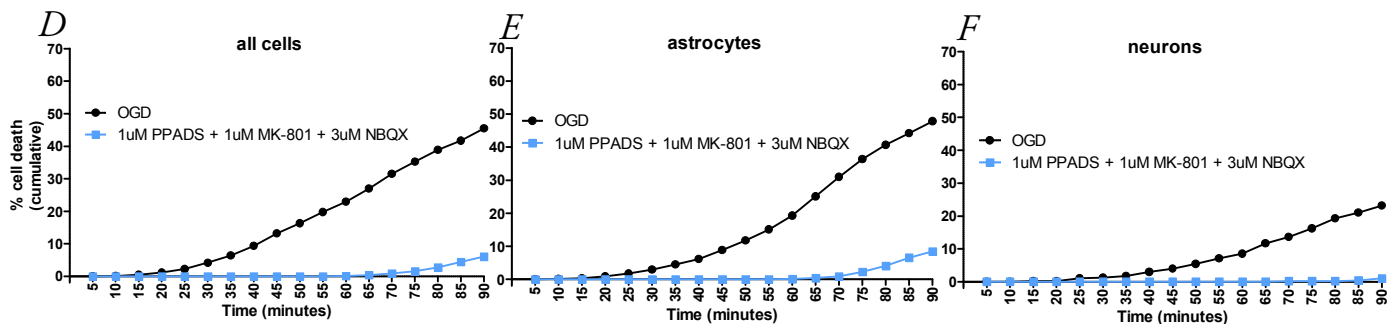
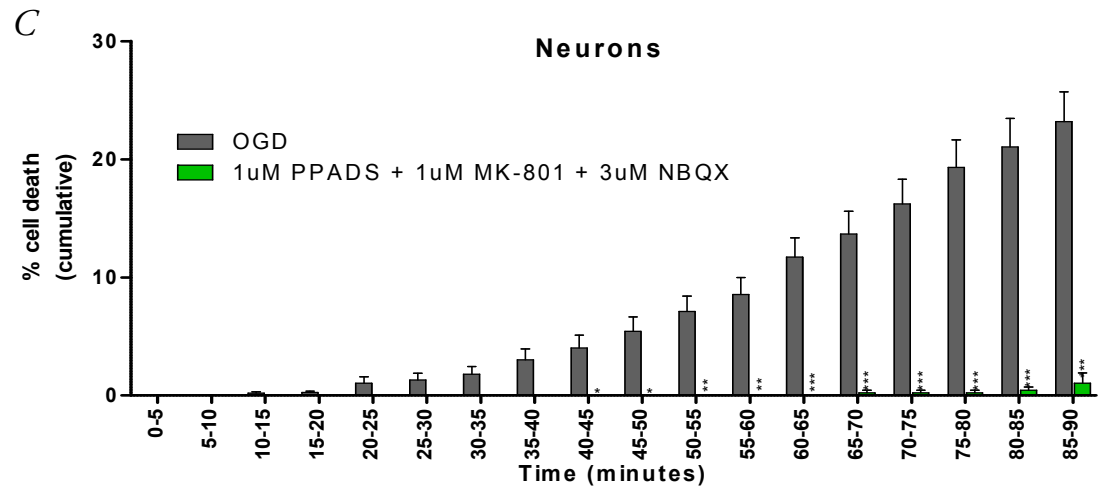
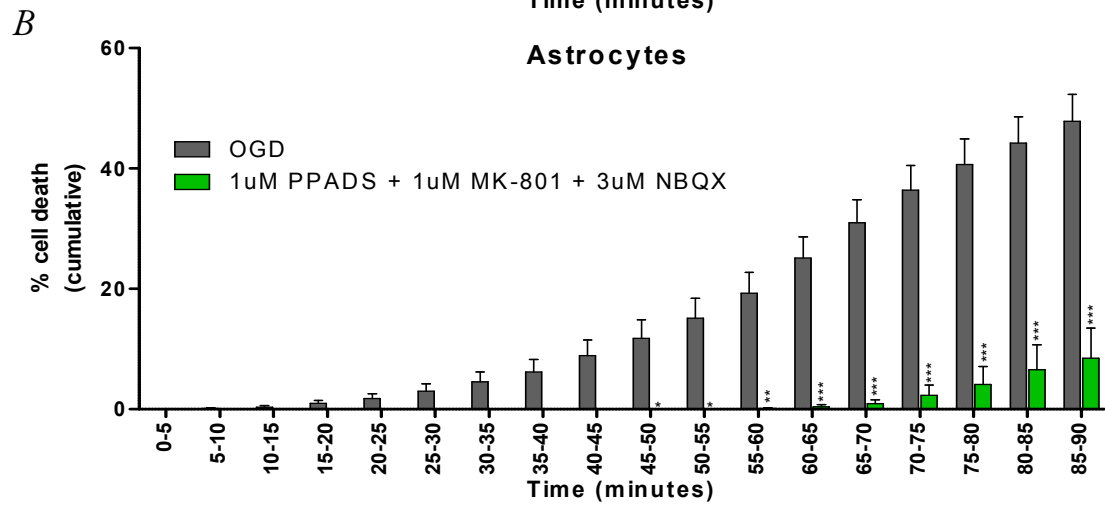
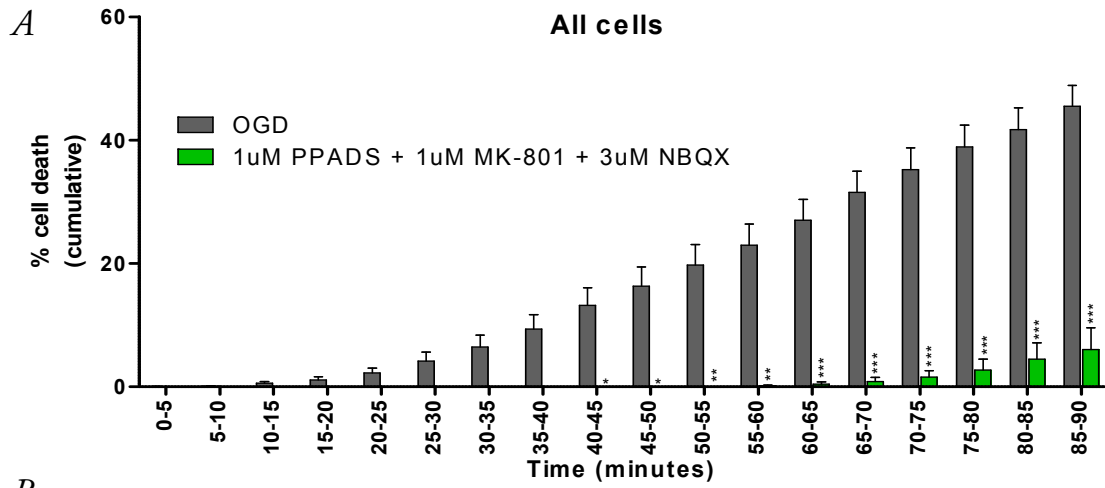
1uM PPADS + 1uM MK-801 + 3uM NBQX significantly reduced overall cell death and neuronal death during OGD after 45 minutes and astrocyte death after 50 minutes, with the protective effect becoming progressively more significant over time.

D,E,F: Linear versions of graphs *A-C*, with error bars removed and uniform y-axis scales for easier comparisons.

*: $p < 0.05$

** : $p < 0.01$

***: $p < 0.001$



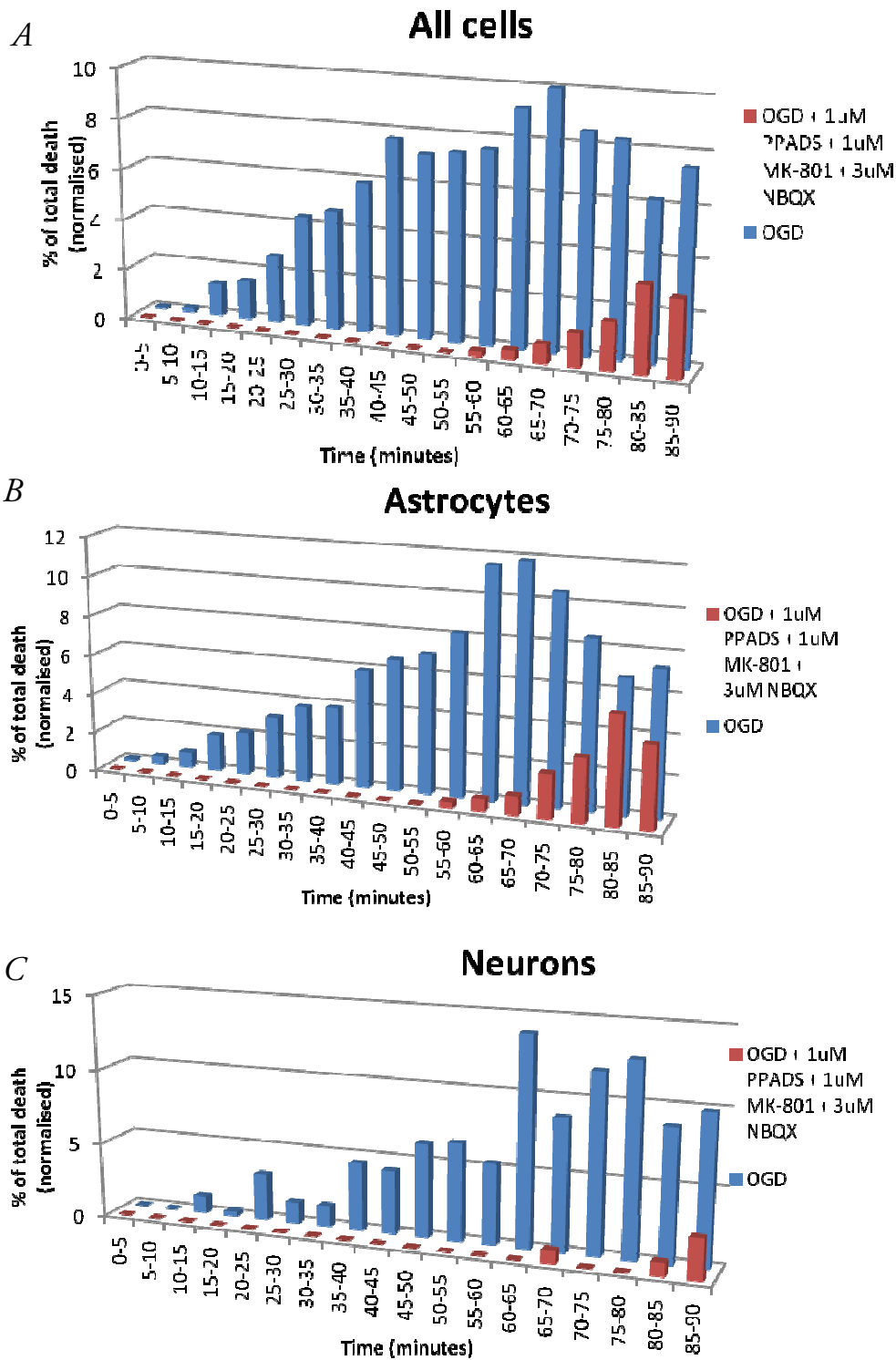


Figure 5-41: Effects of combining P2 and glutamate receptor antagonists during OGD in co-cultures, timescale of cell death

A, B, C: Frequency histogram of cell death of all cells (*A*), astrocytes (*B*) and neurons (*C*)

All three frequency histograms demonstrate that the combination of PPADS + MK-801 + NBQX, even at a reduced concentration, significantly delayed and reduced all types of cell death during OGD in co-cultures.

Summary- P2 and glutamate receptor antagonists during OGD in co-cultures

The findings using all antagonists are summarised in **Figure 5-42**. Overall cell death of all cells combined was significantly reduced by suramin, PPADS, MRS-2179, NBQX, NBQX + MK-801, suramin + NBQX + MK-801 and the combination of 1P1M3N, suggesting a role for P2 receptors, P2Y₁ receptors, and AMPA/Kainate receptors. Astrocyte death was significantly reduced by PPADS, MRS-2179, suramin + NBQX + MK-801 and 1P1M3N, suggesting a role for P2 receptors in general and P2Y₁ receptors in astrocyte death. Neuronal death was significantly reduced by PPADS, suramin, MRS-2179, NBQX, MK-801, NBQX + MK-801, suramin + MK-801 + NBQX and 1P1M3N, suggesting a role for P2 receptors, P2Y₁ receptors, AMPA/kainate receptors and NMDA receptors in neuronal death. The onset of cell death of all cells combined was delayed by suramin, PPADS and 1P1M3N, suggesting a role for P2 receptors in mediating early death. The onset of astrocyte death was only significantly delayed by PPADS and 1P1M3N, suggesting a role for P2 receptors in initiating astrocyte death during OGD. The onset of neuronal death was delayed by suramin, PPADS, KN-62, NBQX, MK-801 + NBQX, and 1P1M3N, suggesting a role for P2 receptors, P2X₇ receptors, and AMPA/kainate receptors in initiating neuronal death during OGD. Finally, the mean time to cell death of all cells combined was delayed by all antagonists used, while astrocyte death was delayed by suramin, PPADS KN-62, NBQX, MK-801 + NBQX and 1P1M3N and neuronal death was delayed by PPADS, KN-62, NBQX, MK-801 + NBQX and 1P1M3N. When all results are combined, it suggests that P2 receptors and P2Y₁ receptors are involved in astrocyte death and neuronal death, with P2X₇ receptors possibly involved in initiating neuronal death as well, while NMDA and AMPA/kainate receptors are involved in neuronal death with AMPA/kainate receptors possibly also involved in the onset of neuronal death. Simultaneously blocking P2 and glutamate receptors is highly protective, significantly delaying and reducing ischaemic cell death, even at reduced concentrations, suggesting a synergistic protective effect of combining these antagonists.

The reader is also referred to **Tables 5-3 and 5-4** for a complete summary of all results presented in this chapter.

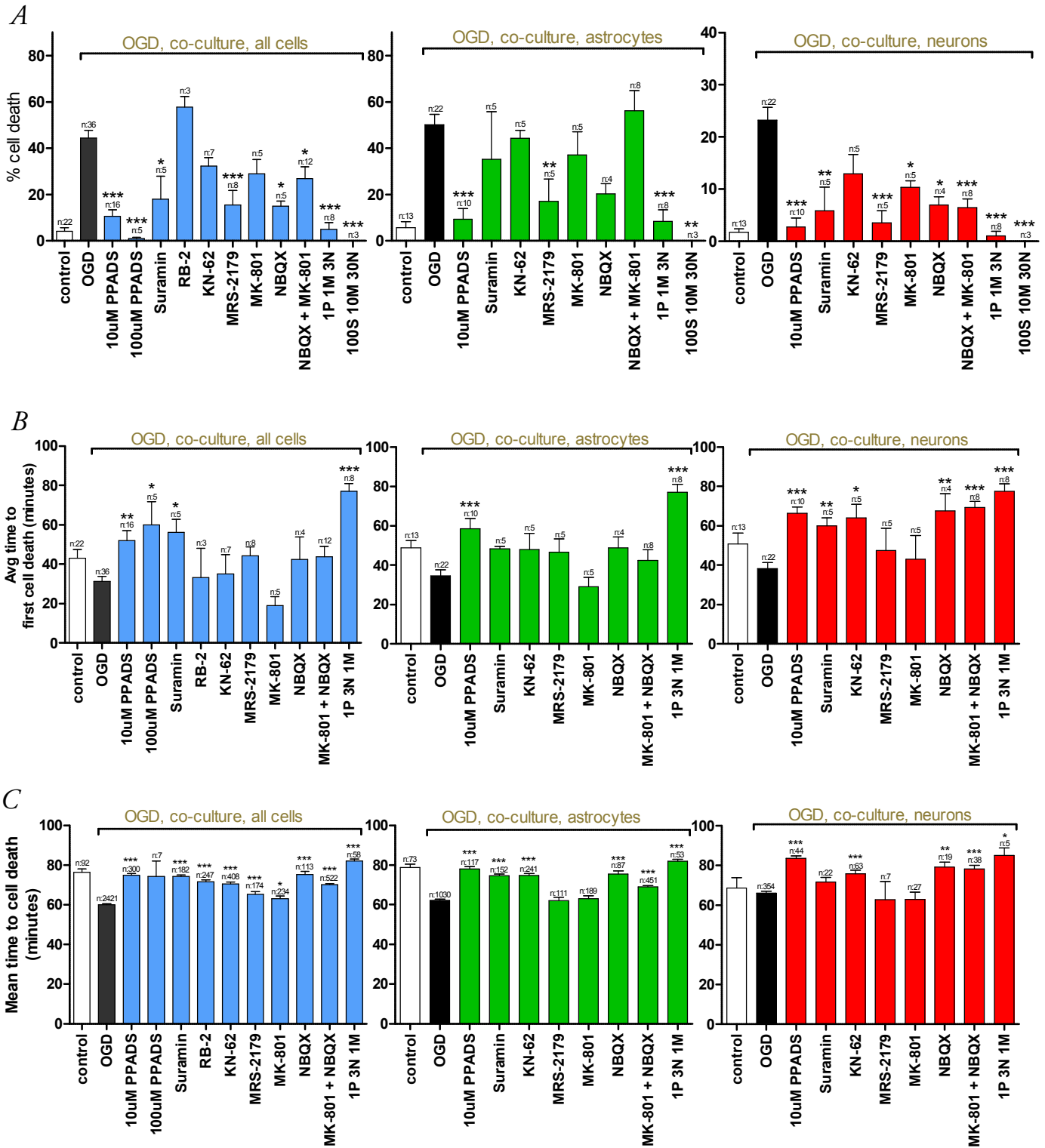


Figure 5-42: Summary of results, P2 and glutamate receptor antagonists during OGD

A: % cell death

B: Average time to first cell death

C: Mean time to cell death

Table 5-3: Summary of results, neuron and astrocyte death in different cultures and effects of long agonist application

		Astrocytes			Neurons			
		OD	MTTD	TTFD	OD	MTTD	TTFD	Transient effects
Astrocyte culture	Control, neurobasal	-	-	-	-	-	-	-
	OGD, neurobasal	↑↑↑ 35	-	↑↑↑	-	-	-	-
	Control, DMEM	-	-	-	-	-	-	-
	OGD, DMEM	↓↓† 35	↓↓↓†	-	-	-	-	-
Neuronal culture	Control	-	-	-	-	-	-	-
	OGD	-	-	-	-	-	-	-
	Control +							
	1uM ATP	-	-	-	-	-	↓	↑ death, 5-10m
	10uM ATP	-	-	-	-	-	-	-
	100uM ATP	-	-	-	-	↓	-	-
	1mM ATP	-	-	-	-	-	-	-
	OGD +							
	100uM ATP	-	-	-	-	↓↓↓	-	-
1mM glutamate	-	-	-	-	-	-	-	
ATP + glutamate	-	-	-	-	↓↓↓	-	↑ death, 5 + 15m	
Co-culture	Control	-	-	↓↓↓*	↓↓*	-	-	-
	OGD	↑↑↑ 45	↑↑*	-	↑↑↑ 50 / ↑↑* 50	↑↑	↑↑	-
	OGD +							
	1uM glutamate	-	↑↑↑	-	-	↑	-	-
	10uM glutamate	↓ 85	-	-	-	-	-	-
	100uM glutamate	↓ 85	↓	-	-	-	-	-
	1mM glutamate	↓↓ 65	-	-	-	↓	-	↑ death, 20m
	100uM ATP	-	↑↑↑	-	-	-	-	-
10nM MRS-2365	-	↑	-	-	-	-	-	

OD: overall cell death; **MTTD:** mean time to cell death; **TTFD:** average time to first death m: minutes

Only differences reaching statistical significance are marked with arrows. Direction of arrows indicates how value shifted compared to relevant control.

The number of arrows indicates p-value (1 arrow: <0.05, 2 arrows: <0.01, 3 arrows <0.001)

Green arrows highlight favourable effect, red arrows highlight detrimental effect

*: compared to pure culture; †: compared to astrocytes in Neurobasal; if not marked by a symbol, results are relative to controls

Numbers in OD columns: time after which difference became significant

Table 5-4: Summary of results, effects of different agonists and antagonists added to co-cultures during OGD

	All cells in co-culture			Astrocytes in co-culture			Neurons in co-culture			
	OD	MTTD	TTFD	OD	MTTD	TTFD	OD	MTTD	TTFD	Transient effects
1uM Glutamate	-	↑↑↑	-	-	↑↑↑	-	-	↑	-	
10uM Glutamate	↓ 85	-	-	↓ 75	-	-	-	-	-	
100uM Glutamate	↓ 85	↓	-	↓ 75	↓	-	-	-	-	
1mM Glutamate	↓↓↓ 70	-	-	↓↓ 65	-	-	-	↓	-	↑ death, 20m
100uM ATP	-	↑↑↑	↑	-	↑↑↑	-	-	-	-	
10nM MRS-2365	-	↑↑	-	-	↑	-	-	-	-	
100uM Suramin	↓ 65	↑↑↑	↑	-	↑↑↑	-	↓↓ 65	-	↑	
100uM PPADS	↓↓↓ 65	-	↑	↓↓↓ 65	na	na	↓↓↓ 65	na	na	
10uM PPADS	↓↓↓ 40	↑↑↑	↑↑	↓↓↓ 50	↑↑↑	↑↑↑	↓↓↓ 50	↑↑↑	↑↑↑	
100uM RB-2	-	↑↑↑	-	na	na	na	na	na	na	
1uM KN-62	-	↑↑↑	-	-	↑↑↑	-	-	↑↑↑	↑	↓ death, 70-80m
10uM MRS-2179	↓↓↓ 65	↑↑↑	-	↓ 85	-	-	↓ 65	-	-	
30uM NBQX	↓ 75	↑↑↑	-	-	↑↑↑	-	↓ 65	↑↑	↑↑	
10uM MK-801	-	↑	-	-	-	-	↓ 90	-	-	
10uM MK-801 + 30uM NBQX	↓	↑↑↑	-	-	↑↑↑	-	↓↓↓ 50	↑↑↑	↑↑↑	
1uM PPADS + 1uM MK-801 + 3uM NBQX	↓↓↓ 45	↑↑↑	↑↑↑	↓↓↓ 50	↑↑↑	↑↑↑	↓↓↓ 45	↑	↑↑↑	
100uM Suramin + 10uM MK-801 + 30uM NBQX	↓↓↓	na	na	↓↓↓	na	na	↓↓↓	na	na	

OD: overall cell death; **MTTD:** mean time to cell death; **TTFD:** average time to first death;

Only differences reaching statistical significance are marked with arrows. Direction of arrows indicates how value shifted compared to OGD.

The number of arrows indicates p-value compared to OGD (1 arrow: <0.05, 2 arrows: <0.01, 3 arrows <0.001)

Green arrows highlight favourable effect, red arrows highlight detrimental effect; na: data not available

Numbers in OD columns: time after which difference became significant; m: minute

DISCUSSION

Astrocytes kept in Neurobasal medium are more sensitive to OGD

In agreement with the majority of studies investigating the susceptibility of primary cultured astrocytes to ischaemia, astrocytes which were grown in the commonly used DMEM-based serum-containing medium (DM) did not develop significant cell death during 90 minutes of OGD (eg: Goldberg and Choi, 1993; Lyons and Kettenmann, 1998; Papadopoulos et al., 1998; Beck et al., 2003; Lenart et al., 2004). However, in astrocytes that were grown to confluence in DM before being placed in Neurobasal medium (Nb), which is serum free, for a minimum of three days prior to imaging, 90 minutes of OGD produced rapid widespread cell death which was significantly increased compared to controls or astrocytes in DM. The timescale and overall percentage of cell death seen in the astrocytes in Nb is similar to what has been reported in cultured and acutely isolated astrocytes undergoing the HAIR protocol (exposure to hypoxic, acidic, ion-shifted ringer solution) and *in situ* rat optic nerve (RON) astrocytes undergoing OGD (Fern, 1998; Bondarenko and Chesler, 2001b; Thomas et al., 2004). For comparison, 46.6% of astrocytes in the RON die after 80 minutes of OGD, while in my experiments 40.65% of astrocytes perished after the same period of time (Fern, 1998). This also mirrors *in vivo* events, where early widespread necrotic astrocyte death within 15-30 minutes of middle cerebral artery occlusion has been documented (Garcia et al., 1993; Davies et al., 1998; Lukaszevicz et al., 2002). Recent papers by our laboratory have highlighted this poor correlation between the time course of ischemic injury reported in cultured astrocytes and astrocytes *in vivo* or *in situ* (Fern, 2001; Shannon et al., 2007).

My results therefore suggest that common culturing protocols using DM may be producing astrocytes which are ‘artificially’ resistant to ischaemia compared to their *in vivo* and *in situ* counterparts. Just to highlight how common the use of this culture medium is, a recent review article comparing astrocyte culturing methods from 110 papers published in 2006 revealed that only 4 of these did not use animal serum (Saura, 2007). Furthermore, when I looked back over many papers documenting a high resistance of cultured astrocytes to ischaemia, all of them used serum-containing medium (Yu et al., 1989; Kaku et al.,

1991; Goldberg and Choi, 1993; Juurlink and Hertz, 1993; Lyons and Kettenmann, 1998; Papadopoulos et al., 1998; Ho et al., 2001; Yu et al., 2001; Beck et al., 2003; Lenart et al., 2004; Danilov and Fiskum, 2008). A similar protective effect of culturing astrocytes in DM has been reported in the context of glutamate induced astrocyte toxicity (Chen et al., 2000). The presence of glutathione (GSH) precursors such as L-cystine in DMEM and serum along with good growth conditions stimulates astrocytes to maintain higher levels of intracellular GSH (Chen et al., 2000). GSH is protective of astrocytes because it helps scavenge for ROS which are formed during metabolic insults such as ischaemia (Papadopoulos et al., 1997; Papadopoulos et al., 1998; Chen et al., 2000; Reichert et al., 2001; Re et al., 2006). Depletion of astrocyte GSH stores increases astrocyte death during hypoglycaemia and OGD (Papadopoulos et al., 1997; Papadopoulos et al., 1998). It can therefore be hypothesised that switching astrocytes to Nb medium lowered intracellular GSH levels, making them more sensitive to ischaemia. However, Neurobasal medium and B-27 supplement both contain GSH precursors and antioxidants such as reduced glutathione, vitamin E, catalase, and superoxide dismutase, which may have counteracted negative effects of serum-deprivation on astrocyte glutathione content (Velasco et al., 2003). In fact, the presence of these compounds in B-27 has been hypothesised to decrease the sensitivity of cultured neurons to glutamate toxicity when these cells were cultured in Nb, compared with DM (Velasco et al., 2003). Interestingly, this study also demonstrated that glial expression of GLAST and GLT-1 was not significantly affected by switching the culture medium to Nb (Velasco et al., 2003). While the exact mechanism by which serum-containing culture media desensitize astrocytes to ischaemic injury remains to be determined, a culturing approach using serum-free media may provide a novel and more representative method by which *in vivo* ischemic astrocyte death can be modeled *in vitro*.

Lack of increased cell death in the neuronal culture by OGD, ATP, and/or glutamate

In the neuronal culture, OGD did not produce significantly more cell death than control conditions. In addition, overall neuronal death after 90 minutes could not be increased by addition of exogenous ATP (during OGD or control) and/or glutamate (during OGD). This may be due to a number of different factors. First of all, it is important to note that two phases of glutamate mediated injury occur during ischaemia

and glutamate receptor agonist application: an initial phase of non-excitotoxic glutamate receptor dependent osmotic lysis (which is not oxygen dependent), followed by the classically described delayed glutamate receptor mediated excitotoxicity which crucially involves toxic oxygen-dependent NO and ROS formation (Ankarcrona et al., 1995; Dubinsky et al., 1995; Chow and Haddad, 1998; Lipton, 1999). While neurons dying during the initial non-excitotoxic phase undergo rapid necrosis (within 20-30min in glutamate exposure experiments) the component of delayed death does not set in until 3 hours later, and can be inhibited by removal of oxygen (Ankarcrona et al., 1995; Dubinsky et al., 1995). It appears therefore that in my experiments we are only seeing the early phase of oxygen-independent non-excitotoxic glutamate and/or ATP-mediated death. In a set of experiments by Dubinsky and colleagues using hippocampal neuron cultures, exposure to hypoxia for 24 hours killed 40% of cells, and this was not further increased when 500uM glutamate was applied during the first 5 minutes of hypoxia, whereas the same glutamate application under normoxic conditions killed 80% of neurons after 24 hours (Dubinsky et al., 1995). Thus it seems plausible that the same neurons which perished during OGD would also have been killed by the glutamate, hence the lack of increased overall death after 90 minutes when the two insults were combined.

Another possible explanation is the fact that sensitivity of cultured embryonic neurons to ischaemic and excitotoxic insults is developmentally regulated (Choi et al., 1987; Choi and Rothman, 1990; Friedman and Haddad, 1993; Witt et al., 1994; Dugan et al., 1995; Marks et al., 1996; Ye and Sontheimer, 1998; Cheng et al., 1999; Sinor et al., 2000; Amadio et al., 2002; Clodfelter et al., 2002; Fogal et al., 2005; King et al., 2006). For example, in hippocampal neuron cultures, the ED₅₀ for glutamate induced cell death is >100uM at <6 DIV, but decreases to around 6uM when cultures are 3 weeks or older (Ye and Sontheimer, 1998). In cultured CGNs, a 15 minute application of 300uM ATP in 9 DIV cultures causes 100% cell death after 2 hours, whereas at ≤7 DIV cells are unaffected (Amadio et al., 2002). Importantly, the *in vitro* development of neuronal sensitivity to ischaemia/excitotoxicity closely resembles *in vivo* events. With increasing age, the predominant mechanism of cell death in hippocampal neurons after hypoxia-ischaemia

shifts from apoptotic to necrotic death (Liu et al., 2004). Similarly, a substantial proportion of acutely isolated CA1 hippocampal neurons from P21-25 rats die within 10-20 minutes of stimulation with 300uM glutamate for 5 minutes, but there is no death in neurons from P6-8 or P1-3 animals within 90 minutes after the same insult, confirming that *in vitro* resistance of young neurons is not simply a culture phenomenon (Marks et al., 1996).

The actual mechanisms for this developmental change in sensitivity are still unclear (especially in relation to ATP induced toxicity), but may involve alterations in glutamate receptor subunit composition, increased ability for relevant stimuli to induce secondary neuronal glutamate release and/or Ca²⁺-induced Ca²⁺-release in older cells, and maturation of the coupling between glutamate receptors and intracellular processes necessary to trigger cell death (Cheng et al., 1999; Sala et al., 2000; Sinor et al., 2000; Sattler and Tymianski, 2001; Clodfelter et al., 2002; Fogal et al., 2005). Looking back through my experimental results, I could not detect an obvious correlation between amount of cell death and age of cultures in the neuronal cultures/co-cultures after up to 17/15 DIV respectively, although the numbers of experiments spread across different time points are insufficient to make any definite conclusions.

Various aspects relating to culture methods may also affect neuronal sensitivity. The density of neuronal cultures critically determines vulnerability to OGD, with less dense cultures becoming more resistant (Dugan et al., 1995). Analyses of animal serum sold for culture purposes have revealed that these routinely contain about 1mM glutamate, so the DMEM based medium I was using possibly contained around 100uM glutamate just from serum (Ye and Sontheimer, 1998). In the neuron culture protocol, I briefly applied this medium to stop the action of trypsin after trituration, so it is theoretically possible that a sufficiently high concentration of glutamate was added to lead to delayed degeneration of glutamate-sensitive neurons, thereby creating a cell culture which is selective for cells which are not vulnerable to glutamate excitotoxicity (Ye and Sontheimer, 1998).

Significant neuronal death during OGD only occurred in co-cultures: importance of astrocyte-neuron interactions?

In the co-culture there was significantly more neuronal death during OGD than control conditions. Moreover, when comparing neuronal death in the co-culture and neuronal culture, there was significantly more neuronal death in the co-culture during OGD but significantly less during control conditions, suggesting that during physiological signalling astrocytes protect neurons whereas during OGD they mediate a damaging effect. A similar set of experiments performed by Dugan and colleagues produced the opposite result. Murine pure neuronal cultures were more sensitive than mixed cultures to OGD, and this was due to the protective effect of astrocyte glutamate uptake, as neuronal death in co-culture could be increased by blocking glial glutamate transporters (Dugan et al., 1995). However, methodological differences can explain this apparent discrepancy: specifically, they measured cell death by LDH accumulation 24 hours after a variable period of OGD followed by re-oxygenation (Dugan et al., 1995). Therefore, 24 hours of reperfusion will have allowed for delayed excitotoxic neuronal death in the neuronal cultures to develop, while at the same time in the co-culture, glial cells can protect neurons from delayed death by, for instance, removing excess extracellular glutamate after a return to normal glutamate transporter operation (Dugan et al., 1995).

Potential mechanisms for the increased neuronal death during OGD in the presence of astrocytes may include: astrocyte glutamate release, astrocyte ATP release and/or the modulation of neuronal NMDA receptor subunit composition *in vitro* (Rossi et al., 2000; Daniels and Brown, 2001; Bal-Price et al., 2002; Mitani and Tanaka, 2003; Feustel et al., 2004; Parkinson and Xiong, 2004; Camacho and Massieu, 2006; Kosugi and Kawahara, 2006; Pedata et al., 2007; Rossi et al., 2007; Gouix et al., 2009). The idea that excessive ATP and glutamate release from astrocytes is causing increased neuronal death is supported by the result that blocking glutamate receptors and/or P2 receptors significantly reduced neuronal death: thus, astrocytes seem to be sensitising or contributing to neurotransmitter dependent toxicity of neurons. Astrocytes have been demonstrated to contribute to neuronal death during severe brain ischaemia by reversal of glutamate

transporters (Rossi et al., 2000; Mitani and Tanaka, 2003; Camacho and Massieu, 2006; Kosugi and Kawahara, 2006). Additionally, glutamate release via reversal of glial glutamate transporters has been shown to preferentially activate extrasynaptic neuronal NMDA receptors, further enhancing neuronal death (Fellin et al., 2004; Gouix et al., 2009). However, transport reversal only occurs when ionic homeostasis is severely compromised, so during less severe ischaemia or after reperfusion, normal operation of glial glutamate transporters enhances neuronal survival by reducing glutamate toxicity (Sugiyama et al., 1989; Rosenberg et al., 1992; Dugan et al., 1995; Rao et al., 2001; Hamann et al., 2002). It is for this reason that GLT-1 knock-out animals actually have increased infarct volumes after MCAO, as the protective effect of glial glutamate uptake in the penumbra is abolished (Rao et al., 2001). Interestingly, the process of astrocyte glutamate transporter reversal may be both harmful or beneficial to astrocytes themselves: induction of transporter reversal during a non-energy deprived state leads to oxidative death of cultured astrocytes (by depleting intracellular GSH), while during ischaemia this process increases astrocyte survival by preventing toxic intracellular Na⁺ accumulation (Re et al., 2003; Kosugi and Kawahara, 2006; Re et al., 2006). Depletion of GSH in astrocytes will also lead to reduced GSH content in neurons, since astrocytic GSH is transported to neurons (Kahlert and Reiser, 2004). As discussed in Chapter 3, astrocytes have been shown to release ATP during ischaemia, even though this could not be detected in my experiments (Parkinson et al., 2002; Zhang et al., 2007; Schock et al., 2008). This ATP could then theoretically activate neuronal P2 receptors, leading to enhanced cell death.

However, since the application of exogenous ATP and/or glutamate during OGD in neuronal cultures failed to increase cell death to the level seen in the co-culture, mechanisms other than astrocyte ATP and/or glutamate release may be involved in the increased neuronal death in co-cultures. An interesting possibility is the modulation of neuronal receptor expression by astrocytes *in vitro*. Cultured CGNs become more sensitive to glutamate toxicity when co-cultured with astrocytes or treated with astrocyte-conditioned culture medium, and this is due to astrocyte regulation of NMDA receptor subunit composition in the neurons (Daniels and Brown, 2001). Conversely, a different

paper found no direct modulation of NMDA receptor subunit expression by astrocytes in CGN culture, instead reporting a reduction of sensitivity to glutamate toxicity and increased neuronal viability when astrocytes were present (Beaman-Hall et al., 1998). To my knowledge, modulation of P2 receptor expression in neurons by astrocytes has not yet been investigated. One final possibility to consider is that the extensive amount of necrotic astrocyte death in the co-culture in itself might have led to increased neuronal death: large amounts of toxic molecules accumulating in dying astrocytes would suddenly be released upon loss of cell membrane integrity, and could theoretically kill neurons. However, during OGD, astrocytes and neurons reached levels of significant death after the same amount of time in the co-culture, so astrocyte death did not precede neuronal death. Furthermore, a number of different antagonists reduced neuronal death without preventing astrocyte death. An additional comment can be made regarding the result that in the astrocyte culture, compared to the co-culture, astrocyte death was significantly increased transiently after 40-55 minutes and the mean time to cell death was significantly reduced, presenting the intriguing possibility that neurons protect astrocytes.

[Ca²⁺]_i changes during OGD

Over the past decades, a number of hypotheses have been proposed relating changes in [Ca²⁺]_i to the outcome of cellular fate during conditions such as OGD and glutamate excitotoxicity. Initially, a unifying Ca²⁺ hypothesis was put forward stating that high [Ca²⁺]_i is a common pathway for cell death, and this has so far been demonstrated to hold true for all CNS cell types (Siesjo and Bengtsson, 1989; Goldberg and Choi, 1993; Choi, 1995; Duffy and MacVicar, 1996; Silver et al., 1997; Fern, 1998; Arundine and Tymianski, 2003; Martinez-Sanchez et al., 2004; Pringle, 2004). In agreement with this, death of all cell types during my experiments, regardless of conditions, was always preceded by a large sharp increase in [Ca²⁺]_i. Nonetheless, many studies have found that there is no simple correlation between the magnitude of [Ca²⁺]_i increases and later cell death or dysfunction, and sustained [Ca²⁺]_i elevations do not necessarily predict cell death (Dubinsky and Rothman, 1991; Frandsen and Schousboe, 1992, 1993; Witt et al., 1994; Sattler et al., 1998). Again, results from my experiments support this. In neuronal

cultures, adding the combination of ATP + glutamate during OGD caused large early $[Ca^{2+}]_i$ rises in a significantly higher proportion of cells than OGD alone, OGD + ATP, or OGD + glutamate, but this did not correlate with increased levels of cell death after 90 minutes, although it did result in significantly more early death (after 5 and 15 minutes, but not later).

The above result does present a paradox which is difficult to explain. On the one hand, results of antagonist experiments clearly demonstrated that blocking P2 and glutamate receptors during ischaemia was protective, suggesting that $[Ca^{2+}]_i$ accumulation via these pathways may be linked to increased cell death. On the other hand, deliberate activation of these pathways during OGD produced $[Ca^{2+}]_i$ rises in neuronal cultures which did not correlate with increased cell death. This runs counter to the source-specificity hypothesis, which states that the specific route of Ca^{2+} influx rather than overall $[Ca^{2+}]_i$ load predicts the outcome of $[Ca^{2+}]_i$ accumulation: for example, in cultured murine cortical neurons, Ca^{2+} influx through NMDA receptors causes cell death, whereas an identical $[Ca^{2+}]_i$ load produced via influx through VGCCs is innocuous (Sattler et al., 1998). The mechanistic explanation behind this theory is that $[Ca^{2+}]_i$ triggers neurotoxic processes in the cell depending on the vicinity of a route of influx (such as an NMDA receptor) to the intracellular site at which the Ca^{2+} then activates a cytotoxic cascade (Sattler et al., 1998). Alternatively, a threshold system has also been suggested, whereby once a cell reaches a particular $[Ca^{2+}]_i$, it is invariably destined for death (Tymianski et al., 1993a; Witt et al., 1994). It may be that ATP and glutamate mediated non-excitotoxic mechanisms of cell death were causing cell death in these experiments.

A closer analysis of the $[Ca^{2+}]_i$ changes before cell death revealed a pattern of an early initial $[Ca^{2+}]_i$ rise followed by a second, often larger $[Ca^{2+}]_i$ rise which immediately preceded cell death. This occurred in both neurons and astrocytes. Similarly large $[Ca^{2+}]_i$ rises, as well as mechanistically dissociated early and late components, have been reported in both astrocytes and neurons during OGD and/or glutamate excitotoxicity (Duffy and MacVicar, 1996; Silver et al., 1997; Fern, 1998; Diarra et al., 1999; Aarts et al., 2003;

Chinopoulos et al., 2004). In astrocytes subjected to OGD, the early phase of Ca^{2+} entry was found to be mediated mainly by T-type VGCCs, while during ischaemia in neurons it can be prevented by blocking a combination of ionotropic glutamate receptors and VGCCs (Fern, 1998; Aarts et al., 2003).

Comparing astrocytes and neurons, the early $[\text{Ca}^{2+}]_i$ rise in astrocytes tended to be smaller than in neurons. This suggests that the balance of $[\text{Ca}^{2+}]_i$ extrusion and influx pathways active during the early part of OGD is different in both cell types. For example, neurons but not astrocytes expressed highly Ca^{2+} permeable glutamate receptors which are probably activated early during ischaemia, while at the same time astrocytes are generally better able to maintain intracellular ATP levels during early ischaemia and hence continue active transport of Ca^{2+} out of the cell (by Ca^{2+} -ATPase and $\text{Na}^+/\text{Ca}^{2+}$ -exchanger activity) or Ca^{2+} sequestration into the ER (SERCA activity), reducing early $[\text{Ca}^{2+}]_i$ loading (Duffy and MacVicar, 1996; Fern, 1998; Aarts et al., 2003). A similar theory was put forth by Duffy and MacVicar, who compared the $[\text{Ca}^{2+}]_i$ changes induced by hypoxia-hypoglycaemia (HH) in acutely isolated hippocampal astrocytes and neurons (Duffy and MacVicar, 1996). In neurons, HH caused rapid increases in $[\text{Ca}^{2+}]_i$, usually within 3-4 minutes after onset of HH, and these were not reversed by removal of external Ca^{2+} (Duffy and MacVicar, 1996). Astrocytes showed slower and more modest increases in $[\text{Ca}^{2+}]_i$, and external Ca^{2+} removal reversed HH induced $[\text{Ca}^{2+}]_i$ elevations (Duffy and MacVicar, 1996). The authors suggest that during ischaemia, Ca^{2+} extrusion mechanisms are still functional in astrocytes, while in neurons they are either inhibited or overpowered by further influx (Duffy and MacVicar, 1996).

However, the late $[\text{Ca}^{2+}]_i$ rises immediately preceding cell death were comparable in both astrocytes and neurons, suggesting that a similar process occurs in both cell types at this point. In cultured murine hippocampal neurons, this late rise could not be prevented by blocking ionotropic glutamate receptors or VGCCs, but rather was mediated by 2 members of the melastatin subfamily of transient receptor potential (TRP) channels: TRPM2 and TRPM7 (Aarts et al., 2003). TRP channels are a large class of non-specific

cation channels which are expressed abundantly in the mammalian brain (Aarts and Tymianski, 2005). Importantly, TRPM7 knock-down using siRNAs significantly protected neurons exposed to up to 3 hours of OGD against cell death (Aarts et al., 2003). However, in neonatal RON astrocytes, these later $[Ca^{2+}]_i$ rises are mediated by L-type VGCCs (Fern, 1998). Interestingly, the paper by Fern also reported a complete block of all $[Ca^{2+}]_i$ rises in the majority of astrocytes as well as a significant reduction in overall cell death during ischaemia by La^{3+} , a metal ion which has since been shown to potently inhibit TRPMs, suggesting that this channel may also be an interesting target for investigation in the context of astroglial death during ischaemia (Fern, 1998; Aarts and Tymianski, 2005).

Finally, complete prevention of Ca^{2+} accumulation during ischaemia may actually promote delayed apoptotic cell death (Gwag et al., 1995). Thus, it has been proposed that various thresholds linking intracellular Ca^{2+} levels to a specific cellular outcome may exist during ischaemia (at least in neurons), such that very high $[Ca^{2+}]_i$ loading leads to necrotic death and complete prevention of $[Ca^{2+}]_i$ rises leads to delayed apoptosis, while intermediate $[Ca^{2+}]_i$ elevation actually prevents delayed apoptosis (Yoon et al., 2003; Canzoniero et al., 2004).

Exogenous ATP and glutamate application

One of the methods used to examine the potential contributions of ATP and glutamate signalling to ischaemic cell death was to monitor the effects of exogenously added ATP and glutamate. Cultured neurons are highly susceptible to ATP induced toxicity (Amadio et al., 2002; Amadio et al., 2005). However, immediate effects upon ATP exposure, such as early cell death, have not been well documented. As discussed above, continuous application of 1uM, 10uM, 100uM or 1mM ATP to the neuronal cultures did not induce significant cell death after 90 minutes. Despite the lack of effects in terms of overall death, 1uM ATP significantly increased neuronal death transiently after 5 and 10 minutes and reduced the average time to first cell death, while 100uM ATP significantly reduced the mean time to cell death, suggesting at least some increased toxicity with added ATP under these conditions.

The level of ATP-induced neuronal death was far less dramatic than findings by Amadio and colleagues, which report that cultured CGNs exposed to 500uM ATP start to die within 15 minutes, with almost 100% cell death apparent after 120 minutes (Amadio et al., 2002). Similar rates of cell death were evident in striatal and organotypic hippocampal cultures; effects on cortical cultures, though, have not been reported (Amadio et al., 2002). Interestingly, various NMDA receptor antagonists protected against ATP induced cell death in CGN cultures: MK-801 reduced cell death by 85-90%, implying that ATP was causing glutamate release which in turn caused cell death (Amadio et al., 2002). This is further suggested by their result that only P2 antagonists with known activity at glutamate receptors (RB-2 and Suramin) are protective against ATP-toxicity, while PPADS, oxATP or KN-62, which do not block glutamate receptors, are ineffective (Balcar et al., 1995; Nakazawa et al., 1995; Price and Raymond, 1996; Ong et al., 1997; Gu et al., 1998; Peoples and Li, 1998; Zona et al., 2000; Amadio et al., 2002; Suzuki et al., 2004).

Continuous application of 100uM ATP during OGD also failed to significantly influence overall rates of cell death in the neuronal culture or the co-culture. However, there were divergent results in terms of the temporal dynamics of cell death between the two cultures: in the neuronal culture, ATP reduced the mean time to cell death (due to reduced late death), while in the co-culture it increased the mean time to cell death (all cells and astrocytes) and time to first death (all cells). These results suggest a more protective rather than harmful effect of ATP application during ischaemia in the co-culture. In stark contrast to these observations, 500uM ATP application during hypoglycaemia significantly augments cell death in cultured CGNs compared to hypoglycaemia alone, as determined by LDH release (Cavaliere et al., 2002). Moreover, 5mM ATP application during 40 minutes of OGD and for 2 hours thereafter in a unique organotypic cortical/striatal/subventricular zone culture increases cell death by 50% compared to OGD alone (Cavaliere et al., 2005). A similar augmentation of cell death after OGD was also seen with 10uM 2MeS-ATP and 100uM ATPgS application, suggesting P2 receptor involvement in the effect (Cavaliere et al., 2005). However, these two studies used higher concentrations of ATP and they

measured cell death after 20-24 hours, making it difficult to directly compare their results to mine.

Various lines of evidence in the literature support the idea that excessive extracellular ATP accumulation may also exert potentially protective effects during ischaemia. Such protective effects may be mediated by ATP itself or by its enzymatic breakdown product adenosine. In rat hippocampal slices, degradation of exogenously applied ATP to adenosine causes an inhibition of neurotransmission (measured by a reduction in the amplitude of field excitatory postsynaptic potentials (fEPSP) and population spikes (PS)), as demonstrated by the fact that the inhibitory effect of ATP is blocked by a selective A₁ adenosine receptor antagonist, although a minor component of the inhibitory effect was also mediated by P2 receptors (Coppi et al., 2007). A similar study corroborated this finding: 10uM ATP application in hippocampal slices exerts an inhibitory action on fEPSPs, although in this study it was independent of its degradation to adenosine (Pedata et al., 2007). The application of 100uM ATP or the P2 receptor agonist α,β -MeATP (but not adenosine) accelerates functional recovery of synaptic transmission after 20 minutes of OGD in hippocampal slices (Aihara et al., 2002). This protective effect of ATP is produced by an increase in P2 receptor mediated GABA release from neurons but not astrocytes (Aihara et al., 2002). Alternatively, the finding that ATP itself can directly modulate NMDA receptors provides a further possible explanation for the protective effect of exogenously applied ATP in these cultures during OGD. ATP may act as a direct antagonist at NMDA receptors and has been shown to attenuate NMDA-mediated excitotoxicity in cultured hippocampal neurons (Ortinou et al., 2003). Furthermore, ATP can act as a competitive antagonist and positive allosteric modulator at recombinant NMDA receptors (Kloda et al., 2004).

It may be that in the co-culture, increased cellular density/surface area produced greater ectonucleotidase activity and hence increased adenosine formation from ATP than in the neuronal culture. Adenosine acting on the different adenosine receptor subtypes (A₁, A_{2a}, A_{2b}, A₃) has long been known to influence cell fate during ischaemia via a number of

mechanisms, including inhibition of neuronal activity by decreasing excitatory amino acid release and Ca^{2+} influx, stabilisation of the membrane potential through hyperpolarisation, increased *in vivo* oxygen supply by vasodilation, and inhibition of free radical production (Bona et al., 1997; Schubert et al., 1997; Fredholm, 2007). Numerous studies using *in vitro* and *in vivo* models, as well as specific adenosine receptor subtype antagonists and knock-out animals, have created a general consensus that A_1 , A_{2b} and A_3 receptor activation is protective during brain ischaemia while antagonists at A_{2a} are protective (Phillis, 1995; Bona et al., 1997; Chen et al., 1999; Aden et al., 2003; Almeida et al., 2003; Marcoli et al., 2003; Yu et al., 2004; Pedata et al., 2005; Bjorklund et al., 2008). Importantly, these effects appear to extend to glia as well as neurons (Schubert et al., 1997; Nishizaki, 2004; Bjorklund et al., 2008). NTPDase (nucleoside triphosphate diphosphohydrolase: a type of ectonucleotidase) knock-out mice, characterised by a significantly reduced ability of brain and other tissues to break down extracellular ATP and ADP, have significantly increased infarct volumes following *in vivo* transient focal cerebral ischaemia, an effect which is reversed by the administration of a recombinant soluble form of the enzyme (Pinsky et al., 2002; Marcus et al., 2003). This result suggests a protective effect of enzymatic breakdown products of nucleosides such as ATP and/or damaging effect of not breaking down ATP/ADP, although a vascular effect of breakdown inhibition cannot be discounted as a factor in this result, since cerebral perfusion was significantly altered in NTPDase $-/-$ animals (Pinsky et al., 2002). It would have been interesting to further investigate whether ischaemic ATP release in the co-culture also resulted in the formation and accumulation of adenosine. For example, ectonucleotidase inhibitors could have been applied during OGD and/or ATP application, as this could in theory enhance effects of ATP at P2 receptors while preventing degradation to and subsequent effects of adenosine.

Glutamate was applied to neuronal cultures and co-cultures during OGD. In the neuronal culture, 100uM glutamate did not affect the amount of cell death, although the average time to first death was significantly reduced. In the co-culture, glutamate had a similar effect on neurons, with 1mM glutamate (but not 1,10, or 100uM) reducing the mean time to cell death and increasing cell death transiently after 20 minutes. In

combination, these results show that glutamate was speeding up the onset of neuronal death. Interestingly, simultaneously adding ATP and glutamate to the neuronal culture during OGD further enhanced early death, producing significantly increased death after 5 and 15 minutes, suggesting a summative effect by both ligands on cell death. As discussed earlier, the classically reported glutamate mediated excitotoxicity which causes widespread death in so many *in vitro* neuronal preparations requires oxygen to induce significant cell death (Dubinsky et al., 1995). In hippocampal neuron cultures, glutamate application does not cause a significant increase in cell death during hypoxia, even after 24 hours, although the hypoxic conditions themselves caused about 40% cell death during this time period (Dubinsky et al., 1995). The lack of overall increased neuronal death in these cultures was therefore not unexpected. Moreover, even in the presence of oxygen, only a relatively small subset of cells die during the first 3 hours of glutamate application, with the majority of cells instead perishing later: in CGN cultures, 20-30% of neurons die during a 30 minute continuous exposure to 100uM glutamate, but this does not increase further until about 3 hours after removal of glutamate (Ankarcrona et al., 1995). Overall, this is consistent with the idea that a subset of neurons exists in cell cultures which are particularly sensitive to early death in response to glutamate excitotoxicity, regardless of oxygenation. This concept explains why cell death was only affected by glutamate application at earlier time-points. Furthermore, it seems likely that those cells which died earlier when glutamate was applied were the same ones which would have died later on as ischaemia progressed, hence the lack of increased overall cell death by glutamate application during OGD.

A particularly surprising and novel finding was the significant reduction in astrocyte death when exogenous glutamate was added to the co-culture during OGD. This was concentration dependent, with 1uM providing no protection while 10uM, 100uM and 1mM glutamate reduced astrocyte death during OGD by approximately 84%. By contrast, a toxic effect of glutamate has been described in astrocyte cultures, where constant exposure to 100uM glutamate for 24 hours leads to increased LDH release after 24 hours (but not earlier) (Chen et al., 2000). However, they found that the damaging effect was linked to

glutamate uptake, which is severely impaired during OGD. Interestingly, pharmacologically induced reversal of glutamate transporters leads to oxidative cell death in astrocyte cultures secondary to intracellular GSH depletion, and the application of exogenous glutamate ($\geq 500\mu\text{M}$) prevents both GSH depletion and cell death under these circumstances (Re et al., 2003; Re et al., 2006). Theoretically then glutamate may have protected astrocytes during ischaemia by preventing GSH depletion.

Another possible explanation is glutamate-induced receptor desensitization. In immature oligodendrocytes, the addition of 1mM glutamate during OGD significantly reduces cell death via receptor desensitization (Fern and Moller, 2000). In cultured cortical astrocytes, 500 μM glutamate application does not produce any change in cell viability after 24-48 hours, but when AMPA receptor desensitization is blocked there is significant cell death within 30 minutes (David et al., 1996). However, functional AMPA receptor expression could not be detected in astrocyte cultures (Chapter 4), and this seems unlikely to be due to quick desensitization since functional AMPA receptor responses were very much evident in neurons. Furthermore, there is no reason to suggest that desensitization would not occur during ischaemia, and the application of NBQX did not significantly reduce astrocyte death. Alternatively, exogenous glutamate may have been protective via metabotropic glutamate receptor (mGluR) activation. mGluR agonists are protective in various models of ischaemia and excitotoxicity (Koh et al., 1991; Chiamulera et al., 1992; Opitz and Reymann, 1993; Maiese et al., 1996; Henrich-Noack et al., 1998; Sagara and Schubert, 1998; Kingston et al., 1999; Schroder et al., 1999). More specifically, activation of group 2 and 3 mGluRs (which are linked to a reduction in cyclic AMP formation) appears to be protective, while group 1 mGluR activation (coupled to increased PLC formation) is damaging (Rauca et al., 1998). For example, the administration of (S)-4C3HPG, which acts as an antagonist at group 1 and agonist at group 2 and 3 mGluRs, reduces infarct size and improves functional recovery after *in vivo* ischaemia (Henrich-Noack et al., 1998; Rauca et al., 1998). Group 2 mGluR agonists protect against NMDA-excitotoxicity (Kingston et al., 1999). However, I am unaware of any studies describing specific protection of astrocytes by mGluR activation, with most focusing on neuronal

effects, although it can be speculated that since infarct size was reduced by mGluR manipulations during *in vivo* ischaemia, astrocytes may have also been protected.

Glutamate receptor antagonists prevent neuronal but not astrocyte death

Blocking NMDA and AMPA/kainate receptors separately or in combination provided significant protective effects in neurons but not astrocytes during OGD. The protection of neurons but not astrocytes by NMDA and non-NMDA receptor antagonists during ischaemic insults has been previously documented, and correlates well with the patterns of glutamate receptor expression described in Chapter 4 (Goldberg et al., 1987; Monyer et al., 1989; Choi and Rothman, 1990; Kaku et al., 1991; Goldberg and Choi, 1993; Kaku et al., 1993; Newell et al., 1995; Fern, 1998; Lipton, 1999). Analysis of the time course of cell death revealed that the reduction in neuronal death by MK-801 alone only reached statistical significance after 90 minutes of OGD, and did not reduce the mean time to cell death or average time to first death. On the other hand, the addition of NBQX alone or in combination with MK-801 significantly reduced cell death after just 60-65 minutes of OGD, and also significantly delayed the mean time to cell death and average time to first death, suggesting that AMPA/kainate receptor activation may be involved in early cell death. In agreement with this, NMDA receptor antagonists have been shown to be less effective than AMPA/kainate receptor antagonists during prolonged and/or more severe ischaemia (reviewed in: Lipton, 1999). For instance, in a model of severe transient forebrain ischaemia using adult rats, blocking AMPA but not NMDA receptors prevents CA1 hippocampal injury (Buchan et al., 1991a; Buchan et al., 1991b). However, during less severe focal ischaemia in cats, both AMPA and NMDA receptor antagonists are neuroprotective (Bullock et al., 1990; Bullock et al., 1994).

Although not apparent in my experiments, a synergistic protective effect of combining NMDA and non-NMDA receptor antagonists during OGD has been reported. In cortical neuron cultures, cell death following prolonged (90-105 minutes) OGD is significantly attenuated by a combination of MK-801 and CNQX but not by either antagonist alone, although in this study cell death was only assessed 20 hours afterwards (Kaku et al., 1991; Kaku et al., 1993). In rat optic nerves, blocking both receptors

simultaneously but not individually significantly improves functional recovery after 20 minutes of OGD, as determined by recording the compound action potential, although in this white matter preparation effects are mediated principally by protection of oligodendrocytes and axons (Bakiri et al., 2008). Strategies aimed at reducing activation of both receptors simultaneously during ischaemia may therefore be more beneficial.

Broad-spectrum P2 receptor antagonists prevent death of both neurons and astrocytes

To investigate a possible contribution of P2 receptor activation to ischaemic death of astrocytes and neurons, various broad-spectrum P2 antagonists were applied to the co-culture during OGD. PPADS (10 and 100uM), suramin (100uM) and RB-2 (100uM) were used. It is important to reiterate that suramin and RB-2 are both known to have many non-specific effects, including activity at glutamate receptors, while PPADS, especially at the reduced concentration of 10uM, is highly selective for P2 receptors (Balcar et al., 1995; Nakazawa et al., 1995; Price and Raymond, 1996; Ong et al., 1997; Gu et al., 1998; Peoples and Li, 1998; Lambrecht, 2000; Zona et al., 2000; Suzuki et al., 2004; Lammer et al., 2006). RB-2 did not significantly affect overall cell death rates, although it did delay the mean time to cell death of all cells combined. Suramin significantly reduced neuronal but not astrocyte death, and also increased the average time to first death and mean time to cell death of neurons. PPADS was the most protective, significantly reducing death of both neurons and astrocytes. 100uM PPADS virtually eliminated all cell death, while 10uM reduced astrocytic and neuronal death by about 80%, while also significantly delaying the average time to first death and mean time to cell death for both cell types. These results suggest that P2 receptor activation plays an important role in the ischaemic demise of both neurons and astrocytes.

The protection of neurons by suramin and PPADS mirrors results presented by numerous recent *in vitro* and *in vivo* studies (the reader is referred back to **Tables 5-1** and **5-2** in this chapter's introduction for summaries of said studies). Suramin and PPADS significantly reduce neuronal death in various different dissociated primary neuron cultures and slice cultures, as measured by propidium iodide uptake 20-24 hours after a variable period of hypoglycaemia or OGD (Cavaliere et al., 2001b; Cavaliere et al., 2003; Cavaliere

et al., 2005). A similar protective effect of very low concentrations of PPADS (5uM) has also been reported in hippocampal slice cultures, although in this study cell death was only assessed 12-48 hours after 32 minutes of OGD (Runden-Pran et al., 2005). However, these studies only provide insight into the combined early and delayed death produced by ischaemia, whereas my results confirm that these antagonists are able to reduce neuronal death occurring during the first 90 minutes of ischaemia, before reperfusion. Protection against early neuronal dysfunction during ischemia by P2 antagonists has also been suggested by a functional study using hippocampal slices, where PPADS (at 30uM but not 10uM) and suramin (at 100uM but not 10uM) both prevent failure of neurotransmission induced by a 7 minute period of OGD (Coppi et al., 2007).

The lack of protection by RB-2 may be due to its non-specific effects. Alternatively, RB-2 might have a greater protective effect against delayed ischaemic cell death rather than the immediate necrotic death which I was investigating, since all the studies documenting a neuroprotective effect of this antagonist have shown that it prevents death 24 hours after a less severe ischaemic insult (Cavaliere et al., 2001a; Cavaliere et al., 2003; Melani et al., 2006). RB-2 also has some toxic effects: in CGN cultures, 24 hour incubation with 100uM RB-2 causes the death of 30% of cells (Volonte et al., 1999).

The significant prevention of ischaemic astrocyte death by PPADS is a novel finding of this study. Only a few mechanisms have so far been described which may explain why P2 antagonism during ischaemia protects astrocytes. Astrocytes transiently upregulate P2Y₁ and P2Y₂ immediately after a short period of OGD, leading to enhanced intracellular Ca²⁺ signalling and Ca²⁺ wave propagation (Iwabuchi and Kawahara, 2009a, b). One could speculate then that PPADS protects astrocytes by preventing such P2 receptor mediated Ca²⁺ signalling during ischaemia. Alternatively, P2 receptor activation has been linked to ROS formation in astrocytes (Murakami et al., 2003; Guerra et al., 2007; Kahlert et al., 2007). Whether or not this process occurs during ischaemia and contributes to P2 receptor activation induced astrocyte death is yet to be determined. Regardless of the mechanism(s) which may be involved, the combined protection of

astrocytes as well as neurons makes PPADS a particularly promising candidate for neuroprotection. Indeed, such a combined protective effect against astrocytic and neuronal death may explain why PPADS and the less selective P2 antagonists suramin and RB-2 significantly reduce the functional and/or histological sequelae of focal cerebral ischaemia *in vivo* (Kharlamov et al., 2002; Lammer et al., 2006; Melani et al., 2006).

P2X₇ receptor: possible contribution to neuronal death during OGD

Blocking P2X₇ receptors with KN-62 did not significantly reduce overall cell death of either astrocytes or neurons after 90 minutes of OGD. However, detailed analysis of KN-62 induced alterations to the dynamics of cell death revealed a potential contribution of P2X₇ receptors to OGD induced neuronal death. In the presence of KN-62, neuronal death was transiently significantly reduced after 75 and 80 minutes of ischaemia, and the mean time to cell death and average time to first cell death were both significantly delayed in neurons, suggesting that P2X₇ receptor activation may be involved in the early stages and/or initiation of neuronal death during OGD. A similar contribution of P2X₇ receptors to neuronal dysfunction early during OGD has been reported in rat hippocampal slices, where blocking P2X₇ receptors with the selective antagonist brilliant blue G (BBG) significantly delays the onset of anoxic depolarisation and prevents failure of neurotransmission in the CA1 region during a short 7 minute period of OGD (Coppi et al., 2007).

In agreement with the finding that overall cell death was not affected after 90 minutes of OGD, the intracerebroventricular administration of either BzATP or the irreversible selective P2X₇ antagonist 2',3',-Dialdehyde ATP (oxATP) failed to significantly influence the infarct volume following middle cerebral artery occlusion (MCAO) (Le Feuvre et al., 2003). A similar lack of protection *in vivo* against ischaemic injury was reported by the same group using P2X₇ knock-out (-/-) mice, with no reductions in infarct volumes measured after either 30 or 60 minutes of reversible MCAO followed by 24 hours of reperfusion or permanent MCAO (Le Feuvre et al., 2002; Le Feuvre et al., 2003). Furthermore, the sizes of excitotoxic lesions induced by the NMDA receptor agonist

methano-glutamate *in vivo* were not reduced in P2X₇ *-/-* animals or by three different selective P2X₇ antagonists, suggesting that these receptors are not involved in glutamate neurotoxicity (Le Feuvre et al., 2002; Le Feuvre et al., 2003). By contrast, a different study reported a complete prevention of OGD induced cellular damage by oxATP in organotypic hippocampal cultures, as demonstrated by reduced propidium iodide uptake 20 hours after 40 minutes of OGD (Cavaliere et al., 2004a).

These apparently contradictory results may be at least partially explained by the hypothesis that P2X₇ receptor activation causes the release of damaging glutamate or neuroprotective GABA from neurons depending on whether or not neurons in the culture/CNS region are predominantly glutamatergic or GABAergic (Wirkner et al., 2005). OGD causes increased P2X₇ receptor mediated GABA release in a population of predominantly GABAergic cultured cortical neurons during OGD (Wirkner et al., 2005). In the *in vivo* ischaemia experiments by Le Feuvre and colleagues mentioned above, infarcts following MCAO occurred in the predominantly GABAergic parietal cortex, so blocking P2X₇ receptors would have reduced GABA release, preventing its protective effects (Le Feuvre et al., 2002; Le Feuvre et al., 2003). The *in vitro* experiments by Cavaliere and colleagues used organotypic hippocampal cultures/slices containing much larger populations of glutamatergic neurons, so prevention of P2X₇ mediated glutamate release may theoretically account for the protective effect of antagonists here (Cavaliere et al., 2004a; Coppi et al., 2007). In further agreement with this theory, P2X₇ receptor blockade significantly reduces OGD induced glutamate release from hippocampal slices and improves functional/histological recovery following trauma to the spinal cord trauma: both of these structures contain little GABAergic innervation (Wang et al., 2004; Sperlagh et al., 2007). Mixed glial/neuronal cortical cell cultures similar to the ones I used may contain a large GABAergic population, so this could explain the relative lack of protection by KN-62 as well as the result that P2 receptors were not contributing significantly to glutamate release during OGD, although pure cortical neuron cultures have been demonstrated to be mainly glutamatergic (Kovacs et al., 2001; Milius et al., 2008; Fischer et al., 2009).

Another plausible explanation for why potentially neuroprotective effects of P2X₇ receptor blockade *in vitro* do not translate into reduced infarct volumes *in vivo* is the lack of protection against astrocyte death apparent in my experiments. The percentage of astrocyte death was not reduced at any time point during OGD, and there was no change in the mean time to cell death or average time to first cell death. In support of this hypothesis, Cavaliere and colleagues report that in rat organotypic hippocampal slice cultures, P2X₇ receptor expression 1 or 24 hours after 40-60 minutes of OGD is localized exclusively to neurites, while being absent in oligodendrocytes, astrocytes and neuronal cell bodies (Cavaliere et al., 2004a). Similarly, in cortical mixed cultures, 2 or 12 hours of OGD causes significant upregulation of P2X₇ expression in neurons but not astrocytes (Milius et al., 2008). Furthermore, *in vivo* studies have reported a localisation and upregulation of P2X₇ receptors exclusively on penumbral microglia 24 hours after focal ischaemia, with neuronal and astrocytic P2X₇ expression only becoming apparent 4 or 7 days after the insult (Collo et al., 1997; Franke et al., 2004; Melani et al., 2006). It appears therefore that there may be important differences relating to P2X₇ receptor signalling during ischaemia between *in vivo* and *in vitro* models of ischaemia as well as different CNS regions and cell types which warrant further investigation.

Several natural polymorphisms and two functional P2X₇ receptor splice variants have been described thus far which may at least partly account for some of the discrepancies and controversy surrounding many experimental findings pertaining to this receptor (Cheewatrakoolpong et al., 2005; Nicke et al., 2009). The first functional P2X₇ splice variant to be characterised lacks the C-terminus, is highly expressed in the human brain and maintains its ability to respond to ATP with cation movements although it is unable to produce large pore formation (Cheewatrakoolpong et al., 2005). Furthermore, it is not detected by the majority of commercial antibodies, which are directed towards the C-terminus (Cheewatrakoolpong et al., 2005). A second functional splice variant was recently described (P2X₇k) which contains an alternative N-terminus and first transmembrane domain (Nicke et al., 2009). P2X₇k undergoes pore dilation more rapidly and at lower agonist concentrations, and is widely expressed in the brain (Nicke et al., 2009). Moreover,

the receptor is still present and functional in one of the available P2X₇ *-/-* animals, highlighting one of the potential pitfalls of using knock-out models (Nicke et al., 2009). This is not the same mouse model used in the studies mentioned above which demonstrated a lack of changes in infarct volumes in P2X₇ *-/-* animals (Le Feuvre et al., 2002; Le Feuvre et al., 2003). Finally, an allelic mutation present in some commonly used strains of mice (C57BL/6 and DBA/2) has been shown to drastically reduce sensitivity of the receptor to ATP-induced large pore formation (Adriouch et al., 2002). Importantly, this study reports that BALB/c mice (the strain used for this project) do not carry this mutation (Adriouch et al., 2002). Similar impairment-of-function single amino acid substitution polymorphisms have been demonstrated in humans (reviewed in: Adriouch et al., 2009). These findings further emphasise the potential functional diversity of P2 receptors.

Potent reduction of OGD induced neuron and astrocyte death by P2Y₁ antagonism

A further novel finding of this study was the highly protective effect of blocking P2Y₁ receptors. Coppi and colleagues recently reported a protective effect of blocking P2Y₁ receptors during OGD: in hippocampal slices, MRS-2179 significantly delays and/or reduces the onset of anoxic depolarisation and failure of neurotransmission during a 7 minute exposure to OGD (Coppi et al., 2007). However, my results are the first to show that blocking P2Y₁ receptors can actually reduce cell death, even during prolonged OGD, and that both neurons and astrocytes are protected.

A number of other findings further support a therapeutic potential of P2Y₁ receptors during and after ischaemic brain injury. P2Y₁ receptor activation stimulates glutamate release from cultured hippocampal and spinal cord astrocytes but not neurons, and P2Y₁ receptor inhibition reduces ATP induced glutamate release from astrocytes (Domercq et al., 2006; Zeng et al., 2008b; Zeng et al., 2008a). Blocking P2Y₁ receptors may therefore theoretically reduce glutamate excitotoxicity, particularly in sensitive glutamatergic areas of the brain such as the hippocampus, even though this did not seem to be occurring in my preparation since PPADS did not reduce ischaemic glutamate efflux

from the co-culture (Chapter 3). Also, it has been suggested recently that blocking P2Y₁ receptors may reduce detrimental while increasing beneficial effects of reactive astrogliosis following ischaemia (Sun et al., 2008). MRS-2179 application *in vivo* or *in vitro* during transient ischaemic insults decreases post-ischaemic GFAP expression (a marker of astrogliosis) and increases glial-derived neurotrophic factor (GDNF) production (Sun et al., 2008). In addition, a heteromeric association and functional coupling of P2Y₁ and A₁ receptors has been demonstrated in neurons and astrocytes from rats as well as human astrocytes (Tonazzini et al., 2007; Tonazzini et al., 2008). Specifically, P2Y₁ receptor activation leads to heterologous desensitisation of A₁ receptor responses (Tonazzini et al., 2008). Prevention of A₁ receptor desensitisation may therefore be a potential mechanism by which P2Y₁ antagonists are protective during ischaemia, since A₁ receptor activation under such conditions is protective.

Continuously applying the P2Y₁ agonist MRS-2365 during OGD in co-cultures did not significantly affect cell death rates, although it significantly delayed the mean time to cell death of neurons. MRS-2365 has been shown to induce rapid desensitisation of P2Y₁ receptors in human platelets, so perhaps MRS-2365 only induced P2Y₁ receptor activation for a short period in these experiments (Bourdon et al., 2006). However, P2Y₁ receptor activation may also mediate protective effects of relevance to ischaemic injury. When cultured astrocytes are subjected to a period of sub-lethal OGD (ischaemic preconditioning), they become more resistant to a further prolonged ischaemic insult the following day (Iwabuchi and Kawahara, 2009b). This effect is partly mediated by P2Y₁ receptor activation, since the application of MRS-2179 during sub-lethal OGD significantly attenuates the protective effect of preconditioning (Iwabuchi and Kawahara, 2009b). The protective effects of P2Y₁ receptor activation after preconditioning are produced by enhanced expression of phosphorylated ERK1/2, signals which are known to promote cell proliferation and suppress death signals (Iwabuchi and Kawahara, 2009b). Furthermore, a neuroprotective effect of P2Y₁ receptor activation in preventing H₂O₂ induced neuronal and astrocyte death has been described (Fujita et al., 2009). Specifically, ATP application protects astrocytes in monoculture or co-culture and neurons in co-

cultures but not neurons in monoculture from H₂O₂ injury, and this is prevented by MRS-2179 or P2Y₁-selective siRNAs (Fujita et al., 2009). As neurons are only protected by ATP when co-cultured with astrocytes or grown in astrocyte conditioned medium, a diffusible factor released by astrocytes is mediating the effect: this was found to be IL-6 (Fujita et al., 2009). Therefore, given the therapeutic potential suggested by my results, effects of P2Y₁ antagonists during ischaemia need to be further investigated, in particular to find out whether the protective effect which was apparent during 90 minutes of OGD will translate into a protective effect after periods of reperfusion and during *in vivo* ischaemia.

Synergistic protective effect of P2 and glutamate receptor antagonists during ischaemia

Finally, the combined effect of blocking P2 and glutamate receptors simultaneously was tested. Initially, suramin (100uM), NBQX (30uM) and MK-801 (10uM) were added to the co-culture together: this combination completely prevented cell death during 90 minutes of OGD, and was significantly more protective than either suramin or the combination of NBQX + MK-801, suggesting a synergistic protective effect. To further investigate the possibility of synergistic protection by blocking P2 and ionotropic glutamate receptors, a combination of PPADS (1uM), NBQX (3uM) and MK-801 (1uM) was applied: by using PPADS instead of suramin and reduced concentrations of the antagonists, non-specific effects are highly unlikely. This combination was also significantly protective, reducing cell death of astrocytes and neurons by 83%/95% respectively, whilst also significantly delaying the onset and mean time to cell death more than any other antagonist combination, confirming the synergistic protective effect of blocking P2 and NMDA/non-NMDA receptors.

A similar combinatorial protective effect was suggested in a study by Runden-Pran and colleagues, where the combination of suramin (200uM) and MK-801 (100uM) significantly attenuates cell death in hippocampal slice cultures undergoing a protocol of 32 minutes of OGD followed by up to 48 hours of re-oxygenation, with cell death being assessed by propidium iodide uptake (Runden-Pran et al., 2005). However, this was not

significantly more protection than was afforded by either antagonist on its own, and the use of such a high concentration of suramin does not provide specific insight into P2 receptor mediated events (Runden-Pran et al., 2005). Furthermore, OGD exclusively injured neurons in the CA1 region of hippocampus, and significant cell death only occurred 3 hours after reperfusion (Runden-Pran et al., 2005). Therefore my data is the first to confirm that a combinatorial approach blocking P2 and ionotropic glutamate receptors provides synergistic protection against the ischaemic death of astrocytes and neurons.

Final Summary

Ischaemia caused significant death of both astrocytes and neurons in co-cultures, with astrocytes playing a crucial part in the pathogenesis of neuronal death. Cell death in both neurons and astrocytes was always preceded by a large rise in $[Ca^{2+}]_i$. The application of exogenous ATP and/or glutamate during control and ischaemic conditions in neuronal cultures and co-cultures revealed complex effects of these two substances, suggesting that they may mediate both harmful and beneficial components. The significant degree of protection afforded by various P2 receptor antagonists strongly suggest that P2 receptor activation plays an important part in mediating the early necrotic phase of astrocyte and neuronal death occurring during severe ischaemia. P2Y₁ receptors in particular appear to be involved in the death of both neurons and astrocytes, while P2X₇ receptors may contribute to the onset of neuronal death. The application of NMDA and non-NMDA receptor antagonists confirmed that these receptors are only involved in neuronal death. Finally, a highly protective synergistic effect of blocking P2 receptors and ionotropic glutamate receptors simultaneously during ischaemia was revealed. In conclusion, these results provide evidence that parallel pathways of P2 and glutamate receptor mediated excitotoxicity produce astrocyte and neuronal death, and that protective strategies aimed at preventing them both may provide superior outcomes after CNS ischaemia.

Chapter 6:
Final conclusions, discussion and perspectives

In this thesis I investigated the possible contributions of ATP and glutamate mediated excitotoxicity to the death of cultured cortical neurons and astrocytes during the first 90 minutes of a severe ischaemic insult (OGD). Cultures of neurons, astrocytes or co-cultures of both cell types were used to determine the relative contributions of these two cell types as well as the importance of astrocyte-neuron interactions to the processes involved in ischaemic cell death.

Summary of results

For ATP and glutamate mediated excitotoxic cascades to exist, cells must release excessive ATP and glutamate during ischaemia. As described in Chapter 3, ATP and glutamate efflux was measured from different cultures using biosensor microelectrodes, allowing for a uniquely detailed comparison of the dynamics of glutamate and ATP release during ischaemia. OGD induced significant release of both ATP and glutamate from co-cultures. Both substances were released soon after the onset of OGD, although direct comparison revealed that ATP levels were lower and reached statistical significance later than glutamate. Astrocytes, but not neurons, contributed the majority of glutamate release during OGD, since significant glutamate release only occurred from the astrocyte cultures and co-cultures. Furthermore, glutamate release from co-cultures could not be attenuated by PPADS, suggesting that P2 receptor activation was not contributing to ischaemic glutamate release. Excessive ischaemic ATP release was only consistently detectable in the co-culture, giving rise to the novel suggestion that astrocytes and neurons interact/co-operate by an unknown mechanism to release ATP or enhance extracellular ATP accumulation during ischaemia.

A second pre-requisite for ATP and glutamate mediate excitotoxicity is the functional expression of P2 and glutamate receptors on neurons and astrocytes. This was investigated in Chapter 4, where functional receptor responses were detected using Fura-2 Ca^{2+} imaging. This also allowed the efficacy of a range of P2 and glutamate receptor antagonists to be tested in these cells. Results revealed widespread ionotropic and metabotropic glutamate receptor responses in neuronal cultures, while only a very small

percentage of cultured astrocytes expressed functional glutamate receptors, which were mostly metabotropic. Additionally, cortical cultured neurons and astrocytes expressed a variety of functional P2 receptors, with 100% of astrocytes and approximately 60% of neurons responding. In both cell types, there was a dominant contribution of P2Y over P2X receptors. Although far from exhaustive, a limited P2 receptor subtype expression profile obtained using multiple P2 agonists/antagonists and P2Y₁^{-/-} astrocytes suggested the functional expression on neurons and astrocytes of P2Y₁ and P2Y₆, with a possibility of P2Y₂ and/or P2Y₄, while astrocytes in particular probably also expressed functional P2X₇ receptors.

Contributions of purinergic and glutamatergic signaling to early ischaemic cell death were investigated in Chapter 5. Ischaemia caused significant death of both astrocytes and neurons in co-cultures, with astrocytes playing a crucial role in the pathogenesis of ischaemic neuronal death. Cell death of both neurons and astrocytes was always preceded by a large rise in [Ca²⁺]_i. The application of exogenous ATP and/or glutamate during control and ischaemic conditions in neuronal cultures and co-cultures revealed complex effects of these two substances, suggesting that they may mediate both harmful and beneficial components. The significant degree of protection afforded by various P2 receptor antagonists strongly suggest that P2 receptor activation plays an important part in mediating the early necrotic phase of astrocyte and neuronal death occurring during severe ischaemia. P2Y₁ receptors in particular appear to be involved in the death of both neurons and astrocytes, while P2X₇ receptors may contribute to the onset of neuronal death. The application of NMDA and non-NMDA receptor antagonists confirmed that these receptors are only involved in neuronal death. Finally, a highly protective synergistic effect of blocking P2 receptors and ionotropic glutamate receptors simultaneously during ischaemia was revealed.

A final model summarising results regarding the purinergic and glutamatergic events involved in astrocyte and neuronal death during OGD is presented in **Figure 6-1**.

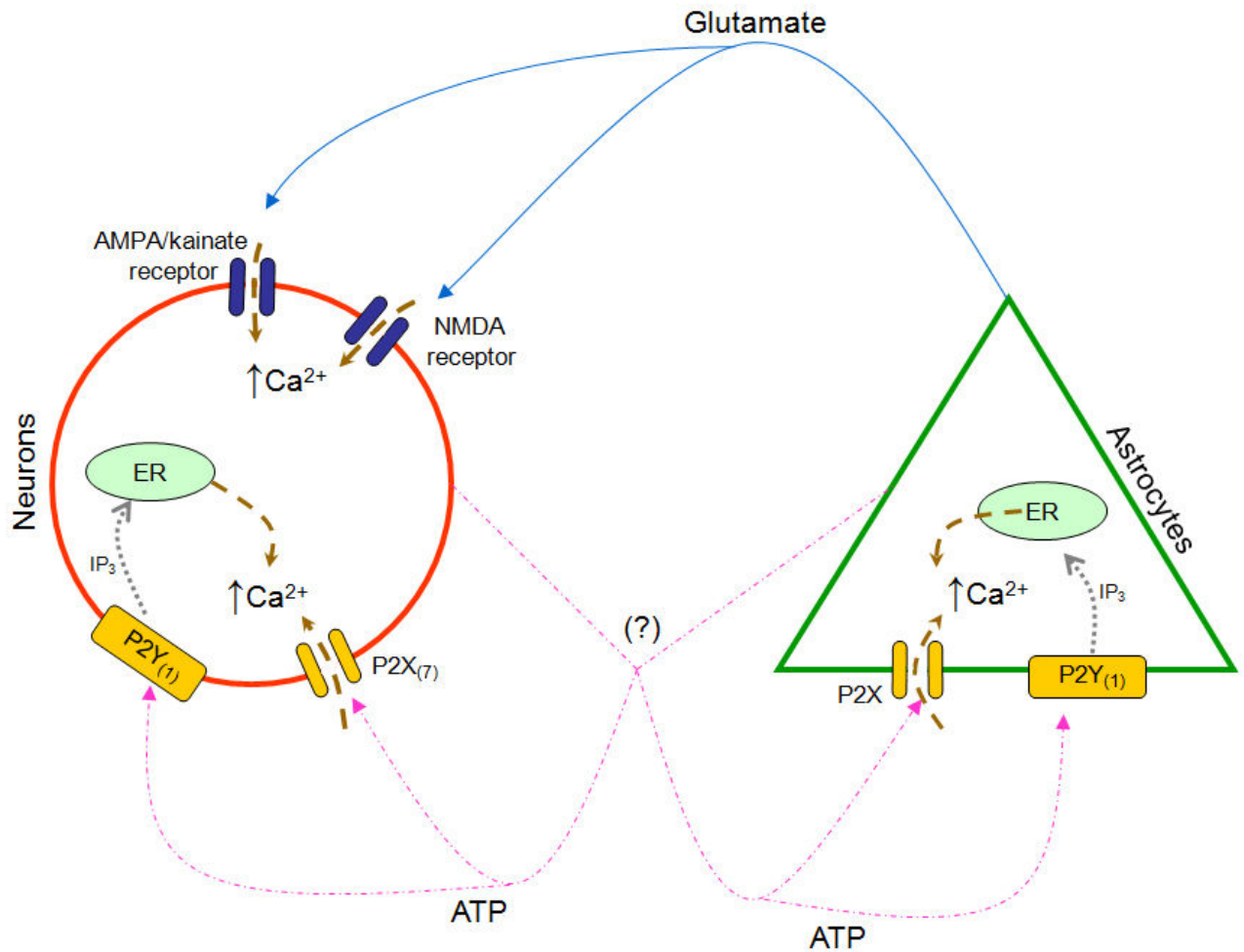


Figure 6-1: Final model of purinergic and glutamatergic events involved in astrocyte and neuronal death during OGD

Within a few minutes of onset of ischaemia, excess glutamate and ATP accumulate in the extracellular space. Glutamate is released by astrocytes, while the source of ATP is less clear.

Glutamate causes increased neuronal death by gating AMPA/kainate and NMDA receptors, leading to Ca²⁺ influx.

ATP activates P2 receptors on both astrocytes and neurons, leading to Ca²⁺ release from intracellular stores (P2Y receptors) and/or Ca²⁺ influx through P2X ion channels. P2Y₁ receptors in particular were present on both cell types and mediated cell death. P2X₇ receptors may be involved in early neuronal but not astrocyte death. Other P2 receptor subtypes may be involved but this will need to be further investigated as and when newer more selective agonists/antagonists become available.

Protective effect of P2 receptor antagonists does not appear to be mediated by interference with glutamate excitotoxicity

The protective effect of P2 receptor antagonists is unlikely to have been linked to glutamate excitotoxicity in my experiments for a number of reasons. First of all, PPADS application did not reduce ischaemic glutamate release from co-cultures, thus removing the possibility that P2 antagonists were protective during ischaemia by preventing glutamate release. Secondly, glutamate receptor antagonists only significantly reduced neuronal ischaemic death, while P2 antagonists also protected astrocytes, mirroring the functional receptor expression profile. Various non-selective P2 antagonists, including suramin and RB-2 have been shown to block or otherwise modulate ionotropic glutamate receptor functions (Balcar et al., 1995; Nakazawa et al., 1995; Price and Raymond, 1996; Ong et al., 1997; Gu et al., 1998; Peoples and Li, 1998; Zona et al., 2000; Ortinau et al., 2003; Suzuki et al., 2004). However, neither PPADS nor MRS-2179 interferes directly with glutamate receptors (Volonte et al., 1999; Lin et al., 2005). In my experiments, both MRS-2179 and PPADS, the latter even at reduced concentrations, significantly attenuated cell death despite having no activity at glutamate receptors. Finally, when glutamate and P2 receptor antagonists were combined, the protective effect was synergistic. Thus, ATP and glutamate excitotoxic cascades appear to operate in parallel rather than in unison during ischaemia.

Potential roles of purinergic signaling beyond the initial phase of necrotic cell death

Having established their importance in mediating early ischaemic cell death, it would be important to investigate the role of purinergic mechanisms in cell death and survival after reperfusion or during infarct maturation. In rat hippocampal slices, extracellular ATP levels increase to almost 3 times the already significant level reached during a prior 15 minute period of OGD, suggesting that ATP-mediated excitotoxicity may be further exacerbated during reperfusion (Freguelli et al., 2007). Furthermore, P2 receptors appear to be intimately involved in the regulation of ROS formation in both astrocytes and neurons, a process which contributes to cell death particularly after reperfusion (Kahlert et al., 2007). Finally, further evidence is provided by the finding that

P2 receptor antagonists prevent delayed neuronal death in various models of ischaemia + reperfusion (Cavaliere et al., 2003; Cavaliere et al., 2004a; Cavaliere et al., 2005; Runden-Pran et al., 2005; Cavaliere et al., 2007).

Purinergic signaling may also be crucial to the reparative/reactive processes activated after ischaemia. For instance, P2 receptor stimulation appears to be intimately involved in astrogliosis, a process producing both harmful and beneficial effects in the post-ischaemic brain (Neary et al., 1994a; Neary et al., 1994b; Franke et al., 2001; Neary et al., 2006). *In vitro* application of ATP or P2 agonists causes stellation, increased GFAP expression and proliferation of astrocytes (Neary et al., 1994a; Neary et al., 1994b; Neary et al., 2006). Furthermore, the direct application of a variety of P2 agonists in the nucleus acumbens *in vivo* produces an astroglial reaction characterized by hypertrophy of astrocytes, elongation of astrocyte processes and up-regulation of GFAP, all of which can be reduced by the application of P2 antagonists (Franke et al., 2001). Growth promoting and inhibiting factors, cytokines and other mitogens and morphogens are produced by reactive astrocytes, some of which may impede axonal regeneration, while others are involved in axonal guidance and neuronal survival (Neary et al., 2006). Harmful and beneficial effects may be differentially regulated by different P2 receptor subtypes (Neary et al., 2006).

It appears therefore that P2 receptor antagonists used for ischaemia treatment may produce complex and varied actions at different time points during and after the acute ischaemic event. More detailed studies into the roles of purinergic signaling during such events will be required to produce a more complete perspective of how different interventions will affect harmful and/or beneficial processes after ischaemia, such that treatment can be tailored to produce maximal neuroprotection.

Potential for ATP-mediated excitotoxicity in white matter and oligodendrocytes

Since P2 receptor antagonists were highly protective of astrocytes, they may have significant potential in reducing white matter injury, as this tissue is rich in glial cells. In a BSc project I undertook prior to starting my PhD, I found that suramin was able to

significantly attenuate OGD induced astrocyte death in the neonatal RON (Vermehren, 2005). Oligodendrocytes are a further important component of white matter, and these cells are known to be exquisitely sensitive to ischaemic injury (Lyons and Kettenmann, 1998; Fern and Moller, 2000; Tekkok and Goldberg, 2001; Wilke et al., 2004; Salter and Fern, 2005). Oligodendrocytes and myelin express functional P2X₇ receptors which can mediate cell death *in vitro* and *in vivo* following prolonged ATP or BzATP application (James and Butt, 2001, 2002; Matute et al., 2007). They have also been shown to express other P2 receptors including both P2X subtypes and P2Y_{1,2,12} (reviewed in: James and Butt, 2002). However, whether or not ATP mediated excitotoxicity contributes to oligodendrocyte injury and/or death during ischaemic insults is yet to be determined, but protection of white matter against ischaemic and excitotoxic injury has therapeutic potential in many disorders.

Possible contributions of microglia to ischaemic cell death

It is important to consider the possibility that even the relatively small numbers of microglia present in my cultures may contribute significantly to cytotoxicity during OGD (Saura, 2007). Microglia are rapidly activated by even small changes in the local environment, a process leading to varying degrees of proliferation, migration, electrophysiological changes, and perhaps most importantly the secretion of soluble products including cytokines, proteases, free radicals and growth factors which all play an important role in determining cell death or survival following CNS injury (Ferrari et al., 1997; Cavaliere et al., 2005; Pinteaux et al., 2006; Skaper et al., 2006; Thornton et al., 2006; Hailer, 2008; Kaushal and Schlichter, 2008; Wang et al., 2008; Montero et al., 2009). There is strong evidence that microglia have the potential to contribute to neuronal death. One study reports that glutamate released during OGD by neurons activates co-cultured microglia via group II metabotropic glutamate receptors, which in turn initiates a neurotoxic activity of microglia mediated by tumor necrosis factor- α (TNF- α) release which in turn activates both caspase-8 and caspase-3 in neurons leading to apoptosis (Kaushal and Schlichter, 2008).

Purinergic mechanisms may also be involved. Microglia are known to strongly express P2 receptors, including P2X₇ receptors, making them highly sensitive to P2-agonist mediated toxicity (Ferrari et al., 1997; Inoue, 2008; Crain et al., 2009). P2X₇ activation by BzATP in microglia co-cultured with neurons leads to neuronal injury, as neuronal injury is prevented when microglia but not neurons are derived from P2X₇ -/- mice, or when P2X₇ receptors are pharmacologically blocked, with the damaging effects of microglia at least partly mediated by ROS (Skaper et al., 2006). In agreement, P2X₇ receptor activation on primary microglia has been shown to stimulate the release of copious amounts of superoxide (Parvathenani et al., 2003). Furthermore, P2X₇ receptors appear to be intimately involved with the process of microglial proliferation, as blockage or down-regulation of the receptor severely decreases microglial proliferation while over-expressing it enhances proliferation (Bianco et al., 2006; Monif et al., 2009). However, it must also be taken into account that microglia have the capacity to secrete factors which can promote neuronal survival or regeneration, so it is still uncertain whether the net effect of microglial contributions during acute CNS injury is protective or damaging (reviewed in: Hailer, 2008). For example, hippocampal slice cultures depleted of microglia demonstrated significantly increased neuronal death and astrogliosis one day after OGD compared with cultures where microglial numbers were not reduced, suggesting a neuroprotective role of microglia after OGD (Montero et al., 2009). It is essential to note though that most of the potential mechanisms by which microglia have been shown to influence cell death or survival during ischaemia are unlikely to contribute significantly within the short time window that was being observed in my experiments.

Considerations regarding stroke therapy: prophylactic neuroprotective strategies using a combination of glutamate and P2 receptor antagonists

The disappointing or mixed outcomes of the majority of preclinical trials testing non-vascular neuroprotective strategies in humans have fostered a nihilistic view of acute stroke therapies (O'Collins et al., 2006; Besancon et al., 2008; Ginsberg, 2008). These strategies have generally focused on reducing delayed cell death in the penumbra, an area which has classically been viewed as most amenable to therapeutic interventions,

particularly as the time window during which interventions may still theoretically produce benefit stretches up to 4-6 hours after the onset of ischaemia (Ginsberg, 2008). However, the administration of neuroprotectants within even such a prolonged time window has proven difficult in clinical practice (Ginsberg, 2008). Furthermore, neurological deficits in stroke patients are the consequence of massive tissue destruction in the infarct core, while selective neuronal injury in the penumbra is unlikely to contribute to the severity of stroke outcome (Nedergaard and Dirnagl, 2005). Therefore, targeting mechanisms involved in the pan-necrotic death of all cell types in an ischaemic core may provide enhanced neuroprotective strategies (Nedergaard and Dirnagl, 2005). Cells within the infarct core become irreversibly injured within 30 minutes of stroke onset (Garcia et al., 1993). Additionally, the progression from selective neuronal loss to pan-cellular necrosis within an infarct and at the edge of the penumbra depends on the fate and function of astrocytes (Chesler, 2005). As a result, strategies aimed at mitigating cell death in this area would need to target astrocytes and neurons as well as requiring a prophylactic rather than reactionary treatment protocol, since the therapeutic window for interventions after the onset of ischaemia would be in the order of minutes rather than hours.

The identification of patients at a high stroke risk already currently forms a vital component of their management (Hankey and Eikelboom). Presently, prophylactic pharmacological interventions in stroke therapy are focused on the prevention of thrombotic events, using drugs such as aspirin and warfarin (Hankey and Eikelboom). It seems conceivable that medication aimed at reducing the extent of necrotic cell death could be added to such a prophylactic regimen in this group of patients. However, prophylaxis will require medication with acceptable side-effect profiles. This has been one of the major problems with ionotropic glutamate receptor antagonists for stroke therapy: therapeutic levels are accompanied by unacceptable psychotropic side-effects (Ikonomidou and Turski, 2002; Besancon et al., 2008). For instance, synaptic transmission by NMDA receptors is essential for neuronal survival, so complete block is unwanted (Ikonomidou et al., 2000; Ikonomidou and Turski, 2002). Thus, many neuroprotective drugs have failed to live up

to their promise due to side effects caused by their interference with normal brain functions (Lipton, 2007).

ATP appears to be involved vitally in glial-glial and neuron-glial signalling, so drugs which interfere with this may produce similar consequences to the glutamate receptor antagonists. Moreover, when one considers the widespread expression of many P2 receptor subtypes throughout various tissues and organs, the potential is there for unwanted side-effects (Burnstock and Knight, 2004). Currently, the only clinically available P2 receptor antagonists are a group of P2Y₁₂ antagonists used as anti-platelet agents (eg. Clopidogrel). These are widely used and generally well tolerated, but the active metabolites do not cross the blood brain barrier (Founztopoulous et al., 2007). Nonetheless, some information about potential side effects can be garnered from different P2 receptor knockout (ko) models. Although the vast majority are viable and not obviously distinguishable from wild-type mice, some phenotypic abnormalities have been described. For example, P2X₁ ko males are infertile due to reduced vas deferens contractility, P2Y₂ ko mice suffer from salt-resistant arterial hypertension, and P2Y₁ ko mice have inhibited platelet aggregation/increased bleeding time/resistance to thromboembolism (Homolya et al., 1999; Leon et al., 1999; Mulryan et al., 2000; Solle et al., 2001; Cockayne et al., 2005; Abbracchio et al., 2006; Sim et al., 2006; Rieg et al., 2007). P2Y₁ receptors may also be involved in motivation-related behaviour and anxiety (reviewed in: Kittner et al., 2004).

A number of strategies may be used to minimize the impact of neuroprotective agents on normal brain functions. The NMDA receptor antagonist memantine circumvents this problem thanks to its unique pharmacological properties: memantine blocks NMDA receptors by binding uncompetitively to a cryptic allosteric site which only becomes exposed during pathological over-activation of the receptor, and once the binding site is no longer exposed the drug can no longer produce blockade due to its fast off-rate (Lipton, 2007). Importantly, memantine has been shown to be neuroprotective against ischaemic grey and white matter injury *in situ* and *in vivo* in rats, and is already licensed for use in humans (Chen et al., 1998; Xiong et al., 2004; Bakiri et al., 2008; Manning et al.,

2008). This type of approach should allow for the development of drugs which preferentially inhibit pathological activation of their targets while preserving normal brain functions (Lipton, 2007). Alternatively, downstream effectors of receptor induced neurotoxicity could be targeted for neuroprotection, as this approach should theoretically prevent unwanted impediment of normal physiological functions, thereby reducing side-effects. For example, NMDA receptors have been shown to be linked via a protein called PSD-95 to neuronal nitric oxide synthase (nNOS), and a PSD-95 inhibitory peptide protected cultured neurons from glutamate excitotoxicity and dramatically reduced cerebral infarct volumes and improved neurological functions in rats subjected to transient focal cerebral ischaemia (Aarts et al., 2002). The downstream effectors of P2 receptor toxicity during ischaemia remain to be elucidated, but may offer interesting targets.

A further potential method for reducing side-effects may be provided by using a combination of drugs targeting different cell death pathways at reduced concentrations. My results demonstrating synergistic protection by a combination of PPADS, MK-801 and NBQX supports this theory. Synergistic neuroprotection has previously been demonstrated for combinatorial therapies *in vitro* and *in vivo*: for example, blocking a combination of NMDA and P2 receptors as well as mitogen activated protein kinases provides virtually complete protection in hippocampal slice cultures subjected to OGD, while a combination of caspase inhibitors and MK-801 produced synergistic protection and prolonged the therapeutic windows in mice subjected to 2 hours of MCAO (Ma et al., 1998; Runden-Pran et al., 2005). An important next step will therefore involve validation of the protective effect of combining of P2 and ionotropic glutamate receptor antagonists at reduced concentrations using *in vivo* models of ischaemia.

Final thoughts

Over the past few years, numerous new subtype-selective P2 receptor agonists and antagonists have become available (some have been included in **Tables 4-2 to 4-5** for future reference). This includes antagonists with good oral bioavailability and brain penetration which may be useful for future *in vivo* work (Stokes et al., 2006; Carroll et al.,

2009; Jacobson et al., 2009; Jarvis and Khakh, 2009). Furthermore, P2 receptor knockout animals are available now for almost all receptor subtypes. Therefore, the combined use of new antagonists and knock-out animals in future studies should allow for detailed investigations into which P2 receptors are involved in mediating ischaemic injury.

In conclusion, this thesis presents data which suggests that parallel pathways of ATP and glutamate excitotoxicity operate during ischaemia, which require the co-operation of both astrocytes and neurons, and that concomitant blockade of both at the receptor level provides synergistic neuroprotection by preventing both astrocyte and neuronal death during the initial phase of a severe ischaemic insult. My hope is that these findings will provide a platform for further studies which will ideally produce novel and powerful strategies for neuroprotection, perhaps via a prophylactic approach, to reduce the mortality and morbidity associated with cerebral ischaemic events.

Bibliography

- Aarts M, Iihara K, Wei WL, Xiong ZG, Arundine M, Cerwinski W, MacDonald JF, Tymianski M (2003) A key role for TRPM7 channels in anoxic neuronal death. *Cell* 115:863-877.
- Aarts M, Liu Y, Liu L, Besshoh S, Arundine M, Gurd JW, Wang YT, Salter MW, Tymianski M (2002) Treatment of ischemic brain damage by perturbing NMDA receptor- PSD-95 protein interactions. *Science* 298:846-850.
- Aarts MM, Tymianski M (2005) TRPMs and neuronal cell death. *Pflugers Arch* 451:243-249.
- Abbracchio MP, Burnstock G, Verkhratsky A, Zimmermann H (2009) Purinergic signalling in the nervous system: an overview. *Trends Neurosci* 32:19-29.
- Abbracchio MP, Burnstock G, Boeynaems JM, Barnard EA, Boyer JL, Kennedy C, Knight GE, Fumagalli M, Gachet C, Jacobson KA, Weisman GA (2006) International Union of Pharmacology LVIII: update on the P2Y G protein-coupled nucleotide receptors: from molecular mechanisms and pathophysiology to therapy. *Pharmacol Rev* 58:281-341.
- Abdullaev IF, Rudkouskaya A, Schools GP, Kimelberg HK, Mongin AA (2006) Pharmacological comparison of swelling-activated excitatory amino acid release and Cl⁻ currents in cultured rat astrocytes. *J Physiol* 572:677-689.
- Adamchik Y, Baskys A (2000) Glutamate-mediated neuroprotection against N-methyl-D-aspartate toxicity: a role for metabotropic glutamate receptors. *Neuroscience* 99:731-736.
- Aden U, Halldner L, Lagercrantz H, Dalmau I, Ledent C, Fredholm BB (2003) Aggravated brain damage after hypoxic ischemia in immature adenosine A2A knockout mice. *Stroke* 34:739-744.
- Adriouch S, Dox C, Welge V, Seman M, Koch-Nolte F, Haag F (2002) Cutting edge: a natural P451L mutation in the cytoplasmic domain impairs the function of the mouse P2X7 receptor. *J Immunol* 169:4108-4112.
- Adriouch S, Scheuplein F, Bähring R, Seman M, Boyer O, Koch-Nolte F, Haag F (2009) Characterisation of the R276A gain-of-function mutation in the ectodomain of murine P2X7. *Purinergic Signal* 5:151-161.
- Aihara H, Fujiwara S, Mizuta I, Tada H, Kanno T, Tozaki H, Nagai K, Yajima Y, Inoue K, Kondoh T, Motooka Y, Nishizaki T (2002) Adenosine triphosphate accelerates recovery from hypoxic/hypoglycemic perturbation of guinea pig hippocampal neurotransmission via a P(2) receptor. *Brain Res* 952:31-37.
- Alexander SP, Mathie A, Peters JA (2008) Guide to Receptors and Channels (GRAC), 3rd edition. *Br J Pharmacol* 153 Suppl 2:S1-209.
- Almeida T, Rodrigues RJ, de Mendonca A, Ribeiro JA, Cunha RA (2003) Purinergic P2 receptors trigger adenosine release leading to adenosine A2A receptor activation and facilitation of long-term potentiation in rat hippocampal slices. *Neuroscience* 122:111-121.
- Amadio S, D'Ambrosi N, Cavaliere F, Murra B, Sancesario G, Bernardi G, Burnstock G, Volonte C (2002) P2 receptor modulation and cytotoxic function in cultured CNS neurons. *Neuropharmacology* 42:489-501.
- Amadio S, D'Ambrosi N, Trincavelli ML, Tuscano D, Sancesario G, Bernardi G, Martini C, Volonte C (2005) Differences in the neurotoxicity profile induced by ATP and ATP_γS in cultured cerebellar granule neurons. *Neurochem Int* 47:334-342.
- Anderson CM, Swanson RA (2000) Astrocyte glutamate transport: review of properties, regulation, and physiological functions. *Glia* 32:1-14.
- Ankarcrona M, Dypbukt JM, Bonfoco E, Zhivotovsky B, Orrenius S, Lipton SA, Nicotera P (1995) Glutamate-induced neuronal death: a succession of necrosis or apoptosis depending on mitochondrial function. *Neuron* 15:961-973.
- Araque A, Perea G (2004) Glial modulation of synaptic transmission in culture. *Glia* 47:241-248.
- Arcuino G, Lin JH, Takano T, Liu C, Jiang L, Gao Q, Kang J, Nedergaard M (2002) Intercellular calcium signaling mediated by point-source burst release of ATP. *Proc Natl Acad Sci U S A* 99:9840-9845.
- Arundine M, Tymianski M (2003) Molecular mechanisms of calcium-dependent neurodegeneration in excitotoxicity. *Cell Calcium* 34:325-337.

- Atterbury-Thomas AE, Leon C, Gachet C, Forsythe ID, Evans RJ (2008) Contribution of P2Y(1) receptors to ADP signalling in mouse spinal cord cultures. *Neurosci Lett* 435:190-193.
- Auld DS, Robitaille R (2003) Glial cells and neurotransmission: an inclusive view of synaptic function. *Neuron* 40:389-400.
- Ayoub AE, Salm AK (2003) Increased morphological diversity of microglia in the activated hypothalamic supraoptic nucleus. *J Neurosci* 23:7759-7766.
- Baker DA, McFarland K, Lake RW, Shen H, Tang XC, Toda S, Kalivas PW (2003) Neuroadaptations in cystine-glutamate exchange underlie cocaine relapse. *Nat Neurosci* 6:743-749.
- Bakiri Y, Hamilton NB, Karadottir R, Attwell D (2008) Testing NMDA receptor block as a therapeutic strategy for reducing ischaemic damage to CNS white matter. *Glia* 56:233-240.
- Bakiri Y, Burzomato V, Frugier G, Hamilton NB, Karadottir R, Attwell D (2009) Glutamatergic signaling in the brain's white matter. *Neuroscience* 158:266-274.
- Bal-Price A, Moneer Z, Brown GC (2002) Nitric oxide induces rapid, calcium-dependent release of vesicular glutamate and ATP from cultured rat astrocytes. *Glia* 40:312-323.
- Balcar VJ, Dias LS, Li Y, Bennett MR (1995) Inhibition of [³H]CGP 39653 binding to NMDA receptors by a P2 antagonist, suramin. *Neuroreport* 7:69-72.
- Banker BQ, Larroche JC (1962) Periventricular leukomalacia of infancy. A form of neonatal anoxic encephalopathy. *Arch Neurol* 7:386-410.
- Bano D, Nicotera P (2007) Ca²⁺ signals and neuronal death in brain ischemia. *Stroke* 38:674-676.
- Barres BA (1991) Glial ion channels. *Curr Opin Neurobiol* 1:354-359.
- Baurand A, Raboisson P, Freund M, Leon C, Cazenave JP, Bourguignon JJ, Gachet C (2001) Inhibition of platelet function by administration of MRS2179, a P2Y1 receptor antagonist. *Eur J Pharmacol* 412:213-221.
- Beaman-Hall CM, Leahy JC, Benmansour S, Vallano ML (1998) Glia modulate NMDA-mediated signaling in primary cultures of cerebellar granule cells. *J Neurochem* 71:1993-2005.
- Beck J, Lenart B, Kintner DB, Sun D (2003) Na-K-Cl cotransporter contributes to glutamate-mediated excitotoxicity. *J Neurosci* 23:5061-5068.
- Beindl W, Mitterauer T, Hohenegger M, Ijzerman AP, Nanoff C, Freissmuth M (1996) Inhibition of receptor/G protein coupling by suramin analogues. *Mol Pharmacol* 50:415-423.
- Bennett GC, Ford AP, Smith JA, Emmett CJ, Webb TE, Boarder MR (2003) P2Y receptor regulation of cultured rat cerebral cortical cells: calcium responses and mRNA expression in neurons and glia. *Br J Pharmacol* 139:279-288.
- Benveniste H (1991) The excitotoxin hypothesis in relation to cerebral ischemia. *Cerebrovasc Brain Metab Rev* 3:213-245.
- Benveniste H, Drejer J, Schousboe A, Diemer NH (1984) Elevation of the extracellular concentrations of glutamate and aspartate in rat hippocampus during transient cerebral ischemia monitored by intracerebral microdialysis. *J Neurochem* 43:1369-1374.
- Besancon E, Guo S, Lok J, Tymianski M, Lo EH (2008) Beyond NMDA and AMPA glutamate receptors: emerging mechanisms for ionic imbalance and cell death in stroke. *Trends Pharmacol Sci* 29:268-275.
- Bevensee MO, Schwiening CJ, Boron WF (1995) Use of BCECF and propidium iodide to assess membrane integrity of acutely isolated CA1 neurons from rat hippocampus. *J Neurosci Methods* 58:61-75.
- Bianchi BR, Lynch KJ, Touma E, Niforatos W, Burgard EC, Alexander KM, Park HS, Yu H, Metzger R, Kowaluk E, Jarvis MF, van Biesen T (1999) Pharmacological characterization of recombinant human and rat P2X receptor subtypes. *Eur J Pharmacol* 376:127-138.
- Bianco F, Colombo A, Saglietti L, Lecca D, Abbracchio MP, Matteoli M, Verderio C (2009) Different properties of P2X(7) receptor in hippocampal and cortical astrocytes. *Purinergic Signal* 5:233-240.
- Bianco F, Ceruti S, Colombo A, Fumagalli M, Ferrari D, Pizzirani C, Matteoli M, Di Virgilio F, Abbracchio MP, Verderio C (2006) A role for P2X7 in microglial proliferation. *J Neurochem* 99:745-758.
- Bjorklund O, Shang M, Tonazzini I, Dare E, Fredholm BB (2008) Adenosine A1 and A3 receptors protect astrocytes from hypoxic damage. *Eur J Pharmacol* 596:6-13.
- Bodin P, Burnstock G (2001) Purinergic signalling: ATP release. *Neurochem Res* 26:959-969.
- Bolanos JP, Heales SJ, Peuchen S, Barker JE, Land JM, Clark JB (1996) Nitric oxide-mediated mitochondrial damage: a potential neuroprotective role for glutathione. *Free Radic Biol Med* 21:995-1001.

- Bona E, Aden U, Gilland E, Fredholm BB, Hagberg H (1997) Neonatal cerebral hypoxia-ischemia: the effect of adenosine receptor antagonists. *Neuropharmacology* 36:1327-1338.
- Bondarenko A, Chesler M (2001a) Calcium dependence of rapid astrocyte death induced by transient hypoxia, acidosis, and extracellular ion shifts. *Glia* 34:143-149.
- Bondarenko A, Chesler M (2001b) Rapid astrocyte death induced by transient hypoxia, acidosis, and extracellular ion shifts. *Glia* 34:134-142.
- Bondarenko A, Svichar N, Chesler M (2005) Role of Na⁺-H⁺ and Na⁺-Ca²⁺ exchange in hypoxia-related acute astrocyte death. *Glia* 49:143-152.
- Bourdon DM, Mahanty SK, Jacobson KA, Boyer JL, Harden TK (2006) (N)-methanocarba-2MeSADP (MRS2365) is a subtype-specific agonist that induces rapid desensitization of the P2Y1 receptor of human platelets. *J Thromb Haemost* 4:861-868.
- Bowman CL, Kimelberg HK (1984) Excitatory amino acids directly depolarize rat brain astrocytes in primary culture. *Nature* 311:656-659.
- Bowser DN, Khakh BS (2007) Vesicular ATP is the predominant cause of intercellular calcium waves in astrocytes. *J Gen Physiol* 129:485-491.
- Boyer JL, Mohanram A, Camaioni E, Jacobson KA, Harden TK (1998) Competitive and selective antagonism of P2Y1 receptors by N6-methyl 2'-deoxyadenosine 3',5'-bisphosphate. *Br J Pharmacol* 124:1-3.
- Brake AJ, Wagenbach MJ, Julius D (1994) New structural motif for ligand-gated ion channels defined by an ionotropic ATP receptor. *Nature* 371:519-523.
- Brenner M, Kisseberth WC, Su Y, Besnard F, Messing A (1994) GFAP promoter directs astrocyte-specific expression in transgenic mice. *J Neurosci* 14:1030-1037.
- Brough D, Le Feuvre RA, Iwakura Y, Rothwell NJ (2002) Purinergic (P2X7) receptor activation of microglia induces cell death via an interleukin-1-independent mechanism. *Mol Cell Neurosci* 19:272-280.
- Brouns R, De Deyn PP (2009) The complexity of neurobiological processes in acute ischemic stroke. *Clin Neurol Neurosurg* 111:483-495.
- Bruno V, Battaglia G, Casabona G, Copani A, Caciagli F, Nicoletti F (1998) Neuroprotection by glial metabotropic glutamate receptors is mediated by transforming growth factor-beta. *J Neurosci* 18:9594-9600.
- Bruno VM, Goldberg MP, Dugan LL, Giffard RG, Choi DW (1994) Neuroprotective effect of hypothermia in cortical cultures exposed to oxygen-glucose deprivation or excitatory amino acids. *J Neurochem* 63:1398-1406.
- Buchan A, Li H, Pulsinelli WA (1991a) The N-methyl-D-aspartate antagonist, MK-801, fails to protect against neuronal damage caused by transient, severe forebrain ischemia in adult rats. *J Neurosci* 11:1049-1056.
- Buchan AM, Li H, Cho S, Pulsinelli WA (1991b) Blockade of the AMPA receptor prevents CA1 hippocampal injury following severe but transient forebrain ischemia in adult rats. *Neurosci Lett* 132:255-258.
- Bullock R, Graham DI, Swanson S, McCulloch J (1994) Neuroprotective effect of the AMPA receptor antagonist LY-293558 in focal cerebral ischemia in the cat. *J Cereb Blood Flow Metab* 14:466-471.
- Bullock R, Graham DI, Chen MH, Lowe D, McCulloch J (1990) Focal cerebral ischemia in the cat: pretreatment with a competitive NMDA receptor antagonist, D-CPP-ene. *J Cereb Blood Flow Metab* 10:668-674.
- Burnstock G (1972) Purinergic nerves. *Pharmacol Rev* 24:509-581.
- Burnstock G (1976) Purinergic receptors. *J Theor Biol* 62:491-503.
- Burnstock G (2006a) Purinergic signalling--an overview. *Novartis Found Symp* 276:26-48; discussion 48-57, 275-281.
- Burnstock G (2006b) Historical review: ATP as a neurotransmitter. *Trends Pharmacol Sci* 27:166-176.
- Burnstock G, Kennedy C (1985) Is there a basis for distinguishing two types of P2-purinoceptor? *Gen Pharmacol* 16:433-440.
- Burnstock G, Knight GE (2004) Cellular distribution and functions of P2 receptor subtypes in different systems. *Int Rev Cytol* 240:31-304.
- Burnstock G, Campbell G, Bennett M, Holman ME (1963) Inhibition of the Smooth Muscle on the Taenia Coli. *Nature* 200:581-582.

- Burnstock G, Campbell G, Bennett M, Holman ME (1964) Innervation of the Guinea-Pig *Taenia Coli*: Are There Intrinsic Inhibitory Nerves Which Are Distinct from Sympathetic Nerves? *Int J Neuropharmacol* 3:163-166.
- Burnstock G, Campbell G, Satchell D, Smythe A (1970) Evidence that adenosine triphosphate or a related nucleotide is the transmitter substance released by non-adrenergic inhibitory nerves in the gut. *Br J Pharmacol* 40:668-688.
- Calvert JA, Atterbury-Thomas AE, Leon C, Forsythe ID, Gachet C, Evans RJ (2004) Evidence for P2Y1, P2Y2, P2Y6 and atypical UTP-sensitive receptors coupled to rises in intracellular calcium in mouse cultured superior cervical ganglion neurons and glia. *Br J Pharmacol* 143:525-532.
- Camacho A, Massieu L (2006) Role of glutamate transporters in the clearance and release of glutamate during ischemia and its relation to neuronal death. *Arch Med Res* 37:11-18.
- Canzoniero LM, Babcock DJ, Gottron FJ, Grabb MC, Manzerra P, Snider BJ, Choi DW (2004) Raising intracellular calcium attenuates neuronal apoptosis triggered by staurosporine or oxygen-glucose deprivation in the presence of glutamate receptor blockade. *Neurobiol Dis* 15:520-528.
- Carroll WA, Donnelly-Roberts D, Jarvis MF (2009) Selective P2X(7) receptor antagonists for chronic inflammation and pain. *Purinergic Signal* 5:63-73.
- Castillo J, Davalos A, Naveiro J, Noya M (1996) Neuroexcitatory amino acids and their relation to infarct size and neurological deficit in ischemic stroke. *Stroke* 27:1060-1065.
- Cavaliere F, Dinkel K, Reymann K (2005) Microglia response and P2 receptor participation in oxygen/glucose deprivation-induced cortical damage. *Neuroscience* 136:615-623.
- Cavaliere F, Sancesario G, Bernardi G, Volonte C (2002) Extracellular ATP and nerve growth factor intensify hypoglycemia-induced cell death in primary neurons: role of P2 and NGFRp75 receptors. *J Neurochem* 83:1129-1138.
- Cavaliere F, D'Ambrosi N, Sancesario G, Bernardi G, Volonte C (2001a) Hypoglycaemia-induced cell death: features of neuroprotection by the P2 receptor antagonist basilen blue. *Neurochem Int* 38:199-207.
- Cavaliere F, Amadio S, Sancesario G, Bernardi G, Volonte C (2004a) Synaptic P2X7 and oxygen/glucose deprivation in organotypic hippocampal cultures. *J Cereb Blood Flow Metab* 24:392-398.
- Cavaliere F, Amadio S, Dinkel K, Reymann KG, Volonte C (2007) P2 receptor antagonist trinitrophenyl-adenosine-triphosphate protects hippocampus from oxygen and glucose deprivation cell death. *J Pharmacol Exp Ther* 323:70-77.
- Cavaliere F, Amadio S, Angelini DF, Sancesario G, Bernardi G, Volonte C (2004b) Role of the metabotropic P2Y(4) receptor during hypoglycemia: cross talk with the ionotropic NMDAR1 receptor. *Exp Cell Res* 300:149-158.
- Cavaliere F, D'Ambrosi N, Ciotti MT, Mancino G, Sancesario G, Bernardi G, Volonte C (2001b) Glucose deprivation and chemical hypoxia: neuroprotection by P2 receptor antagonists. *Neurochem Int* 38:189-197.
- Cavaliere F, Florenzano F, Amadio S, Fusco FR, Viscomi MT, D'Ambrosi N, Vacca F, Sancesario G, Bernardi G, Molinari M, Volonte C (2003) Up-regulation of P2X2, P2X4 receptor and ischemic cell death: prevention by P2 antagonists. *Neuroscience* 120:85-98.
- Centemeri C, Bolego C, Abbracchio MP, Cattabeni F, Puglisi L, Burnstock G, Nicosia S (1997) Characterization of the Ca²⁺ responses evoked by ATP and other nucleotides in mammalian brain astrocytes. *Br J Pharmacol* 121:1700-1706.
- Chang K, Hanaoka K, Kumada M, Takuwa Y (1995) Molecular cloning and functional analysis of a novel P2 nucleotide receptor. *J Biol Chem* 270:26152-26158.
- Charlton SJ, Brown CA, Weisman GA, Turner JT, Erb L, Boarder MR (1996a) Cloned and transfected P2Y4 receptors: characterization of a suramin and PPADS-insensitive response to UTP. *Br J Pharmacol* 119:1301-1303.
- Charlton SJ, Brown CA, Weisman GA, Turner JT, Erb L, Boarder MR (1996b) PPADS and suramin as antagonists at cloned P2Y- and P2U-purinoreceptors. *Br J Pharmacol* 118:704-710.
- Chaumont S, Khakh BS (2008) Patch-clamp coordinated spectroscopy shows P2X2 receptor permeability dynamics require cytosolic domain rearrangements but not Panx-1 channels. *Proc Natl Acad Sci U S A* 105:12063-12068.
- Cheewatrakoolpong B, Gilchrest H, Anthes JC, Greenfeder S (2005) Identification and characterization of splice variants of the human P2X7 ATP channel. *Biochem Biophys Res Commun* 332:17-27.

- Chen CJ, Liao SL, Kuo JS (2000) Gliotoxic action of glutamate on cultured astrocytes. *J Neurochem* 75:1557-1565.
- Chen HS, Wang YF, Rayudu PV, Edgecomb P, Neill JC, Segal MM, Lipton SA, Jensen FE (1998) Neuroprotective concentrations of the N-methyl-D-aspartate open-channel blocker memantine are effective without cytoplasmic vacuolation following post-ischemic administration and do not block maze learning or long-term potentiation. *Neuroscience* 86:1121-1132.
- Chen JF, Huang Z, Ma J, Zhu J, Moratalla R, Standaert D, Moskowitz MA, Fink JS, Schwarzschild MA (1999) A(2A) adenosine receptor deficiency attenuates brain injury induced by transient focal ischemia in mice. *J Neurosci* 19:9192-9200.
- Chen Y, Swanson RA (2003) Astrocytes and brain injury. *J Cereb Blood Flow Metab* 23:137-149.
- Chen Y, Vartiainen NE, Ying W, Chan PH, Koistinaho J, Swanson RA (2001) Astrocytes protect neurons from nitric oxide toxicity by a glutathione-dependent mechanism. *J Neurochem* 77:1601-1610.
- Cheng C, Fass DM, Reynolds IJ (1999) Emergence of excitotoxicity in cultured forebrain neurons coincides with larger glutamate-stimulated $[Ca^{2+}]_i$ increases and NMDA receptor mRNA levels. *Brain Res* 849:97-108.
- Chesler M (2005) Failure and function of intracellular pH regulation in acute hypoxic-ischemic injury of astrocytes. *Glia* 50:398-406.
- Chessell IP, Simon J, Hibell AD, Michel AD, Barnard EA, Humphrey PP (1998) Cloning and functional characterisation of the mouse P2X7 receptor. *FEBS Lett* 439:26-30.
- Chhatrivala M, Ravi RG, Patel RI, Boyer JL, Jacobson KA, Harden TK (2004) Induction of novel agonist selectivity for the ADP-activated P2Y1 receptor versus the ADP-activated P2Y12 and P2Y13 receptors by conformational constraint of an ADP analog. *J Pharmacol Exp Ther* 311:1038-1043.
- Chiamulera C, Albertini P, Valerio E, Reggiani A (1992) Activation of metabotropic receptors has a neuroprotective effect in a rodent model of focal ischaemia. *Eur J Pharmacol* 216:335-336.
- Chidekel AS, Friedman JE, Haddad GG (1997) Anoxia-induced neuronal injury: role of Na^+ entry and Na^+ -dependent transport. *Exp Neurol* 146:403-413.
- Chinopoulos C, Gerencser AA, Doczi J, Fiskum G, Adam-Vizi V (2004) Inhibition of glutamate-induced delayed calcium deregulation by 2-APB and La^{3+} in cultured cortical neurones. *J Neurochem* 91:471-483.
- Cho Y, Bannai S (1990) Uptake of glutamate and cysteine in C-6 glioma cells and in cultured astrocytes. *J Neurochem* 55:2091-2097.
- Choi DW (1985) Glutamate neurotoxicity in cortical cell culture is calcium dependent. *Neurosci Lett* 58:293-297.
- Choi DW (1995) Calcium: still center-stage in hypoxic-ischemic neuronal death. *Trends Neurosci* 18:58-60.
- Choi DW, Rothman SM (1990) The role of glutamate neurotoxicity in hypoxic-ischemic neuronal death. *Annu Rev Neurosci* 13:171-182.
- Choi DW, Maulucci-Gedde M, Kriegstein AR (1987) Glutamate neurotoxicity in cortical cell culture. *J Neurosci* 7:357-368.
- Choi DW, Koh JY, Peters S (1988) Pharmacology of glutamate neurotoxicity in cortical cell culture: attenuation by NMDA antagonists. *J Neurosci* 8:185-196.
- Chow E, Haddad GG (1998) Differential effects of anoxia and glutamate on cultured neocortical neurons. *Exp Neurol* 150:52-59.
- Clodfelter GV, Porter NM, Landfield PW, Thibault O (2002) Sustained Ca^{2+} -induced Ca^{2+} -release underlies the post-glutamate lethal Ca^{2+} plateau in older cultured hippocampal neurons. *Eur J Pharmacol* 447:189-200.
- Cockayne DA, Dunn PM, Zhong Y, Rong W, Hamilton SG, Knight GE, Ruan HZ, Ma B, Yip P, Nunn P, McMahon SB, Burnstock G, Ford AP (2005) P2X2 knockout mice and P2X2/P2X3 double knockout mice reveal a role for the P2X2 receptor subunit in mediating multiple sensory effects of ATP. *J Physiol* 567:621-639.
- Coco S, Calegari F, Pravettoni E, Pozzi D, Taverna E, Rosa P, Matteoli M, Verderio C (2003) Storage and release of ATP from astrocytes in culture. *J Biol Chem* 278:1354-1362.
- Collo G, Neidhart S, Kawashima E, Kosco-Vilbois M, North RA, Buell G (1997) Tissue distribution of the P2X7 receptor. *Neuropharmacology* 36:1277-1283.

- Collo G, North RA, Kawashima E, Merlo-Pich E, Neidhart S, Surprenant A, Buell G (1996) Cloning OF P2X5 and P2X6 receptors and the distribution and properties of an extended family of ATP-gated ion channels. *J Neurosci* 16:2495-2507.
- Communi D, Parmentier M, Boeynaems JM (1996a) Cloning, functional expression and tissue distribution of the human P2Y6 receptor. *Biochem Biophys Res Commun* 222:303-308.
- Communi D, Robaye B, Boeynaems JM (1999) Pharmacological characterization of the human P2Y11 receptor. *Br J Pharmacol* 128:1199-1206.
- Communi D, Motte S, Boeynaems JM, Piroton S (1996b) Pharmacological characterization of the human P2Y4 receptor. *Eur J Pharmacol* 317:383-389.
- Conti F, Minelli A, Brecha NC (1994) Cellular localization and laminar distribution of AMPA glutamate receptor subunits mRNAs and proteins in the rat cerebral cortex. *J Comp Neurol* 350:241-259.
- Conti F, DeBiasi S, Minelli A, Melone M (1996) Expression of NR1 and NR2A/B subunits of the NMDA receptor in cortical astrocytes. *Glia* 17:254-258.
- Conti F, Minelli A, DeBiasi S, Melone M (1997) Neuronal and glial localization of NMDA receptors in the cerebral cortex. *Mol Neurobiol* 14:1-18.
- Conti F, Barbaresi P, Melone M, Ducati A (1999) Neuronal and glial localization of NR1 and NR2A/B subunits of the NMDA receptor in the human cerebral cortex. *Cereb Cortex* 9:110-120.
- Contreras JE, Sanchez HA, Veliz LP, Bukauskas FF, Bennett MV, Saez JC (2004) Role of connexin-based gap junction channels and hemichannels in ischemia-induced cell death in nervous tissue. *Brain Res Brain Res Rev* 47:290-303.
- Contreras JE, Sanchez HA, Eugenin EA, Speidel D, Theis M, Willecke K, Bukauskas FF, Bennett MV, Saez JC (2002) Metabolic inhibition induces opening of unapposed connexin 43 gap junction hemichannels and reduces gap junctional communication in cortical astrocytes in culture. *Proc Natl Acad Sci U S A* 99:495-500.
- Cooper EH (1994) Neuron-specific enolase. *Int J Biol Markers* 9:205-210.
- Coppi E, Pugliese AM, Stephan H, Muller CE, Pedata F (2007) Role of P2 purinergic receptors in synaptic transmission under normoxic and ischaemic conditions in the CA1 region of rat hippocampal slices. *Purinergic Signal* 3:203-219.
- Cotrina ML, Lin JH, Lopez-Garcia JC, Naus CC, Nedergaard M (2000) ATP-mediated glia signaling. *J Neurosci* 20:2835-2844.
- Cotrina ML, Lin JH, Alves-Rodrigues A, Liu S, Li J, Azmi-Ghadimi H, Kang J, Naus CC, Nedergaard M (1998) Connexins regulate calcium signaling by controlling ATP release. *Proc Natl Acad Sci U S A* 95:15735-15740.
- Crain JM, Nikodemova M, Watters JJ (2009) Expression of P2 nucleotide receptors varies with age and sex in murine brain microglia. *J Neuroinflammation* 6:24.
- Cui Y, Zhang L, Utsunomiya K, Yanase H, Mitani A, Kataoka K (1999) Ischemia-induced glutamate release in the dentate gyrus. A microdialysis study in the gerbil. *Neurosci Lett* 271:191-194.
- D'Antoni S, Berretta A, Bonaccorso CM, Bruno V, Aronica E, Nicoletti F, Catania MV (2008) Metabotropic Glutamate Receptors in Glial Cells. *Neurochem Res*.
- Dale N, Pearson T, Frenguelli BG (2000) Direct measurement of adenosine release during hypoxia in the CA1 region of the rat hippocampal slice. *J Physiol* 526 Pt 1:143-155.
- Dale N, Hatz S, Tian F, Llaudet E (2005) Listening to the brain: microelectrode biosensors for neurochemicals. *Trends Biotechnol* 23:420-428.
- Dallas M, Boycott HE, Atkinson L, Miller A, Boyle JP, Pearson HA, Peers C (2007) Hypoxia suppresses glutamate transport in astrocytes. *J Neurosci* 27:3946-3955.
- Danbolt NC (2001) Glutamate uptake. *Prog Neurobiol* 65:1-105.
- Daniels M, Brown DR (2001) Astrocytes regulate N-methyl-D-aspartate receptor subunit composition increasing neuronal sensitivity to excitotoxicity. *J Biol Chem* 276:22446-22452.
- Danilov CA, Fiskum G (2008) Hyperoxia promotes astrocyte cell death after oxygen and glucose deprivation. *Glia* 56:801-808.
- Darby M, Kuzmiski JB, Panenka W, Feighan D, MacVicar BA (2003) ATP released from astrocytes during swelling activates chloride channels. *J Neurophysiol* 89:1870-1877.
- David JC, Yamada KA, Bagwe MR, Goldberg MP (1996) AMPA receptor activation is rapidly toxic to cortical astrocytes when desensitization is blocked. *J Neurosci* 16:200-209.

- Davies CA, Loddick SA, Stroemer RP, Hunt J, Rothwell NJ (1998) An integrated analysis of the progression of cell responses induced by permanent focal middle cerebral artery occlusion in the rat. *Exp Neurol* 154:199-212.
- Decleves X, Regina A, Laplanche JL, Roux F, Boval B, Launay JM, Scherrmann JM (2000) Functional expression of P-glycoprotein and multidrug resistance-associated protein (Mrp1) in primary cultures of rat astrocytes. *J Neurosci Res* 60:594-601.
- Deng W, Rosenberg PA, Volpe JJ, Jensen FE (2003) Calcium-permeable AMPA/kainate receptors mediate toxicity and preconditioning by oxygen-glucose deprivation in oligodendrocyte precursors. *Proc Natl Acad Sci U S A* 100:6801-6806.
- Deng W, Wang H, Rosenberg PA, Volpe JJ, Jensen FE (2004) Role of metabotropic glutamate receptors in oligodendrocyte excitotoxicity and oxidative stress. *Proc Natl Acad Sci U S A* 101:7751-7756.
- Di Virgilio F, Chiozzi P, Falzoni S, Ferrari D, Sanz JM, Venketaraman V, Baricordi OR (1998) Cytolytic P2X purinoceptors. *Cell Death Differ* 5:191-199.
- Diarra A, Sheldon C, Brett CL, Baimbridge KG, Church J (1999) Anoxia-evoked intracellular pH and Ca²⁺ concentration changes in cultured postnatal rat hippocampal neurons. *Neuroscience* 93:1003-1016.
- Dingledine R, Borges K, Bowie D, Traynelis SF (1999) The glutamate receptor ion channels. *Pharmacol Rev* 51:7-61.
- Dixon SJ, Yu R, Panupinthu N, Wilson JX (2004) Activation of P2 nucleotide receptors stimulates acid efflux from astrocytes. *Glia* 47:367-376.
- Dolphin AC, Prestwich SA (1985) Pertussis toxin reverses adenosine inhibition of neuronal glutamate release. *Nature* 316:148-150.
- Domercq M, Brambilla L, Pilati E, Marchaland J, Volterra A, Bezzi P (2006) P2Y1 receptor-evoked glutamate exocytosis from astrocytes: control by tumor necrosis factor- α and prostaglandins. *J Biol Chem* 281:30684-30696.
- Donnelly-Roberts DL, Namovic MT, Han P, Jarvis MF (2009) Mammalian P2X7 receptor pharmacology: comparison of recombinant mouse, rat and human P2X7 receptors. *Br J Pharmacol* 157:1203-1214.
- Doyle KP, Simon RP, Stenzel-Poore MP (2008) Mechanisms of ischemic brain damage. *Neuropharmacology* 55:310-318.
- Duan S, Neary JT (2006) P2X(7) receptors: properties and relevance to CNS function. *Glia* 54:738-746.
- Duan S, Anderson CM, Keung EC, Chen Y, Swanson RA (2003) P2X7 receptor-mediated release of excitatory amino acids from astrocytes. *J Neurosci* 23:1320-1328.
- Dubinsky JM, Rothman SM (1991) Intracellular calcium concentrations during "chemical hypoxia" and excitotoxic neuronal injury. *J Neurosci* 11:2545-2551.
- Dubinsky JM, Kristal BS, Elizondo-Fournier M (1995) An obligate role for oxygen in the early stages of glutamate-induced, delayed neuronal death. *J Neurosci* 15:7071-7078.
- Duffy S, MacVicar BA (1996) In vitro ischemia promotes calcium influx and intracellular calcium release in hippocampal astrocytes. *J Neurosci* 16:71-81.
- Dugan LL, Kim-Han JS (2004) Astrocyte mitochondria in in vitro models of ischemia. *J Bioenerg Biomembr* 36:317-321.
- Dugan LL, Bruno VM, Amagasa SM, Giffard RG (1995) Glia modulate the response of murine cortical neurons to excitotoxicity: glia exacerbate AMPA neurotoxicity. *J Neurosci* 15:4545-4555.
- Dunn PM, Blakeley AG (1988) Suramin: a reversible P2-purinoceptor antagonist in the mouse vas deferens. *Br J Pharmacol* 93:243-245.
- Dunwiddie TV, Diao L, Proctor WR (1997) Adenine nucleotides undergo rapid, quantitative conversion to adenosine in the extracellular space in rat hippocampus. *J Neurosci* 17:7673-7682.
- Durkin JP, Tremblay R, Chakravarthy B, Mealing G, Morley P, Small D, Song D (1997) Evidence that the early loss of membrane protein kinase C is a necessary step in the excitatory amino acid-induced death of primary cortical neurons. *J Neurochem* 68:1400-1412.
- Edwards FA, Gibb AJ, Colquhoun D (1992) ATP receptor-mediated synaptic currents in the central nervous system. *Nature* 359:144-147.
- Egan TM, Khakh BS (2004) Contribution of calcium ions to P2X channel responses. *J Neurosci* 24:3413-3420.
- Eng LF, Ghirnikar RS, Lee YL (2000) Glial fibrillary acidic protein: GFAP-thirty-one years (1969-2000). *Neurochem Res* 25:1439-1451.

- Enkvist MO, Holopainen I, Akerman KE (1989) Glutamate receptor-linked changes in membrane potential and intracellular Ca²⁺ in primary rat astrocytes. *Glia* 2:397-402.
- Erecinska M, Silver IA (1990) Metabolism and role of glutamate in mammalian brain. *Prog Neurobiol* 35:245-296.
- Fam SR, Gallagher CJ, Kalia LV, Salter MW (2003) Differential frequency dependence of P2Y₁- and P2Y₂-mediated Ca²⁺ signaling in astrocytes. *J Neurosci* 23:4437-4444.
- Fan D, Grooms SY, Araneda RC, Johnson AB, Dobrenis K, Kessler JA, Zukin RS (1999) AMPA receptor protein expression and function in astrocytes cultured from hippocampus. *J Neurosci Res* 57:557-571.
- Fellin T, Pozzan T, Carmignoto G (2006a) Purinergic receptors mediate two distinct glutamate release pathways in hippocampal astrocytes. *J Biol Chem* 281:4274-4284.
- Fellin T, Pascual O, Gobbo S, Pozzan T, Haydon PG, Carmignoto G (2004) Neuronal synchrony mediated by astrocytic glutamate through activation of extrasynaptic NMDA receptors. *Neuron* 43:729-743.
- Fellin T, Sul JY, D'Ascenzo M, Takano H, Pascual O, Haydon PG (2006b) Bidirectional astrocyte-neuron communication: the many roles of glutamate and ATP. *Novartis Found Symp* 276:208-217; discussion 217-221, 233-207, 275-281.
- Fern R (1998) Intracellular calcium and cell death during ischemia in neonatal rat white matter astrocytes in situ. *J Neurosci* 18:7232-7243.
- Fern R (2001) Ischemia: astrocytes show their sensitive side. *Prog Brain Res* 132:405-411.
- Fern R, Moller T (2000) Rapid ischemic cell death in immature oligodendrocytes: a fatal glutamate release feedback loop. *J Neurosci* 20:34-42.
- Ferraguti F, Shigemoto R (2006) Metabotropic glutamate receptors. *Cell Tissue Res* 326:483-504.
- Ferrari D, Chiozzi P, Falzoni S, Dal Susino M, Collo G, Buell G, Di Virgilio F (1997) ATP-mediated cytotoxicity in microglial cells. *Neuropharmacology* 36:1295-1301.
- Ferrari D, Pizzirani C, Adinolfi E, Lemoli RM, Curti A, Idzko M, Panther E, Di Virgilio F (2006) The P2X₇ receptor: a key player in IL-1 processing and release. *J Immunol* 176:3877-3883.
- Feustel PJ, Jin Y, Kimelberg HK (2004) Volume-regulated anion channels are the predominant contributors to release of excitatory amino acids in the ischemic cortical penumbra. *Stroke* 35:1164-1168.
- Fields RD, Burnstock G (2006) Purinergic signalling in neuron-glia interactions. *Nat Rev Neurosci* 7:423-436.
- Fischer KG, Saueressig U, Jacobshagen C, Wichelmann A, Pavenstadt H (2001) Extracellular nucleotides regulate cellular functions of podocytes in culture. *Am J Physiol Renal Physiol* 281:F1075-1081.
- Fischer W, Krugel U (2007) P2Y receptors: focus on structural, pharmacological and functional aspects in the brain. *Curr Med Chem* 14:2429-2455.
- Fischer W, Franke H, Scheibler P, Allgaier C, Illes P (2002) AMPA-induced Ca²⁺ influx in cultured rat cortical nonpyramidal neurones: pharmacological characterization using fura-2 microfluorimetry. *Eur J Pharmacol* 438:53-62.
- Fischer W, Appelt K, Grohmann M, Franke H, Norenberg W, Illes P (2009) Increase of intracellular Ca²⁺ by P2X and P2Y receptor-subtypes in cultured cortical astroglia of the rat. *Neuroscience* 160:767-783.
- Fleidervish IA, Gebhardt C, Astman N, Gutnick MJ, Heinemann U (2001) Enhanced spontaneous transmitter release is the earliest consequence of neocortical hypoxia that can explain the disruption of normal circuit function. *J Neurosci* 21:4600-4608.
- Flynn RW, MacWalter RS, Doney AS (2008) The cost of cerebral ischaemia. *Neuropharmacology* 55:250-256.
- Fogal B, Trettel J, Uliasz TF, Levine ES, Hewett SJ (2005) Changes in secondary glutamate release underlie the developmental regulation of excitotoxic neuronal cell death. *Neuroscience* 132:929-942.
- Fok-Seang J, Miller RH (1992) Astrocyte precursors in neonatal rat spinal cord cultures. *J Neurosci* 12:2751-2764.
- Fountzopoulos E, Mavroudis C, Nadar SK, Gunning MG (2007) Case report: An unusual complication of clopidogrel. *Int J Cardiol* 115:e27-28.
- Frandsen A, Schousboe A (1992) Mobilization of dantrolene-sensitive intracellular calcium pools is involved in the cytotoxicity induced by quisqualate and N-methyl-D-aspartate but not by 2-amino-3-(3-

- hydroxy-5-methylisoxazol-4-yl)propionate and kainate in cultured cerebral cortical neurons. *Proc Natl Acad Sci U S A* 89:2590-2594.
- Frandsen A, Schousboe A (1993) Excitatory amino acid-mediated cytotoxicity and calcium homeostasis in cultured neurons. *J Neurochem* 60:1202-1211.
- Franke H, Illes P (2006) Involvement of P2 receptors in the growth and survival of neurons in the CNS. *Pharmacol Ther* 109:297-324.
- Franke H, Krugel U, Illes P (2006) P2 receptors and neuronal injury. *Pflugers Arch* 452:622-644.
- Franke H, Krugel U, Schmidt R, Grosche J, Reichenbach A, Illes P (2001) P2 receptor-types involved in astrogliosis in vivo. *Br J Pharmacol* 134:1180-1189.
- Franke H, Gunther A, Grosche J, Schmidt R, Rossner S, Reinhardt R, Faber-Zuschratter H, Schneider D, Illes P (2004) P2X7 receptor expression after ischemia in the cerebral cortex of rats. *J Neuropathol Exp Neurol* 63:686-699.
- Fredholm BB (2007) Adenosine, an endogenous distress signal, modulates tissue damage and repair. *Cell Death Differ* 14:1315-1323.
- Freguelli BG, Llaudet E, Dale N (2003) High-resolution real-time recording with microelectrode biosensors reveals novel aspects of adenosine release during hypoxia in rat hippocampal slices. *J Neurochem* 86:1506-1515.
- Freguelli BG, Wigmore G, Llaudet E, Dale N (2007) Temporal and mechanistic dissociation of ATP and adenosine release during ischaemia in the mammalian hippocampus. *J Neurochem* 101:1400-1413.
- Freguelli BL, E; Dale, N (2005) ATP release during ischemia as a harbinger of cell death? In: *Neuroscience*. Washington, D.C.
- Friedman JE, Haddad GG (1993) Major differences in Ca²⁺ response to anoxia between neonatal and adult rat CA1 neurons: role of Ca²⁺ and Na⁺. *J Neurosci* 13:63-72.
- Fujita T, Tozaki-Saitoh H, Inoue K (2009) P2Y1 receptor signaling enhances neuroprotection by astrocytes against oxidative stress via IL-6 release in hippocampal cultures. *Glia* 57:244-257.
- Fumagalli M, Brambilla R, D'Ambrosi N, Volonte C, Matteoli M, Verderio C, Abbracchio MP (2003) Nucleotide-mediated calcium signaling in rat cortical astrocytes: Role of P2X and P2Y receptors. *Glia* 43:218-203.
- Garcia-Guzman M, Stuhmer W, Soto F (1997a) Molecular characterization and pharmacological properties of the human P2X3 purinoceptor. *Brain Res Mol Brain Res* 47:59-66.
- Garcia-Guzman M, Soto F, Gomez-Hernandez JM, Lund PE, Stuhmer W (1997b) Characterization of recombinant human P2X4 receptor reveals pharmacological differences to the rat homologue. *Mol Pharmacol* 51:109-118.
- Garcia JH, Yoshida Y, Chen H, Li Y, Zhang ZG, Lian J, Chen S, Chopp M (1993) Progression from ischemic injury to infarct following middle cerebral artery occlusion in the rat. *Am J Pathol* 142:623-635.
- Gargett CE, Wiley JS (1997) The isoquinoline derivative KN-62 a potent antagonist of the P2Z-receptor of human lymphocytes. *Br J Pharmacol* 120:1483-1490.
- Gebhardt C, Korner R, Heinemann U (2002) Delayed anoxic depolarizations in hippocampal neurons of mice lacking the excitatory amino acid carrier 1. *J Cereb Blood Flow Metab* 22:569-575.
- Geeraerts MD, Ronveaux-Dupal MF, Lemasters JJ, Herman B (1991) Cytosolic free Ca²⁺ and proteolysis in lethal oxidative injury in endothelial cells. *Am J Physiol* 261:C889-896.
- Gegg ME, Clark JB, Heales SJ (2005) Co-culture of neurones with glutathione deficient astrocytes leads to increased neuronal susceptibility to nitric oxide and increased glutamate-cysteine ligase activity. *Brain Res* 1036:1-6.
- Gever JR, Cockayne DA, Dillon MP, Burnstock G, Ford AP (2006) Pharmacology of P2X channels. *Pflugers Arch* 452:513-537.
- Giaume C, Kirchhoff F, Matute C, Reichenbach A, Verkhratsky A (2007) Glia: the fulcrum of brain diseases. *Cell Death Differ* 14:1324-1335.
- Giffard RG, Monyer H, Choi DW (1990) Selective vulnerability of cultured cortical glia to injury by extracellular acidosis. *Brain Res* 530:138-141.
- Ginsberg MD (2008) Neuroprotection for ischemic stroke: past, present and future. *Neuropharmacology* 55:363-389.

- Glaum SR, Holzwarth JA, Miller RJ (1990) Glutamate receptors activate Ca²⁺ mobilization and Ca²⁺ influx into astrocytes. *Proc Natl Acad Sci U S A* 87:3454-3458.
- Globus MY, Busto R, Dietrich WD, Martinez E, Valdes I, Ginsberg MD (1988) Effect of ischemia on the in vivo release of striatal dopamine, glutamate, and gamma-aminobutyric acid studied by intracerebral microdialysis. *J Neurochem* 51:1455-1464.
- Globus MY, Busto R, Martinez E, Valdes I, Dietrich WD, Ginsberg MD (1991) Comparative effect of transient global ischemia on extracellular levels of glutamate, glycine, and gamma-aminobutyric acid in vulnerable and nonvulnerable brain regions in the rat. *J Neurochem* 57:470-478.
- Goldberg MP, Choi DW (1990) Intracellular free calcium increases in cultured cortical neurons deprived of oxygen and glucose. *Stroke* 21:III75-77.
- Goldberg MP, Choi DW (1993) Combined oxygen and glucose deprivation in cortical cell culture: calcium-dependent and calcium-independent mechanisms of neuronal injury. *J Neurosci* 13:3510-3524.
- Goldberg MP, Weiss JH, Pham PC, Choi DW (1987) N-methyl-D-aspartate receptors mediate hypoxic neuronal injury in cortical culture. *J Pharmacol Exp Ther* 243:784-791.
- Gordon JW, Scangos GA, Plotkin DJ, Barbosa JA, Ruddle FH (1980) Genetic transformation of mouse embryos by microinjection of purified DNA. *Proc Natl Acad Sci U S A* 77:7380-7384.
- Gouix E, Leveille F, Nicole O, Melon C, Had-Aissouni L, Buisson A (2009) Reverse glial glutamate uptake triggers neuronal cell death through extrasynaptic NMDA receptor activation. *Mol Cell Neurosci* 40:463-473.
- Gourine AV, Llaudet E, Dale N, Spyer KM (2005a) Release of ATP in the ventral medulla during hypoxia in rats: role in hypoxic ventilatory response. *J Neurosci* 25:1211-1218.
- Gourine AV, Llaudet E, Dale N, Spyer KM (2005b) ATP is a mediator of chemosensory transduction in the central nervous system. *Nature* 436:108-111.
- Gourine AV, Dale N, Korsak A, Llaudet E, Tian F, Huckstepp R, Spyer KM (2008) Release of ATP and glutamate in the nucleus tractus solitarius mediate pulmonary stretch receptor (Breuer-Hering) reflex pathway. *J Physiol* 586:3963-3978.
- Griffin S, Clark JB, Canevari L (2005) Astrocyte-neurone communication following oxygen-glucose deprivation. *J Neurochem* 95:1015-1022.
- Gryniewicz G, Poenie M, Tsien RY (1985) A new generation of Ca²⁺ indicators with greatly improved fluorescence properties. *J Biol Chem* 260:3440-3450.
- Gu JG, Bardoni R, Magherini PC, MacDermott AB (1998) Effects of the P₂-purinoceptor antagonists suramin and pyridoxal-phosphate-6-azophenyl-2',4'-disulfonic acid on glutamatergic synaptic transmission in rat dorsal horn neurons of the spinal cord. *Neurosci Lett* 253:167-170.
- Guerra AN, Gavala ML, Chung HS, Bertics PJ (2007) Nucleotide receptor signalling and the generation of reactive oxygen species. *Purinergic Signal* 3:39-51.
- Guo C, Masin M, Qureshi OS, Murrell-Lagnado RD (2007) Evidence for functional P₂X₄/P₂X₇ heteromeric receptors. *Mol Pharmacol* 72:1447-1456.
- Guo Y, Su M, McNutt MA, Gu J (2009) Expression and distribution of cystic fibrosis transmembrane conductance regulator in neurons of the spinal cord. *J Neurosci Res* 87:3611-3619.
- Gwag BJ, Lobner D, Koh JY, Wie MB, Choi DW (1995) Blockade of glutamate receptors unmasks neuronal apoptosis after oxygen-glucose deprivation in vitro. *Neuroscience* 68:615-619.
- Haak LL, Heller HC, van den Pol AN (1997) Metabotropic glutamate receptor activation modulates kainate and serotonin calcium response in astrocytes. *J Neurosci* 17:1825-1837.
- Haberg A, Qu H, Sonnewald U (2006) Glutamate and GABA metabolism in transient and permanent middle cerebral artery occlusion in rat: importance of astrocytes for neuronal survival. *Neurochem Int* 48:531-540.
- Haberg A, Qu H, Saether O, Unsgard G, Haraldseth O, Sonnewald U (2001) Differences in neurotransmitter synthesis and intermediary metabolism between glutamatergic and GABAergic neurons during 4 hours of middle cerebral artery occlusion in the rat: the role of astrocytes in neuronal survival. *J Cereb Blood Flow Metab* 21:1451-1463.
- Hagberg H, Lehmann A, Sandberg M, Nystrom B, Jacobson I, Hamberger A (1985) Ischemia-induced shift of inhibitory and excitatory amino acids from intra- to extracellular compartments. *J Cereb Blood Flow Metab* 5:413-419.

- Hailer NP (2008) Immunosuppression after traumatic or ischemic CNS damage: it is neuroprotective and illuminates the role of microglial cells. *Prog Neurobiol* 84:211-233.
- Hamann M, Rossi DJ, Marie H, Attwell D (2002) Knocking out the glial glutamate transporter GLT-1 reduces glutamate uptake but does not affect hippocampal glutamate dynamics in early simulated ischaemia. *Eur J Neurosci* 15:308-314.
- Hamilton N, Vayro S, Kirchhoff F, Verkhatsky A, Robbins J, Gorecki DC, Butt AM (2008) Mechanisms of ATP- and glutamate-mediated calcium signaling in white matter astrocytes. *Glia* 56:734-749.
- Hankey GJ, Eikelboom JW Antithrombotic drugs for patients with ischaemic stroke and transient ischaemic attack to prevent recurrent major vascular events. *Lancet Neurol* 9:273-284.
- Hansen AJ, Nedergaard M (1988) Brain ion homeostasis in cerebral ischemia. *Neurochem Pathol* 9:195-209.
- Hardingham GE, Fukunaga Y, Bading H (2002) Extrasynaptic NMDARs oppose synaptic NMDARs by triggering CREB shut-off and cell death pathways. *Nat Neurosci* 5:405-414.
- Hassinger TD, Guthrie PB, Atkinson PB, Bennett MV, Kater SB (1996) An extracellular signaling component in propagation of astrocytic calcium waves. *Proc Natl Acad Sci U S A* 93:13268-13273.
- Haun SE, Murphy EJ, Bates CM, Horrocks LA (1992) Extracellular calcium is a mediator of astroglial injury during combined glucose-oxygen deprivation. *Brain Res* 593:45-50.
- Hausmann R, Rettinger J, Gerevich Z, Meis S, Kassack MU, Illes P, Lambrecht G, Schmalzing G (2006) The suramin analog 4,4',4'',4'''-(carbonylbis(imino-5,1,3-benzenetriylbis (carbonylimino)))tetra-kis-benzenesulfonic acid (NF110) potently blocks P2X3 receptors: subtype selectivity is determined by location of sulfonic acid groups. *Mol Pharmacol* 69:2058-2067.
- Hayes AJ, Hall A, Brown L, Tubo R, Caterson B (2007) Macromolecular organization and in vitro growth characteristics of scaffold-free neocartilage grafts. *J Histochem Cytochem* 55:853-866.
- Henrich-Noack P, Hatton CD, Reymann KG (1998) The mGlu receptor ligand (S)-4C3HPG protects neurons after global ischaemia in gerbils. *Neuroreport* 9:985-988.
- Hertz L (2008) Bioenergetics of cerebral ischemia: a cellular perspective. *Neuropharmacology* 55:289-309.
- Hertz L, Peng L, Lai JC (1998) Functional studies in cultured astrocytes. *Methods* 16:293-310.
- Hibell AD, Kidd EJ, Chessell IP, Humphrey PP, Michel AD (2000) Apparent species differences in the kinetic properties of P2X(7) receptors. *Br J Pharmacol* 130:167-173.
- Hirrlinger PG, Scheller A, Braun C, Quintela-Schneider M, Fuss B, Hirrlinger J, Kirchhoff F (2005) Expression of reef coral fluorescent proteins in the central nervous system of transgenic mice. *Mol Cell Neurosci* 30:291-303.
- Hisanaga K, Onodera H, Kogure K (1986) Changes in levels of purine and pyrimidine nucleotides during acute hypoxia and recovery in neonatal rat brain. *J Neurochem* 47:1344-1350.
- Ho C, Hicks J, Salter MW (1995) A novel P2-purinoceptor expressed by a subpopulation of astrocytes from the dorsal spinal cord of the rat. *Br J Pharmacol* 116:2909-2918.
- Ho MC, Lo AC, Kurihara H, Yu AC, Chung SS, Chung SK (2001) Endothelin-1 protects astrocytes from hypoxic/ischemic injury. *FASEB J* 15:618-626.
- Holzwarth JA, Gibbons SJ, Brorson JR, Philipson LH, Miller RJ (1994) Glutamate receptor agonists stimulate diverse calcium responses in different types of cultured rat cortical glial cells. *J Neurosci* 14:1879-1891.
- Homolya L, Watt WC, Lazarowski ER, Koller BH, Boucher RC (1999) Nucleotide-regulated calcium signaling in lung fibroblasts and epithelial cells from normal and P2Y(2) receptor (-/-) mice. *J Biol Chem* 274:26454-26460.
- Honore T, Drejer J (1988) Chaotropic ions affect the conformation of quisqualate receptors in rat cortical membranes. *J Neurochem* 51:457-461.
- Honore T, Davies SN, Drejer J, Fletcher EJ, Jacobsen P, Lodge D, Nielsen FE (1988) Quinoxalinediones: potent competitive non-NMDA glutamate receptor antagonists. *Science* 241:701-703.
- Humphreys BD, Rice J, Kertesz SB, Dubyak GR (2000) Stress-activated protein kinase/JNK activation and apoptotic induction by the macrophage P2X7 nucleotide receptor. *J Biol Chem* 275:26792-26798.
- Humphreys BD, Virginio C, Surprenant A, Rice J, Dubyak GR (1998) Isoquinolines as antagonists of the P2X7 nucleotide receptor: high selectivity for the human versus rat receptor homologues. *Mol Pharmacol* 54:22-32.
- Hyrn KL, Bownik JM, Goldberg MP (2000) Ionic selectivity of low-affinity ratiometric calcium indicators: mag-Fura-2, Fura-2FF and BTC. *Cell Calcium* 27:75-86.

- Ikeda M (2007) Characterization of functional P2X(1) receptors in mouse megakaryocytes. *Thromb Res* 119:343-353.
- Ikonomidou C, Turski L (2002) Why did NMDA receptor antagonists fail clinical trials for stroke and traumatic brain injury? *Lancet Neurol* 1:383-386.
- Ikonomidou C, Stefovská V, Turski L (2000) Neuronal death enhanced by N-methyl-D-aspartate antagonists. *Proc Natl Acad Sci U S A* 97:12885-12890.
- Illes P, Alexandre Ribeiro J (2004) Molecular physiology of P2 receptors in the central nervous system. *Eur J Pharmacol* 483:5-17.
- Innocenti B, Parpura V, Haydon PG (2000) Imaging extracellular waves of glutamate during calcium signaling in cultured astrocytes. *J Neurosci* 20:1800-1808.
- Inoue K (2008) Purinergic systems in microglia. *Cell Mol Life Sci* 65:3074-3080.
- Iwabuchi S, Kawahara K (2009a) Oxygen-glucose deprivation-induced enhancement of extracellular ATP-P2Y purinoceptors signaling for the propagation of astrocytic calcium waves. *Biosystems* 96:35-43.
- Iwabuchi S, Kawahara K (2009b) Possible involvement of extracellular ATP-P2Y purinoceptor signaling in ischemia-induced tolerance of astrocytes in culture. *Neurochem Res* 34:1542-1554.
- Iwata-Ichikawa E, Kondo Y, Miyazaki I, Asanuma M, Ogawa N (1999) Glial cells protect neurons against oxidative stress via transcriptional up-regulation of the glutathione synthesis. *J Neurochem* 72:2334-2344.
- Jabs R, Kirchhoff F, Kettenmann H, Steinhauser C (1994) Kainate activates Ca(2+)-permeable glutamate receptors and blocks voltage-gated K⁺ currents in glial cells of mouse hippocampal slices. *Pflugers Arch* 426:310-319.
- Jacobson KA, Ivanov AA, de Castro S, Harden TK, Ko H (2009) Development of selective agonists and antagonists of P2Y receptors. *Purinergic Signal* 5:75-89.
- Jaiswal JK, Fix M, Takano T, Nedergaard M, Simon SM (2007) Resolving vesicle fusion from lysis to monitor calcium-triggered lysosomal exocytosis in astrocytes. *Proc Natl Acad Sci U S A* 104:14151-14156.
- James G, Butt AM (1999) Adenosine 5' triphosphate evoked mobilization of intracellular calcium in central nervous system white matter of adult mouse optic nerve. *Neurosci Lett* 268:53-56.
- James G, Butt AM (2001) P2X and P2Y purinoreceptors mediate ATP-evoked calcium signalling in optic nerve glia in situ. *Cell Calcium* 30:251-259.
- James G, Butt AM (2002) P2Y and P2X purinoceptor mediated Ca²⁺ signalling in glial cell pathology in the central nervous system. *Eur J Pharmacol* 447:247-260.
- Janssens N, Lesage AS (2001) Glutamate receptor subunit expression in primary neuronal and secondary glial cultures. *J Neurochem* 77:1457-1474.
- Jarvis MF, Khakh BS (2009) ATP-gated P2X cation-channels. *Neuropharmacology* 56:208-215.
- Jensen AM, Chiu SY (1990) Fluorescence measurement of changes in intracellular calcium induced by excitatory amino acids in cultured cortical astrocytes. *J Neurosci* 10:1165-1175.
- Jensen AM, Chiu SY (1991) Differential intracellular calcium responses to glutamate in type 1 and type 2 cultured brain astrocytes. *J Neurosci* 11:1674-1684.
- Jentsch TJ, Stein V, Weinreich F, Zdebik AA (2002) Molecular structure and physiological function of chloride channels. *Physiol Rev* 82:503-568.
- Jeremic A, Jeftinija K, Stevanovic J, Glavaski A, Jeftinija S (2001) ATP stimulates calcium-dependent glutamate release from cultured astrocytes. *J Neurochem* 77:664-675.
- Jessen KR (2006) A brief look at glial cells. *Novartis Found Symp* 276:5-14; discussion 54-17, 275-281.
- Jiang X, Tian F, Mearow K, Okagaki P, Lipsky RH, Marini AM (2005) The excitoprotective effect of N-methyl-D-aspartate receptors is mediated by a brain-derived neurotrophic factor autocrine loop in cultured hippocampal neurons. *J Neurochem* 94:713-722.
- Jimenez AI, Castro E, Communi D, Boeynaems JM, Delicado EG, Miras-Portugal MT (2000) Coexpression of several types of metabotropic nucleotide receptors in single cerebellar astrocytes. *J Neurochem* 75:2071-2079.
- Johnston MV, Nakajima W, Hagberg H (2002) Mechanisms of hypoxic neurodegeneration in the developing brain. *Neuroscientist* 8:212-220.
- Jones CA, Chessell IP, Simon J, Barnard EA, Miller KJ, Michel AD, Humphrey PP (2000) Functional characterization of the P2X(4) receptor orthologues. *Br J Pharmacol* 129:388-394.

- Jones KA, Baughman RW (1991) Both NMDA and non-NMDA subtypes of glutamate receptors are concentrated at synapses on cerebral cortical neurons in culture. *Neuron* 7:593-603.
- Jorgensen MB, Diemer NH (1982) Selective neuron loss after cerebral ischemia in the rat: possible role of transmitter glutamate. *Acta Neurol Scand* 66:536-546.
- Jourdain P, Bergersen LH, Bhaukaurally K, Bezzi P, Santello M, Domercq M, Matute C, Tonello F, Gundersen V, Volterra A (2007) Glutamate exocytosis from astrocytes controls synaptic strength. *Nat Neurosci* 10:331-339.
- Juranyi Z, Sperlagh B, Vizi ES (1999) Involvement of P2 purinoceptors and the nitric oxide pathway in [3H]purine outflow evoked by short-term hypoxia and hypoglycemia in rat hippocampal slices. *Brain Res* 823:183-190.
- Juurlink BH, Hertz L (1993) Ischemia-induced death of astrocytes and neurons in primary culture: pitfalls in quantifying neuronal cell death. *Brain Res Dev Brain Res* 71:239-246.
- Kahlert S, Reiser G (2004) Glial perspectives of metabolic states during cerebral hypoxia--calcium regulation and metabolic energy. *Cell Calcium* 36:295-302.
- Kahlert S, Zundorf G, Reiser G (2005) Glutamate-mediated influx of extracellular Ca²⁺ is coupled with reactive oxygen species generation in cultured hippocampal neurons but not in astrocytes. *J Neurosci Res* 79:262-271.
- Kahlert S, Blaser T, Tulapurkar M, Reiser G (2007) P2Y receptor-activating nucleotides modulate cellular reactive oxygen species production in dissociated hippocampal astrocytes and neurons in culture independent of parallel cytosolic Ca(2+) rise and change in mitochondrial potential. *J Neurosci Res* 85:3443-3456.
- Kaku DA, Goldberg MP, Choi DW (1991) Antagonism of non-NMDA receptors augments the neuroprotective effect of NMDA receptor blockade in cortical cultures subjected to prolonged deprivation of oxygen and glucose. *Brain Res* 554:344-347.
- Kaku DA, Giffard RG, Choi DW (1993) Neuroprotective effects of glutamate antagonists and extracellular acidity. *Science* 260:1516-1518.
- Kang J, Kang N, Lovatt D, Torres A, Zhao Z, Lin J, Nedergaard M (2008) Connexin 43 hemichannels are permeable to ATP. *J Neurosci* 28:4702-4711.
- Karadottir R, Cavalier P, Bergersen LH, Attwell D (2005) NMDA receptors are expressed in oligodendrocytes and activated in ischaemia. *Nature* 438:1162-1166.
- Karadottir R, Hamilton NB, Bakiri Y, Attwell D (2008) Spiking and nonspiking classes of oligodendrocyte precursor glia in CNS white matter. *Nat Neurosci* 11:450-456.
- Kaushal V, Schlichter LC (2008) Mechanisms of microglia-mediated neurotoxicity in a new model of the stroke penumbra. *J Neurosci* 28:2221-2230.
- Kettenmann H, Schachner M (1985) Pharmacological properties of gamma-aminobutyric acid-, glutamate-, and aspartate-induced depolarizations in cultured astrocytes. *J Neurosci* 5:3295-3301.
- Kettenmann H, Backus KH, Schachner M (1984) Aspartate, glutamate and gamma-aminobutyric acid depolarize cultured astrocytes. *Neurosci Lett* 52:25-29.
- Kew JN, Kemp JA (2005) Ionotropic and metabotropic glutamate receptor structure and pharmacology. *Psychopharmacology (Berl)* 179:4-29.
- Khakh BS (2009) ATP-gated P2X receptors on excitatory nerve terminals onto interneurons initiate a form of asynchronous glutamate release. *Neuropharmacology* 56:216-222.
- Kharlamov A, Jones SC, Kim DK (2002) Suramin reduces infarct volume in a model of focal brain ischemia in rats. *Exp Brain Res* 147:353-359.
- Kimelberg HK (2004) Increased release of excitatory amino acids by the actions of ATP and peroxynitrite on volume-regulated anion channels (VRACs) in astrocytes. *Neurochem Int* 45:511-519.
- Kimelberg HK (2005) Astrocytic swelling in cerebral ischemia as a possible cause of injury and target for therapy. *Glia* 50:389-397.
- Kimelberg HK, Nestor NB, Feustel PJ (2004) Inhibition of release of taurine and excitatory amino acids in ischemia and neuroprotection. *Neurochem Res* 29:267-274.
- Kimelberg HK, Goderie SK, Higman S, Pang S, Waniewski RA (1990) Swelling-induced release of glutamate, aspartate, and taurine from astrocyte cultures. *J Neurosci* 10:1583-1591.

- Kimelberg HK, Cai Z, Rastogi P, Charniga CJ, Goderie S, Dave V, Jalonon TO (1997) Transmitter-induced calcium responses differ in astrocytes acutely isolated from rat brain and in culture. *J Neurochem* 68:1088-1098.
- King AE, Chung RS, Vickers JC, Dickson TC (2006) Localization of glutamate receptors in developing cortical neurons in culture and relationship to susceptibility to excitotoxicity. *J Comp Neurol* 498:277-294.
- King BF, Neary JT, Zhu Q, Wang S, Norenberg MD, Burnstock G (1996) P2 purinoceptors in rat cortical astrocytes: expression, calcium-imaging and signalling studies. *Neuroscience* 74:1187-1196.
- Kingston AE, O'Neill MJ, Bond A, Bruno V, Battaglia G, Nicoletti F, Harris JR, Clark BP, Monn JA, Lodge D, Schoepp DD (1999) Neuroprotective actions of novel and potent ligands of group I and group II metabotropic glutamate receptors. *Ann N Y Acad Sci* 890:438-449.
- Kirchhoff F, Dringen R, Giaume C (2001) Pathways of neuron-astrocyte interactions and their possible role in neuroprotection. *Eur Arch Psychiatry Clin Neurosci* 251:159-169.
- Kittner H, Hoffmann E, Krugel U, Illes P (2004) P2 receptor-mediated effects on the open field behaviour of rats in comparison with behavioural responses induced by the stimulation of dopamine D2-like and by the blockade of ionotropic glutamate receptors. *Behav Brain Res* 149:197-208.
- Kloda A, Clements JD, Lewis RJ, Adams DJ (2004) Adenosine triphosphate acts as both a competitive antagonist and a positive allosteric modulator at recombinant N-methyl-D-aspartate receptors. *Mol Pharmacol* 65:1386-1396.
- Koh JY, Palmer E, Cotman CW (1991) Activation of the metabotropic glutamate receptor attenuates N-methyl-D-aspartate neurotoxicity in cortical cultures. *Proc Natl Acad Sci U S A* 88:9431-9435.
- Koizumi S, Fujishita K, Tsuda M, Shigemoto-Mogami Y, Inoue K (2003) Dynamic inhibition of excitatory synaptic transmission by astrocyte-derived ATP in hippocampal cultures. *Proc Natl Acad Sci U S A* 100:11023-11028.
- Koizumi S, Saito Y, Nakazawa K, Nakajima K, Sawada JI, Kohsaka S, Illes P, Inoue K (2002) Spatial and temporal aspects of Ca²⁺ signaling mediated by P2Y receptors in cultured rat hippocampal astrocytes. *Life Sci* 72:431-442.
- Kondoh T, Nishizaki T, Aihara H, Tamaki N (2001) NMDA-responsible, APV-insensitive receptor in cultured human astrocytes. *Life Sci* 68:1761-1767.
- Koshimizu T, Tomic M, Van Goor F, Stojilkovic SS (1998) Functional role of alternative splicing in pituitary P2X2 receptor-channel activation and desensitization. *Mol Endocrinol* 12:901-913.
- Kosugi T, Kawahara K (2006) Reversed astrocytic GLT-1 during ischemia is crucial to excitotoxic death of neurons, but contributes to the survival of astrocytes themselves. *Neurochem Res* 31:933-943.
- Kovacs AD, Cebere G, Cebere A, Moreira T, Liljequist S (2001) Cortical and striatal neuronal cultures of the same embryonic origin show intrinsic differences in glutamate receptor expression and vulnerability to excitotoxicity. *Exp Neurol* 168:47-62.
- Kozlov AS, Angulo MC, Audinat E, Charpak S (2006) Target cell-specific modulation of neuronal activity by astrocytes. *Proc Natl Acad Sci U S A* 103:10058-10063.
- Kriegstein AR, Dichter MA (1983) Morphological classification of rat cortical neurons in cell culture. *J Neurosci* 3:1634-1647.
- Krugel U, Schraft T, Regenthal R, Illes P, Kittner H (2004) Purinergic modulation of extracellular glutamate levels in the nucleus accumbens in vivo. *Int J Dev Neurosci* 22:565-570.
- Kukley M, Barden JA, Steinhauser C, Jabs R (2001) Distribution of P2X receptors on astrocytes in juvenile rat hippocampus. *Glia* 36:11-21.
- Lalo U, Kostyuk P (1998) Developmental changes in purinergic calcium signalling in rat neocortical neurones. *Brain Res Dev Brain Res* 111:43-50.
- Lalo U, Voitenko N, Kostyuk P (1998) Iono- and metabotropically induced purinergic calcium signalling in rat neocortical neurons. *Brain Res* 799:285-291.
- Lalo U, Verkhatsky A, Pankratov Y (2007) Ivermectin potentiates ATP-induced ion currents in cortical neurones: evidence for functional expression of P2X4 receptors? *Neurosci Lett* 421:158-162.
- Lalo U, Pankratov Y, Kirchhoff F, North RA, Verkhatsky A (2006) NMDA receptors mediate neuron-to-glia signaling in mouse cortical astrocytes. *J Neurosci* 26:2673-2683.

- Lalo U, Pankratov Y, Wichert SP, Rossner MJ, North RA, Kirchhoff F, Verkhratsky A (2008) P2X1 and P2X5 subunits form the functional P2X receptor in mouse cortical astrocytes. *J Neurosci* 28:5473-5480.
- Lambrecht G (2000) Agonists and antagonists acting at P2X receptors: selectivity profiles and functional implications. *Naunyn Schmiedebergs Arch Pharmacol* 362:340-350.
- Lambrecht G, Friebe T, Grimm U, Windscheif U, Bungardt E, Hildebrandt C, Baumert HG, Spatz-Kumbel G, Mutschler E (1992) PPADS, a novel functionally selective antagonist of P2 purinoceptor-mediated responses. *Eur J Pharmacol* 217:217-219.
- Lammer A, Gunther A, Beck A, Krugel U, Kittner H, Schneider D, Illes P, Franke H (2006) Neuroprotective effects of the P2 receptor antagonist PPADS on focal cerebral ischaemia-induced injury in rats. *Eur J Neurosci* 23:2824-2828.
- Lazarowski ER, Rochelle LG, O'Neal WK, Ribeiro CM, Grubb BR, Zhang V, Harden TK, Boucher RC (2001) Cloning and functional characterization of two murine uridine nucleotide receptors reveal a potential target for correcting ion transport deficiency in cystic fibrosis gallbladder. *J Pharmacol Exp Ther* 297:43-49.
- Le Feuvre R, Brough D, Rothwell N (2002) Extracellular ATP and P2X7 receptors in neurodegeneration. *Eur J Pharmacol* 447:261-269.
- Le Feuvre RA, Brough D, Touzani O, Rothwell NJ (2003) Role of P2X7 receptors in ischemic and excitotoxic brain injury in vivo. *J Cereb Blood Flow Metab* 23:381-384.
- Le KT, Babinski K, Seguela P (1998a) Central P2X4 and P2X6 channel subunits coassemble into a novel heteromeric ATP receptor. *J Neurosci* 18:7152-7159.
- Le KT, Villeneuve P, Ramjaun AR, McPherson PS, Beaudet A, Seguela P (1998b) Sensory presynaptic and widespread somatodendritic immunolocalization of central ionotropic P2X ATP receptors. *Neuroscience* 83:177-190.
- Lechner SG, Boehm S (2004) Regulation of neuronal ion channels via P2Y receptors. *Purinergic Signal* 1:31-41.
- Lemasters JJ, DiGuseppi J, Nieminen AL, Herman B (1987) Blebbing, free Ca²⁺ and mitochondrial membrane potential preceding cell death in hepatocytes. *Nature* 325:78-81.
- Lenart B, Kintner DB, Shull GE, Sun D (2004) Na-K-Cl cotransporter-mediated intracellular Na⁺ accumulation affects Ca²⁺ signaling in astrocytes in an in vitro ischemic model. *J Neurosci* 24:9585-9597.
- Lenertz LY, Gavala ML, Hill LM, Bertics PJ (2009) Cell signaling via the P2X(7) nucleotide receptor: linkage to ROS production, gene transcription, and receptor trafficking. *Purinergic Signal* 5:175-187.
- Lenz G, Gottfried C, Luo Z, Avruch J, Rodnight R, Nie WJ, Kang Y, Neary JT (2000) P(2Y) purinoceptor subtypes recruit different mek activators in astrocytes. *Br J Pharmacol* 129:927-936.
- Leon C, Hechler B, Vial C, Leray C, Cazenave JP, Gachet C (1997) The P2Y1 receptor is an ADP receptor antagonized by ATP and expressed in platelets and megakaryoblastic cells. *FEBS Lett* 403:26-30.
- Leon C, Hechler B, Freund M, Eckly A, Vial C, Ohlmann P, Dierich A, LeMeur M, Cazenave JP, Gachet C (1999) Defective platelet aggregation and increased resistance to thrombosis in purinergic P2Y(1) receptor-null mice. *J Clin Invest* 104:1731-1737.
- Lester RA, Clements JD, Westbrook GL, Jahr CE (1990) Channel kinetics determine the time course of NMDA receptor-mediated synaptic currents. *Nature* 346:565-567.
- Li JH, Wang YH, Wolfe BB, Krueger KE, Corsi L, Stocca G, Vicini S (1998a) Developmental changes in localization of NMDA receptor subunits in primary cultures of cortical neurons. *Eur J Neurosci* 10:1704-1715.
- Li S, Mealing GA, Morley P, Stys PK (1999) Novel injury mechanism in anoxia and trauma of spinal cord white matter: glutamate release via reverse Na⁺-dependent glutamate transport. *J Neurosci* 19:RC16.
- Li WE, Nagy JI (2000) Connexin43 phosphorylation state and intercellular communication in cultured astrocytes following hypoxia and protein phosphatase inhibition. *Eur J Neurosci* 12:2644-2650.
- Li WE, Ochalski PA, Hertzberg EL, Nagy JI (1998b) Immunorecognition, ultrastructure and phosphorylation status of astrocytic gap junctions and connexin43 in rat brain after cerebral focal ischaemia. *Eur J Neurosci* 10:2444-2463.

- Lin CH, Chen PS, Gean PW (2008a) Glutamate preconditioning prevents neuronal death induced by combined oxygen-glucose deprivation in cultured cortical neurons. *Eur J Pharmacol* 589:85-93.
- Lin JH, Lou N, Kang N, Takano T, Hu F, Han X, Xu Q, Lovatt D, Torres A, Willecke K, Yang J, Kang J, Nedergaard M (2008b) A central role of connexin 43 in hypoxic preconditioning. *J Neurosci* 28:681-695.
- Lin Y, Desbois A, Jiang S, Hou ST (2005) P2 receptor antagonist PPADS confers neuroprotection against glutamate/NMDA toxicity. *Neurosci Lett* 377:97-100.
- Lipton P (1999) Ischemic cell death in brain neurons. *Physiol Rev* 79:1431-1568.
- Lipton SA (2007) Pathologically activated therapeutics for neuroprotection. *Nat Rev Neurosci* 8:803-808.
- Liu CL, Siesjo BK, Hu BR (2004) Pathogenesis of hippocampal neuronal death after hypoxia-ischemia changes during brain development. *Neuroscience* 127:113-123.
- Liu D, Smith CL, Barone FC, Ellison JA, Lysko PG, Li K, Simpson IA (1999) Astrocytic demise precedes delayed neuronal death in focal ischemic rat brain. *Brain Res Mol Brain Res* 68:29-41.
- Liu GJ, Kalous A, Werry EL, Bennett MR (2006a) Purine release from spinal cord microglia after elevation of calcium by glutamate. *Mol Pharmacol* 70:851-859.
- Liu HT, Sabirov RZ, Okada Y (2008) Oxygen-glucose deprivation induces ATP release via maxi-anion channels in astrocytes. *Purinergic Signal* 4:147-154.
- Liu HT, Tashmukhamedov BA, Inoue H, Okada Y, Sabirov RZ (2006b) Roles of two types of anion channels in glutamate release from mouse astrocytes under ischemic or osmotic stress. *Glia* 54:343-357.
- Llaudet E, Hatz S, Droniou M, Dale N (2005) Microelectrode biosensor for real-time measurement of ATP in biological tissue. *Anal Chem* 77:3267-3273.
- Longuemare MC, Swanson RA (1995) Excitatory amino acid release from astrocytes during energy failure by reversal of sodium-dependent uptake. *J Neurosci Res* 40:379-386.
- Lucas DR, Newhouse JP (1957) The toxic effect of sodium L-glutamate on the inner layers of the retina. *AMA Arch Ophthalmol* 58:193-201.
- Lucius R, Sievers J (1996) Postnatal retinal ganglion cells in vitro: protection against reactive oxygen species (ROS)-induced axonal degeneration by cocultured astrocytes. *Brain Res* 743:56-62.
- Lukaszevicz AC, Sampaio N, Guegan C, Benchoua A, Couriaud C, Chevalier E, Sola B, Lacombe P, Onteniente B (2002) High sensitivity of protoplasmic cortical astroglia to focal ischemia. *J Cereb Blood Flow Metab* 22:289-298.
- Lundy PM, Hamilton MG, Mi L, Gong W, Vair C, Sawyer TW, Frew R (2002) Stimulation of Ca(2+) influx through ATP receptors on rat brain synaptosomes: identification of functional P2X(7) receptor subtypes. *Br J Pharmacol* 135:1616-1626.
- Lustig KD, Shiau AK, Brake AJ, Julius D (1993) Expression cloning of an ATP receptor from mouse neuroblastoma cells. *Proc Natl Acad Sci U S A* 90:5113-5117.
- Lutz PL, Kabler S (1997) Release of adenosine and ATP in the brain of the freshwater turtle (*Trachemys scripta*) during long-term anoxia. *Brain Res* 769:281-286.
- Luzzati F, De Marchis S, Fasolo A, Peretto P (2006) Neurogenesis in the caudate nucleus of the adult rabbit. *J Neurosci* 26:609-621.
- Lynch KJ, Touma E, Niforatos W, Kage KL, Burgard EC, van Biesen T, Kowaluk EA, Jarvis MF (1999) Molecular and functional characterization of human P2X(2) receptors. *Mol Pharmacol* 56:1171-1181.
- Lyons SA, Kettenmann H (1998) Oligodendrocytes and microglia are selectively vulnerable to combined hypoxia and hypoglycemia injury in vitro. *J Cereb Blood Flow Metab* 18:521-530.
- Ma J, Endres M, Moskowitz MA (1998) Synergistic effects of caspase inhibitors and MK-801 in brain injury after transient focal cerebral ischaemia in mice. *Br J Pharmacol* 124:756-762.
- Maiese K, Swiriduk M, TenBroeke M (1996) Cellular mechanisms of protection by metabotropic glutamate receptors during anoxia and nitric oxide toxicity. *J Neurochem* 66:2419-2428.
- Malarkey EB, Parpura V (2008) Mechanisms of glutamate release from astrocytes. *Neurochem Int* 52:142-154.
- Mamedova LK, Gao ZG, Jacobson KA (2006) Regulation of death and survival in astrocytes by ADP activating P2Y1 and P2Y12 receptors. *Biochem Pharmacol* 72:1031-1041.

- Manning SM, Talos DM, Zhou C, Selip DB, Park HK, Park CJ, Volpe JJ, Jensen FE (2008) NMDA receptor blockade with memantine attenuates white matter injury in a rat model of periventricular leukomalacia. *J Neurosci* 28:6670-6678.
- Marcoli M, Cervetto C, Castagnetta M, Saffi P, Maura G (2004a) 5-HT control of ischemia-evoked glutamate efflux from human cerebrocortical slices. *Neurochem Int* 45:687-691.
- Marcoli M, Raiteri L, Bonfanti A, Monopoli A, Ongini E, Raiteri M, Maura G (2003) Sensitivity to selective adenosine A1 and A2A receptor antagonists of the release of glutamate induced by ischemia in rat cerebrocortical slices. *Neuropharmacology* 45:201-210.
- Marcoli M, Bonfanti A, Roccatagliata P, Chiamonte G, Ongini E, Raiteri M, Maura G (2004b) Glutamate efflux from human cerebrocortical slices during ischemia: vesicular-like mode of glutamate release and sensitivity to A(2A) adenosine receptor blockade. *Neuropharmacology* 47:884-891.
- Marcus AJ, Broekman MJ, Drosopoulos JH, Islam N, Pinsky DJ, Sesti C, Levi R (2003) Metabolic control of excessive extracellular nucleotide accumulation by CD39/ecto-nucleotidase-1: implications for ischemic vascular diseases. *J Pharmacol Exp Ther* 305:9-16.
- Margaill I, Parmentier S, Callebert J, Allix M, Boulu RG, Plotkine M (1996) Short therapeutic window for MK-801 in transient focal cerebral ischemia in normotensive rats. *J Cereb Blood Flow Metab* 16:107-113.
- Marks JD, Friedman JE, Haddad GG (1996) Vulnerability of CA1 neurons to glutamate is developmentally regulated. *Brain Res Dev Brain Res* 97:194-206.
- Marteau F, Le Poul E, Communi D, Labouret C, Savi P, Boeynaems JM, Gonzalez NS (2003) Pharmacological characterization of the human P2Y13 receptor. *Mol Pharmacol* 64:104-112.
- Martin LJ, Blackstone CD, Levey AI, Hagan RL, Price DL (1993) AMPA glutamate receptor subunits are differentially distributed in rat brain. *Neuroscience* 53:327-358.
- Martin LJ, Al-Abdulla NA, Brambrink AM, Kirsch JR, Sieber FE, Portera-Cailliau C (1998) Neurodegeneration in excitotoxicity, global cerebral ischemia, and target deprivation: A perspective on the contributions of apoptosis and necrosis. *Brain Res Bull* 46:281-309.
- Martin LJ, Brambrink AM, Lehmann C, Portera-Cailliau C, Koehler R, Rothstein J, Traystman RJ (1997) Hypoxia-ischemia causes abnormalities in glutamate transporters and death of astroglia and neurons in newborn striatum. *Ann Neurol* 42:335-348.
- Martinez-Sanchez M, Striggow F, Schroder UH, Kahlert S, Reymann KG, Reiser G (2004) Na(+) and Ca(2+) homeostasis pathways, cell death and protection after oxygen-glucose-deprivation in organotypic hippocampal slice cultures. *Neuroscience* 128:729-740.
- Masse K, Bhamra S, Eason R, Dale N, Jones EA (2007) Purine-mediated signalling triggers eye development. *Nature* 449:1058-1062.
- Matsumoto K, Lo EH, Pierce AR, Halpern EF, Newcomb R (1996) Secondary elevation of extracellular neurotransmitter amino acids in the reperfusion phase following focal cerebral ischemia. *J Cereb Blood Flow Metab* 16:114-124.
- Matute C, Domercq M, Sanchez-Gomez MV (2006) Glutamate-mediated glial injury: mechanisms and clinical importance. *Glia* 53:212-224.
- Matute C, Alberdi E, Ibarretxe G, Sanchez-Gomez MV (2002) Excitotoxicity in glial cells. *Eur J Pharmacol* 447:239-246.
- Matute C, Torre I, Perez-Cerda F, Perez-Samartin A, Alberdi E, Etxebarria E, Arranz AM, Ravid R, Rodriguez-Antiguedad A, Sanchez-Gomez M, Domercq M (2007) P2X(7) receptor blockade prevents ATP excitotoxicity in oligodendrocytes and ameliorates experimental autoimmune encephalomyelitis. *J Neurosci* 27:9525-9533.
- McDonald JW, Althomsons SP, Hyrc KL, Choi DW, Goldberg MP (1998) Oligodendrocytes from forebrain are highly vulnerable to AMPA/kainate receptor-mediated excitotoxicity. *Nat Med* 4:291-297.
- Melani A, Turchi D, Vannucchi MG, Cipriani S, Gianfriddo M, Pedata F (2005) ATP extracellular concentrations are increased in the rat striatum during in vivo ischemia. *Neurochem Int* 47:442-448.
- Melani A, Pantoni L, Corsi C, Bianchi L, Monopoli A, Bertorelli R, Pepeu G, Pedata F (1999) Striatal outflow of adenosine, excitatory amino acids, gamma-aminobutyric acid, and taurine in awake freely moving rats after middle cerebral artery occlusion: correlations with neurological deficit and histopathological damage. *Stroke* 30:2448-2454; discussion 2455.

- Melani A, Amadio S, Gianfriddo M, Vannucchi MG, Volonte C, Bernardi G, Pedata F, Sancesario G (2006) P2X7 receptor modulation on microglial cells and reduction of brain infarct caused by middle cerebral artery occlusion in rat. *J Cereb Blood Flow Metab* 26:974-982.
- Mendoza-Fernandez V, Andrew RD, Barajas-Lopez C (2000) ATP inhibits glutamate synaptic release by acting at P2Y receptors in pyramidal neurons of hippocampal slices. *J Pharmacol Exp Ther* 293:172-179.
- Meucci O, Fatatis A, Holzwarth JA, Miller RJ (1996) Developmental regulation of the toxin sensitivity of Ca(2+)-permeable AMPA receptors in cortical glia. *J Neurosci* 16:519-530.
- Micu I, Jiang Q, Coderre E, Ridsdale A, Zhang L, Woulfe J, Yin X, Trapp BD, McRory JE, Rehak R, Zamponi GW, Wang W, Stys PK (2006) NMDA receptors mediate calcium accumulation in myelin during chemical ischaemia. *Nature* 439:988-992.
- Milius D, Sperlagh B, Illes P (2008) Up-regulation of P2X7 receptor-immunoreactivity by *in vitro* ischemia on the plasma membrane of cultured rat cortical neurons. *Neurosci Lett*.
- Mitani A, Tanaka K (2003) Functional changes of glial glutamate transporter GLT-1 during ischemia: an *in vivo* study in the hippocampal CA1 of normal mice and mutant mice lacking GLT-1. *J Neurosci* 23:7176-7182.
- Mitani A, Andou Y, Matsuda S, Arai T, Sakanaka M, Kataoka K (1994) Origin of ischemia-induced glutamate efflux in the CA1 field of the gerbil hippocampus: an *in vivo* brain microdialysis study. *J Neurochem* 63:2152-2164.
- Mongin AA, Kimelberg HK (2002) ATP potently modulates anion channel-mediated excitatory amino acid release from cultured astrocytes. *Am J Physiol Cell Physiol* 283:C569-578.
- Monif M, Reid CA, Powell KL, Smart ML, Williams DA (2009) The P2X7 receptor drives microglial activation and proliferation: a trophic role for P2X7R pore. *J Neurosci* 29:3781-3791.
- Montana V, Malarkey EB, Verderio C, Matteoli M, Parpura V (2006) Vesicular transmitter release from astrocytes. *Glia* 54:700-715.
- Montero M, Gonzalez B, Zimmer J (2009) Immunotoxic depletion of microglia in mouse hippocampal slice cultures enhances ischemia-like neurodegeneration. *Brain Res* 1291:140-152.
- Monyer H, Goldberg MP, Choi DW (1989) Glucose deprivation neuronal injury in cortical culture. *Brain Res* 483:347-354.
- Moore D, Chambers J, Waldvogel H, Faull R, Emson P (2000) Regional and cellular distribution of the P2Y(1) purinergic receptor in the human brain: striking neuronal localisation. *J Comp Neurol* 421:374-384.
- Moro S, Guo D, Camaioni E, Boyer JL, Harden TK, Jacobson KA (1998) Human P2Y1 receptor: molecular modeling and site-directed mutagenesis as tools to identify agonist and antagonist recognition sites. *J Med Chem* 41:1456-1466.
- Motin L, Bennett MR (1995) Effect of P2-purinoreceptor antagonists on glutamatergic transmission in the rat hippocampus. *Br J Pharmacol* 115:1276-1280.
- Mulryan K, Gitterman DP, Lewis CJ, Vial C, Leckie BJ, Cobb AL, Brown JE, Conley EC, Buell G, Pritchard CA, Evans RJ (2000) Reduced vas deferens contraction and male infertility in mice lacking P2X1 receptors. *Nature* 403:86-89.
- Murakami K, Nakamura Y, Yoneda Y (2003) Potentiation by ATP of lipopolysaccharide-stimulated nitric oxide production in cultured astrocytes. *Neuroscience* 117:37-42.
- Nakase T, Fushiki S, Naus CC (2003) Astrocytic gap junctions composed of connexin 43 reduce apoptotic neuronal damage in cerebral ischemia. *Stroke* 34:1987-1993.
- Nakatsuka T, Gu JG (2001) ATP P2X receptor-mediated enhancement of glutamate release and evoked EPSCs in dorsal horn neurons of the rat spinal cord. *J Neurosci* 21:6522-6531.
- Nakatsuka T, Tsuzuki K, Ling JX, Sonobe H, Gu JG (2003) Distinct roles of P2X receptors in modulating glutamate release at different primary sensory synapses in rat spinal cord. *J Neurophysiol* 89:3243-3252.
- Nakayama R, Yano T, Ushijima K, Abe E, Terasaki H (2002) Effects of dantrolene on extracellular glutamate concentration and neuronal death in the rat hippocampal CA1 region subjected to transient ischemia. *Anesthesiology* 96:705-710.

- Nakazawa K, Inoue K, Ito K, Koizumi S (1995) Inhibition by suramin and reactive blue 2 of GABA and glutamate receptor channels in rat hippocampal neurons. *Naunyn Schmiedebergs Arch Pharmacol* 351:202-208.
- Namura S, Maeno H, Takami S, Jiang XF, Kamichi S, Wada K, Nagata I (2002) Inhibition of glial glutamate transporter GLT-1 augments brain edema after transient focal cerebral ischemia in mice. *Neurosci Lett* 324:117-120.
- Narcisse L, Scemes E, Zhao Y, Lee SC, Brosnan CF (2005) The cytokine IL-1beta transiently enhances P2X7 receptor expression and function in human astrocytes. *Glia* 49:245-258.
- Neary JT, Baker L, Jorgensen SL, Norenberg MD (1994a) Extracellular ATP induces stellation and increases glial fibrillary acidic protein content and DNA synthesis in primary astrocyte cultures. *Acta Neuropathol* 87:8-13.
- Neary JT, Whittemore SR, Zhu Q, Norenberg MD (1994b) Synergistic activation of DNA synthesis in astrocytes by fibroblast growth factors and extracellular ATP. *J Neurochem* 63:490-494.
- Neary JT, Kang Y, Shi YF, Tran MD, Wanner IB (2006) P2 receptor signalling, proliferation of astrocytes, and expression of molecules involved in cell-cell interactions. *Novartis Found Symp* 276:131-143; discussion 143-137, 233-137, 275-181.
- Nedergaard M, Dirnagl U (2005) Role of glial cells in cerebral ischemia. *Glia* 50:281-286.
- Nedergaard M, Ransom B, Goldman SA (2003) New roles for astrocytes: redefining the functional architecture of the brain. *Trends Neurosci* 26:523-530.
- Nellgard B, Wieloch T (1992) Postischemic blockade of AMPA but not NMDA receptors mitigates neuronal damage in the rat brain following transient severe cerebral ischemia. *J Cereb Blood Flow Metab* 12:2-11.
- Newell DW, Barth A, Papermaster V, Malouf AT (1995) Glutamate and non-glutamate receptor mediated toxicity caused by oxygen and glucose deprivation in organotypic hippocampal cultures. *J Neurosci* 15:7702-7711.
- Nicke A, Kuan YH, Masin M, Rettinger J, Marquez-Klaka B, Bender O, Gorecki DC, Murrell-Lagnado RD, Soto F (2009) A functional P2X7 splice variant with an alternative transmembrane domain 1 escapes gene inactivation in P2X7 knock-out mice. *J Biol Chem* 284:25813-25822.
- Nishizaki T (2004) ATP- and adenosine-mediated signaling in the central nervous system: adenosine stimulates glutamate release from astrocytes via A2a adenosine receptors. *J Pharmacol Sci* 94:100-102.
- Nobile M, Monaldi I, Alloisio S, Cugnoli C, Ferroni S (2003) ATP-induced, sustained calcium signalling in cultured rat cortical astrocytes: evidence for a non-capacitative, P2X7-like-mediated calcium entry. *FEBS Lett* 538:71-76.
- Noctor SC, Ivic L, Martinez-Cerdeno V, Kriegstein AR (2005) The role of neurogenic astroglial cells in the developing and adult central nervous system. In: *Neuroglia*, 2nd edition Edition (Kettenmann H, Ransom B, eds), pp 101-111. Oxford: Oxford University Press.
- Nolte C, Matyash M, Pivneva T, Schipke CG, Ohlemeyer C, Hanisch UK, Kirchhoff F, Kettenmann H (2001) GFAP promoter-controlled EGFP-expressing transgenic mice: a tool to visualize astrocytes and astrogliosis in living brain tissue. *Glia* 33:72-86.
- North RA (2002) Molecular physiology of P2X receptors. *Physiol Rev* 82:1013-1067.
- North RA, Verkhratsky A (2006) Purinergic transmission in the central nervous system. *Pflugers Arch* 452:479-485.
- O'Collins VE, Macleod MR, Donnan GA, Horkey LL, van der Worp BH, Howells DW (2006) 1,026 experimental treatments in acute stroke. *Ann Neurol* 59:467-477.
- Obenaus A, Ashwal S (2008) Magnetic resonance imaging in cerebral ischemia: focus on neonates. *Neuropharmacology* 55:271-280.
- Olney JW (1969) Brain lesions, obesity, and other disturbances in mice treated with monosodium glutamate. *Science* 164:719-721.
- Olney JW, Sharpe LG (1969) Brain lesions in an infant rhesus monkey treated with monosodium glutamate. *Science* 166:386-388.
- Olney JW, Ho OL, Rhee V (1971) Cytotoxic effects of acidic and sulphur containing amino acids on the infant mouse central nervous system. *Exp Brain Res* 14:61-76.

- Ong WY, Motin LG, Hansen MA, Dias LS, Ayrout C, Bennett MR, Balcar VJ (1997) P2 purinoceptor blocker suramin antagonises NMDA receptors and protects against excitatory behaviour caused by NMDA receptor agonist (RS)-(tetrazol-5-yl)-glycine in rats. *J Neurosci Res* 49:627-638.
- Ooboshi H, Ibayashi S, Takano K, Sadoshima S, Kondo A, Uchimura H, Fujishima M (2000) Hypothermia inhibits ischemia-induced efflux of amino acids and neuronal damage in the hippocampus of aged rats. *Brain Res* 884:23-30.
- Opitz T, Reymann KG (1993) (1S, 3R)-ACPD protects synaptic transmission from hypoxia in hippocampal slices. *Neuropharmacology* 32:103-104.
- Ortinou S, Laube B, Zimmermann H (2003) ATP inhibits NMDA receptors after heterologous expression and in cultured hippocampal neurons and attenuates NMDA-mediated neurotoxicity. *J Neurosci* 23:4996-5003.
- Otis TS, Sofroniew MV (2008) Glia get excited. *Nat Neurosci* 11:379-380.
- Ottersen OP, Laake JH, Reichelt W, Haug FM, Torp R (1996) Ischemic disruption of glutamate homeostasis in brain: quantitative immunocytochemical analyses. *J Chem Neuroanat* 12:1-14.
- Ozawa S, Kamiya H, Tsuzuki K (1998) Glutamate receptors in the mammalian central nervous system. *Prog Neurobiol* 54:581-618.
- Pangrsic T, Potokar M, Stenovec M, Kreft M, Fabbretti E, Nistri A, Pryazhnikov E, Khirouq L, Giniatullin R, Zorec R (2007) Exocytotic release of ATP from cultured astrocytes. *J Biol Chem* 282:28749-28758.
- Pankratov Y, Lalo U, Krishtal O, Verkhratsky A (2003) P2X receptor-mediated excitatory synaptic currents in somatosensory cortex. *Mol Cell Neurosci* 24:842-849.
- Pankratov Y, Lalo U, Verkhratsky A, North RA (2006) Vesicular release of ATP at central synapses. *Pflugers Arch* 452:589-597.
- Pankratov Y, Lalo U, Verkhratsky A, North RA (2007) Quantal release of ATP in mouse cortex. *J Gen Physiol* 129:257-265.
- Pankratov YV, Lalo UV, Krishtal OA (2002) Role for P2X receptors in long-term potentiation. *J Neurosci* 22:8363-8369.
- Papadopoulos MC, Koumenis IL, Dugan LL, Giffard RG (1997) Vulnerability to glucose deprivation injury correlates with glutathione levels in astrocytes. *Brain Res* 748:151-156.
- Papadopoulos MC, Koumenis IL, Yuan TY, Giffard RG (1998) Increasing vulnerability of astrocytes to oxidative injury with age despite constant antioxidant defenses. *Neuroscience* 82:915-925.
- Papp L, Vizi ES, Sperlagh B (2004) Lack of ATP-evoked GABA and glutamate release in the hippocampus of P2X7 receptor^{-/-} mice. *Neuroreport* 15:2387-2391.
- Paredes RM, Etzler JC, Watts LT, Zheng W, Lechleiter JD (2008) Chemical calcium indicators. *Methods* 46:143-151.
- Parkinson FE, Xiong W (2004) Stimulus- and cell-type-specific release of purines in cultured rat forebrain astrocytes and neurons. *J Neurochem* 88:1305-1312.
- Parkinson FE, Sinclair CJ, Othman T, Haughey NJ, Geiger JD (2002) Differences between rat primary cortical neurons and astrocytes in purine release evoked by ischemic conditions. *Neuropharmacology* 43:836-846.
- Parvathenani LK, Tertysnikova S, Greco CR, Roberts SB, Robertson B, Posmantur R (2003) P2X7 mediates superoxide production in primary microglia and is up-regulated in a transgenic mouse model of Alzheimer's disease. *J Biol Chem* 278:13309-13317.
- Pascual O, Casper KB, Kubera C, Zhang J, Revilla-Sanchez R, Sul JY, Takano H, Moss SJ, McCarthy K, Haydon PG (2005) Astrocytic purinergic signaling coordinates synaptic networks. *Science* 310:113-116.
- Pasti L, Zonta M, Pozzan T, Vicini S, Carmignoto G (2001) Cytosolic calcium oscillations in astrocytes may regulate exocytotic release of glutamate. *J Neurosci* 21:477-484.
- Pausch MH, Lai M, Tseng E, Paulsen J, Bates B, Kwak S (2004) Functional expression of human and mouse P2Y12 receptors in *Saccharomyces cerevisiae*. *Biochem Biophys Res Commun* 324:171-177.
- Pearson T, Damian K, Lynas RE, Frenguelli BG (2006) Sustained elevation of extracellular adenosine and activation of A1 receptors underlie the post-ischaemic inhibition of neuronal function in rat hippocampus in vitro. *J Neurochem* 97:1357-1368.

- Pedata F, Gianfriddo M, Turchi D, Melani A (2005) The protective effect of adenosine A2A receptor antagonism in cerebral ischemia. *Neurol Res* 27:169-174.
- Pedata F, Melani A, Pugliese AM, Coppi E, Cipriani S, Traini C (2007) The role of ATP and adenosine in the brain under normoxic and ischemic conditions. *Purinergic Signal* 3:299-310.
- Pelegrin P, Surprenant A (2006) Pannexin-1 mediates large pore formation and interleukin-1 β release by the ATP-gated P2X7 receptor. *EMBO J* 25:5071-5082.
- Pelegrin P, Surprenant A (2009) The P2X(7) receptor-pannexin connection to dye uptake and IL-1 β release. *Purinergic Signal* 5:129-137.
- Pellegatti P, Falzoni S, Pinton P, Rizzuto R, Di Virgilio F (2005) A novel recombinant plasma membrane-targeted luciferase reveals a new pathway for ATP secretion. *Mol Biol Cell* 16:3659-3665.
- Pellerin L, Magistretti PJ (2004) Neuroenergetics: calling upon astrocytes to satisfy hungry neurons. *Neuroscientist* 10:53-62.
- Peoples RW, Li C (1998) Inhibition of NMDA-gated ion channels by the P2 purinoceptor antagonists suramin and reactive blue 2 in mouse hippocampal neurones. *Br J Pharmacol* 124:400-408.
- Persson L, Valtysson J, Enblad P, Warne PE, Cesarini K, Lewen A, Hillered L (1996) Neurochemical monitoring using intracerebral microdialysis in patients with subarachnoid hemorrhage. *J Neurosurg* 84:606-616.
- Petito CK, Olarte JP, Roberts B, Nowak TS, Jr., Pulsinelli WA (1998) Selective glial vulnerability following transient global ischemia in rat brain. *J Neuropathol Exp Neurol* 57:231-238.
- Petralia RS, Wenthold RJ (1992) Light and electron immunocytochemical localization of AMPA-selective glutamate receptors in the rat brain. *J Comp Neurol* 318:329-354.
- Phillis JW (1995) The effects of selective A1 and A2a adenosine receptor antagonists on cerebral ischemic injury in the gerbil. *Brain Res* 705:79-84.
- Phillis JW, O'Regan MH, Perkins LM (1993) Adenosine 5'-triphosphate release from the normoxic and hypoxic in vivo rat cerebral cortex. *Neurosci Lett* 151:94-96.
- Phillis JW, Smith-Barbour M, O'Regan MH (1996) Changes in extracellular amino acid neurotransmitters and purines during and following ischemias of different durations in the rat cerebral cortex. *Neurochem Int* 29:115-120.
- Phillis JW, Ren J, O'Regan MH (2000) Transporter reversal as a mechanism of glutamate release from the ischemic rat cerebral cortex: studies with DL-threo-beta-benzyloxyaspartate. *Brain Res* 880:224.
- Pinheiro P, Mülle C (2006) Kainate receptors. *Cell Tissue Res* 326:457-482.
- Pinsky DJ, Broekman MJ, Peschon JJ, Stocking KL, Fujita T, Ramasamy R, Connolly ES, Jr., Huang J, Kiss S, Zhang Y, Choudhri TF, McTaggart RA, Liao H, Drosopoulos JH, Price VL, Marcus AJ, Maliszewski CR (2002) Elucidation of the thromboregulatory role of CD39/ectoapyrase in the ischemic brain. *J Clin Invest* 109:1031-1040.
- Pinteaux E, Rothwell NJ, Boutin H (2006) Neuroprotective actions of endogenous interleukin-1 receptor antagonist (IL-1ra) are mediated by glia. *Glia* 53:551-556.
- Porter JT, McCarthy KD (1995) GFAP-positive hippocampal astrocytes in situ respond to glutamatergic neuroligands with increases in [Ca²⁺]_i. *Glia* 13:101-112.
- Porter JT, McCarthy KD (1997) Astrocytic neurotransmitter receptors in situ and in vivo. *Prog Neurobiol* 51:439-455.
- Praetorius HA, Leipziger J (2009) ATP release from non-excitabile cells. *Purinergic Signal*.
- Price CJ, Raymond LA (1996) Evans blue antagonizes both alpha-amino-3-hydroxy-5-methyl-4-isoxazolepropionate and kainate receptors and modulates receptor desensitization. *Mol Pharmacol* 50:1665-1671.
- Prieto M, Alonso G (1999) Differential sensitivity of cultured tanycytes and astrocytes to hydrogen peroxide toxicity. *Exp Neurol* 155:118-127.
- Pringle AK (2004) In, out, shake it all about: elevation of [Ca²⁺]_i during acute cerebral ischaemia. *Cell Calcium* 36:235-245.
- Pringle AK, Iannotti F, Wilde GJ, Chad JE, Seeley PJ, Sundstrom LE (1997) Neuroprotection by both NMDA and non-NMDA receptor antagonists in in vitro ischemia. *Brain Res* 755:36-46.
- Pulsinelli WA, Brierley JB, Plum F (1982) Temporal profile of neuronal damage in a model of transient forebrain ischemia. *Ann Neurol* 11:491-498.

- Queiroz G, Gebicke-Haerter PJ, Schobert A, Starke K, von Kugelgen I (1997) Release of ATP from cultured rat astrocytes elicited by glutamate receptor activation. *Neuroscience* 78:1203-1208.
- Queiroz G, Meyer DK, Meyer A, Starke K, von Kugelgen I (1999) A study of the mechanism of the release of ATP from rat cortical astroglial cells evoked by activation of glutamate receptors. *Neuroscience* 91:1171-1181.
- Raff MC, Abney ER, Cohen J, Lindsay R, Noble M (1983) Two types of astrocytes in cultures of developing rat white matter: differences in morphology, surface gangliosides, and growth characteristics. *J Neurosci* 3:1289-1300.
- Ralevic V, Burnstock G (1998) Receptors for purines and pyrimidines. *Pharmacol Rev* 50:413-492.
- Rao VL, Dogan A, Todd KG, Bowen KK, Kim BT, Rothstein JD, Dempsey RJ (2001) Antisense knockdown of the glial glutamate transporter GLT-1, but not the neuronal glutamate transporter EAAC1, exacerbates transient focal cerebral ischemia-induced neuronal damage in rat brain. *J Neurosci* 21:1876-1883.
- Rauca C, Henrich-Noack P, Schafer K, Holtt V, Reymann KG (1998) (S)-4C3HPG reduces infarct size after focal cerebral ischemia. *Neuropharmacology* 37:1649-1652.
- Rawanduzy A, Hansen A, Hansen TW, Nedergaard M (1997) Effective reduction of infarct volume by gap junction blockade in a rodent model of stroke. *J Neurosurg* 87:916-920.
- Re DB, Boucraut J, Samuel D, Birman S, Kerkerian-Le Goff L, Had-Aissouni L (2003) Glutamate transport alteration triggers differentiation-state selective oxidative death of cultured astrocytes: a mechanism different from excitotoxicity depending on intracellular GSH contents. *J Neurochem* 85:1159-1170.
- Re DB, Nafia I, Melon C, Shimamoto K, Kerkerian-Le Goff L, Had-Aissouni L (2006) Glutamate leakage from a compartmentalized intracellular metabolic pool and activation of the lipoxygenase pathway mediate oxidative astrocyte death by reversed glutamate transport. *Glia* 54:47-57.
- Reichenbach A, Wolburg H (2005) Astrocytes and ependymal glia. In: *Neuroglia*, 2nd edition Edition (Kettenmann H, Ransom B, eds), pp 19-35. Oxford: Oxford University Press.
- Reichert SA, Kim-Han JS, Dugan LL (2001) The mitochondrial permeability transition pore and nitric oxide synthase mediate early mitochondrial depolarization in astrocytes during oxygen-glucose deprivation. *J Neurosci* 21:6608-6616.
- Reifel Saltzberg JM, Garvey KA, Keirstead SA (2003) Pharmacological characterization of P2Y receptor subtypes on isolated tiger salamander Muller cells. *Glia* 42:149-159.
- Reigada D, Lu W, Mitchell CH (2006) Glutamate acts at NMDA receptors on fresh bovine and on cultured human retinal pigment epithelial cells to trigger release of ATP. *J Physiol* 575:707-720.
- Rieg T, Bunday RA, Chen Y, Deschenes G, Junger W, Insel PA, Vallon V (2007) Mice lacking P2Y2 receptors have salt-resistant hypertension and facilitated renal Na⁺ and water reabsorption. *FASEB J* 21:3717-3726.
- Roberts JA, Vial C, Digby HR, Agboh KC, Wen H, Atterbury-Thomas A, Evans RJ (2006) Molecular properties of P2X receptors. *Pflugers Arch* 452:486-500.
- Robson SC, Kaczmarek E, Siegel JB, Candinas D, Koziak K, Millan M, Hancock WW, Bach FH (1997) Loss of ATP diphosphohydrolase activity with endothelial cell activation. *J Exp Med* 185:153-163.
- Rodrigues RJ, Almeida T, Richardson PJ, Oliveira CR, Cunha RA (2005) Dual presynaptic control by ATP of glutamate release via facilitatory P2X1, P2X2/3, and P2X3 and inhibitory P2Y1, P2Y2, and/or P2Y4 receptors in the rat hippocampus. *J Neurosci* 25:6286-6295.
- Rosenberg PA, Aizenman E (1989) Hundred-fold increase in neuronal vulnerability to glutamate toxicity in astrocyte-poor cultures of rat cerebral cortex. *Neurosci Lett* 103:162-168.
- Rosenberg PA, Amin S, Leitner M (1992) Glutamate uptake disguises neurotoxic potency of glutamate agonists in cerebral cortex in dissociated cell culture. *J Neurosci* 12:56-61.
- Rossi DJ, Oshima T, Attwell D (2000) Glutamate release in severe brain ischaemia is mainly by reversed uptake. *Nature* 403:316-321.
- Rossi DJ, Brady JD, Mohr C (2007) Astrocyte metabolism and signaling during brain ischemia. *Nat Neurosci* 10:1377-1386.
- Rubini P, Pinkwart C, Franke H, Gerevich Z, Norenberg W, Illes P (2006) Regulation of intracellular Ca²⁺ by P2Y1 receptors may depend on the developmental stage of cultured rat striatal neurons. *J Cell Physiol* 209:81-93.

- Rubio ME, Soto F (2001) Distinct Localization of P2X receptors at excitatory postsynaptic specializations. *J Neurosci* 21:641-653.
- Runden-Pran E, Tanso R, Haug FM, Ottersen OP, Ring A (2005) Neuroprotective effects of inhibiting N-methyl-D-aspartate receptors, P2X receptors and the mitogen-activated protein kinase cascade: a quantitative analysis in organotypical hippocampal slice cultures subjected to oxygen and glucose deprivation. *Neuroscience* 136:795-810.
- Russman BS, Ashwal S (2004) Evaluation of the child with cerebral palsy. *Semin Pediatr Neurol* 11:47-57.
- Ryu JK, Kim J, Choi SH, Oh YJ, Lee YB, Kim SU, Jin BK (2002) ATP-induced in vivo neurotoxicity in the rat striatum via P2 receptors. *Neuroreport* 13:1611-1615.
- Sagara Y, Schubert D (1998) The activation of metabotropic glutamate receptors protects nerve cells from oxidative stress. *J Neurosci* 18:6662-6671.
- Sala C, Rudolph-Correia S, Sheng M (2000) Developmentally regulated NMDA receptor-dependent dephosphorylation of cAMP response element-binding protein (CREB) in hippocampal neurons. *J Neurosci* 20:3529-3536.
- Saliba E, Marret S (2001) Cerebral white matter damage in the preterm infant: pathophysiology and risk factors. *Semin Neonatol* 6:121-133.
- Salter MG, Fern R (2005) NMDA receptors are expressed in developing oligodendrocyte processes and mediate injury. *Nature* 438:1167-1171.
- Salter MG, Fern R (2008) The mechanisms of acute ischemic injury in the cell processes of developing white matter astrocytes. *J Cereb Blood Flow Metab* 28:588-601.
- Sasaki Y, Hoshi M, Akazawa C, Nakamura Y, Tsuzuki H, Inoue K, Kohsaka S (2003) Selective expression of Gi/o-coupled ATP receptor P2Y12 in microglia in rat brain. *Glia* 44:242-250.
- Sattler R, Tymianski M (2001) Molecular mechanisms of glutamate receptor-mediated excitotoxic neuronal cell death. *Mol Neurobiol* 24:107-129.
- Sattler R, Charlton MP, Hafner M, Tymianski M (1998) Distinct influx pathways, not calcium load, determine neuronal vulnerability to calcium neurotoxicity. *J Neurochem* 71:2349-2364.
- Saura J (2007) Microglial cells in astroglial cultures: a cautionary note. *J Neuroinflammation* 4:26.
- Schipke CG, Ohlemeyer C, Matyash M, Nolte C, Kettenmann H, Kirchhoff F (2001) Astrocytes of the mouse neocortex express functional N-methyl-D-aspartate receptors. *FASEB J* 15:1270-1272.
- Schock SC, Leblanc D, Hakim AM, Thompson CS (2008) ATP release by way of connexin 36 hemichannels mediates ischemic tolerance in vitro. *Biochem Biophys Res Commun* 368:138-144.
- Schock SC, Munyao N, Yakubchik Y, Sabourin LA, Hakim AM, Ventureyra EC, Thompson CS (2007) Cortical spreading depression releases ATP into the extracellular space and purinergic receptor activation contributes to the induction of ischemic tolerance. *Brain Res* 1168:129-138.
- Scholz KP, Miller RJ (1992) Inhibition of quantal transmitter release in the absence of calcium influx by a G protein-linked adenosine receptor at hippocampal synapses. *Neuron* 8:1139-1150.
- Schroder UH, Opitz T, Jager T, Sabelhaus CF, Breder J, Reymann KG (1999) Protective effect of group I metabotropic glutamate receptor activation against hypoxic/hypoglycemic injury in rat hippocampal slices: timing and involvement of protein kinase C. *Neuropharmacology* 38:209-216.
- Schubert P, Ogata T, Marchini C, Ferroni S, Rudolph K (1997) Protective mechanisms of adenosine in neurons and glial cells. *Ann N Y Acad Sci* 825:1-10.
- Schulze-Lohoff E, Hugo C, Rost S, Arnold S, Gruber A, Brune B, Sterzel RB (1998) Extracellular ATP causes apoptosis and necrosis of cultured mesangial cells via P2Z/P2X7 receptors. *Am J Physiol* 275:F962-971.
- Seifert G, Steinhauser C (1995) Glial cells in the mouse hippocampus express AMPA receptors with an intermediate Ca²⁺ permeability. *Eur J Neurosci* 7:1872-1881.
- Seifert G, Steinhauser C (2001) Ionotropic glutamate receptors in astrocytes. *Prog Brain Res* 132:287-299.
- Seki Y, Feustel PJ, Keller RW, Jr., Tranmer BI, Kimelberg HK (1999) Inhibition of ischemia-induced glutamate release in rat striatum by dihydrokinate and an anion channel blocker. *Stroke* 30:433-440.
- Sellers LA, Simon J, Lundahl TS, Cousens DJ, Humphrey PP, Barnard EA (2001) Adenosine nucleotides acting at the human P2Y1 receptor stimulate mitogen-activated protein kinases and induce apoptosis. *J Biol Chem* 276:16379-16390.

- Shannon C, Salter M, Fern R (2007) GFP imaging of live astrocytes: regional differences in the effects of ischaemia upon astrocytes. *J Anat* 210:684-692.
- Sheldon AL, Robinson MB (2007) The role of glutamate transporters in neurodegenerative diseases and potential opportunities for intervention. *Neurochem Int* 51:333-355.
- Shigeri Y, Seal RP, Shimamoto K (2004) Molecular pharmacology of glutamate transporters, EAATs and VGLUTs. *Brain Res Brain Res Rev* 45:250-265.
- Sibson NR, Dhankhar A, Mason GF, Rothman DL, Behar KL, Shulman RG (1998) Stoichiometric coupling of brain glucose metabolism and glutamatergic neuronal activity. *Proc Natl Acad Sci U S A* 95:316-321.
- Siesjo BK (1988) Historical overview. Calcium, ischemia, and death of brain cells. *Ann N Y Acad Sci* 522:638-661.
- Siesjo BK (1990) Calcium in the brain under physiological and pathological conditions. *Eur Neurol* 30 Suppl 2:3-9; discussion 39-41.
- Siesjo BK, Bengtsson F (1989) Calcium fluxes, calcium antagonists, and calcium-related pathology in brain ischemia, hypoglycemia, and spreading depression: a unifying hypothesis. *J Cereb Blood Flow Metab* 9:127-140.
- Silver IA, Deas J, Erecinska M (1997) Ion homeostasis in brain cells: differences in intracellular ion responses to energy limitation between cultured neurons and glial cells. *Neuroscience* 78:589-601.
- Sim JA, Broomhead HE, North RA (2008) Ectodomain lysines and suramin block of P2X1 receptors. *J Biol Chem* 283:29841-29846.
- Sim JA, Young MT, Sung HY, North RA, Surprenant A (2004) Reanalysis of P2X7 receptor expression in rodent brain. *J Neurosci* 24:6307-6314.
- Sim JA, Chaumont S, Jo J, Ulmann L, Young MT, Cho K, Buell G, North RA, Rassendren F (2006) Altered hippocampal synaptic potentiation in P2X4 knock-out mice. *J Neurosci* 26:9006-9009.
- Simon J, Webb TE, Barnard EA (1997) Distribution of [³⁵S]dATP alpha S binding sites in the adult rat neuraxis. *Neuropharmacology* 36:1243-1251.
- Sinor JD, Du S, Venneti S, Blitzblau RC, Leszkiewicz DN, Rosenberg PA, Aizenman E (2000) NMDA and glutamate evoke excitotoxicity at distinct cellular locations in rat cortical neurons in vitro. *J Neurosci* 20:8831-8837.
- Skaper SD, Facci L, Culbert AA, Evans NA, Chessell I, Davis JB, Richardson JC (2006) P2X(7) receptors on microglial cells mediate injury to cortical neurons in vitro. *Glia* 54:234-242.
- Sladeczek F, Pin JP, Recasens M, Bockaert J, Weiss S (1985) Glutamate stimulates inositol phosphate formation in striatal neurones. *Nature* 317:717-719.
- Sofroniew MV, Vinters HV (2009) Astrocytes: biology and pathology. *Acta Neuropathol*.
- Solle M, Labasi J, Perregaux DG, Stam E, Petrushova N, Koller BH, Griffiths RJ, Gabel CA (2001) Altered cytokine production in mice lacking P2X(7) receptors. *J Biol Chem* 276:125-132.
- Soto F, Garcia-Guzman M, Gomez-Hernandez JM, Hollmann M, Karschin C, Stuhmer W (1996) P2X4: an ATP-activated ionotropic receptor cloned from rat brain. *Proc Natl Acad Sci U S A* 93:3684-3688.
- Sperlagh B, Zsilla G, Baranyi M, Illes P, Vizi ES (2007) Purinergic modulation of glutamate release under ischemic-like conditions in the hippocampus. *Neuroscience* 149:99-111.
- Sperlagh B, Kofalvi A, Deuchars J, Atkinson L, Milligan CJ, Buckley NJ, Vizi ES (2002) Involvement of P2X7 receptors in the regulation of neurotransmitter release in the rat hippocampus. *J Neurochem* 81:1196-1211.
- Spillson AB, Russell JW (2003) Metabotropic glutamate receptor regulation of neuronal cell death. *Exp Neurol* 184 Suppl 1:S97-105.
- Spray DC, Ye ZC, Ransom BR (2006) Functional connexin "hemichannels": a critical appraisal. *Glia* 54:758-773.
- Sprinkle TJ (1989) 2',3'-cyclic nucleotide 3'-phosphodiesterase, an oligodendrocyte-Schwann cell and myelin-associated enzyme of the nervous system. *Crit Rev Neurobiol* 4:235-301.
- Stokes L, Jiang LH, Alcaraz L, Bent J, Bowers K, Fagura M, Furber M, Mortimore M, Lawson M, Theaker J, Laurent C, Braddock M, Surprenant A (2006) Characterization of a selective and potent antagonist of human P2X(7) receptors, AZ11645373. *Br J Pharmacol* 149:880-887.
- Stout CE, Costantin JL, Naus CC, Charles AC (2002) Intercellular calcium signaling in astrocytes via ATP release through connexin hemichannels. *J Biol Chem* 277:10482-10488.

- Strasser U, Fischer G (1995) Protection from neuronal damage induced by combined oxygen and glucose deprivation in organotypic hippocampal cultures by glutamate receptor antagonists. *Brain Res* 687:167-174.
- Strijbos PJ, Leach MJ, Garthwaite J (1996) Vicious cycle involving Na⁺ channels, glutamate release, and NMDA receptors mediates delayed neurodegeneration through nitric oxide formation. *J Neurosci* 16:5004-5013.
- Suadicani SO, Brosnan CF, Scemes E (2006) P2X7 receptors mediate ATP release and amplification of astrocytic intercellular Ca²⁺ signaling. *J Neurosci* 26:1378-1385.
- Suarez-Huerta N, Pouillon V, Boeynaems J, Robaye B (2001) Molecular cloning and characterization of the mouse P2Y₄ nucleotide receptor. *Eur J Pharmacol* 416:197-202.
- Sugiyama K, Brunori A, Mayer ML (1989) Glial uptake of excitatory amino acids influences neuronal survival in cultures of mouse hippocampus. *Neuroscience* 32:779-791.
- Suh SW, Bergher JP, Anderson CM, Treadway JL, Fosgerau K, Swanson RA (2007) Astrocyte glycogen sustains neuronal activity during hypoglycemia: studies with the glycogen phosphorylase inhibitor CP-316,819 ([R-R*,S*]-5-chloro-N-[2-hydroxy-3-(methoxymethylamino)-3-oxo-1-(phenylmethyl)propyl]-1H-indole-2-carboxamide). *J Pharmacol Exp Ther* 321:45-50.
- Sun JJ, Liu Y, Ye ZR (2008) Effects of P2Y₁ receptor on glial fibrillary acidic protein and glial cell line-derived neurotrophic factor production of astrocytes under ischemic condition and the related signaling pathways. *Neurosci Bull* 24:231-243.
- Surprenant A, Rassendren F, Kawashima E, North RA, Buell G (1996) The cytolytic P2Z receptor for extracellular ATP identified as a P2X receptor (P2X₇). *Science* 272:735-738.
- Surprenant A, Schneider DA, Wilson HL, Galligan JJ, North RA (2000) Functional properties of heteromeric P2X_(1/5) receptors expressed in HEK cells and excitatory junction potentials in guinea-pig submucosal arterioles. *J Auton Nerv Syst* 81:249-263.
- Suzuki E, Kessler M, Montgomery K, Arai AC (2004) Divergent effects of the purinoceptor antagonists suramin and pyridoxal-5'-phosphate-6-(2'-naphthylazo-6'-nitro-4',8'-disulfonate) (PPNDS) on alpha-amino-3-hydroxy-5-methyl-4-isoxazolepropionic acid (AMPA) receptors. *Mol Pharmacol* 66:1738-1747.
- Suzuki R, Watanabe J, Arata S, Funahashi H, Kikuyama S, Shioda S (2003) A transgenic mouse model for the detailed morphological study of astrocytes. *Neurosci Res* 47:451-454.
- Swanson RA, Choi DW (1993) Glial glycogen stores affect neuronal survival during glucose deprivation in vitro. *J Cereb Blood Flow Metab* 13:162-169.
- Swanson RA, Farrell K, Stein BA (1997) Astrocyte energetics, function, and death under conditions of incomplete ischemia: a mechanism of glial death in the penumbra. *Glia* 21:142-153.
- Szatkowski M, Barbour B, Attwell D (1990) Non-vesicular release of glutamate from glial cells by reversed electrogenic glutamate uptake. *Nature* 348:443-446.
- Takano T, Oberheim N, Cotrina ML, Nedergaard M (2009) Astrocytes and ischemic injury. *Stroke* 40:S8-12.
- Tekkok SB, Goldberg MP (2001) Ampa/kainate receptor activation mediates hypoxic oligodendrocyte death and axonal injury in cerebral white matter. *J Neurosci* 21:4237-4248.
- Thomas R, Salter MG, Wilke S, Husen A, Allcock N, Nivison M, Nnoli AN, Fern R (2004) Acute ischemic injury of astrocytes is mediated by Na-K-Cl cotransport and not Ca²⁺ influx at a key point in white matter development. *J Neuropathol Exp Neurol* 63:856-871.
- Thornton P, Pinteaux E, Gibson RM, Allan SM, Rothwell NJ (2006) Interleukin-1-induced neurotoxicity is mediated by glia and requires caspase activation and free radical release. *J Neurochem* 98:258-266.
- Tian F, Gourine AV, Huckstepp RT, Dale N (2009) A microelectrode biosensor for real time monitoring of L-glutamate release. *Anal Chim Acta* 645:86-91.
- Tonazzini I, Trincavelli ML, Montali M, Martini C (2008) Regulation of A₁ adenosine receptor functioning induced by P2Y₁ purinergic receptor activation in human astroglial cells. *J Neurosci Res* 86:2857-2866.
- Tonazzini I, Trincavelli ML, Storm-Mathisen J, Martini C, Bergersen LH (2007) Co-localization and functional cross-talk between A₁ and P2Y₁ purine receptors in rat hippocampus. *Eur J Neurosci* 26:890-902.

- Torres GE, Haines WR, Egan TM, Voigt MM (1998) Co-expression of P2X1 and P2X5 receptor subunits reveals a novel ATP-gated ion channel. *Mol Pharmacol* 54:989-993.
- Towfighi J, Mauger D, Vannucci RC, Vannucci SJ (1997) Influence of age on the cerebral lesions in an immature rat model of cerebral hypoxia-ischemia: a light microscopic study. *Brain Res Dev Brain Res* 100:149-160.
- Tymianski M, Charlton MP, Carlen PL, Tator CH (1993a) Secondary Ca²⁺ overload indicates early neuronal injury which precedes staining with viability indicators. *Brain Res* 607:319-323.
- Tymianski M, Wallace MC, Spigelman I, Uno M, Carlen PL, Tator CH, Charlton MP (1993b) Cell-permeant Ca²⁺ chelators reduce early excitotoxic and ischemic neuronal injury in vitro and in vivo. *Neuron* 11:221-235.
- Ueda Y, Obrenovitch TP, Lok SY, Sarna GS, Symon L (1992) Efflux of glutamate produced by short ischemia of varied severity in rat striatum. *Stroke* 23:253-259.
- Valera S, Hussy N, Evans RJ, Adami N, North RA, Surprenant A, Buell G (1994) A new class of ligand-gated ion channel defined by P2x receptor for extracellular ATP. *Nature* 371:516-519.
- Van den Bergh V, Boens N, De Schryver FC, Ameloot M, Steels P, Gallay J, Vincent M, Kowalczyk A (1995) Photophysics of the fluorescent Ca²⁺ indicator Fura-2. *Biophys J* 68:1110-1119.
- Velasco I, Velasco-Velazquez MA, Salazar P, Lajud N, Tapia R (2003) Influence of serum-free medium on the expression of glutamate transporters and the susceptibility to glutamate toxicity in cultured cortical neurons. *J Neurosci Res* 71:811-818.
- Verkhrasky A, Krishtal OA, Burnstock G (2009) Purinoceptors on neuroglia. *Mol Neurobiol* 39:190-208.
- Verkhratsky A, Kirchhoff F (2007) NMDA Receptors in glia. *Neuroscientist* 13:28-37.
- Vermehren P (2005) Intracellular calcium and cell death in neonatal rat white matter astrocytes and neurons during ischaemia: protective effects of suramin and glutamate receptor blockers and the importance of astrocyte neuronal interactions. In: Department of Cell Physiology and Pharmacology, Faculty of Medicine and Biological Sciences, p 64. Leicester: University of Leicester.
- Vexler ZS, Ferriero DM (2001) Molecular and biochemical mechanisms of perinatal brain injury. *Semin Neonatol* 6:99-108.
- Vigne P, Hechler B, Gachet C, Breitmayer JP, Frelin C (1999) Benzoyl ATP is an antagonist of rat and human P2Y1 receptors and of platelet aggregation. *Biochem Biophys Res Commun* 256:94-97.
- Virginio C, MacKenzie A, Rassendren FA, North RA, Surprenant A (1999) Pore dilation of neuronal P2X receptor channels. *Nat Neurosci* 2:315-321.
- Volonte C, Merlo D (1996) Selected P2 purinoceptor modulators prevent glutamate-evoked cytotoxicity in cultured cerebellar granule neurons. *J Neurosci Res* 45:183-193.
- Volonte C, Ciotti MT, D'Ambrosi N, Lockhart B, Spedding M (1999) Neuroprotective effects of modulators of P2 receptors in primary culture of CNS neurones. *Neuropharmacology* 38:1335-1342.
- Volonte C, Amadio S, Cavaliere F, D'Ambrosi N, Vacca F, Bernardi G (2003) Extracellular ATP and neurodegeneration. *Curr Drug Targets CNS Neurol Disord* 2:403-412.
- Volpe JJ (2001) Neurobiology of periventricular leukomalacia in the premature infant. *Pediatr Res* 50:553-562.
- Volpe JJ (2003) Cerebral white matter injury of the premature infant-more common than you think. *Pediatrics* 112:176-180.
- Volpe JJ (2009) Brain injury in premature infants: a complex amalgam of destructive and developmental disturbances. *Lancet Neurol* 8:110-124.
- Volterra A, Meldolesi J (2005) Astrocytes, from brain glue to communication elements: the revolution continues. *Nat Rev Neurosci* 6:626-640.
- von Kugelgen I (2006) Pharmacological profiles of cloned mammalian P2Y-receptor subtypes. *Pharmacol Ther* 110:415-432.
- Vornov JJ (1995) Toxic NMDA-receptor activation occurs during recovery in a tissue culture model of ischemia. *J Neurochem* 65:1681-1691.
- Vornov JJ, Tasker RC, Coyle JT (1994) Delayed protection by MK-801 and tetrodotoxin in a rat organotypic hippocampal culture model of ischemia. *Stroke* 25:457-464; discussion 464-455.
- Waldo GL, Harden TK (2004) Agonist binding and Gq-stimulating activities of the purified human P2Y1 receptor. *Mol Pharmacol* 65:426-436.

- Wall MJ, Dale N (2007) Auto-inhibition of rat parallel fibre-Purkinje cell synapses by activity-dependent adenosine release. *J Physiol* 581:553-565.
- Wang P, Rothwell NJ, Pinteaux E, Brough D (2008) Neuronal injury induces the release of pro-interleukin-1beta from activated microglia in vitro. *Brain Res* 1236:1-7.
- Wang X, Arcuino G, Takano T, Lin J, Peng WG, Wan P, Li P, Xu Q, Liu QS, Goldman SA, Nedergaard M (2004) P2X7 receptor inhibition improves recovery after spinal cord injury. *Nat Med* 10:821-827.
- Wang XF, Cynader MS (1999) Effects of astrocytes on neuronal attachment and survival shown in a serum-free co-culture system. *Brain Res Brain Res Protoc* 4:209-216.
- Warr O, Takahashi M, Attwell D (1999) Modulation of extracellular glutamate concentration in rat brain slices by cystine-glutamate exchange. *J Physiol* 514 (Pt 3):783-793.
- Watano T, Matsuoka I, Kimura J (2002) Characteristics of ATP-induced current through P2X7 receptor in NG108-15 cells: unique antagonist sensitivity and lack of pore formation. *Jpn J Pharmacol* 88:428-435.
- Watkins JC, Jane DE (2006) The glutamate story. *Br J Pharmacol* 147 Suppl 1:S100-108.
- Weinberger JM (2006) Evolving therapeutic approaches to treating acute ischemic stroke. *J Neurol Sci* 249:101-109.
- White TD (1977) Direct detection of depolarisation-induced release of ATP from a synaptosomal preparation. *Nature* 267:67-68.
- Wigley R, Hamilton N, Nishiyama A, Kirchhoff F, Butt AM (2007) Morphological and physiological interactions of NG2-glia with astrocytes and neurons. *J Anat* 210:661-670.
- Wildman SS, Unwin RJ, King BF (2003) Extended pharmacological profiles of rat P2Y2 and rat P2Y4 receptors and their sensitivity to extracellular H⁺ and Zn²⁺ ions. *Br J Pharmacol* 140:1177-1186.
- Wilke S, Thomas R, Allcock N, Fern R (2004) Mechanism of acute ischemic injury of oligodendroglia in early myelinating white matter: the importance of astrocyte injury and glutamate release. *J Neuropathol Exp Neurol* 63:872-881.
- Wirkner K, Koles L, Thummler S, Luthardt J, Poelchen W, Franke H, Furst S, Illes P (2002) Interaction between P2Y and NMDA receptors in layer V pyramidal neurons of the rat prefrontal cortex. *Neuropharmacology* 42:476-488.
- Wirkner K, Kofalvi A, Fischer W, Gunther A, Franke H, Groger-Arndt H, Norenberg W, Madarasz E, Vizi ES, Schneider D, Sperlagh B, Illes P (2005) Supersensitivity of P2X receptors in cerebrocortical cell cultures after in vitro ischemia. *J Neurochem* 95:1421-1437.
- Witt MR, Dekermendjian K, Frandsen A, Schousboe A, Nielsen M (1994) Complex correlation between excitatory amino acid-induced increase in the intracellular Ca²⁺ concentration and subsequent loss of neuronal function in individual neocortical neurons in culture. *Proc Natl Acad Sci U S A* 91:12303-12307.
- Wong EH, Kemp JA, Priestley T, Knight AR, Woodruff GN, Iversen LL (1986) The anticonvulsant MK-801 is a potent N-methyl-D-aspartate antagonist. *Proc Natl Acad Sci U S A* 83:7104-7108.
- Wu X, Zhu D, Jiang X, Okagaki P, Mearow K, Zhu G, McCall S, Banaudha K, Lipsky RH, Marini AM (2004) AMPA protects cultured neurons against glutamate excitotoxicity through a phosphatidylinositol 3-kinase-dependent activation in extracellular signal-regulated kinase to upregulate BDNF gene expression. *J Neurochem* 90:807-818.
- Xing J, Lu J, Li J (2008) Purinergic P2X receptors presynaptically increase glutamatergic synaptic transmission in dorsolateral periaqueductal gray. *Brain Res* 1208:46-55.
- Xiong ZG, Zhu XM, Chu XP, Minami M, Hey J, Wei WL, MacDonald JF, Wemmie JA, Price MP, Welsh MJ, Simon RP (2004) Neuroprotection in ischemia: blocking calcium-permeable acid-sensing ion channels. *Cell* 118:687-698.
- Xu L, Sapolsky RM, Giffard RG (2001) Differential sensitivity of murine astrocytes and neurons from different brain regions to injury. *Exp Neurol* 169:416-424.
- Yan Z, Li S, Liang Z, Tomic M, Stojilkovic SS (2008) The P2X7 receptor channel pore dilates under physiological ion conditions. *J Gen Physiol* 132:563-573.
- Yao H, Haddad GG (2004) Calcium and pH homeostasis in neurons during hypoxia and ischemia. *Cell Calcium* 36:247-255.
- Ye ZC, Sontheimer H (1998) Astrocytes protect neurons from neurotoxic injury by serum glutamate. *Glia* 22:237-248.

- Ye ZC, Wyeth MS, Baltan-Tekkok S, Ransom BR (2003) Functional hemichannels in astrocytes: a novel mechanism of glutamate release. *J Neurosci* 23:3588-3596.
- Yoon WJ, Won SJ, Ryu BR, Gwag BJ (2003) Blockade of ionotropic glutamate receptors produces neuronal apoptosis through the Bax-cytochrome C-caspase pathway: the causative role of Ca²⁺ deficiency. *J Neurochem* 85:525-533.
- Yu AC, Gregory GA, Chan PH (1989) Hypoxia-induced dysfunctions and injury of astrocytes in primary cell cultures. *J Cereb Blood Flow Metab* 9:20-28.
- Yu AC, Wong HK, Yung HW, Lau LT (2001) Ischemia-induced apoptosis in primary cultures of astrocytes. *Glia* 35:121-130.
- Yu L, Huang Z, Mariani J, Wang Y, Moskowitz M, Chen JF (2004) Selective inactivation or reconstitution of adenosine A2A receptors in bone marrow cells reveals their significant contribution to the development of ischemic brain injury. *Nat Med* 10:1081-1087.
- Zamzow CR, Xiong W, Parkinson FE (2008) Astrocytes affect the profile of purines released from cultured cortical neurons. *J Neurosci Res* 86:2641-2649.
- Zeevalk GD, Davis N, Hyndman AG, Nicklas WJ (1998) Origins of the extracellular glutamate released during total metabolic blockade in the immature retina. *J Neurochem* 71:2373-2381.
- Zeng JW, Liu XH, Zhang JH, Wu XG, Ruan HZ (2008a) P2Y1 receptor-mediated glutamate release from cultured dorsal spinal cord astrocytes. *J Neurochem* 106:2106-2118.
- Zeng JW, Liu XH, He WJ, Du L, Zhang JH, Wu XG, Ruan HZ (2008b) Inhibition of ATP-induced glutamate release by MRS2179 in cultured dorsal spinal cord astrocytes. *Pharmacology* 82:257-263.
- Zhang FL, Luo L, Gustafson E, Palmer K, Qiao X, Fan X, Yang S, Laz TM, Bayne M, Monsma F, Jr. (2002) P2Y₁₃: identification and characterization of a novel Galphai-coupled ADP receptor from human and mouse. *J Pharmacol Exp Ther* 301:705-713.
- Zhang RL, Zhang ZG, Chopp M (2008) Ischemic stroke and neurogenesis in the subventricular zone. *Neuropharmacology* 55:345-352.
- Zhang Z, Chen G, Zhou W, Song A, Xu T, Luo Q, Wang W, Gu XS, Duan S (2007) Regulated ATP release from astrocytes through lysosome exocytosis. *Nat Cell Biol* 9:945-953.
- Zhao G, Flavin MP (2000) Differential sensitivity of rat hippocampal and cortical astrocytes to oxygen-glucose deprivation injury. *Neurosci Lett* 285:177-180.
- Zhu Y, Kimelberg HK (2001) Developmental expression of metabotropic P2Y₁ and P2Y₂ receptors in freshly isolated astrocytes from rat hippocampus. *J Neurochem* 77:530-541.
- Zhuo L, Sun B, Zhang CL, Fine A, Chiu SY, Messing A (1997) Live astrocytes visualized by green fluorescent protein in transgenic mice. *Dev Biol* 187:36-42.
- Ziak D, Chvatal A, Sykova E (1998) Glutamate-, kainate- and NMDA-evoked membrane currents in identified glial cells in rat spinal cord slice. *Physiol Res* 47:365-375.
- Ziganshin AU, Hoyle CH, Lambrecht G, Mutschler E, Bumert HG, Burnstock G (1994) Selective antagonism by PPADS at P2X-purinoceptors in rabbit isolated blood vessels. *Br J Pharmacol* 111:923-929.
- Zimmermann H (1996) Biochemistry, localization and functional roles of ecto-nucleotidases in the nervous system. *Prog Neurobiol* 49:589-618.
- Zimmermann H (2006) Ectonucleotidases in the nervous system. *Novartis Found Symp* 276:113-128; discussion 128-130, 233-117, 275-181.
- Zona C, Marchetti C, Volonte C, Mercuri NB, Bernardi G (2000) Effect of P2 purinoceptor antagonists on kainate-induced currents in rat cultured neurons. *Brain Res* 882:26-35.